Acta Neurochirurgica Supplement 118

Yoichi Katayama · Takeshi Maeda
Toshihiko Kuroiwa *Editors*

Brain Edema XV

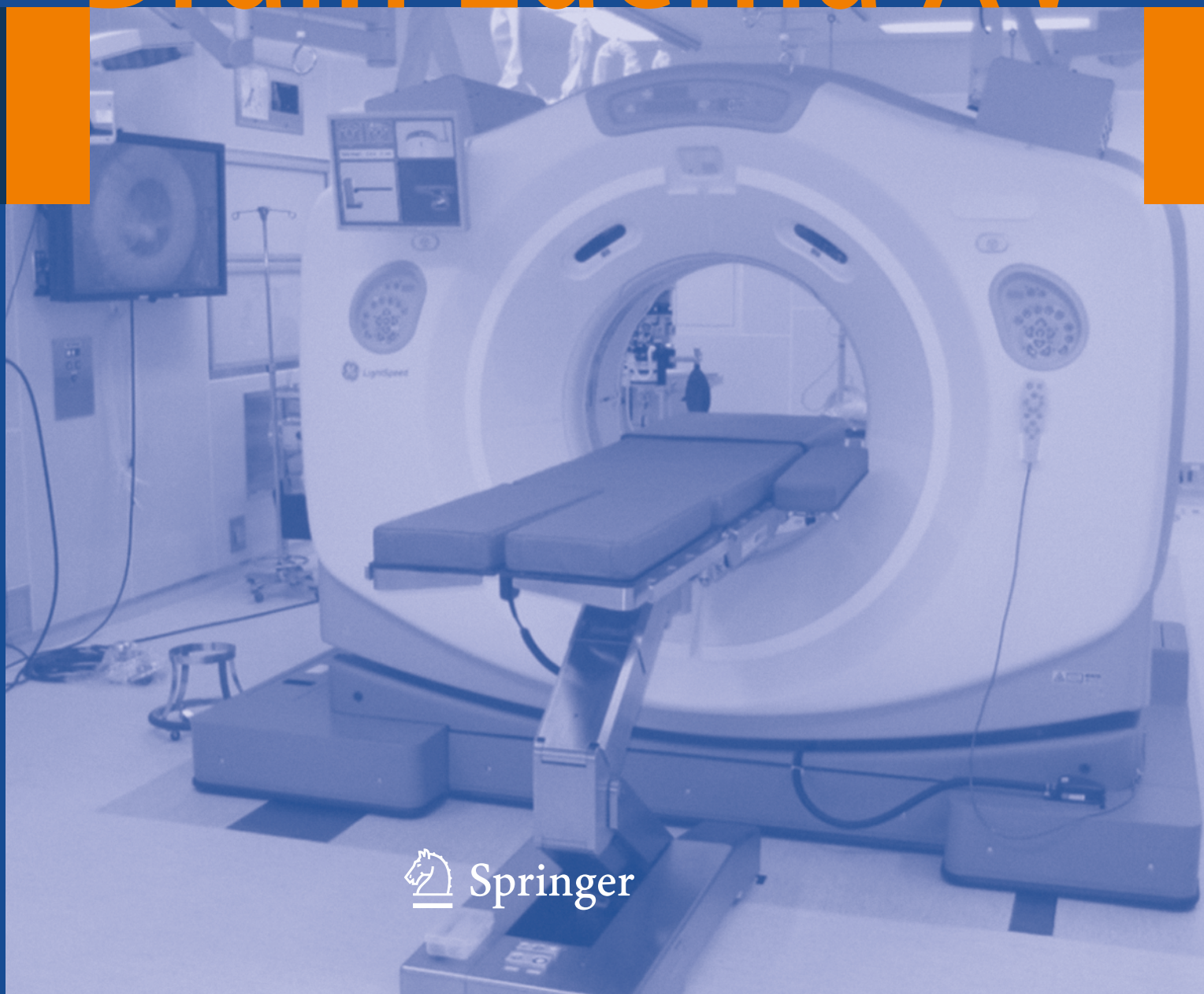

Springer

Acta Neurochirurgica
Supplements

Editor: H.-J. Steiger

Brain Edema XV

Edited by
Yoichi Katayama, Takeshi Maeda, and Toshihiko Kuroiwa

Acta Neurochirurgica
Supplement 118

Springer

Yoichi Katayama
Department of Neurological Surgery
Nihon University
School of Medicine
Tokyo, Japan

Takeshi Maeda
Departments of Neurological Surgery
and Anesthesiology
Nihon University
School of Medicine
Tokyo, Japan

Toshihiko Kuroiwa
Laboratory of Clinical Medicine
Namegata District
General Hospital
Ibaraki, Japan

Typesetting: SPI, Pondichery, India
Printed on acid-free and chlorine-free bleached paper

Library of Congress Control Number: 2013936438

With 46 (partly coloured) Figures

ISSN 0065-1419
ISBN 978-3-7091-1433-9 ISBN 978-3-7091-1434-6 (eBook)
DOI 10.1007/978-3-7091-1434-6
Springer Wien Heidelberg New York Dordrecht London

Preface

I am delighted to be able to hold and scrutinize this book, the 15th volume in the series of proceedings which covers the official symposia of the International Brain Edema Society. The first symposium was held in Vienna in 1965 under the auspices of Drs. Igor Klazo and Franz Seitelberger. The 15th symposium (Brain Edema 2011, The XVth International Symposium of Brain Edema and Cellular Injury), on which this volume is based, took place in Tokyo, on 22–24 October 2011. During this 46-year period the various proceedings have continued to offer up-to-date information in the field of brain edema research. Since the eighth symposium, which was held in Bern by Dr. Hans-J Reulen, the proceedings of each symposium have been published as a supplement to *Acta Neurochirurgica*. The present advisory board decided to continue this tradition.

On 11 March 2011, the northwestern part of Japan's main island was struck by a massive earthquake and tsunami, which subsequently led to serious problems in the region's nuclear power plants. As a result, Japan and the Japanese people suffered great emotional as well as economic depression. This was not an atmosphere in which we felt able to welcome our expected guests from outside Japan. It thus became very difficult for us, the local organizing committee, to decide whether or not the 15th symposium should be held as planned. However, warm encouragement was given to us by participants from many countries outside Japan, such as Dr. Alexander Baethmann who was our guest of honor for the symposium, and we thank them all for the support. Their unchanged intentions to participate in the symposium led us to decide proceed as planned. The 15th symposium thus took place because of their unflinching determination to be there with us.

Dr. Anthony Marmarou passed away after the last symposium, which was held in Warsaw by Dr. Zbigniew Czernicki. On the occasion of the 15th symposium, in order to commemorate the works of Dr. Marmarou, Dr. Katsuji Shima was honored to present a lecture named after him, and Dr. Hari Shanker Sharma was elected as recipient of the Anthony Marmarou Award.

It is clearly evident that our field of endeavor has undergone rapid development through close cooperation and association between neurosurgeons and basic scientists. The 15th symposium placed an emphasis on identifying and defining the roles of neurosurgeons within the broad multi-disciplinary spectrum of brain edema research, and on reviewing recent advances across a wide range of surgical and non-surgical techniques that can contribute to improvement of the patient's outcome. To facilitate communication and cooperation among neurosurgeons and scientists within the field of brain edema research, the 15th symposium was supported and co-sponsored by the Japan Neurosurgical Society (JNSS) and organized in conjunction with the 17th annual meeting of the Japan Neuromonitoring Society. We are very grateful for the cooperation provided by these societies.

As expected, the 15th symposium provided an excellent opportunity to share knowledge among neurosurgeons and basic scientists. The symposium drew strong attention and interest among neurosurgeons regarding recent progress in the relevant fields of basic sciences, and helped basic scientists to discuss their achievements in the context of a clearer understanding of recent developments in surgical techniques. We would like to express our gratitude to all participants at the 15th symposium and contributors to this volume for providing an excellent opportunity for everyone to interact with each other.

We greatly acknowledge Dr. Czernicki, who contributed to the International Society of Brain Edema as President during the period 2008–2011, for his unfailing support so generously given to us in holding the 15th symposium. We also express our acknowledgement to Nihon University and its medical alumni association who granted funds and provided indispensable support for this symposium.

Tokyo, January 2013 Yoichi Katayama
Tokyo, January 2013 Takeshi Maeda

Anthony Marmarou, PhD, 1934–2010

Dr. Anthony Marmarou was born on 15 March 1934 in Philadelphia, Pennsylvania, USA. He attended Drexel University, receiving a Bachelor of Science in Electrical Engineering. He continued his education at the University of Pennsylvania, where he received his Master's in Control Engineering, and finally, Temple University School of Medicine, where he completed an NIH Special Research Fellowship and a PhD. in Biomedical Engineering. His scientific exploration of intracranial pressure (ICP) dynamics in traumatic brain injury (TBI) began at Albert Einstein Medical in the Bronx, New York, and was continued during his 27 years with the Virginia Commonwealth University (VCU) Department of Neurosurgery in Richmond, Virginia. Well known for his commitment to research on TBI and normal pressure hydrocephalus (NPH), Dr. Marmarou was considered a world authority on fluid dynamics within the brain and spinal cord. His tireless efforts to communicate the results of his scientific studies on a global stage earned him an international reputation as an outstanding scholar and scientist. Dr. Marmarou, in collaboration with his long-standing research partner, Dr. Harold Young, Chairman of the Department of Neurosurgery at VCU, led an international team in developing the first clinical guidelines for the diagnosis and treatment of idiopathic NPH. Their tireless efforts have resulted in our current standard of care for patients with NPH. Dr. Marmarou's statement that "Patients should explore all their options because there is always hope" has earned him the unerring devotion of these patients and his staff. Dr. Marmarou was one of those unique researchers who could bring basic laboratory research directly to the bedside to improve patient care and treatment. Also noteworthy were his collaborative basic research studies targeting mechanisms of cellular injury following TBI and stroke in collaboration with Dr. John Povlishock, Professor and Chairman of Anatomy and Neurobiology at VCU, and Dr. Ross Bullock, Professor of Neurosurgery at the University of Miami. Their efforts on the experimental front have led the way to novel therapies currently being evaluated to attenuate the devastating effects of human head injury. Dr. Marmarou was a leader in the scientific community and was honored for his work by the Brazilian, English, French, German, Greek,

Dr. Anthony Marmarou in his laboratory.

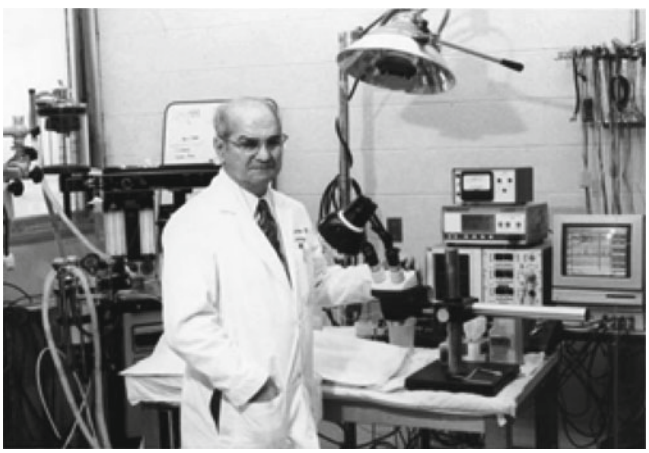

Dr. Marmarou in discussion with Dr. Povlishock.

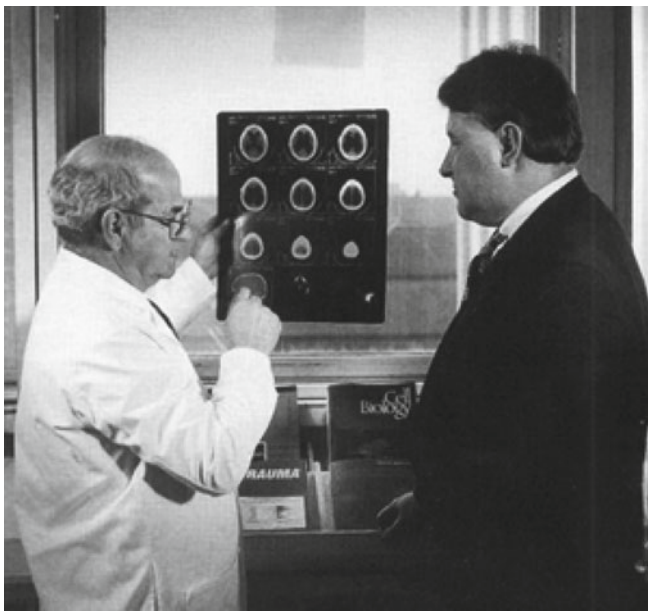

Japanese, and Turkish Neurosurgical Societies. In particular, his collaborative efforts with Dr. Katsuji Shima, Professor and Chairman of Neurosurgery at the National Defense Institute in Japan, established global standards for the care and management of ICP following TBI. His scientific legacy remains assured, since it will live on through the dedication of over 200 neurosurgical fellows he has trained throughout his scientific career. We will miss his wisdom and humanity as well as his tireless devotion to scientific advancement for patients.

Acknowledgments

The editors would like to express their sincere thanks to those who made the 15th International Symposium of Brain Edema possible. We give thanks especially to the Executive and Emeritus Board Member of the International Brain Edema Society.

Executive Board Member of the International Brain Edema Society
(*21 October 2011–*)

R. Bullock
Z. Czernicki
Y. Katayama
O. Kempski
T. Kuroiwa
D. Mendelow
N. Plesnila
R. Suzuki
G. Xi
J. Zhang

Emeritus Board Member
A. Baethmann
U. Ito

Contents

Trauma (Clinical)

Cerebral Hemorrhage

Neuromonitoring & Neuroimaging

Treatments

International Brain Edema Symposia 1967–2011

Toshihiko Kuroiwa

Abstract This is a brief review of previous international brain edema symposia. The symposia that took place from 1965 to 1999 were summarized by Igor Klatzo and A. Marmarou in the proceedings Brain Edema XI [1]. In this article the author summarized the symposia, including latest five. Images from previous symposia such as the cover pages of the proceedings and snapshots of organizers were included. The outline and key words of the symposia were summarized in tables. The name of the prize winner and the title of the memorial lectures in recent symposia were also summarized in a table.

Keywords Brain edema • International brain edema symposia • Proceedings • Symposia organizers • Prize winner • Memorial lecture

This is a brief review of previous international brain edema symposia. The symposia that took place from 1965 to 1999 were summarized by Igor Klatzo and A. Marmarou in the proceedings Brain Edema XI [1]. In this article the author summarized the symposia, including latest five. Images from previous symposia such as the cover pages of the proceedings and snapshots of organizers were included (Figs. 1, 2). The outline and key words of the symposia were summarized in tables (Tables 1, 2). The name of the prize winner and the title of the memorial lectures in recent symposia were also summarized in a table (Table 3).

The first brain edema symposium was organized by Franz Seitelberger and Igor Klatzo in 11–13 September 1965 in Vienna. The symposium was planned by the Österreichische Arbeitsgemeinschaft für Neuropathologie and by the Problem Commission for Neuropathology of the World Federation of Neurology. Fifty-eight participants, including Milton W. Brightman, Konstantin Alexander Hossmann, Asao Hirano, and Kraus Joachim Zülch are listed in the proceedings [2]. The importance of a multidisciplinary approach and studies on ultrastructural/molecular levels were emphasized in the symposium. Kraus Joachim Zülch described the differences between brain swelling (an intracellular increase in fluid or protein) and brain edema (an intercellular accumulation of fluid). Asao Hirano presented extracellular accumulation of edema fluid in the white matter after polysaccharide implantation and experimental allergic encephalomyelitis. The importance of active endothelial transport in edema development was presented. A round table discussion chaired by R.D. Adams summarized the symposium. The proceedings were published by Springer, Vienna/New York in 1967.

The second brain edema symposium was organized by Hans Jürgen Reulen and Kurt Schürmann. The symposium was held in Mainz, 19–21 June 1972. The main topic was the effect of steroids on brain edema, i.e., 22 out of 29 papers in the proceedings dealt with steroids. Other topics included the role of free radicals in the development of brain edema and the therapeutic effect of antioxidants. Hypertonic blood-brain barrier opening was presented. Classification of brain edema into the cytotoxic type and the vasogenic type by Igor Klatzo [3] was widely accepted. A round table discussion summarized the symposium. The proceedings were published by Springer, Berlin/Heidelberg/New York in 1972 [4].

The third brain edema symposium was organized by Hanna M. Pappius and William Feindel, 25–29 June 1976, in Montreal. One of the main topics was the function and dysfunction of the blood–brain barrier. About half of the papers were included in the chapters on the blood brain–barrier and vasogenic edema. Increased pinocytosis was observed after seizures and post-irradiation edema. Bulk flow and colloid osmotic pressure, the pathophysiology of

T. Kuroiwa, M.D.
Laboratory of Clinical Medicine, Namegata District General Hospital, 98-8 Inouefujii, Namegata, Ibaraki 311-3516, Japan
e-mail: tkuroiwa-nsu@umin.ac.jp

Y. Katayama et al. (eds.), *Brain Edema XV*, Acta Neurochirurgica Supplement, Vol. 118,
DOI 10.1007/978-3-7091-1434-6_1,

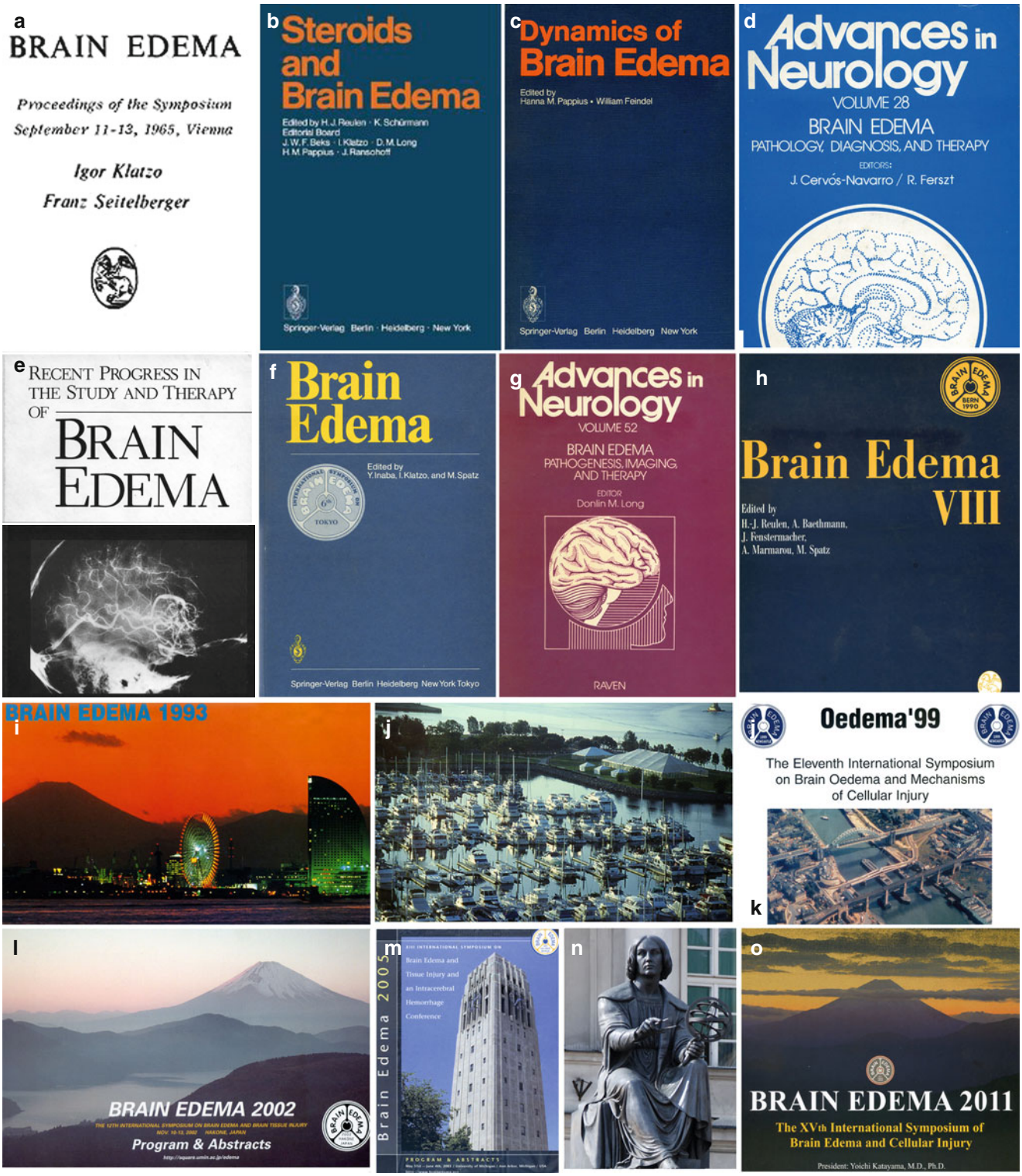

Fig. 1 Images from past brain edema symposia. (**a**) Inside cover of the proceedings of brain edema I. (**b**–**h**) Covers of the proceedings of brain edema II, III, IV, V, VI, VII, and VIII. (**i**) Poster of brain edema IX. (**j**) Yacht harbor in San Diego, brain edema X. (**k**) Poster of brain edema XI. (**l**) Cover of the abstracts book for brain edema XII. (**m**) Poster of brain edema XIII, (**n**) Statue of Copernicus in front of a building of the Polish Academy of Science, brain edema XIV. (**o**) Cover of the abstracts book, brain edema XV

early ischemic edema, and various animal models of ischemia were the other main topics of the symposium. Computed tomography findings of brain edema were presented in the brain symposium for the first time. The proceedings were published by Springer, Berlin/Heidelberg/New York in 1976 [5].

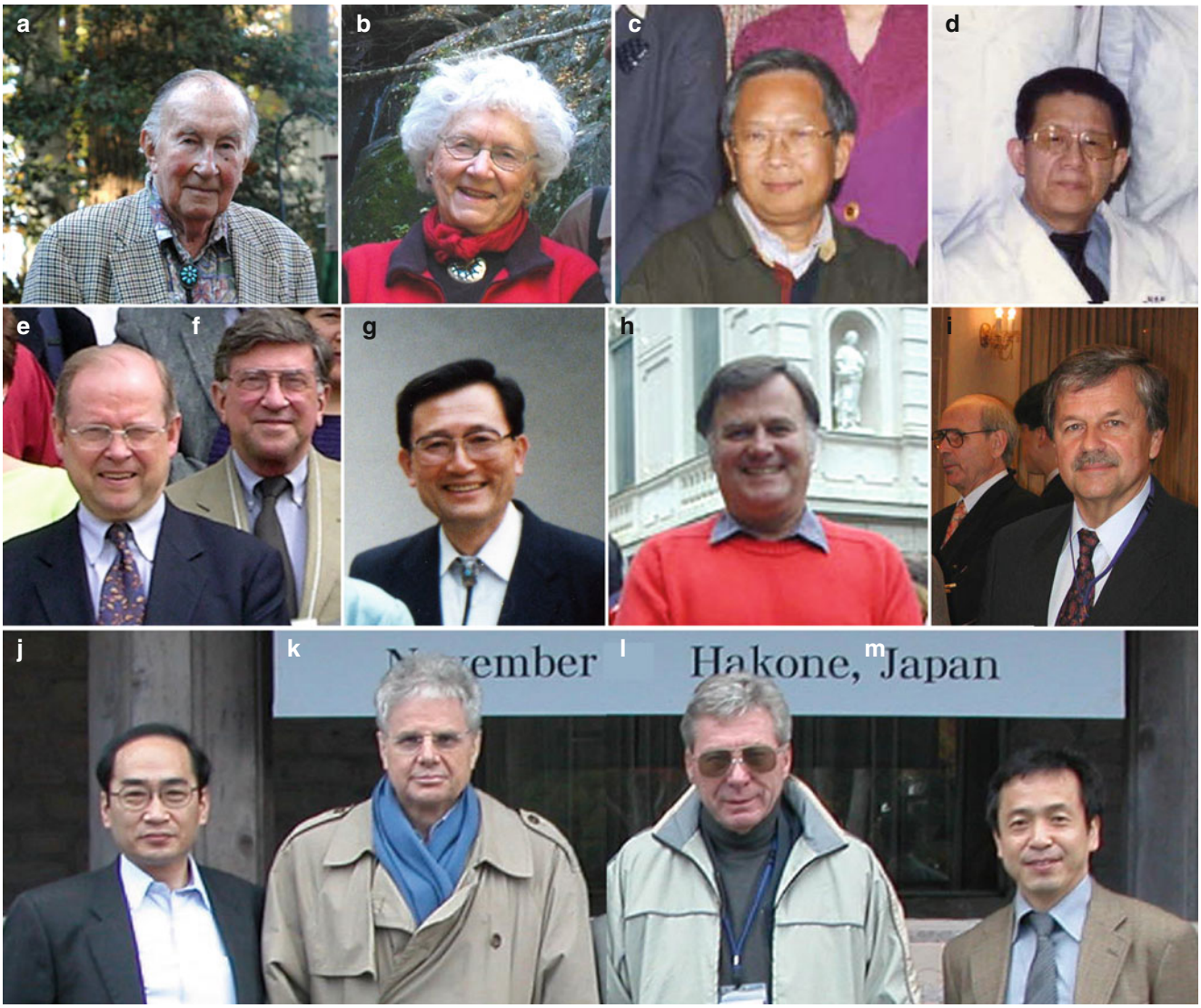

Fig. 2 Organizers of brain edema symposia. (**a**) Igor Klatzo, Brain edema I. (**b**) Hanna M. Pappius, brain edema II. (**c**) K.G.G., brain edema V. (**d**) Yutaka Inaba, brain edema VI. (**e**) Julian T. Hoff, brain edema XIII. (**f**) Hector James, brain edema X. (**g**) Umeo Ito, brain edema IX. (**h**) A. David Mendelow, brain edema XI. (**i**) Zbigniew Czernicki brain edema XIV. (**j**) Yoichi Katayama, brain edema XV. (**k**) Alexander Baethmann, editor of brain edema proceedings. (**l**) Hans J. Reulen, brain edema VIII. (**m**) Toshihiko Kuroiwa, brain edema XII

The fourth symposium was organized by Jordi Cervós-Navarro and R. Ferszt in Berlin in 1980. Ultrastructural tracer study on change in the blood–brain barrier in various pathological situations showed increased vesicular transport. Brain edema factors, such as serotonin, fatty acids, and glutamate, were discussed. Biomechanics of edema and the mechanism of the resolution of edema were other topics on offer. Several papers dealt with computed tomography findings on various types of brain edema. Positron emission tomography was emerging as a potentially powerful tool for brain edema research. The proceedings were published by Raven Press, New York in 1980 [6].

The fifth symposium was organized by K.G. Go and Jan Beks in the Martinihal Center in Groningen, 10–12 June 1982. Several new areas of investigation that had been introduced into brain edema research were reported, which included nuclear magnetic resonance imaging and ^{14}C deoxyglucose autoradiography. Several clinical studies on brain edema using positron emission tomography were also presented. Cerebral endothelial cell culture, calcium antagonists, anti-inflammatory drugs, and prostaglandin synthesis were some of the other topics. The proceedings were published by Plenum Press, New York/London in 1982 [7].

The sixth symposium was organized by Yutaka Inaba in 7–10 November 1984 in Tokyo. The symposium was for the first time held in Asia. A series of invited lectures were given by Igor Klatzo, Asao Hirano, Stanley I. Rapoport, Bo K. Siesjö, Hanna M. Pappius, Konstantin Alexander Hossmann, and Donlin M. Long. B.K. Siesjö presented the mechanism of cytotoxic edema and intracellular pH. K.A. Hossmann reported the mechanism of post-ischemic edema and S.I. Rapoport the mechanism of vasogenic brain edema. A finite

Table 1 Date, venue, and organizers, title, publisher, year of publication, the number of papers in the proceedings/presentations in the symposium

	Date	Venue	Organizer(s)	Book title/publisher/year	No. of papers
1	Sept 11–13, 1965	Vienna	Igor Klatzo, Franz Seitelberger	Brain edema *proceedings of the symposium 11–13 September 1965, Vienna*/Springer/Vienna, New York/1967	48/–
2	June 19–21, 1972	Mainz	Hans-J. Reulen, K. Schürmann	Steroids and brain edema/Springer/Berlin, Heidelberg, New York	29/
3	June 25–29, 1976	Montreal	Hanna M. Pappius, William Feindel	Dynamics of brain edema/Springer/Berlin, Heidelberg, New York/1976	53/–
4	Sept 12–15, 1979	Berlin	J. Cervós-Navarro, R. Ferszt	Brain edema pathology diagnosis and therapy, Advances in Neurology, vol. 28/Raven Press/New York/1980	38/–
5	June 10–12, 1982	Groningen, The Netherlands	K.G. Go, Jan Beks	Recent progress in the study and therapy of brain edema/Plenum Press/New York, London/1982	69/–
6	Nov 7–10, 1984	Tokyo	Yutaka Inaba	Brain edema/Springer/Berlin, Heidelberg, New York, Tokyo/1985	101/112
7	1987	Baltimore, MD	Donlin M. Long	Brain edema pathogenesis, imaging, and therapy, Advances in Neurology, vol 52/Raven Press/New York/1987	68/90[a]
8	June 17–20, 1990	Bern	Hans-J. Reulen	Brain edema VIII, Acta Neurochirurgica supplement 50/Springer/Vienna, New York/1990	139/158
9	May 16–19, 1993	Yokohama	Umeo Ito	Brain edema IX, Acta Neurochirurgica supplement 60/Springer/Vienna, New York/1994	149/190
10	October 20–23, 1996	San Diego	Hector E. James	Brain edema X, Acta Neurochirurgica supplement 70/Springer/Vienna, New York/1997	92/108
11	June 6–10, 1999	Newcastle	A. David Mendelow	Brain edema XI, Acta Neurochirurgica supplement 80/Springer/Vienna, New York/2000	117/151
12	Nov 10–13, 2002	Hakone, Japan	Toshihiko Kuroiwa	Brain edema XII, Acta Neurochirurgica supplement 86/Springer/Vienna, New York/2003	119/155
13	June 1–3, 2005	Ann Arbor Michigan	Julian T. Hoff	Brain edema XIII, Acta Neurochirurgica supplement 96 Springer/Vienna, New York/2006	95/109
14	June 11–14, 2008	Warsaw	Zbigniew Czernicki	Brain edema XIV, Acta Neurochirurgica supplement 106/Springer/Vienna, New York/2009	65/104
15	Oct 22–24, 2011	Tokyo	Yoichi Katayama	Brain edema XV, Acta Neurochirurgica supplement/Springer/Vienna, New York/2011	–/119

[a]The number of papers in the proceedings/presentations in the abstract book

element method was introduced for computer simulation of the propagation of vasogenic brain edema. The symposium had many participants from Asia, i.e., 51 papers from Japan and two from China. The logo of the brain edema symposium was designed by Dr. Inaba. It was decided that the symposium would be held in order of United States, Europe, and Japan, by advisor Committee. The proceedings were published by Springer, Berlin/Heidelberg/New York/Tokyo in 1985 [8].

The seventh symposium was organized by Donlin M. Long in Baltimore in 1987. Molecular mechanism of glial swelling, the effect of superoxide dismutase and free radical scavengers were some of the topics discussed in the symposium. A keynote address entitled "Peritumoral brain edema" was given by H.J. Reulen, i.e., a clinical study visualizing the spread and resolution of edema by repeated dynamic CT. Sixty-eight papers and 22 abstracts were included in the proceedings, published by Raven Press, New York in 1990 [9].

The eighth symposium was organized by Hans Jürgen Reulen in Bern, 17–20 June 1990. Klaus Joachim Zülch died in 1988 and Igor Klatzo started the symposium with a lecture

Table 2 Keywords and phrases of the symposia

	Year	Venue	Keywords/phrases
1	1965	Vienna	The first brain edema symposium, brain swelling and brain edema, electron microscopy, active transendothelial transport, round table discussion, Springer, Vienna
2	1972	Mainz	Steroids, free radicals, antioxidants, classification of brain edema, hypertonic blood–brain barrier opening
3	1976	Montreal	BBB function and dysfunction, increased pinocytosis, bulk flow and colloid osmotic pressure, early ischemic edema, computed tomography
4	1979	Berlin	Ultrastrucutural tracer study on blood–brain barrier change, development and resolution of edema, brain edema factors, serotinin, glutamate, biomechanics of edema, positron emission tomography
5	1982	Groningen	Magnetic resonance imaging, ^{14}C deoxyglucose antoradiography, cerebral endothelial cell culture, anti-inflammatory drugs and prostaglandin synthesis, calcium antagonists
6	1984	Tokyo	The first meeting in Asia, invited lecture series by Klatzo Siesjö, Hossmann, etc., cytotoxic edema and intracellular pH, mechanism of postischemic edema, finite element method, logo of the symposium
7	1987	Baltimore	Molecular mechanism of glial swelling, superoxide dismutase, free radical scavenger, keynote address, peritumoral brain edema
8	1990	Bern	K.J. Zülch Memorial lecture, experimental and clinical application of magnetic resonance imaging, ischemic brain edema, atrial natriuretic peptide, publication of proceedings within 6 months, Springer, Vienna
9	1993	Yokohama	Glutamate and glial swelling, NMR diffusion imaging, vascular endothelial growth factor, anisotropic swelling, the largest symposium in the history of brain edema symposia, International Society for Brain Edema Research
10	1996	San Diego	J. Douglas Miller memorial lecture, hypothermia, hyperthermia, ischemia and traumatic edema, NMDA antagonists, magnetic transfer contrast imaging
11	1999	Newcastle	Magnetic resonance spectroscopy, spreading depression, human brain microvascular endothelial cell culture, hypothermia, aquaporin 4, clinical monitoring of traumatic edema, cannabinoids
12	2002	Hakone	Aquaporins in the formation and resolution of edema, high-throughput gene profiling, surgical decompression for the treatment of ICH, Hakone best presentation award, sponsored sessions, round-table discussion
13	2005	Ann Arbor	Satellite intracranial hemorrhage conference, neurovascular unit after hemorrhage, multimodal approaches to brain injury, surgical management of cerebral contusion, convection-enhanced drug distribution, STICH trial
14	2008	Warsaw	The first edema symposium in the former Eastern European countries, Igor Klatzo lecture, clinical papers on the diagnosis and treatment of edema, decompressive craniectomy, nanoparticles,
15	2011	Tokyo	Symposium held 7 months after great earthquake in eastern Japan, A. Marmarou award, student's award, neurovascular mechanisms after stroke, neuromonitoring, pathomechanisms and treatment of traumatic brain edema

to commemorate Zülch. Results of experimental or clinical study using magnetic resonance imaging on brain edema were reported from many institutions. Papers on atrial natriuretic peptide were presented by several laboratories. The proceedings were published in 1990 within 6 months of the symposium by Springer [10], much faster than for previous

proceedings. The proceedings were divided into chapters such as pathophysiology, tumor, ischemia, trauma, hypertension, and hydrocephalus. The process and the style of the publication were inherited by subsequent symposia.

The ninth symposium was organized by Umeo Ito in Yokohama, 16–19 May 1993. There were four guidelines, namely (1) blood-parenchymal cell border injury, (2) neuroglial interactions and injury, (3) formation, propagation, and resolution of edema, and (4) treatment. Sessions of these themes started with the keynote lecture, e.g., "Neuron-Glial Interactions During Injury and Edema of the CNS" by Oliver Kempski in the session "Neuron-Glial Cell Injury and Edema." Some of the topics of the symposium were glutamate and glial swelling, NMR diffusion imaging, vascular endothelial growth factor, anisotropic swelling, and NMDA antagonists. There were 190 presentations, which was the largest number in the history of international brain symposia. The establishment of the International Society for Brain Edema Research was proposed by Dr. Ito. The proceedings were published by Springer in 1994 [11].

The tenth symposium was organized by Hector E. James near the beautiful yacht harbor in the city of San Diego, 20–23 October 1996. The J. Douglas Miller memorial lecture on traumatic brain injury was given by A. Marmarou at the beginning of the symposium. About half of the papers were on ischemic edema or traumatic edema. Edema associated with hypothermia or hyperthermia was another main topic of the symposium. New imaging methods such as magnetic transfer contrast imaging were reported. Several new therapeutic substances were also reported. The proceedings were published in 1997 by Springer [12].

The 11th symposium was organized by A. David Mendelow in Newcastle-upon-Tyne, 6–10 June 1999. Some of the topics were magnetic resonance spectroscopy, spread of depression, human brain microvascular endothelial cell culture, and hypothermia. Aquaporin 4 mRNA expression following cerebral ischemia was reported. The session on traumatic edema was the largest in the symposium, where mechanisms of secondary damage after trauma and clinical monitoring were the foci of discussion. New neuroprotective agents such as growth factors and cannabinoids were described. There was a summary at the beginning of each chapter of the proceedings, which allowed the reader a quick overview of each topic. The proceedings were published by Springer in 2000 [13].

The 12th symposium was organized by Toshihiko Kuroiwa, 10–13 November 2002. The symposium was held on the shores of Lake Ashi in the Fuji-Hakone-Izu National Park. Some of the topics included the role of aquaporins in the formation and resolution of edema, high-throughput gene profiling, and surgical decompression for the treatment of intracerebral hemorrhage. Two short sessions were sponsored by pharmaceutical and medical equipment companies. Six papers were selected by an international board chaired by A. David Mendelow for the Hakone Best Presentation award at the end of the symposium (Fig. 3; Table 3). A round table discussion summarized the symposium. The proceedings were published by Springer in 2003 [14].

The 13th symposium was organized by Julian T. Hoff in Ann Arbor, 31 May—to 3 June 2005, succeeded by a 1-day satellite conference on intracerebral hemorrhage (ICH) on 4 June. Some of the topics of keynote lectures were neurovascular unit after hemorrhage, multimodal approaches to brain injury, surgical management of cerebral contusion and convection-enhanced drug distribution. Some results from the STICH trial were presented by the Newcastle group in the satellite conference. The proceedings were published in 2006 by Springer [15]. Papers from the satellite conference were included in the proceedings. The second ICH symposium was organized by Liang-Fu Zhou, 10–11 November 2007, in Shanghai.

The 14th symposium was organized by Zbigniew Czernicki in Warsaw, 11–14 June, 2008. This was the first brain edema symposium organized in one of the former Eastern European countries. The meeting was held in a building of the Polish Academy of Science near the very beautiful old town of Starówka, Warsaw. Dr. Igor Klatzo died in 2007 and a lecture named after him was presented by Hans-Jürgen Reulen. The title was "Bulk Flow and Diffusion Revisited, and Clinical Application." A few more papers were dedicated to the memory of Igor Klatzo. Many clinical papers on the diagnosis and treatment of brain edema, including papers on decompressive craniectomy for the treatment of posttraumatic intracranial hypertension were presented. Nanoparticles was a new topic at the brain symposia. The proceedings were published by Springer in 2010 [16].

The 15th symposium was organized by Yoichi Katayama in Tokyo, 22–24 October 2011. After the great earthquake disaster in east Japan, and the subsequent accident at the Fukushima nuclear power plant, many international conferences were cancelled. However, Dr. Katayama and his colleague succeeded in going ahead with the brain edema symposium. The symposium was scientifically very fruitful, and the symposium was larger than the previous one. There were 119 presentations including 11 keynote lectures. Some of the topics of the lectures were neurovascular mechanisms after stroke, neuromonitoring, pathomechanisms, and treatment of traumatic brain edema. The Anthony Marmarou award and the student's award (Travel Award) were given to eight recipients (Fig. 3; Table 3). The proceedings will be published by Springer in 2013.

The 16th symposium will be held in Loma Linda, California, USA, in 2014. The symposium will be organized by Dr. John Zhang, Professor and Director of Neurosurgical Research at Loma Linda University.

Fig. 3 (**a**) Dr. M.C. Papadopoulos (*right*) received the Hakone Best Presentation Award from Dr. A.D. Mendelow (*left*). (**b**) Certificate of the Hakone Best Presentation Award in brain edema XII. (**c**) Dr. H. Kawai (*right*) received the student's award from Dr. Y. Katayama (*left*) (**d**). Trophy of the student's award (Travel Award) in brain edema XV

Brain edema has been a major focus of therapeutic research in neurology and neurosurgery for dozens of years. There have been many important discoveries and technical improvements in the diagnosis and treatment. However, brain edema is still a fatal disorder for many neurological patients, and therefore we need to continue research into brain edema. Both clinical studies and fundamental research have been reported in balanced manner in the past international brain edema symposia. Translational research was the main constituent of fundamental research. These points constitute the charm of the international brain edema meeting, and I think that this is a reason why it has continued until now. It is important that the international brain edema symposium remains attractive to clinicians and basic scientists. Efforts to publish the proceedings as soon as possible should be continued in future. In addition, the round-table discussion summarizing the results of the symposium is very effective and should be continued. In recent brain edema symposia, several awards were given to young investigators to promote their research activities in brain edema (Fig. 3; Table 3). The author believes that these efforts are also important for the future of brain edema research and international brain edema symposia.

Conflict of Interest We declare that we have no conflict of interest.

Table 3 Memorial lecture, awards for young investigators in recent symposia

Symposium	Award/lecture	Presenter/author	Title
VIII Bern	K.J. Zülch Lecture	Klatzo I.	Prof. Dr. DR.h.c. Klaus Joachim Zülch In Memoriam
X San Diego	J. Douglas Miller Memorial Lecture	Marmarou A.	
XII Hakone	Hakone Best Presentation Award	Kawai N.	Treatment of cold injury-induced brain edema with a nonspecific matrix metalloproteinase inhibitor MMI1270 in rats
		Kawahra N.	DNA microarray-based expression analysis for induced ischemic tolerance and delayed neuronal death following transient global ischemia in rats
		Papadopolous M.C.	Role of water channel proteins (aquaporins) in brain tumor edema
		Otani N.	Temporal and spatial profile of phosphorylated mitogen-activated protein kinase (MAPK) pathways following lateral percussion brain injury in rats
		Tanaka Y.	Recovery of apparent diffusion coefficient in a rat model of embolic stroke does not mean complete salvage from ischemic neuronal injury
		Akiyama C.	Src family kinase inhibitor PPI improves most functions by reducing edema after spinal cord contusion in rats
XIV Warsaw	Igor Klatzo Lecture	Reulen Hans-J.	Bulk flow and diffusion revisited, and clinical application
XV Tokyo	A Marmarou Award	Sharma H.S.	Astrocytes are sensitive indicators of hypothermia-induced brain edema in normal and in Cu nanoparticles-treated rats
		Takeuchi S.	Cerebrospinal fluid congestion in the perioptic space
	Travel Award	Kawai H.	Induced pluripotent stem cells transplanted in mouse ischemic brain
		Menon P.K.	A combination of CNTF, GDNF, and BDNF applied topically over the injured spinal cord reduces heme oxygenase-2 (HO_2) expression, blood–spinal cord barrier permeability, edema formation, and cellular damage in the rat
		Mullah Habib E. Rasul S.	A selective adenosine A2A receptor antagonist SCH58261 ameliorated hyperlocomotion in an animal model of lateral fluid percussion brain injury
		Santos E.	Cortical spreading depressions dynamics can be studied using intrinsic optical imaging on gyrencephalic animal cortex
		Ponten E.	Propofol induces dose-related upregulation of blood–brain barrier breakdown and heat shock protein (HSP 72 kd) response in the developing mice brain
		Bhattacharya P.	Heat stress modulates aquaporin-4 expression, induces edema formation and brain pathology in rats. Neuroprotective effects of cerebrolysin

References

1. Klatzo I, Marmarou A, A Brief Review of the Previous Brain Edema Symposite in: Mendelow AD, et al (eds) (2000) Brain Edema XI, vol 76. Acta neurochiurgica suppl. Springer, Vienna/New York
2. Klatzo I, Seitelberger F (eds) (1967) Brain edema: Proceedings of the symposium september 11–13, 1965, Vienna. Springer, Vienna/New York
3. Klatzo I (1967) Presidential address. Neuropathological aspects of brain edema. J Neuropathol Exp Neurol 26:1–14
4. Reulen HJ, Schürmann K (eds) (1972) Steroids and brain edema. Proceedings of the second international workshop, Mainz, W. Germany, June 19–21, 1972. Springer, Berlin/Heidelberg/New York
5. Pappius HM, Feindel WF (eds) (1978) Dynamics of brain edema. Springer, Berlin/Heidelberg/New York
6. Cervós-Navarro J, Ferszt R (eds) (1980) Brain edema pathology, diagnosis and therapy, advances in neurology, vol 28. Raven Press, New York
7. Go KG, Baethmann A (eds) (1982) Recent progress in the study and therapy of brain edema. Plenum Press, New York/London
8. Inaba Y, Klatzo I, Spatz M (eds) (1985) Brain edema. Springer, Berlin/Heidelberg/New York/Tokyo
9. Long DM (ed) (1990) Brain edema pathogenesis, imaging and therapy, advances in neurology, vol 52. Raven Press, New York
10. Reulen HJ, Baethmann A, Fenstermacher J, Marmarou A, Spatz M (eds) (1990) Brain edema VIII, vol 51, Acta neurochirurgica supplement. Springer, Vienna/New York

11. Ito U, Baethmann A, Hossmann K-A, Kuroiwa T, Marmarou A, Reulen HJ, Takakura K (eds) (1994) Brain edema IX, vol 60, Acta neurochirurgica supplement. Springer, Vienna/New York
12. James HE, Marshall LF, Reulen HJ, Baethmann A, Marmarou A, Ito U, Hoff JT, Kuroiwa T, Czernicki Z, Czernicki Z (eds) (1997) Brain edema X, vol 70, Acta neurochirurgica Supplement. Springer, Vienna/New York
13. Mendelow AD, Baethmann A, Czernicki Z, Hoff JT, Ito U, James HE, Kuroiwa T, Marmarou A, Marshall LF, Reulen HJ (eds) (2000) Brain edema XI, vol 76, Acta neurochirurgica Supplement. Springer, Vienna/New York
14. Kuroiwa T, Baethmann A, Czernicki Z, Hoff JT, Ito U, Katayama Y, Marmarou A, Mendelow AD, Reulen HJ (eds) (2003) Brain edema XII, vol 86, Acta neurochirurgica supplement. Springer, Vienna/New York
15. Hoff JT, Keep RF, Xi G, Hua Y (eds) (2006) Brain edema XIII, vol 96, Acta neurochirurgica supplement. Springer, Vienna/New York
16. Czernicki Z, Baethmann A, Ito U, Katayama Y, Kuroiwa T, Mendelow D (eds) (2009) Brain edema XIV, vol 106, Acta neurochirurgica supplement. Springer, Vienna/New York

Brain Edema and Blood–Brain Barrier Opening After Photothrombotic Ischemia in Rat

Toshihiko Kuroiwa, Guohua Xi, Ya Hua, Tavarekere N. Nagaraja, Joseph D. Fenstermacher, and Richard F. Keep

Abstract We have examined the time course of brain edema and the blood–brain barrier opening in rat after basal ganglia ischemia induced by photothrombotic occlusion of the small vessels within the caudate–putamen. Male SD rats were anesthetized, and Rose Bengal dye was intravenously injected. The left caudo-putamen was exposed to cold white light for 5–10 min via a stereotaxically implanted optic fiber. Ischemic brain edema and the blood–brain barrier, as well as the histological changes, were assessed at various times during the following 6 weeks. Local cerebral blood flow was measured 90 min after photothrombosis by quantitative autoradiography. A round infarct with thrombosed parenchymal vessels surrounded by a layer of selective neuronal death was formed within the caudo-putamen. The ischemic lesion turned into a lacune over a period of 6 weeks. A central zone of markedly reduced blood flow and a surrounding oligemic zone were observed 90 min after light exposure. Early blood–brain barrier opening with edema was observed as early as 4 h after photothrombosis, peaked at day 1, and disappeared at 7 days after photothrombosis. In a model of lacunar infarction, we observed an early and transient brain edema and blood–brain opening after onset of ischemia.

Keywords Photothrombosis • Caudo-putamen • Histology Cerebral blood flow • Blood–brain barrier and brain edema

T. Kuroiwa, MD (✉)
Laboratory of Clinical Medicine,
Namegata District General Hospital,
98-8 Inouefujii, Namegata, Ibaraki, 311-3516, Japan

Department of Neurosurgery, University of Michigan,
Ann Arbor, MI, USA
e-mail: tkuroiwa-nsu@umin.ac.jp

G. Xi, MD, Y. Hua, MD and R.F. Keep
Department of Neurosurgery, University of Michigan Medical School,
Ann Arbor, MI, USA

T.N. Nagaraja and J.D. Fenstermacher
Department of Anesthesiology, Henry Ford Health System,
Detroit, MI, USA

Introduction

Small infarctions in deep brain structures are typically caused by occlusion of small parenchymal arteries and are referred to as lacunes. Stroke-prone spontaneous hypertensive (SHRSP) rat has been shown to develop small infarcts in the basal ganglia, but the unpredictable onset, size, and location of the ischemic lesions in this model make it difficult to use in mechanistic and therapeutic studies [3, 13]. Photothrombosis has been widely used to induce ischemia in the cortex, but not deep brain structures [1, 11]. We have developed an animal model of photothrombotic ischemia within the caudo-putamen in rat, and examined the time course of brain edema and blood–brain barrier opening after basal ganglia photothrombosis [5].

Materials and Methods

Male SD rats were anesthetized, and Rose Bengal dye (20 mg/kg) was intravenously injected. The left caudo-putamen was exposed to cold white light for 5–10 min via a stereotaxically implanted optic fiber (0.5 mm diameter, Eska CK-20; Mitsubishi Rayon, Tokyo, Japan; Fig. 1a, b) [5, 9]. For histopathology, rats were re-anesthetized with 4 % isoflurane and transcardially perfused with 4 % paraformaldehyde in 0.1 mol/l phosphate-buffered saline at various times from 4 h to 6 weeks following photothrombosis. The fixed brains were removed and kept in 4 % paraformaldehyde for 6 h. A coronal slab of brain tissue containing the center of the lesion was cut, embedded in paraffin, sectioned, and prepared for hematoxylin and eosin staining. Electron microscopy was also performed on tissue from the 4 h group. The rats underwent transcardiac perfusion with 4 % glutaraldehyde. Specimens containing the photothrombosis-induced lesion were excised, embedded in epon, and prepared for

Y. Katayama et al. (eds.), *Brain Edema XV*, Acta Neurochirurgica Supplement, Vol. 118,
DOI 10.1007/978-3-7091-1434-6_2, © Springer-Verlag Wien 2013

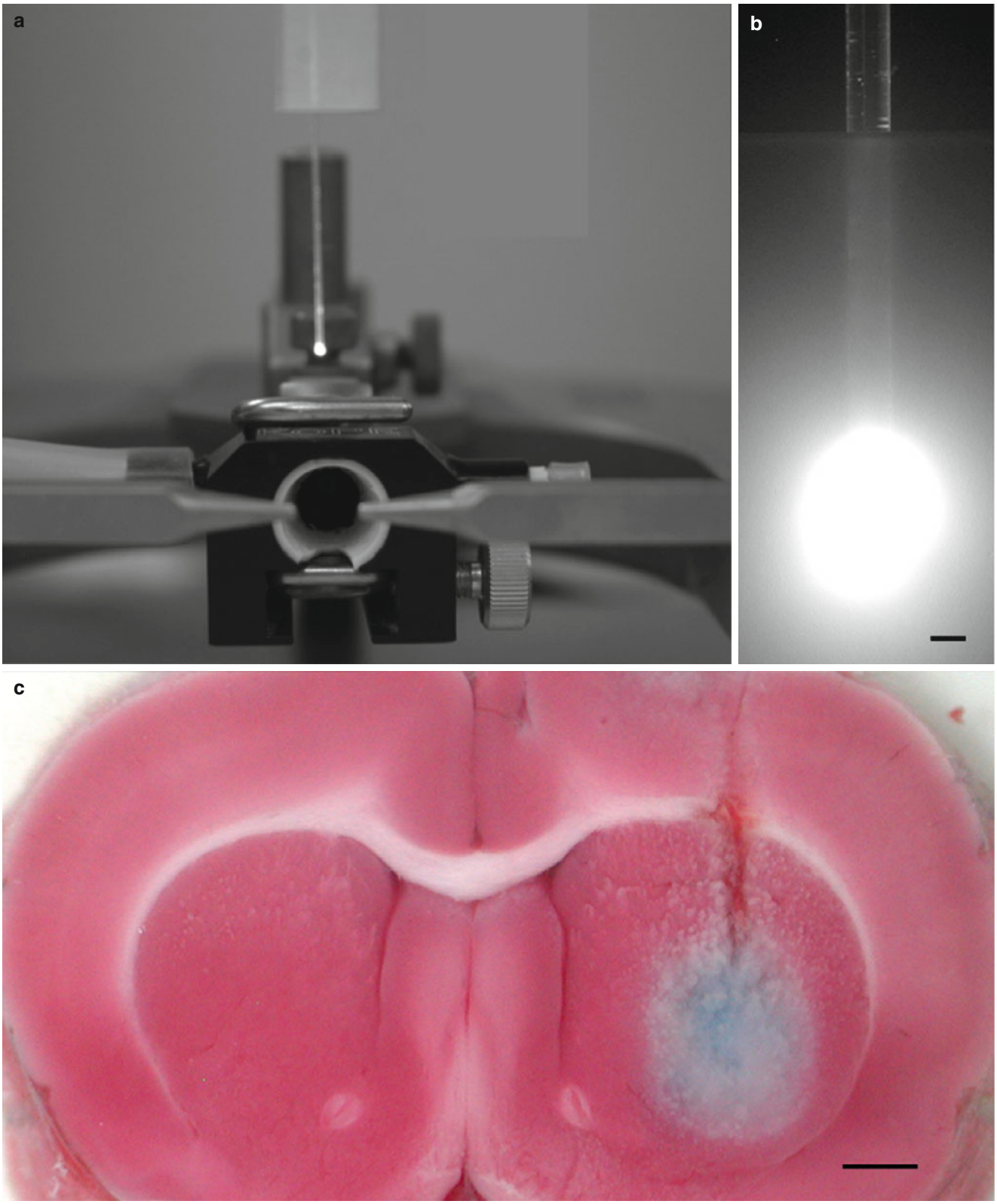

Fig. 1 (**a**) A stereotaxic device with a polymethylmethacrylate optic fiber coated with polyethylene measuring 0.5 mm in diameter (Eska CK-20, Mitsubishi Rayon, Tokyo, Japan) (**b**) Optic fiber with sharp beveled edge connected to a light source (bar = 0.5 mm) (**c**) Typical TTC-stained coronal section of brain at the level of the optic fiber 1 day after photothrombosis (bar = 1.0 mm). A clearly demarcated (*white*) lesion indicative of infarction is seen in the center of the caudo-putamen around the end of the needle track. In this animal, Evans Blue was injected i.v. before sacrifice and an area of *blue* staining is seen (indicating blood–brain barrier leakage to Evans Blue-tagged albumin) within the 2,3,5-triphenyl tetrazolium chloride (TTC)-demarcated lesion

ultrastructural examination. For the assessment of brain edema and blood–brain barrier permeability, animals were anesthetized and injected with Evans Blue solution. After 1 h, brains were removed and cut coronally on a brain-slicing matrix at the level of optic fiber implantation. Tissue samples of the photothrombotic lesion and corresponding site in the contralateral caudate were excised and dropped into a kerosene/monobromobenzene gradient column for specific gravity measurement, and the water content was calculated [2, 7]. An adjacent section was stained with 2,3,5-triphenyl tetrazolium chloride (TTC) to visualize the area of infarction and Evans Blue leakage (Fig. 1c) [6]. Local cerebral blood flow was measured 90 min after photothrombosis by quantitative autoradiography [8]. Ultrastructural assessment of blood–brain barrier change was performed in the 4 h group. One milliliter of saline with 25 mg horseradish peroxide (HRP; Sigma Type II) was injected i.v. into the animals 30 min before the animals were perfused with the fixative. Fixed brains were processed for enzyme histochemical reactions [10].

Results

A round infarct with thrombosed parenchymal vessels surrounded by a layer of selective neuronal death was formed within the caudo-putamen around the tip of the optic fiber (Fig. 2a). The ischemic lesion turned into a cystic cavity (lacune) over a period of 6 weeks. Four hours after photothrombosis, the histology of the periphery of the lesion was abnormal with pyknotic and eosinophilic neurons and numerous microvacuoles. The latter structures are swollen astrocytic and neuronal processes within the neuropil. Platelet thrombus formation within parenchymal small vessels, dark neurons, and hydropic swelling of astrocytes and oligodendrocytes were evident at this time (Fig. 2b, c). Multiple HRP vesicles were present in the endothelia of small vessels in the lesion in the 4 h group (Fig. 2d, e). By day 1, neuronal destruction and neuropilar microvacuolation became more evident in the center of the lesion. At the lesion periphery, marked neutrophil infiltration was seen 3 days after photothrombosis, whereas macrophage infiltration peaked at

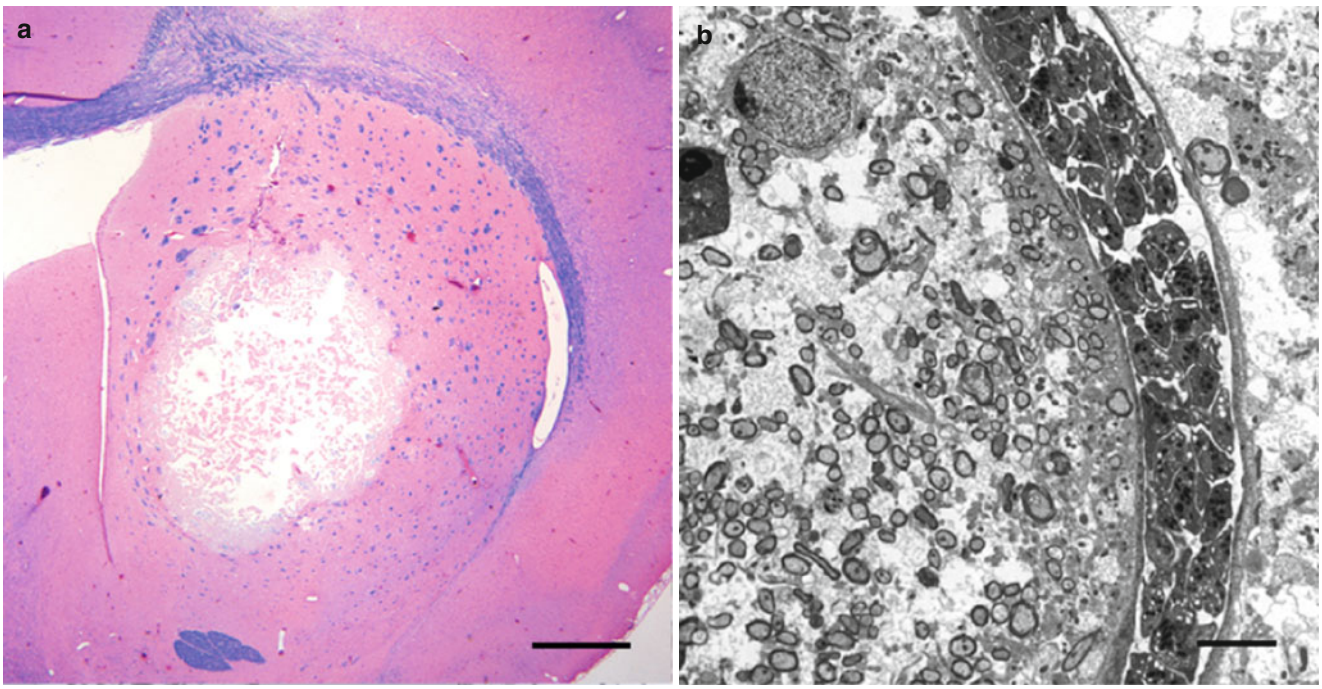

Fig. 2 (**a**) Typical lesion 1 day after photothrombosis (10 min exposure; Luxol Fast Blue and Eosin staining; scale bar = 1.0 mm). There is a round lesion in the center of the caudo-putamen. The area of central infarction was surrounded by a thin layer of selective neuronal death. (**b**) Typical electron micrograph of a small microvessel within the periphery at 4 h after light exposure. The vessel is filled with platelets and is surrounded by swollen perivascular cells, mostly astrocytic end-feet (bar = 10 μm). (**c**) An example of a triangulated ischemic neuron within the ischemic periphery (bar = 10 μm). The neuron is surrounded by several swollen perineuronal astrocytic processes. (**d**) Horseradish peroxide (HRP) vesicles detected in the endothelium of microvessels in the ischemic region, indicating increased blood–brain barrier permeability (bar = 1 μm). (**e**) Higher magnification of the capillary endothelium with HRP vesicles (bar = 0.1 μm)

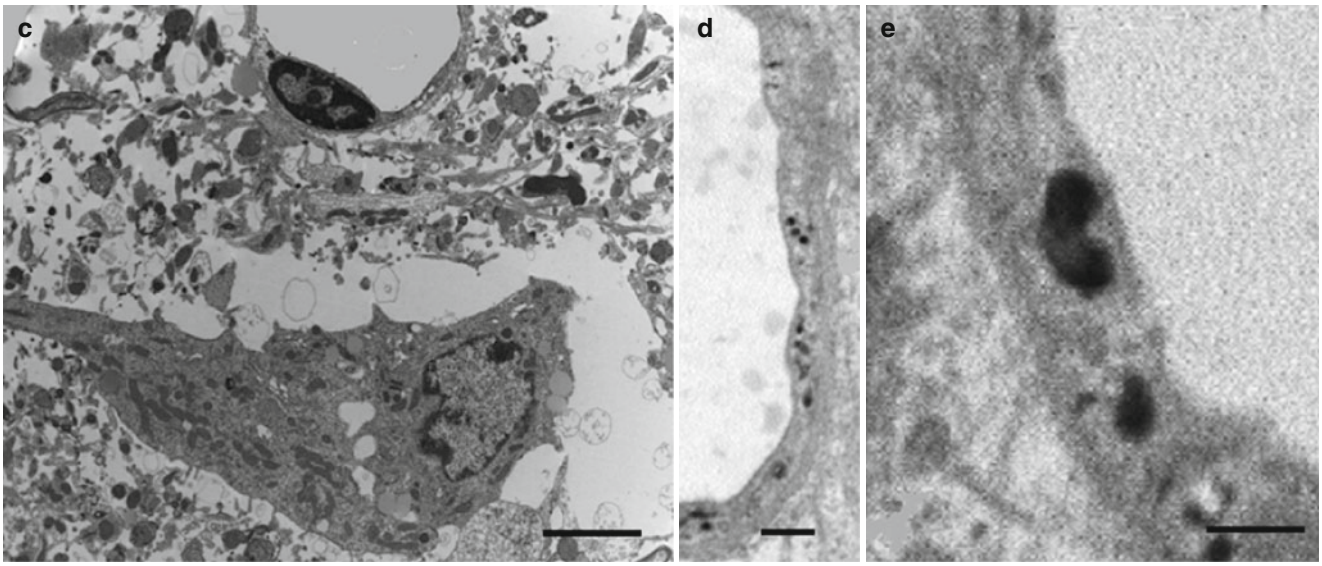

Fig. 2 (continued)

2 weeks after photothrombosis. Reactive astrocytosis and new capillary formation were also evident in the lesion periphery at 2 weeks. A small cyst with a thin layer of gliosis was observed 6 weeks after light exposure. The color-coded maps of lCBF at 1.5 h after photothrombosis indicated a large portion of the ipsilateral caudo-putamen with very low flow (approximately 10–15 ml/100 g/min) compared with contralateral (approximately 80 ml/100 g/min). Evans Blue leakage was observed at 1.5 h in 3 out of 6 animals, 4 h in 6 out of 6 animals, 1 day in 6 out of 6 animals, 4 days in 4 out of 6, 7 days in 1 out of 6 animals after photothrombosis, but not at all at 6 weeks. Brain edema was detectable by 1.5 h, peaked at 1 day, and was resolved by 6 weeks (Fig. 3).

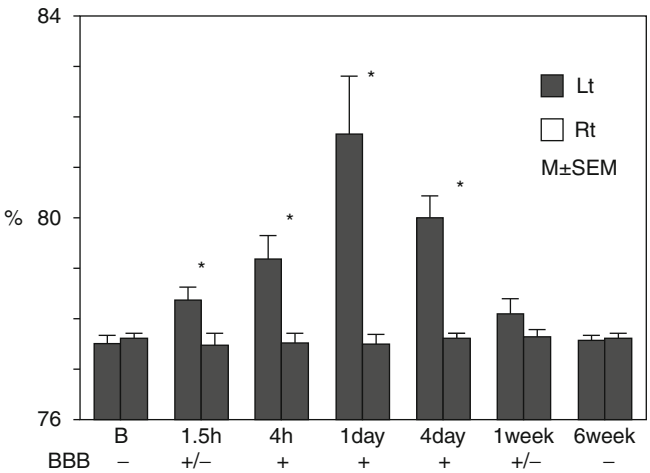

Fig. 3 Time course of tissue water content and blood–brain barrier permeability change after photothrombosis. Water content (%, vertical axis) was measured in the left and right caudate. $*P<0.05$ versus contralateral. Evans Blue leakage was observed at 1.5 h, 4 h, 1 day, 4 days, and 7 days after photothrombosis, but not at 6 weeks. Brain edema was detectable by 1.5 h, peaked at 1 day, and was resolved by 6 weeks

Conclusion

Watson et al. developed a method of inducing photothrombotic infarction in the cerebral cortex that has the advantage of precise control of the size and location of the infarct [11]. Current study aimed to establish a reproducible model of a deep small infarction in the caudo-putamen using a stereotaxically implanted optic fiber. Polymethylmethacrylate optic fibers are suitable for cold lighting because they transmit very little infrared light. Histological examination early after light exposure after Rose Bengal dye infusion showed an almost spherical infarct around the tip of the fiber optic surrounded by a peripheral area of selective neuronal death and ischemic edema. Thrombotic occlusion of small parenchymal vessels was found in the center and periphery of the lesion, and lCBF was decreased by about 85 % in the lesion center. This is, thus, a model of deep, localized brain ischemia that induces subsequent infarction. Blood–brain barrier opening takes place shortly after lesioning in this model. Early BBB opening was found in an air embolus model of ischemia [12]. In both models, occlusion of small parenchymal vessels is probably an important factor in early BBB opening, which is different from the delayed BBB opening that often occurs after large artery occlusion [4]. In summary, an animal model of photothrombotic caudo-putamen infarction with histological changes similar to those found in lacunar infarcts has been developed.

Opening of the BBB and ischemic edema were found at an early stage after onset. This model can be employed to test differences in the effects of potential therapeutic agents between large and small vessels (lacunar) ischemia or among sites of ischemic injury.

Conflict of Interest We declare that we have no conflict of interest.

References

1. Boquillon M, Boquillon JP, Bralet J (1992) Photochemically induced, graded cerebral infarction in the mouse by laser irradiation evolution of brain edema. J Pharmacol Toxicol Methods 27:1–6
2. Fujiwara K, Nitsch C, Suzuki R, Klatzo I (1981) Factors in the reproducibility of the gravimetric method for evaluation of edematous changes in the brain. Neurol Res 3:345–361
3. Hossmann KA (2005) Experimental models of focal cerebral ischemia. In: Kalimo H (ed) Pathology & genetics of cerebrovascular diseases. ISN Neuropath Press, Basel, pp 227–235
4. Ito U, Go KG, Walker JT Jr, Spatz M, Klatzo I (1976) Experimental cerebral ischemia in Mongolian gerbils III. Behaviour of the blood-brain barrier. Acta Neuropathol 34:1–6
5. Kuroiwa T, Xi G, Hua Y, Nagaraja TN, Fenstermacher JD, Keep RF (2009) Development of a rat model of photothrombotic ischemia and infarction within the caudoputamen. Stroke 40: 248–253
6. Lippold HJ (1982) Quantitative succinic dehydrogenases histochemistry. A comparison of different tetrazolium salts. Histochemistry 76:381–405
7. Marmarou A, Tanaka K, Shulman K (1982) An improved gravimetric measure of cerebral edema. J Neurosurg 56:246–253
8. Obrenovitch TP, Clayton CB, Strong AJ (1987) A double-radionuclide autoradiographic method using N-isopropyl-iodoamphetamine for sequential measurements of local cerebral blood flow. J Cereb Blood Flow Metab 7:356–365
9. Paxinos G, Watson C (1986) The rat brain in stereotaxic coordinates, 2nd edn. Academic, San Diego
10. Reese TS, Karnovsky MJ (1967) Fine structural localization of a blood-brain barrier to exogenous peroxidase. J Cell Biol 34: 207–217
11. Watson BD, Dietrich WD, Busto R, Wachtel MS, Ginsberg MD (1985) Induction of reproducible brain infarction by photochemically initiated thrombosis. Ann Neurol 17:497–504
12. Wolman M, Klatzo I, Chui E, Wilmes F, Nishimoto K, Fujiwara K, Spatz M (1981) Evaluation of the dye-protein tracers in pathophysiology of the blood-brain barrier. Acta Neuropathol 54:55–61
13. Yamori Y, Horie R, Handa H, Sato M, Fukase M (1976) Pathogenetic similarity of strokes in stroke-prone spontaneously hypertensive rats and humans. Stroke 7:46–53

Cerebral Ischemia Model Using Mongolian Gerbils—Comparison Between Unilateral and Bilateral Carotid Occlusion Models

Umeo Ito, Yoji Hakamata, Takekane Yamaguchi, and Kikuo Ohno

Abstract We permanently occluded unilaterally and/or bilaterally the carotid arteries of anesthetized Mongolian gerbils (60–80 g) and compared the two models. In the former, stroke-positive animals were selected by calculating the stroke index score of the conscious animals. Selection was not made in the latter. We measured the rCBF of the cerebral cortex, hippocampus, and diencephalon using the ^{3}H-nicotine scintillation method; analyzed the EEG using the wave-form recognition method (Fujimori); measured ATP, PCr (phosphocreatine), lactate, and glucose content in the cerebral hemisphere using the Lowry method; and measured infarct size on HE-stained coronal sections. All parameter values were uniform in the gerbils of the unilateral model, whereas great variation was observed in the right and left cerebral cortex, hippocampus, and diencephalon in the bilateral occlusion model. Therefore, we have discarded the bilateral model and used the stroke-positive unilateral model only.

By changing the length of time of the unilateral carotid occlusions and intervals, we found that two 10-min unilateral carotid occlusions with a 5-h interval between them achieved a threshold ischemic insult in gerbils, which produced uniform cortical focal infarctions that evolved in the maturing DSNN on the coronal surface sectioned at the chiasmatic level (Face A). This model showed a marked reduction in the occurrence of ischemic epilepsy and death.

Keywords Unilateral and bilateral carotid occlusion • Stroke index score • Stroke-positive Mongolian gerbil

Introduction

Studies on human pathological anatomy have not been able to elucidate the pathological changes that occur in the cerebrum in the acute phase after stroke onset. Until the early 1970s, although there was a different vulnerability depending on the neuron, neurons had been thought to die soon, even after a short period of ischemia. Except in the case of the Levine preparation using ischemia and hypoxia on gerbils [9], investigations into the acute phase of neuronal changes and/or evolution of an infarction after ischemic stroke have mainly used large animals such as cats and rhesus monkeys for focal ischemia, and rabbits for total ischemia. Owing to the difficulty in operative manipulation to produce ischemic lesions, the precise temporal profile of different grades of pure ischemic insult was not investigated until the appearance of the ischemic model using rodents. In 1972, Kahn [7] reported the selection of stroke-positive gerbils by using the stroke index score, which measures the various behaviors shown by animals after unilateral carotid occlusion. Therefore, we switched from using rhesus monkeys to using Mongolian gerbils at the NIH to investigate the precise histo-pathological temporal profile of various parts of the cerebral hemisphere after various durations of temporary ischemia. After investigating thousands of gerbils, we discovered that the rapid death of neurons did not occur soon

U. Ito, MD, PhD, FAHA (✉)
Laboratory for Neurodegenerative Pathology,
Department of Sensory and Motor Systems,
Tokyo Metropolitan Institute of Medical Science,
Tokyo, Japan

Division of Neuropathology,
Department of Brain Disease Research, Shinshu University,
School of Medicine, Nagano, Japan
e-mail: umeo-ito@nn.iij4u.or.jp

Y. Hakamata, DVM, PhD
Department of Basic Science,
School of Veterinary Nursing and Technology,
Faculty of Veterinary Science,
Nippon Veterinary and Life Science University,
Tokyo, Japan
e-mail: yhakama@nvlu.ac.jp

T. Yamaguchi, MD, PhD and K. Ohno, MD, PhD
Department of Neurosurgery,
Tokyo Medical and Dental University,
Tokyo, Japan
e-mail: yamguchi@toshima-hp.metro.tokyo.jp; ohno.nsrg@tmd.ac.jp

Y. Katayama et al. (eds.), *Brain Edema XV*, Acta Neurochirurgica Supplement, Vol. 118,
DOI 10.1007/978-3-7091-1434-6_3,

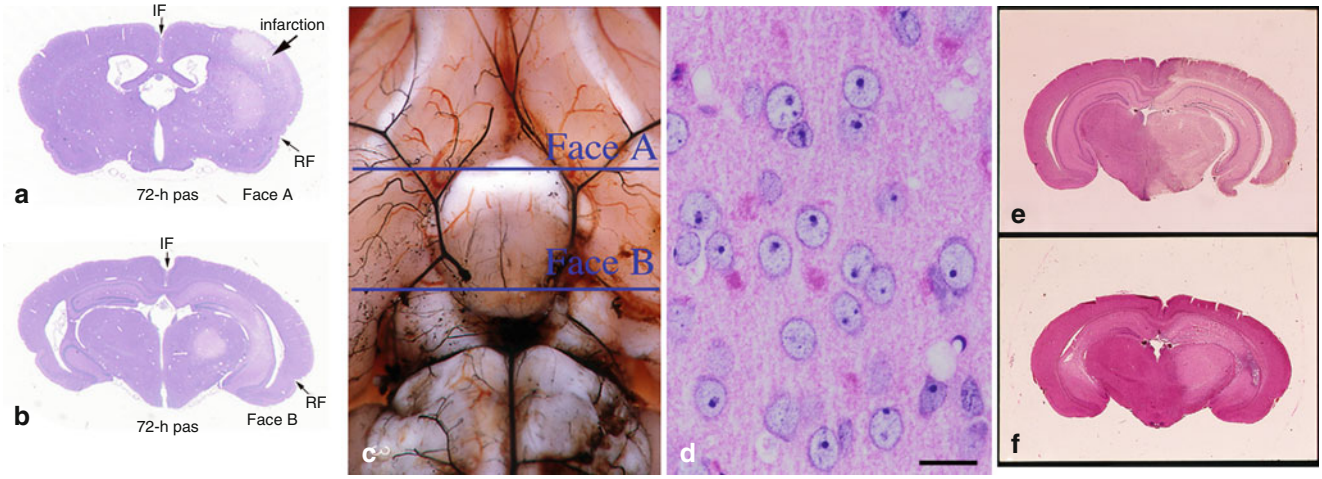

Fig. 1 Coronal sections at (**a**) the chiasmatic (*Face A*) and (**b**) the infundibular (*Face B*) levels, 72 h post-ischemia; PAS staining. (**c**) Carbon-black perfused Willis's circle of a stroke-positive, unilaterally carotid-occluded gerbil, and the cutting line of *Face A* and *B*. Right anterior and bilateral posterior communications are lacking. (**d**) Light microscopy of post-ischemic cerebral cortex (*Face B*), 8 weeks; PAS staining: Bar = 12.5 μm. The PAS-positive dead neurons (ghost cells) are seen in disseminated fashion among the surviving, normal-appearing neurons. (**e**) Homogeneous infarction in the left cerebral hemisphere. Unilateral left carotid occlusion for 5 h. H&E staining. (**f**) Heterogeneous focal infarctions in the bilateral cerebral hemisphere. Five hours after temporary bilateral carotid occlusion for 20 min. HE staining

after the ischemic insult. Rather, the animals suffered various post-ischemic neuronal changes ranging from degeneration and recovery to death, and further to focal infarction beyond the threshold of the ischemic insult. Also, the intensities of ischemic injuries and the speed of their appearance were directly related to the duration of ischemia. We referred to this phenomenon as the "maturation phenomenon of ischemic injuries" [3]. Later, using a bilateral carotid occlusion model of gerbils, Kirino reported the same kinds of changes confined to CA1 pyramidal cells of the hippocampus and described this process as "delayed neuronal death" [8]. This phenomenon provided a therapeutic window and boosted research in this field to rescue dying neurons and to reduce the size of the infarction. In this present study, we compared gerbils in which the unilateral carotid artery was permanently occluded and stroke-positive animals were selected by calculating the stroke index score [12], and gerbils in which bilateral carotid arteries were permanently occluded but the selection was not made.

Materials and Methods, Results, and Discussion

Unilaterally Carotid-Occluded, Stroke-Positive Model

As the cerebral arterial system lacks various anterior and posterior communicating arteries at the Willis circle (Fig. 1c), permanent occlusion of the unilateral occlusion of the carotid artery induced infarction uniformly involving the caudal two thirds of the cerebral hemisphere in only about 40 % of animals (Fig. 1e).

Table 1 Modified stroke index

Signs	Stroke index
Hair roughed up or tremor	1
Obtundent or paucity of movement	1
Hypesthesia of ear	1
Head cocked	3
Eye fixed open	3
Ptosis	1
A splayed out hind limb	3
Circulation movement	3
Seizures or abrupt explosive movement	3
Extreme weakness	6
Total	25

After C.P. McGraw

During various surgical procedures, light anesthesia with ether and air or 2 % halothane or 3 % isoflurane in a mixed gas of 70 % nitrous oxide and 30 % oxygen was applied. The unilateral cerebral ischemia induced various abnormal behaviors of the conscious animals. Each behavior could be scored as points, and the total score of each animal was calculated (maximal total score: 25 points; Table 1). We classified the gerbils according to the total score: 0 as stroke-negative, 1–9 as pseudo-positive, and more than 10 as stroke-positive animals. Of the 282 animals evaluated, 42–43 % were positive for stroke, 47–53 % were negative, and the

remainder were indefinite. We permanently occluded the left common carotid arteries of male Mongolian gerbils of 60–80 g and various ages. After recovery of the animals from anesthesia and determination of McGraw's modified stroke index score [12], we compared the percentage of stroke-positive and -negative animals between the 6-week age group and the 25- to 32-week age group. There was no statistical difference in the occurrence of stroke-positive and -negative animals between these different age groups. At 1 h after permanent unilateral cerebral occlusion of five stroke-positive animals, 1.0 ml of carbon-black suspension (Pelican, carbon-black ink) was perfused from a femoral vein for 30 s prior to decapitation, and then their brains were immediately immersion-fixed in 10 % phosphate-buffered formaldehyde. All five animals showed a non-perfused area involving the caudal two thirds of their left cerebral hemisphere. Animals that survived more than 5 h after left carotid occlusion were investigated. We examined 109 animals microscopically by observing HE-stained coronal sections of brains from animals perfusion-fixed via the heart with 10 % phosphate-buffered formaldehyde. All 35 stroke-positive animals showed a homogeneous cerebral infarction involving the caudal two thirds of the left cerebral hemisphere (Fig. 1e). In the 50 gerbils in the stroke-negative group, 48 of them showed no infarction, with the other 2 animals having small foci of infarcts. Of the 24 animals in the indefinite group, 2 of them showed large infarctions, 7 showed small infarctions in their left cerebral hemisphere, and 15 had no infarction.

1. We measured the rCBF of the cerebral cortex, hippocampus, and diencephalon of conscious animals by using the ^{3}H-nicotine scintillation method [12] at 1 h after the start of permanent ischemia due to left carotid occlusion. In the control group (six animals), the rCBF was 1.099 ± 0.189 ml/g/min in the cerebral cortex, 0.575 ± 0.056 ml/g/min in the hippocampus, and 0.686 ± 0.035 ml/g/min in the diencephalon. In the stroke-positive group (five animals), the corresponding values were 0.091 ± 0.016, 0.035 ± 0.22, and 0.149 ± 0.014 ml/g/min, respectively. All values of the stroke-positive group were less than 10 % of those of the control group, and they showed minimal variation. In the stroke-negative group (five animals), all values of these three portions of the cerebral hemisphere showed only a slight decrease. In the indefinite group (three animals), there was a large variety among animals. In the right non-ischemic hemisphere of the stroke-positive animals, there was a slight decrease in rCBF in all portions. All data were presented as the average ± SEM.
2. We analyzed the EEG using the computerized wave-form recognition method [4, 11] in five stroke-positive animals in the awake state at 1 h after the start of permanent ischemia induced by the left carotid occlusion. After the injection of a muscle relaxant and with controlled respiration, mono polar electrodes were placed on the bilateral parietal dura mater; and the EEG was recorded bilaterally for 1 min. We analyzed by computer the average number of waves multiplied by the average amplitude in the lower frequency (0.5–8.5 Hz) and higher frequency (9.0–30Hz) groups. For the left hemisphere of the control group, the above value for the entire frequency range (0.5–30 Hz) was 1,029 ± 180, whereas in the stroke-positive group, it had decreased to 370 ± 124 with minimal variation. The stroke-negative group showed a very slight decrease, whereas the indefinite group showed marked variation. In the right non-ischemic hemisphere of the stroke-positive animals, the above value for the control group was 1,052 ± 152, whereas in the stroke-negative group, there was a moderate decrease to 739.4 ± 153.
3. We measured various parameters of energy metabolism by using the Lowry method at 1 h after permanent ischemia had been established in conscious animals. Each animal brain was fixed instantaneously by using microwave irradiation, and the posterior two thirds of the left ischemic and right non-ischemic hemisphere were homogenized. We measured ATP, PCr (phosphocreatine), lactate, and glucose content in the cerebral cortex, hippocampus and diencephalon of each cerebral hemisphere [10]. We measured these values in five animals in each group. In the control group, the ATP content was 9.25 ± 0.14 μmol/g protein; PCr, 17.76 ± 0.56 μmol/g protein; lactate, 6.04 ± 0.57 μmol/g protein; and glucose, 6.26 ± 0.76 μmol/g protein. In the stroke-positive group, the ATP value decreased to 1.72 ± 0.20 μmol/g protein; PCr, to 3.08 ± 0.48 μmol/g protein; and glucose, to 2.23 ± 0.10 μmol/g protein. In contrast, the lactate increased to 25.22 ± 3.58 μmol/g protein. Thus, we found a marked decrease in the values of ATP and PCr and a marked increase in lactate. In the right non-ischemic hemisphere, a slight decrease in ATP to 6.74 ± 0.61 μmol/g protein and a slight decrease in PCr to 12.17 ± 1.57 μmol/g protein occurred. In the stroke-negative group, all values for the ischemic hemisphere were almost the same as those of the control group.

Bilaterally Carotid-Occluded Model (Without Selection of Stroke-Positive Gerbils)

Under light anesthesia (the same as for unilateral occlusion), bilateral carotid arteries were permanently occluded. Immediately after occlusion, all 66 ischemic animals showed abnormal respiration and cyanosis owing to paralysis of their respiratory muscles, which are innervated bilaterally from the cerebral cortex, and 32 % of them died within 20 min. The surviving animals showed abnormal hyper-respiration.

At 15 min after bilateral carotid occlusion of 10 animals, we perfused each of them with 1.0 ml of carbon-black

Table 2 rCBF measurement with ^{3}H-nicotine at 1 h of ischemia (bilateral carotid occlusion)

Side of cerebral hemisphere	Gerbil number	Part of cerebral hemisphere		
		Cortex	Hippocampus	Diencephalon
	Control	1.099 ± 0.189	0.575 ± 0.056	0.686 ± 0.035
Left	Cbb 1	0.21	0.18	0.28
	Cbb 2	0.01	0.02	0.28
	Cbb 3	0.06	0.02	0.14
	Cbb 4	0.56	0.34	0.50
Right	Cbb 1	0.41	0.32	0.44
	Cbb 2	0.01	0.01	0.40
	Cbb 3	0.50	0.32	0.44
	Cbb 4	0.15	0.12	0.12

suspension (Pelican, carbon-black ink) via a femoral vein for 30 s prior to decapitation, and then immediately immersion-fixed the brains in 10 % phosphate-buffered formaldehyde. Carbon-black was perfused in various parts of the cerebral cortex and the diencephalon irregularly, depending on the animal and the hemisphere, right or left.

As the percentage of animal deaths was very high in the bilateral occlusion group, we temporarily occluded the bilateral carotid arteries for 20 min and then selected 43 animals that survived for more than 5 h. We investigated all 43 brains by microscopically observing HE-stained sections cut coronally at three different levels, i.e., pre-chiasma, infundibulum, and caudal to the mammillary body (Fig. 1c). We measured the size of the infarct foci in each cerebral hemisphere (Fig. 1f), and classified them into one of two categories: (1) large infarction involving the cortex, hippocampus, diencephalon, and basal ganglia; and (2) small infarction covering less than two of the above three cerebral portions. A large infarction evolved in the bilateral hemispheres of 7 animals; and a small infarction, in those of 25 animals. A small infarction also evolved in the right or left hemisphere of 4 animals. In the remaining 7 animals, a small infarction evolved in either the right or left hemisphere, and a large infarction in the opposite hemisphere. Thus, we were unable to obtain a homogeneous distribution of infarctions in the bilateral carotid occlusion model.

1. In the same way as in the left unilateral carotid occlusion model, we measured the rCBF of the cerebral cortex, hippocampus, and diencephalon after 10 min of permanent ischemia of the bilateral carotid occlusion in four gerbils. In one of them, the rCBF of the left cerebral cortex was 0.56 ml/g/min, whereas that of the right cerebral cortex was 0.15 ml/g/min. In another gerbil, the rCBF of the left cerebral cortex was 0.01, while that of the right cerebral cortex was 0.01 ml/g/min. The decrease in the rCBF of the cerebral cortex thus showed quite a difference with respect to the animal and to the right or left side (Table 2).
2. In the same way as in the left unilateral carotid occlusion model, we obtained the EEG of five conscious, bilaterally occluded animals at 30 min after permanent ischemia. In one gerbil, the number of waves over the entire frequency (0.5–30 Hz) was 446 in the left hemisphere, but 965 in the right. In another gerbil, these numbers were 148 and 44 respectively. The decrease in the number of waves of the entire frequency from the control value were quite different according to the animal and to the right or left side. The values of the number of waves multiplied by the amplitudes showed the same tendencies as the number of waves, but were exaggerated.
3. In the same way as in the left unilateral carotid occlusion model, after 20 min of permanent ischemia due to bilateral carotid occlusion, we measured various parameters of energy metabolism of six stroke-positive conscious animals by using the Lowry method. In one animal, the ATP content was 7.18 μmol/g protein in the left hemisphere, and 2.37 μmol/g protein in the right. The respective PCr contents were 12.52 and 2.38 μmol/g protein. In another animal, ATP was 0.79 μmol/g protein in the left hemisphere and 1.93 μmol/g protein in the right; and PCr was 0.81 in the left, and 3.92 in the right. These values were quite different according to the animal as well as to the hemisphere involved (Table 3).

Conclusion

1. Infarction size, decrease in rCBF, in the number of waves in the EEG, and in the various parameters of the energy state showed great variation in each animal and in each portion and side of the cerebral hemisphere in the bilateral carotid occlusion model. However, all parameters were uniform among the gerbils of the unilateral carotid occlusion model using stroke-positive gerbils, and the operative manipulation of this model does not injure the cerebral cortex.
2. The death rate of animals due to impaired respiration was very high in the bilateral carotid occlusion model. For these reasons, we have discontinued the use of the bilateral model.

Table 3 Energy metabolism 20 min after ischemia (bilateral carotid occlusion)

Side of cerebral hemisphere	Gerbil number	ATP	PCr	Lactate	Glucose
	Control	9.25 ± 0.14	17.76 ± 0.56	6.04 ± 0.57	6.76 ± 0.76
Left	246	1.08	0.82	57.39	2.33
	248	2.53	5.55	67.62	2.73
	251	0.79	0.81	50.34	6.13
	255	4.78	5.62	46.98	2.90
	257	7.18	12.52	6.89	17.3
	259	1.19	1.92	24.91	2.25
Right	246	1.26	2.07	50.7	2.62
	248	1.64	3.43	72.37	4.02
	251	1.93	3.92	48.15	5.59
	255	3.80	3.24	31.95	1.75
	257	2.37	2.38	50.7	2.50
	259	1.08	2.26	23.24	1.82

Modified Unilateral Carotid-Occlusion Model

We have had to answer a question regarding the maturation phenomenon of ischemic injury after temporary ischemia, i.e., whether the transition from maturing disseminated selective neuronal necrosis (DSNN) (Fig. 1d) to the abrupt onset of focal infarction (Fig. 1a) is continuous or not after temporary ischemia [1]. As the mechanism of the transition is an enigma, we devised a gerbil model suitable for studying the transition after the threshold level of ischemic injury in inducing focal infarction had been reached. By changing the duration of the unilateral carotid occlusions and intervals, we found that two 10-min unilateral carotid occlusions with a 5-h interval between them achieved a threshold ischemic insult for producing uniform cortical focal infarctions at the coronal surface sectioned at the chiasmatic level (Fig. 1a) that evolved in the maturing DSNN (Fig. 1d) [2]. This model showed a marked reduction in the occurrence of ischemic epilepsy and death, which had long been considered as a problem with the use of the unilateral carotid occlusion model of gerbils. With this model we found that a focal cerebral–cortical infarction developed in the maturing DSNN after temporary ischemia. This infarction was induced by the delayed occurrence of the temporary microvascular obstruction due to compression of micro-vessels by swollen astrocytic end-feet at 3 ~ to 8 h after the restoration of blood flow, and it later resulted in tissue pan-necrosis at 12 ~ to 24 h post-ischemia [5, 6]. By changing time length of each of the two occlusions and the interval between them, we could obtain a different intensity of maturing ischemic injuries [1, 2].

Conflict of Interest We declare that we have no conflict of interest.

References

1. Hanyu S, Ito U, Hakamata Y, Yoshida M (1995) Transition from ischemic neuronal necrosis to infarction in repeated ischemia. Brain Res 686:44–48
2. Hanyu S, Ito U, Hakamata Y, Nakano I (1997) Topographical analysis of cortical neuronal loss associated with disseminated selective neuronal necrosis and infarction after repeated ischemia. Brain Res 767:154–157
3. Ito U, Spatz M, Jr Walker J, Klatzo I (1975) Experimental cerebral ischemia in Mongolian gerbils. I. Light microscopic observations Experimental cerebral ischemia in Mongolian gerbils. Acta Neuropathol 32:209–223
4. Ito U, Tomita H, Matsuura M, Yamazaki S, Takada Y, Inaba Y (1985) Computer-analyzed EEG before and after bypass surgery. Quantification by a computerized wave form recognition method. Clin Neurol Neurosurg 87:267–274
5. Ito U, Hakamata Y, Kawakami E, Oyanagi K (2009) Degeneration of astrocytic processes and their mitochondria in cerebral cortical regions peripheral to the cortical infarction: heterogeneity of their disintegration is closely associated with disseminated selective neuronal necrosis and maturation of injury. Stroke 40:2173–2181
6. Ito U, Hakamata Y, Kawakami E, Oyanagi K (2011) Temporary cerebral ischemia results in swollen astrocytic end-feet that compress microvessels and lead to delayed focal cortical infarction. J Cereb Blood Flow Metab 31:328–338
7. Kahn K (1972) The natural course of experimental cerebral infarction in the gerbil. Neurology 22:510–515
8. Kirino T (1982) Delayed neuronal death in the gerbil hippocampus following ischemia. Brain Res 239:57–69
9. Levine S, Payan H (1966) Effects of ischemia and other procedures on the brain and retina of the gerbil (Meriones unguiculatus). Exp Neurol 16:255–262
10. Lowry OH, Passonneau JV (1972) A flexible system of enzymatic analysis. Academic, New York
11. Matsuura M, Yamamoto K, Fukuzawa H, Okubo Y, Uesugi H, Moriiw M, Kojima T, Shimazono Y (1985) Age development and sex differences of various EEG elements in healthy children and adults – quantification by a computerized wave form recognition method. Electroencephalogr Clin Neurophysiol 60:394–406
12. Ohno K, Ito U, Inaba Y (1984) Regional cerebral blood flow and stroke index after left carotid artery ligation in the conscious gerbil. Brain Res 297:151–157

Astrocytic Involvement in the Maturation Phenomenon After Temporary Cerebral Ischemia

Umeo Ito, Yoji Hakamata, Kazuhiko Watabe, and Kiyomitsu Oyanagi

Abstract Astrocytes support neuronal functions by regulating the extracellular ion homeostasis and levels of neurotransmitters, and by providing fuel such as lactate to the neurons via their processes (APs). After two 10-min unilateral carotid occlusions with a 5-h interval in gerbils, we investigated maturing disseminated selective neuronal necrosis (DSNN) on the coronal surface sectioned at the infundibular level. We chronologically counted the normal appearing, degenerated, and dead neurons and astrocytes in the cerebral cortex; observed the ultrastructure of APs, and counted the number of their cut-ends and mitochondria in the neuropil; determined the percentage volume of APs according to Weibel's point-counting method; compared the number of cut-ends and mitochondria and percentage volume of APs around the astrocytes and around the normal-appearing, degenerated, and dead neurons. Heterogeneous degeneration of APs was concluded to be closely associated with the maturation of DSNN.

Using the same model, at the coronally sectioned surface on the chiasmatic level, we investigated the mechanism of development of focal infarction in the maturing DSNN. Same as in the above study, we chronologically counted various neurons and astrocytes; observed and measured the area of the ultrastructure of astrocytic end-feet; counted the number of carbon-black-suspension-perfused microvessels. We concluded that after temporary cerebral ischemia, secondary focal ischemia was induced by microvascular obstruction compressed by swollen astrocytic end-feet, resulting in delayed focal infarction.

Keywords Maturation phenomenon • Delayed neuronal death • Selective neuronal necrosis • Development of infarction Temporally cerebral ischemia • Astrocyte • Astrocytic process • End-feet • tPA • Vascular stenting

U. Ito, MD, PhD, FAHA (✉)
Laboratory for Neurodegenerative Pathology,
Department of Sensory and Motor Systems,
Tokyo Metropolitan Institute of Medical Science,
Tokyo, Japan

Division of Neuropathology,
Department of Brain Disease Research,
Shinshu University, School of Medicine,
Nagano, Japan
e-mail: umeo-ito@nn.iij4u.or.jp

Y. Hakamata, DVM, PhD
Department of Basic Science, School of Veterinary Nursing and Technology, Faculty of Veterinary Science,
Nippon Veterinary and Life Science University,
Tokyo, Japan
e-mail: yhakama@nvlu.ac.jp

K. Watabe, MD, PhD
Department of Sensory and Motor Systems,
Tokyo Metropolitan Institute of Medical Science,
Tokyo, Japan
e-mail: watabe-kz@igakuken.or.jp

K. Oyanagi, MD, PhD
Division of Neuropathology, Department of Brain Disease Research,
Shinshu University, School of Medicine,
Nagano, Japan
e-mail: k123ysm@shinshu-u.ac.jp

Introduction

Until the early 1970s, although a difference in their vulnerability was known, neurons had been thought to die soon even after a short period of ischemia. After the unilateral occlusion model of Mongolian gerbils was reported in 1972 by Kahn [10], who selected stroke-positive animals according to the stroke index score counted by behaviors of unilaterally carotid-occluded gerbils, different intensities (time length) of ischemic insult became easier to test in these animals than in larger animals, such as monkeys and cats. Using this model, we compared ischemic injuries after various recirculation times such as 5 s, 1, 5, 20 h or 1 or 2 weeks following temporary occlusion of 5, 15 or 30 min or 1, 3 or 6 h duration, and found that neurons are not killed outright

Y. Katayama et al. (eds.), *Brain Edema XV*, Acta Neurochirurgica Supplement, Vol. 118,
DOI 10.1007/978-3-7091-1434-6_4,

after an ischemic insult, but suffer various post-ischemic neuronal changes ranging from degeneration to death and to the recovery of injured neurons, and further to focal infarctions beyond a threshold of the insult. The intensity of ischemic injuries and the speed of their appearance are directly related to the duration of ischemia, and we referred to these changes as the "maturation phenomenon" [3]. Delayed neuronal death [11] of CA1 pyramidal cells of the hippocampus is a classic example of this phenomenon (see Figs. 6 and 7 in Ito et al. [3]). This phenomenon has provided a therapeutic window, and has encouraged research in this field toward the goal of rescuing dying neurons and development of infarction.

Astrocytes support neuronal functions by regulating the extra cellular ion homeostasis and levels of neurotransmitters, and by providing fuel such as lactate to the neurons via astrocytic processes (APs). Recently, purinergic signaling in neuron–glial interactions has been investigated [12].

After two 10-min unilateral carotid occlusions of gerbils with a 5-h interval between them, we were able to obtain a uniform distribution of disseminated selective neuronal necrosis (DSNN) and to determine the threshold amount of ischemic insult to produce a focal infarction in the cerebral cortex with almost no epileptic death of the animals [1, 2]. Using this model, we earlier investigated (1) the involvement of APs in maturing disseminated selective neuronal necrosis (DSNN) at the coronal surface sectioned at the infundibular level (Face B) [7], and (2) the involvement of astrocytic end-feet in the development of focal infarctions at the coronal surface sectioned at the chiasmatic level (Face A) (Fig. 1a) [8].

Materials and Methods

Ischemia-positive animals were selected based on having a modified stroke index score of over 10 points [13]. These animals were killed at 0, 0.5, 3, 5, 12, 24, 48 or 72 h after the second ischemic insult, by transcardiac perfusion. The animals were perfused with diluted fixative (1 % paraformaldehyde and 1.25 % glutaraldehyde in a 0.1 mol/L cacodylate buffer) for 5 min, followed by perfusion with concentrated fixative (4 % paraformaldehyde and 5 % glutaraldehyde in the same buffer) for 20 min for EM (three animals for each time group) or with 10 % phosphate-buffered formaldehyde fixative for 30 min for LMS (four animals for each time group).

For the LMS and EM studies we performed the following morphometric investigations on all cortical layers along a 1-mm-wide path at the point one-third of the distance from the rhinal fissure in Face B, as well at the point midway between the rhinal and interhemispheric fissures of the left cerebral cortex in Face A (Fig. 1a).

Number of Normal-Appearing Neurons, Dead Neurons, and Astrocytes (Light Microscopy)

Using an eye-piece micrometer (U-OCMSQ10/10) under 400-power magnification, we counted the number of astrocytes (PAS staining) and normal-appearing, degenerated, and dead neurons (HE staining) in all six cortical layers in four adjacent columns by vertically and horizontally moving the specimen along a 0.25-mm-wide × 4 path of the cortex.

Area and Number of Mitochondria in the Astrocytic Cytoplasm and End-Feet (Electron Microscopy)

Using a computer-assisted digitizer (Measure-5; System Supply, Nagano, Japan), we measured the area (μm^2) and number of mitochondria in the astrocytic cytoplasm and in the end-feet in three animals from each time group on 4,050- to 10,800-fold magnified EM photographs.

Percentage Volume of One Cut-End and Numbers of Cut-Ends of Astrocytic Processes and Mitochondria in Them in the Various Parts of the Neuropil (Electron Microscopy)

Placing a 1.0 × 1.0 or 0.5 × 0.5 cm^2 quadratic lattice on each variously enlarged EM photograph of a neuropil from three animals for each time group, we determined the percentage volume of the APs in the neuropil by using the point-counting method [14] to evaluate the swelling. We also measured the numbers of cut-ends of APs and their mitochondria in the same area of the EM pictures. The counted number was converted to the number per 100- or 25-cm^2 area of each EM picture (21.53, 28.20 or 38.33 μm^2, after correcting for magnification by real size) and expressed them as the average per time point. We calculated the percentage volume and the number of mitochondria per cut-end of APs, whose values were obtained by dividing the measured value of each parameter by the number of the cut-ends of the APs.

Number of Carbon-Black-Suspension-Perfused Micro-vessels (Light Microscopy)

Under anesthesia, gerbils were perfused for 30 s with 1.0 mL of carbon black suspension (Platina, Tokyo, Japan) through a

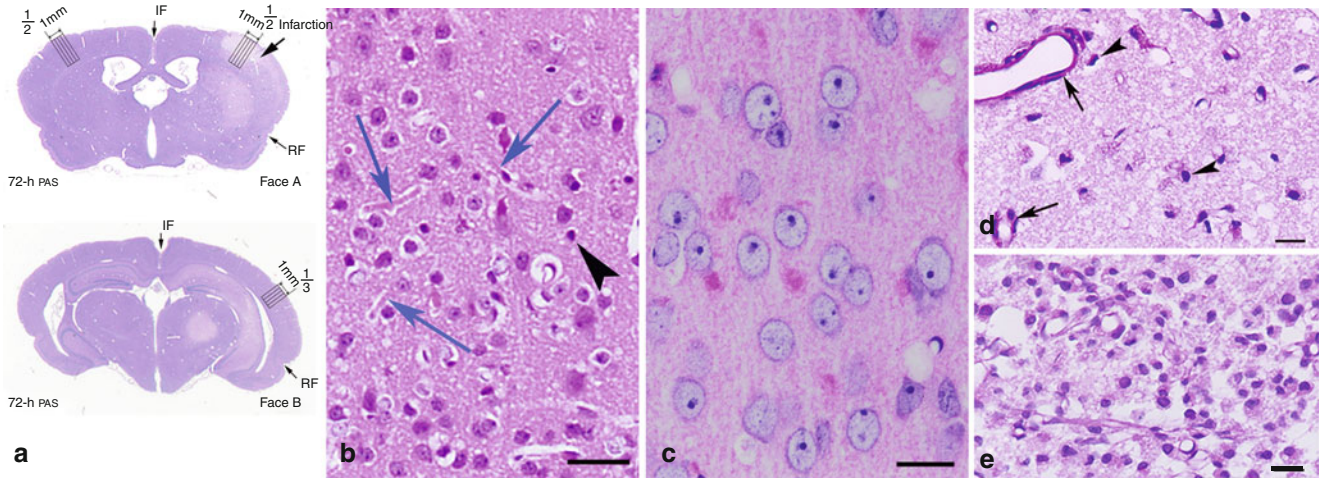

Fig. 1 Light microscopic findings in the cerebral cortex. (**a**) Coronal sections at the chiasmatic (*Face A*) and infundibular levels (*Face B*), 72 h post-ischemia, PAS staining. The four cortical columns counted, each 0.25 μm in width, are indicated at the midpoint 1/2 in Face A, and 1/3 points from *RF* in Face B between the rhinal (RF) and the inter-hemispheric fissure (*IF*). (**b**) 5-h; HE staining of Face A: Bar = 30.4 μm. Dead neurons are seen among the normal-appearing neurons (*arrowhead*), along with microvascular stasis (*blue arrows*). (**c**) 8 weeks post-ischemia; PAS staining of Face B: Bar = 12.5 μm. The PAS-positive dead neurons (ghost cells) are seen among the surviving normal-looking neurons. (**d**) 48 h; HE staining of Face A: Bar = 12.5 μm. The cortical tissue is necrotic and many macrophages (*arrowheads*) are extravasated around the proliferating microvessels (*arrows*). (**e**) 1 week; *PAS* staining of Face A: Bar = 15.2 μm. Multiple foamy cells are evident in the liquefied infarction

femoral vein. Thereafter, each animal was decapitaded immediately; the brain was then removed and immersion-fixed in 10 % phosphate-buffered formaldehyde for 3 days. Using an eye-piece micrometer (U-OCMSQ10/10) under 400-power magnification, we counted the number of carbon-black-suspension-perfused micro-vessels (CBSPm) in the four columns of the left ischemic and symmetrically located right non-ischemic cerebral hemisphere of Face A.

Statistical Analysis

We analyzed the statistical difference between each time group by using analysis of variance, followed by the Bonferroni–Dunn test. All data in the text and in the figures were presented as the average ± SD, and statistical significance was accepted as being $P < 0.05$.

1. Results and Conclusion

After a threshold ischemic insult to produce a focal infarction, in the present ischemic model, focal infarction evolved in the area of the maturing disseminated selective neuronal necrosis (DSNN) in the rostral cerebral cortex of the left cerebral hemisphere, where infarctions were observed on the coronally cut surface at the chiasmatic level (Face A; Fig. 1a), whereas DSNN without infarction matured in the cerebral cortex on the coronally cut surface at the infundibular level (Face B; Fig. 1a).

I. Maturation of DSNN in Face B

Degradation of neurons with a halo of swollen APs and a few dead neurons appeared in disseminated fashion (DSNN) among the normal-appearing neurons at 5 h post-ischemia (Fig.1b). Thereafter, dead neurons increased in number among the normal-appearing neurons, which decreased in number, 5–48 h after ischemia (Fig. 2 I-a). Instead of the homogeneous degradation of all the insulted neurons, each neuron became degraded heterogeneously in a disseminated fashion (Fig. 1c). To explain this phenomenon, a possible secondary damage of DNA, such as occurs in apoptosis, has been considered. However, we had earlier observed no ultrastructural changes in the neuronal nucleus specific to apoptosis in previous studies, which were conducted until 24 weeks after temporary ischemia [5, 6]. Therefore, we investigated ultrastructurally the involvement of the APs in the neurons that became degraded in a disseminated fashion. In spite of the degradation of neurons, the astrocytic number remained constant from 5 to 48 h post-ischemia (Fig. 2 I-a).

On EM pictures, the astrocytic cytoplasm (Fig. 3a) and end-feet (Fig. 3b) were swollen and showed an increased number of glycogen granules at 5 h post-ischemia. Mitochondrial number and size also increased by elongation, branching, and budding. The spaces between cristae

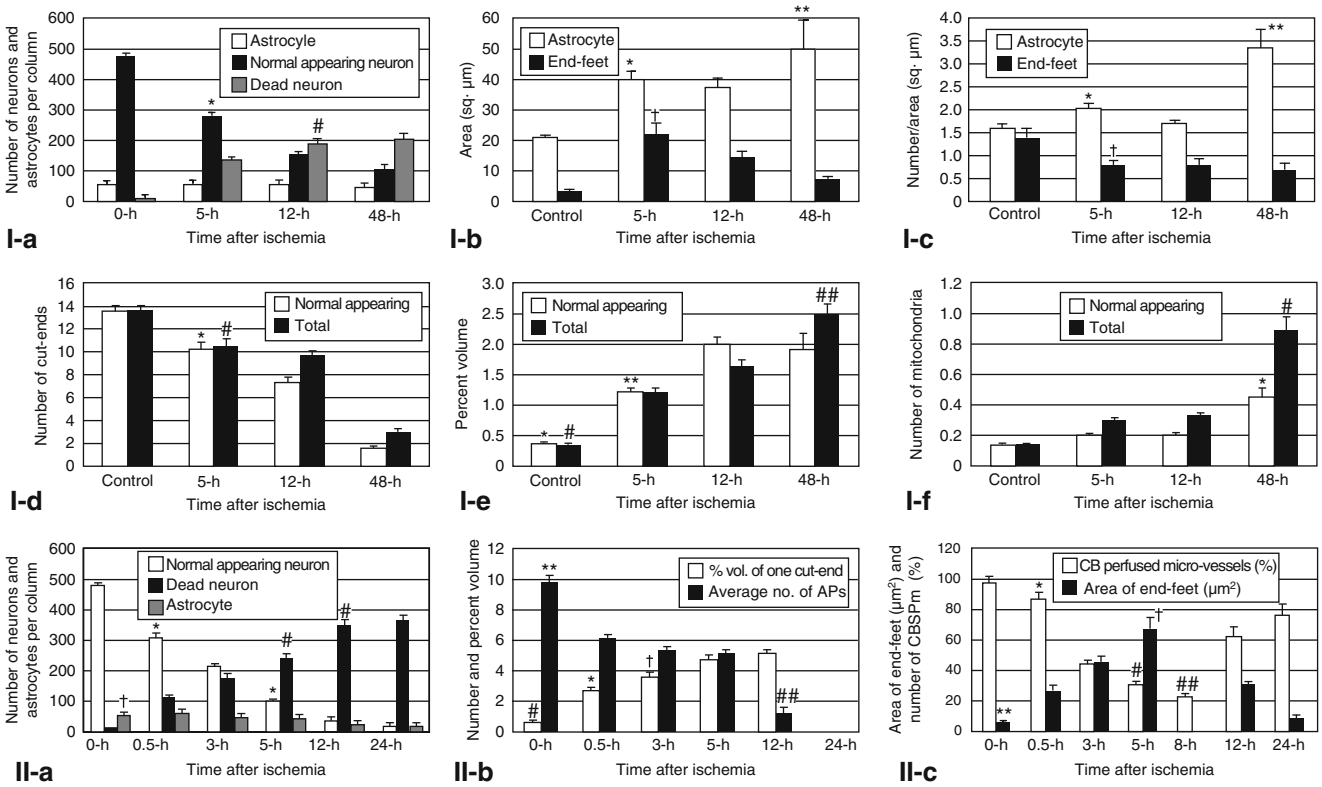

Fig. 2 (**I-a**) Number of neurons and astrocytes per column: Normal-appearing neuron, $*P<0.05$ vs 0, 12, 48 h. Dead neuron, $^{\#}P<0.05$ vs 0, 5, 48 h. (**I-b**) Area of astrocytes and end-feet: Astrocytes, $*P<0.05$ vs 0, 48 h; $**P<0.05$ vs 0, 5, 12 hr. End-feet, $P<0.05$ vs 0, 12, 48 h. (**I-c**) Number of mitochondria in astrocytic cytoplasm and end-feet: Astrocytic cytoplasm, $*P<0.05$ vs 0 h; $**P<0.05$ vs 0 to 12 h. End-feet, $^{\dagger}P<0.05$ vs 0, 12, 48 h. (**I-d**) Number of cut-ends of APs in neuropil (in 28.20 μm²): Normal-appearing APs,$*P<0.05$ vs 0, 12, 48 h: Total APs, $^{\#}P<0.05$ vs 0, 12, 48 hr. (**I-e**) Percentage volume of one cut-end of APs: Normal-appearing APs, $*P<0.05$ vs 5, 12, 48 h; $**P<0.05$ vs 12, 24 h. Total APs, $^{\#}P<0.05$ vs 0, 5, 12, 24 h. (**I-f**) Number of mitochondria in one cut-end of APs: Normal-appearing mitochondria, $*P<0.05$ vs 0, 5, 12 h. Total mitochondria, $^{\#}P<0.05$ vs $*P<0.05$ vs 0, 5, 12 h. (**II-a**) Number of normal-appearing and dead neurons, as well astrocytes per cortical column of 0.25 width: Normal-appearing neurons, $*P<0.05$ vs 0, 3,12 h. Dead neuron $^{\#}P<0.05$ vs 0, 0.5, 12, 24 h. (**II-b**) Number of cut-ends of normal appearing APs in a neuropil area of 21.53 μm² and percentage volume of one cut-end of APs: Average number of cut-ends of APs, $**P<0.05$ vs 0.5, 3, 5, 12 h. Percentage volume of one cut-end of APs, $^{\#}P<0.05$ vs 0.5, 3, 5, 12 h; $*P<0.05$ vs 5, 12 h; $^{\dagger}P<0.05$ vs 5, 12 h. (**II-c**) Area of end-feet (μm²) and percentage of carbon black suspension-perfused microvessels: Percentage ratio of carbon black suspension-perfused microvessels (CBSPm), $*P<0.05$ vs 3, 5, 8, 12 h; $^{\#\#}P<0.05$ vs 0, 0.5, 3, 5, 12, 24 h; $^{\#}P<0.05$ vs 0, 12, 24 h. Area of end-feet, $**P<0.05$ vs 0.5, 3, 5, 12 h; $^{\dagger}P<0.05$ vs 0, 0.5, 3, 12, 24 h

were dilated with an electron-dense matrix. Five to 12 h post-ischemia, the area of the astrocytic cytoplasm and the number of mitochondria in it did not change; but then both values increased at 48 h (Fig. 3f), whereas the end-feet gradually thinned out, showing a decreased number of mitochondria and being surrounded by degenerated APs (Fig. 2 I-b, c). At 48 h post-ischemia, the APs around the astrocytes degenerated and became swollen, and the number of mitochondria, glycogen granules, and glial fibrils increased in the enlarged swollen cytoplasm of the astrocytes (Fig. 3f).

On EM pictures, we measured and compared the number and percentage volume of the cut-ends of APs, and the number of mitochondria in the cut-ends in the neuropil in various areas and at various times after ischemia.

1. When we compared APs in the inter-cellular neuropil at 0, 5, 12, and 48 h post-ischemia, the number of cut-ends of APs decreased; whereas the percentage volume of APs increased from 5 to 48 h (Figs. 2 I-d, e and 3c). However, the number of normal-appearing mitochondria decreased at 5 h and did not change prominently until 48 h, when they increased (Fig. 2 I-f).
2. We compared APs in the neuropil around the normal-appearing, degenerated, and dead neurons at 12 h post-ischemia. The number of cut-ends of normal-appearing APs decreased from 4.36 ± 0.52, 2.86 ± 0.52 to 1.56 ± 0.17 in order around normal-appearing, degenerated, and dead neurons respectively. For the percentage volume of one cut-end of the normal-appearing APs, the value increased from 1.99 ± 0.23, 2.78 ± 0.23 to 3.18 ± 0.34 respectively. The number of mitochondria in one cut-end of APs increased from 0.25 ± 0.03, 0.45 ± 0.06 to 0.65 ± 0.09 respectively (Fig. 3d, e).

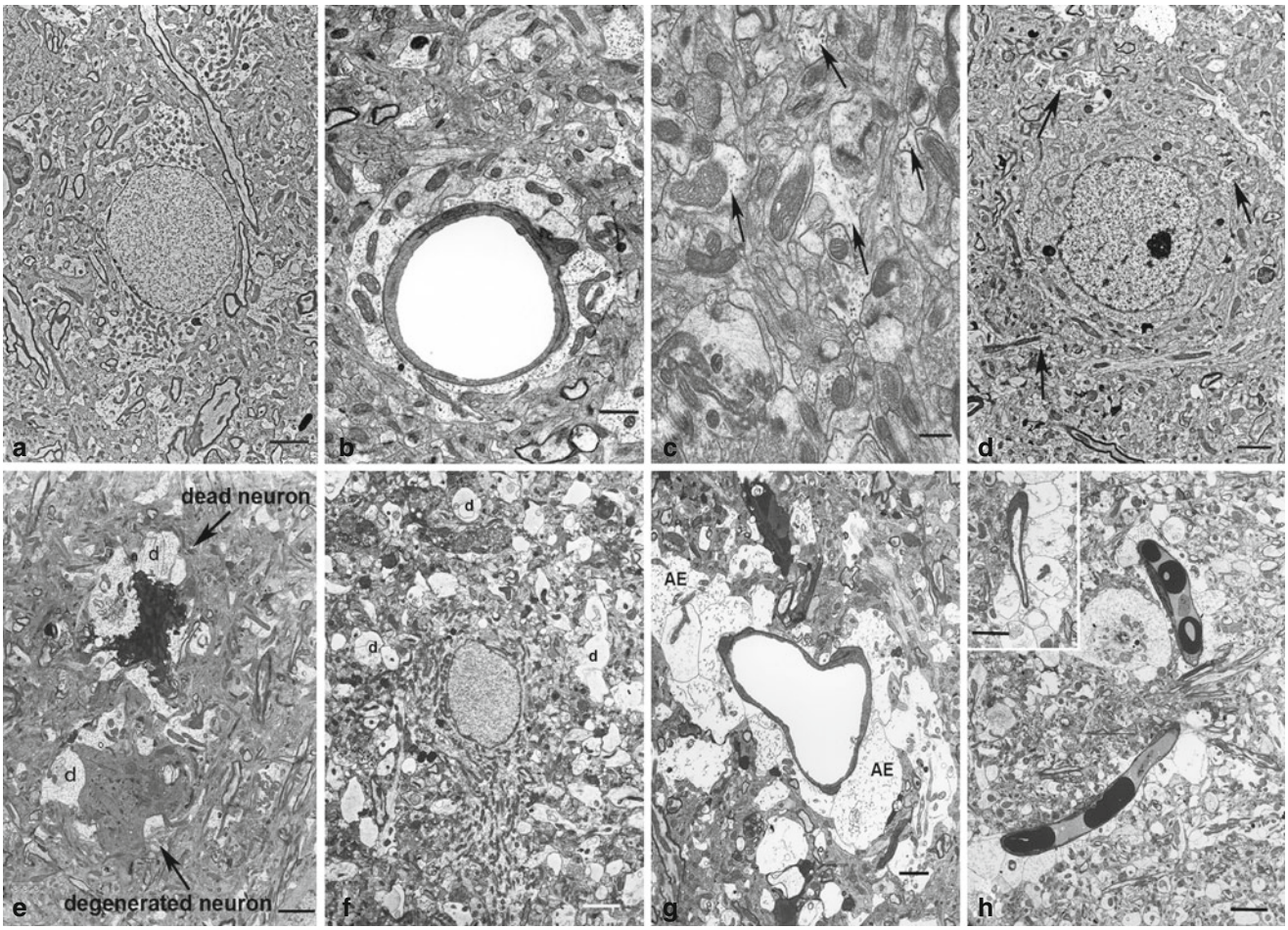

Fig. 3 Electron-microscopic findings in the cerebral cortex: (**a**–**f**) Face B; (**g**, **h**) Face A. (**a**) 5 h. Swollen astrocytic cytoplasm with increased number of mitochondria: Bar = 1.22 μm. (**b**) 5 h. Swollen end-feet: Bar = 1.85 μm. (**c**) 5 h. Swollen, normal-appearing APs with a decreased number of mitochondria (*arrows*): Bar = 0.64 μm. (**d**) 12 h. Not changed APs around the normal-appearing neuron; Bar = 1.73 μm. (**e**) 12 h. Swollen degenerated APs around the degenerated and dead neurons: Bar = 2.06 μm. (**f**) 48 h. Enlarged astrocytic cytoplasm rich in mitochondria is surrounded by swollen degenerated APs (*d*), Bar = 1.67 μm. (**g**) 5 h. Remarkably swollen end-feet (*AE*) compressed the microvessels: Bar = 0.64 μm. (**h**) 5 h. Microvascular stasis. Stagnated plasma, erythrocytes, and platelets are seen: Bar = 4.22 μm. *Inset*: Obstructed microvascular lumen compressed by swollen end-feet. Bar = 3.0 μm

3. We compared APs in the neuropil around the astrocytes at 5 and 48 h post-ischemia. The number of cut-ends of normal-appearing and total APs decreased from12.30 ± 4.36 to 1.70 ± 0.23 and from 14.23 ± 0.86 to 5.14 ± 0.36 in 38.33 μm^2 of the neuropil area respectively, around the astrocytes from 5 to 48 h post-ischemia. The percentage volume of one cut-end of normal-appearing and total APs increased from 0.85 ± 0.09 to 3.16 ± 1.00 and from 0.82 ± 0.07 to 3.19 ± 0.26 respectively, from 5 to 48 h post-ischemia (Fig. 3a, f).

The above chronological and comparative ultrastructural observations on APs suggested that the degenerated swollen APs first appeared around the degenerated/dead neurons, spread in the neuropil with a decrease in number and an increase in swelling. Finally, swollen APs surrounded still viable astrocytes that did not decrease in number, but increased in size owing to swelling at 48-h post-ischemia. After temporary ischemia, all neurons were normal-appearing, but in a necro-biotic state induced by neuronal hyper-excitation. The heterogeneous degeneration of the APs around the neurons of various degrees of viability induced further neuronal injuries and death by the secondary decrease in the energy supply to the necro-biotic neurons and by derangement of the glutamate–glutamine cycle and ion homeostasis, and the possible derangement of purinergic signaling in neuron–glial interactions. This heterogeneous degeneration of APs is closely associated with disseminated selective neuronal necrosis (DSNN) and its maturation [7].

II. Evolution of Focal Infarction in Maturing DSNN in Face A

After temporary ischemia, brief moderate ischemia induces DSNN, whereas longer and more severe ischemia produces

an infarction. Excitatory amino acids are thought to lead to DSNN by neuronal hyper-excitation and by metabolic tissue acidosis, to an infarction. The question to be answered regarding the maturation phenomenon of ischemic injury after temporary ischemia is whether or not the transition from maturing DSNN to abrupt onset of focal infarction is a continuous metabolic process [1]. For vascular reopening therapy by tPA or stenting in the case of acute stroke, prevention of the evolution of a focal infarction after restoration of blood flow is of paramount importance for a better recovery.

By LMS observations, DSNN was found to have matured in the cerebral cortex of Face A (Fig. 1a), where degenerating neurons with a halo of swollen APs and dead neurons appeared and increased in number in disseminated fashion (DSNN) among the normal-appearing neurons at 0.5 and 5 h post-ischemia (Fig. 1b), as was observed in Face B (*I.*), while there was a decrease in the number of normal-appearing neurons (Fig. 2 II-a). Astrocytes slightly decreased in number over 24 h, but there were no statistical differences among 0-, 0.5-, and 3-h values (Fig. 2 II-a).

The cut-ends of APs in the intercellular neuropil decreased in number over 12 h. However, there were no statistical differences among 0.5-, 3-, and 5-h values. Their number decreased remarkably at 12 h, and the cut-ends had disappeared by 24 h owing to the development of the infarction. However, the percentage volume of one cut-end of APs increased from 0 to 12 h because of the swelling (Fig. 2 II-b).

At 3 h post-ischemia, we compared astrocytic processes (APs) in the neuropil of the EM pictures taken around the normal-appearing, degenerated and dead neurons. In these areas, where DSNN was maturing in the cerebral cortex of Face A, the swelling and degeneration of the APs in the neuropil were observed in the same way as in Face B (Fig. 3d, e), but appeared much earlier stage, i.e., at 3 h post-ischemia compared with 12 h in Face B (*I.*-2, page 26).

The end-feet also showed increased swelling at 0.5, 3 and 5 h (Fig. 3g) and then decreased from 12 to 24 h (Fig. 2 II-b). Conversely, the percentage of CBSPm in Face A decreased in over 5 h, further decreasing 8 h post-ischemia, and then increased up to 12 h and further up to 24 h (Fig. 2 II-c). This later increase in CBSPm was due to the decrease in the number of vessel-compressing astrocytic end-feet, resulting from the decrease in the number of astrocytes during the developement of the infarction. Necrotic end-feet were also observed at 12 h. During the decrease in percentage of CBSPm, we observed obstructed micro-vessels of various shapes that had been compressed by swollen end-feet and had developed micro-vascular stasis (Figs. 1b and 3h). Evolution of focal infarction developed later than 12 h post-ischemia (Fig. 1d, e).

Immediately after temporary 30-min unilateral carotid-occlusion of gerbils, we previously investigated the no-reflow phenomenon by perfusion with carbon black suspension and by performing C^{14}-antipyrine autoradiography. We found that the phenomenon was very transient, as it continued for less than 0.5 min after re-canalization; and the regional cerebral blood flow (rCBF) then returned to normal [4].

The ratio of the normal blood flow to the blood flow at the threshold necessary to induce infarction remains roughly constant across species at 3:1. In the present study, the carbon black suspension perfused microvessels (CBSPm) were reduced to 32 and 24 % of normal at 5 and 8 h post-ischemia respectively. An infarction evolves, occurring with a delay of 3–4 h along a rising sigmoid function between rCBF and the duration of the delay [9].

In the present study, we found that the focal cerebral–cortical infarction evolved in the maturing DSNN. It was induced by delayed occurrence of temporary microvascular obstruction due to compression of microvessels by swollen end-feet at 3 ~ to 8 h after restoration of blood flow, and it later resulted in tissue pan-necrosis at 12 ~ to 24 h post-ischemia [8].

Therefore, before evolution of an infarction, strategies to prevent the swelling of end-feet should commence immediately after the reopening of the obstructed major vessels, but before infarction evolution.

Conflict of Interest We declare that we have no conflict of interest.

References

1. Hanyu S, Ito U, Hakamata Y, Yoshida M (1995) Transition from ischemic neuronal necrosis to infarction in repeated ischemia. Brain Res 686:44–48
2. Hanyu S, Ito U, Hakamata Y, Nakano I (1997) Topographical analysis of cortical neuronal loss associated with disseminated selective neuronal necrosis and infarction after repeated ischemia. Brain Res 767:154–157
3. Ito U, Spatz M, Jr WJ, Klatzo I (1975) Experimental cerebral ischemia in Mongolian gerbils. I. Light microscopic observations experimental cerebral ischemia in Mongolian gerbils. Acta Neuropathol 32:209–223
4. Ito U, Ohno K, Yamaguchi T, Tomita H, Inaba Y, Kashima M (1980) Transitional appearance of "no-reflow" phenomenon in Mongolian gerbils. Stroke 11:517–521
5. Ito U, Kuroiwa T, Nagasao J, Kawakami E, Oyanagi K (2006) Temporal profiles of axon terminals. Synapses and spines in the ischemic penumbra of the cerebral cortex. Ultrastructure of neuronal remodeling. Stroke 37:2134–2213
6. Ito U, Nagasao J, Kawakami E, Oyanagi K (2007) Fate of disseminated dead neurons in the cortical ischemic penumbra: ultrastructure indicating a novel scavenger mechanism of microglia and astrocytes. Stroke 38:2577–2583
7. Ito U, Hakamata Y, Kawakami E, Oyanagi K (2009) Degeneration of astrocytic processes and their mitochondria in cerebral cortical regions peripheral to the cortical infarction: heterogeneity of their

disintegration is closely associated with disseminated selective neuronal necrosis and maturation of injury. Stroke 40:2173–2181
8. Ito U, Hakamata Y, Kawakami E, Oyanagi K (2011) Temporary cerebral ischemia results in swollen astrocytic end-feet that compress microvessels and lead to delayed focal cortical infarction. J Cereb Blood Flow Metab 31:328–338
9. Jones TH, Morawetz RB, Crowell RM, Marcoux FW, FitzGibbon SJ, DeGirolami U, Ojemann RG (1981) Thresholds of focal cerebral ischemia in awake monkeys. J Neurosurg 54:773–782
10. Kahn K (1972) The natural course of experimental cerebral infarction in the gerbil. Neurology 22:510–515
11. Kirino T (1982) Delayed neuronal death in the gerbil hippocampus following ischemia. Brain Res 239:57–69
12. Novartis F (2006) Purinergic signaling in neuron-glial interactions. Wiley, Ontario, pp 1–291
13. Ohno K, Ito U, Inaba Y (1984) Regional cerebral blood flow and stroke index after left carotid artery ligation in the conscious gerbil. Brain Res 297:151–157
14. Weibel ER (1963) Morphometry of the human lung. Springer, Berlin/Gowttingen/Heidelberg, pp 19–22

High-Mobility Group Box 1: An Amplifier of Stem and Progenitor Cell Activity After Stroke

Kazuhide Hayakawa, Loc-Duyen D. Pham, Ken Arai, and Eng H. Lo

Abstract Stroke induces a highly complex web of pathophysiology that usually leads to serious long-term disability. Molecules from the damage-associated molecular pattern (DAMP) family immediately increase after stroke. DAMPs are known to cause massive inflammation and brain damage. Thus, they may be targets for neuroprotection. However, emerging data now suggest that DAMPs may not always be detrimental. The high-mobility group box1 (HMGB1) protein is discussed as an example of this idea. During the acute phase after stroke, HMGB1 amplifies neuroinflammation. But during the brain remodeling phase of stroke recovery, HMGB1 can mediate beneficial plasticity and enhance stem and progenitor cell recruitment, proliferation, and differentiation within damaged brain. These emerging findings support the hypothesis that HMGB1 might be an important molecule for regulating stem and progenitor cell therapies in stroke patients.

Keywords Stroke • HMGB1 • Inflammation • Stem cells • Brain remodeling

Introduction

Stroke is the second leading cause of death worldwide and is a very challenging clinical and scientific problem. Therapeutic options for stroke patients are still limited. For example, in ischemic stroke, acute treatments are limited to reperfusion with tissue plasminogen activator or mechanical catheter devices [56]. Many targets and drugs seem exciting at the level of molecular, cellular and animal models. But it has been exceedingly difficult to translate these pre-clinical ideas into clinical efficacy [47, 57].

The biological processes after cerebral ischemia are complicated. Energy deprivation and excitotoxicity are the main causes of the initial tissue damage. In response to initial injury, damage-associated molecular patterns (DAMPs) released into the extracellular micro-environment amplify the secondary processes of blood–brain barrier (BBB) disruption and post-ischemic inflammation [50]. Nevertheless, damaged brain can be surprisingly plastic, and neurogenesis, angiogenesis, and dendritic and axonal remodeling may all provide substrates for compensation and repair. A paradigm shift from symptomatic control for secondary prevention against stroke to amplifying brain regenerative mechanisms may provide a therapeutic opportunity to improve long-term disability after stroke [57].

As a potential concept in brain regenerative medicine, cell-based therapies may become an exciting new frontier for promoting endogenous brain plasticity after stroke [10, 44]. Accumulating evidence suggests that the recruitment of endogenous stem and progenitor cells or exogenously transplanted cells may support brain remodeling following stroke. Intriguingly, high-mobility group box 1 (HMGB1, a member of the DAMP family) can act as a key regulator of stem cell migration, proliferation and differentiation. In this mini-review, we discuss multi-potential actions of HMGB1 (also known as amphoterin or HMG1) as a "case study" for how endogenous mediators might regulate and influence cell-based stroke therapies.

HMGB1 in the Acute Phase After Stroke

HMGB1, a highly conserved non-histone nuclear DNA-binding protein, is widely expressed in most eukaryotic cells, including neural cells in several animal species including humans [87]. Nuclear HMGB1 is able to bind to DNA to

K. Hayakawa, L-D.D. Pham, K. Arai, and E.H. Lo (✉)
Neuroprotection Research Laboratory,
Harvard Medical School, Massachusetts General Hospital East,
149-2401, Charlestown, MA 02129, USA
e-mail: lo@helix.mgh.harvard.edu

Y. Katayama et al. (eds.), *Brain Edema XV*, Acta Neurochirurgica Supplement, Vol. 118,
DOI 10.1007/978-3-7091-1434-6_5, © Springer-Verlag Wien 2013

stabilize nucleosome formation and maintains nuclear homeostasis. HMGB1 enables bending of DNA and facilitates transcription to regulate gene expression [66, 69, 89]. Genetic knockout of HMGB1 causes severe energy deficits, and mice die shortly after birth owing to hypoglycemia caused by impaired glucocorticoid receptor [87]. Overall, intracellular HMGB1 plays an essential role in regulating activation of basal transcriptional machinery [20, 83] and energy homeostasis. Although the function of HMGB1 in the nucleus is not quite understood, the role of extracellular HMGB1 has been extensively studied.

Traditionally, HMGB1 has acted as a nuclear and cellular danger signal [50]. HMGB1 exerts different functions depending on its cellular localization. It can be passively released from damaged cells or actively secreted from stimulated cells. Release of HMGB1 is observed after traumatic brain injury and ischemic stroke. In rodent middle cerebral artery occlusion models, levels of HMGB1 in the ischemic core are immediately decreased, and in turn, serum HMGB1 is rapidly increased [24, 36, 70]. In clinical stroke patients, HMGB1 is upregulated in serum up to day 7 after stroke onset [59]. HMGB1 is also increased in cerebrospinal fluid of subarachnoid hemorrhage patients on days 3, 7, and 14 after onset [59]. In addition, plasma HMGB1 in patients is acutely elevated 30 min after severe trauma in comparison to healthy subjects [17]. These findings suggest that HMGB1 might be highly relevant to human stroke.

Extracellular HMGB1 binds to its receptors and activates a downstream pathway that leads to upregulation of cytokines and other pro-inflammatory molecules. HMGB1 acts as and acts in an autocrine/paracrine fashion. It is secreted by activated macrophage [11], natural killer cells [73], and myeloid dendritic cells [19] in response to endotoxin and other inflammatory stimuli. Besides active secretion, HMGB1 can be released into the extracellular space from damaged cells or necrotic cells [36, 70]. In this case, the membranes of necrotic or damaged cells become "leaky" and HMGB1, which is normally bound loosely to chromatin, diffuses from nucleus to cytoplasm, then into the extracellular matrix. Interestingly, most cytokines start to increase a few hours after stroke [51], while HMGB1 release occurs in the ischemic core of striatum as early as 30 min after artery occlusion [36]. Furthermore, blockade of HMGB1 reduces inflammation and BBB disruption [36, 45, 90]. These results suggest that HMGB1 might be an early mediator that triggers inflammatory cascades.

HMGB1 may signal via its putative receptors, such as receptor for advanced glycation end products (RAGE), toll-like receptor-2 (TLR2), and TLR4. These receptors are expressed in brain cells [13, 27, 79]. RAGE expression is usually low under normal conditions, but enhanced expression of RAGE was observed in diabetic vasculature and other inflammatory diseases [8]. TLR2 and TLR4 have been shown to play a critical role in infectious diseases [79]. Higher constitutive expression levels of TLR4 have been found in brain regions that lack a tight BBB, such as the circumventricular organs and choroid plexus [40, 54]. Activation of HMGB1 receptors leads to activation of NF-κB and MAP kinase [29]. Blockade of either RAGE or TLR4 results in a reduction of cytokine and nitric oxide production and a decrease in inflammation [36, 58, 79], suggesting that HMGB1 might potently contribute to the induction of inflammation.

HMGB1 in Recovery and Remodeling

Most stroke patients show some degree of recovery over time. Damaged brain can be surprisingly plastic, and cross-talk between various types of remodeling brain cells takes place after brain injury [15, 16]. In the late phase after cerebral ischemia, the generation of new blood vessels underlies a highly coupled neurorestorative process that links neurogenesis, synaptogenesis, and angiogenesis [77, 92]. These phenomena are clinically relevant – markers of neurogenesis and angiogenesis have been observed in the adult human brain [39, 53].

In recent years, emerging data suggest that neurovascular repair might be induced by dynamic interactions among cerebral endothelial cells, glia, neurons, and extracellular matrix from days to weeks after stroke [3]. Of these neurovascular cells, astrocytes are the most numerous non-neuronal cell type in the mammalian brain [81]. Traditionally, it was assumed that reactive astrocytes after stroke or brain injury contribute to glial scarring, which impedes neuronal remodeling and recovery [75]. However, it is now recognized that reactive astrocytes may also release many trophic factors, such as nerve growth factor, basic fibroblast growth factor, platelet-derived growth factor, brain-derived neurotrophic factor, ciliary neurotrophic factor, neuropilin-1, vascular endothelial growth factor, and others [55, 76, 80]. Many of these trophic factors may in fact be beneficial in that they promote neuronal survival and synaptogenesis, neurogenesis, and angiogenesis after stroke or brain injury [26, 65].

In contrast to its negative effects, as described in the earlier sections, HMGB1 may also possess beneficial actions. HMGB1 signaling can promote endothelial activation [82] and sprouting [72], and it has also been reported that HMGB1 may increase neurite outgrowth and cell survival in neurons [30, 31, 67]. Intriguingly, stimulated astrocytes have been shown to induce and release HMGB1 protein into the extracellular medium [23, 67]. In a recent study, we showed that low levels of IL-1β potently upregulate HMGB1 in astrocytes. The prototypical MAP kinase ERK provided the upstream signal. The nuclear export protein chromosome region maintenance 1 (CRM1) enabled nuclear HMGB1 to

translocate from nucleus to cytoplasm before release [23]. In vivo study, HMGB1 immunoreactivity was also observed in reactive astrocytes, which are concentrated in the ischemic penumbra in an in vivo ischemic model [35]. Importantly, metabolic inhibition of reactive astrocytes suppressed HMGB1-positive astrocytes in peri-infarct cortex, and that disrupted various neurovascular markers, such as CD31, synaptophysin, and PSD95, which correlated with functional recovery after cerebral ischemia in a mouse focal ischemia model [25]. These findings suggest that reactive astrocytes produce HMGB1, which may promote neurovascular repair in brain after stroke.

Stem and Progenitor Cells Research in Stroke

Over the past two decades, cell-based therapy has been widely proposed as a way of repairing damaged brain after stroke. A variety of cell types, such as hematopoietic stem cells (HSCs) [12, 78], mesenchymal stem cells (MSCs) [6, 85, 86], endothelial progenitor cells (EPCs) [21, 88], very small embryonic-like cells (VSELs) [71], and neuronal stem cells (NSCs) [2, 7, 74] have all been demonstrated to show therapeutic potential in stroke. More recently, human umbilical tissue-derived stem cells (hUTCs) [43, 91] and induced pluripotent stem cells (iPSCs) [33, 34] have been considered to be a candidate source of cells for restorative therapy in stroke. The strategies for stem cell therapy show that different stem cells and their derivatives of rodent and human origin can survive, differentiate into neurons, astrocytes and oligodendrocytes, and induce brain remodeling after stroke (Fig. 1) [44].

Emerging data suggest that stem cells might repair the damaged brain by increasing blood supply by the creation of new vessels, reducing inflammation and ongoing brain cell death, enhancing endogenous repair mechanisms. For example, intravenous injection of human NSCs has been shown to induce improvements after hemorrhagic stroke in rats through anti-inflammatory actions [41]. Intravenously administered human MSCs have been found to reduce stroke-induced deficits in rats by inducing angiogenesis and improving cerebral blood flow [61]. Human ES cell-derived MSCs injected intravenously in rats have been shown to migrate to the infarct region, express neuronal and endothelial cell markers, provide neuroprotection, and improve recovery [46]. Importantly, mouse NSCs delivered intravenously 3 days after stroke in mice have been shown to suppress inflammation

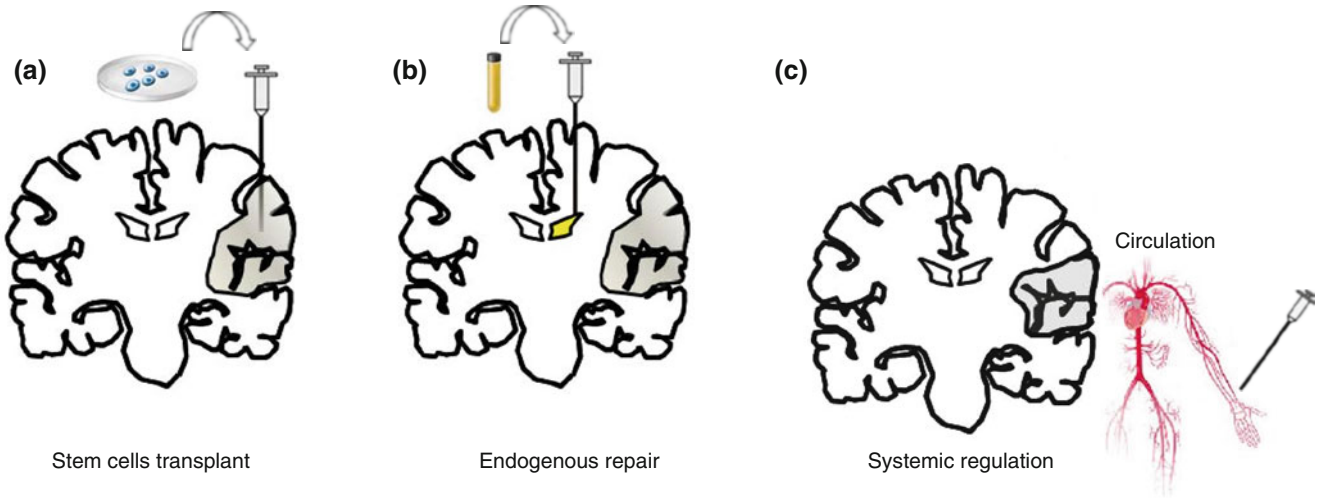

Stem cell therapy

(a). Neuron precursors or neuroblasts generated from stem cells

(b). Compounds to enhance endogenous neurogenesis and angiogenesis

(c). Stem cells for neuroprotection and modulation of inflammation

Fig. 1 Overall strategy of cell-based therapies for stroke. Stroke induces multiple cell death in neurons, astrocytes, oligodendrocytes, and endothelial cells in the cortex and subcortical regions. (**a**) Stem cell-based therapy could be used to repair damaged tissue by transplanting neuronal stem cells/multipotent stem cells. (**b**) Exogenous molecules could be infused to promote neurogenesis, axonal regeneration, and angiogenesis. (**c**) Stem and progenitor cells could be injected systemically for neuroprotection and modulation of inflammation. HMGB1 provides an example of how molecular regulation of these cell therapies may be critically important in optimizing these approaches for clinical utility

and glial scar formation and give rise to delayed neuroprotection and improved functional recovery, starting 18 days after the insult [4]. Clinical reports of MSC transplantation in stroke patients reveal that MSCs may improve the functional recovery of patients without adverse side effects [5]. Accumulating evidence now suggests that stem and progenitor cell-based therapy might hold promise for regenerative medicine, even beyond stroke per se.

A few initial clinical trials delivering stem cells in stroke have been completed [48]. For example, an immortalized human teratocarcinoma cell line implanted into ischemic/hemorrhagic infarcts affecting the basal ganglia and in some cases also the cerebral cortex [37, 38, 60] – these effects may be related to slight improvements in some patients. No substantial clinical improvements were detected after intravenous injection of autologous MSCs in patients with an ischemic lesion in the territory supplied by the middle cerebral artery [5]. Several clinical studies using intravenous or intra-arterial (into damaged territory) infusion of autologous bone marrow-derived stem cells in stroke patients are ongoing or planned (www.clinicaltrials.gov). The company ReNeuron, based in the United Kingdom, is planning a clinical trial in stroke patients involving transplantation of clonal, conditionally immortalized NSCs isolated from human fetal cortex.

Role of HMGB1 on Various Stem and Progenitor Cells Activation

HMGB1 has also had a beneficial effect under a number of pathological conditions in terms of its ability to recruit stem cells and promote their proliferation [62]. HMGB1 was found to enable endothelial progenitor cells to home to ischemic muscle in animal models of hind limb ischemia [14]. If HMGB1 was injected into the infarct area of the heart, it promoted tissue regeneration, and a significant recovery of cardiac performance was indeed mediated by RAGE signaling [22, 42]. More recently, it was reported that endogenous HMGB1 was crucial for ischemia-induced angiogenesis and that HMGB1 protein administration enhanced collateral blood flow in the ischemic hind limbs of diabetic mice through a VEGF-dependent mechanism [9]. It is now recognized that HMGB1 may have beneficial effects on tissue regeneration and remodeling through the recruitment of stem and progenitor cells.

Recent findings suggest that HMGB1 might be a key regulator for MSC activity [68]. It has been demonstrated that HMGB1 not only attract MSCs, but also enhances the proliferation of MSCs and inhibits the ability of MSCs to produce the IFN-γ-induced immunosuppressive molecule indoleamine-2,3-dioxygenase (IDO). These phenomena mediated by HMGB1 were neutralized by specific polyclonal antibodies to HMGB1 or by the soluble receptor for advanced glycation end products (sRAGE) [49]. On the other hand, others reported that HMGB1 inhibited the proliferation of MSCs, but promoted migration and differentiation into osteoblasts. Moreover, HMGB1-treated MSCs displayed unchanged suppressive activity on in vitro lymphocyte cell proliferation elicited by ConA [52]. Hence, there may also be involvement of TLR2 and/or TLR4 receptors in the stimulation of MSC migration mediated by HMGB1 [52]. Indeed, MSCs may be a target of HMGB1 signaling, but many more studies are needed to properly define the mechanisms involved.

In terms of connections between brain and blood, HMGB1 is also an essential factor of non-cell-autonomous enhancement in hematopoietic stem cell (HSC) activity [18]. HMGB1 released by MSCs after treatment with 12 Gy gamma-ray irradiation induced the proliferation and differentiation capacities of cord blood hematopoietic stem cells. This effect was partially inhibited by TLR2 and TLR4 antibodies [84]. In addition, HMGB1 promoted endothelial progenitor cells (EPCs) to home to ischemic muscle in animal models of hind limb ischemia [14]. HMGB1 increased EPC adhesion to the immobilized integrin ligands intercellular adhesion molecule-1 and fibronectin in a RAGE-dependent manner, suggesting that HMGB1-RAGE signaling in EPCs might be a novel target for improving vascular remodeling after stroke.

Migration of mesoangioblast stem cells may also involve HMGB1. Full-length HMGB1 and a fragment that lacks only the acidic tail chemoattracts mesoangioblast stem cells in a concentration-dependent manner [64], whereas the individual boxes (box A or box B), or both boxes (box A + B) had no significant chemotactic effect, suggesting that the segment from the end of box B to the beginning of the acidic tail (amino acids 165–185) might be necessary for the chemotactic effect in mesoangioblast stem cells [64]. Interestingly, this segment significantly corresponded to the surface recognized on HMGB1 by the RAGE [28, 32]. In transmigration assay of mesoangioblast stem cells, HMGB1 in the lower compartment induced a higher number of mesoangioblasts to migrate across the endothelial monolayer and filter than in the presence of VEGF [62]. In vivo migration assay also showed that HMGB1 could chemoattract both mesoangioblast stem cells and DiI-labeled lin^- hematopoietic stem cells [62]. The cell signaling of HMGB1-induced mesoangioblast migration may be involved in the nuclear factor kappaB pathway via extracellular signal-regulated kinase phosphorylation [63].

What makes HMGB1 particularly important is its pleiotropic actions in harnessing the power of stem and progenitor cells. Multiple cell sources may be affected. In zebrafish brain development, HMGB1 may be a critical factor enabling survival and proliferation of neural progenitors in amphoterin-induced gene and orf (AMIGO) dependent manner [93]. Neuronal progenitors have the capacity to replace lost neurons and enhance neurogenesis, angiogenesis,

axonal sprouting, and synaptogenesis. HMGB1 multipotency may contribute to neuronal regeneration by enhancing the potential of neuronal progenitor cells after stroke.

Perspective for Stem and Progenitor Cells Therapy in Stroke

To date, cell-based approaches have been extensively investigated as potential treatments for neurodegenerative disorders. Indeed, transplantation of stem cells or their derivatives in animal models of neurodegenerative diseases can improve function by replacing the lost neurons and glial cells and by mediating remyelination, trophic actions, and modulation of inflammation. Endogenous stem and progenitor cells are also potential therapeutic targets for producing neurons, glial cells, and endothelial cells in response to injury. However, in order to translate stem cell therapy into clinical reality, many hurdles still remain. For example, it is necessary to determine the optimal cell types to use. Perhaps even more importantly, we need to learn how to control/regulate the proliferation, survival, migration, differentiation, and functional integration of transplanted and/or endogenous cells or factors (i.e., HMGB1) in the damaged brain after stroke. Ultimately, however strong the biology, we may also need to develop procedures and criteria for cell delivery, scaling up, appropriate manufacturing and quality control of target cells, optimal functional recovery, and patient selection and assessment [1]. Clearly, longer-term studies are needed to translate cell transplantation therapy to the clinic in a timely but safe and effective manner so that the remarkable potential already shown for cell transplantation to aid recovery from experimental stroke can become a reality for the patients [10].

Conclusion

Extensive data from molecular, cellular, and animal models support the existence of a potent pro-inflammatory effect of HMGB1 in acute ischemic stroke. In fact, therapeutically beneficial effects of monoclonal HMGB1 antibody have been described in several animal models of cerebral ischemia. However, it is now important to realize that HMGB1 might possess biphasic actions during stroke, brain injury, and neurodegeneration. During delayed phases of stroke recovery, extracellular HMGB1 may not only enhance the crosstalk among neurovascular cells such as neurons, astrocytes, and endothelial cells, but may also contribute to stem cell migration into the ischemic region and promote stroke recovery through neurogenesis, vasculogenesis, and angiogenesis. Ultimately, a more nuanced approach to modifying the HMGB1 response after stroke may be needed in order to optimize inhibition during acute stages of injury without interfering with the beneficial mechanisms of neurovascular remodeling driven by stem and progenitor cells.

Acknowledgments Supported in part by NIH grants, the American Heart Association, the Deane Institute.

Conflict of Interest We declare that we have no conflict of interest.

References

1. Wechsler L, Steindler D, Borlongan C, Chopp M, Savitz S, Deans R, Caplan L, Hess D, Mays RW, Boltze J, Boncoraglio G, Borlongan CV, Caplan LR, Carmichael ST, Chopp M, Davidoff AW, Deans RJ, Fisher M, Hess DC, Kondziolka D, Mays RW, Norrving B, Parati E, Parent J, Reynolds BA, Gonzalez-Rothi LJ, Savitz S, Sanberg P, Schneider D, Sinden JD, Snyder E, Steinberg GK, Steindler D, Wechsler L, Weiss MD, Weiss S, Victor S, Zheng T. Stem Cell Therapies as an Emerging Paradigm in Stroke (STEPS): bridging basic and clinical science for cellular and neurogenic factor therapy in treating stroke (2009) Stroke 40:510–515.
2. Andres RH, Horie N, Slikker W, Keren-Gill H, Zhan K, Sun G, Manley NC, Pereira MP, Sheikh LA, McMillan EL, Schaar BT, Svendsen CN, Bliss TM, Steinberg GK (2011) Human neural stem cells enhance structural plasticity and axonal transport in the ischaemic brain. Brain 134:1777–1789
3. Arai K, Lok J, Guo S, Hayakawa K, Xing C, Lo EH (2011) Cellular mechanisms of neurovascular damage and repair after stroke. J Child Neurol 26:1193–1198
4. Bacigaluppi M, Pluchino S, Peruzzotti-Jametti L, Kilic E, Kilic U, Salani G, Brambilla E, West MJ, Comi G, Martino G, Hermann DM (2009) Delayed post-ischaemic neuroprotection following systemic neural stem cell transplantation involves multiple mechanisms. Brain 132:2239–2251
5. Bang OY, Lee JS, Lee PH, Lee G (2005) Autologous mesenchymal stem cell transplantation in stroke patients. Ann Neurol 57: 874–882
6. Bao X, Wei J, Feng M, Lu S, Li G, Dou W, Ma W, Ma S, An Y, Qin C, Zhao RC, Wang R (2011) Transplantation of human bone marrow-derived mesenchymal stem cells promotes behavioral recovery and endogenous neurogenesis after cerebral ischemia in rats. Brain Res 1367:103–113
7. Barkho BZ, Zhao X (2011) Adult neural stem cells: response to stroke injury and potential for therapeutic applications. Curr Stem Cell Res Ther 6(4):327–338
8. Barlovic DP, Soro-Paavonen A, Jandeleit-Dahm KA (2011) RAGE biology, atherosclerosis and diabetes. Clin Sci (Lond) 121:43–55
9. Biscetti F, Straface G, De Cristofaro R, Lancellotti S, Rizzo P, Arena V, Stigliano E, Pecorini G, Egashira K, De Angelis G, Ghirlanda G, Flex A (2010) High-mobility group box-1 protein promotes angiogenesis after peripheral ischemia in diabetic mice through a VEGF-dependent mechanism. Diabetes 59:1496–1505
10. Bliss T, Guzman R, Daadi M, Steinberg GK (2007) Cell transplantation therapy for stroke. Stroke 38:817–826
11. Bonaldi T, Talamo F, Scaffidi P, Ferrera D, Porto A, Bachi A, Rubartelli A, Agresti A, Bianchi ME (2003) Monocytic cells hyperacetylate chromatin protein HMGB1 to redirect it towards secretion. EMBO J 22:5551–5560
12. Boy S, Sauerbruch S, Kraemer M, Schormann T, Schlachetzki F, Schuierer G, Luerding R, Hennemann B, Orso E, Dabringhaus A, Winkler J, Bogdahn U (2011) Mobilisation of hematopoietic CD34+ precursor cells in patients with acute stroke is safe–results of an open-labeled non randomized phase I/II trial. PLoS One 6:e23099

13. Caso JR, Pradillo JM, Hurtado O, Lorenzo P, Moro MA, Lizasoain I (2007) Toll-like receptor 4 is involved in brain damage and inflammation after experimental stroke. Circulation 115: 1599–1608
14. Chavakis E, Hain A, Vinci M, Carmona G, Bianchi ME, Vajkoczy P, Zeiher AM, Chavakis T, Dimmeler S (2007) High-mobility group box 1 activates integrin-dependent homing of endothelial progenitor cells. Circ Res 100:204–212
15. Chen Y, Swanson RA (2003) Astrocytes and brain injury. J Cereb Blood Flow Metab 23:137–149
16. Chopp M, Zhang ZG, Jiang Q (2007) Neurogenesis, angiogenesis, and MRI indices of functional recovery from stroke. Stroke 38:827–831
17. Cohen MJ, Brohi K, Calfee CS, Rahn P, Chesebro BB, Christiaans SC, Carles M, Howard M, Pittet JF (2009) Early release of high mobility group box nuclear protein 1 after severe trauma in humans: role of injury severity and tissue hypoperfusion. Crit Care 13:R174
18. Deneault E, Cellot S, Faubert A, Laverdure JP, Frechette M, Chagraoui J, Mayotte N, Sauvageau M, Ting SB, Sauvageau G (2009) A functional screen to identify novel effectors of hematopoietic stem cell activity. Cell 137:369–379
19. Dumitriu IE, Bianchi ME, Bacci M, Manfredi AA, Rovere-Querini P (2007) The secretion of HMGB1 is required for the migration of maturing dendritic cells. J Leukoc Biol 81:84–91
20. Ellwood KB, Yen YM, Johnson RC, Carey M (2000) Mechanism for specificity by HMG-1 in enhanceosome assembly. Mol Cell Biol 20:4359–4370
21. Fan Y, Shen F, Frenzel T, Zhu W, Ye J, Liu J, Chen Y, Su H, Young WL, Yang GY (2010) Endothelial progenitor cell transplantation improves long-term stroke outcome in mice. Ann Neurol 67:488–497
22. Germani A, Limana F, Capogrossi MC (2007) Pivotal advances: high-mobility group box 1 protein – a cytokine with a role in cardiac repair. J Leukoc Biol 81:41–45
23. Hayakawa K, Arai K, Lo EH (2010) Role of ERK map kinase and CRM1 in IL-1beta-stimulated release of HMGB1 from cortical astrocytes. Glia 58:1007–1015
24. Hayakawa K, Mishima K, Nozako M, Hazekawa M, Mishima S, Fujioka M, Orito K, Egashira N, Iwasaki K, Fujiwara M (2008) Delayed treatment with minocycline ameliorates neurologic impairment through activated microglia expressing a high-mobility group box1-inhibiting mechanism. Stroke 39:951–958
25. Hayakawa K, Nakano T, Irie K, Higuchi S, Fujioka M, Orito K, Iwasaki K, Jin G, Lo EH, Mishima K, Fujiwara M (2010) Inhibition of reactive astrocytes with fluorocitrate retards neurovascular remodeling and recovery after focal cerebral ischemia in mice. J Cereb Blood Flow Metab 30:871–882
26. Horner PJ, Gage FH (2000) Regenerating the damaged central nervous system. Nature 407:963–970
27. Hua F, Ma J, Ha T, Xia Y, Kelley J, Williams DL, Kao RL, Browder IW, Schweitzer JB, Kalbfleisch JH, Li C (2007) Activation of toll-like receptor 4 signaling contributes to hippocampal neuronal death following global cerebral ischemia/reperfusion. J Neuroimmunol 190:101–111
28. Huttunen HJ, Fages C, Kuja-Panula J, Ridley AJ, Rauvala H (2002) Receptor for advanced glycation end products-binding COOH-terminal motif of amphoterin inhibits invasive migration and metastasis. Cancer Res 62:4805–4811
29. Huttunen HJ, Fages C, Rauvala H (1999) Receptor for advanced glycation end products (RAGE)-mediated neurite outgrowth and activation of NF-kappaB require the cytoplasmic domain of the receptor but different downstream signaling pathways. J Biol Chem 274:19919–19924
30. Huttunen HJ, Kuja-Panula J, Rauvala H (2002) Receptor for advanced glycation end products (RAGE) signaling induces CREB-dependent chromogranin expression during neuronal differentiation. J Biol Chem 277:38635–38646
31. Huttunen HJ, Kuja-Panula J, Sorci G, Agneletti AL, Donato R, Rauvala H (2000) Coregulation of neurite outgrowth and cell survival by amphoterin and S100 proteins through receptor for advanced glycation end products (RAGE) activation. J Biol Chem 275:40096–40105
32. Huttunen HJ, Rauvala H (2004) Amphoterin as an extracellular regulator of cell motility: from discovery to disease. J Intern Med 255:351–366
33. Jiang M, Lv L, Ji H, Yang X, Zhu W, Cai L, Gu X, Chai C, Huang S, Sun J, Dong Q (2011) Induction of pluripotent stem cells transplantation therapy for ischemic stroke. Mol Cell Biochem 354:67–75
34. Kawai H, Yamashita T, Ohta Y, Deguchi K, Nagotani S, Zhang X, Ikeda Y, Matsuura T, Abe K (2010) Tridermal tumorigenesis of induced pluripotent stem cells transplanted in ischemic brain. J Cereb Blood Flow Metab 30:1487–1493
35. Kim JB, Lim CM, Yu YM, Lee JK (2008) Induction and subcellular localization of high-mobility group box-1 (HMGB1) in the postischemic rat brain. J Neurosci Res 86:1125–1131
36. Kim JB, Sig Choi J, Yu YM, Nam K, Piao CS, Kim SW, Lee MH, Han PL, Park JS, Lee JK (2006) HMGB1, a novel cytokine-like mediator linking acute neuronal death and delayed neuroinflammation in the postischemic brain. J Neurosci 26:6413–6421
37. Kondziolka D, Steinberg GK, Wechsler L, Meltzer CC, Elder E, Gebel J, Decesare S, Jovin T, Zafonte R, Lebowitz J, Flickinger JC, Tong D, Marks MP, Jamieson C, Luu D, Bell-Stephens T, Teraoka J (2005) Neurotransplantation for patients with subcortical motor stroke: a phase 2 randomized trial. J Neurosurg 103:38–45
38. Kondziolka D, Wechsler L, Goldstein S, Meltzer C, Thulborn KR, Gebel J, Jannetta P, DeCesare S, Elder EM, McGrogan M, Reitman MA, Bynum L (2000) Transplantation of cultured human neuronal cells for patients with stroke. Neurology 55:565–569
39. Krupinski J, Kaluza J, Kumar P, Kumar S, Wang JM (1993) Some remarks on the growth-rate and angiogenesis of microvessels in ischemic stroke. Morphometric and immunocytochemical studies. Patol Pol 44:203–209
40. Laflamme N, Echchannaoui H, Landmann R, Rivest S (2003) Cooperation between toll-like receptor 2 and 4 in the brain of mice challenged with cell wall components derived from gram-negative and gram-positive bacteria. Eur J Immunol 33: 1127–1138
41. Lee ST, Chu K, Jung KH, Kim SJ, Kim DH, Kang KM, Hong NH, Kim JH, Ban JJ, Park HK, Kim SU, Park CG, Lee SK, Kim M, Roh JK (2008) Anti-inflammatory mechanism of intravascular neural stem cell transplantation in haemorrhagic stroke. Brain 131: 616–629
42. Limana F, Germani A, Zacheo A, Kajstura J, Di Carlo A, Borsellino G, Leoni O, Palumbo R, Battistini L, Rastaldo R, Muller S, Pompilio G, Anversa P, Bianchi ME, Capogrossi MC (2005) Exogenous high-mobility group box 1 protein induces myocardial regeneration after infarction via enhanced cardiac C-kit + cell proliferation and differentiation. Circ Res 97:e73–e83
43. Lin YC, Ko TL, Shih YH, Lin MY, Fu TW, Hsiao HS, Hsu JY, Fu YS (2011) Human umbilical mesenchymal stem cells promote recovery after ischemic stroke. Stroke 42:2045–2053
44. Lindvall O, Kokaia Z (2010) Stem cells in human neurodegenerative disorders – time for clinical translation? J Clin Invest 120:29–40
45. Liu K, Mori S, Takahashi HK, Tomono Y, Wake H, Kanke T, Sato Y, Hiraga N, Adachi N, Yoshino T, Nishibori M (2007) Anti-high mobility group box 1 monoclonal antibody ameliorates brain infarction induced by transient ischemia in rats. FASEB J 21: 3904–3916
46. Liu YP, Seckin H, Izci Y, Du ZW, Yan YP, Baskaya MK (2009) Neuroprotective effects of mesenchymal stem cells derived from human embryonic stem cells in transient focal cerebral ischemia in rats. J Cereb Blood Flow Metab 29:780–791

47. Lo EH (2008) Experimental models, neurovascular mechanisms and translational issues in stroke research. Br J Pharmacol 153(Suppl 1):S396–S405
48. Locatelli F, Bersano A, Ballabio E, Lanfranconi S, Papadimitriou D, Strazzer S, Bresolin N, Comi GP, Corti S (2009) Stem cell therapy in stroke. Cell Mol Life Sci 66:757–772
49. Lotfi R, Eisenbacher J, Solgi G, Fuchs K, Yildiz T, Nienhaus C, Rojewski MT, Schrezenmeier H (2011) Human mesenchymal stem cells respond to native but not oxidized damage associated molecular pattern molecules from necrotic (tumor) material. Eur J Immunol 41:2021–2028
50. Lotze MT, Tracey KJ (2005) High-mobility group box 1 protein (HMGB1): nuclear weapon in the immune arsenal. Nat Rev Immunol 5:331–342
51. Maddahi A, Edvinsson L (2010) Cerebral ischemia induces microvascular pro-inflammatory cytokine expression via the MEK/ERK pathway. J Neuroinflammation 7:14
52. Meng E, Guo Z, Wang H, Jin J, Wang J, Wu C, Wang L (2008) High mobility group box 1 protein inhibits the proliferation of human mesenchymal stem cells and promotes their migration and differentiation along osteoblastic pathway. Stem Cells Dev 17:805–813
53. Minger SL, Ekonomou A, Carta EM, Chinoy A, Perry RH, Ballard CG (2007) Endogenous neurogenesis in the human brain following cerebral infarction. Regen Med 2:69–74
54. Mishra BB, Mishra PK, Teale JM (2006) Expression and distribution of toll-like receptors in the brain during murine neurocysticercosis. J Neuroimmunol 181:46–56
55. Mocchetti I, Wrathall JR (1995) Neurotrophic factors in central nervous system trauma. J Neurotrauma 12:853–870
56. Molina CA (2011) Reperfusion therapies for acute ischemic stroke: current pharmacological and mechanical approaches. Stroke 42:S16–S19
57. Moskowitz MA, Lo EH, Iadecola C (2010) The science of stroke: mechanisms in search of treatments. Neuron 67:181–198
58. Muhammad S, Barakat W, Stoyanov S, Murikinati S, Yang H, Tracey KJ, Bendszus M, Rossetti G, Nawroth PP, Bierhaus A, Schwaninger M (2008) The HMGB1 receptor RAGE mediates ischemic brain damage. J Neurosci 28:12023–12031
59. Nakahara T, Tsuruta R, Kaneko T, Yamashita S, Fujita M, Kasaoka S, Hashiguchi T, Suzuki M, Maruyama I, Maekawa T (2009) High-mobility group box 1 protein in CSF of patients with subarachnoid hemorrhage. Neurocrit Care 11:362–368
60. Nelson PT, Kondziolka D, Wechsler L, Goldstein S, Gebel J, DeCesare S, Elder EM, Zhang PJ, Jacobs A, McGrogan M, Lee VM, Trojanowski JQ (2002) Clonal human (hNT) neuron grafts for stroke therapy: neuropathology in a patient 27 months after implantation. Am J Pathol 160:1201–1206
61. Onda T, Honmou O, Harada K, Houkin K, Hamada H, Kocsis JD (2008) Therapeutic benefits by human mesenchymal stem cells (hMSCs) and Ang-1 gene-modified hMSCs after cerebral ischemia. J Cereb Blood Flow Metab 28:329–340
62. Palumbo R, Bianchi ME (2004) High mobility group box 1 protein, a cue for stem cell recruitment. Biochem Pharmacol 68: 1165–1170
63. Palumbo R, Galvez BG, Pusterla T, De Marchis F, Cossu G, Marcu KB, Bianchi ME (2007) Cells migrating to sites of tissue damage in response to the danger signal HMGB1 require NF-kappaB activation. J Cell Biol 179:33–40
64. Palumbo R, Sampaolesi M, De Marchis F, Tonlorenzi R, Colombetti S, Mondino A, Cossu G, Bianchi ME (2004) Extracellular HMGB1, a signal of tissue damage, induces mesoangioblast migration and proliferation. J Cell Biol 164:441–449
65. Panickar KS, Norenberg MD (2005) Astrocytes in cerebral ischemic injury: morphological and general considerations. Glia 50:287–298
66. Pasqualini JR, Sterner R, Mercat P, Allfrey VG (1989) Estradiol enhanced acetylation of nuclear high mobility group proteins of the uterus of newborn guinea pigs. Biochem Biophys Res Commun 161:1260–1266
67. Passalacqua M, Patrone M, Picotti GB, Del Rio M, Sparatore B, Melloni E, Pontremoli S (1998) Stimulated astrocytes release high-mobility group 1 protein, an inducer of LAN-5 neuroblastoma cell differentiation. Neuroscience 82:1021–1028
68. Pistoia V, Raffaghello L (2011) Damage-associated molecular patterns (DAMPs) and mesenchymal stem cells: a matter of attraction and excitement. Eur J Immunol 41:1828–1831
69. Prendergast P, Onate SA, Christensen K, Edwards DP (1994) Nuclear accessory factors enhance the binding of progesterone receptor to specific target DNA. J Steroid Biochem Mol Biol 48:1–13
70. Qiu J, Nishimura M, Wang Y, Sims JR, Qiu S, Savitz SI, Salomone S, Moskowitz MA (2008) Early release of HMGB-1 from neurons after the onset of brain ischemia. J Cereb Blood Flow Metab 28:927–938
71. Ratajczak J, Zuba-Surma E, Paczkowska E, Kucia M, Nowacki P, Ratajczak MZ (2011) Stem cells for neural regeneration – a potential application of very small embryonic-like stem cells. J Physiol Pharmacol 62:3–12
72. Schlueter C, Weber H, Meyer B, Rogalla P, Roser K, Hauke S, Bullerdiek J (2005) Angiogenetic signaling through hypoxia: HMGB1: an angiogenetic switch molecule. Am J Pathol 166: 1259–1263
73. Semino C, Angelini G, Poggi A, Rubartelli A (2005) NK/iDC interaction results in IL-18 secretion by DCs at the synaptic cleft followed by NK cell activation and release of the DC maturation factor HMGB1. Blood 106:609–616
74. Shen CC, Lin CH, Yang YC, Chiao MT, Cheng WY, Ko JL (2010) Intravenous implanted neural stem cells migrate to injury site, reduce infarct volume, and improve behavior after cerebral ischemia. Curr Neurovasc Res 7:167–179
75. Silver J, Miller JH (2004) Regeneration beyond the glial scar. Nat Rev Neurosci 5:146–156
76. Strauss S, Otten U, Joggerst B, Pluss K, Volk B (1994) Increased levels of nerve growth factor (NGF) protein and mRNA and reactive gliosis following kainic acid injection into the rat striatum. Neurosci Lett 168:193–196
77. Sun Y, Jin K, Xie L, Childs J, Mao XO, Logvinova A, Greenberg DA (2003) VEGF-induced neuroprotection, neurogenesis, and angiogenesis after focal cerebral ischemia. J Clin Invest 111:1843–1851
78. Taguchi A, Soma T, Tanaka H, Kanda T, Nishimura H, Yoshikawa H, Tsukamoto Y, Iso H, Fujimori Y, Stern DM, Naritomi H, Matsuyama T (2004) Administration of CD34+ cells after stroke enhances neurogenesis via angiogenesis in a mouse model. J Clin Invest 114:330–338
79. Tang SC, Arumugam TV, Xu X, Cheng A, Mughal MR, Jo DG, Lathia JD, Siler DA, Chigurupati S, Ouyang X, Magnus T, Camandola S, Mattson MP (2007) Pivotal role for neuronal toll-like receptors in ischemic brain injury and functional deficits. Proc Natl Acad Sci U S A 104:13798–13803
80. Tokita Y, Keino H, Matsui F, Aono S, Ishiguro H, Higashiyama S, Oohira A (2001) Regulation of neuregulin expression in the injured rat brain and cultured astrocytes. J Neurosci 21:1257–1264
81. Tower DB, Young OM (1973) The activities of butyrylcholinesterase and carbonic anhydrase, the rate of anaerobic glycolysis, and the question of a constant density of glial cells in cerebral cortices of various mammalian species from mouse to whale. J Neurochem 20:269–278
82. Treutiger CJ, Mullins GE, Johansson AS, Rouhiainen A, Rauvala HM, Erlandsson-Harris H, Andersson U, Yang H, Tracey KJ, Andersson J, Palmblad JE (2003) High mobility group 1 B-box mediates activation of human endothelium. J Intern Med 254:375–385
83. Verrijdt G, Haelens A, Schoenmakers E, Rombauts W, Claessens F (2002) Comparative analysis of the influence of the high-mobility

group box 1 protein on DNA binding and transcriptional activation by the androgen, glucocorticoid, progesterone and mineralocorticoid receptors. Biochem J 361:97–103
84. Wang XB, Chen X, Song KD, Wang J, Yao W, Liu HL, Sun ZM (2010) Effects of HMGB1 on human cord blood CD34(+) hematopoietic stem cells proliferation and differentiation in vitro. Zhonghua Xue Ye Xue Za Zhi 31:88–91
85. Xin H, Li Y, Shen LH, Liu X, Hozeska-Solgot A, Zhang RL, Zhang ZG, Chopp M (2011) Multipotent mesenchymal stromal cells increase tPA expression and concomitantly decrease PAI-1 expression in astrocytes through the sonic hedgehog signaling pathway after stroke (in vitro study). J Cereb Blood Flow Metab 31(11):2181–2188
86. Xin H, Li Y, Shen LH, Liu X, Wang X, Zhang J, Pourabdollah-Nejad DS, Zhang C, Zhang L, Jiang H, Zhang ZG, Chopp M (2010) Increasing tPA activity in astrocytes induced by multipotent mesenchymal stromal cells facilitate neurite outgrowth after stroke in the mouse. PLoS One 5:e9027
87. Yang H, Wang H, Czura CJ, Tracey KJ (2005) The cytokine activity of HMGB1. J Leukoc Biol 78:1–8
88. Yip HK, Chang LT, Chang WN, Lu CH, Liou CW, Lan MY, Liu JS, Youssef AA, Chang HW (2008) Level and value of circulating endothelial progenitor cells in patients after acute ischemic stroke. Stroke 39:69–74
89. Zhang CC, Krieg S, Shapiro DJ (1999) HMG-1 stimulates estrogen response element binding by estrogen receptor from stably transfected HeLa cells. Mol Endocrinol 13:632–643
90. Zhang J, Takahashi HK, Liu K, Wake H, Liu R, Maruo T, Date I, Yoshino T, Ohtsuka A, Mori S, Nishibori M (2011) Anti-high mobility group box-1 monoclonal antibody protects the blood-brain barrier from ischemia-induced disruption in rats. Stroke 42:1420–1428
91. Zhang L, Li Y, Zhang C, Chopp M, Gosiewska A, Hong K (2011) Delayed administration of human umbilical tissue-derived cells improved neurological functional recovery in a rodent model of focal ischemia. Stroke 42:1437–1444
92. Zhang ZG, Zhang L, Jiang Q, Zhang R, Davies K, Powers C, Bruggen N, Chopp M (2000) VEGF enhances angiogenesis and promotes blood-brain barrier leakage in the ischemic brain. J Clin Invest 106:829–838
93. Zhao X, Kuja-Panula J, Rouhiainen A, Chen YC, Panula P, Rauvala H (2011) High mobility group box-1 (HMGB1; amphoterin) is required for zebrafish brain development. J Biol Chem 286: 23200–23213

Geldanamycin Treatment During Cerebral Ischemia/Reperfusion Attenuates p44/42 Mitogen-Activated Protein Kinase Activation and Tissue Damage

Murat Karabiyikoglu, Ya Hua, Richard F. Keep, and Guohua Xi

Abstract *Background*: Heat-shock protein 90 (Hsp90) inhibitor geldanamycin was found to be neuroprotective in various experimental models of brain disease. The effect was attributed to the induction of heat-shock proteins and/or disruption of cellular signaling. *Methods*: In Sprague–Dawley rats, the middle cerebral artery was occluded for 90 min using the intraluminal suture method. Geldanamycin (300 mg/kg) or vehicle was injected intraperitoneally 15 min before onset of ischemia or reperfusion. Animals were sacrificed at 2, 4 or 24 h after ischemia onset and brain samples were processed for infarct volume measurement, Western blot analysis or immunofluorescent staining of Hsp90, Raf-1, p38, and p44/42 mitogen-activated protein kinases (MAPKs). *Results*: Geldanamycin treatment during ischemia or reperfusion reduced infarct volume by 79 and 61 % respectively. Geldanamycin decreased Raf-1 and activated p44/42 MAPK proteins, but did not alter levels of activated p38 MAPK during early reperfusion. Hsp90 was co-localized with Raf-1 and activated p44/42 MAPK in the cytoplasm of ischemic neurons. *Conclusion*: Geldanamycin-induced protection against transient focal cerebral ischemia may in part be based upon depletion of Raf-1 and blockade of p44/42 MAPK activation.

Keywords Cerebral ischemia • Geldanamycin • Mitogen-activated protein kinase • Raf • Hsp90 • Rat

M. Karabiyikoglu
Department of Neurosurgery, University of Michigan, Ann Arbor, MI, USA

Y. Hua, MD, R.F. Keep, and G. Xi, MD (✉)
Department of Neurosurgery,
University of Michigan Medical School,
5018 BSRB, 109 Zina Pitcher Pl,
Ann Arbor, MI 48109-2200, USA
e-mail: guohuaxi@umich.edu

Introduction

The ubiquitous heat-shock protein 90 (Hsp90)-based chaperone system is an essential component of several signal transduction pathways in eukaryotic cells. Hsp90 is markedly expressed throughout neuronal subpopulations of adult rat brain, but not in non-neuronal cells [7]. The Hsp90 inhibitor geldanamycin (GA), upon binding Hsp90, releases heat-shock factor (HSF1) and induces heat-shock proteins (HSPs) [2, 5]. An injection of GA 24 h before focal ischemia in rat was neuroprotective, the effect being attributed to the induction of Hsp70 [12]. However, an earlier study found that GA protected a mouse hippocampal cell line against glutamate toxicity even when given 4 h after the insult [23]. In this paradigm, GA increased the degradation of Raf-1, the central component of a mitogen-activated protein kinase (MAPK) cascade, as well as inducing Hsp90. Thus, it is likely that various cell-signaling pathways may be altered by pharmaceutical inhibition of Hsp90 chaperone function during cerebral ischemia and reperfusion.

In this study, we tested the efficacy of a GA dose given just before ischemia or reperfusion in a rat model of focal cerebral ischemia. We also investigated the effects of these GA treatments on p38 and p44/42 MAPK signaling pathways.

Materials and Methods

Animal Model and Treatment Groups

The protocols for the animal studies were approved by the University of Michigan Committee on the Use and Care of Animals. A total of 57 male Sprague–Dawley rats (275–325 g; Charles River Laboratories, Portage, MI, USA) were used. The animals were fasted for 4 h before surgery, but had free access to water. Anesthesia was induced by inhalation of

Y. Katayama et al. (eds.), *Brain Edema XV*, Acta Neurochirurgica Supplement, Vol. 118,
DOI 10.1007/978-3-7091-1434-6_6,

5 % isoflurane in a 70 % nitrous oxide/30 % oxygen mixture and maintained by 1.5 % isoflurane administered through a face mask. A blood sample was collected from the tail artery to measure PaO_2, $PaCO_2$, pH, hematocrit, and glucose. Rectal temperature was maintained at 37.5 °C using a feedback-controlled heating pad. Transient focal cerebral ischemia was induced using the intraluminal suture method [13]. Ninety minutes after ischemia induction the animal was re-anesthetized and the intraluminal suture was removed. The sham operation was identical except that the intraluminal suture was not advanced beyond 15 mm.

Two GA (Sigma, St. Louis, MO, USA) treatment regimens were used: the GA ischemia regimen consisted of an intraperitoneal injection of 300 mg/kg GA 15 min before induction of ischemia, and the GA reperfusion regimen consisted of the same dose injected 15 min before reperfusion. Vehicle-treated animals received an equal volume intraperitoneal injection of 20 % dimethylsulfoxide 15 min before the induction of ischemia. Animals were sacrificed 2 or 4 h after ischemia onset (0.5 or 2.5 h of reperfusion) for Western blot analysis, or 24 h after ischemia onset for determination of tissue damage.

Morphometric Measurement of Tissue Damage

To identify the tissue damage fresh brain tissue was cut into 2-mm-thick coronal sections and incubated in 2 % 2,3,5-triphenyltetrazolium chloride (TTC). The infarct area was measured with NIH Image 1.62 software, and the volume was calculated by multiplying the distance between sections.

Western Blot Analysis

Animals were perfused with saline. Ischemic tissue in the left hemisphere was sampled using a 6-mm cork borer and divided into cortex and caudate. Western blot analysis was performed as previously described [22]. Primary antibodies were anti-Raf-1 (1:500; Santa Cruz Biotechnology, Santa Cruz, CA, USA) and anti-phospho-p44/42 MAPK (1:1,000; Cell Signaling Technology, Boston, MA, USA).

Immunofluorescence Staining

Another set of animals that were exposed to 90-min transient MCA occlusion without any treatment were sacrificed at 2 and 4 h after ischemia onset and were perfused with saline followed by 4 % paraformaldehyde. The brains were removed and immersed in 4 % paraformaldehyde and 25 % sucrose for 24 h at 4 °C. The tissue was frozen, embedded in OCT compound (Sakura Finetek, Torrance, CA, USA), and sectioned at 40-μm thickness on a cryostat. Floating sections were microwaved in distilled water and single- or double-stained using anti-Hsp90 (1:400; StressGen Biotechnologies, San Diego, CA, USA), anti-phospho-p44/42 MAPK (1:200), and anti-Raf-1 (1:100) primary antibodies. Secondary antibodies were fluorescein-conjugated anti-mouse (1:100; Vector Laboratories, Burlingame, CA, USA) and rhodamine-conjugated anti-rabbit (1:100; Chemicon, Billerica, MA, USA) [22]. All solutions were buffered using Tris base. Stained sections were mounted using Vectashield (Vector Laboratories) and visualized under an Olympus FV-500 confocal microscope.

Statistical Analysis

All quantitative data were presented as mean ± standard deviation and compared using analysis of variance (ANOVA) with Student's *t* test. Differences were considered significant at the $P<0.05$ level.

Results

Physiological data were measured immediately after induction of ischemia. Blood pH, PaO_2, $PaCO_2$, glucose, and hematocrit were within the normal range.

Both treatment regimens, GA ischemia and GA reperfusion, reduced infarct volume significantly compared with the vehicle group ($n=24$; 56 ± 37 mm^3 and 105 ± 67 mm^3 vs 267 ± 97 mm^3, $P<0.005$). The protective effect of GA was more pronounced in the cortex (Fig. 1).

The phosphorylated active forms of p38 (p-p38) and p44/42 (p-p44/42) MAPKs detected by Western blotting were increased both in the ischemic caudate and cortex at 2 and 4 h after ischemia onset. The average increase in p-p38 MAPK was 1.6-fold, whereas p-p44/42 MAPK increased an average of 24-fold. Raf-1 was unchanged at 2 h, but decreased at 4 h after ischemia onset compared with the pre-ischemic levels (data not shown). GA ischemia and GA reperfusion significantly attenuated p-p44/42 MAPK in ischemic caudate ($n=12$: 386 ± 60 and $1{,}091\pm187$ vs $2{,}333\pm314$ %, $P<0.005$), and even more so in the ischemic cortex (103 ± 34 % and 163 ± 31 % vs $2{,}468\pm306$ %, $P<0.0005$) at 4 h after ischemia compared with the vehicle. Both treatment regimens of GA also decreased Raf-1 levels in ischemic regions at 2 h after ischemia compared with

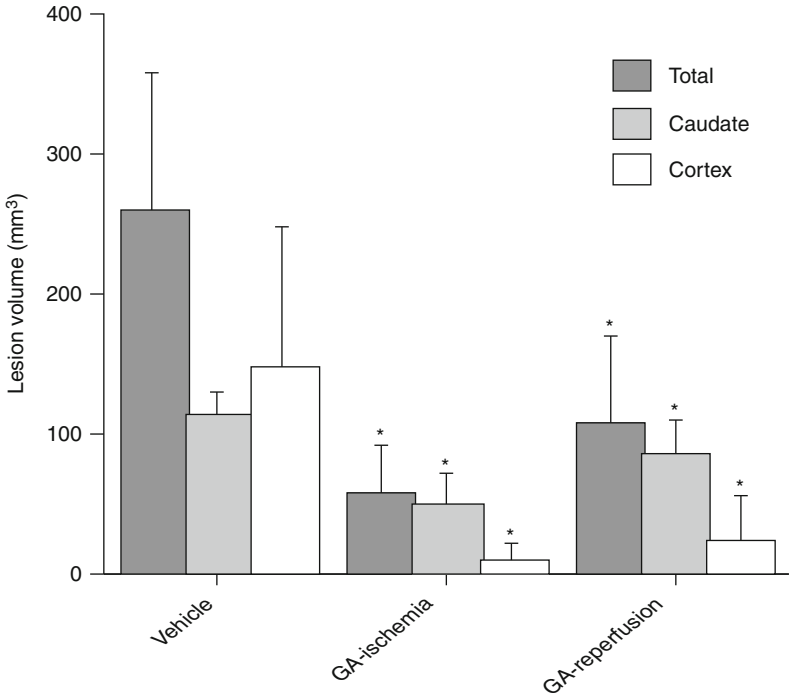

Fig. 1 A dose of geldanamycin (GA) given 15 min before the onset of ischemia (GA ischemia) or reperfusion (GA reperfusion) reduced infarct volume (detected 24 h after ischemia) compared with the vehicle-injected group by 79 and 61 % respectively. $n=8$, $^*P<0.05$ vs vehicle

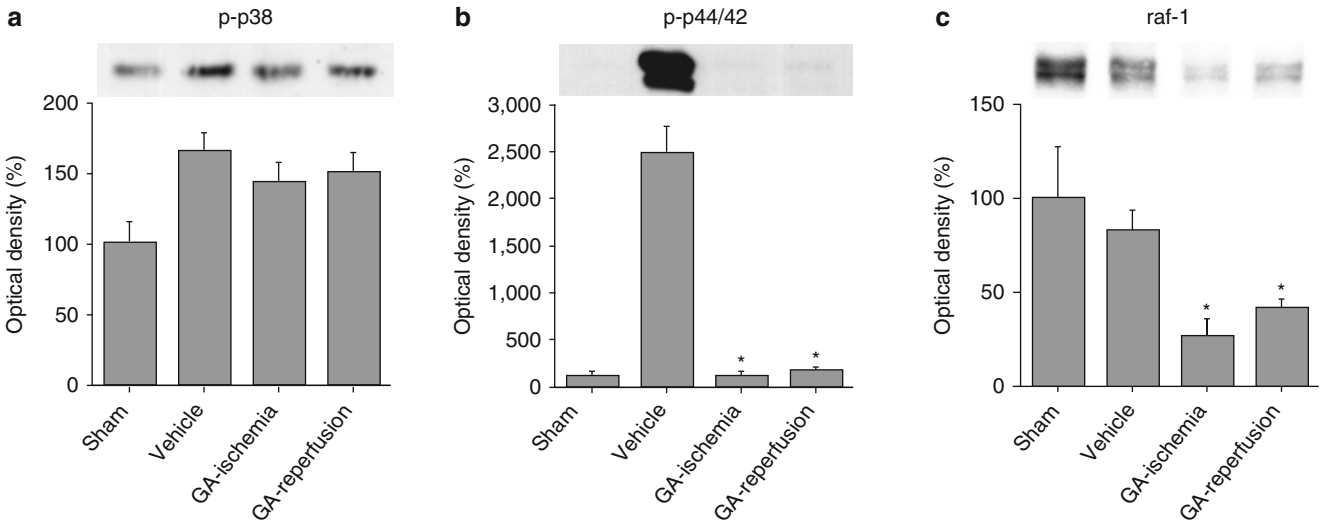

Fig. 2 The GA treatment regimens did not significantly alter p38 MAPK activation (**a**), but effectively blocked p44/42 MAPK activation (**b**) in the ischemic cortex 4 h after ischemia onset. Premature depletion of Raf-1 by GA treatment in the same region 2 h after ischemia onset (**c**) may explain the downstream blockage of p44/42 MAPK phosphorylation. $n=4$, $^*P<0.05$ vs vehicle

vehicle. Although GA-treated animals showed slightly reduced p38 MAPK activation, the effect was not significant (Fig. 2).

Hsp90 was predominantly located in the nucleus of neurons in normal rat brain, with little cytoplasmic staining detected by immunofluorescence. The cytoplasm of these neurons also stained positive for Raf-1 in double-labeled sections. Normal rat brain parenchyma showed no p-p44/42 MAPK staining. Two hours after ischemia onset (0.5 h after reperfusion), Hsp90 was increased in the cytoplasm of neurons in the ischemic core and co-localized with Raf-1 and p-p44/42 MAPK. Four hours after ischemia onset (2.5 h after reperfusion), Hsp90 co-localized with Raf-1 and p-p44/42 MAPK in the cytoplasm of neurons in the penumbral regions. In contrast, there was decreased Hsp90 and Raf-1 staining in the ischemic core at this time point.

However, neurons in the ischemic core were still positive for p-p44/42 MAPK.

Conclusion

The present study shows that inhibition of Hsp90 with GA during ischemia or early reperfusion protects adult rat brain against focal ischemic damage. This treatment is also associated with a rapid decrease in Raf-1 protein levels and attenuation of p44/42 MAPK activation, whereas the p38 MAPK activation is not altered significantly.

The MAPKs comprise a group of signaling proteins that play a prominent role in regulating cell proliferation, differentiation, and adaptation. Both p38 and p44/42 MAPKs have been implicated in neuronal injury and disease (reviewed in Chu et al. [4], Harper and Wilkie [8], and Irving and Bamford [10]). Following ischemia many factors are released, including glutamate, free radicals, growth factors, cytokines, and thrombin, all of which are known to stimulate MAPK pathways. Ischemia rapidly induces p38 and p44/42 MAPK activation in rodent neurons and inhibition of these kinase systems reduces ischemic brain damage [1, 3, 6, 9, 11, 14, 19–21]. Our Western blot and immunofluorescence staining data also showed increased levels of activated p38 and p44/42 MAPKs in affected neurons at 0.5 and 2.5 h following 90 min of MCA occlusion. GA treatment during ischemia or reperfusion, while reducing brain injury, blocked p44/42 MAPK activation, but did not significantly affect p38 MAPK activation.

The Raf-MEK-p44/42 MAPK signaling module is the best characterized of the three main MAPK cascades and is emerging as an important regulator of neuronal responses to both functional (learning and memory) and pathological (regulated cell death) stimuli. Raf-1 is targeted to the cell membrane by Ras and integrates extracellular signals by phosphorylating the dual specificity kinase MEK (MAPK kinase), which in turn phosphorylates p44/42 MAPK. Activation of p44/42 MAPK leads to activation of other downstream kinases, as well as several transcription factors. Raf-1 is primarily cytosolic in location and exists in a native heterocomplex with Hsp90 [18]. Treatment by GA disrupts Raf-1 complex formation with Hsp90, leading to aberrant intracellular trafficking and increased degradation of Raf-1 [15, 16]. It is also shown that Raf-1 is the only component of the p44/42 MAPK signaling pathway that is depleted by GA and Raf-1 depletion by GA is sufficient to interdict signaling through this pathway [17]. In our experiments, GA treatment during ischemia/reperfusion decreased Raf-1 protein levels at 2 h after ischemia onset, which, in turn, may account for the reduced p44/42 MAPK activation observed at 4 h. Our confocal microscopic data demonstrated temporal co-localization of Hsp90, Raf-1, and p-p44/42 in the cytoplasm of neurons located in the ischemic core and penumbra.

The small lipophilic drug GA readily crosses the blood–brain barrier and is a promising option for the treatment of clinical stroke. GA treatment induces HSPs and blocks the activation of p44/42 MAPK in experimental stroke, which may in part account for the resulting neuroprotection. However, alterations in HSPs and MAPKs may also be the result of alterations in ischemic damage, complicating definitive conclusions. More detailed investigations of the involvement of HSP90 in ischemic neurodegeneration and the specific consequences of MAPK activation in this paradigm are necessary to fully reveal the mechanism of GA-induced neuroprotection.

Acknowledgments This study was supported by grants NS-017760, NS-039866. and NS-057539 from the National Institutes of Health (NIH) and 0840016 N from the American Heart Association (AHA). The content is solely the responsibility of the authors and does not necessarily represent the official views of the NIH and AHA.

Conflict of Interest We declare that we have no conflict of interest.

References

1. Alessandrini A, Namura S, Moskowitz MA, Bonventre JV (1999) MEK1 protein kinase inhibition protects against damage resulting from focal cerebral ischemia. Proc Natl Acad Sci U S A 96: 12866–12869
2. Ali A, Bharadwaj S, O'Carroll R, Ovsenek N (1998) HSP90 interacts with and regulates the activity of heat shock factor 1 in Xenopus oocytes. Mol Cell Biol 18:4949–4960
3. Barone FC, Irving EA, Ray AM, Lee JC, Kassis S, Kumar S, Badger AM, Legos JJ, Erhardt JA, Ohlstein EH, Hunter AJ, Harrison DC, Philpott K, Smith BR, Adams JL, Parsons AA (2001) Inhibition of p38 mitogen-activated protein kinase provides neuroprotection in cerebral focal ischemia. Med Res Rev 21:129–145
4. Chu CT, Levinthal DJ, Kulich SM, Chalovich EM, DeFranco DB (2004) Oxidative neuronal injury. The dark side of ERK1/2. Eur J Biochem 271:2060–2066
5. Conde AG, Lau SS, Dillmann WH, Mestril R (1997) Induction of heat shock proteins by tyrosine kinase inhibitors in rat cardiomyocytes and myogenic cells confers protection against simulated ischemia. J Mol Cell Cardiol 29:1927–1938
6. Ferrer I, Friguls B, Dalfo E, Planas AM (2003) Early modifications in the expression of mitogen-activated protein kinase (MAPK/ERK), stress-activated kinases SAPK/JNK and p38, and their phosphorylated substrates following focal cerebral ischemia. Acta Neuropathol 105:425–437
7. Gass P, Schroder H, Prior P, Kiessling M (1994) Constitutive expression of heat shock protein 90 (HSP90) in neurons of the rat brain. Neurosci Lett 182:188–192
8. Harper SJ, Wilkie N (2003) MAPKs: new targets for neurodegeneration. Expert Opin Ther Targets 7:187–200

9. Hu BR, Liu CL, Park DJ (2000) Alteration of MAP kinase pathways after transient forebrain ischemia. J Cereb Blood Flow Metab 20:1089–1095
10. Irving EA, Bamford M (2002) Role of mitogen- and stress-activated kinases in ischemic injury. J Cereb Blood Flow Metab 22:631–647
11. Irving EA, Barone FC, Reith AD, Hadingham SJ, Parsons AA (2000) Differential activation of MAPK/ERK and p38/SAPK in neurones and glia following focal cerebral ischaemia in the rat. Brain Res Mol Brain Res 77:65–75
12. Lu A, Ran R, Parmentier-Batteur S, Nee A, Sharp FR (2002) Geldanamycin induces heat shock proteins in brain and protects against focal cerebral ischemia. J Neurochem 81:355–364
13. Memezawa H, Smith ML, Siesjo BK (1992) Penumbral tissues salvaged by reperfusion following middle cerebral artery occlusion in rats. Stroke 23:552–559
14. Namura S, Iihara K, Takami S, Nagata I, Kikuchi H, Matsushita K, Moskowitz MA, Bonventre JV, Alessandrini A (2001) Intravenous administration of MEK inhibitor U0126 affords brain protection against forebrain ischemia and focal cerebral ischemia. Proc Natl Acad Sci U S A 98:11569–11574
15. Schulte TW, An WG, Neckers LM (1997) Geldanamycin-induced destabilization of Raf-1 involves the proteasome. Biochem Biophys Res Commun 239:655–659
16. Schulte TW, Blagosklonny MV, Ingui C, Neckers L (1995) Disruption of the Raf-1-Hsp90 molecular complex results in destabilization of Raf-1 and loss of Raf-1-Ras association. J Biol Chem 270:24585–24588
17. Schulte TW, Blagosklonny MV, Romanova L, Mushinski JF, Monia BP, Johnston JF, Nguyen P, Trepel J, Neckers LM (1996) Destabilization of Raf-1 by geldanamycin leads to disruption of the Raf-1-MEK-mitogen-activated protein kinase signalling pathway. Mol Cell Biol 16:5839–5845
18. Stancato LF, Chow YH, Hutchison KA, Perdew GH, Jove R, Pratt WB (1993) Raf exists in a native heterocomplex with hsp90 and p50 that can be reconstituted in a cell-free system. J Biol Chem 268:21711–21716
19. Sugino T, Nozaki K, Takagi Y, Hattori I, Hashimoto N, Moriguchi T, Nishida E (2000) Activation of mitogen-activated protein kinases after transient forebrain ischemia in gerbil hippocampus. J Neurosci 20:4506–4514
20. Wang X, Wang H, Xu L, Rozanski DJ, Sugawara T, Chan PH, Trzaskos JM, Feuerstein GZ (2003) Significant neuroprotection against ischemic brain injury by inhibition of the MEK1 protein kinase in mice: exploration of potential mechanism associated with apoptosis. J Pharmacol Exp Ther 304:172–178
21. Wu DC, Ye W, Che XM, Yang GY (2000) Activation of mitogen-activated protein kinases after permanent cerebral artery occlusion in mouse brain. J Cereb Blood Flow Metab 20:1320–1330
22. Xi G, Keep RF, Hua Y, Xiang J, Hoff JT (1999) Attenuation of thrombin-induced brain edema by cerebral thrombin preconditioning. Stroke 30:1247–1255
23. Xiao N, Callaway CW, Lipinski CA, Hicks SD, DeFranco DB (1999) Geldanamycin provides posttreatment protection against glutamate-induced oxidative toxicity in a mouse hippocampal cell line. J Neurochem 72:95–101

Evaluation of the Stage of Hemorrhage Using Optical Diffuse Reflectance Spectroscopy: An In Vivo Study

Satoru Takeuchi, Satoko Kawauchi, Shunichi Sato, Hiroshi Nawashiro, Kimihiro Nagatani, Hiroaki Kobayashi, Naoki Otani, Hideo Osada, Kojiro Wada, and Katsuji Shima

Abstract Intracerebral hemorrhage (ICH) is a common and often fatal subtype of stroke. Estimation of the stage of hemorrhage allows clinicians to know when the hemorrhage occurred, even in unconscious patients, enabling decisions to be made about the optimal management and treatment strategy. After ICH, oxidative denaturation of the hemoglobin progresses, and deoxyhemoglobin is gradually converted to methemoglobin. MRI has been used to estimate the stage of hemorrhage by evaluating the status of hemoglobin. However, there is currently no bedside device that can be used for the measurement of hemoglobin derivatives in patients with hematomas. The aim of the present study was to investigate the validity of using optical diffuse reflectance spectroscopy (ODRS) for bedside evaluation of the stage of hemorrhage. An ICH model was generated in adult Sprague–Dawley male rats by stereotactically injecting 50 μl of autologous blood into the right caudate nucleus. To analyze the hemoglobin derivatives in the hematomas, ODRS measurement was performed for the rats in vivo. In all rats, we found increased absorption at around 630 nm, which indicated the formation of methemoglobin. In conclusion, the results of the present study suggest that ODRS allows clinicians to more easily evaluate the stage of hemorrhage at the patient's bedside.

Keywords Intracerebral hemorrhage • Optical diffuse reflectance spectroscopy • In vivo • Monitoring

S. Takeuchi (✉), H. Nawashiro, K. Nagatani, H. Kobayashi
N. Otani, MD, H. Osada, K. Wada, and K. Shima
Department of Neurosurgery, National Defense Medical College,
3-2 Namiki, Tokorozawa, Saitama 359-8513, Japan
e-mail: s.takeuchi@room.ocn.ne.jp

S. Kawauchi and S. Sato
Division of Biomedical Information Sciences,
National Defense Medical College,
3-2 Namiki, Tokorozawa, Saitama 359-8513, Japan

Introduction

Intracerebral hemorrhage (ICH) is a common and often fatal subtype of stroke [16]. Estimation of the stage of hemorrhage allows clinicians to determine when the hemorrhage occurred, even in unconscious patients, thereby enabling appropriate decisions to be made about the optimal management and treatment strategy. After ICH, oxidative denaturation of hemoglobin progresses, and deoxyhemoglobin is gradually converted to methemoglobin [13–15]. Magnetic resonance imaging (MRI) has been used to estimate the stage of hemorrhage by evaluating the state of hemoglobin conversion, i.e., the age of the hematoma [1, 2, 4, 6, 7, 16]. However, MRI is often difficult to perform, especially in patients who require mechanical ventilation and/or who need to be monitored continuously, and a bedside device is therefore needed for the measurement of hemoglobin derivatives in hematomas.

Recently, non-invasive diffuse optical spectroscopy has been demonstrated to have the potential to non-invasively monitor physiological and biochemical characteristics of tissue [8–12]. Methemoglobin has an absorption peak at around 630 nm [3, 11], and recent studies have shown that diffuse optical spectroscopy can be an attractive non-invasive tool for the in vivo monitoring of methemoglobin formation [11].

The aim of the present study was to investigate the validity of using optical diffuse reflectance spectroscopy (ODRS) for the bedside evaluation of the stage of hemorrhage.

Materials and Methods

Animal Preparation and Intracerebral Infusion

All experimental procedures were approved by the Animal Care and Use Committee of the National Defense Medical College. Six adult male Sprague–Dawley rats (weighing

Y. Katayama et al. (eds.), *Brain Edema XV*, Acta Neurochirurgica Supplement, Vol. 118,
DOI 10.1007/978-3-7091-1434-6_7, © Springer-Verlag Wien 2013

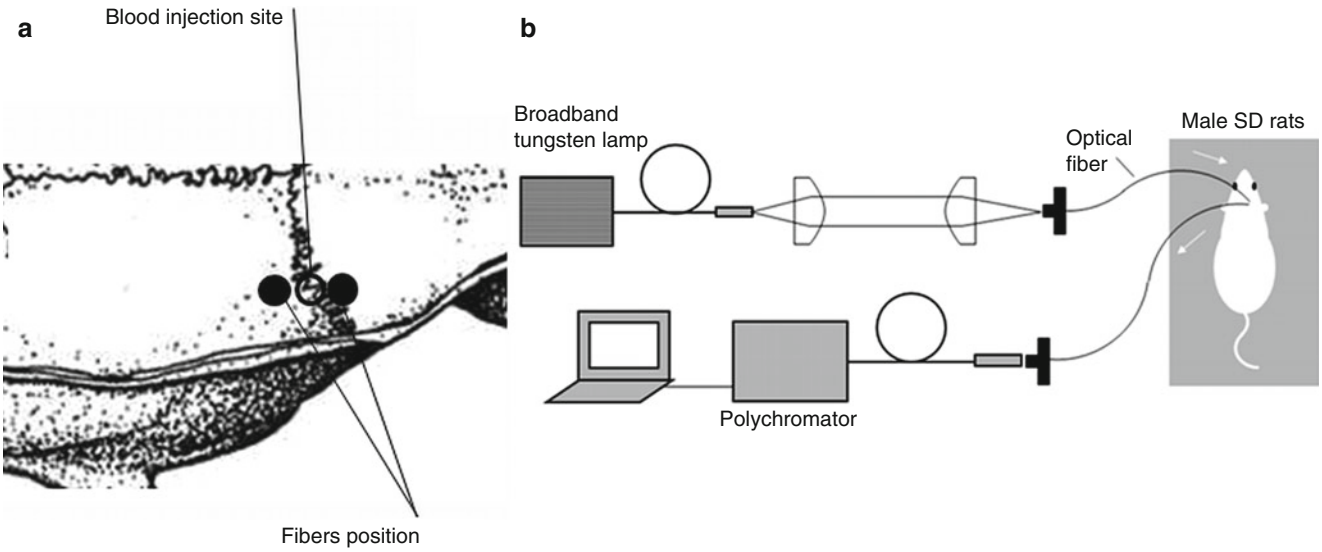

Fig. 1 The positions of the fibers on the skull (**a**), and the experimental set-up (**b**)

between 300 and 400 g) were used for the study. The rats were housed in individual cages under controlled environmental conditions (12/12 h light/dark cycle; 20–22 °C room temperature) with food and water freely available for 1 week before the experimental procedure. All of the rats were anesthetized with sodium pentobarbital (50 mg/kg, intraperitoneally), and the right femoral artery was catheterized to monitor arterial blood pressure and to sample the blood for intracerebral infusion. The rats were positioned using a stereotaxic frame, and a cranial burr hole (1 mm) was drilled into the skull (1 mm anterior and 4 mm lateral to the bregma). Next, a 27-gauge needle was lowered stereotactically into the right caudate nucleus (5 mm ventral from the skull surface). Autologous whole blood (50 μl with no anticoagulants) was injected at a rate of 10 μl/min using a microinfusion pump. The needle remained in place for an additional 10 min after injection to prevent back-leakage. After needle removal, the burr hole was sealed with bone wax.

Optical Diffuse Reflectance Spectroscopy Measurement

To analyze the hemoglobin derivatives in the hematomas, ODRS measurements were performed for rats in vivo (Fig. 1) as follows:

1. A pair of optical fibers with a core diameter of 800 μm and a center-to-center separation of 4 mm were placed on the exposed parietal bone of the right hemisphere above the blood injection site (as a control, measurements were performed at the contralateral site [1 mm anterior and 4 mm lateral to the bregma]).
2. A tungsten lamp with a long wavelength-absorbing filter was used as a light source at an output power of 45 μW.
3. Diffuse light reflectance was measured with a polychromator. Measurements were performed at 30 min, 2, 6, 12, 24, and 48 h after blood injection.

Evaluation of Hematoma Distribution

Following the ODRS measurement at 48 h after blood injection, the rats were euthanized by decapitation under intraperitoneal anesthesia. The brain was removed immediately and fixed with 4 % phosphate-buffered paraformaldehyde. Fixed brains were cut coronally through the needle entry site, and then serial slices (1 mm thick) both anterior and posterior to the needle entry site were obtained. Digital photographs of the serial slices were taken, and the hematoma distributions were evaluated.

Results

At the contralateral site, no time-dependent changes in the diffuse reflectance spectra were observed. At the site of blood infusion, on the other hand, a small dip appeared at around 630 nm in the spectrum beginning at 6 h after blood infusion (Fig. 2). This indicated the formation of methemoglobin. Hematomas were mainly observed in the basal ganglia, and partially extended into the corpus callosum (Fig. 3). The distance from the brain surface to the hematoma was approximately 2.5 mm in each rat.

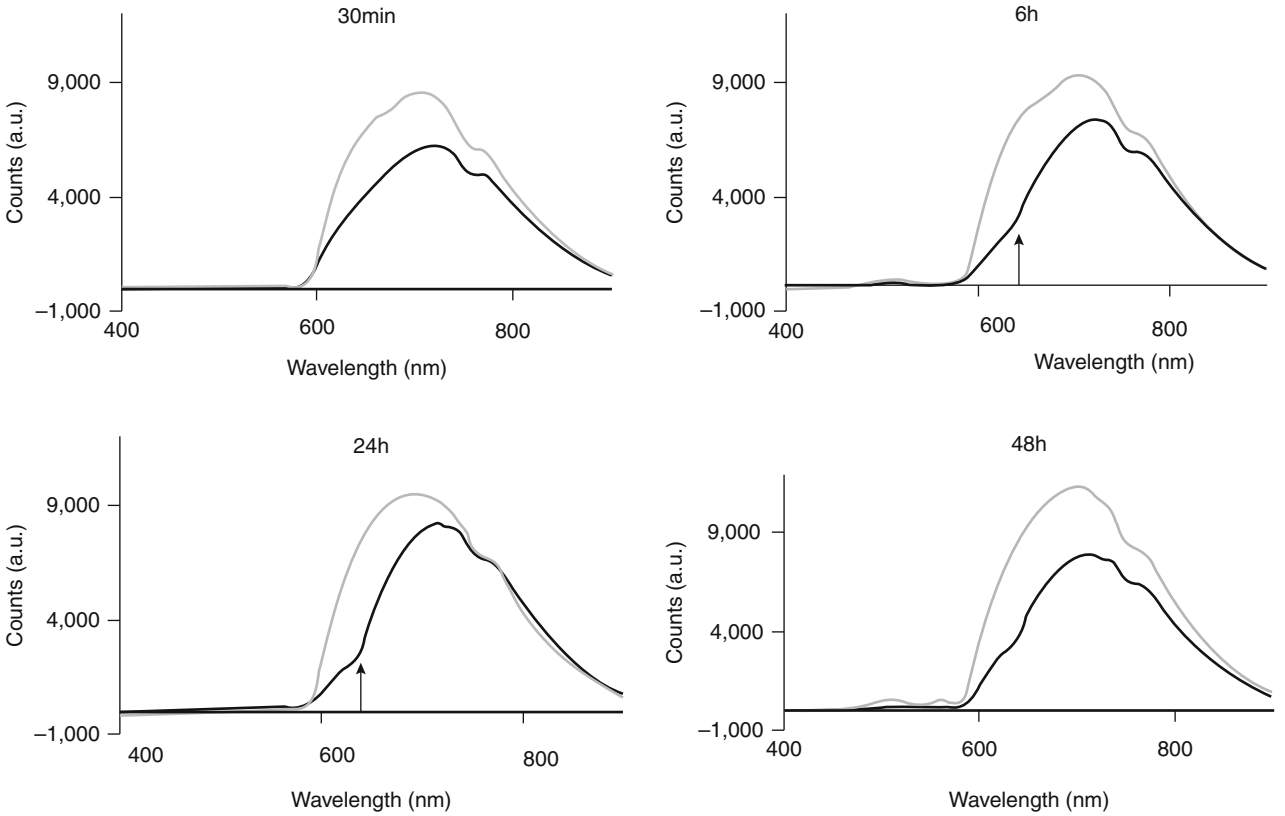

Fig. 2 Representative serial results of optical diffuse reflectance spectroscopy measurements. At the contralateral site, no time-dependent change in the diffuse reflectance spectra was observed. At the site of blood infusion, a small dip appeared at around 630 nm in the spectrum beginning 6 h after blood infusion. *Black line*, the spectra at the blood infusion site; *gray line*, the spectra at the contralateral site. The *arrows* indicate the point of 630 nm

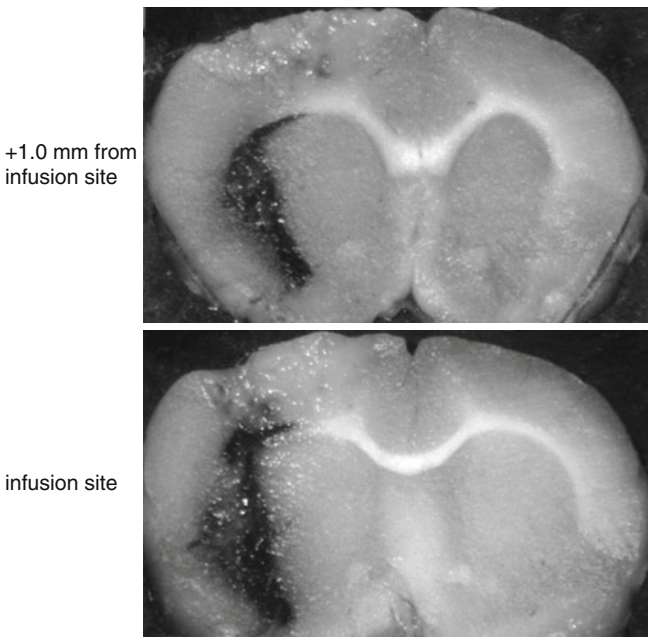

Fig. 3 Representative photographs taken 48 h after blood infusion. Hematomas were mainly found in the basal ganglia and partially extended into the corpus callosum

Conclusion

Patients with ICH should be closely observed for at least 6 h after the onset [5], because the risk of hematoma growth in this period is high. However, if the patient is unconscious and no witnesses to the event are available, then clinicians cannot obtain sufficient information regarding when the hemorrhage occurred. As a result, accurately estimating the stage of hemorrhage is extremely important for clinicians to appropriately manage patients with ICH.

In humans, in the early hours following ICH, oxyhemoglobin is converted to deoxyhemoglobin as the red cells lose their oxygen [15, 16]. In 2 or 3 days, deoxyhemoglobin is spontaneously oxidized to methemoglobin, which is initially formed intracellularly, and then becomes extracellular as the red blood cells lyse [15, 16]. Thereafter, macrophages and phagocytes begin transforming the methemoglobin to hemosiderin and ferritin on around day 7 [15, 16]. In rats, these changes occur more rapidly than in humans [15].

Magnetic resonance imaging can identify the age of hematomas based on five stages: hyperacute (intracellular oxyhemoglobin, long T1 and T2), acute (intracellular

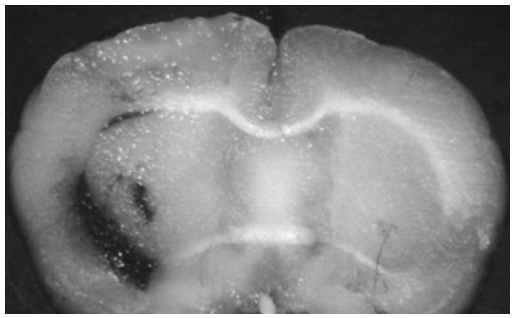

Fig. 3 (continued)

deoxyhemoglobin, long T1, short T2), early subacute (intracellular methemoglobin, short T1, short T2), late subacute (extracellular methemoglobin, short T1, long T2), and chronic (ferritin and hemosiderin, short T2) [4]. However, MRI is difficult to perform in some cases, especially in critical patients.

The present preliminary study showed that the time-dependent formation of methemoglobin can be detected by ODRS measurement in vivo. These results suggest that ODRS would allow clinicians to more easily evaluate the stage of hemorrhage in the brain at the patient's bedside. The quantitative analysis of hemoglobin derivatives should be the subject of future investigations.

Acknowledgements This study was supported by a research grant from The General Insurance Association of Japan.

Conflict of Interest We declare that we have no conflict of interest.

References

1. Armstrong P, Keevil SF (1991) Magnetic resonance imaging – 2: clinical uses. BMJ 303:105–109
2. Atlas SW, Thulborn KR (2002) Intracranial hemorrhage. In: Atlas SW (ed) Magnetic resonance imaging of the brain and spine, 3rd edn. Lippincott Williams & Wilkins, Philadelphia, pp 773–832
3. Bjerre S (1967) Determination of abnormal hemoglobin pigments by spectrophotometry. Clin Biochem 1:299–310
4. Bradley WG Jr (1993) MR appearance of hemorrhage in the brain. Radiology 189:15–26
5. Fujii Y, Tanaka R, Takeuchi S, Koike T, Minakawa T, Sasaki O (1994) Hematoma enlargement in spontaneous intracerebral hemorrhage. J Neurosurg 80:51–57
6. Gomori JM, Grossman RI, Goldberg HI, Zimmerman RA, Bilaniuk LT (1985) Intracranial hematomas: imaging by high-field MR. Radiology 157:87–93
7. Greenberg MS (2010) Handbook of neurosurgery, 7th edn. Thieme, New York, pp 1118–1142
8. Kawauchi S, Sato S, Ooigawa H, Nawashiro H, Ishihara M, Kikuchi M (2008) Simultaneous measurement of changes in light absorption due to the reduction of cytochrome c oxidase and light scattering in rat brains during loss of tissue viability. Appl Opt 47:4164–4176
9. Kawauchi S, Sato S, Ooigawa H, Nawashiro H, Ishihara M, Kikuchi M (2009) Light scattering change precedes loss of cerebral adenosine triphosphate in a rat global ischemic brain model. Neurosci Lett 459:152–156
10. Kawauchi S, Sato S, Uozumi Y, Nawashiro H, Ishihara M, Kikuchi M (2011) Light-scattering signal may indicate critical time zone to rescue brain tissue after hypoxia. J Biomed Opt 16:027002
11. Lee J, El-Abaddi N, Duke A, Cerussi AE, Brenner M, Tromberg BJ (2006) Noninvasive in vivo monitoring of methemoglobin formation and reduction with broadband diffuse optical spectroscopy. J Appl Physiol 100:615–622
12. Lee J, Kim JG, Mahon S, Tromberg BJ, Mukai D, Kreuter K, Saltzman D, Patino R, Goldberg R, Brenner M (2009) Broadband diffuse optical spectroscopy assessment of hemorrhage- and hemoglobin-based blood substitute resuscitation. J Biomed Opt 14:044027
13. Leung G, Moody AR (2010) MR imaging depicts oxidative stress induced by methemoglobin. Radiology 257:470–476
14. Sadrzadeh SM, Anderson DK, Panter SS, Hallaway PE, Eaton JW (1987) Hemoglobin potentiates central nervous system damage. J Clin Invest 79:662–664
15. Wagner KR, Sharp FR, Ardizzone TD, Lu A, Clark JF (2003) Heme and iron metabolism: role in cerebral hemorrhage. J Cereb Blood Flow Metab 23:629–652
16. Warach S, Kidwell CS, Baird AE (2004) Magnetic resonance imaging. In: Mohr J, Weir B, Choi D, Wolf P, Grotta J (eds) Stroke: pathophysiology, diagnosis and management, 4th edn. Churchill Livingstone, Philadelphia, pp 461–479

Establishment and Characterization of Primary Adult Microglial Culture in Mice

Hirokazu Ohtaki, Tomomi Tsumuraya, Dandan Song, Atsushi Sato, Kenji Ohara, Kazuyuki Miyamoto, Hiroyasu Nakano, Keisuke Kiriyama, Kenji Dohi, Yutaka Hiraizumi, Masaji Matsunaga, and Seiji Shioda

Abstract Microglial cells account for approximately 12–15 % of the cells in the central nervous system (CNS). Microglial cells are polarized by pathological stimuli such as cytokines, chemokines, and growth factors, and play important roles in the deterioration and repair of the CNS. Here, we established cultures of primary microglial cells isolated from the brains of adult C57/BL6 mice using Percoll density gradients. The cells were cultured and stained with antibodies against CD11b, glial fibrillary acidic protein, myelin basic protein and NeuN to determine microglial, astroglial, oligodendroglial, and neuronal cells respectively. Moreover, the cells were exposed to interferon-γ (IFNγ) plus interleukin-1β (IL-1β) or IL-4 for 24 h to demonstrate the activating phenotypes with inducible nitric oxide synthase (iNOS), Ym1, and Iba-1 immunoblotting. At least 95 % of the cultured cells were CD11b-positive and -negative for astroglial, neuronal, and oligodendrocyte markers. IFNγ plus IL-1β treatment resulted in classical activation, which was represented by an increase in iNOS. The cells also displayed alternative activation, which increased Ym1 when treated with IL-4. The present study indicates that the microglial cells isolated as described here are a useful tool for elucidating adult microglial function.

Keywords Microglial cells • Adult primary culture • Classical activation • Alternative activation • Macrophages

H. Ohtaki, PhD (✉), T. Tsumuraya, D. Song, A. Sato, K. Ohara
H. Nakano, K. Kiriyama, and S. Shioda, PhD
Department of Anatomy, Showa University School of Medicine,
1-5-8 Hatanodai, Shinagawa-Ku, Tokyo 142-8555, Japan
e-mail: taki@med.showa-u.ac.jp

K. Miyamoto and K. Dohi
Department of Anatomy, Showa University School of Medicine,
1-5-8 Hatanodai, Shinagawa-Ku, Tokyo 142-8555, Japan

Department of Emergency and Critical Care Medicine,
Showa University School of Medicine,
Shinagawa-Ku, Tokyo 142-8555, Japan

Y. Hiraizumi
Department of Orthopedic Surgery,
Showa University School of Medicine,
Shinagawa-Ku, Tokyo 142-8555, Japan

M. Matsunaga
Gene Trophology Research Institute,
Tokyo 130-0012, Japan

Introduction

Microglial cells account for approximately 12–15% of cells in the central nervous system (CNS) [6, 18, 26]. Microglial cells are the sentries of the brain and continually monitor the brain microenvironment [22] to protect it from infection by pathogens or diverse injury signals. Microglial cells are implicated in host defense, wound healing, debris scavenging, peripheral immune cell recruitment, immune response regulation, and neuro-plasticity [1]. In these roles, the microglial cells are beneficial and support neuronal homeostasis by communicating with CNS cells through the release of growth factors and cytokines [8]. However, the microglial cells can have deleterious effects owing to pro-inflammatory cytokines, excess glutamate responses, and/or free radicals during several pathological conditions, such as stroke traumatic injury, cerebral hemorrhage, auto-immune diseases, and neurodegeneration [5, 14, 19].

Microglial cells were considered to be phenotypically polarized by the microenvironment and the polarized phenotypes of microglial cells were considered to resemble macrophages [16, 20, 29]. However, the polarized microglial cells have not yet been understood in detail. Polarized microglia/macrophage phenotype was broadly classified into two main groups: the classical activated type (also called M1) whose prototypical activating stimuli are interferon-γ (IFNγ) and lipopolysaccharide (LPS), and the alternative activated type (also called M2). The alternative activated type is further subdivided into narrowly defined

Y. Katayama et al. (eds.), *Brain Edema XV*, Acta Neurochirurgica Supplement, Vol. 118,
DOI 10.1007/978-3-7091-1434-6_8,

alternative activated type (or M2a), which is activated by interleukin-4 (IL-4) or IL-13, and innate/acquired deactivated-type (or M2c), which is activated by IL-10 and transforming growth factor-β (TGFβ). Classical activated microglia/macrophages are tissues that have deteriorated because of inflammation and apoptosis to increase inducible NO synthase (iNOS), reactive oxygen species (ROS), and pro-inflammatory cytokines, such as IL-1β, tumor necrosis factor-α (TNFα), and IL-6. Alternative activated microglia/macrophages produce ariginase I, Ym1, FIZZ1/2, and express CD206 (mannose receptor), and function in wound-healing and resolution of inflammation [27]. Innate/acquired deactivated microglia/macrophages produce anti-inflammatory cytokines such as IL-10, TGFβ, and PGE2.

At present, the majority of in vitro studies utilize rodent newborn or neonatal microglia cultures [13, 15, 31] or microglial cell lines such as BV-2 [4], N9 [30], and EOC 20 [33]. Although these cells and cell lines have great proliferative potential in vitro, the cells are not always a perfect model [17] because some of the lines are semi-adherent cells and do not show clear morphological features. Neonatal microglia are likely functionally different from adult microglial cells because newborn/neonatal microglia do not exhibit a ramified morphology, but are instead amoeboid [9, 32]. This suggests that neonatal microglial cells are not functionally mature [11]. Moreover, neonatal microglia exhibit a partially activated phenotype in vitro, as indicated by an intermediate expression level of MHC class II and co-stimulatory molecules [3, 7]. Only a small number of studies have utilized ex vivo isolated adult microglia [2].

Recently, several groups have established microglial cell cultures from adult CNS using density gradient methods [6, 21, 28]. These microglial cells are adherent and showed morphological changes depending on the stimulant. Moreover, the cells were used for flow cytometric analysis, suggesting that the isolation methods might be favorable ex vivo. The disadvantage of using adult microglial cells that have been isolated ex vivo is their tendency to undergo cell death within several days upon culture. In support of this a report by Fischer and Reichmann showed that mouse adult microglia do not proliferate in vitro [12].

In the present paper, we provide an outline of the isolation of microglial cells from adult mouse CNS and present suitable culture methods for maintenance and proliferation of the cultures for long periods. Also, we present the immunocytological features demonstrating the purity of the cultures. Finally, we present a paradigm that shows that the primary cells are able to polarize to different activating phenotypes in response to IFNγ plus IL-1β or IL-4 stimulation.

Materials and Methods

Animals

All animal experimental procedures were approved by the Institutional Animal Care and Use Committee of Showa University (#00138 and 01156). Young adult male and female C57/BL6 mice were used in the present study and the animals were bred at our facility.

Isolation of Primary Adult Microglial Cells

All instruments and reagents should be sterile. Twenty animals were anesthetized with sodium pentobarbital (50 mg/kg, i.p.) and perfused transcardially with ice-cold saline (Otsuka, Tokyo, Japan) to wash out contaminating blood cells from the brain. Brains and/or spinal cords were quickly removed and immersed immediately in ice-cold PBS (-) on ice. The brain of each of five animals was transferred to a small Petri dish containing 2 mL of digesting solution and minced roughly with scissors. The digesting solution [6] contained 0.025 U/mL DNase (Sigma, St. Louis, MO, USA), 0.5 % Dispase II (Roche, Mannheim, Germany), 0.05 % Collagenase D (Roche), and 0.1 μg/mL Nα-Tosyl-L-lysine chloromethyl ketone hydrochloride (TLCK; Sigma) in Hank's balanced salt solution (Invitrogen, Carlsbad, CA, USA). The minced brains were transferred to a 7-mL Dounce-tissue grinder (Weaton, Millville, NJ, USA) and homogenized (ten strokes) in 3 mL of digesting solution. These procedures were repeated four times to homogenize 20 brains. The homogenates were further digested by rocking at 100 rpm in a 50-mL conical tube containing 40 mL (final volume) of digesting solution for 15 min at room temperature and was then allowed to settle for 10–15 min. After filtration with a 100-μm nylon cell strainer (BD Falcon, Bedford, MA, USA), the homogenate was centrifuged at 500×g for 7 min and the supernatant was aspirated. Each pellet was resuspended with HBSS, the suspensions were pooled and centrifuged again. After aspirating the supernatant, the pellet was suspended in 25 mL of 30 % isotonic Percoll (GE, Uppsala, Sweden). Fifteen mL HBSS was gently overlaid on the suspension and the Percoll gradient solution was centrifuged at 200×g for 40 min without breaking. The debris and supernatant were aspirated and the cell pellet was suspended to wash with HBSS and centrifuged at 400×g for 6 min. The pellet was resuspended with 36 mL of 10 % RPMI1640 medium (10 % heat-inactivated fetal calf serum [FCS; Nichirei, Tokyo, Japan], 2 mM L-glutamate, 100 units/mL penicillin, and 100 μg/mL streptomycin in RPMI1640

[all from Invitrogen]). The cell suspension was seeded into three six-well plates and incubated with a change of medium every 3–4 days for 1 month until reaching confluence.

Immunocytochemistry

The epitope profiles of the cells were determined by immunocytostaining. Aliquots of the cell suspension were seeded in four- or eight-well Lab-Tek™ chamber slides (Permanox™; Nunc, Roskilde, Denmark) and cultured with a change of medium every 3–4 days for 3 weeks. The media were removed and the cultures gently washed twice with PBS (-). The cells were fixed with 2 % paraformaldehyde in PBS for 15 min followed by two washes with PBS (-). After blocking with 2.5 % normal horse serum in PBS containing 0.05 % Tween 20 (PBST) for 1 h, the cells were incubated with antibodies against CD11b (1:100; AbD Serotec, Oxford, UK, a microglial marker), Neu N (1:500; Millipore, Billerica, MA, USA, a neuronal marker), GFAP (1:10; DAKO, Glostrup, Denmark, an astroglial marker), and myelin basic protein (1:250; MBP; Millipore, an oligodendroglial marker) overnight at 4 °C. After rinses with PBST, cultures were incubated with Alexa 488-labeled goat anti-rat IgG, Alexa 546-labeled goat anti-mouse or rabbit IgG (all obtained from Invitrogen), for 2 h at room temperature. The cells were rinsed with PBST and counterstained with 4,6-Diamidine-2-phenylindole dihydrochloride (DAPI, 1:10,000; Roche). The fluorescence and immunolabeling were detected using optical sectioning microscopy (Axio Imager with ApoTome; Zeiss, Oberkochen, Germany).

Polarization and Immunoblotting

The cells were cultured in six-well plates in 1 % DMEM (1 % FCS, 2 mM L-glutamate, 100 units/mL penicillin, and 100 μg/mL streptomycin in DMEM [Invitrogen]), containing 10 ng/mL each of recombinant mouse interferon-γ (rmIFNγ) and rm interleukin-1β (rmIL-1β), or 20 ng/mL rmIL-4 (all from PeproTech, Rocky Hill, NJ, USA) was applied for 24 h to induce classical or alternative polarized microglia respectively. The cells were then gently washed twice with PBS (-), and were collected using a cell scraper in lysis buffer (10 mM Tris-HCl [pH 7.4], 0.15M NaCl and 1 % Triton X-100, 1 mM EGTA, 50 mM NaF, 2 mM sodium orthovanadate, 10 mM sodium pyruvate, and protease inhibitor cocktail [Sigma]). The suspension was then sonicated for 10 s twice (Handy Sonic; Tomy Seiko, Tokyo, Japan) and incubated for 30 min on ice. The protein concentration of the samples was determined using a BCA protein assay kit (Thermo Fisher Scientific, Waltham, MA, USA). All samples were stored at −30 °C until use. The samples were reduced by heating in sampling buffer (4× sampling buffer: 0.25M Tris/HCl [pH 6.8], 10 v/v% 2-mercaptoethanol, 8 w/v% glycerol, 4.5 w/v% sodium dodecyl sulfate), 8 μg protein was electrophoresed on a 10 % poly-acrylamide gel (Bio-Rad, Hercules, CA, USA) and was transferred to polyvinylidinene fluoride membranes (Bio-Rad). After blocking with 5 % nonfat milk for 1 h, the membrane was probed with rabbit anti-Iba-1 (1:1,000; Wako, Tokyo, Japan), rabbit anti-nitric oxide synthase 2 (NOS2, also known as iNOS, 1:10,000; Transduction Laboratories, Lexington, KY, USA), rabbit anti-Ym1 antibody (1:1,500; StemCell Tech, Vancouver, BC, Canada) or mouse anti-β-actin (1:4,000, Sigma) overnight at 4 °C. The membrane was rinsed with 10 mM Tris/HCl (pH 7.4)/0.05 % Tween 20 (TBST) and probed with horseradish peroxidase (HRP)-conjugated donkey anti-rabbit IgG (1:3,000, GE Healthcare Bioscience, Little Chalfont, UK) or sheep anti-mouse IgG (1:2,000; GE Healthcare Bioscience). The protein bands were detected by chemiluminescence (SuperSignal West Dura Extended Duration Substrate; Pierce, Rockford, IL, USA) and exposed onto X-ray film (Fuji Film, Tokyo, Japan). For comparison with brain homogenates, homogenate samples from ipsilateral hemispheres of focal ischemic brains [24] were applied to the electrophoresis in the same manner.

Results

Morphological Alteration of Primary Adult Microglial Cells

A few hours after seeding, the microglial cells began to attach to the plate. The next day, some cells were flatly adhered and the majority had an amoeboid-like morphology. In the interspaces of the amoeboid-like cells, small cells had increased gradually in size and had extended foot processes within a week (Fig. 1a). These small cells appeared shiny and had long processes 2 weeks later (Fig. 1b). They appeared to be of the ramified type. The small cells survived trypsinization and were able to be passaged.

Immunocytochemistry of the Microglial Cells

Epitope characteristics of the cells were determined by immunostaining with antibodies against microglial, neural,

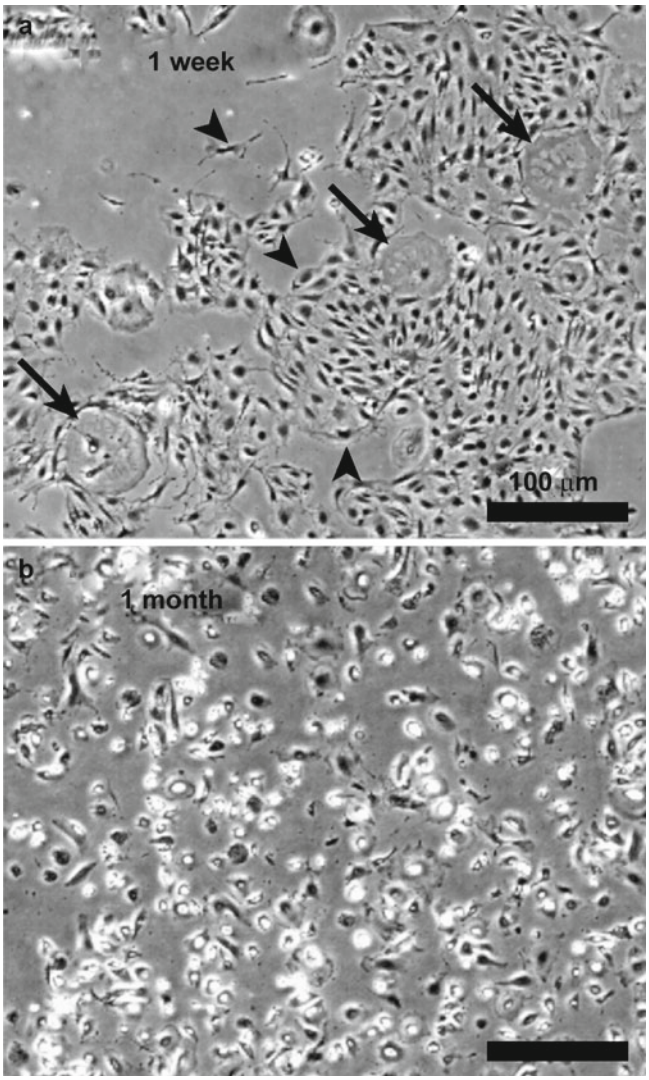

Fig. 1 Morphology of cultured adult microglial cells. Microglial cells were isolated from the CNS of adult C57/BL6 mice and cultured for 1 week (**a**) and 1 month (**b**) in six-well plates. The images were photographed using phase contrast microscopy. (**a**) The microglial cells were flatly adhered and exhibited large size (*arrows*) for the first few days. The microglial cells exhibited other morphology over time in culture.In the interspaces of the large flattened cells, the cells (*arrowheads*) which are small size and had extended foot processes gradually increased the number in the culture plate. (**b**) The small microglial cells proliferated and became shiny at 1 month

astroglial, and oligodendroglial characteristic proteins (Fig. 2). Most of the cells were clearly positive for the microglia marker CD11b. The staining overlapped completely with differential interference contrast (DIC) images and was not present in the DAPI-stained nuclei. No labeling was seen with the astroglial (GFAP) and neuronal (NeuN) antibodies. Oligodendroglial (MBP) marker-positive cells were rarely observed in the cultures. These results suggested that the cultures were at least 95 % pure microglial cells.

Activating Polarization of the Microglial Cell Culture with Cytokine Stimuli

Next, we determined whether the cultured microglial cells were able to be polarized with cytokine stimuli. Cells were incubated in IFNγ plus IL-1β or IL-4 for 24 h and were collected for immunoblotting. The blots were probed with antibodies against microglia, Iba-1, iNOS, a marker for classical activating phenotype, and Ym1, as the alternative activating phenotype marker. We also electrophoresed brain homogenates to assess expression levels in normal and ischemic brains. As shown in Fig. 3, the control microglial cells exposed to vehicle alone (1 % DMEM) expressed the microglial marker Iba-1, but did not express iNOS and Ym1. The cells exposed to IFNγ plus IL-1β clearly increased iNOS expression, but were negative forYm1. These cells tended to increase the Iba-1 level as well. In contrast, the cells exposed to IL-4 displayed increased Ym1 levels, but not iNOS at 24 h. These cells also had decreased Iba-1 levels. In the brain homogenates Iba-1 was not detected, probably because of the low population of microglial cells in the brain. Non-ischemic control brain (0 h) was negative for iNOS, and showed weak levels of Ym1. The Ym1 levels increased 24 h after ischemia. However, no iNOS could be detected 24 h after ischemia. The results were consistent with our previous experiment in that iNOS was not detected even if the 30-μg ischemic brain sample was loaded for electrophoresis (unpublished data) and Ym1 was detected in the hippocampus after ischemia [25].

Conclusion

In this paper we presented a method of isolating primary microglial cells from adult mice CNS. The isolation methods are relatively simple and can be accomplished within a few hours. Moreover, the cells proliferated, although the growth was slow, and did not show obvious autolysis for extended time periods. In fact, we were able to culture the cells for 3 months in basic medium without any supplement (data not shown). The ability to culture these cells long term may be related to the fact that the density of cells at seeding was 60–70 % confluence. Although this is considered high density, lower density cells rapidly exhibited cell death by autolysis. Moreover, the cultured microglial cells changed their morphology from large flat amoeboid-type to small shiny ramified-type over time in culture. The shiny small cells were often able to be lifted and re-plated. The features of the cells are consistent with previous reports [28].

Percoll density gradient methods have been used to isolate microglial cells from adult mice [6, 21, 28]. Cardona et al.,

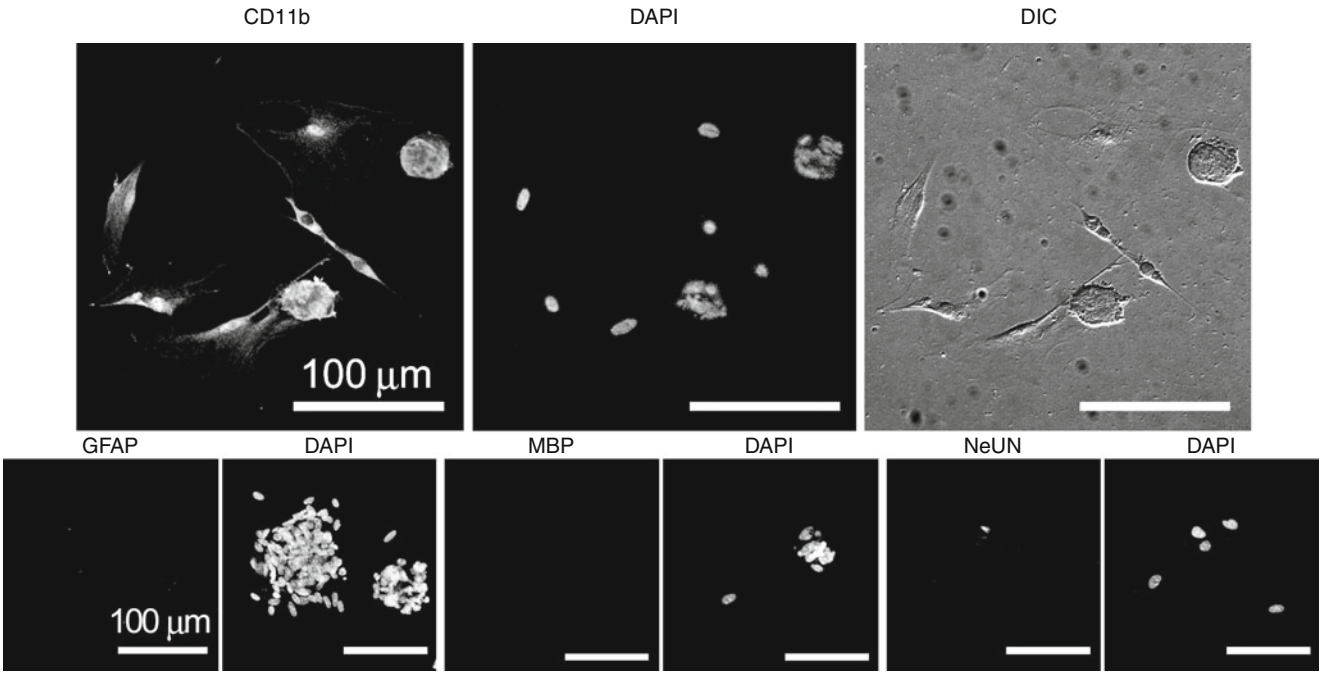

Fig. 2 Immunofluorescence of adult primary microglia performed with optical sectioning microscopy. The adult microglial cells were stained with anti-*CD11b*, *-GFAP*, *-MBP*, and *NeuN* antibodies. The nuclei were counterstained with *DAPI*. The microglial cells were stained with *CD11b* and overlapped completely with differential interference contrast (*DIC*) images. However, few positive staining was observed in *GFAP*, *MBP*, and NeuN antibodies

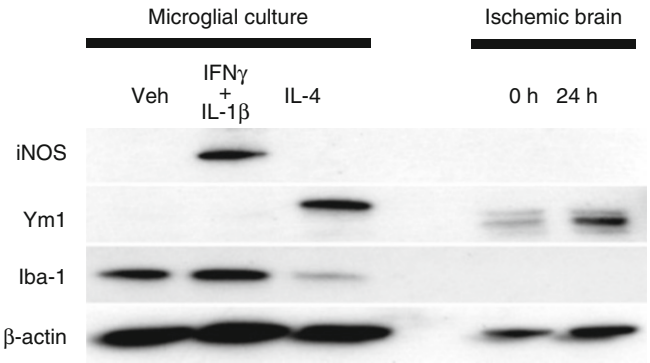

Fig. 3 Immunoblotting analysis of the microglial cells and ischemic brain homogenate. The adult microglial cells were incubated in vehicle (*veh*), *IFNγ* plus *IL-1β* or *IL-4* for 24 h, to induce classical activating or alternative activating phenotype, respectively. The microglial cells, pre-ischemia and 24 h after tMCAO brain homogenates, were electrophoresed for immunoblotting. Then, a microglial marker, *Iba-1*, a classical activating microglial marker, *iNOS*, and an alternative activating marker, *Ym1* were blotted. *β-actin* is an internal control

who recommended the use of flow cytometric analysis and PCR studies used a 70 %/40 % gradient, and the cells were observed at the interphase of 40 and 70 % [6]. Their method obtained a higher purity of cell suspension than ours, but their cell yield s was 20 % of ours. With our methods, although the purity after Percoll density gradient centrifugation is not higher and includes cellular debris and other cells such as red blood cells, this contamination does not adhere to the culture plates. Our immunocytochemical study revealed that most of the adherent cells expressed the microglial marker CD11b, did not include neuronal and astroglial cells, and the cultures were at least 95 % pure.

We then evaluated a function of the microglial cells. The microglial cells were polarized to microglia/macrophage-activated phenotypes by cytokine application according to previous studies [16, 20]. Microglial cells exposed to IFNγ plus IL-1β showed increased expression of iNOS, but not of Ym1, suggesting that the microglial cells polarized to a classical activating phenotype [10, 16]. In contrast, the microglial cells treated with IL-4 showed increased expression of Ym1 but not of iNOS, consistent with polarization to an alternatively activated phenotype [10, 16, 27]. Moreover, Iba-1 was detected in nonstimulated cells, was increased by classical activating polarization and was decreased by alternative activation. For comparison with in vivo microglia, the same amount of protein derived from pre- and 24 h post-ischemic brains was immunoblotted. In both brain samples, Iba-1 was not detectable, probably because of the low population (12–15%) of microglial cells in the brain. Although iNOS could not be detected even after ischemia owing to less gene expression [23], Ym1 signals were detected in the pre-ischemic brain and were enhanced after ischemia; consistent with our previous study [25]. The paradigm indicates that the microglial cells are a useful tool for elucidating adult microglial function.

Acknowledgements The project was supported by a Showa University Grant-in-Aid for Innovative Collaborative Research Projects, and a Grant-in-Aid for Young Scientists (B) from the Japanese Ministry of Education, Culture, Sports, Science and Technology (HO). This work was also supported in part by Research on Health Sciences focusing on Drug Innovation from The Japan Health Sciences Foundation (SS, MM).

Conflict of Interest We declare that we have no conflict of interest.

References

1. Aloisi F (2001) Immune function of microglia. Glia 36:165–179
2. Aloisi F, De Simone R, Columba-Cabezas S, Penna G, Adorini L (2000) Functional maturation of adult mouse resting microglia into an APC is promoted by granulocyte-macrophage colony-stimulating factor and interaction with Th1 cells. J Immunol 164:1705–1712
3. Aloisi F, Ria F, Columba-Cabezas S, Hess H, Penna G, Adorini L (1999) Relative efficiency of microglia, astrocytes, dendritic cells and B cells in naive CD4+ T cell priming and Th1/Th2 cell restimulation. Eur J Immunol 29:2705–2714
4. Blasi E, Barluzzi R, Bocchini V, Mazzolla R, Bistoni F (1990) Immortalization of murine microglial cells by a v-raf/v-myc carrying retrovirus. J Neuroimmunol 27:229–237
5. Brown GC, Neher JJ (2010) Inflammatory neurodegeneration and mechanisms of microglial killing of neurons. Mol Neurobiol 41:242–247
6. Cardona AE, Huang D, Sasse ME, Ransohoff RM (2006) Isolation of murine microglial cells for RNA analysis or flow cytometry. Nat Protoc 1:1947–1951
7. Carson MJ, Reilly CR, Sutcliffe JG, Lo D (1998) Mature microglia resemble immature antigen-presenting cells. Glia 22:72–85
8. Colton CA (2009) Heterogeneity of microglial activation in the innate immune response in the brain. J Neuroimmune Pharmacol 4:399–418
9. de Groot CJ, Huppes W, Sminia T, Kraal G, Dijkstra CD (1992) Determination of the origin and nature of brain macrophages and microglial cells in mouse central nervous system, using non-radioactive in situ hybridization and immunoperoxidase techniques. Glia 6:301–309
10. Dohi K, Ohtaki H, Nakamachi T, Yofu S, Satoh K, Miyamoto K, Song D, Tsunawaki S, Shioda S, Aruga T (2010) Gp91phox (NOX2) in classically activated microglia exacerbates traumatic brain injury. J Neuroinflammation 7:41
11. Draheim HJ, Prinz M, Weber JR, Weiser T, Kettenmann H, Hanisch UK (1999) Induction of potassium channels in mouse brain microglia: cells acquire responsiveness to pneumococcal cell wall components during late development. Neuroscience 89:1379–1390
12. Fischer HG, Reichmann G (2001) Brain dendritic cells and macrophages/microglia in central nervous system inflammation. J Immunol 166:2717–2726
13. Floden AM, Combs CK (2007) Microglia repetitively isolated from in vitro mixed glial cultures retain their initial phenotype. J Neurosci Methods 164:218–224
14. Garden GA, Möller T (2006) Microglia biology in health and disease. J Neuroimmune Pharmacol 1:127–137
15. Giulian D, Baker TJ (1986) Characterization of ameboid microglia isolated from developing mammalian brain. J Neurosci 6:2163–2178
16. Gordon S (2003) Alternative activation of macrophages. Nat Rev Immunol 3:23–35
17. Horvath RJ, Nutile-McMenemy N, Alkaitis MS, Deleo JA (2008) Differential migration, LPS-induced cytokine, chemokine, and NO expression in immortalized BV-2 and HAPI cell lines and primary microglial cultures. J Neurochem 107:557–569
18. Lawson LJ, Perry VH, Dri P, Gordon S (1990) Heterogeneity in the distribution and morphology of microglia in the normal adult mouse brain. Neuroscience 39:151–170
19. Loane DJ, Byrnes KR (2010) Role of microglia in neurotrauma. Neurotherapeutics 7:366–377
20. Martinez FO, Sica A, Mantovani A, Locati M (2008) Macrophage activation and polarization. Front Biosci 13:453–461
21. Moussaud S, Draheim HJ (2010) A new method to isolate microglia from adult mice and culture them for an extended period of time. J Neurosci Methods 187:243–253
22. Nimmerjahn A, Kirchhoff F, Helmchen F (2005) Resting microglial cells are highly dynamic surveillants of brain parenchyma in vivo. Science 308:1314–1318
23. Ohtaki H, Funahashi H, Dohi K, Oguro T, Horai R, Asano M, Iwakura Y, Yin L, Matsunaga M, Goto N, Shioda S (2003) Suppression of oxidative neuronal damage after transient middle cerebral artery occlusion in mice lacking interleukin-1. Neurosci Res 45:313–324
24. Ohtaki H, Nakamachi T, Dohi K, Aizawa Y, Takaki A, Hodoyama K, Yofu S, Hashimoto H, Shintani N, Baba A, Kopf M, Iwakura Y, Matsuda K, Arimura A, Shioda S (2006) Pituitary adenylate cyclase-activating polypeptide (PACAP) decreases ischemic neuronal cell death in association with IL-6. Proc Natl Acad Sci U S A 103:7488–7493
25. Ohtaki H, Ylostalo J, Foraker J, Robinson A, Reger R, Shioda S, Prockop D (2008) Stem/progenitor cells from bone marrow decrease neuronal death in global ischemia by modulation of inflammatory/immune responses. Proc Natl Acad Sci U S A 105:14638–14643
26. Parkhurst CN, Gan WB (2010) Microglia dynamics and function in the CNS. Curr Opin Neurobiol 20:595–600
27. Ponomarev ED, Maresz K, Tan Y, Dittel BN (2007) CNS-derived interleukin-4 is essential for the regulation of autoimmune inflammation and induces a state of alternative activation in microglial cells. J Neurosci 27:10714–10721
28. Ponomarev ED, Novikova M, Maresz K, Shriver LP, Dittel BN (2005) Development of a culture system that supports adult microglial cell proliferation and maintenance in the resting state. J Immunol Methods 300:32–46
29. Ransohoff RM, Perry VH (2009) Microglial physiology: unique stimuli, specialized responses. Annu Rev Immunol 27:119–145
30. Righi M, Mori L, De Libero G, Sironi M, Biondi A, Mantovani A, Donini SD, Ricciardi-Castagnoli P (1989) Monokine production by microglial cell clones. Eur J Immunol 19:1443–1448
31. Santambrogio L, Belyanskaya SL, Fischer FR, Cipriani B, Brosnan CF, Ricciardi-Castagnoli P, Stern LJ, Strominger JL, Riese R (2001) Developmental plasticity of CNS microglia. Proc Natl Acad Sci U S A 98:6295–6300
32. Sierra A, Gottfried-Blackmore AC, McEwen BS, Bulloch K (2007) Microglia derived from aging mice exhibit an altered inflammatory profile. Glia 55:412–424
33. Walker WS (1994) Establishment of mononuclear phagocyte cell lines. J Immunol Methods 174:25–31

Expression and Distribution of Pituitary Adenylate Cyclase-Activating Polypeptide Receptor in Reactive Astrocytes Induced by Global Brain Ischemia in Mice

Tomoya Nakamachi, Jozsef Farkas, Nobuyuki Kagami, Yoshihiro Wada, Motohide Hori, Daisuke Tsuchikawa, Masashi Tsuchida, Akira Yoshikawa, Nori Imai, Tomohiko Hosono, Satoru Atrata, and Seiji Shioda

Abstract Pituitary adenylate cyclase-activating polypeptide (PACAP) is a neuropeptide acting as a neuroprotectant. We previously showed that PACAP receptor (PAC1R) immunoreactivity was elevated in reactive astrocytes after stab wound injury. However, the pattern of PAC1R expression in astrocytes after brain injury is still unknown. In this study, PAC1R expression was evaluated in mouse hippocampal astrocytes after bilateral common carotid artery occlusion. PAC1R mRNA levels in the hippocampus peaked on day 7, and glial fibrillary acidic protein (GFAP) mRNA levels increased from day 3 to day 7 after ischemia. We then observed co-localization of PAC1R and GFAP by double immunostaining. GFAP-immunopositive cells showed signs of hypertrophy 3 days after the ischemia, and by day 7 had fine processes, were hypertrophied, and are known as reactive astrocytes. A low number of PAC1R-immunopositive astrocytes were detectable in the hippocampal area until 3 days after ischemia. PAC1R-positive astrocytes were widely distributed in the hippocampus between day 7 and day 14 after ischemia, and they were converging around the damaged CA1 pyramidal cell layer by day 28. These results suggest that PAC1R might be expressed in the middle to late stage of reactive astrocytes and PACAP plays an important role in the reactive astrocytes after brain injury.

Keywords PACAP receptor • Brain ischemia • Reactive astrocyte • Hippocampus • Mouse • Bilateral common carotid artery occlusion • Real-time PCR • Immunohistochemistry

T. Nakamachi
Department of Anatomy, Showa University School of Medicine, 1-5-8 Hatanodai, Shinagawa-Ku, Tokyo 142-8555, Japan

Center for Biotechnology, Showa University, Shinagawa-Ku, Tokyo 142-8555, Japan

J. Farkas, N. Kagami, Y. Wada, M. Hori, D. Tsuchikawa M. Tsuchida, A. Yoshikawa, and N. Imai
Department of Anatomy, Showa University School of Medicine, 1-5-8 Hatanodai, Shinagawa-Ku, Tokyo 142-8555, Japan

T. Hosono
Institute of Laboratory Animals, Showa University, Shinagawa-Ku, Tokyo 142-8555, Japan

S. Atrata
Center for Biotechnology, Showa University, Shinagawa-Ku, Tokyo 142-8555, Japan

Institute of Laboratory Animals, Showa University, Shinagawa-Ku, Tokyo 142-8555, Japan

S. Shioda PhD (✉)
Department of Anatomy, Showa University School of Medicine, 1-5-8 Hatanodai, Shinagawa-Ku, Tokyo 142-8555, Japan

Institute of Laboratory Animals, Showa University, Shinagawa-Ku, Tokyo 142-8555, Japan
e-mail: shioda@med.showa-u.ac.jp

Introduction

Pituitary adenylate cyclase-activating polypeptide (PACAP) was isolated from ovine hypothalamus, based on its ability to stimulate the accumulation of cAMP in rat pituitary cell cultures [2]. PACAP is a member of the vasoactive intestinal polypeptide (VIP) secretin glucagon family, and its closest analog is VIP. PACAP and VIP share three types of receptors: the PAC1 receptor (PAC1R), and the VPAC1 and VPAC2 receptors (VPAC1R, VPAC2R). The affinity of PAC1R for PACAP is more than 1,000 times higher than its affinity for VIP, indicating that PAC1R is a relatively selective receptor for PACAP [7, 30]. PAC1R is widely distributed in the brain, and is expressed in neurons and astrocytes [1, 21]. PACAP has been shown to have pleiotropic functions, such as neurotransmission, neuroprotection, vasodilatation, and immunomodulation, and it also regulates neural development [10, 20, 25, 31]. PACAP has a great neuroprotective effect on the brain, retina, spinal cord, heart, etc. [4, 12, 18, 24, 28]. The neuroprotective effects of PACAP after infarction appear at a very low concentration after

Y. Katayama et al. (eds.), *Brain Edema XV*, Acta Neurochirurgica Supplement, Vol. 118,
DOI 10.1007/978-3-7091-1434-6_9,

intracerebroventricular or intravenous infusion in the case of global or focal ischemia [21, 29]. We previously showed that PACAP receptor (PAC1R) immunoreactivity was elevated in reactive astrocytes after stab wound injury [26]. However, the expression pattern of PAC1R in ischemic brain has not yet been clarified. Moreover, the astrocytic PAC1R distribution in resting and activated astrocytes after ischemia is unknown. In this study, we examined the expression and distribution of PAC1R in hippocampal regions after global ischemia.

Materials and Methods

Animals

All experimental procedures involving animals were approved by the Institutional Animal Care and Use Committee of the Showa University (51010, 51031). All experiments were performed on male C57BL/6 mice. The animals were housed at 23 °C on a 12-h light/dark cycle with ad libitum access to food and water.

Global Cerebral Ischemia Model

The bilateral common carotid artery occlusion (BCCAO) procedure was carried out as described in our previous report [13]. In brief, mice were anesthetized with 2.0 % sevoflurane in N_2O/O_2. The body temperature was maintained at 37.0–38.0 °C by a heat blanket. The common carotid arteries on both sides were exposed and occluded with Zen temporary clips (Oowa-tusho, Tokyo, Japan). After 15 min the clips were removed for reperfusion.

Real Time PCR

Mice were sacrificed by decapitation and brains were immediately removed on day 0, 3, 7 or 14 after BCCAO. The hippocampi were then collected and immediately frozen by liquid nitrogen, and kept in a deep freezer at −80 °C. Total RNA was extracted using Trisol (Invitrogen, Carlsbad, CA, USA). The total RNA was reverse-transcribed into cDNA and then amplified using the reagents and the protocol of the PrimeScript RT reagent kit (TaKaRa BIO, Kyoto, Japan). RT reaction and the PCR amplification were performed with GeneAmp PCR System 2700 (Perkin-Elmer, Boston, MA, USA). The primers specific for the mouse GFAP, PAC1R, and β-actin primers were purchased from TaKaRa BIO. For quantification of GFAP and PAC1R mRNA levels, real-time PCR was performed in a SYBR Premix Ex Taq II reagent (TaKaRa BIO INC) setting with heating to 95 °C for 30 s followed by 45 amplification cycles of 95 °C for 5 s and 60 °C for 31 s using an ABI PRISM 7900 (Applied Biosystems, Lincoln, CA, USA). Standard curves were generated using a serial dilution of a reference sample and included in each real-time run to correct for possible variations in product amplification. Relative copy numbers were obtained from standard curve values, and were normalized to the values obtained for the house keeping gene, β-actin. The levels of GFAP and PAC1R mRNA were normalized as percentages of the intact controls.

Histology

Mice were anesthetized with sodium pentobarbital (50 mg/kg, i.p.) 0, 1, 3, 7, 14 or 28 days after BCCAO, and brains were fixed by perfusion with saline followed by 2 % paraformaldehyde in 50 mM phosphate buffer. Post-fixation, the brain tissues containing bregma −1.6 to −2.2 mm were embedded in OCT compound after immersion in 20 % sucrose for cytoprotection as a frozen section. The frozen sections (thickness 8 μm) were used for immunostaining.

Double Immunofluorescent Staining

The frozen sections were washed by PBS, incubated, and blocked with 5 % normal horse serum. The sections were then incubated overnight at 4 °C with rabbit anti-PAC1R antibody raised by using the N-terminal residue as an antigen [26] and mouse anti-glial fibrillary acidic protein (GFAP) antibody (1:500; Sigma, St. Louis, MO, USA) as a marker of astrocytes. The immunoreactivity of PAC1R was detected using Alexa 546-labeled goat anti-rabbit IgG, while that of GFAP were detected using Alexa 488-labeled goat anti-mouse or anti-rat IgG antibodies following 90 min incubation at room temperature. Double immunolabeling was detected using a fluorescence microscope.

Results

Hippocampal GFAP and PAC1R mRNA levels after BCCAO were evaluated using real-time PCR. The GFAP mRNA level was significantly elevated and peaked 3 days after ischemia (456 ± 84 %; Fig. 1). It then decreased gradually by day 7 (280 ± 73 %), and reached the basal level on day 14

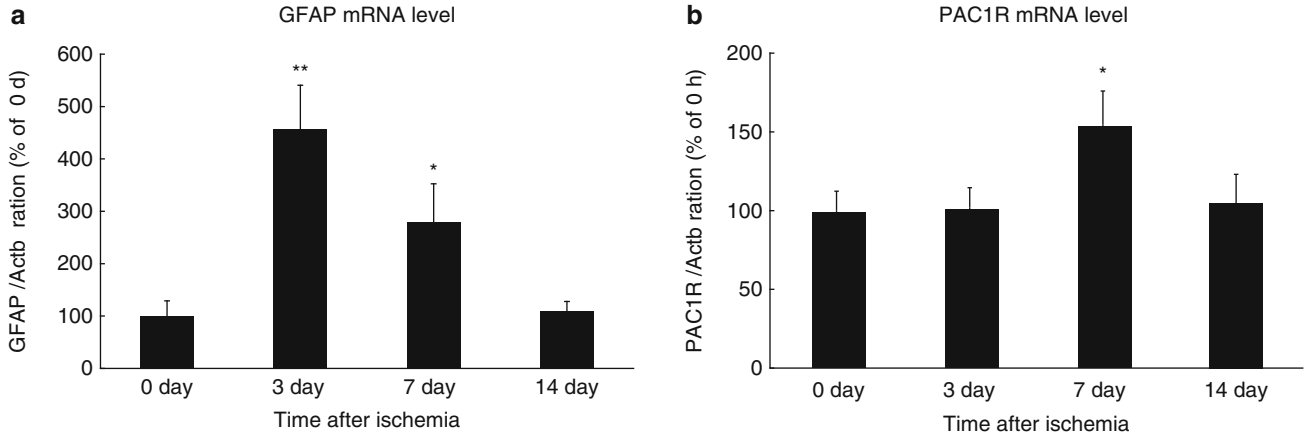

Fig. 1 Glial fibrillary acidic protein (*GFAP*) *mRNA* (**a**) and pituitary adenylate cyclase-activating polypeptide receptor (*PAC1R*) *mRNA* (**b**) levels in mouse hippocampus after global ischemia. Data on the mRNA levels are shown as the mean ± SE ($n=6$). $^{**}P<0.01$, $^{*}P<0.05$ vs 0 day (one-way ANOVA followed by Dunnett's test)

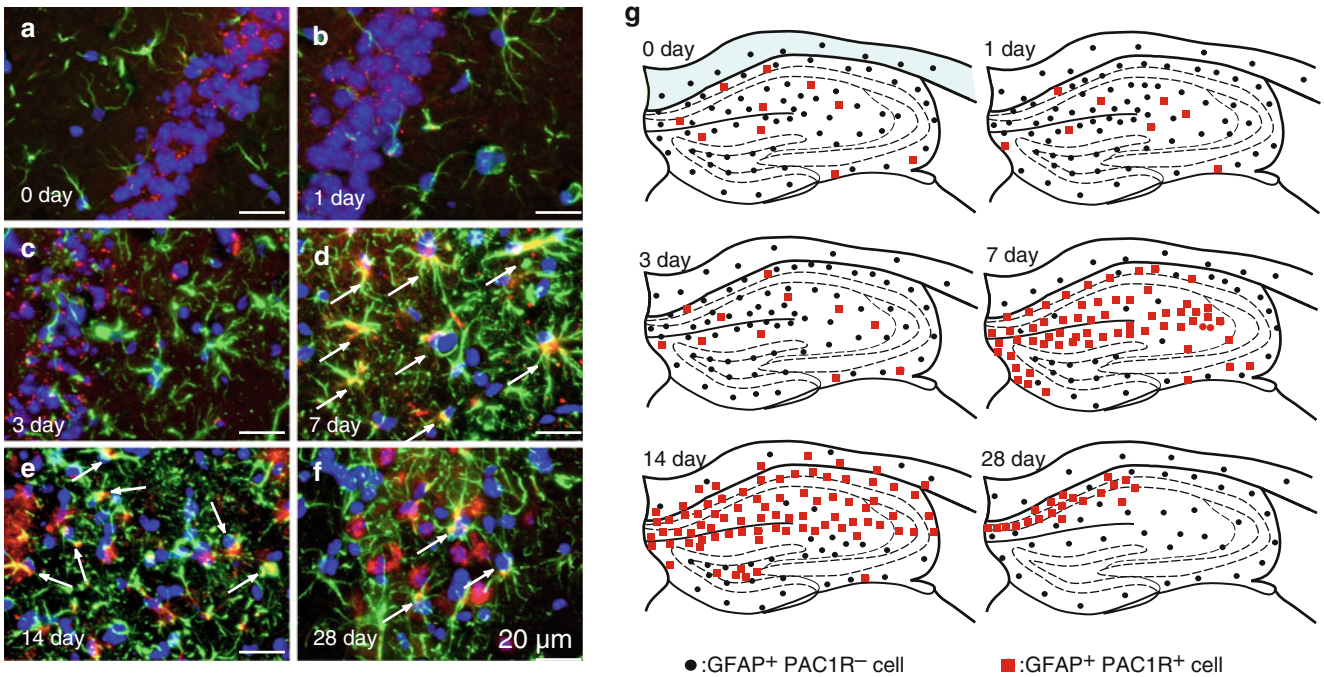

Fig. 2 Distribution of GFAP and PAC1R immunoreactivities in the mouse hippocampal region after global ischemia. (**a**–**f**) Typical hippocampal pictures with GFAP (*green*) and PAC1R (*red*) immunoreactivities in intact mice (**a**) or mice at 1 (**b**), 3 (**c**), 7 (**d**), 14 (**e**), and 28 days (**f**) after bilateral common carotid artery occlusion (BCCAO). Double-immunopositive cells were indicated by *arrows* (**d**–**f**). (**g**) Schematic brain maps indicate the distribution of GFAP-positive and PAC1R-negative cells (*black circles*) and GFAP-positive and PAC1R-positive cells (*red squares*)

(110 ± 18 %; Fig. 1). The PAC1R mRNA level did not change on day 3 (102 ± 13 %), but increased significantly on day 7, where it peaked (155 ± 21 %; Fig. 1).

Immunoreactivity of GFAP and PAC1R was observed in the ischemic mouse hippocampus. GFAP-positive PAC1R-negative cells were observed in the hippocampus, and weak PAC1R immunoreactivity was observed in CA1 pyramidal neurons on 0 (intact) and 1 day after ischemia (Fig. 2a, b). GFAP-immunopositive cells became hypertrophied on day 3 without PAC1R immunoreactivity (Fig. 2c). On day 7, PAC1R immunoreactivity was well co-localized with GFAP-positive cells, which had fine processes and were hypertrophied, and are known as reactive astrocytes (Fig. 2d). GFAP-positive with PAC1R-positive cells were observed around the hippocampal CA1 area, where delayed neuronal death was induced by BCCAO. The double-immunopositive cells were widely distributed from there on day 14 (Fig. 2e), and were only found in the CA1 region on day 28 (Fig. 2f).

Although PAC1R and GFAP double-immunopositive cells were observed in the cerebral cortex, in the amygdala, and in the fimbria hippocampi, the distribution did not change after BCCAO (data not shown). The distribution of GFAP and PAC1R immunoreactivity after BCCAO was summarized in Fig. 2g.

Conclusion

Astrocytes can be activated by central nervous system injury. The activated astrocytes, called reactive astrocytes, form dense scar tissue, known as the glial scar, around the lesion site, which serves to compact inflammatory cells and re-seal the blood–brain barrier after it has been breached by injury [5, 11]. We previously reported that PAC1R-immunopositive astrocytes were observed close to the injury site on day 4 after stab wounding. However, the behavior of PAC1R-immunopositive astrocytes after nervous tissue injury is not well understood. In this study, we used the BCCAO model which resulted in delayed neuronal death in the hippocampal CA1 region on day 4 after injury [13]. As a result, the number of PAC1R and GFAP double-immunopositive cells were elevated on day 7, diffused at 14 days, and converging on the area around the injury site 28 days after BCCAO (Fig. 2). To our knowledge, this is the first report to reveal the distribution and transition of PAC1R-immunopositive astrocytes after brain injury. Interestingly, peaks of the mRNA levels show a time lag: GFAP on day 3 and PAC1R on day 7 (Fig. 1). GFAP is well known as a normal astrocytic marker, but it is also up-regulated when these astrocytes become reactive [9]. Indeed, GFAP-immunopositive cells start hypertrophying on day 3, almost at the same time as neuronal death occurs, but the astrocytes were PAC1R-immunonegative. Between days 7 and 14, matured reactive astrocytes were PAC1R-immunopositive. These data suggest that PAC1R is expressed at the middle or late stage of reactive astrocytosis, but not in the earlier stage.

The effect of PACAP on cultured astrocytes has been reported. A number of growth factors and cytokines are released from reactive astrocytes [23], and it has been reported that PACAP administration induces the expression of neuroprotective proteins, such as ADNF and ADNP [3, 15, 17], and cytokines [6, 14, 27]. Recently, We reported that PAC1R immunoreactivity was observed in IL-6 reactive astrocyte with IL-6 immunoreactivity which is known as an neuroprotective factor associated with PACAP [19]. Neuroprotective effects of PACAP may mediate the release of such PACAP-inducible factors from astrocytes. Moreover, PACAP at a concentration of 10^{-11} to 10^{-13} M potentiates and stimulates the proliferation of resting and reactive astrocytes [8, 16].

We conclude that PAC1R expressed in mature reactive astrocytes may play an important role in glial scar formation. Further studies are required to fully elucidate the role of PACAP in the functional behavior of astrocytes, and to characterize the underlying mechanisms.

Acknowledgments This work was supported in part by a Special Research Grant-in-Aid for Development of Characteristic Education and the High-Technology Research Center Project from the Ministry of Education, Culture, Sports, Science, and Technology (T.N. and S.S.) and Research on Health Sciences focusing on Drug Innovation from The Japan Health Sciences Foundation (S.S).

Conflict of Interest We declare that we have no conflict of interest.

References

1. Arimura A (1998) Perspectives on pituitary adenylate cyclase activating polypeptide (PACAP) in the neuroendocrine, endocrine, and nervous systems. Jpn J Physiol 48:301–331
2. Arimura A, Shioda S (1995) Pituitary adenylate cyclase activating polypeptide (PACAP) and its receptors: neuroendocrine and endocrine interaction. Front Neuroendocrinol 16:53–88
3. Dejda A, Sokolowska P, Nowak JZ (2005) Neuroprotective potential of three neuropeptides PACAP, VIP and PHI. Pharmacol Rep 57:307–320
4. Endo K, Nakamachi T, Seki T, Kagami N, Wada Y, Nakamura K, Kishimoto K, Hori M, Tsuchikawa D, Shinntani N, Hashimoto H, Baba A, Koide R, Shioda S (2011) Neuroprotective effect of PACAP against NMDA-induced retinal damage in the mouse. J Mol Neurosci 43:22–29
5. Fawcett JW, Asher RA (1999) The glial scar and central nervous system repair. Brain Res Bull 49:377
6. Gottschall PE, Tatsuno I, Arimura A (1994) Regulation of interleukin-6 (IL-6) secretion in primary cultured rat astrocytes: synergism of interleukin-1 (IL-1) and pituitary adenylate cyclase activating polypeptide (PACAP). Brain Res 637:197–203
7. Harmar AJ, Arimura A, Gozes I, Journot L, Laburthe M, Pisegna JR, Rawlings SR, Robberecht P, Said SI, Sreedharan SP, Wank SA, Waschek JA (1998) International Union of Pharmacology. XVIII. Nomenclature of receptors for vasoactive intestinal peptide and pituitary adenylate cyclase-activating polypeptide. Pharmacol Rev 50:265–270
8. Hashimoto H, Kunugi A, Arakawa N, Shintani N, Fujita T, Kasai A, Kawaguchi C, Morita Y, Hirose M, Sakai Y, Baba A (2003) Possible involvement of a cyclic AMP-dependent mechanism in PACAP-induced proliferation and ERK activation in astrocytes. Biochem Biophys Res Commun 311:337–343
9. Lin RCS, Matesic DF, Marvin M, McKay RDG, Brüstle O (1995) Re-expression of the intermediate filament nestin in reactive astrocytes. Neurobiol Dis 2:79
10. Matsuno R, Ohtaki H, Nakamachi T, Watanabe J, Yofu S, Hayashi D, Takeda T, Nonaka N, Seki M, Nakamura M, Itabashi K, Shioda S (2008) Distribution and localization of pituitary adenylate cyclase-activating polypeptide-specific receptor (PAC1R) in the rostral migratory stream of the infant mouse brain. Regul Pept 145:80–87
11. Milos P, Michael N (2005) Astrocyte activation and reactive gliosis. Glia 50:427–434
12. Mori H, Nakamachi T, Ohtaki H, Yofu S, Sato A, Endo K, Iso Y, Suzuki H, Takeyama Y, Shintani N, Hashimoto H, Baba A, Shioda

S (2010) Cardioprotective effect of endogenous pituitary adenylate cyclase-activating polypeptide on doxorubicin-induced cardiomyopathy in mice. Circ J 74:1183–1190
13. Nakamachi T, Endo S, Ohtaki H, Yin L, Kenji D, Kudo Y, Funahashi H, Matsuda K, Shioda S (2005) Orexin-1 receptor expression after global ischemia in mice. Regul Pept 126:49–54
14. Nakamachi T, Farkas J, Watanabe J, Ohtaki H, Dohi K, Arata S, Shioda S (2011) Role of PACAP in neural stem/progenitor cell and astrocyte – from neural development to neural repair. Curr Pharm Des 17:973–984
15. Nakamachi T, Li M, Shioda S, Arimura A (2006) Signaling involved in pituitary adenylate cyclase-activating polypeptide-stimulated ADNP expression. Peptides 27:1859–1864
16. Nakamachi T, Nakamura K, Oshida K, Kagami N, Mori H, Watanabe J, Arata S, Yofu S, Endo K, Wada Y, Hori M, Tsuchikawa D, Kato M, Shioda S (2011) Pituitary adenylate cyclase-activating polypeptide (PACAP) stimulates proliferation of reactive astrocytes in vitro. J Mol Neurosci 43:16–21
17. Nakamachi T, Ohtaki H, Yofu S, Dohi K, Watanabe J, Hayashi D, Matsuno R, Nonaka N, Itabashi K, Shioda S (2008) Pituitary adenylate cyclase-activating polypeptide (PACAP) type 1 receptor (PAC1R) co-localizes with activity-dependent neuroprotective protein (ADNP) in the mouse brains. Regul Pept 145:88–95
18. Nakamachi T, Ohtaki H, Yofu S, Dohi K, Watanabe J, Mori H, Sato A, Hashimoto H, Shintani N, Baba A, Shioda S (2010) Endogenous pituitary adenylate cyclase activating polypeptide is involved in suppression of edema in the ischemic brain. Acta Neurochir Suppl 106:43–46
19. Nakamachi T, Tsuchida M, Kagami N, Yofu S, Wada Y, Hori M, Tsuchikawa D, Yoshikawa A, Imai N, Nakamura K, Arata S, Shioda S (2012) IL-6 and PACAP receptor expression and localization after global brain ischemia in mice. J Mol Neurosci 48(3):518–525
20. Ohtaki H, Dohi K, Yofu S, Nakamachi T, Kudo Y, Endo S, Aruga T, Goto N, Watanabe J, Kikuyama S, Shioda S (2004) Effect of pituitary adenylate cyclase-activating polypeptide 38 (PACAP38) on tissue oxygen content – treatment in central nervous system of mice. Regul Pept 123:61–67
21. Ohtaki H, Nakamachi T, Dohi K, Aizawa Y, Takaki A, Hodoyama K, Yofu S, Hashimoto H, Shintani N, Baba A, Kopf M, Iwakura Y, Matsuda K, Arimura A, Shioda S (2006) Pituitary adenylate cyclase-activating polypeptide (PACAP) decreases ischemic neuronal cell death in association with IL-6. Proc Natl Acad Sci U S A 103:7488–7493
22. Reglodi D, Somogyvari-Vigh A, Vigh S, Kozicz T, Arimura A (2000) Delayed systemic administration of PACAP38 is neuroprotective in transient middle cerebral artery occlusion in the rat. Stroke 31:1411–1417
23. Ridet JL, Malhotra SK, Privat A, Gage FH (1997) Reactive astrocytes: cellular and molecular cues to biological function. Trends Neurosci 20:570–577
24. Seki T, Itoh H, Nakamachi T, Endo K, Wada Y, Nakamura K, Shioda S (2011) Suppression of rat retinal ganglion cell death by PACAP following transient ischemia induced by high intraocular pressure. J Mol Neurosci 43:30–34
25. Shioda S, Ohtaki H, Nakamachi T, Dohi K, Watanabe J, Nakajo S, Arata S, Kitamura S, Okuda H, Takenoya F, Kitamura Y (2006) Pleiotropic functions of PACAP in the CNS: neuroprotection and neurodevelopment. Ann N Y Acad Sci 1070:550–560
26. Suzuki R, Arata S, Nakajo S, Ikenaka K, Kikuyama S, Shioda S (2003) Expression of the receptor for pituitary adenylate cyclase-activating polypeptide (PAC1-R) in reactive astrocytes. Brain Res Mol Brain Res 115:10–20
27. Tatsuno I, Morio H, Tanaka T, Uchida D, Hirai A, Tamura Y, Saito Y (1996) Pituitary adenylate cyclase-activating polypeptide (PACAP) is a regulator of astrocytes: PACAP stimulates proliferation and production of interleukin 6 (IL-6), but not nerve growth factor (NGF), in cultured rat astrocyte. Ann N Y Acad Sci 805:482–488
28. Tsuchikawa D, Nakamachi T, Tsuchida M, Wada Y, Hori M, Farkas J, Yoshikawa A, Kagami N, Imai N, Shintani N, Hashimoto H, Atsumi T, Shioda S (2012) Neuroprotective effect of endogenous pituitary adenylate cyclase-activating polypeptide on spinal cord injury. J Mol Neurosci 48(3):508–517
29. Uchida D, Arimura A, Somogyvari-Vigh A, Shioda S, Banks WA (1996) Prevention of ischemia-induced death of hippocampal neurons by pituitary adenylate cyclase activating polypeptide. Brain Res 736:280–286
30. Vaudry D, Gonzalez BJ, Basille M, Yon L, Fournier A, Vaudry H (2000) Pituitary adenylate cyclase-activating polypeptide and its receptors: from structure to functions. Pharmacol Rev 52:269–324
31. Watanabe J, Nakamachi T, Matsuno R, Hayashi D, Nakamura M, Kikuyama S, Nakajo S, Shioda S (2007) Localization, characterization and function of pituitary adenylate cyclase-activating polypeptide during brain development. Peptides 28:1713–1719

The Effect of Hydrogen Gas on a Mouse Bilateral Common Carotid Artery Occlusion

Kimihiro Nagatani, Satoru Takeuchi, Hiroaki Kobayashi, Naoki Otani, Kojiro Wada, Masanori Fujita, Hiroshi Nawashiro, Shoichi Tachibana, and Katsuji Shima

Abstract In recent studies, molecular hydrogen selectively reduced the levels of hydroxyl radicals in vitro and exerted a therapeutic anti-oxidant activity in a rat middle cerebral artery occlusion model. The aim of this study was to investigate the effect of hydrogen gas on a mouse bilateral common carotid artery occlusion (BCCAO) model. Male C57BL/6J mice were subjected to transient BCCAO with a nontraumatic aneurysm clip. The mice were divided into three groups: sham, BCCAO, and BCCAO treated with 1.3 % hydrogen gas. Cerebral blood flow (CBF) in the cortex was measured sequentially for both hemispheres with a noninvasive and noncontact laser Doppler blood perfusion imager during the procedure. Vital signs were also recorded. Oxidative stress evaluated by measuring the level of 8-hydroxy-2'-deoxyguanosine (8-OHdG), neuronal injury in the hippocampal CA1 sector, and brain water content were assessed 24 h after ischemia. The hydrogen gas treatment had no significant effect on vital signs or CBF values. However, the reduction of the expression of 8-OHdG, the decrease in the neuronal injury in the hippocampal CA1 sector, and the attenuation in brain water content were observed in hydrogen-treated mice. In conclusion, hydrogen gas might be effective in a mouse BCCAO model.

Keywords Hydrogen • Bilateral common carotid artery occlusion • Mouse • Ischemia/reperfusion injury • Brain edema

K. Nagatani (✉), S. Takeuchi, H. Kobayashi, N. Otani, MD
K. Wada, H. Nawashiro, and K. Shima
Department of Neurosurgery, National Defense Medical College,
3-2 Namiki, Tokorozawa, Saitama 359-8513, Japan
e-mail: naval.kimi@gmail.com

M. Fujita and S. Tachibana
Division of Environmental Medicine,
Research Institute, National Defense Medical College,
3-2 Namiki, Tokorozawa, Saitama 359-8513, Japan

Introduction

Hydrogen (H_2) gas is one of the antioxidant agents that reduce hydroxyl radicals and peroxynitrite in vitro [5]. Inhalation of H_2 gas has been reported to reduce infarct size in the rat model of myocardial, intestinal, and hepatic I/R injuries [3, 4, 7]. Moreover, H_2 gas exerts a therapeutic antioxidant activity in a focal brain ischemia model in rats [5]. The aim of this study was to investigate the effect of H_2 gas on a mouse bilateral common carotid artery occlusion (BCCAO) model.

Materials and Methods

H_2 Gas Treatment

For gaseous treatment, a tank with high-pressure pre-mixed gases was purchased directly from the manufacturer (Japan Fine Products, Kanagawa, Japan). Concentration of hydrogen (1.3 %), oxygen (30 %), and nitrogen (balanced) was confirmed by the manufacturer. We applied a hydrogen concentration of 1.3 % because it was safer when a high-pressure mixed gas was used with 30 % oxygen. H_2 from the pre-mixed gas tank was delivered to mice via a tight-fitting reservoir face mask. The mice without H_2 treatment inhaled nitrogen-based high-pressure mixed gas with 30 % oxygen (without hydrogen; Japan Fine Products).

BCCAO Model

Male C57BL/6J mice 9–11 weeks of age and weighing 23–27 g (CLEA Japan, Tokyo, Japan) were allowed free access to food and water before experimental use. Mice were divided into three groups: sham surgery (Sham), BCCAO,

Y. Katayama et al. (eds.), *Brain Edema XV*, Acta Neurochirurgica Supplement, Vol. 118,
DOI 10.1007/978-3-7091-1434-6_10,

and BCCAO treated with hydrogen gas (BCCAO + H_2). During surgery and the postoperative period, rectal temperature was maintained at approximately 37.0 °C by means of a heating pad. Mean arterial blood pressure, heart rate, and respiratory rate were recorded. Mice were anesthetized with 20 mg/kg of sodium pentobarbital intraperitoneally. The skull was exposed after a midline scalp and periosteum incision with lidocaine local anesthesia. A mild dose of sodium pentobarbital was used to minimize the effects on cerebral blood flow (CBF). CBF in the cortex was measured semiquantitatively for both hemispheres with a non-invasive and non-contact laser Doppler blood perfusion imager (Periscan PIM II; PeriMed, Stockholm, Sweden). Both common carotid arteries were exposed and occluded by applying non-traumatic small aneurysm clips for 45 min. After 45 min of occlusion, the clips were carefully removed to restore blood flow. CBF was measured sequentially just before, during 5 and 45 min, and at 5, 30, 60, 120, and 180 min after BCCAO. After 180 min of reperfusion, the neck incision was closed, and the mice were allowed to recover. We previously confirmed that mice without the posterior communicating artery showed low residual CBF (less than 30 % of pre-occlusion values) in the same hemisphere during BCCAO by performing an anatomical study [6]. Therefore, mice that showed low residual CBF (less than 30 % of pre-occlusion values) in the same hemisphere were included from further analysis. In the BCCAO + H_2 group, mice inhaled H_2 gas during the 225-min process (45 min occlusion and 180 min reperfusion). Furthermore, H_2 was administered for 3 h a day from 1 to 3 days after surgery. In the BCCAO group, mice inhaled O_2 gas during the entire process, instead of inhaling H_2 gas. Sham-operated mice were treated as described above, but without BCCAO.

Tissue Preparation

After 24 h of reperfusion, mice were anesthetized and transcardially perfused with 0.9 % saline solution, followed by 4 % buffered paraformaldehyde. The brains were removed and embedded in paraffin after fixation in the same fixative for 24 h at 4 °C. Three series of 5-μm-thick coronal sections were cut at the coronal levels of 1.94 mm posterior to the bregma. Each series of sections was used for hematoxylin and eosin staining, Nissl staining, and immunostaining against 8-hydroxy-2'-deoxyguanosine.

Hematoxylin and Eosin Staining, Nissl Staining

Serial coronal sections were stained with hematoxylin and eosin. For Nissl staining, the sections were stained with 0.2 % cresyl violet. The CA1 area of hippocampus from each mouse was captured by using a microscope (Axio Imager. A1; Carl Zeiss, Jena, Germany) equipped with a digital camera system. Histological changes in the sections of the CA1 of the hippocampus were evaluated by a blind rater. For each section, three fields of view (×400) were sequentially selected and the numbers of pyramid cells inside were counted.

8-Hydroxy-2'-Deoxyguanosine Staining

Immunohistochemistry was performed using a Histofine MOUSESTAIN Kit (NICHIREI Co, Tokyo, Japan) according to the manufacturer's instruction. Serial coronal sections were stained overnight at 4 °C with a mouse monoclonal antibody against 8-hydroxy-2'-deoxyguanosine (8-OHdG; 1:100; Japan Institute For the Control of Aging, Shizuoka, Japan) to detect oxidative DNA damage. The immunoreactivity was detected using a diaminobenzidine method. Images were observed and captured with a microscope (Axio Imager. A1; Carl Zeiss). Oxidative DNA damage was quantified in a blinded manner by counting the number of 8-OHdG-positive cells in three areas of the cortex (motor, somatosensory, piriform) at the coronal section (1.94 mm posterior to the bregma). The mean was calculated from the three areas in the cortex.

Brain Water Content

Brain water content was measured using the wet/dry method. Briefly, mice were decapitated after 24 h of reperfusion, and the brain of each mouse was removed. The cerebral cortex of both hemispheres was separated and weighed, and then the tissues were put in an oven at 110 °C for 48 h and reweighed. Brain water content was calculated as follows: (wet weight − dry weight)/wet weight × 100 %.

Statistical Analysis

Comparisons among multiple groups were performed with ANOVA followed by Bonferroni/Dunn test and Fisher's least significant difference test. Comparisons between the two groups were made by the unpaired *t* test. A value of $P < 0.05$ was considered statistically significant.

Results

We carefully monitored several physiological parameters and found no significant differences between the BCCAO group and the BCCAO + H_2 group. In both groups, residual

CBF in both hemispheres after BCCAO was less than 30 % of the pre-occlusion value; the values were not significantly different between the two groups (unpublished data).

No obvious neuronal injury was detected in the sham group. A significant reduction in surviving neurons was observed in the BCCAO group and the BCCAO + H_2 group compared with the sham group (unpublished data). However, a significantly greater increase in the count of surviving neurons was observed in the BCCAO + H_2 group than in the BCCAO group (unpublished data).

We identified oxidative DNA damage by an 8-OHdG antibody. No positive staining was detected in the sham group. After 24 h of reperfusion, strong 8-OHdG immunoreactivity was evident in the nuclei of neurons in the BCCAO group. A significant reduction in 8-OHdG-positive neurons was observed in the BCCAO + H_2 group compared with the BCCAO group (unpublished data).

Twenty-four hours of reperfusion resulted in a significant increase in brain water content in the BCCAO group compared with the sham group (unpublished data). However, inhalation of 1.3 % H_2 significantly reduced the brain water content of BCCAO mice (unpublished data). There was no significant difference in brain water content between the BCCAO + H_2 group and the sham group (unpublished data).

Conclusion

The present study showed that 1.3 % H_2 inhalation significantly increased the number of survival neurons in the hippocampal CA1 sector in BCCAO mice. This was in good agreement with the findings that inhalation of H_2 gas with concentrations between 1 and 4 % reduced the infarct size in the focal cerebral ischemia rats [5], and that H_2 saline treatment significantly increased the number of survival neurons, and reduced the infarct size and the caspase activity in the neonatal cerebral hypoxia–ischemia rats [1]. Our study also showed that 1.3 % H_2 inhalation significantly attenuates the brain edema in BCCAO mice after 24 h of reperfusion. Chen et al. reported that H_2 gas reduced the hemorrhagic transformation in focal cerebral ischemia in rats and that the reduction of oxidative agents might contribute to increased survivability of the endothelial cells [2]. To the best of our knowledge, this is the first report showing that H_2 gas treatment attenuated the brain edema in BCCAO mice. We believe that the attenuation of brain edema may result from the protection of endothelial cells via reduction of oxidative stress by H_2 gas. However, more evidence is needed to support the precise mechanistic action of hydrogen gas on the brain edema.

In summary, inhalation of 1.3 % H_2 gas attenuated oxidative stress, neuronal injury in the hippocampal CA1 sector, and brain edema in BCCAO mice.

Acknowledgments This study was supported by a research grant from The General Insurance Association of Japan.

Conflict of Interest We declare that we have no conflict of interest.

References

1. Cai J, Kang Z, Liu K, Liu W, Li R, Zhang JH, Luo X, Sun X (2009) Neuroprotective effects of hydrogen saline in neonatal hypoxia-ischemia rat model. Brain Res 1256:129–137
2. Chen CH, Manaenko A, Zhan Y, Liu WW, Ostrowki RP, Tang J, Zhang JH (2010) Hydrogen gas reduced acute hyperglycemia-enhanced hemorrhagic transformation in a focal ischemia rat model. Neuroscience 169:402–414
3. Fukuda K, Asoh S, Ishikawa M, Yamamoto Y, Ohsawa I, Ohta S (2007) Inhalation of hydrogen gas suppresses hepatic injury caused by ischemia/reperfusion through reducing oxidative stress. Biochem Biophys Res Commun 361:670–674
4. Hayashida K, Sano M, Ohsawa I, Shinmura K, Tamaki K, Kimura K, Endo J, Katayama T, Kawamura A, Kohsaka S, Makino S, Ohta S, Ogawa S, Fukuda K (2008) Inhalation of hydrogen gas reduces infarct size in the rat model of myocardial ischemia-reperfusion injury. Biochem Biophys Res Commun 373:30–35
5. Ohsawa I, Ishikawa M, Takahashi K, Watanabe M, Nishimaki K, Yamagata K, Katsura K, Katayama Y, Asoh S, Ohta S (2007) Hydrogen acts as a therapeutic antioxidant by selectively reducing cytotoxic oxygen radicals. Nat Med 13:688–694
6. Uozumi Y, Nawashiro H, Sato S, Kawauchi S, Shima K, Kikuchi M (2010) Targeted increase in cerebral blood flow by transcranial near-infrared laser irradiation. Lasers Surg Med 42:566–576
7. Zheng X, Mao Y, Cai J, Li Y, Liu W, Sun P, Zhang JH, Sun X, Yuan H (2009) Hydrogen-rich saline protects against intestinal ischemia/reperfusion injury in rats. Free Radic Res 43:478–484

Simultaneous Measurement of Cytosolic and Mitochondrial Ca^{2+} During Ischemia in Mice Whole-Brain Slice Preparation and Its Application to Drug Evaluation

Takahisa Nishiyama, Erika Hasegawa, Shigeru Yanagi, Yoshihisa Kudo, Ryuta Hamada, Noriko Matsumura, Mikiko Tomino, Yukio Muromachi, Kiyoshi Hatakeyama, and Hiroyuki Uchino

Abstract We developed a conventional imaging method to measure Ca^{2+} concentration in cytosol (using FuraRed as an indicator) and mitochondria (using Rhod-2 as an indicator), simultaneously, by alternative excitation with specific wave length. After confirming the availability of the method in Hela cells, we applied it to mouse whole-brain slice preparation, which was exposed to oxygen- and glucose-deprived artificial cerebrospinal fluid (ischemic ACSF) for 12 min. The fluorescence (>570 nm) at the cerebral cortex and hippocampus due to FuraRed (excited by 480 ± 10 nm) decreased (indicating the increase in cytosolic Ca^{2+}-concentration), while the fluorescence due to Rhod-2 (excited by 560 ± 10 nm) increased (indicating the increase in mitochondrial Ca^{2+} concentration) during exposure to ischemic conditions. We found the characteristic protective effects of cyclosporine A (10^{-6} M), a known blocker for mitochondrial permeability transition, and SEA0400 (10^{-6} M), a blocker for Na^+/Ca^{2+} exchanger, on the abnormal Ca^{2+} increase in cytosol. We confirmed that the present method will be useful for future pathological and pharmacological studies on ischemia-induced brain damage.

Keywords Ischemia • Cytosol • Mitochondria • Fluorescence Ca^{2+} indicator • Rhod-2 • FuraRed • Cyclosporine A SEA0400 • Na^+/Ca^{2+}exchanger • Mitochondrial permeability transition

T. Nishiyama (✉)
Department of Anesthesiology, Tokyo Medical University,
6-7-1 Nishishinjuku, Shinjuku, Tokyo 160-0023, Japan

Department of Anesthesiology,
Hachioji Medical Center, Tokyo Medical University,
1163 Tate-machi Hachioji City, Shinjuku, Tokyo 193-0998, Japan

Department of Anesthesiology, Kimura Hospital,
Tokyo, Japan
e-mail: nishiyat@tokyo-med.ac.jp

E. Hasegawa
Laboratory of Biochemistry,
Tokyo University of Pharmacy and Life Sciences,
1432-1 Horinouchi Hachioji, Tokyo 192-0392, Japan

S. Yanagi, R. Hamada, N. Matsumura, M. Tomino, and Y. Muromachi
Department of Anesthesiology, Tokyo Medical University,
6-7-1 Nishishinjuku, Shinjuku, Tokyo 160-0023, Japan

Y. Kudo
Department of Anesthesiology,
Tokyo Medical University, Tokyo, Japan

K. Hatakeyama
Department of Anesthesiology, Tokyo Medical University,
6-7-1 Nishishinjuku, Shinjuku, Tokyo 160-0023, Japan

Department of Anesthesiology,
Hachioji Medical Center, Tokyo Medical University,
1163 Tate-machi Hachioji City, Shinjuku, Tokyo, 193-0998, Japan

Department of Anesthesiology, Toda Central General Hospital,
Toda, Japan

Department of Anesthesiology, Toda Chuo General Hospital,
Toda, Japan

H. Uchino, MD, PhD
Department of Anesthesiology, Tokyo Medical University,
6-7-1 Nishishinjuku, Shinjuku, Tokyo 160-0023, Japan

Department of Anesthesiology,
Hachioji Medical Center, Tokyo Medical University,
1163 Tate-machi Hachioji City, Shinjuku, Tokyo 193-0998, Japan

Introduction

Brain tissue has been known to require a very large amount of energy. Embolism or infarction of cerebral blood vessels and also accidental hypoxia and hypoglycemia cause encephalopathies, which are sometimes fatal or have severe sequelae depending upon the sites attacked. The mechanisms of acute neuronal cell death due to the energy deficit have been demonstrated to be dependent upon the massive increase in intracellular Ca^{2+} concentration. The increased Ca^{2+} subsequently triggers the Ca^{2+}-dependent process to produce superoxides and cascade activation of many kinds of proteases, which cause the severe breakdown of functional molecules inside the cell, cytoskeleton, and plasma membrane [1]. Abnormal Ca^{2+} concentration increase during ischemia

Y. Katayama et al. (eds.), *Brain Edema XV*, Acta Neurochirurgica Supplement, Vol. 118,
DOI 10.1007/978-3-7091-1434-6_11, © Springer-Verlag Wien 2013

seemed to be one of the most important targets for developing new drugs to protect the brain from the damage due to ischemia. Since we know mitochondria is one of the most important organelles for controlling the intracellular Ca^{2+} concentration, it seems very important to not only the cytosolic Ca^{2+} concentration, but also the mitochondrial Ca^{2+} concentration during and after the ischemia. Nowadays, many kinds of Ca^{2+} indicators are commercially available. Almost all indicators are known to distribute inside cytosol, but an indicator called Rhod-2, a derivative of rhodamine, has been proven to distribute in mitochondria preferentially [4]. In the present study, we tried to develop a conventional method for simultaneous measurement of cytosolic and mitochondrial Ca^{2+} concentration and attempted to apply the method for drug evaluation.

Materials and Methods

Experimental Procedures for Simultaneous Detection of Cytosolic and Mitochondrial Ca^{2+} Concentration

The peak excitation wave length of Rhod-2, a mitochondrial Ca^{2+} indicator, is 560 nm, and the peak fluorescence due to the excitation is observed at around 590 nm. As for an indicator for cytosolic Ca^{2+} dynamics, we selected FuraRed/AM, which distributes in cytosol [2]. The peak excitation wave length of the dye is around 500 nm, which induces fluorescence with a peak wave length of around 650 nm. We loaded those two types of Ca^{2+} indicators onto the cells in culture or the mouse brain slices simultaneously. Using a conventional epifluorescence inverted microscope (Olympus IX81) with an automatic excitation filter exchange system, we detected the fluorescence due to those two different indicators with almost simultaneous timing (within 0.1 s of excitation filter exchange) through a dichroic mirror of 570 nm and a long-pass emission filter (>575 nm). The fluorescence images were detected by a highly sensitive digital CCD camera (ORCA ER, Hamamatsu Photonics) and fed into an image analysis system (AQUACOSMOS, Hamamatsu Photonics). The fluorescence signals obtained from two different indicators were analyzed separately and provided as cytosolic and mitochondrial signals respectively.

Procedure for Preparing Cultured Hela Cells and for Loading Ca^{2+} Indicators

Hela cells are maintained in Dulbecco's modified Eagle's medium (DMEM) supplemented with 10 % fetal bovine serum (FBS) at 37 °C under 5 % CO_2 on a glass-bottomed culture dish (IWAKI, 3931-035). Two days later, the cultured cells on the dish were rinsed with the balanced salt solution (BSS), and then exchanged with the BSS containing FuraRed/AM (5 μM) and Rhod-2/AM (5 μM). After 45 min of incubation at room temperature (27 ± 1 °C), the cells were rinsed with fresh BSS and kept for another 30 min at room temperature to allow breakdown of the ester form by the intrinsic esterase. The cells on the glass-bottomed dish were perfused continuously at a rate of 2 mL/min. The fluorescence images of the cells were observed × 40 lens and fed into the above-mentioned image analysis system.

Procedure for Preparing Fresh Mice Brain Slice Preparations and for Loading Ca^{2+} Indicators

An adult mouse (C57 BK, 20–30 g) was decapitated under deep ether anesthesia. Whole brain was isolated quickly and kept in ice-cold aerobic artificial cerebrospinal fluid (ACSF; bubbled constantly with 95 % O_2 and 5 % CO_2) for 10 min. Then the 300 μM horizontal brain slices including the hippocampus and cerebral cortex were prepared by a tissue slicer (Dohsaka DTK-1000). The brain slices were placed in the aerated ACSF containing FuraRed/AM (10 μM) and Rhod-2/AM (5 μM) for 60 min, and then in a large volume of fresh ACSF at room temperature for 30 min. The slice preparation was placed on the glass-bottomed recording chamber. The slice was perfused with aerated ACSF at a rate of 2 mL/min at 32 ± 1 °C. The fluorescence images of the slice preparation were detected by × 4 objective lens and fed into the image analysis system.

Protocol for Exposing the Slice Preparation to Ischemia and the Evaluation of Drug Effects

To expose the slice preparation to the ischemic conditions, normal aerobic ACSF was replaced for 12 min by the ischemic ACSF containing 2-deoxy-D-glucose, bubbled with 95 % N_2 and 5 % CO_2) at 31 ± 1 °C. Drug effects on the slice preparation were evaluated by administration from 10 min before exposure to the end of the experiment.

Drugs Used

SEA0400 was kindly supplied by Taisho Pharmaceutical (Saitama, Tokyo, Japan). Cyclosporine A, ionomycin, rotenone, and histamine were purchased from Sigma-Aldrich (St. Louis, MO, USA). Rhod-2/AM was purchased from

Dojindo Molecular Technologies. (Kumamoto, Japan), and FuraRed.AM was purchased from Invitrogen, Molecular probes (Eugene, OR, USA).

Results

Confirmation of Differential Distribution of FuraRed and Rhod-2 in Hela Cells

As shown in Fig. 1a, the cells loaded with FuraRed and Rhod-2 showed different fluorescence images (>570 nm) when excited by 500 and 560 nm, alternately. The fluorescence intensity of the cells obtained by 500-nm excitation was almost homogeneous, while that excited by 560 nm was concentrated in specific filamentous structures in the cell. The Rhod-2 fluorescence images seemed to show the structure of living mitochondria. We applied histamine (10^{-5} M) to the cells and examined their fluorescence by alternate excitation with 500 and 560 nm. As shown in Fig. 1b, the fluorescence due to 500-nm excitation decreased, which indicated an increase in cytosolic Ca^{2+} concentration, while the fluorescence due to 560-nm excitation increased, which indicated an increase in mitochondrial Ca^{2+} concentration.

We applied ionomycin (10^{-6} M), a Ca^{2+} ionophore, for 1 min, and observed a large increase in Ca^{2+} in both cytosol and mitochondria. In the cells treated with rotenone, a mitochondrial Ca^{2+} uptake blocker, we were able to observe an increase in cytosolic Ca^{2+} concentration, while the increase in mitochondria was largely reduced (data not shown).

These results indicate that the present method can be used to detect the specific Ca^{2+} dynamics in both cytosol and mitochondria simultaneously.

Examination of the Drugs Affecting the Ca^{2+} Dynamics in Hela Cells

We examined the effects of two types of drugs affecting Ca^{2+} dynamics. Cyclosporine A (CsA) has been proven to have a strong protective effect on mitochondrial permeability transition [5], which will occur during Ca^{2+} overloading in mitochondria. Another drug is SEA0400 (SEA), which has been demonstrated to inhibit the activity of the Na^{+}/Ca^{2+} exchanger in plasma and mitochondrial membrane [3].

The drugs were administered on Hela cells by perfusion 5 min before the exposure to ionomycin (10^{-6} M) for 1 min, which caused a massive increase in cytosolic and mitochondrial Ca^{2+}. We evaluated the effects of the drugs according to the percentage recovery from the extensive increase in Ca^{2+} concentration in cytosol and mitochondria 1 min after exposure to ionomycin. As shown in Fig. 2, CsA (0–10^{-5} M) and SEA (0–10^{-5} M) showed dose-dependent protective effects on the ionomycin-induced severe Ca^{2+} increase in both cytosol and mitochondria.

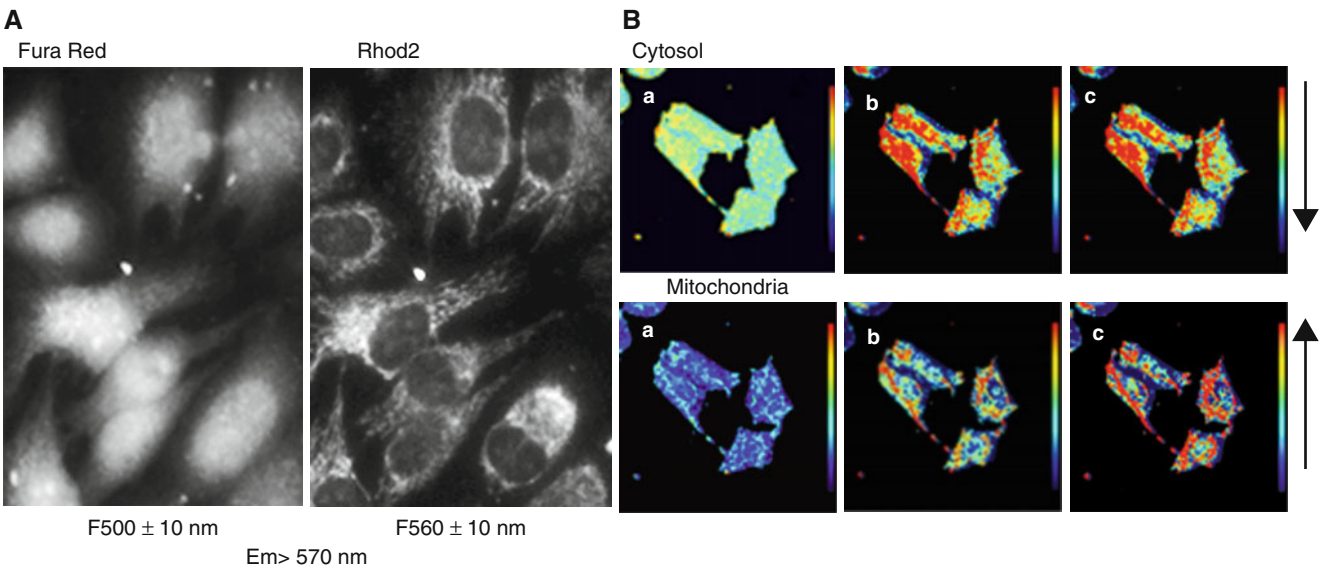

Fig. 1 Fluorescence images and Ca^{2+} dynamics in Hela cells loaded with both FuraRed/AM and Rhod-2. (**A**) Differential fluorescence images (>570 nm) of FuraRed and Rhod-2 in the same cells. (**B**) Pseudocolor images of cytosolic and mitochondrial Ca^{2+} concentrations. **a**, **b** and **c** indicate before, during, and after histamine (10^{-5} M) administration. *Arrows* indicate the direction of color change due to an increase in Ca^{2+} concentration

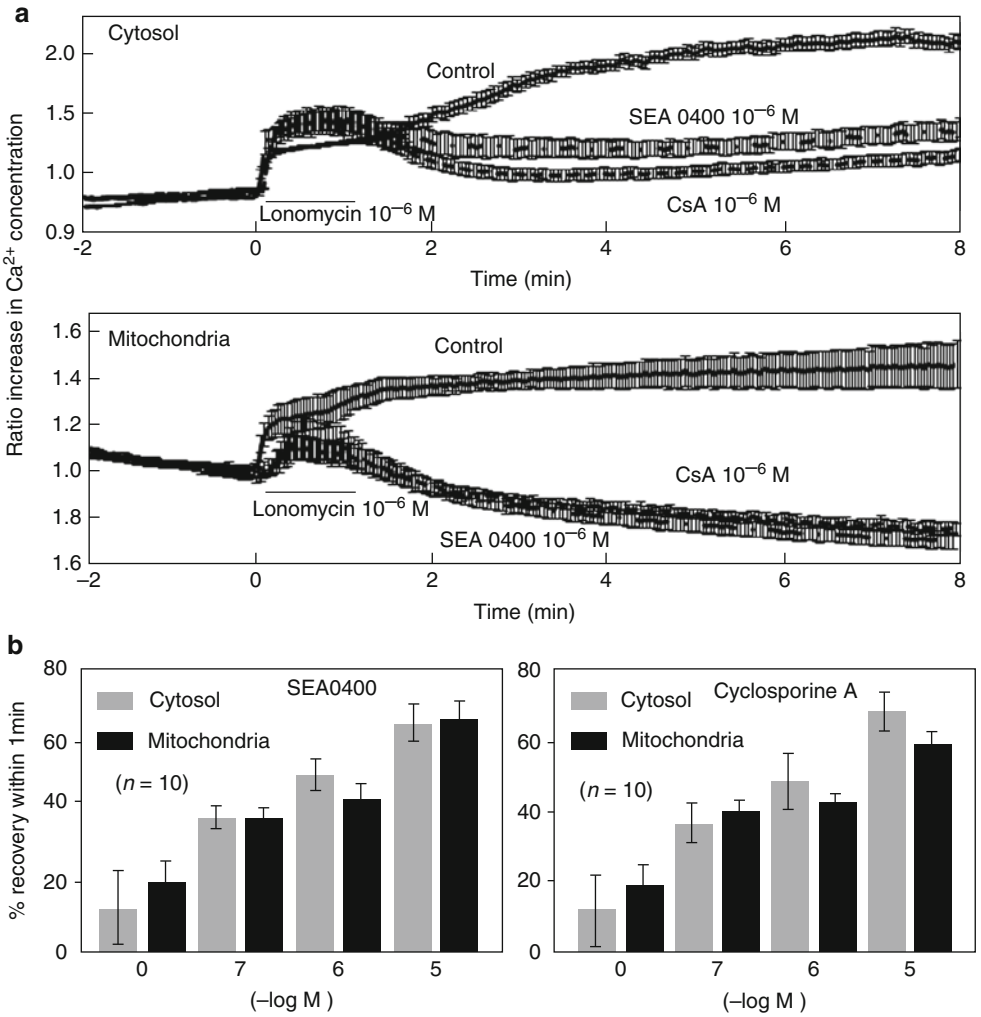

Fig. 2 Effects of SEA0400 and cyclosporine A on the ionomycin-induced Ca^{2+} increase in cytosol and mitochondria in Hela cells. (**a**) Averaged time courses of the Ca^{2+} dynamics and the protective effects of SEA0400 (10^{-6} M) and cyclosporine A on cytosol (*upper panel*) and mitochondria (*lower panel*; $n = 10$, SE indicated). The fluorescence signals in cytosol were reversed to compare them with mitochondria. (**b**) The dose response relationships to the effects of SEA0400 and cyclosporine A

Application of the Method to Mouse Brain Slices

We applied the method to the mouse brain-slice preparations. Our preliminary experiments showed that the loading of Rhod-2 to the brain-slice preparation was more efficient than FuraRed and that the excitation for FuraRed was more effective at a shorter wave length of 480 nm than in the Hela cell experiments. Thus, we decided the loading concentration for the brain-slice preparation to be 10 μM for FuraRed/AM and 5 μM for Rhod-2/AM. The excitation wave length for FuraRed was fixed at 480 nm.

We confirmed the availability of the method for the brain-slice preparation by administering a high potassium ACSF (50 K; 50 mM, isotonic like normal ACSF by exchanging sodium for potassium). During 5-min administration of 50 K to the slice preparation, we were able to observe the decrease in FuraRed and the increase in Rhod-2 fluorescence, suggesting that our method successfully detected the increase in cytosolic and mitochondrial Ca^{2+} respectively.

Examination of Ca^{2+} Dynamics During Ischemia and the Effects of Drugs

Under the above-mentioned experimental conditions, we examined the Ca^{2+} dynamics in cytosol and mitochondria during exposure to 12 min of ischemia. We were able to

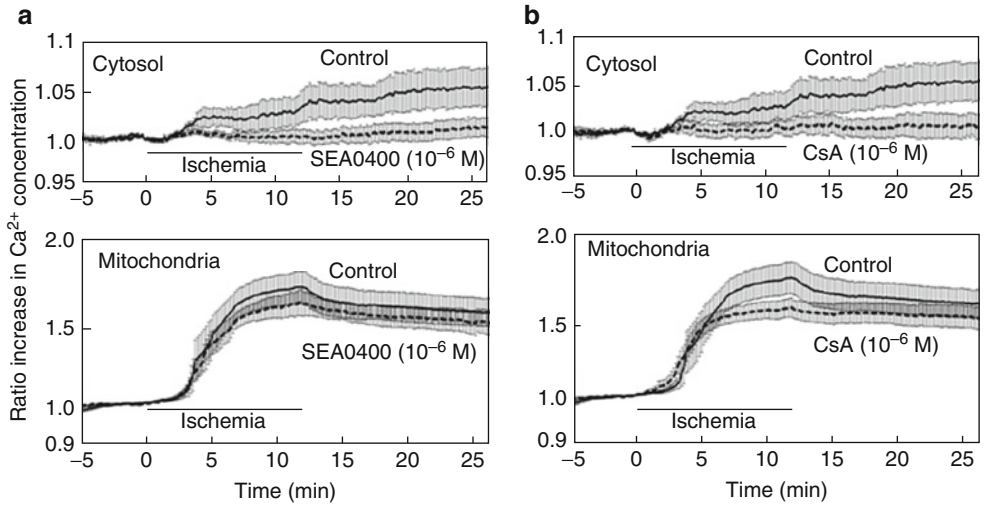

Fig. 3 The time courses of Ca^{2+} dynamics in cytosol and mitochondria in mouse brain slices because of a 12-min exposure to ischemic conditions, and the effects of SEA0400 and CsA. The time courses of Ca^{2+} dynamics observed during exposure to ischemia in the hippocampal CA1 region, and the effects of SEA0400 (10^{-6} M) (**a**) and CsA (10^{-6} M) (**b**). Each graph shows the average time course ($n=5$, SE indicated)

observe a characteristic Ca^{2+} increase in the whole brain during ischemia. Figure 3 shows the changes that occurred in the hippocampal CA1 region. The increase in the cytosolic and mitochondrial Ca^{2+} concentrations began within 5 min, and developed progressively during exposure to the ischemic conditions. The increase in cytosolic Ca^{2+} was apparently irreversible, but mitochondrial Ca^{2+} seemed to be partially reversible. We administered CsA and SEA by pretreatment for 10 min before the onset of ischemia. As shown in Fig. 3, CsA (10^{-6} M) and SEA (10^{-6} M) significantly depressed the increase in cytosolic Ca^{2+} increase during ischemia. CsA seemed to reduce the increase in mitochondrial Ca^{2+}, but the inhibition was not significant.

Conclusion

In the present study, we established a conventional method of measuring cytosolic and mitochondrial Ca^{2+} dynamics in culture cells and brain-slice preparation simultaneously. The simultaneous measurement of mitochondria and cytosol using laser confocal microscopy has been reported in isolated pancreatic acinar cells [6]. However, we ventured to develop an image analysis system equipped with an epifluorescence microscope with an automatic excitation filter exchanger, which is more popular in laboratories and easier to handle. We confirmed that the present method worked effectively on the cells in culture. We were able to observe the dramatic rescuing effects of SAE0400 and CsA on cells exposed to ionomycin, which induced a massive increase in cytosolic and mitochondrial Ca^{2+} concentration and caused acute cell death. The pharmacological profiles of the two drugs seemed to be similar from a Ca^{2+} dynamics point of view.

Although the dynamics of Ca^{2+} in cytosol and mitochondria may show different profiles under abnormal conditions in energy production such as ischemia, few studies discussing the difference between the Ca^{2+} dynamics in the two compartments during ischemia have been published so far. We expected the efficiency of the present method on observing the ischemia-induced Ca^{2+} abnormality and the effects of drugs on it. We found that the simultaneous observation of Ca^{2+} dynamics in both cytosol and mitochondria provides important clues in searching for drugs effective for preventing severe brain damage due to Ca^{2+} overloading. However, we are not satisfied with the present results. The signal observed as cytosolic Ca^{2+} in the slice preparation was unexpectedly low. We should therefore search for the most relevant experimental conditions suitable for brain-slice preparations in order to increase reliability.

Conflict of Interest We declare that we have no conflict of interest.

References

1. Kristian T, Siesjo BK (1998) Calcium in ischemic cell death. Stroke 29(3):705–718
2. Kurebayashi N, Harkins AB, Baylor SM (1993) Use of FuraRed as an intracellular calcium indicator in frog skeletal muscle fibers. Biophys J 64(6):1934–1960
3. Matsuda T, Arakawa N, Takuma K, Kishida Y, Kawasaki Y, Sakaue M, Takahashi K, Takahashi T, Suzuki T, Ota T, Hamano-Takahashi

A, Onishi M, Tanaka Y, Kameo K, Baba A (2001) SEA0400, a novel and selective inhibitor of the Na^+-Ca^{2+} exchanger, attenuates reperfusion injury in the in vitro and in vivo cerebral ischemic models. J Pharmacol Exp Ther 298:249–256

4. Minta A, Kao JP, Tsien RY (1989) Fluorescent indicators for cytosolic calcium based on rhodamine and fluorescein chromophores. J Biol Chem 264(14):8171–8178
5. Uchino H, Elmér E, Uchino K, Lindvall O, Siesjö BK (1995) Cyclosporine A dramatically ameliorates CA1 hippocampal damage following transient forebrain ischemia in the rat. Acta Physiol Scand 155(4):469–471
6. Voronia S, Sukhomlin T, Johnson PR, Erdemili G, Petersen OH, Tepkin A (2002) Correlation of NADH and Ca^{2+} signals in mouse pancreatic acinar cells. J Physiol 539:41–52

Repetitive Cerebral Blood Flow Measurements Using Laser Speckle Imaging in a Transient Cerebral Ischemic Mouse Model

Michihiro Murozono, Morika Suzuki, Aiko Kubota, Chihiro Ando, Kazuto Miyata, Toshimi Arai, Takahisa Nishiyama, and Kiyoshi Hatakeyama

Abstract Using laser speckle imaging (LSI), which can visualize quadratic distribution of blood flow, we measured blood flow changes in transient cerebral ischemic mice, and compared these results with data obtained using laser Doppler flowmetry (LDF). In addition, we examined the relationship between ischemic damage and blood flow change. ICR mice ($n = 22$) were subjected to transient middle cerebral artery occlusion using a 6-0 monofilament under general anesthesia. LSI was performed before ischemia, during ischemia, and 30 min, 3 h, 24 h, 7 days, and 28 days after ischemia. LDF was monitored continuously from pre-ischemia to 10 min after ischemia commenced. The level of cerebral blood flow (CBF) measured by LSI was less than that using LDF. LSI was able to measure CBF quantitatively and repeatedly. Blood flow measurements using LSI revealed that recovery of cerebral cortical blood flow after ischemia in mice without cortical infarction was earlier than that seen in mice with cortical infarction. This study indicates that LSI is a useful technique for analyzing the relationship between tissue damage and cerebral blood flow change following cerebral ischemia.

Keywords Brain ischemia • Cerebral blood flow • Mice • Laser speckle image

M. Murozono (✉), A. Kubota, and T. Arai
Department of Anesthesiology,
Tokyo Medical University Ibaraki Medical Center,
3-20-1 Chuo Ami-machi, Inashiki-gun, Ami,
Ibaraki 300-0395, Japan
e-mail: murozono@tokyo-med.ac.jp

M. Suzuki, C. Ando, and K. Miyata
Department of Anesthesiology,
Tokyo Medical University,
Tokyo, Japan

T. Nishiyama
Department of Anesthesiology, Kimura Hospital,
Tokyo, Japan

K. Hatakeyama
Department of Anesthesiology, Toda Chuo General Hospital,
Toda, Japan

Introduction

Various methods have been used to measure cerebral blood flow after cerebral ischemia. Moreover, many studies have described cerebral blood flow (CBF) changes following cerebral ischemia. We have been using laser Doppler flowmetry (LDF) to monitor cerebral blood flow during brain ischemia. However, this method had several limitations, which included single point measurements, poor reproducibility, and difficulty with fixed-quantity analysis. Therefore, we attempted to use laser speckle imaging (LSI), which visualizes the quadratic distribution of cerebral blood flow in mice, and also allows sequential monitoring of blood flow pre-ischemia, during ischemia, and post-ischemia in the mouse cerebral hemispheres. In this paper, we reviewed the availability of LSI and compared it with LDF. In addition, we also discuss blood flow changes after transient cerebral ischemia using this measurement technique.

Materials and Methods

Animals

Experiments were performed using male ICR mice (6 weeks of age, Charles River Japan, Atsugi, Japan). The experimental protocol was approved by the Tokyo Medical University Institutional Review Committee for the Use of Animal Subjects.

Y. Katayama et al. (eds.), *Brain Edema XV*, Acta Neurochirurgica Supplement, Vol. 118,
DOI 10.1007/978-3-7091-1434-6_12, © Springer-Verlag Wien 2013

Transient Focal Cerebral Ischemia

As previously reported [5], a 6-0 siliconized filament (PDS II; Ethicon, NJ, USA) was inserted into the external carotid artery and the filament was advanced through the origin of the anterior cerebral artery so as to occlude the right middle cerebral artery (MCA). Anesthesia was maintained with 1.5–2.0 % (v/v) isoflurane in 67 % N_2O and 34 % O_2 employing an inhalation mask during the surgical procedure. During ischemia, anesthesia was continued. After a 30-min occlusion period, reperfusion was accomplished by withdrawing the intraluminal filament from the right external carotid artery. After the operation, anesthesia was discontinued and all mice were placed in a recovery box maintained at 34 °C for 3 h to prevent hypothermia.

Measurement of CBF

By both of LDF and LSI, we measure the blood flow in the brain cortical surface. It is possible to measure the blood flows in the whole brain surface simultaneously by LSI. Figure 2 shows the measured values by LSI at the same sites measured by LDF.

CBF Measurements by LSI

Cerebrospinal fluid was recorded for 10 s using the LSI system (Omegazone, Omegawave, Tokyo, Japan) in anesthetized and prone-positioned mice whose skull was exposed and covered with plastic wrap. The skull surface was diffusely illuminated using a 780-nm laser light. The scattered light was filtered and detected using a CCD camera positioned above the head. The filter detected only scattered light that had a perpendicular polarization to the incident light. The current experimental settings allowed CBF measurements on the dorsal surface of the cerebrum, such as the motor cortex and parietal cortex including the primary somatosensory cortex. Raw speckle images were recorded using a video capture card and software. The raw speckle images were used to compute speckle contrast, which corresponds to the number and velocity of moving red blood cells, i.e., CBF. Signal processing was performed using the algorithm developed by Forrester et al. [2]. Color-coded blood flow images were obtained using the high-resolution mode (638 × 480 pixels: 1 image/s). One blood flow image was generated by averaging 20 consecutive raw speckle images. CBF data in a region of interest, which corresponds to the area of the LDF measurement, was obtained using pallet software installed in the Omegazone imaging system. CBF measurements by LSI were carried out pre-ischemia, during ischemia, and at five time points post-ischemia (30 min, 3 h, 24 h, 1 week, and 4 weeks). In this experiment, measurements using LSI were obtained in a 1-mm diameter circle, which included the area used for LDF measurements in the ischemic hemisphere.

CBF Measurements by LDF

An LDF probe (EG fine probe, OMEGAWAVE, Tokyo, Japan) was fixed to the skull (2 mm posterior and 5 mm lateral to the bregma) with superglue. The analog laser Doppler signals (FLO-C1, OMEGAWAVE, Tokyo, Japan) were collected using a computerized data acquisition system (Mac Lab chart v3.5/s: AD instruments, using a Macintosh computer). CBF measurements by LDF were carried out continuously from pre-ischemia to 10 min after ischemia commenced.

Neurological Assessment

Neurological changes after ischemia were evaluated at 3 and 24 h, and 4 weeks after ischemia by a masked observer. We quantified the severity of the neurological deficit using a modified four-point scale as follows: 0, no observable neurological deficits (normal); 1, failure to extend left forepaw (mild); 2, circling to the left or right side (moderate); 3, loss of walking ability or right reflex (severe).

Immunostaining and Evaluation of Brain Infarction

Four weeks after reperfusion, all mice were deeply anesthetized with 5 % (v/v) isoflurane with 67 % N_2O and 33 % O_2 in a box. The brain was fixed with 4 % (w/v) paraformaldehyde through the heart. After fixation, 40-μm coronal sections were cut using a cryostat. These sections were stained with a mouse monoclonal antibody against mouse neuronal nuclei (NeuN, Chemicon) for identification of the infarct area. Each mouse was assigned to two groups, namely the CI group and the non-CI group, depending on the presence or absence of cortical infarction (CI).

Statistical Analysis

Values are expressed as the means ± SD in the text and figures. One-way ANOVA followed by Sheffe's test was used to compare CBF and LSI measurement within each group. The Mann–Whitney *U* test was used to compare CBF and LSI measurements, and neurological scores between groups at each time point. The paired Student's *t* test was employed to compare the change in CBF during ischemia between the LSI and LDF measurement groups. A value of $P < 0.05$ was considered to be statistically significant.

Results

We performed experiments on 22 mice. During the 28-day experimental period, 6 mice died. They were excluded from the data. Eleven animals were assigned to the cortical infarction group (CI group), and 5 animals were assigned to the group without cortical infarction (non-CI group; Fig. 1). No significant difference was observed in the neurological score between the two groups 3 h after ischemia (CI group: 1.64 ± 0.51; non-CI group: 1.4 ± 0.55). However, 24 h after ischemia, the neurological score in the non-CI group (0.6 ± 0.55) was significantly lower ($P < 0.05$) than that of the CI group (1.18 ± 0.41) mice. In contrast, 4 weeks after ischemia, the neurological scores of both groups decreased and were not significantly different (non-CI group: 0.20 ± 0.45; CI group: 0.72 ± 0.47). During ischemia, CBF measured by LDF (21.1 ± 10 % of the pre-ischemic value) was significantly low compared with that measured by LSI (39.5 ± 8.2 % of the pre-ischemic value). In the CI group, during ischemia and 30 min after ischemia, CBF measured by LSI was less than 20 mL/100 g/min, and was significantly lower compared with the pre-ischemic value (Fig. 2). In the non-CI group, CBF measured by LSI during ischemia was significantly reduced compared with the pre-ischemic value, and 30 min after ischemia, CBF by LSI increased more than 20 mL/100 g/min (Figs. 2 and 3). At other time points, CBF was not significantly different from the pre-ischemic value in the non-CI group. Furthermore, CBF 30 min and 4 weeks after ischemia was significantly different in the two groups when measured by LSI.

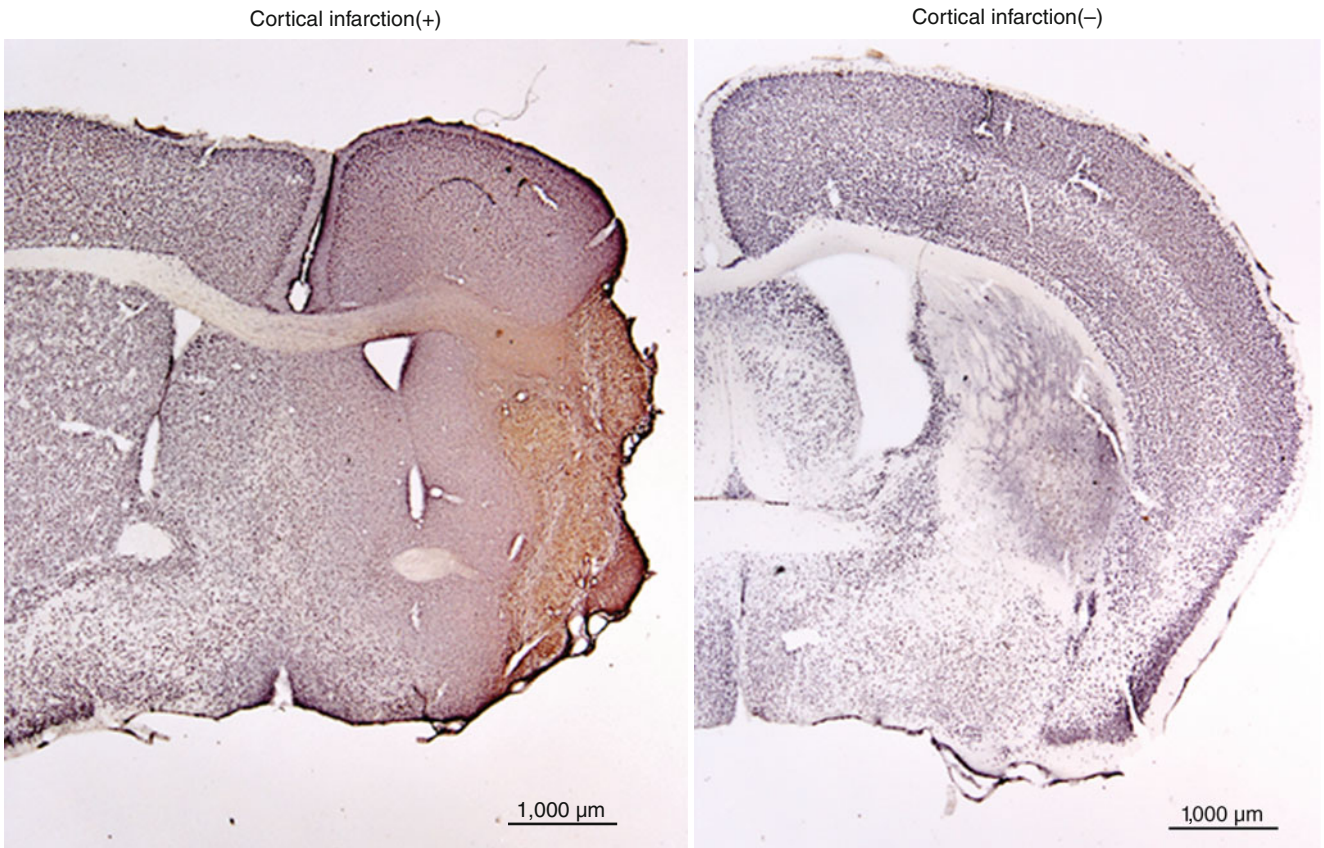

Fig. 1 Representative coronal sections stained with NeuN 4 weeks after ischemia in mice. We quantified the extent of cortical infarction and assigned each mouse to one of two groups

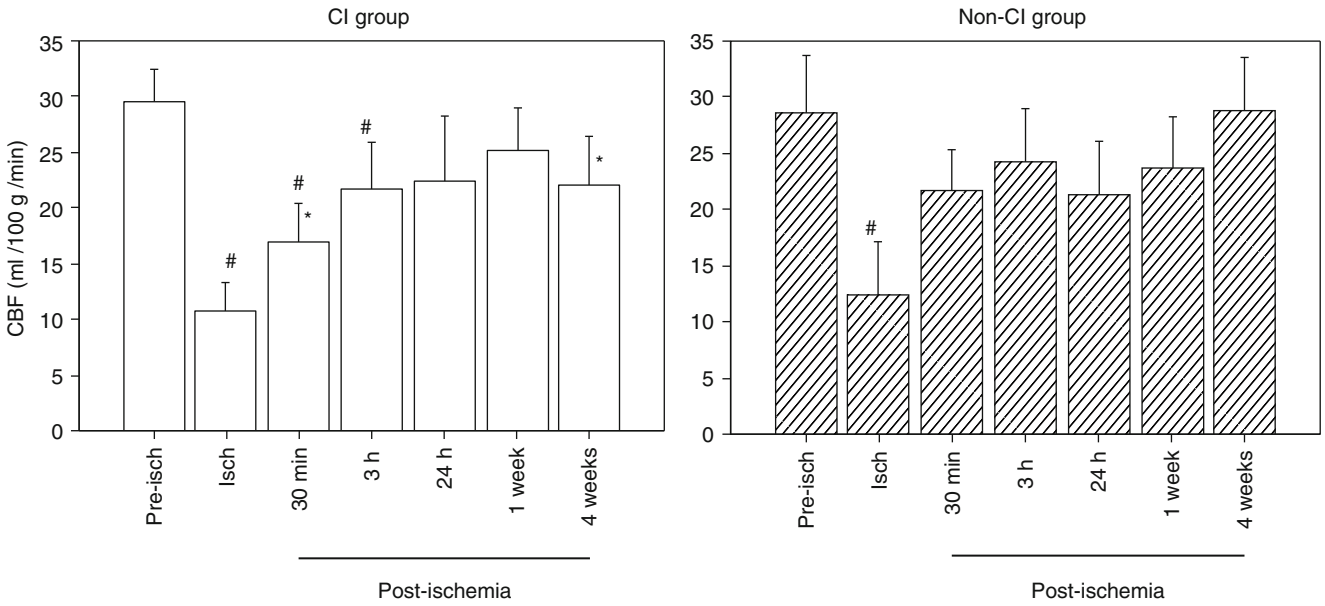

Fig. 2 Graph showing changes in cerebrospinal fluid (CBF) using laser speckle imaging (LSI) during the experimental period. The measurement area for LSI was a 1-mm diameter circle including the area used for laser Doppler flowmetry (LDF) measurements in the ischemic hemisphere. #$P<0.05$ vs pre-ischemia. *$P<0.05$ vs non-CI (cortical infarction) group at the same time point

Conclusion

We measured changes in CBF during local cerebral ischemia over a long period using LSI. We found that LSI can be used as a stable repeated-measures technique. During ischemia, the rate of decline in CBF by LSI was lower than that by LDF. However, in other reports, changes in CBF using LSI in the MCA occlusion model were similar [3]. Blood flow measurements by LDF are less informative owing to measurement being recorded at only one point, and are therefore not suitable for long-term repeated measurements. In addition, LDF is not suitable for quantitative measurement. These limitations can be resolved by LSI. In this study, we divided mice into two groups depending on the absence or presence of a cortical infarct, and investigated changes in CBF following transient focal cerebral ischemia. In the group without cortical infarction, CBF could be recovered earlier after ischemia than in the group with cortical infarction. This information is useful in predicting the damage caused by ischemia. In previous studies, it has been documented that CBF below 10–15 mL/100 g/min for 2–3 h leads to irreversible damage to neuronal tissue [1, 4]. In this experiment, CBF was below 20 mL/100 g/min for 1–3 h, resulting in cortical infarction. Our results are slightly different from those of previous studies, which may be due to the difference in measurement sites and measurement methods. However, further studies need to be performed in order to understand the potential advantages of LSI.

Conflict of Interest We declare that we have no conflict of interest.

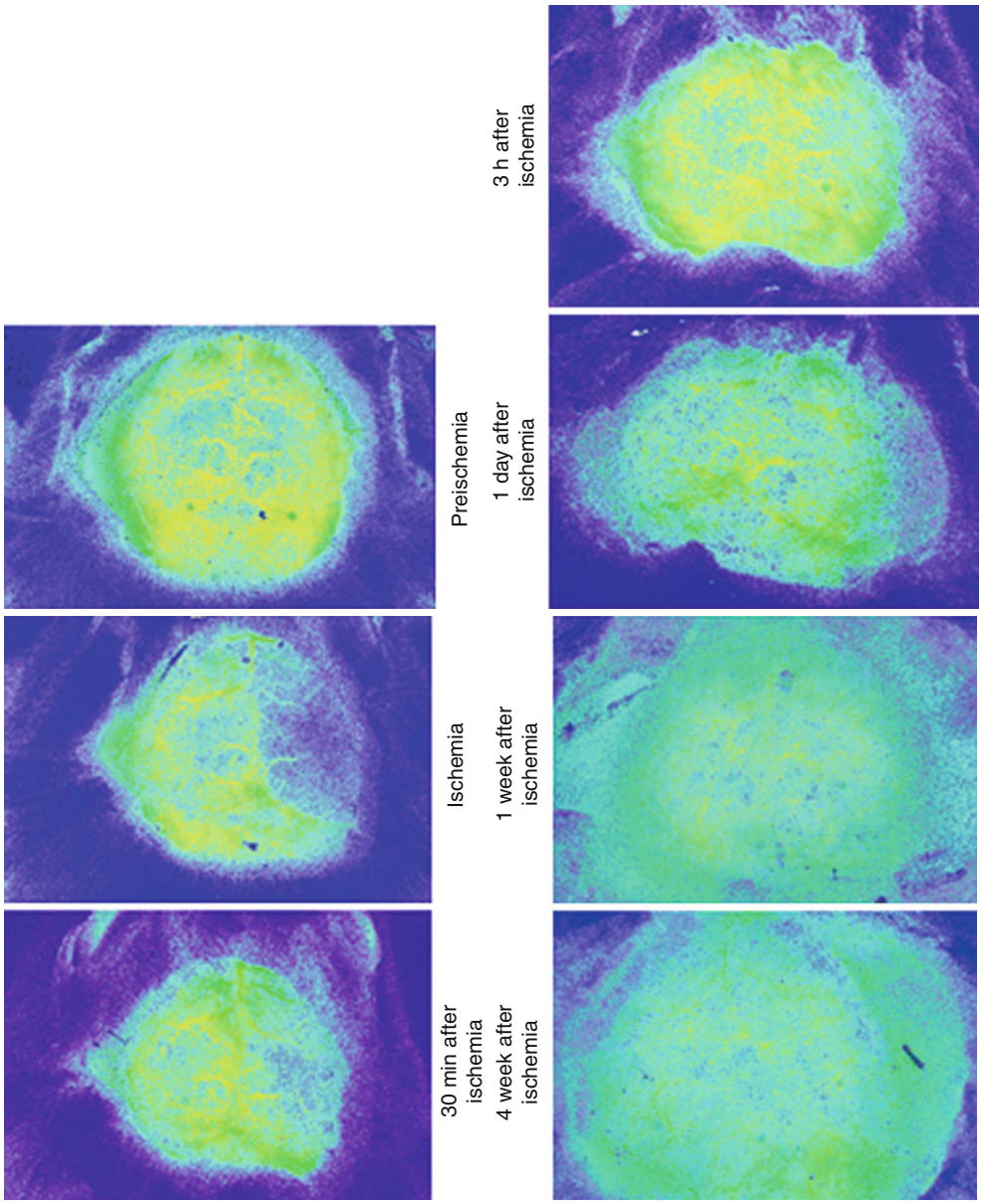

Fig. 3 Color-coded laser speckle images taken from a representative animal pre-ischemia to 4 weeks post-ischemia. This mouse was included in the non-CI group

References

1. Astrup J, Siesjo BK, Symon L (1981) Thresholds in cerebral ischemia – the ischemic penumbra. Stroke 2(6):723–725
2. Forrester KR et al (2002) Comparison of laser speckle and laser Doppler perfusion imaging: measurement in human skin and rabbit articular tissue. Med Biol Eng Comput 40(6):687–697
3. Guo Q, Wang G, Namura S (2010) Fenofibrate improves cerebral blood flow after middle cerebral artery occlusion in mice. J Cereb Blood Flow Metab 30(1):70–78
4. Hossmann KA (1994) Viability thresholds and the penumbra of focal ischemia. Ann Neurol 36(4):557–565
5. Murozono M et al (2004) Neuroprotective and neurotoxic effects of cyclosporine A on transient focal ischemia in mdr1a knockout mice. Eur J Pharmacol 498(1–3):115–118

Preoperative-Induced Mild Hypothermia Attenuates Neuronal Damage in a Rat Subdural Hematoma Model

Shoji Yokobori, Ross Bullock, Shyam Gajavelli, Stephen Burks, Stefania Mondello, Jixiang Mo, Kevin K.W. Wang, Ronald L. Hayes, Helen Bramlett, and Dalton Dietrich

Abstract Post-traumatic hypothermia has been effective for traumatic brain injury in the laboratory setting. However, hypothermia has not shown efficacy in clinical trials. With the results of a recent clinical trial, we hypothesized that hypothermia might reduce neuronal damage in acute subdural hematoma (ASDH) by blunting the effects of reperfusion injury. Twenty rats were induced with ASDH and placed into one of four groups. The normothermia group was maintained at 37 °C throughout. In the early hypothermia group, brain temperature was reduced to 33 °C 30 min prior to craniotomy. In the late hypothermia group, brain temperature was lowered to 33 °C 30 min after decompression. The sham group had no ASDH and underwent only craniotomy with normothermia. For estimation of glial and neuronal cell damage, we analyzed serum and microdialysate (using a 100kD probe) concentrations of: glial fibrillary acidic protein (GFAP) and ubiquitin carboxyl-terminal hydrolase -L1 (UCH-L1). Hypothermia induced early significantly reduced the concentration of MD UCH-L1. In conclusion, hypothermia induced early may reduce neuronal cell damage in the reperfusion injury, which was induced after ASDH removal. MD UCH-L1 seems like a good candidate for a sensitive microdialysate biomarker for neuronal injury and outcome.

S. Yokobori, MD, PhD (✉), R. Bullock, MD, PhD, and S. Gajavelli, PhD
Department of Neurosurgery,
University of Miami Miller School of Medicine,
1095 NW 14th terrace, Miami, FL 33136, USA
e-mail: syokobori@med.miami.edu

S. Burks, BA, H. Bramlett, PhD, and D. Dietrich, PhD
Department of Neurosurgery,
University of Miami Miller School of Medicine,
1095 NW 14th terrace, Miami, FL 33136, USA

S. Mondello, MD, PhD, J. Mo, PhD, K.K.W. Wang, PhD,
and R.L. Hayes, PhD
Center of Innovate Research, Banyan Biomarkers, Inc.,
Alachua, FL, USA

Keywords Hypothermia • Traumatic brain injury Microdialysis • Biomarkers

Introduction

One therapeutic method, post-traumatic hypothermia, has been shown in previous studies to improve histopathological and behavioral consequences of traumatic brain injury (TBI) using various experimental models [6]. Unfortunately, therapeutic hypothermia has not shown efficacy in multi-center trials owing to the heterogeneous nature of TBI patients [4, 21]. In a recent clinical trial, the utility of hypothermia was not confirmed as a primary neuroprotective strategy in severe TBI patients [5]. On the other hand, this study demonstrated the possibility that early induced hypothermia might have a beneficial effect on patients with ischemic/reperfusion injury (I/R), such as that seen in acute subdural hematomas [15].

With data from the Clifton study in mind, we hypothesized that hypothermia might be beneficial in the rat ASDH model by blunting the effects of reperfusion injury. The main aim of our study was to test the efficacy of temperature management in reducing brain damage after ASDH. "Brain biomarkers" of groups with normothermia, with pre-craniotomy hypothermia (early), and with post-craniotomy hypothermia (late) were compared.

For a more direct estimation of brain damage, the microdialysis (MD) technique can be utilized. MD has demonstrated promise in the neuromonitoring of severely brain injured patients. Extracellular biomarkers, such as lactate and pyruvate, have been measured with 20 kD cut-off MD probes in the clinical setting. Lactate/pyruvate ratio (LPR) has been said to be effective in the detection of ischemic events [22]. The LPR, however, is influenced by general conditions, and it is difficult to interpret the meaning of LPR values completely [14]. For a more direct understanding of neuronal viability, we decided to measure some extracellular

Y. Katayama et al. (eds.), *Brain Edema XV*, Acta Neurochirurgica Supplement, Vol. 118,
DOI 10.1007/978-3-7091-1434-6_13, © Springer-Verlag Wien 2013

biomarkers with 100 kD cut-off MD probes in this rat ASDH model. In this study, we applied glial fibrillary acidic protein (GFAP) and ubiquitin carboxyl-terminal hydrolase-L1 (UCH-L1) as markers of glial and neuronal cell damage respectively. GFAP is said to be one of the most clinically reliable serum biomarkers for head injury [8]. UCH-L1 has also been said to be a sensitive and specific neuronal cell biomarker, able to predict injury severity and mortality after severe TBI [16]. In the past there have been no studies, laboratory or clinically based, that correlate MD levels of UCH-L1 and GFAP with their predictive ability. Our secondary aim was to analyze these biomarkers in serum and extracellular fluid (measured with MD), to compare their levels before and after craniotomy and to establish their value in this I/R brain injury model.

Materials and Methods

Twenty male Sprague–Dawley rats were randomly divided into four groups. They underwent subdural hematoma induction, surgical procedure, and temperature manipulation as seen below: (1) In the normothermia group brain temperature was maintained at normothermic levels (37 °C) during the course of the experiment. (2) The early hypothermia group underwent hypothermic management (33 °C) 30 min prior to decompressive craniotomy and removal of coagulated blood to mimic a clinical situation in which hypothermia induction could be started when ASDH is diagnosed and while the operating room is prepared. Hypothermic treatment was continued for 3 h after decompression. (3) The late hypothermia group received hypothermic management (33 °C) 30 min after decompression surgery and it was maintained for 3 h. (4) The sham group did not receive induced subdural hematoma, but underwent craniotomy. Their brain temperature was maintained at normothermic levels (37 °C) during the course of the experiment. All animals were anesthetized and intubated as previously described [12]. The tail artery was cannulated with a polyethylene catheter for blood pressure monitoring, blood sampling, and obtaining the autologous blood needed for ASDH induction. A PaO_2 of around 100–150 mmHg and a $PaCO_2$ of 30–40 mmHg were aimed for. The brain temperature was maintained at 33 °C in the early- and late- hypothermia groups by a combination of the water blanket and heating system. In normothermia and the sham rat group, brain and rectal temperatures were maintained at 37 °C during the course of the experiment. Brain temperature was estimated using temporalis muscle temperature, as previously discussed [10]. A midline scalp incision was made and a burrhole of 3 mm diameter was drilled 2 mm to the left of the sagittal suture and 3 mm behind the coronal suture. The dura was incised and a blunt-tipped, J-shaped, No. 23 gauge needle inserted into the subdural space. A cyanoacrylate glue was used to set the needle and seal the burrhole. The hematoma was induced by injecting 350 µl of nonheparinized autologous blood into the subdural space, allowing it to clot in situ. In the sham-treated group, the needle was set in place, but no blood was injected. Two and a half hours after induction of the subdural hematoma, a craniotomy measuring 15 × 6 mm was made using a dental drill. The hematoma was removed using saline irrigation and forceps after widely opening the dura. The scalp was closed over the craniotomy without replacing the bone to mimic clinical practice.

We used a CMA 12 MD probe (CMA Microdialysis, Solna, Sweden), which had a molecular weight cut-off at 100 kD. One hour before ASDH induction, a second burrhole was drilled 2 mm to the left of the sagittal suture and 2 mm behind the lambdoid suture for microdialysis probe insertion. The probe was inserted into this burrhole at 10° from the horizontal plane and at a depth of 6 mm, as previously described [13]. The dialysis probes were continuously perfused with physiological saline with 4 % BSA added at 0.3 µl/min. Microdialysis sampling was delayed by 1 h after insertion to allow the brain to adapt to the presence of the probe. Dialysate samples of 36 µl were then produced over 2 h periods, 2.5 h before and 0.5 h after craniotomy, and stored at −80 °C. Frozen microdialysate vials was later analyzed for biomarkers. At the end of each MD sampling period, 0.6 ml of blood was collected, and centrifuged at 2,500 rpm for 10 min. From these centrifuged blood samples, serum was saved and stored at −80 °C for biomarker analyses.

Quantitative detection of UCH-L1 in serum and microdialysate was performed using proprietary SW enzyme-linked immunosorbent assay (ELISA) and recombinant UCH-L1 as standard [20]. For quantification of GFAP in serum and microdialysate, sandwich ELISA kits from BioVendor were used according to the manufacturer's instructions.

Values from demographic and clinical data, and all biomarker quantification data, were expressed as Mean ± SE, and assessed by using repeated analysis of variance (ANOVA) measures. Statistical significance was set at $p < 0.05$.

Results

Over the course of the experiment, mean arterial blood pressure and $PaCO_2$ did not differ significantly among any of the groups. General circulation, oxygenation, and ventilation statuses were also stable. All physiological parameters in each treatment group were within the normal range throughout the experiments. Brain temperatures were smoothly maintained at 37 °C in normothermia and sham group, and at

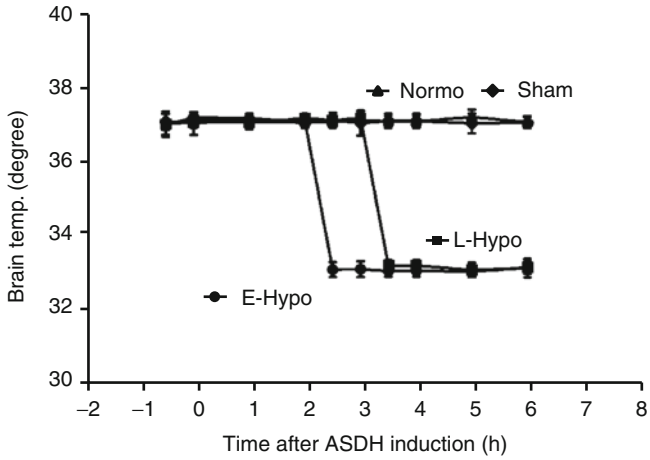

Fig. 1 Brain temperature manipulation. In the early hypothermia group, mild hypothermia (33 °C) was induced 30 min before craniotomy. In the late hypothermia group, cooling began 30 min after craniotomy. At the time of decompressive craniotomy, brain temperature of the early and late hypothermia groups was significantly different. Values are expressed as mean ± SE. *ASDH* acute subdural hematoma, *E-Hypo* early hypothermia therapy (33 °C), l-*Hypo* late hypothermia therapy, *Normo* normothermia therapy, *Sham* sham-operated group

33 °C in the early hypothermia and late hypothermia group (Fig. 1). Global analysis between the four treatment groups for each biomarker showed no significant differences. In one sub-group, however, a significant difference was seen; in the early hypothermia treatment group, the extracellular UCH-L1 concentration measured by MD was significantly decreased after craniotomy (statistics with paired *t* test, $p = 0.0240$, in Table 1). With the focus on UCH-L1 MD, we analyzed the degree of change from baseline (sample collected pre-craniotomy) and determined that only hypothermia induced early could reduce the concentration of UCH L1 MD (Fig. 2).

Discussion

In our study, we were able to detect a significant decrease in microdialysate levels of UCH-L1 before and after craniotomy in the early hypothermia group alone (Fig. 2). Using UCH-L1 as a marker of neuronal injury, this finding clearly supports the idea that hypothermia induced early is effective in reducing neuronal cell damage in I/R pathophysiology, as seen in the ASDH model.

In a multicenter trial of hypothermia for neuroprotection [4], 392 patients with acute brain injury were randomized to normothermia or surface-induced hypothermia; hypothermia did not improve outcome. However, there was some weak evidence of improved outcomes in patients who were hypothermic on admission and treated with continued hypothermia [4]. This same group then tried to confirm the efficacy of very early hypothermia in patients with severe brain injury, the National Acute Brain Injury Study: Hypothermia II (NABISH: II) [5]. In NABISH-II, the hypothermia that was induced early was not efficacious with regard to mortality and morbidity data. On the other hand, in a sub-populational analysis differentiating the diffuse brain injury patients from those with surgical hematoma evacuation, hypothermia induced early did prove efficacious for the latter group. The authors concluded that one explanation was the differences in pathophysiology between diffuse brain injury and hematoma. In experimental models, ischemia occurs during acute subdural hematoma expansion followed by reperfusion after removal [12]. This is similar to the pathophysiology of that seen in patients with cardiac arrest—a group that has been successfully treated with hypothermia [9]. Experimentally, intra-ischemic hypothermia, prior to hematoma removal is associated with improved outcome [3]. Diffuse brain injury is not characterized by ischemia in in vitro studies and may not be a good candidate for hypothermia treatment. After consideration of previous studies, we decided to test hypothermia induced early in the setting of an acute subdural hematoma rat model, which would stimulate I/R injury to the brain.

The pathology of I/R injury can be separated into two mechanisms that play out over two time scales: hypothermia-induced cellular dysfunction and reperfusion-induced free radical production. Reperfusion following ischemia results in a short period of excessive free radical production. Experimental measurements of post I/R free radical production demonstrate that oxygen- and carbon-centered free radical production peaks within 5 min of reperfusion [2] and that hydroxyl generation peaks within 15 min [11]. Thus, mitochondrial free radical production is an important target and provides the first window of opportunity for hypothermia treatment. Intra-ischemic cooling was likely necessary in our model because it ensured proper blood temperature at the time of reperfusion. A second window of opportunity for hypothermia targets the inflammatory cascade and cell death pathways of apoptosis and necrosis. These probably center on mitochondrial dysfunction and previous data have suggested that a transition in mitochondrial permeability may be the "point of no return" in both cell death pathways [17]. Apoptosis is ATP dependent, whereas necrosis is not. Both processes play out over hours to days and are associated with poor calcium and sodium management. Activation of caspases and proteases, and the release of mitochondrial cytochrome C, are features of the more organized apoptosis [17]. These cell death processes represent the second window of treatment with hypothermia.

Despite large amounts of basic and clinical research into I/R brain injury, the mechanisms of neuronal protection in hypothermia therapy remain unknown. Currently, therapeutic

Table 1 Concentrations of biomarkers in serum and cerebral extracellular microdialysate (mean ± SE)

	UCH-L1 MD			GFAP MD			UCH-L1 serum			GFAP serum		
	Normo	Early	Late	Normo	Early	Late	Normo	Early	Late	Normo	Early	Late
Pre craniotomy (ng/ml)	64.84 ± 38.37	20.75 ± 5.77	45.67 ± 14.59	9.05 ± 4.32	6.84 ± 2.77	5.62 ± 2.79	0.17 ± 0.02	0.29 ± 0.16	0.22 ± 0.90	1.04 ± 0.21	1.04 ± 0.35	0.82 ± 0.31
Post craniotomy (ng/ml)	68.74 ± 37.19	4.29 ± 1.36	39.52 ± 17.28	7.24 ± 4.58	7.06 ± 4.24	9.55 ± 5.35	0.18 ± 0.03	0.41 ± 0.18	0.31 ± 0.15	0.57 ± 0.13	1.28 ± 0.20	0.96 ± 0.28
P value*	0.9436	0.0240*	0.7904	0.7805	0.9652	0.5099	0.6766	0.6372	0.6158	0.0905	0.5595	0.7545
	Sham			Sham			Sham			Sham		
Pre craniotomy (ng/ml)	1.81 ± 1.26			4.92 ± 1.53			0.18 ± 0.03			0.72 ± 0.31		
Post craniotomy (ng/ml)	1.11 ± 0.66			3.54 ± 1.91			0.76 ± 0.35			0.64 ± 0.23		
P value*	0.6351			0.5867			0.1414			0.8382		

UCH-L1 ubiquitin carboxyl-terminal hydrolase-L1, *GFAP* glial fibrillary acidic protein, *MD* microdialysate, *Normo* normothermia group, *Early* early hypothermia group, *Late* late hypothermia group, *Sham* sham-operated group

*$p < 0.05$; significant difference existed between pre- and post-craniotomy (unpaired *t* test)

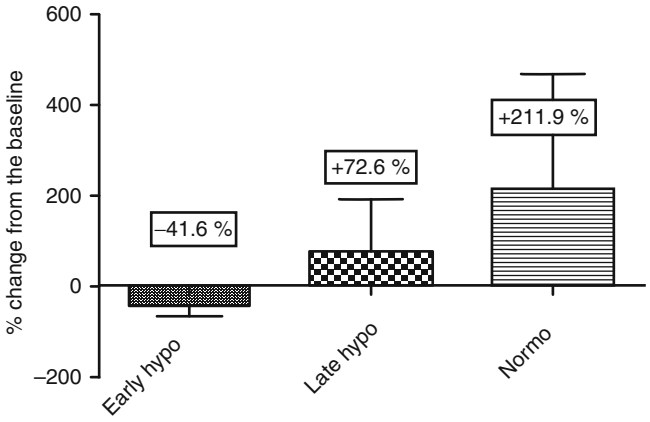

Fig. 2 Relative change (%) in UCH-L1 MD concentration from baseline. This graph shows the relative ratio of ubiquitin carboxyl-terminal hydrolase-L1 concentration in microdialysates (UCH-L1 MD) from baseline (pre-craniotomy) levels. A significantly negative ratio was observed in only the early hypothermia group. In the late hypothermia and normothermia groups, the relative ratios were positive. *Early Hypo* early hypothermia therapy, *Late Hypo* late hypothermia therapy, *Normo* normothermia therapy

hypothermia is believed to confer protection against I/R injury through multiple mechanisms. Among the many pathways cited a central hypothesis is that hypothermia reduces cellular metabolism and oxygen demand while maintaining acceptable ATP levels [7]. Additionally, hypothermia attenuates abnormal free radical production [19], improves cellular ion handling, and improves cellular pH balance [18]. Hypothermia also reduces cell death and inflammatory signaling [23]. Although different tissues have different sensitivities to ischemia, I/R injury has been observed in many tissue types [1].

In our results, we were able to show the beneficial effects of hypothermia induced early in brain damage associated with an acute subdural hematoma. This neuro-protective effect is likely the result of the mechanisms described above. The important thing is that the hypothermia period should be initiated before reperfusion injury.

Our group is planning to transition this study into the clinical setting, exploring hypothermia induced early in subdural hematoma patients using MD sampling for similar biomarkers. Previously, we used a 20-kD cut-off in our MD sampling with the primary goal of measuring LPR, which has been said to be the most sensitive ischemic biomarker. Problematically, LPR values are influenced by many conditions, and it may be difficult to interpret the data [14]. Therefore, we advocate the use of UCH-L1 MD as a good candidate for the next generation of MD sampling, as it offers a high degree of sensitivity and specificity for detecting brain damage, especially ischemic injury.

We conclude that UCH-L1 MD is a reliable biomarker, especially in ischemic traumatic head injury. Using this

sensitive biomarker with the MD technique, we were able to demonstrate the efficacy of early, pre-reperfusional mild hypothermia through its capacity to reduce neuronal cell damage in this I/R model, created by an ASDH. Clinical, multicenter trials are needed to further examine the efficacy of very early, preoperatively induced hypothermia.

Acknowledgments This work was supported by funds from NINDS RO1 NS 042133 and the Miami Project to Cure Paralysis.

Author Disclosure Statement Dr. Mondello and Dr. Mo are employees of Banyan Biomarkers, Inc.; Dr. Wang owns stock, receive royalties from, and is a former officer of Banyan Biomarkers Inc., and as such may benefit financially as a result of the outcomes of this research or work reported in this publication.

References

1. Becker LB (2004) New concepts in reactive oxygen species and cardiovascular reperfusion physiology. Cardiovasc Res 61:461–470
2. Bolli R, Jeroudi MO, Patel BS, Aruoma OI, Halliwell B, Lai EK, McCay PB (1989) Marked reduction of free radical generation and contractile dysfunction by antioxidant therapy begun at the time of reperfusion. Evidence that myocardial "stunning" is a manifestation of reperfusion injury. Circ Res 65:607–622
3. Burger R, Bendszus M, Vince GH, Solymosi L, Roosen K (2004) Neurophysiological monitoring, magnetic resonance imaging, and histological assays confirm the beneficial effects of moderate hypothermia after epidural focal mass lesion development in rodents. Neurosurgery 54:701–711; discussion 711–702
4. Clifton GL, Miller ER, Choi SC, Levin HS, McCauley S, Smith KR Jr, Muizelaar JP, Wagner FC Jr, Marion DW, Luerssen TG, Chesnut RM, Schwartz M (2001) Lack of effect of induction of hypothermia after acute brain injury. N Engl J Med 344:556–563
5. Clifton GL, Valadka A, Zygun D, Coffey CS, Drever P, Fourwinds S, Janis LS, Wilde E, Taylor P, Harshman K, Conley A, Puccio A, Levin HS, McCauley SR, Bucholz RD, Smith KR, Schmidt JH, Scott JN, Yonas H, Okonkwo DO (2011) Very early hypothermia induction in patients with severe brain injury (the National Acute Brain Injury Study: Hypothermia II): a randomised trial. Lancet Neurol 10:131–139
6. Dietrich WD, Bramlett HM (2010) The evidence for hypothermia as a neuroprotectant in traumatic brain injury. Neurotherapeutics 7:43–50
7. Erecinska M, Thoresen M, Silver IA (2003) Effects of hypothermia on energy metabolism in mammalian central nervous system. J Cereb Blood Flow Metab 23:513–530
8. Honda M, Tsuruta R, Kaneko T, Kasaoka S, Yagi T, Todani M, Fujita M, Izumi T, Maekawa T (2010) Serum glial fibrillary acidic protein is a highly specific biomarker for traumatic brain injury in humans compared with S-100B and neuron-specific enolase. J Trauma 69:104–109
9. Janata A, Holzer M (2009) Hypothermia after cardiac arrest. Prog Cardiovasc Dis 52:168–179
10. Jiang JY, Lyeth BG, Clifton GL, Jenkins LW, Hamm RJ, Hayes RL (1991) Relationship between body and brain temperature in traumatically brain-injured rodents. J Neurosurg 74:492–496
11. Khalid MA, Ashraf M (1993) Direct detection of endogenous hydroxyl radical production in cultured adult cardiomyocytes during anoxia and reoxygenation. Is the hydroxyl radical really the most damaging radical species? Circ Res 72:725–736
12. Kuroda Y, Bullock R (1992) Local cerebral blood flow mapping before and after removal of acute subdural hematoma in the rat. Neurosurgery 30:687–691
13. Kwon TH, Sun D, Daugherty WP, Spiess BD, Bullock MR (2005) Effect of perfluorocarbons on brain oxygenation and ischemic damage in an acute subdural hematoma model in rats. J Neurosurg 103:724–730
14. Larach DB, Kofke WA, Le Roux P (2011) Potential non-hypoxic/ischemic causes of increased cerebral interstitial fluid lactate/pyruvate ratio: a review of available literature. Neurocrit Care 15(3):609–622
15. Miller JD, Bullock R, Graham DI, Chen MH, Teasdale GM (1990) Ischemic brain damage in a model of acute subdural hematoma. Neurosurgery 27:433–439
16. Mondello S, Robicsek SA, Gabrielli A, Brophy GM, Papa L, Tepas J, Robertson C, Buki A, Scharf D, Jixiang M, Akinyi L, Muller U, Wang KK, Hayes RL (2010) AlphaII-spectrin breakdown products (SBDPs): diagnosis and outcome in severe traumatic brain injury patients. J Neurotrauma 27:1203–1213
17. Neumar RW (2000) Molecular mechanisms of ischemic neuronal injury. Ann Emerg Med 36:483–506
18. Polderman KH (2009) Mechanisms of action, physiological effects, and complications of hypothermia. Crit Care Med 37:S186–S202
19. Shao ZH, Sharp WW, Wojcik KR, Li CQ, Han M, Chang WT, Ramachandran S, Li J, Hamann KJ, Vanden Hoek TL (2010) Therapeutic hypothermia cardioprotection via Akt- and nitric oxide-mediated attenuation of mitochondrial oxidants. Am J Physiol Heart Circ Physiol 298:H2164–H2173
20. Svetlov SI, Prima V, Kirk DR, Gutierrez H, Curley KC, Hayes RL, Wang KK (2010) Morphologic and biochemical characterization of brain injury in a model of controlled blast overpressure exposure. J Trauma 69:795–804
21. Timmons SD (2010) Current trends in neurotrauma care. Crit Care Med 38:S431–S444
22. Timofeev I, Carpenter KL, Nortje J, Al-Rawi PG, O'Connell MT, Czosnyka M, Smielewski P, Pickard JD, Menon DK, Kirkpatrick PJ, Gupta AK, Hutchinson PJ (2011) Cerebral extracellular chemistry and outcome following traumatic brain injury: a microdialysis study of 223 patients. Brain 134:484–494
23. Yang D, Guo S, Zhang T, Li H (2009) Hypothermia attenuates ischemia/reperfusion-induced endothelial cell apoptosis via alterations in apoptotic pathways and JNK signaling. FEBS Lett 583: 2500–2506

Cerebral Hemorrhage, Brain Edema, and Heme Oxygenase-1 Expression After Experimental Traumatic Brain Injury

Shuichi Okubo, Guohua Xi, Richard F. Keep, Karin M. Muraszko, and Ya Hua

Abstract Intracranial bleeding is a common and serious consequence of traumatic brain injury (TBI). In the present study, we investigated cerebral hematoma occurrence, brain edema formation, blood–brain barrier (BBB) disruption, and heme oxygenase-1 (HO-1) expression after TBI. Moderate severity (1.8–2.2 atmospheres [ATM]) TBI was induced by lateral fluid percussion in male adult Sprague–Dawley rats. Sham rats underwent only a craniotomy. Rats were euthanized 24 h later for brain histology and immunoblotting analysis. We found TBI-induced cerebral hematomas and iron deposition in the ipsilateral hemisphere in all rats. TBI also caused marked BBB disruption ($p<0.05$) and brain swelling ($p<0.05$). HO-1, a key enzyme for heme degradation, was upregulated significantly after TBI (419 ± 89 vs 194 ± 59 pixels in the sham, $p<0.05$). These results suggest that cerebral hematomas might play a role in brain injury after TBI. Future studies should determine the role of iron released from the cerebral hematoma in TBI.

Keywords Brain edema • Cerebral hemorrhage • Iron • Traumatic brain injury

S. Okubo
Department of Neurosurgery,
University of Michigan Medical School,
R5018 Biomedical Science Research Building,
109 Zina Pitcher Place, Ann Arbor, MI, 48109-2200, USA

Department of Neurosurgery,
Kagawa Medical University,
Kagawa, Japan

G. Xi, MD, R.F. Keep, K. M. Muraszko, and Y. Hua, MD (✉)
Department of Neurosurgery,
University of Michigan Medical School,
R5018 Biomedical Science Research Building,
109 Zina Pitcher Place, Ann Arbor, MI, 48109-2200, USA
e-mail: yahua@umich.edu

Introduction

Each year in the United States, approximately 1.6 million people suffer a traumatic brain injury (TBI) and there are more than 5 million Americans currently living with TBI-related disabilities [10]. There are currently no effective therapies for TBI patients. Intracranial bleeding is a common and serious consequence of TBI. MRI has shown a preponderance of hemorrhagic lesions and few ischemic lesions in the acute phase and 56 % of TBI patients were reported to have at least one intracranial bleed [12]. The release of iron from the breakdown of hemoglobin during hematoma resolution may result in a build-up of non-heme iron in brain tissue and brain damage.

In the present study we established a TBI model with cerebral hematoma. The lateral fluid percussion (LFP) model produces both focal and diffuse injury with vascular disruption, neuronal cell death and glial proliferation [1, 2, 7, 14, 15, 17, 20].

Materials and Methods

Animal Preparation and Experimental Group

The protocols for these animal studies were approved by the University of Michigan Committee on the Use and Care of Animals at the University of Michigan. Adult male Sprague–Dawley rats (Charles River Laboratories, Portage, MI, USA) weighing 260–340 g were used in this study. Animals were euthanized at 24 h post-TBI or sham operation for brain histology and Western blot analysis.

Y. Katayama et al. (eds.), *Brain Edema XV*, Acta Neurochirurgica Supplement, Vol. 118,
DOI 10.1007/978-3-7091-1434-6_14,

Lateral Fluid Percussion Injury

Traumatic brain injury was induced by lateral fluid percussion injury, as described previously [3, 15]. In brief, rats were anesthetized with pentobarbital (50 mg/kg, i.p.), and rectal temperature was maintained at 37.5 °C by using a feedback-controlled heating pad. The animals were placed in a stereotaxic frame, and the scalp and temporal muscle were reflected. A 4.8-mm diameter hole was drilled between the bregma and lambda on the right convexity (anterior edge 2.0 mm posterior to the bregma; lateral edge adjacent to the left lateral ridge), and a hollow female Luer–Lock fitting secured with dental cement. Lateral fluid percussion injury was induced by a transient (21–23 ms) fluid pulse impact against the exposed dura by using a fluid-percussion device (AmScien Instruments, Richmond, VA, USA). The impact pressure was measured by an extra-cranial transducer and controlled to 1.8–2.2 atmospheres (ATM). After impact, the dura was checked to ensure that it had remained intact. Sham-operated control animals underwent all surgical procedures, except the fluid-percussion impact. Animals that did not survive the injury were predetermined to be excluded from the study.

Histological and Immunohistochemical Study

Rats were reanesthetized with pentobarbital (60 mg/kg, i.p.), followed by intracardiac perfusion with 4 % paraformaldehyde in 0.1 mol/L phosphate-buffered saline, pH 7.4. Brains were removed, kept in 4 % paraformaldehyde for 24 h, and immersed in 25 % sucrose for 3–4 days at 4 °C. The brains were then embedded in an optimal cutting temperature compound (Sakura Finetek USA, Torrance, CA, USA) and sectioned on a cryostat (18 μm). Brain swelling was assessed morphometrically. Coronal sections from 1 mm posterior to the anterior edge of the craniotomy site were stained with hematoxylin and eosin. On the microscopic images, the area of the ipsilateral or contralateral hemisphere was measured using ImageJ software. Brain swelling was estimated by the ratio of the volume of (ipsilateral – contralateral)/contralateral hemisphere. Immunohistochemical staining was performed using avidin–biotin complex technique. The primary antibody was polyclonal rabbit anti-rat HO-1 IgG (1:200 dilution, StressGene) and the secondary antibody was biotinylated goat anti-rabbit IgG (1:500 dilution, Vector Laboratories). Normal rabbit IgG was used as negative control. Brain iron deposition was determined by enhanced Perls' reaction [22].

Western Blot Analysis

Animals were anesthetized before undergoing transcardiac perfusion with 0.1 mol/L phosphate-buffered saline. The brains were removed and a 4-mm thick coronal brain slice was cut approximately 5 mm from the frontal pole. The slice was separated into ipsilateral or contralateral cortex and basal ganglia. Western blot analysis was performed as previously described [24]. The primary antibodies were polyclonal rabbit anti-rat HO-1 IgG antibody (1:2,500 dilution; StressGen, Farmingdale, NY, USA) and polyclonal sheep anti-rat albumin antibody (1:20,000 dilution; Bethyl Lab, Montgomery, USA). The secondary antibodies were peroxidase-conjugated goat anti-rabbit antibody (Bio-Rad Laboratories, Hercules, CA, USA) and rabbit anti-sheep antibody (Millipore, Billerica, MA, USA).

Statistical Analysis

All data in this study are presented as mean ± standard deviation. Data were analyzed using Student's t test or Kruskal–Wallis test. Statistical significance was set at $p < 0.05$.

Results

All animals undergoing lateral fluid percussion had intracerebral hematomas in the ipsilateral cortex and caudate at 24 h (Fig. 1a). TBI caused ipsilateral brain swelling (3.3 ± 0.9 % vs −0.04 ± 1.2 % in the sham group, $p < 0.05$, Fig. 1b). Release of iron from the degradation of heme occurred around clots 24 h after brain trauma, as indicated by Perls' staining. Iron-positive cells were found in the ipsilateral hemisphere, especially around hematomas (Fig. 2a). TBI also resulted in blood–brain barrier disruption. Albumin levels were increased in the ipsilateral hemisphere of TBI rats (1,248 ± 710 vs 204 ± 171 pixels in the sham group, $p < 0.05$, Fig. 2b).

Immunoreactivity of HO-1 was increased markedly in the ipsilateral cortex and caudate of TBI rats (Fig. 3a, b). Most HO-1 positive cells were microglia-like cells. HO-1 protein levels were determined by Western blot analysis and we found that HO-1 levels in the ipsilateral cortex were significantly higher in TBI rats (419 ± 89 vs 194 ± 59 pixels in the sham, $p < 0.05$, Fig. 3c).

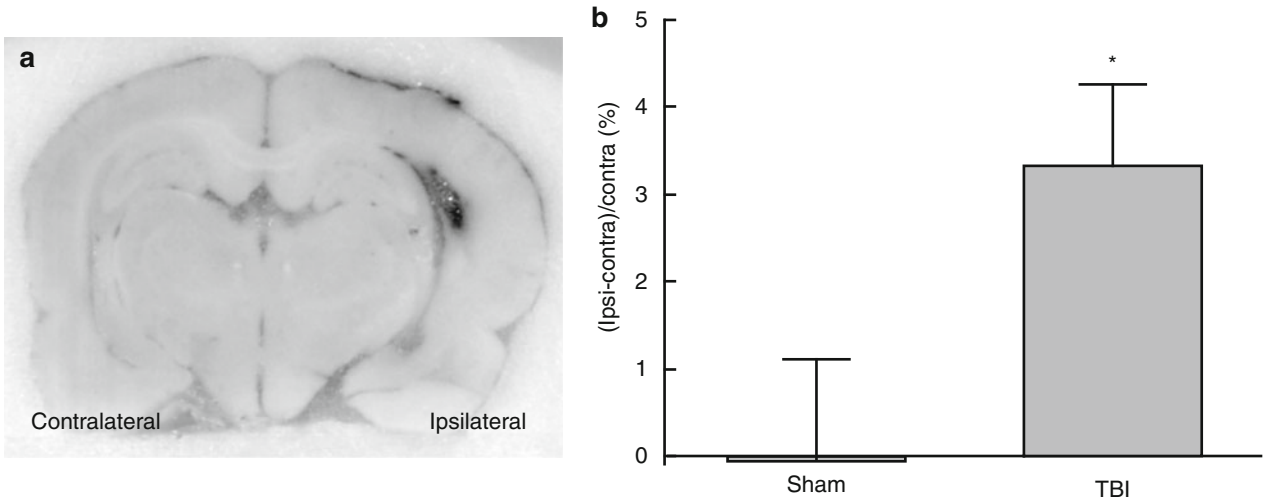

Fig. 1 (**a**) Cerebral hematomas in the coronal brain section of a rat. The rat had lateral fluid percussion-induced traumatic brain injury (TBI). (**b**) Brain swelling was expressed as the volume of (ipsilateral – contralateral)/contralateral hemisphere. Values are mean ± SD, $n=4–5$, $^*p<0.05$ vs sham

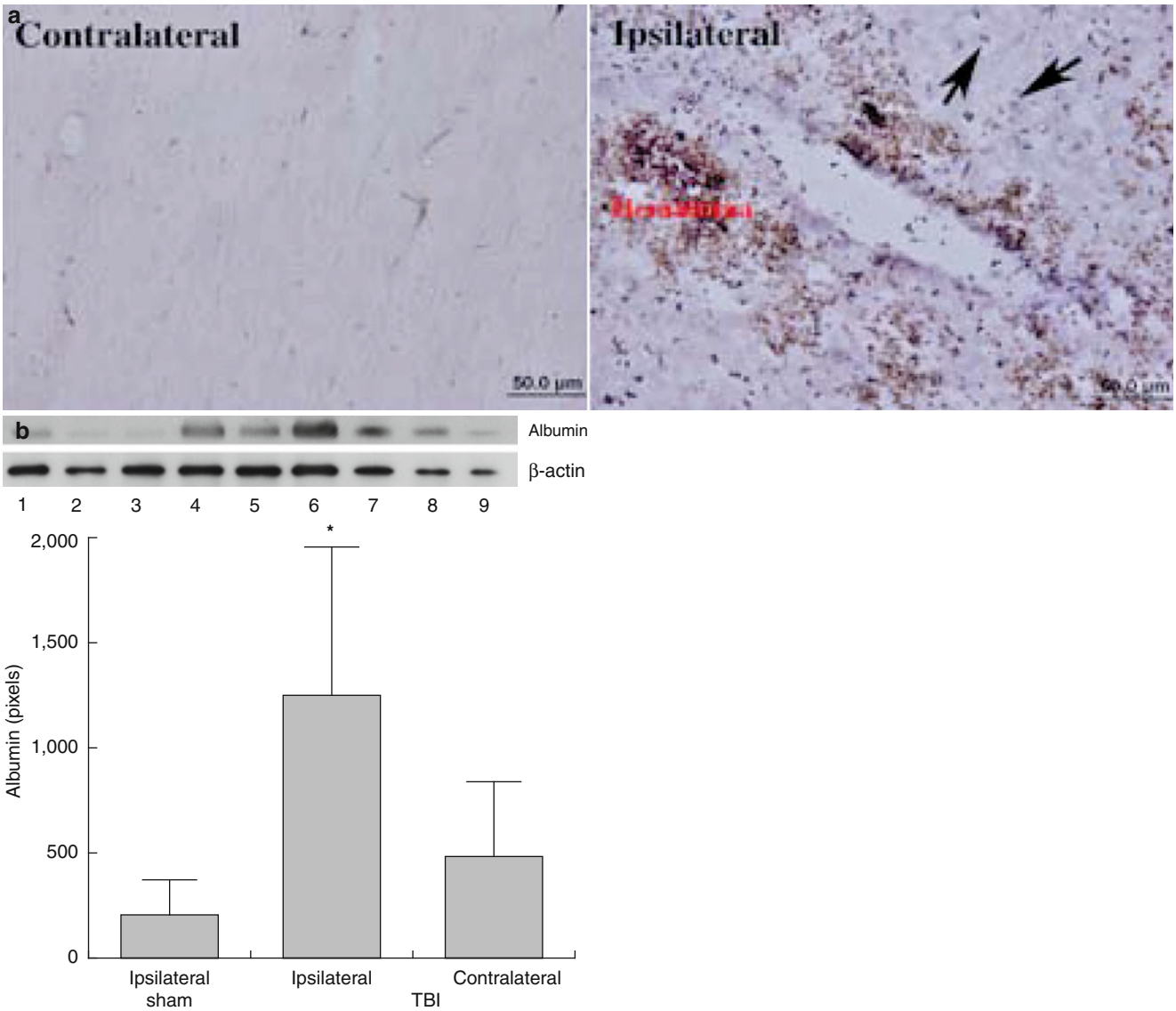

Fig. 2 (**a**) Perls' staining showing iron deposition in the ipsilateral hemisphere 24 h after TBI, scale bar = 50 μm; (**b**) Albumin levels in the ipsilateral hemisphere of sham rats (lanes 1–3) or in the ipsilateral hemisphere (lanes 4–6) or in the contralateral hemisphere (lanes 7–9) of TBI rats. Values are mean ± SD, $n=3$, $^*p<0.05$ vs sham. *Arrows* indicate perls' positive cells

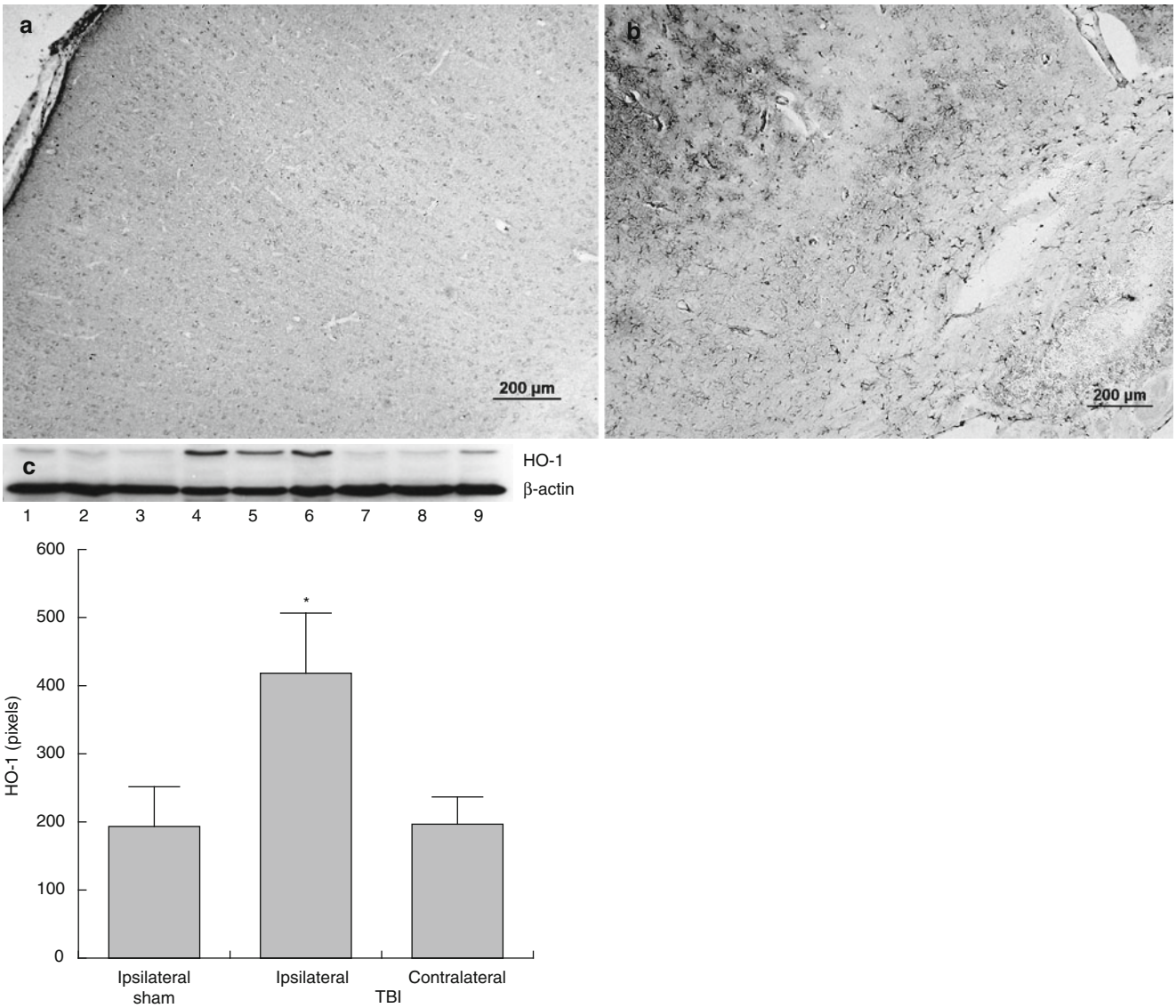

Fig. 3 HO-1 immunoreactivity in the ipsilateral cortex of sham rat (**a**) or TBI rat (**b**). Scale bar = 200 μm. HO-1 protein levels (**c**) in the ipsilateral hemisphere of sham-operated rats (lanes 1–3) and in the ipsilateral hemisphere (lanes 4–6) and the contralateral hemisphere (lanes 7–9) of TBI rats at 24 h. Values are mean ± SD, $n = 3$, $^*p < 0.05$ vs the other groups

Conclusion

In this study, we found that TBI resulted in cerebral hematomas, brain swelling, and BBB disruption. HO-1 upregulation and brain iron deposition were also found in the ipsilateral hemisphere 24 h after TBI.

Intracranial bleeding is a common and serious consequence of TBI and contributes to the injury. The primary brain injury after trauma may manifest as diffuse axonal injury, intraparenchymal contusions, intracranial hematomas, diffused axonal injury, and skull fractures [9, 12]. Brain edema after TBI is a common and serious consequence of severe traumatic brain injury [6]. BBB disruption was reported previously after TBI [4, 19]. A brain contusion results in immediate cell death in a limited region of the brain. But secondary cell loss and chronic atrophy can occur at sites other than at or near the primary injury [13]. It may be related to regional metabolic distress that was mediated by accumulated iron-induced oxidative stress and metabolic dysfunction [25].

Iron deposition occurs in TBI brain, as indicated in this study using Perls' staining. We have gathered substantial evidence that iron plays a major role in brain injury after intracerebral hemorrhage and subarachnoid hemorrhage. The release

of iron from the breakdown of hemoglobin during hematoma resolution in the rat results in a build-up in the levels of non-heme iron in brain tissue. The high level of non-heme iron remains in the brain for at least 28 days [22]. Through enhanced Perls' reaction, iron-positive cells were found in the perihematomal zone as early as the 1st day [22], as found in our study with TBI. Increases in brain iron levels cause brain edema, oxidative stress, BBB disruption, brain atrophy, and neurological deficits following intracranial hemorrhage (ICH) [8, 16, 21, 23]. Our previous studies showed that free iron levels in cerebrospinal fluid (CSF) increase almost 14-fold on the third day after ICH, and remain high for at least 28 days after experimental ICH [18]. The duration of iron overload after lateral fluid percussion remains to be elucidated.

Brain HO-1 levels are increased after TBI. HO-1, also called heat shock protein 32, is an enzyme for heme degradation into iron, carbon monoxide, and biliverdin. It can be induced in the brain by heat shock, heme and hemoglobin, a variety of oxidants [23], and TBI [5]. In the rat, marked HO-1 upregulation at day 3 accompanied by the elevation of nonheme iron, transferrin, transferrin receptor, and ferritin levels after subarachnoid hemorrhage [11].

In conclusion, TBI induced cerebral hematomas, brain edema formation, BBB disruption, and iron deposition. Cerebral hematomas and brain iron overload could be therapeutic targets for TBI.

Acknowledgments This study was supported by grants NS-017760, NS-039866, and NS-057539 from the National Institutes of Health (NIH) and 0840016 N from the American Heart Association (AHA). The content is solely the responsibility of the authors and does not necessarily represent the official views of the NIH and AHA.

Conflict of Interest We declare that we have no conflict of interest.

References

1. Bramlett HM, Dietrich WD (2002) Quantitative structural changes in white and gray matter 1 year following traumatic brain injury in rats. Acta Neuropathol 103:607–614
2. Cortez SC, McIntosh TK, Noble LJ (1989) Experimental fluid percussion brain injury: vascular disruption and neuronal and glial alterations. Brain Res 482:271–282
3. Dixon CE, Lyeth BG, Povlishock JT, Findling RL, Hamm RJ, Marmarou A, Young HF, Hayes RL (1987) A fluid percussion model of experimental brain injury in the rat. J Neurosurg 67:110–119
4. Fukuda K, Panter SS, Sharp FR, Noble LJ (1995) Induction of heme oxygenase-1 (HO-1) after traumatic brain injury in the rat. Neurosci Lett 199:127–130
5. Fukuda K, Richmon JD, Sato M, Sharp FR, Panter SS, Noble LJ (1996) Induction of heme oxygenase-1 (HO-1) in glia after traumatic brain injury. Brain Res 736:68–75
6. Ghajar J (2000) Traumatic brain injury. Lancet 356:923–929
7. Hicks R, Soares H, Smith D, McIntosh T (1996) Temporal and spatial characterization of neuronal injury following lateral fluid-percussion brain injury in the rat. Acta Neuropathol 91:236–246
8. Hua Y, Nakamura T, Keep R, Wu J, Schallert T, Hoff J, Xi G (2006) Long-term effects of experimental intracerebral hemorrhage: the role of iron. J Neurosurg 104:305–312
9. Khoshyomn S, Tranmer BI (2004) Diagnosis and management of pediatric closed head injury. Semin Pediatr Surg 13:80–86
10. Langlois JA, Rutland-Brown W, Wald MM (2006) The epidemiology and impact of traumatic brain injury: a brief overview. J Head Trauma Rehabil 21:375–378
11. Lee JY, Keep RF, He Y, Sagher O, Hua Y, Xi G (2010) Hemoglobin and iron handling in brain after subarachnoid hemorrhage and the effect of deferoxamine on early brain injury. J Cereb Blood Flow Metab 30:1793–1803
12. Maas AI, Stocchetti N, Bullock R (2008) Moderate and severe traumatic brain injury in adults. Lancet Neurol 7:728–741
13. Marcoux J, McArthur DA, Miller C, Glenn TC, Villablanca P, Martin NA, Hovda DA, Alger JR, Vespa PM (2008) Persistent metabolic crisis as measured by elevated cerebral microdialysis lactate-pyruvate ratio predicts chronic frontal lobe brain atrophy after traumatic brain injury. Crit Care Med 36:2871–2877
14. Marmarou A, Foda MA, van den Brink W, Campbell J, Kita H, Demetriadou K (1994) A new model of diffuse brain injury in rats. Part I: pathophysiology and biomechanics. Neurosurg 80:291–300
15. McIntosh TK, Vink R, Noble L, Yamakami I, Fernyak S, Soares H, Faden AL (1989) Traumatic brain injury in the rat: characterization of a lateral fluid-percussion model. Neuroscience 28:233–244
16. Nakamura T, Keep RF, Hua Y, Schallert T, Hoff JT, Xi G (2004) Deferoxamine-induced attenuation of brain edema and neurological deficits in a rat model of intracerebral hemorrhage. J Neurosurg 100:672–678
17. Pierce JE, Trojanowski JQ, Graham DI, Smith DH, McIntosh TK (1996) Immunohistochemical characterization of alterations in the distribution of amyloid precursor proteins and beta-amyloid peptide after experimental brain injury in the rat. J Neurosci 16:1083–1090
18. Wan S, Hua Y, Keep RF, Hoff JT, Xi G (2006) Deferoxamine reduces CSF free iron levels following intracerebral hemorrhage. Acta Neurochir Suppl 96:215–218
19. Schmidt RH, Grady MS (1993) Regional patterns of blood-brain barrier breakdown following central and lateral fluid percussion injury in rodents. J Neurotrauma 10:415–430
20. Thompson HJ, Lifshitz J, Marklund N, Grady MS, Graham DI, Hovda DA, McIntosh TK (2005) Lateral fluid percussion brain injury: a 15-year review and evaluation. J Neurotrauma 22:42–75
21. Wu J, Hua Y, Keep R, Schallert T, Hoff J, Xi G (2002) Oxidative brain injury from extravasated erythrocytes after intracerebral hemorrhage. Brain Res 953:45
22. Wu J, Hua Y, Keep RF, Nakamura T, Hoff JT, Xi G (2003) Iron and iron-handling proteins in the brain after intracerebral hemorrhage. Stroke 34:2964–2969
23. Xi G, Keep RF, Hoff JT (2006) Mechanisms of brain injury after intracerebral haemorrhage. Lancet Neurol 5:53–63
24. Xi G, Keep RF, Hua Y, Xiang JM, Hoff JT (1999) Attenuation of thrombin-induced brain edema by cerebral thrombin preconditioning. Stroke 30:1247–1255
25. Xu Y, McArthur DL, Alger JR, Etchepare M, Hovda DA, Glenn TC, Huang S, Dinov I, Vespa PM (2010) Early nonischemic oxidative metabolic dysfunction leads to chronic brain atrophy in traumatic brain injury. J Cereb Blood Flow Metab 30: 883–894

A Selective Adenosine A2A Receptor Antagonist Ameliorated Hyperlocomotion in an Animal Model of Lateral Fluid Percussion Brain Injury

Saad Habib-E-Rasul Mullah, Motoki Inaji, Tadashi Nariai, Satoru Ishibashi, and Kikuo Ohno

Abstract Increased concentration of extracellular adenosine after brain injury is supposed to be one of the causes of secondary brain damage. The purpose of the present study is to examine whether or not administration of adenosine A2A receptor antagonist may be efficacious in ameliorating neurological symptoms by blocking secondary brain damage through cascades initiated by adenosine A2a receptor.

Mongolian gerbils were divided into four groups: the trauma-medication (T-M), trauma-saline (T-S), sham-medication (S-M), and sham-saline (S-S) groups. Trauma groups received lateral fluid percussion injury. Medication groups received i.p. injection of SCH58261 (selective adenosine A2A receptor antagonist) until the fifth post-injury day. Open-field locomotion test and grabbing test were conducted before and 1, 3, 5, 7, and 9 days after injury.

The total distance of movement in the T-S group was significantly greater than in the other three groups at all time points. In the T-M group, administration of SCH58261 significantly blocked hyperlocomotion, which was observed in the T-S group. There was no significant difference in the total distance among the T-M, S-M, and S-S groups. In the grabbing test, grabbing time was significantly increased in the T-S group 3, 5, 7, and 9 days after the operation. SCH58261 also improved grabbing time in the T-M group.

Adenosine A2A antagonist successfully suppressed the trauma-induced hyperlocomotion, presumably by blocking secondary brain damage.

S.H. Mullah, MD, PhD, M. Inaji, MD, PhD (✉), T. Nariai, MD, PhD, and K. Ohno, MD, PhD
Department of Neurosurgery, Tokyo Medical and Dental University, 1-5-45, Yushima, Bunkyo-ku, Tokyo, 113-8519, Japan
e-mail: inaji.nsrg@tmd.ac.jp

S. Ishibashi, MD, PhD
Department of Neurology, Tokyo Medical and Dental University, Tokyo, Japan

Keywords Lateral fluid percussion model gerbil • Adenosine A2A receptor • Hyper locomotion

Introduction

Primarily traumatic brain injury leads to mechanical events, such as laceration, contusion, shearing, and axonal stretching. Secondary brain injuries, which result from complex biochemical and physiological hazardous pathways working over a period of hours to days, is also substantially attributable to the chronic neurological symptoms of TBI patients [1, 2]. Therefore, knowledge of secondary brain injury after TBI must be important as it may be achieved by the clinician's hand to prevent patients from suffering from additional damage other than the initial impact.

Adenosine is supposed to be one of the causes of secondary brain damage. The concentration of extracellular adenosine rises markedly in response to ischemia, hypoxia, toxicity, inflammation, and other brain insults [6]. Previously, Alessia Melani et al. reported that SCH 58261, a specific adenosine A2A receptor antagonist, improved neurological and behavioral outcome after focal ischemia in Mongolian gerbils [5]. They also reported that SCH58261 reduced elevation of the extracellular concentration of amino acids, GABA, and other neurotransmitters. Another previous report demonstrated that 3 weeks' pretreatment with caffeine improved the neurological outcome in a trauma model of mice [3]. The protective effect of specific adenosine A2A antagonist to traumatic brain injury, however, has not yet been examined.

The purpose of the present study is to examine whether post-traumatic administration of adenosine A2A receptor antagonist is efficacious in ameliorating neurological symptoms by blocking the secondary brain damage in a lateral fluid percussion neurotrauma model in Mongolian gerbils.

Y. Katayama et al. (eds.), *Brain Edema XV*, Acta Neurochirurgica Supplement, Vol. 118,
DOI 10.1007/978-3-7091-1434-6_15,

Materials and Methods

Animals

All experimental protocols were based on the NIH Guide for the Care and Use of Laboratory Animals and were approved by the Animal Experiment Committee of Tokyo Medical and Dental University. Adult Mongolian Gerbils of 23–37 (weighing 60–100 g) were housed in groups of three or four and maintained on a 14/10 h light/dark cycle with unlimited access to food and water.

Animals were divided into the following four groups: the trauma-medication (T-M), trauma-saline (T-S), sham-medication (S-M), and sham-saline (S-S) groups.

Surgical Procedure for Lateral Fluid Percussion Injury

Moderate brain injury was induced with a lateral fluid percussion device as described previously [4] in T-S and T-M groups. In short, each animal was anesthetized with sodium pentobarbital (50 mg/kg i.p.). Once a surgical level of anesthesia was achieved, animals were placed in a stereotaxic frame, an incision was made along the midline of the scalp, a round craniotomy (3.5 mm diameter) was made on the right parietal bone with the center coordinating midway between the bregma and lambda and 2.5 mm lateral to the midline. A 10-cm-long firm silicone tube with an inner diameter of 2 mm attached to a fluid percussion injury device (Dragonfly R&D, Ridgeley, WV, USA) was placed over the intact dura, and was bonded to the skull with Aron-Alpha cement (Konishi Co, Osaka, Japan). Lateral fluid percussion injuries (LFPIs) induced with a pressure of 20–30 psi have shown hyperactivity, as described in a previous study. Animals in the S-M and S-S groups received anesthesia and underwent a similar surgical procedure except for the delivery of the pressure pulse. Following injury, the injury tube was removed from the skull and the scalp was sutured using nylon.

Open Field Test

For behavioral evaluation, an open field locomotion test and grabbing test were conducted in all animals, before and 1, 3, 5, 7, and 9 days after the LFPI and sham operations.

Animals were placed individually in an open field apparatus (85 × 85 cm at the bottom) and allowed to start from one of the four corners selected randomly by the experimenter. After 1 min all the movements were tracked and measured for 10 min using a video tracking system and smart software (Bio Research Center, Nagoya, Japan). We then analyzed the total distance moved (cm/10 min) by each animal, which represents spontaneous locomotor activity.

Grabbing Test

A 40-gram net whose rods were ~3 mm in diameter (suitable for the gerbils' grip) was used in this study. Each gerbil was passed over the net, and lifted by its tail. The number of times the gerbils held the net freely was recorded and used for evaluation. Each trial was applied six times at 15-min intervals.

Results

Open Field Test

The total distance of movement in the T-S group significantly increased after LFPI surgery ($p < 0.05$). On the other hand, in the other three groups, the distance did not change during the whole experimental period. In the T-M group, administration of SCH58261 significantly blocked hyperlocomotion, which was observed in the T-S group ($p < 0.05$). The total distance of movement in the T-S group was significantly larger than in the other three groups at all time points ($p < 0.05$). There was no significant difference among the T-M, S-M, and S-S groups (Fig. 1). Figure 2 shows a representative alternation of the movement track in each group.

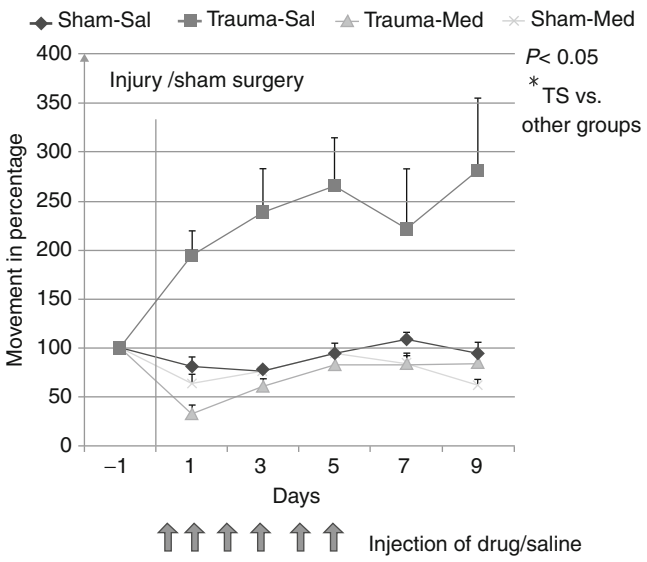

Fig. 1 Open field test: the trauma-saline group moved a greater total distance on all post-trauma days. Administration of SCH58261 reduced hyperlocomotion in the trauma-medication group

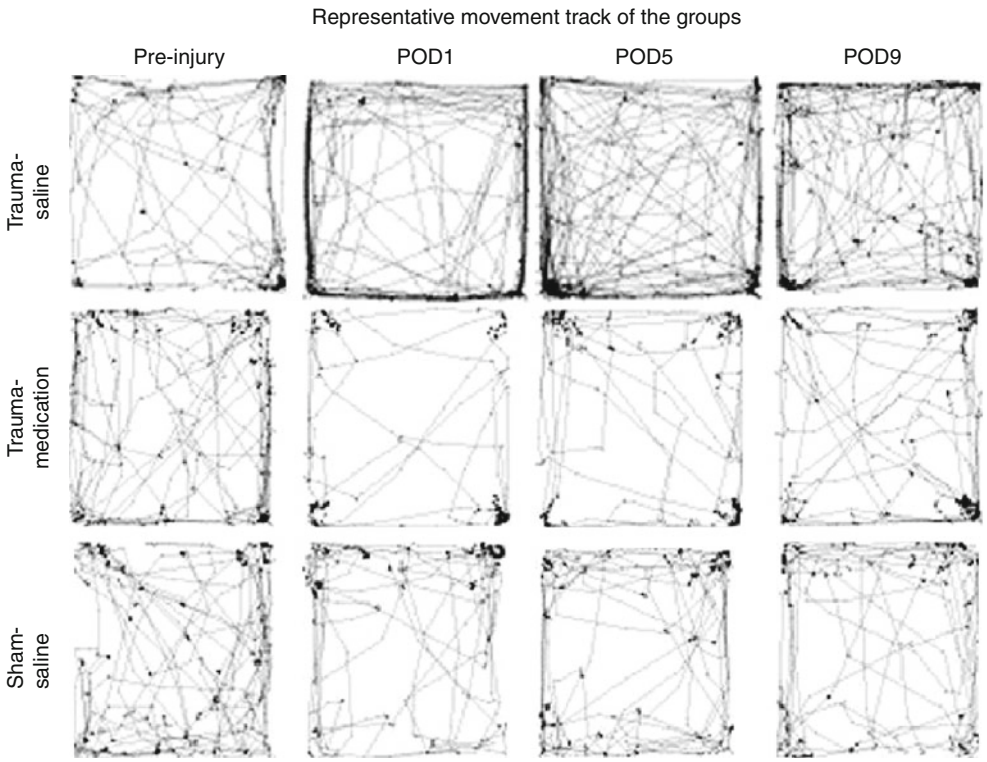

Fig. 2 Representative alteration of the track in each group: the track of the trauma-saline group showed an increase in the locomotion after lateral fluid percussion injury (LFPI). The track of the trauma-medication group showed no alteration over the whole experimental period, similar to that of the sham-saline group

Grabbing Test

Holding time in the T-S group increased significantly on days 3, 5, and 7 ($p<0.05$). In the T-M, S-M, and S-S groups, the time did not change over the whole experimental period. In the T-M group, administration of SCH58261 also significantly blocked the elevation of holding time that was observed in the T-S group ($p<0.05$). The time in the T-S group was significantly longer than in the other three groups at days 3, 5, and 7($p<0.05$). There was no significant difference among the T-M, S-M, and S-S groups (Fig. 3).

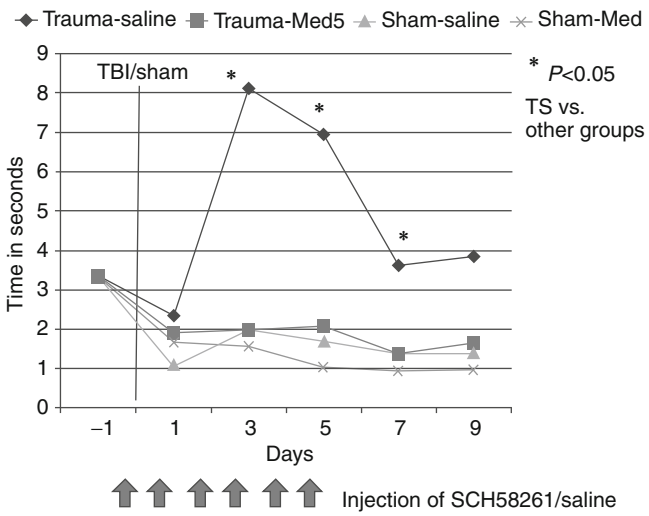

Fig. 3 Grabbing test: the trauma-saline group grabbed the weight for a significantly longer time from 3, 5, and 7 days post-injury compared with the other groups. Medication maintained the grabbing time at a similar length to the sham groups

Conclusion

Traumatic brain injury causes physical, neurological, and emotional/behavioral impairments, which can last for a long period and may prevent the patients returning to normal activity. Development of a new therapeutic method to improve post-traumatic cognitive dysfunction is required to improve patients' outcome, but the effect of the initial impact cannot be managed by medical practices. Therefore, we must have enough knowledge concerning secondary brain damage that might be preventable after patients arrive at the emergency hospital. In the present study, we tried to seek one of biochemical pathways in relation to secondary brain damage through the adenosine A2a receptor.

In the present animal study, we applied two behavioral tests, the open field locomotion test and the grabbing test. Both were established tests for evaluating hyperactivity in Mongolian gerbils. The Hyperactivity in animals is considered to represent a model of the psychological status of human anxiety, lack of inhibition, and working memory impairment. Development of maneuvers to prevent hyperactivity in animal models, therefore, is considered to lead to the development of maneuvers to prevent patients' higher

cognitive dysfunction. In the present study, the adenosine A2a antagonist, SCH58261, improved post-traumatic hyperactivity in two behavioral tests. It suggested that SCH58261 might possess such potential in improving cognitive dysfunction elicited by traumatic brain injury through blocking the pathway to causing secondary brain damage.

Adenosine is supposed to be one of the causes of secondary brain damage. The concentration of extracellular adenosine rises markedly in response to ischemia, hypoxia, toxicity, inflammation, and other brain insults [4], as a result of the depletion of intracellular ATP. Alessia Melani et al. reported that SCH 58261, a specific adenosine A2A receptor antagonist, improved neurological and behavioral outcome after focal ischemia in Mongolian gerbils [5]. They also reported that SCH58261 reduced the elevated extracellular concentration of amino acids, GABA, and other neurotransmitters. It is suggested that an increase in the extracellular adenosine levels might lead to an increase in various neurotransmitters that initiate various hazardous cascades. The mechanism by which SCH58261 improves cognitive impairment is still unclear. We expected SCH58261 to block the binding of increased extracellular adenosine to adenosine A2A receptors, and it caused normalization of the secondary interaction of such neurotransmitter cascades. To clarify this hypothesis, further experiments must be performed.

A specific adenosine A2A receptor antagonist, SCH58261, successfully suppressed the trauma-induced hyperactivity in LFPI gerbils. It suggested that SCH58261 might possess the potential to ameliorate the cognitive dysfunction seen after traumatic brain injury by blocking secondary brain damage.

Acknowledgment This study was supported in part by a medical research grant on traffic accidents from *The General Insurance Association of Japan*.

Conflict of Interest We declare that we have no conflict of interest.

References

1. Dekosky ST, Kochanek PM, Clark RS, Ciallella JR, Dixon CE (1998) Secondary injury after head trauma: subacute and long-term mechanisms. Semin Clin Neuropsychiatry 3:176–185
2. Faden AI (1997) Experimental neurobiology of central nervous system trauma. Crit Rev Neurobiol 7:175–186
3. Li W, Dai S, An J, Li P, Chen X, Xiong R, Liu P, Wang H, Zhao Y, Zhu M, Liu X, Zhu P, Chen JF, Zhou Y (2007) Chronic but not acute treatment with caffeine attenuates traumatic brain injury in the mouse cortical impact model. Neuroscience 151:1198–1207
4. Li S, Kuroiwa T, Katsumata N, Ishihashi S, Sun LY, Endo S, Ohno K (2006) Transient versus prolonged hyperlocotion following lateral fluid percussuion injury in Mongolian gerbils. J Neurosci Res 83:292–300
5. Melani A, Pantone L, Bordoni F, Gianfriddo M, Bianchi L, Vannucchi MG, Bertorelli R, Monopoli A, Pedata F (2003) The selective A2A receptor antagonist SCH 58261 reduces striatal transmitter outflow, turning behavior and ischemic brain damage induced by permanent focal ischemia in the rat. Brain Res 959:243–250
6. Pedata F, Corsi C, Melani A, Bordoni F, Latini S (2001) Adenosine extracellular brain concentrations and role of A2A receptors in ischemia. Ann NY Acad Sci 939:74–84

Cortical Spreading Depression Dynamics Can Be Studied Using Intrinsic Optical Signal Imaging in Gyrencephalic Animal Cortex

Edgar Santos, Michael Schöll, Renan Sanchez-Porras, Modar Kentar, Berk Orakcioglu, Andreas Unterberg, Hartmut Dickhaus, and Oliver W. Sakowitz

Abstract *Objective*: The aim of this study was to co-record electrical changes using electrocorticography (ECoG) and blood volume changes using intrinsic optical signal (IOS) imaging during the induction, propagation, and termination of cortical spreading depolarizations (CSDs).

Methods: Anesthetized male swine were craniotomized and monitored over 16–20 h. A ten-contact electrode strip was placed on the cortex of one hemisphere for ECoG. An optical imaging recording was implemented using a camera with an optical bandpass filter (564 nm, FWHM:15 nm) and a full spectrum light source. CSDs were induced by mechanical and KCl stimulation. Co-occurrences of ECoG baseline shifts and blood volume changes around electrodes were identified.

Results: A mean of 3 CSDs per hour were induced, in a total of 4 swine during 80 h of recording. The propagation of the CSDs increased progressively over the monitoring time. IOS enabled us to clearly visualize the induction, propagation, and termination of CSDs with a spatial resolution within the sub-millimeter range. Every CSD recorded using ECoG could also be observed in IOS imaging, although some blood volume changes of CSDs were observed that terminated before reaching any of the ECoG electrodes.

Conclusion: IOS imaging enables an in vivo evaluation of CSD dynamics over a large surface of gyrencephalic brain.

Keywords Brain ischemia • Cerebral blood flow • Cortical spreading depolarization • Cortical spreading depression • Brain ischemia • Intrinsic optical imaging

Introduction

Cortical spreading depolarization (CSD) is a slowly propagating wave of neuronal and glial depolarization in brain gray matter, at a rate of 2–5 mm/min for several minutes [10]. CSD is observed in the electrocorticogram (ECoG) as a suppression of fast potential changes with an amplitude of 15–30 mV lasting for approximately 1 min in each channel. The electrical changes occurring during CSD are coupled with neurotransmitter-mediated vascular reactions that are translated into changes in regional cerebral blood flow (rCBF). In the physiological scenario, rCBF increased by more than 100 %, which is called spreading hyperemia. In pathological scenarios, such as the hypoperfused area surrounding an infarction, an inverse coupling can occur, leading to vasoconstriction and tissue ischemia, increasing the size of the infarcts [7].

Although research into CSDs started in 1944, most of the physiological knowledge that we have is from lissencephalic brains [13]. Electrophysiological evidence has only just recently clarified that CSDs can occur in human neocortex affected by traumatic or ischemic injury [14]. Since that discovery, CSDs have been extensively documented in stroke [4], subarachnoid hemorrhage [6], and head trauma [8].

The CSD dynamics, especially with regard to how the CSD travels through a gyrencepalic brain, is not well known. Basically, gyrencephalic brains have a different gray and white matter configuration, and different proportions of glial cells and sulcus that could prevent CSD

E. Santos, MD (✉)
Department of Neurosurgery, University Hospital Heidelberg, Im Neuenheimer Feld 400, 69120 Heidelberg, Germany
e-mail: edgar.santos@med.uni-heidelberg.de

M. Schöll and H. Dickhaus
Department of Neurosurgery, University Hospital Heidelberg, Heidelberg, Germany

R. Sanchez-Porras, M. Kentar, B. Orakcioglu, A. Unterberg, and O.W. Sakowitz
Department of Neurosurgery, University Hospital Heidelberg, Heidelberg, Germany

The authors Edgar Santos and Michael Schoell contributed equally to this chapter

Y. Katayama et al. (eds.), *Brain Edema XV*, Acta Neurochirurgica Supplement, Vol. 118,
DOI 10.1007/978-3-7091-1434-6_16, © Springer-Verlag Wien 2013

propagation [13]. In the cat and monkey there are some regions where CSDs could not be detected, so maybe some parts of the brain are less prone to CSD propagation [11, 15] and CSD propagation decelerates in the sulci of gyrencephalic porcine brain [1].

The movement and dynamics of cortical spreading depolarizations (CSDs) in gyrencephalic brain have been unknown up to now. It is likely that the use of swine gyrencephalic brain, rather than rodent lissencephalic brain, provides closer comparability to the human cerebral cortex.

An optical method is required to evaluate the CSD dynamics through the gyrencephalic cortex, since all that we know about the CSD dynamics in humans are simple theoretical deductions based on animal brain experiments (mostly lissencephalic), chicken retinas, and fMRI in humans [3].

The objective of this work is to pilot test a visual method, intrinsic optical signal (IOS) imaging, to detect hemoglobin differences as a surrogate for cerebral blood volume changes in the cortex surface of swine brains during CSD induction.

Materials and Methods

Animal Preparation

Animal protocols for the experiments were approved by the Institutional Animal Care and Use Committee. A standardized operative set-up was followed, as described elsewhere [12].

Four male swine with an average mean weight of 30 kg were anesthetized with midazolam (8 mg/kg) and azaperone (60 mg/kg) administered by intramuscular injection, followed by a 10- to 20-mg intravenous application of midazolam. Animals were orally intubated and mechanically ventilated ($FiO_2 = 0.3$). Anaesthesia was maintained using 1.5 % isoflurane inhalation. Rectal and brain temperature were continuously monitored. Rectal temperature was maintained between 35.5 and 37 °C. After surgical exposure of the right femoral artery a 4-Fr catheter was placed for permanent monitoring of mean arterial blood pressure. A venous line was placed in the right ear vein and capillary oxygen saturation (SO_2) was monitored from one ear.

Operative Procedure

An extensive craniectomy and dura mater excision were performed to visualize the subarachnoidal space unilaterally or bilaterally in two animals each. The heads of the animals were firmly held in a self-made head holder. The brains were perfused for 5 min once, with an elevated K + concentration (7 mMol/L) in the standard ringer lactate solution at the beginning of the experiment, to make the brain more prone to CSD induction as proposed by Bowyer [1]. A strip of ten electrodes was placed on the cortex surface. The brains were regularly perfused with simple ringer lactate solution throughout the entire experiment to avoid water loss from the tissue.

Monitoring

All relevant physiological parameters, such as mean arterial pressure, brain and rectal temperature, heart rate and oxygen saturation, were continuously recorded. Blood–gas analyses were performed every 2–3 h.

Electrocorticography monitoring at 1,024 Hz sampling rate was recorded using a DC amplifier (Refa 8, TMSi) and the recording was saved with the PortiLab 2 software. A 1 W full-spectrum white light LED illumination was used to illuminate the brain surface. An optical bandpass filter (564 nm, 15 nm FWHM) was fixed in front of the objective of a camera (Giganetix GigE Vision Kamera, 1/1.8" Sony CCD, S/W, 1,628 × 1,236 (UXGA), 25 fps). The camera with the filter was fixed 20–30 cm above the head. Two 8-bit gray-scale images of 2 megapixels were taken every second.

CSD Induction

The CSD were induced mechanically using a 0.5-mm diameter wire with a small drop of KCl (7 mMol/L) at the tip. The inductions were carried out three times per hour throughout the entire experiment, in the first and second experiments. They were induced only during the initial 6 h during the third and fourth experiments.

Analysis

The sequence of pictures was matched to a manually chosen reference image to compensate for motion artifacts caused by mechanical ventilation and heartbeat. The differences in image intensities caused by cortical blood volume changes were amplified by differentiation along the time axis and

multiplication with a scaling factor to emphasise the wave front of the CSD. Our software allowed us to analyze IOS imaging and ECoG at the same time.

Results

In total 80 h of monitoring time were obtained from four swine in the first and second experiments, the cortex was chemically stimulated approximately three times per hour. The first CSD was detected 4 and 6 h after preconditioning. Since the success of CSD induction and distance of propagation increased over time, in the third and fourth experiments, the time between one stimulation and the next was increased after 12 h from three times per hour to once per hour and ceased after 16 h. Here, the first CSDs were detected within the range of 6–8 h after preconditioning. Some CSDs were even detected some hours after the last stimulation. The duration of each experiment was within the range of 19–24 h.

Using both methods simultaneously, 52 CSDs were detected. However, there were some more CSDs that could be visualized using IOS imaging and were not reflected in any of the electrodes because the CSD stopped propagation before reaching an electrode.

Intrinsic optical signal optical imaging enabled us to clearly visualize the induction, propagation, and termination of CSDs over a large cortex surface with a spatial resolution in millimeters (Fig. 1). It was possible to zoom in and focus on some areas of interest. During the analysis, the intensity of the signal in proportion to a reference picture could be quantified in given areas. In all cases, when a CSD was recorded using ECoG, a corresponding change in gray-scale intensity was observed in the surrounding area of the corresponding electrode (Fig. 2). Most of these waves were biphasic with an initial episode of brief hypoperfusion followed by sustained hyperperfusion.

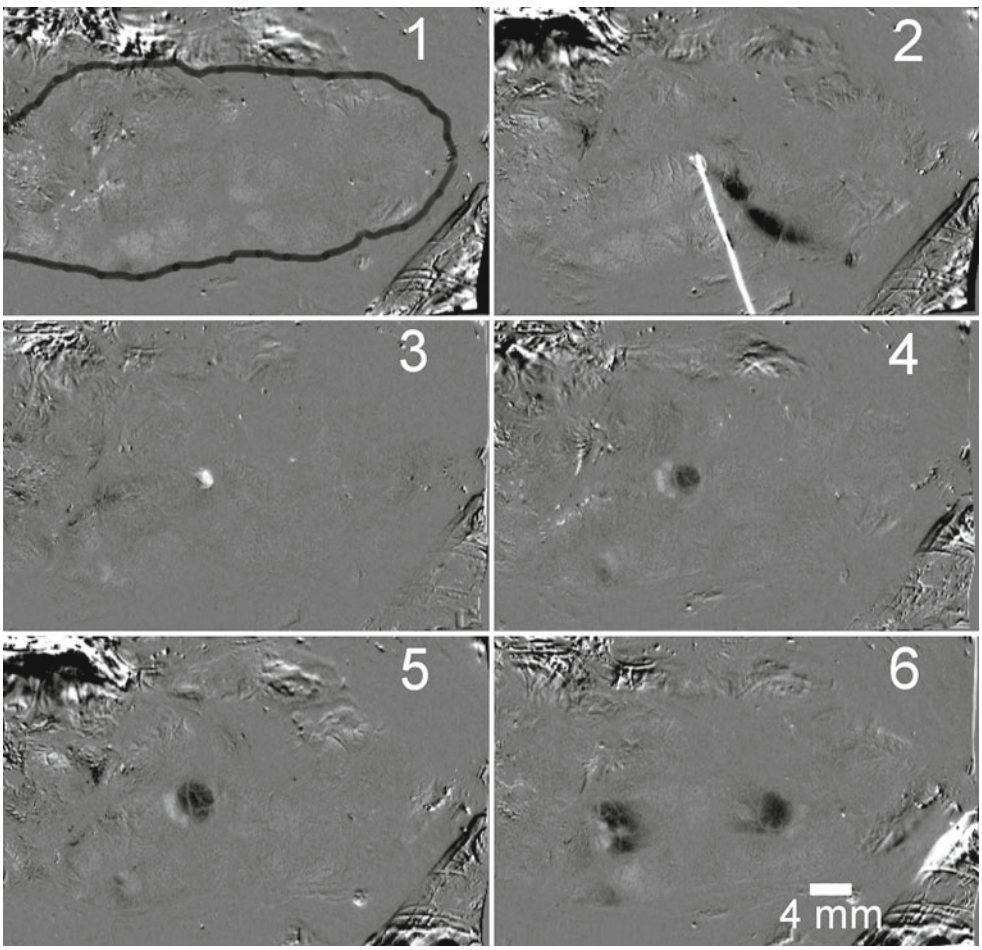

Fig. 1 This is a sequence of 30-s interval pictures. Intensities reflect changes in the cortical blood volume in comparison to cortical blood volume at a time point 20 s before the current picture. Higher intensity reflects the lower blood volume and vice versa. The electrodes were removed to allow better visualization of the phenomenon. *1*: The left hemisphere seen from above. *2*: The metal wire touched the brain surface and created a black shadow. *3*: A vasoconstriction response occurred at the location previously stimulated. *4* and *5*: A vasodilatation wave is orientated in the ventral direction, followed by hyperemia. *6*: A second component of the wave appears on the other side of a sulcus propagating in the opposite direction

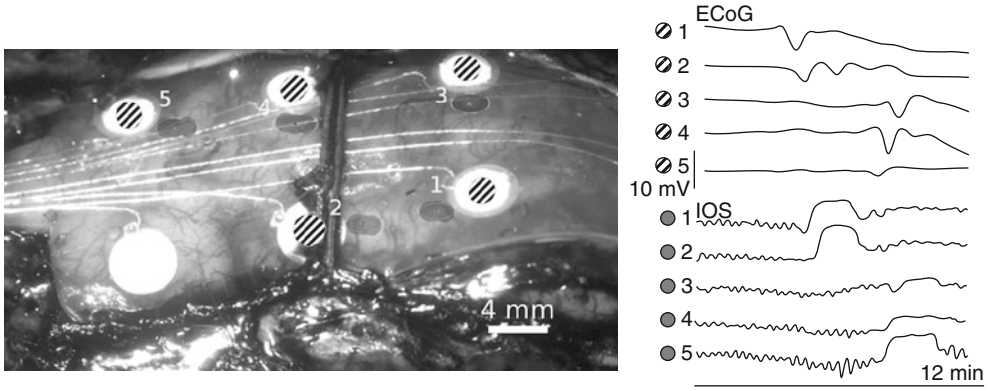

Fig. 2 Reference image, in which we can see the position of six electrodes. The electrocorticography (*ECoG*) recording over 12 min is presented using a slow-pass filter (0.05 Hz). Simultaneously, the black intensity difference (blood volume difference) was quantified and presented simultaneously with the ECoG recording at some points close to the electrodes, using intrinsic optical signal (*IOS*) imaging. Biphasic waves can be seen in channels *1* and *5*. All waves documented by IOS imaging had such a good correlation with the ECoG changes

Conclusion

We have shown that it is possible to detect the change in blood volume associated with CSDs using a visual method that uses a camera with band-pass filter. Problems caused by motion artifacts could be eliminated by custom-developed software that compensates for all movements throughout all the experiments.

We found a perfect correlation between the electrophysiological detection of CSD and the visual detection of the hyperemic wave, with a biphasic component that reflects fast vasoconstriction followed by prolonged vasodilatation. This method enhances the study of the CSD dynamics in the gyrencephalic brain in vivo and demonstrates that CSD can be monitored over several square centimeters of brain surface.

Although CSDs could be detected reliably, some conditions were required beforehand. The first CSD typically did not appear until several hours after preconditioning with high K + solution (7 mMol/L). In general, the brain became more prone to CSDs and the distance that CSDs traveled tended to be longer at the end of the experiment. In the last two experiments, we decreased the frequency of the CSD stimulation and at some point we stopped the stimulation and continued recording. Surprisingly, we observed that some CSDs appeared spontaneously and other CSDs travelled a longer distance (more than 10 cm) and were able to cycle and return to the same place. One possibility that may explain the fact that the brain was more prone to CSDs at the end of the experiment, is the neurotoxic potential of the high K + concentrations, which typically produces a prolonged DC potential depression initiated by a periodic burst of unstable CSD [9]. A second explanation could be brain injury created simply by prolonged exposure of the brain to air during the experiment. Although the brain was periodically perfused with lactated Ringer's solution, this unphysiologic condition could have caused some dehydratation of brain tissues. A third explanation could be the facilitating effect of initial CSDs. CSD is able to increase the pericellular K + concentration and concentrations as high as 60–80 mMol/L can be reached [2].

In agreement with the literature, CSD tended to be limited by deep sulci and fissures [13]. CSDs did not always pass through them. When many CSDs originated spontaneously it was not possible to see whether the CSDs were the continuation of one wave or the initiation of a new one. Movement of CSDs was defined mainly by the shape of the gyri.

We detected biphasic waves of blood volume changes by IOS imaging. A small component of hypoperfusion was seen in most of the waves and was followed by a longer lasting hyperperfusion component. This technique could be useful in detecting spreading ischemia and the factors associated with the inverse hemodynamic response [5–7].

A major disadvantage of this method in comparison to the ECoG is that a craniotomy and exposure of the subarachnoid space is required to visualize the blood changes described. A second disadvantage is that the presence of subarachnoid blood prevents blood volume detection on the brain surface. Nevertheless, in our experiments we avoided areas with even minimal subarachnoid hemorrhage (e.g., because of the surgical preparation of the dura mater).

This method may enable the investigation of the modulation of the spatio-temporal properties of CSD by pharmacological compounds in the gyrencephalic brain in vivo.

In summary, we are able to detect changes in blood volume associated with CSDs, employing an imaging technique to visualize intrinsic optical (hemoglobin) signals. This enables in vivo identification of CSD dynamics with high spatial and temporal resolution

Conflict of Interest We declare that we have no conflict of interest.

References

1. Bowyer SM, Tepley N, Papuashvili N, Kato S, Barkley GL, Welch KM, Okada YC (1999) Analysis of MEG signals of spreading cortical depression with propagation constrained to a rectangular cortical strip. II. Gyrencephalic swine model. Brain Res 843:79–86
2. Canals S, Makarova I, López-Aguado L, Largo C, Ibarz JM, Herreras O (2005) Longitudinal depolarization gradients along the somatodendritic axis of CA1 pyramidal cells: a novel feature of spreading depression. J Neurophysiol 94:943–951
3. Dahlem MA, Hadjikhani N (2009) Migraine aura: retracting particle-like waves in weakly susceptible cortex. PLoS One 4:e5007
4. Dohmen C, Sakowitz OW, Fabricius M, Bosche B, Reithmeier T, Ernestus RI, Brinker G, Dreier JP, Woitzik J, Strong AJ, Graf R (2008) Spreading depolarizations occur in human ischemic stroke with high incidence. Ann Neurol 63:720–728
5. Dreier JP, Major S, Manning A, Woitzik J, Drenckhahn C, Steinbrink J, Tolias C, Oliveira-Ferreira AI, Fabricius M, Hartings JA, Vajkoczy P, Lauritzen M, Dirnagl U, Bohner G, Strong AJ (2009) Cortical spreading ischaemia is a novel process involved in ischaemic damage in patients with aneurysmal subarachnoid haemorrhage. Brain 132:1866–1881
6. Dreier JP, Petzold G, Tille K, Lindauer U, Arnold G, Heinemann U, Einhäupl KM, Dirnagl U (2001) Ischaemia triggered by spreading neuronal activation is inhibited by vasodilators in rats. J Physiol 531:515–526
7. Dreier JP (2011) The role of spreading depression, spreading depolarization and spreading ischemia in neurological disease. Nat Med 17:439–447
8. Hartings JA, Watanabe T, Bullock MR, Okonkwo DO, Fabricius M, Woitzik J, Dreier JP, Puccio A, Shutter LA, Pahl C, Strong AJ (2011) Spreading depolarizations have prolonged direct current shifts and are associated with poor outcome in brain trauma. Brain 134:1529–1540
9. Herreras O, Somjen GG (1993) Effects of prolonged elevation of potassium on hippocampus of anesthetized rats. Brain Res 617:194–204
10. Leão AAP (1978) Spreading depression of activity in the cerebral cortex. J Neurophysiol 7:359–390
11. Marshall WH (1959) Spreading cortical depression of Leao. Physiol Rev 39:239–279
12. Orakcioglu B, Sakowitz OW, Neumann JO, Kentar MM, Unterberg A, Kiening KL (2010) Evaluation of a novel brain tissue oxygenation probe in an experimental swine model. Neurosurgery 67:1716–1722
13. Smith JM, Bradley DP, James MF, Huang CL (2006) Physiological studies of cortical spreading depression. Biol Rev Camb Philos Soc 81:457–481
14. Strong AJ, Fabricius M, Boutelle MG, Hibbins SJ, Hopwood SE, Jones R, Parkin MC, Lauritzen M (2002) Spreading and synchronous depressions of cortical activity in acutely injured human brain. Stroke 33:2738–2743
15. Tower DB, Young OM (1973) The activities of butyrylcholinesterase and carbonic anhydrase, the rate of anaerobic glycolysis, and the question of a constant density of glial cells in cerebral cortices of various mammalian species from mouse to whale. J Neurochem 20:269–278

A Better Mild Traumatic Brain Injury Model in the Rat

Satoru Takeuchi, Hiroshi Nawashiro, Shunichi Sato, Satoko Kawauchi, Kimihiro Nagatani, Hiroaki Kobayashi, Naoki Otani, Hideo Osada, Kojiro Wada, and Katsuji Shima

Abstract The primary pathology associated with mild traumatic brain injury (TBI) is selective axonal injury, which may characterize the vast majority of blast-induced TBIs. Axonal injuries in cases of mild TBI have been considered to be the main factors responsible for the long-lasting memory or attentional impairment in affected subjects. Among these axonal injuries, recent attention has been focused on the cingulum bundle (CB). Furthermore, recent studies with diffusion tensor MR imaging have shown the presence of injuries of the CB in cases of mild TBI in humans. This study aimed to provide a better laboratory model of mild TBI.

Sprague–Dawley rats were subjected to mild TBI using laser-induced shock waves (LISW) (sham, 0.5 J/cm2, or 1.0 J/cm2; n = 4 per group). Bodian-stained brain sections 14 days after LISW at 0.5 J/cm2 or 1.0 J/cm2 showed a decrease in the CB axonal density compared with the sham group, whereas there were no differences in the axonal density of the corpus callosum.

The present study shows that this model is capable of reproducing the histological changes associated with mild TBI.

Keywords Traumatic brain injury • Cingulum bundle • Laser-induced shock wave • Animal model

S. Takeuchi (✉), H. Nawashiro, K. Nagatani, H. Kobayashi
N. Otani, H. Osada, K. Wada, and K. Shima
Department of Neurosurgery,
National Defense Medical College,
3-2 Namiki, Tokorozawa, Saitama 359-8513, Japan
e-mail: s.takeuchi@room.ocn.ne.jp

S. Sato and S. Kawauchi
Division of Biomedical Information Sciences,
National Defense Medical College,
3-2 Namiki, Tokorozawa, Saitama 359-8513, Japan

Introduction

Identification of mild traumatic brain injury (TBI) is challenging. The primary pathology associated with mild TBI is selective axonal injury, which may characterize the vast majority of blast-induced TBIs [2, 8, 9]. Axonal injuries in blast-induced TBIs have been considered to be the main factors responsible for the long-term memory or attentional impairment observed in affected subjects [4, 8, 15]. Among these axonal injuries, recent attention has been focused on the cingulum bundle (CB), because the CB connects the anterior thalamic nuclei with the hippocampal region and is involved in attention, emotions, spatial orientation, and memory. Furthermore, recent studies with diffusion tensor MR imaging have shown the presence of injuries of the CB in cases of mild TBI in humans [8, 13, 15]. The aim of this study was to generate a new model of blast-induced TBI.

Materials and Methods

Animal Procedure

All experimental procedures were approved by the Animal Care and Use Committee of the National Defense Medical College. Adult male Sprague–Dawley rats (weighing 300–400 g) were used. Rats were housed in individual cages under controlled environmental conditions (12/12 h light/dark cycle, 20–22 °C; room temperature) with food and water freely available, for 1 week before the experimental procedure. The rats were anesthetized with sodium pentobarbital (50 mg/kg, intraperitoneally) prior to the procedure.

A 4.8-mm craniectomy was made over the right parietal cortex, midway between the bregma and lambda, thereby leaving the dura mater intact. We used a laser-induced shock waves (LISW) to induce TBI in rats after randomly dividing

Y. Katayama et al. (eds.), *Brain Edema XV*, Acta Neurochirurgica Supplement, Vol. 118,
DOI 10.1007/978-3-7091-1434-6_17,

the rats into three groups (sham, 0.5 J/cm^2, or 1.0 J/cm^2; $n=4$ per group). An LISW was generated by the irradiation of an elastic laser target with 532-nm nanosecond laser pulses of a Q-switched Nd:YAG laser [3, 11].

Following these procedures, the scalp was sutured, and the rats were returned to their home cages with food and water available ad libitum.

Neuropathology

Fourteen days after the LISW application, after the intraperitoneal injection of pentobarbital sodium, the rats were transcardially perfused with normal saline, followed by 4 % buffered paraformaldehyde. The brains were removed just after perfusion and immersed in 4 % buffered paraformaldehyde overnight, and were then embedded in paraffin. The 5 μm-thick coronal sections 3.8 mm posterior to the bregma were used for Bodian silver staining.

Results

A macroscopic examination of the brains showed no abnormalities of the cerebral cortex in any of the animals. Bodian-stained brain sections 14 days after the application of a 0.5 J/cm^2 or 1.0 J/cm^2 LISW showed a decrease in the CB axonal density compared with the sham group, whereas there were no differences in the axonal density of the corpus callosum (Fig. 1).

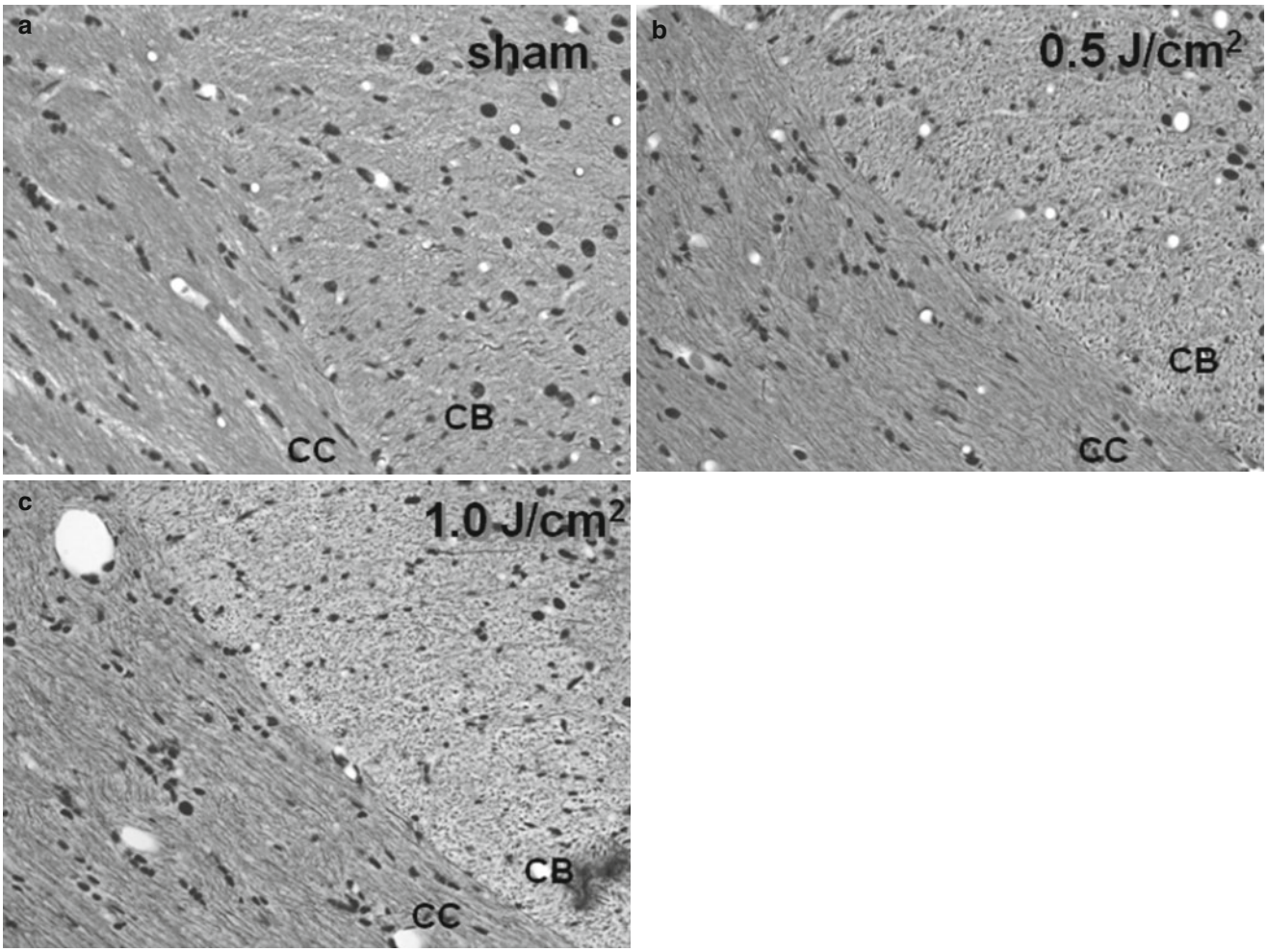

Fig. 1 Bodian silver immunostaining 14 days after laser-induced shock waves (LISW) (**a**: sham, **b**: 0.5 J/cm^2, and **c**: 1.0 J/cm^2). *CB* cingulum bundle, *CC* corpus callosum

Conclusion

Mild TBI is a major medical concern [8, 9]. The primary pathology associated with mild TBI is selective axonal injury, which characterizes the vast majority of blast-induced TBIs [2, 9]. Recent trends in global terrorism raise significant concerns about the potential increases in civilian casualties, as well as the effects on soldiers, caused by blast-induced TBI [8, 9, 14].

According to the US Centers for Disease Control and Prevention, blast injury involves four different phases: (1) a primary injury phase resulting from blast overpressure waves; (2) a secondary injury phase occurring from the penetration of shrapnel due to the blast; (3) a tertiary phase from head movement or acceleration due to blast wind and the resulting impact; and (4) a quaternary phase of injury resulting from toxic gases or thermal burn injuries. Clinical studies suggest that primary blast exposure causes blast-induced TBI and subsequent neuropsychiatric impairment [5].

Memory or attentional impairment is the most frequent cognitive sequela long after blast-induced TBI [4, 9, 15]. However, the identification of the causative lesion is challenging, because in many cases, common CT or MRI is unable to detect the abnormality. Recent studies using diffusion tensor MR imaging have indicated that the CB is vulnerable to mild TBI and may contribute to the cognitive sequelae [15].

Many animal models of TBI have been reported. However, although cerebral contusions can be often seen in those models, they cannot mimic the mild TBI in patients whose common CT and MRI show normal findings [1, 6, 7, 12]. Therefore, a new animal model is required to investigate the pathophysiology of blast-induced TBI.

The present study showed that LISW can reproduce the histological changes of blast-induced mild TBI, without resulting in any cerebral contusions. The apparatus used to generate the LISW is more compact, easier to use, and more readily controllable than other devices [3]. Neave et al. reported that the disruption of the CB was responsible for impairments in the T-maze and radial-arm maze performance by rats [10]. These maze tests can also be used to investigate the neurological behavior in our model.

In conclusion, the present study shows that the LISW-based rat model is capable of reproducing the histological changes associated with blast-induced TBIs. This model may therefore help to elucidate the mechanisms responsible for the sequelae of blast-induced TBIs, and may also assist in the development of new therapeutic approaches.

Acknowledgments This study was supported by a research grant from The General Insurance Association of Japan.

Conflict of Interest We declare that we have no conflict of interest.

References

1. Cheng J, Gu J, Ma Y, Yang T, Kuang Y, Li B, Kang J (2010) Development of a rat model for studying blast-induced traumatic brain injury. J Neurol Sci 294:23–28
2. Desmoulin GT, Dionne JP (2009) Blast-induced neurotrauma: surrogate use, loading mechanisms, and cellular responses. J Trauma 67:1113–1122
3. Hatano B, Matsumoto Y, Otani N, Saitoh D, Tokuno S, Satoh Y, Nawashiro H, Matsushita Y, Sato S (2011) Traumatic brain injury caused by laser-induced shock wave in rats: a novel laboratory model for studying blast-induced traumatic brain injury. Proc SPIE 7897:78971V. doi:10.1117/12.875909
4. Hicks RR, Fertig SJ, Desrocher RE, Koroshetz WJ, Pancrazio JJ (2010) Neurological effects of blast injury. J Trauma 68:1257–1263
5. Kocsis JD, Tessler A (2009) Pathology of blast-related brain injury. J Rehabil Res Dev 46:667–672
6. Koliatsos VE, Cernak I, Xu L, Song Y, Savonenko A, Crain BJ, Eberhart CG, Frangakis CE, Melnikova T, Kim H, Lee D (2011) A mouse model of blast injury to brain: initial pathological, neuropathological, and behavioral characterization. J Neuropathol Exp Neurol 70:399–416
7. Long JB, Bentley TL, Wessner KA, Cerone C, Sweeney S, Bauman RA (2009) Blast overpressure in rats: recreating a battlefield injury in the laboratory. J Neurotrauma 26:827–840
8. Mac Donald CL, Johnson AM, Cooper D, Nelson EC, Werner NJ, Shimony JS, Snyder AZ, Raichle ME, Witherow JR, Fang R, Flaherty SF, Brody DL (2011) Detection of blast-related traumatic brain injury in U.S. military personnel. N Engl J Med 364: 2091–2100
9. Matsumoto Y, Hatano B, Matsushita Y, Nawashiro H, Shima K (2010) The characteristics of blast traumatic brain injury. No Shinkei Geka 38:695–702
10. Neave N, Nagle S, Aggleton JP (1997) Evidence for the involvement of the mammillary bodies and cingulum bundle in allocentric spatial processing by rats. Eur J Neurosci 9:941–955
11. Satoh Y, Sato S, Saitoh D, Tokuno S, Hatano B, Shimokawaji T, Kobayashi H, Takishima K (2010) Pulmonary blast injury in mice: a novel model for studying blast injury in the laboratory using laser-induced stress waves. Lasers Surg Med 42:313–318
12. Svetlov SI, Prima V, Kirk DR, Gutierrez H, Curley KC, Hayes RL, Wang KK (2010) Morphologic and biochemical characterization of brain injury in a model of controlled blast overpressure exposure. J Trauma 69:795–804
13. Takeuchi S, Nawashiro H (2011) Atrophy after traumatic axonal injury. Arch Neurol 68:1090
14. Walilko T, North C, Young LA, Lux WE, Warden DL, Jaffee MS, Moore DF (2009) Head injury as a PTSD predictor among Oklahoma City bombing survivors. J Trauma 67:1311–1319
15. Wu TC, Wilde EA, Bigler ED, Yallampalli R, McCauley SR, Troyanskaya M, Chu Z, Li X, Hanten G, Hunter JV, Levin HS (2010) Evaluating the relationship between memory functioning and cingulum bundles in acute mild traumatic brain injury using diffusion tensor imaging. J Neurotrauma 27:303–307

Edaravone Increases Regional Cerebral Blood Flow After Traumatic Brain Injury in Mice

Kazuyuki Miyamoto, Hirokazu Ohtaki, Kenji Dohi, Tomomi Tsumuraya, Hiroyasu Nakano, Keisuke Kiriyama, Dandan Song, Tohru Aruga, and Seiji Shioda

Abstract Traumatic brain injury (TBI) is a major cause of preventable death and serious morbidity, with subsequent low cerebral blood flow (CBF) considered to be associated with poor prognosis. In the present study, we demonstrated the effect of the free radical scavenger edaravone on regional CBF (rCBF) after TBI. Male mice (C57/BL6) were subjected to TBI using a controlled cortical impactor device. Immediately after TBI, the animals were intravenously administered 3.0 mg/kg of edaravone or a vehicle saline solution. Two-dimensional rCBF images were acquired before and 24 h post-TBI, and were quantified in the ipsilateral and contralateral hemispheres ($n=5$ animals per group). CBF in the vehicle-treated animals decreased broadly over the ipsilateral hemisphere, with the region of low rCBF spreading from the frontal cortex to the occipital lobe. The zone of lowest rCBF matched that of the contusion area. The mean rCBF at 24 h for a defined elliptical region between the bregma and lambda was 73.7 ± 5.8 %. In comparison, the reduction of rCBF in edaravone-treated animals was significantly attenuated (93.4 ± 5.7 %, $p<0.05$). The edaravone-treated animals also exhibited higher rCBF in the contralateral hemisphere compared with that seen in vehicle-treated animals. It is suggested that edaravone reduces neuronal damage by scavenging reactive oxygen species (ROS) and by maintaining intact the autoregulation of the cerebral vasculature.

Keywords TBI • Regional cerebral blood flow • Edaravone • Nitric oxide • Autoregulation

Introduction

Traumatic brain injury (TBI) is a major cause of preventable death and serious morbidity in affected persons for which no effective treatment exists other than supportive care [7]. It has been recognized that low cerebral blood flow (CBF) and low cerebral perfusion pressure (CPP) are associated with poor prognosis after TBI [36]. Cerebral blood pressure is maintained at a homeostatic level as a consequence of the autoregulation of cerebral vasculature across a wide range (50–150 mmHg) of mean arterial blood pressure (MAP) values. However, the autoregulation of the cerebral circulation is disrupted in about 30–80 % of patients following the onset of severe TBI, and delayed recovery of the autoregulation is associated with poor prognosis, even though hypoperfusion may have recovered somewhat in the first 2 weeks after injury [4, 32]. Previous studies have reported that rats exhibited decreased regional CBF (rCBF) after TBI, and may suffer from neuronal damage owing to the ischemic condition [8, 26, 28, 38]. These results suggested that the ischemic condition after TBI might be involved in the induction of neuronal cell death.

Edaravone (3-Methyl-1-phenyl-2-pyrazolin-5-one) is the only medicine approved for use in Japan as a potent free radical scavenger for the treatment of acute cerebral infarction [17, 35]. Edaravone reduces the reactive oxygen species (ROS) and reactive oxygen nitrogen (RON) content, and protects against neuronal cell injury [30, 40]. We have previously reported that edaravone treatment suppressed neuronal

K. Miyamoto
Department of Anatomy, Showa University School of Medicine, 1-5-8 Hatanodai, Shinagawa-Ku, Tokyo 142-8555, Japan

Department of Emergency and Critical Care Medicine, Showa University School of Medicine, Shinagawa-Ku, Tokyo 142-8555, Japan

H. Ohtaki, T. Tsumuraya, H. Nakano, K. Kiriyama, D. Song, and S. Shioda (✉)
Department of Anatomy, Showa University School of Medicine, 1-5-8 Hatanodai, Shinagawa-Ku, Tokyo 142-8555, Japan
e-mail: shioda@med.showa-u.ac.jp

K. Dohi and T. Aruga
Department of Emergency and Critical Care Medicine, Showa University School of Medicine, Shinagawa-Ku, Tokyo 142-8555, Japan

Y. Katayama et al. (eds.), *Brain Edema XV*, Acta Neurochirurgica Supplement, Vol. 118,
DOI 10.1007/978-3-7091-1434-6_18, © Springer-Verlag Wien 2013

damage after TBI in addition to reducing the level of ROS [10]. Other animal studies also supported our findings by showing that edaravone suppressed retinal damage, spinal cord injury, and TBI by decreasing the level of oxidative stress [2, 15, 34].

Recently, several studies have suggested that edaravone increases blood flow. In coronary arthrosclerosis patients, for example, edaravone treatment increased the acetylcholine-mediated coronary blood flow response [27]. Edaravone also increased microvascular nitric oxide (NO) levels in response to exposure to acetylcholine, and preserved blood flow via coronary microvasculature dilation after cardiac ischemia/reperfusion in dogs [31]. It is also known that administration of L-arginine, which is a substrate for NO synthesis, and the calcium channel antagonist verapamil, improves rCBF and reduces neuronal cell injury, thereby improving outcomes in many rodent models of TBI [9, 12, 14, 19, 22, 33].

However, the effect of edaravone on rCBF after TBI has yet to be determined [3]. The aim of the present study was to use a rodent TBI model to determine rCBF after TBI, and to examine the capacity of edaravone to improve rCBF in this model.

Materials and Methods

Animals

Young adult male C57/BL6J mice (aged 8–12 weeks) purchased from the Oriental Yeast Co., Ltd (Tokyo, Japan) were used in the studies. The animals were allowed free access to food and water and were maintained on a 12-h light/dark cycle at 23 ºC with constant humidity (40 ± 15 %). All experimental procedures involving animals were approved by the Institutional Animal Care and Use Committee of Showa University (#00158).

Controlled Cortical Impact Model

Anesthesia was induced by inhalation of 2.0 % sevoflurane in 70 % N_2O and 30 % O_2. Anesthetized mice were mounted on a computer-guided stereotaxic system (Leica Angle Two; Leica Microsystems, Wetzlar, Germany) fitted with an electromagnetic controlled cortical impact (CCI) device (Benchmark Stereotaxic Impactor; Leica Microsystems). Following a midline scalp incision, the bregma was identified, and a 4-mm^2 craniotomy was drilled over the right parietotemporal cortex 3.0 mm laterally from the sagittal suture and 2.0 mm caudally from the bregma (Fig. 1). The CCI device, which has a rounded tip of 1.0 mm in diameter, was positioned on the exposed dura mater. The CCI was at a depth of 1.0 mm from the dura mater with a 3.7-ms stroke velocity [6]. After the impact, bleeding was carefully controlled using a cotton swab, a small piece of artificial dura (4 mm in diameter; GORE Preclude; W.L. Gore & Associates, Newark, NJ, USA) was placed over the brain injury site, and the skull was closed with a plate of dental cement measuring 5 mm in diameter (GC Fuji I; GC Corporation, Tokyo, Japan). The core body temperature of the animals was maintained at 37 ºC during the experiment.

Administration of Edaravone

The free radical scavenger edaravone, a gift from Mitsubishi Tanabe Pharma (Osaka, Japan), was dissolved in sterile saline solution on the day of use. Immediately after TBI by CCI, anesthetized animals were administered 3.0 mg/kg body weight of edaravone (total volume: 100–150 μL volume) or vehicle into the left jugular vein and then left to recover.

Measurement of rCBF

The rCBF in the cerebrum of mice ($n = 5$ in each group) was measured before and 24 h after TBI using a laser Doppler perfusion imager (PeriScan PIMII; Perimed, Järfälla, Sweden). The laser probe (0.1 mm in diameter) of the scanning imager was centered between the bregma and the lambda, 14 cm above the skull. The region to be scanned and scanning time were 40 × 45 mm and 90 s respectively. The mouse under investigation was laid in a prone position and anesthetized with 2.0 % sevoflurane by inhalation. The head was positioned within a three-dimensional stereotaxic frame and the pre-TBI rCBF was measured three times to give an average. The animal was then subjected to TBI as described above and then placed into a recovery cage. Twenty-four hours after TBI, the rCBF was again measured in the same manner. To determine the positional relationship between the brain injury and the rCBF images, black dots measuring 0.5 mm in diameter were marked with black felt pen on the bregma and lambda; the rCBF cannot be detected here because the infrared laser light is absorbed by the black dots. Then, comparison of rCBF in the contralateral and ipsilateral hemispheres was performed as follows. An ellipse (4.0 × 2.0 mm) was drawn 3.0 mm laterally from the sagittal suture and 2.0 mm caudally to the bregma on each side (Fig. 1). The rCBF was then measured from 185 to 187 CBF data points and calculated as a percentage of the control value.

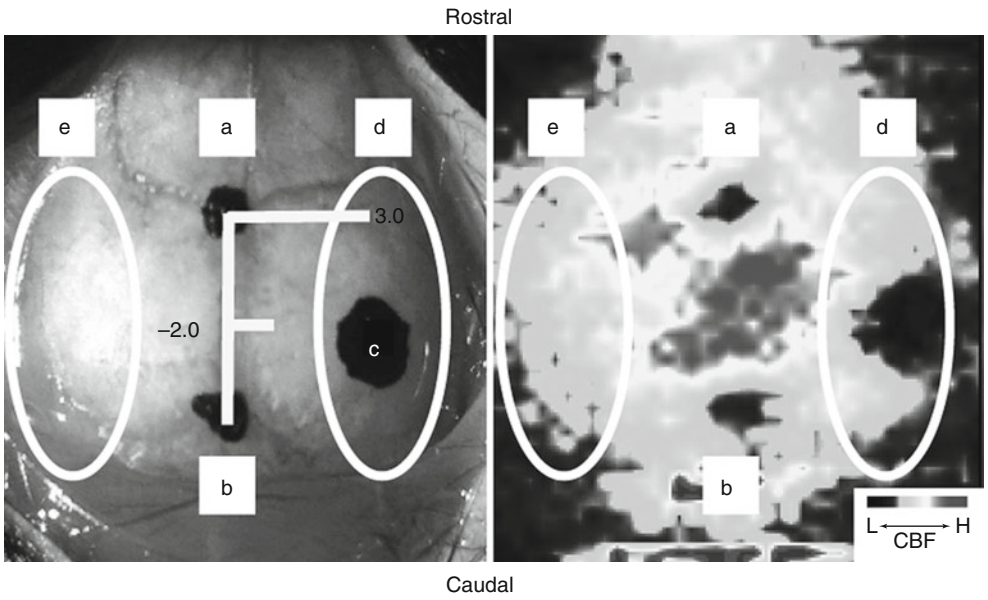

Fig. 1 Brain image (*left*) was photographed and compared with a scanned cerebral blood flow (CBF) image (*right*) to identify a positional relationship. The bregma (*a*) and lambda (*b*) were marked using the black felt pen with a black dot, which prevented detection of the regional cerebral blood flow (rCBF) signal. The contusion was applied 2.0 mm caudally from the bregma and 3.0 mm laterally from the midline (*c*). The position of contusion (*d*) is colored black for descriptive purposes in this figure. A laser probe was used to measure the CBF, which was obtained from three rostral to caudal scans of the parietal brain as described in "Materials and Methods." The rCBF value of the ipsilateral (*d*) and contralateral (*e*) hemispheres was calculated for the ellipsoidal area (4 × 2 mm), which included 185–187 CBF data points

Statistical Analysis

Data were expressed as mean ± SEM. Statistical comparisons were made using two-tailed Student's *t* test. A value of $p < 0.05$ was considered statistically significant.

Results

Edaravone Increases rCBF in the Ipsilateral and Contralateral Hemispheres 24 h After TBI

No animals died during as a result of the surgical procedures. Scanned images showing rCBF highlight a region of low blood flow between the bregma and lambda, which matched with the superior sagittal sinus. The rCBF of other regions was relatively homogeneously distributed with some minor differences at specific points prior to TBI (Fig. 2). There were no differences between the ipsilateral and contralateral hemispheres among the experimental groups prior to TBI, and no major differences among the average baseline rCBF images (data not shown).

Twenty four hours after TBI, the rCBF level in the vehicle-treated animals was decreased broadly across the ipsilateral hemisphere. The region of low rCBF spread from the frontal cortex to the occipital lobe, with the center of this region matching that of the contusion point; here, the rCBF was much lower compared with all other brain areas. In contrast, no differences in the rCBF in the contralateral hemisphere, cerebellum or superior sagittal sinus regions were evident before or 24 h after TBI. Therefore, the reduction in rCBF in the ipsilateral hemisphere was considered to be due to TBI.

Compared with control animals, a reduction in the size of the rCBF area was evident in edaravone-treated animals, with low rCBF levels observed only around the contusion area. The rCBF in the edaravone-treated animals was thus significantly higher than that in vehicle-treated animals in the ipsilateral hemisphere 24 h post TBI, with no differences apparent for either group with respect to the contralateral hemisphere, cerebellum or superior sagittal sinus.

The mean rCBF values before and 24 h after TBI in the ipsilateral and contralateral hemispheres were quantified and compared among the groups (Fig. 3). There were no significant differences between the ipsilateral and contralateral hemispheres with respect to rCBF levels for the vehicle- and edaravone-treated groups before TBI (see Fig. 2). The rCBF in the ipsilateral hemisphere of vehicle-treated animals decreased to 73.7 ± 5.8 % 24 h after TBI, but was unchanged in the contralateral hemisphere (94.0 ± 2.5 %; Fig. 3). However, the rCBF in the ipsilateral hemisphere of edaravone-treated animals (93.4 ± 5.7 %, $p < 0.05$) was significantly higher than that of vehicle-treated animals. Moreover, edaravone also significantly increased rCBF in the contralateral hemisphere 24 h post-TBI (124.3 ± 4.5 %, $p < 0.01$) compared with the vehicle-treated group.

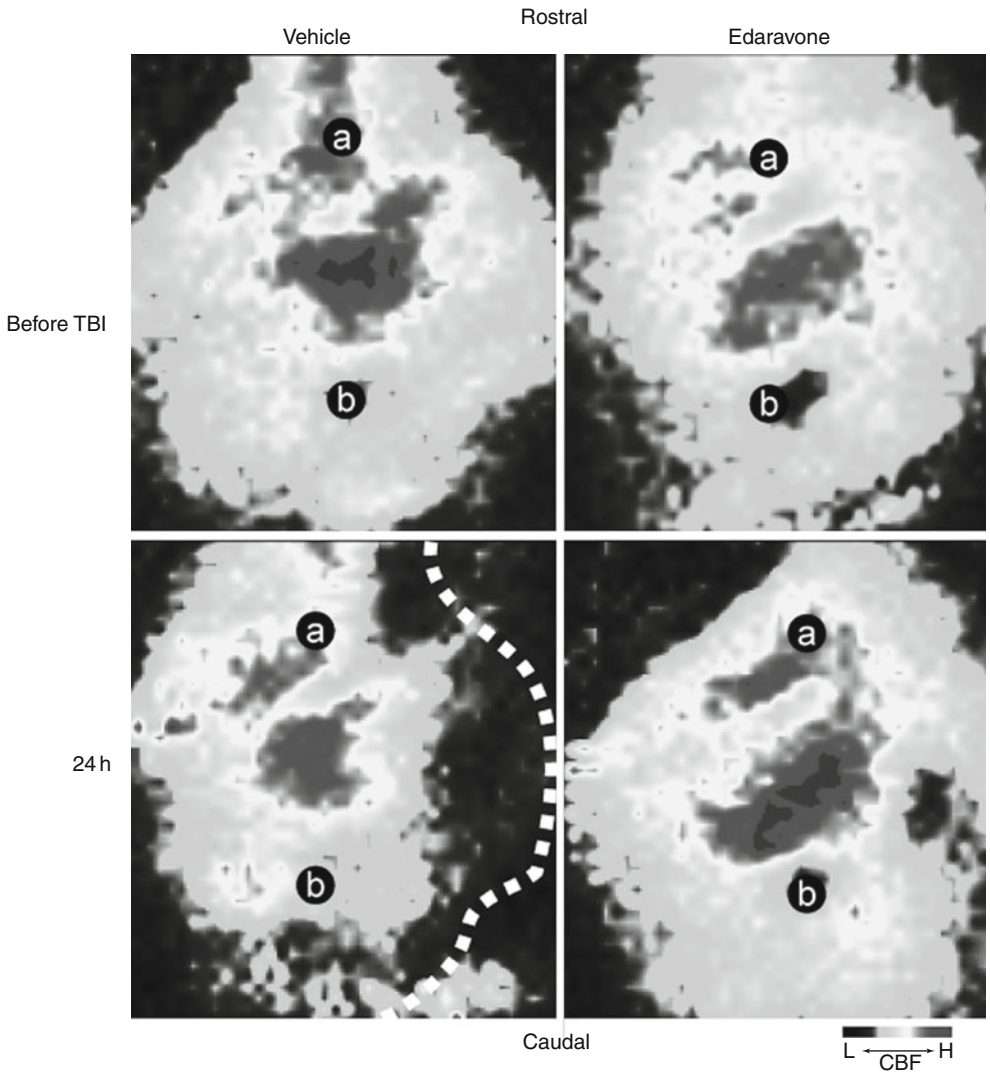

Fig. 2 rCBF images of the brain before and 24 h after traumatic brain injury (TBI) in vehicle- and edaravone-treated animals. Prior to TBI, there was no difference among the groups, whereas 24 h after TBI the rCBF in vehicle-treated animals was extensively decreased in the ipsilateral hemisphere. In the edaravone-treated animals, in contrast, decreased rCBF was observed only in the contusion area, but it still remained higher than that measured in the vehicle-treated group. The positions of the bregma and lambda are indicated by *a* and *b* respectively

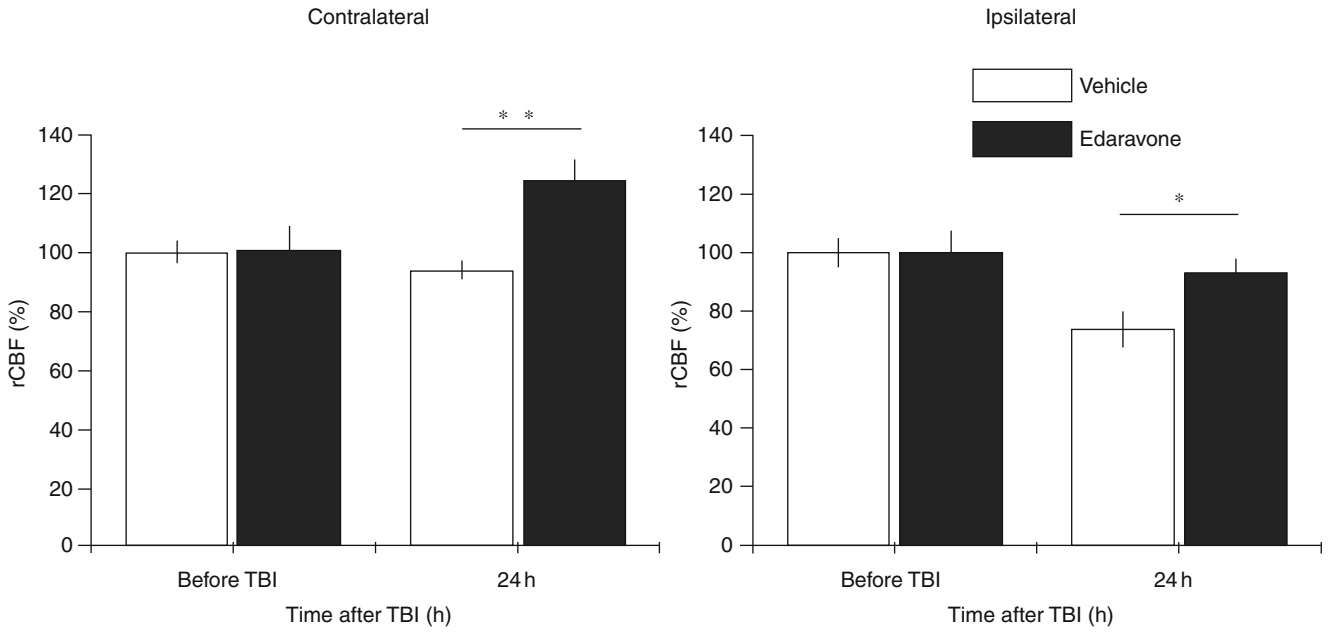

Fig. 3 Edaravone increases rCBF after TBI. Mean rCBF was quantified from rCBF images before and 24 h after TBI in the ipsilateral and contralateral hemispheres. Prior to TBI, no significant differences for either hemisphere were apparent between the experimental groups. The rCBF in the ipsilateral hemispheres of vehicle-treated animals decreases after TBI to 74 % of the pre-TBI value, but no changes in the contralateral hemisphere are seen. However rCBF in the edaravone-treated animals is greater than that seen in the vehicle-treated group for both the ipsilateral and contralateral hemispheres. Values are expressed as mean ± SE ($n = 5$). *$p < 0.05$, **$p < 0.01$, versus vehicle-treated mice (Student's t-test)

Conclusion

In the present study we have demonstrated that rCBF in the ipsilateral hemisphere was significantly and broadly decreased in mice after TBI, and that the TBI-induced hypoperfused condition persisted for at least 1 day. Moreover, we determined that the free radical scavenger edaravone significantly improved the reduction in rCBF induced by TBI.

It has been reported that the autoregulation of cerebral circulation is compromised in 30–80 % of patients after severe TBI [4]. In the rodent model of TBI, the disrupted autoregulation resulted in a reduction in CBF and CPP, and hence the ischemic condition, which was attributable to the development of neuronal cell death [24]. rCBF in the contused cortical region after TBI decreased to a level indicative of ischemic disease after 3 h, and extended from the center to the peripheral areas within 6 h. Thereafter, the ischemic condition gradually recovered and was restricted to the contused cortical region a few days post-trauma [13, 21]. Cerebral vascular endothelial function is impaired by TBI and cerebrovascular damage leads to further reductions of rCBF [1, 21, 22, 24]. Therefore, the reduction in CBF and CPP after TBI is suggested to play an important role in the development of secondary cerebral damage. Our results showed that rCBF after TBI in vehicle-treated animals clearly decreased not only in the contusion area, but also across much of the ipsilateral hemisphere. We also found that rCBF after TBI in vehicle-treated animals did not change in the cerebellum or superior sagittal sinus, and was not influenced in the contralateral hemisphere. These findings suggest that the reduction in rCBF in the ipsilateral hemisphere might be a local response due to dysfunction of the autoregulatory mechanism leading to impairment of vasculature patency, and not as a result of changes to systemic circulatory dynamics.

In the present study, we examined the effect of edaravone on rCBF after TBI, and determined that this free radical scavenger increased rCBF in both hemispheres. Previously, we have reported that edaravone rescued cortical tissues after TBI and decreased alkoxy-radical levels [10], while other studies have suggested that edaravone might modulate blood flow [16, 27, 31]. In a dog model treatment for cardiac ischemia/reperfusion with edaravone increased NO and preserved coronary microvascular dilation in response to acetylcholine [31]. Other studies also suggested that edaravone increased coronary blood flow in patients with coronary endothelial dysfunction mediated by NO and acetylcholine [27]. Moreover, edaravone-treatment increased forearm blood flow as a consequence of endothelium-dependent vasodilation in smokers [16]. However, there have been no reports that edaravone increases rCBF in response to TBI. In the present study, treatment by the intravenous administration of edaravone to mice immediately after TBI accounted

for an improved rCBF at 24 h compared with vehicle-treated animals. Because rCBF increased in both the ipsilateral and contralateral hemispheres, this effect was considered to be due to a systemic response to the edaravone. rCBF and CPP are maintained at homeostatic levels by the autoregulation of cerebral circulation, which in turn is regulated by the cerebral vasculature and mean arterial blood pressure (MAP). Although we have not examined the effect of edaravone on MAP and cardiac output, previous studies [16, 27, 31] support our findings that edaravone influences the endothelial pathway.

An increase in rCBF improves outcome and reduces neuronal damage after TBI. For example, the L-type calcium channel antagonist verapamil increases vasoreactivity and rCBF post-TBI [22], while administration of the NO synthase (NOS) substrate L-arginine post-TBI also improved both rCBF in the contused cortical region and behavioral outcomes [19, 33]. We have reported that nucleoprotamine obtained from salmon soft roe reduces hippocampal neural cell death after global ischemia by increasing rCBF during the ischemic episode. This effect was considered to depend on the protamine, which is rich in L-arginine-containing protein [23].

In contrast, we have also reported the results of electron spin resonance experiments showing that edaravone directly scavenges NO radicals in vitro [30]. However, it has also been reported that edaravone increases endothelial NOS (eNOS) and decreases the neuronal and inducible forms of NOS. To this extent, edaravone inhibits oxidation and enhances NO production derived from increased eNOS expression and reduced CBF [40]. It remains unclear how edaravone regulates the effect of vasculature dilation and what its possible effects might be on MAP and cardiac output.

It is well known that ROS contribute to endothelial damage [20, 25, 37, 39]. TBI enhances inflammatory responses, which include ROS induction, leukocyte recruitment, cytokine production, and local cerebral hemorrhage. These responses further increase ROS production and result in vasculature damage and dysfunction of the autoregulation mechanism [5, 11, 29]. Edaravone treatment protects the neurovascular unit, which involves neurons, astrocytes and microvasculature of the blood–brain barrier, from oxidative stress after stroke [18]. In the present study, we did not evaluate the neuroprotective effect of edaravone, although we have previously shown that decreasing ROS improves outcomes in the TBI rat model [10]. As edaravone also decreases vasculature damage, it may help to maintain intact the autoregulation of cerebral circulation. Further studies are needed to demonstrate the effect of edaravone on rCBF and on neuroprotection.

In summary, we have shown that rCBF in the ipsilateral hemisphere was severely decreased by TBI, and that intravenous treatment with edaravone improved rCBF in the affected areas. It is suggested that edaravone might reduce neuronal damage by scavenging ROS and sustaining the autoregulation of the cerebral vasculature.

Acknowledgments The project was supported by a Grant-in-Aid for Young Scientists (Start-up) from the Japanese Ministry of Education, Culture, Sports, Science and Technology (KM). This work was also supported in part by a grant from the Research on Health Sciences focusing on Drug Innovation program funded by The Japan Health Sciences Foundation (SS).

Conflict of Interest We declare that we have no conflict of interest.

References

1. Alagarsamy S, DeWitt DS, Johnson KM (1998) Effects of moderate, central fluid percussion traumatic brain injury on nitric oxide synthase activity in rats. J Neurotrauma 15:627–633
2. Aoyama T, Hida K, Kuroda S, Seki T, Yano S, Shichinohe H, Iwasaki Y (2008) Edaravone (MCI-186) scavenges reactive oxygen species and ameliorates tissue damage in the murine spinal cord injury model. Neurol Med Chir (Tokyo) 48:539–545; discussion 545
3. Armstead WM, Kiessling JW, Kofke WA, Vavilala MS (2010) SNP improves cerebral hemodynamics during normotension but fails to prevent sex dependent impaired cerebral autoregulation during hypotension after brain injury. Brain Res 1330:142–150
4. Bouma GJ, Muizelaar JP, Bandoh K, Marmarou A (1992) Blood pressure and intracranial pressure-volume dynamics in severe head injury: relationship with cerebral blood flow. J Neurosurg 77: 15–19
5. Bramlett HM, Dietrich WD (2004) Pathophysiology of cerebral ischemia and brain trauma: similarities and differences. J Cereb Blood Flow Metab 24:133–150
6. Brody DL, Mac Donald C, Kessens CC, Yuede C, Parsadanian M, Spinner M, Kim E, Schwetye KE, Holtzman DM, Bayly PV (2007) Electromagnetic controlled cortical impact device for precise, graded experimental traumatic brain injury. J Neurotrauma 24:657–673
7. Brown AW, Elovic EP, Kothari S, Flanagan SR, Kwasnica C (2008) Congenital and acquired brain injury. 1. Epidemiology, pathophysiology, prognostication, innovative treatments, and prevention. Arch Phys Med Rehabil 89:S3–S8
8. Bryan RM Jr, Cherian L, Robertson C (1995) Regional cerebral blood flow after controlled cortical impact injury in rats. Anesth Analg 80:687–695
9. Cherian L, Hlatky R, Robertson CS (2004) Nitric oxide in traumatic brain injury. Brain Pathol 14:195–201
10. Dohi K, Satoh K, Nakamachi T, Yofu S, Hiratsuka K, Nakamura S, Ohtaki H, Yoshikawa T, Shioda S, Aruga T (2007) Does edaravone (MCI- 186) act as an antioxidant and a neuroprotector in experimental traumatic brain injury? Antioxid Redox Signal 9: 281–287
11. Fisher M (2008) Injuries to the vascular endothelium: vascular wall and endothelial dysfunction. Rev Neurol Dis 5(Suppl 1): S4–S11
12. Gahm C, Danilov A, Holmin S, Wiklund PN, Brundin L, Mathiesen T (2005) Reduced neuronal injury after treatment with NG-nitro-L-arginine methyl ester (L-NAME) or 2-sulfo-phenyl-N-tert-butyl nitrone (S-PBN) following experimental brain contusion. Neurosurgery 57:1272–1281; discussion 1272–1281

13. Hendrich KS, Kochanek PM, Williams DS, Schiding JK, Marion DW, Ho C (1999) Early perfusion after controlled cortical impact in rats: quantification by arterial spin-labeled MRI and the influence of spin-lattice relaxation time heterogeneity. Magn Reson Med 42:673–681
14. Hlatky R, Furuya Y, Valadka AB, Goodman JC, Robertson CS (2002) Comparison of microdialysate arginine and glutamate levels in severely head-injured patient. Acta Neurochir Suppl 81: 347–349
15. Inokuchi Y, Imai S, Nakajima Y, Shimazawa M, Aihara M, Araie M, Hara H (2009) Edaravone, a free radical scavenger, protects against retinal damage in vitro and in vivo. J Pharmacol Exp Ther 329:687–698
16. Jitsuiki D, Higashi Y, Goto C, Kimura M, Noma K, Hara K, Nakagawa K, Oshima T, Chayama K, Yoshizumi M (2004) Effect of edaravone, a novel free radical scavenger, on endothelium-dependent vasodilation in smokers. Am J Cardiol 94:1070–1073
17. Lapchak PA (2010) A critical assessment of edaravone acute ischemic stroke efficacy trials: is edaravone an effective neuroprotective therapy? Expert Opin Pharmacother 11:1753–1763
18. Lee BJ, Egi Y, van Leyen K, Lo EH, Arai K (2010) Edaravone, a free radical scavenger, protects components of the neurovascular unit against oxidative stress in vitro. Brain Res 1307: 22–27
19. Liu H, Goodman JC, Robertson CS (2002) The effects of L-arginine on cerebral hemodynamics after controlled cortical impact injury in the mouse. J Neurotrauma 19:327–334
20. Lukic-Panin V, Deguchi K, Yamashita T, Shang J, Zhang X, Tian F, Liu N, Kawai H, Matsuura T, Abe K (2010) Free radical scavenger edaravone administration protects against tissue plasminogen activator induced oxidative stress and blood brain barrier damage. Curr Neurovasc Res 7:319–329
21. Maeda T, Katayama Y, Kawamata T, Aoyama N, Mori T (1997) Hemodynamic depression and microthrombosis in the peripheral areas of cortical contusion in the rat: role of platelet activating factor. Acta Neurochir Suppl 70:102–105
22. Maeda T, Lee SM, Hovda DA (2005) Restoration of cerebral vasoreactivity by an L-type calcium channel blocker following fluid percussion brain injury. J Neurotrauma 22:763–771
23. Matsunaga M, Ohtaki H, Takaki A, Iwai Y, Yin L, Mizuguchi H, Miyake T, Usumi K, Shioda S (2003) Nucleoprotamine diet derived from salmon soft roe protects mouse hippocampal neurons from delayed cell death after transient forebrain ischemia. Neurosci Res 47:269–276
24. Matsushita Y, Bramlett HM, Kuluz JW, Alonso O, Dietrich WD (2001) Delayed hemorrhagic hypotension exacerbates the hemodynamic and histopathologic consequences of traumatic brain injury in rats. J Cereb Blood Flow Metab 21:847–856
25. Niiya Y, Abumiya T, Yamagishi SI, Takino JI, Takeuchi M (2012) Advanced glycation End products increase permeability of brain microvascular endothelial cells through reactive oxygen species-induced vascular endothelial growth factor expression. J Stroke Cerebrovasc Dis 21(4):293–298
26. Nilsson P, Gazelius B, Carlson H, Hillered L (1996) Continuous measurement of changes in regional cerebral blood flow following cortical compression contusion trauma in the rat. J Neurotrauma 13:201–207
27. Oyama J, Satoh S, Suematsu N, Kadokami T, Maeda T, Sugano M, Makino N (2010) Scavenging free radicals improves endothelial dysfunction in human coronary arteries in vivo. Heart Vessels 25:379–385
28. Ozawa Y, Nakamura T, Sunami K, Kubota M, Ito C, Murai H, Yamaura A, Makino H (1991) Study of regional cerebral blood flow in experimental head injury: changes following cerebral contusion and during spreading depression. Neurol Med Chir (Tokyo) 31: 685–690
29. Pedersen MO, Larsen A, Stoltenberg M, Penkowa M (2009) Cell death in the injured brain: roles of metallothioneins. Prog Histochem Cytochem 44:1–27
30. Satoh K, Ikeda Y, Shioda S, Tobe T, Yoshikawa T (2002) Edarabone scavenges nitric oxide. Redox Rep 7:219–222
31. Sukmawan R, Yada T, Toyota E, Neishi Y, Kume T, Shinozaki Y, Mori H, Ogasawara Y, Kajiya F, Yoshida K (2007) Edaravone preserves coronary microvascular endothelial function after ischemia/reperfusion on the beating canine heart in vivo. J Pharmacol Sci 104:341–348
32. Sviri GE, Aaslid R, Douville CM, Moore A, Newell DW (2009) Time course for autoregulation recovery following severe traumatic brain injury. J Neurosurg 111:695–700
33. Wada K, Chatzipanteli K, Busto R, Dietrich WD (1999) Effects of L-NAME and 7-NI on NOS catalytic activity and behavioral outcome after traumatic brain injury in the rat. J Neurotrauma 16:203–212
34. Wang GH, Jiang ZL, Li YC, Li X, Shi H, Gao YQ, Vosler PS, Chen J (2011) Free-radical scavenger edaravone treatment confers neuroprotection against traumatic brain injury in rats. J Neurotrauma 28(10):2123–2134
35. Watanabe T, Yuki S, Egawa M, Nishi H (1994) Protective effects of MCI-186 on cerebral ischemia: possible involvement of free radical scavenging and antioxidant actions. J Pharmacol Exp Ther 268:1597–1604
36. White H, Venkatesh B (2008) Cerebral perfusion pressure in neurotrauma: a review. Anesth Analg 107:979–988
37. Yagi K, Kitazato KT, Uno M, Tada Y, Kinouchi T, Shimada K, Nagahiro S (2009) Edaravone, a free radical scavenger, inhibits MMP-9-related brain hemorrhage in rats treated with tissue plasminogen activator. Stroke 40:626–631
38. Yamakami I, McIntosh TK (1991) Alterations in regional cerebral blood flow following brain injury in the rat. J Cereb Blood Flow Metab 11:655–660
39. Yamashita T, Deguchi K, Nagotani S, Abe K (2011) Vascular protection and restorative therapy in ischemic stroke. Cell Transplant 20:95–97
40. Yoshida H, Yanai H, Namiki Y, Fukatsu-Sasaki K, Furutani N, Tada N (2006) Neuroprotective effects of edaravone: a novel free radical scavenger in cerebrovascular injury. CNS Drug Rev 12:9–20

Adiponectin and Traumatic Brain Injury

Satoru Takeuchi, Kojiro Wada, Hiroshi Nawashiro, Yoichi Uozumi, Naoki Otani, Hideo Osada, Kimihiro Nagatani, Hiroaki Kobayashi, Takamoto Suzuki, and Katsuji Shima

Abstract Adiponectin, a circulating adipose-derived hormone regulating inflammation and energy metabolism, has beneficial actions on cardiovascular disorders. Recent studies have suggested that adiponectin might be a potential molecular target for ischemic stroke therapy; however, little is known about the effects of adiponectin on traumatic brain injury. The present study examined the immunoactivity of adiponectin.

Adult male Sprague–Dawley rats were subjected to lateral fluid percussion injury using the Dragonfly device. Immunohistochemical studies showed that the adiponectin expression was increased in the cerebral cortex at 24 h after injury and in the hippocampus at 72 h after injury. Our findings suggest that adiponectin might participate in the pathophysiological process occurring after traumatic brain injury.

Keywords Adiponectin • Traumatic brain injury • Lateral fluid percussion • Rat

Introduction

Adiponectin is a hormone secreted exclusively by adipose tissue, and plays an important role in the regulation of tissue inflammation and insulin sensitivity [10, 11]. Because of the effects it has, adiponectin is described as an anti-diabetic and anti-atherogenic adipokine [3]. Additionally, recent experimental studies using a cerebral ischemia–reperfusion model have shown that high levels of adiponectin were detected in the ischemic hemisphere [12], and that adiponectin may exert a cerebroprotective action [7]. However, little is known about the effects of adiponectin on traumatic brain injury (TBI). The aim of the present study was to examine the changes in the plasma adiponectin levels and the expression of adiponectin in the brain after TBI.

S. Takeuchi (✉), K. Wada, H. Nawashiro, Y. Uozumi, N. Otani, H. Osada, K. Nagatani, H. Kobayashi, T. Suzuki, and K. Shima
Department of Neurosurgery, National Defense Medical College, 3-2 Namiki, Tokorozawa, Saitama 359-8513, Japan
e-mail: s.takeuchi@room.ocn.ne.jp

Materials and Methods

Animals and Experimental Procedures

All experimental procedures were approved by the Animal Care and Use Committee of the National Defense Medical College. Sprague–Dawley rats (male, 300–400 g in weight; 9–10 weeks of age) were used for the study. The rats were housed in individual cages under controlled environmental conditions (12/12 h light/dark cycle, 20–22 °C; room temperature) with food and water freely available, for 1 week before the experimental surgery. The rats were anesthetized with isofluorane (1.5 %) in a 30 % oxygen to 70 % nitrous oxide gas mixture via a nose cone and were fixed in a stereotaxic frame for the procedure. A 4.8-mm craniotomy was made over the right parietal cortex (3.8 mm posterior and 2.5 mm lateral to the bregma), keeping the underlying dura intact. A plastic Luer Lock was placed over the opening and secured with dental acrylic cement. The rats were returned to their cages and allowed free access to water overnight. The following day, the rats were anesthetized, intubated, and maintained on a mechanical ventilator after infusion of pancronium bromide (0.1 mg/kg; tidal volume: 2.5–3.0 mL/kg; respiratory rate: 60/min). The femoral artery was cannulated with a polyethylene catheter. The rats' blood pressure was monitored throughout the procedure, and arterial blood samples were intermittently analyzed ($PaCO_2$ was controlled at 30–40 mmHg). The rectal temperature was measured with a rectal probe and maintained at a constant level of approximately 37.0 °C with a heating pad.

Y. Katayama et al. (eds.), *Brain Edema XV*, Acta Neurochirurgica Supplement, Vol. 118,
DOI 10.1007/978-3-7091-1434-6_19,

The rats were subjected to fluid percussion injury at a moderate severity (2.5–3.0 atm, 16 ms in duration) using a Dragonfly fluid percussion device (model HPD-1700; Dragonfly R&D, Silver Spring, MD, USA), as previously described [6]. Following injury, the connection cap was removed, the scalp was sutured, and the rats were returned to their home cages with food and water available *ad libitum*. Sham control animals were subjected to the same procedures except for the actual insult.

Tissue Preparation

The rats were perfused transcardially with normal saline, followed by 4 % buffered paraformaldehyde under intraperitoneal anesthesia 24 or 72 h after injury ($n=3$ per each time point). The brain was removed and embedded in paraffin after fixation in 4 % buffered paraformaldehyde, followed by 0.1 mmol/L PBS (pH 7.4) for 24 h at 4 °C. Serial 5 μm-thick coronal sections were prepared for the analyses.

Immunohistochemistry

The immunohistochemical analyses were performed using the universal immunoperoxidase polymer method. After deparaffinization and hydration, the endogenous peroxidase activity was blocked with 3 % hydrogen peroxidase. The sections were incubated overnight at 4 °C with a polyclonal antibody against adiponectin (1:1,000). The sections were washed with PBS and incubated with a Histofine Simple Stain Rat MAX-PO (Nichirei Co, Tokyo, Japan) for 30 min at room temperature. The sections were rinsed with PBS. Peroxidase activity was demonstrated with diamino benzidine. To evaluate the morphological changes, adjacent sections were counterstained with hematoxylin.

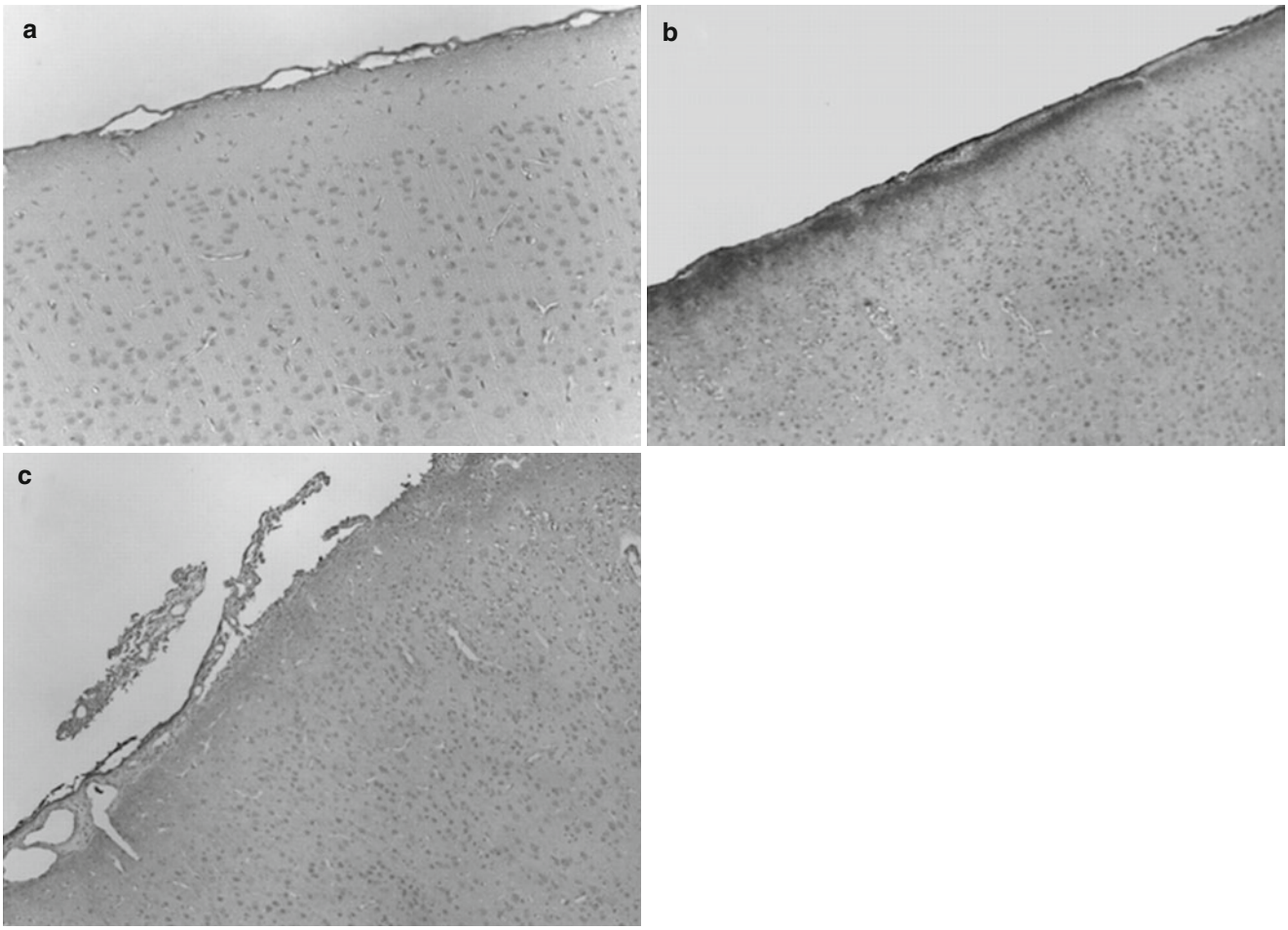

Fig. 1 The serial changes in the expression of adiponectin in the injured cortex. Photomicrographs showed that the adiponectin immunoreactivity in the cortex was only slight before TBI (**a**) and at 72 h after TBI (**c**), but was remarkable at 24 h after TBI (**b**). Original magnifications: ×100

Results

Physiological Data

There were no significant differences in the physiological data of the two groups with regard to the mean arterial blood pressure, pH, pCO_2, pO_2, or body temperature (data not shown).

Expression of Adiponectin in the Cortex After TBI

The alterations of adiponectin immunoreactivity in the cortex are shown in Fig. 1. Immunoreactivity for adiponectin was only slight before TBI and at 72 h after TBI, but was remarkable at 24 h after TBI.

Expression of Adiponectin in the Hippocampus After TBI

The alterations in adiponectin immunoreactivity in the hippocampus (CA3–4) are shown in Fig. 2. Immunoreactivity for adiponectin was only slight before TBI and at 24 h after TBI, but was remarkable at 72 h after TBI.

Conclusion

The present results showed that the adiponectin expression increased in the brain after TBI. Adiponectin is secreted exclusively by adipose tissue, and circulates in the bloodstream [10]. Pertubations in the circulating adiponectin concentrations have been reported to be associated with metabolic syndrome, altered inflammation, and insulin

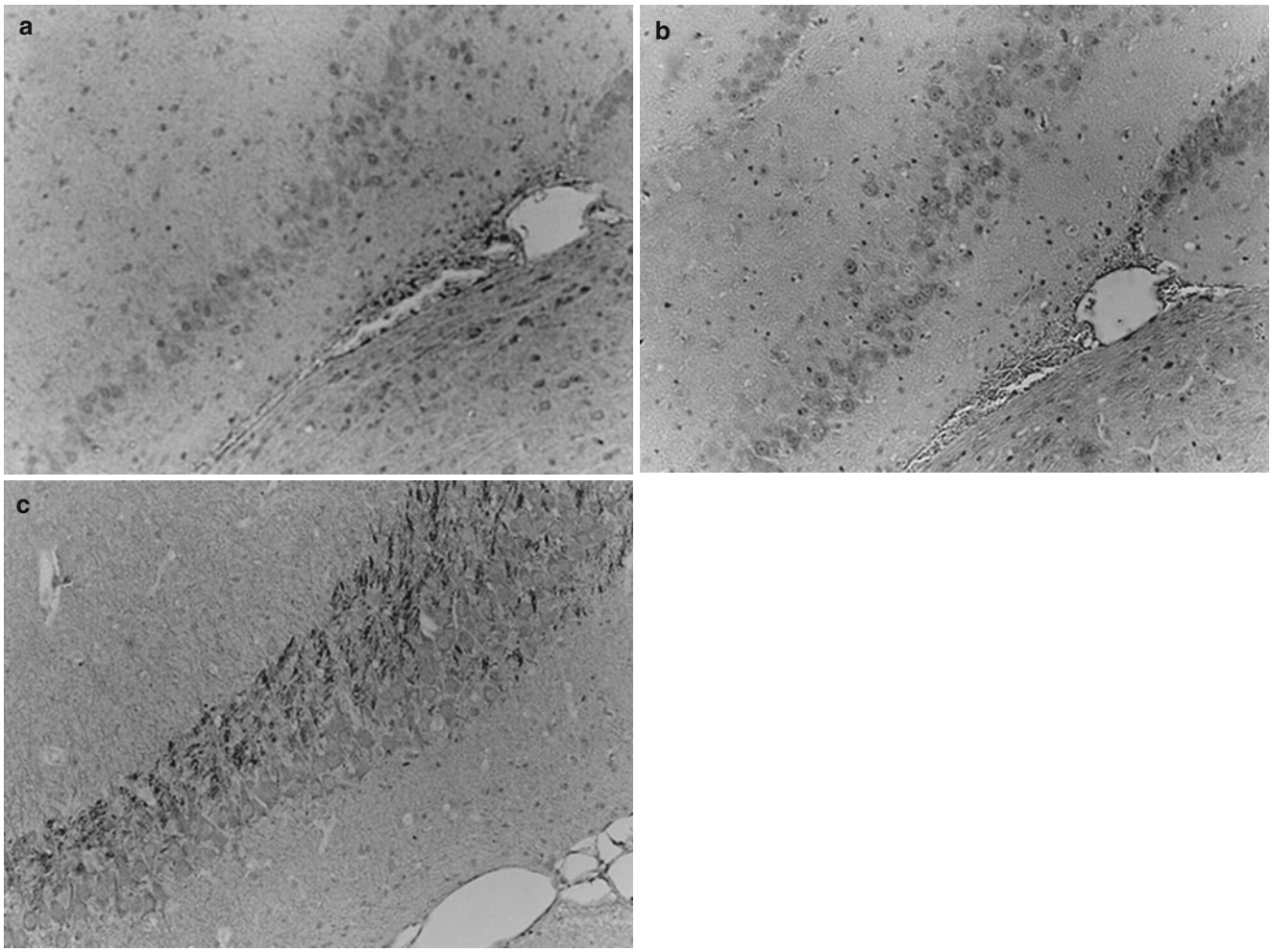

Fig. 2 The serial changes in adiponectin expression in the ipsilateral hippocampus (CA3–4). Photomicrographs showed that the adiponectin immunoreactivity in the hippocampus (CA3–4) was only slight before TBI (**a**) and at 24 h after TBI (**b**), but was remarkable at 72 h after TBI (**c**). Original magnification: ×200

resistance [4]. Furthermore, recent attention has been paid to the role of adiponectin in several acute illnesses in both animals and humans. Yatomi et al. reported that, in a mouse model of ischemia–reperfusion, the plasma adiponectin level decreased significantly until 48 h after reperfusion [12]. Marousi et al. reported that the serum adiponectin level was already significantly suppressed during the early phases of stroke, and that the levels remained unchanged 6 months later in humans [5]. Furthermore, Venkatesh et al. recently reported that the plasma adiponectin levels in critically ill patients, including those with sepsis, burns, and trauma, decreased significantly on days 3 and 7 after injury [9], although they did not describe whether their studies included any patients with TBI.

Several authors have reported a high level of expression of adiponectin in the ischemic hemisphere in mice [8, 12], whereas adiponectin mRNA was not detected in the brain [12]. These results indicate that the expression of adiponectin in the brain reflects not the production, but the accumulation in the injured brain. Additionally, it has been shown that adiponectin exerts a potent cerebroprotective function through its anti-inflammatory actions in the brain ischemia–reperfusion model. We found, for the first time, that the expression of adiponectin increased significantly in the cortex at 24 h after TBI and in the hippocampus (CA3–4) at 72 h after TBI. Conti et al. reported that apoptotic cells increased mostly in the injured cortex at 24 h after TBI in rats [1]. Their study also showed that the apoptosis peak tended to be delayed compared with that in the cortex [1]. It has also been reported that the injured cortex and hippocampus, especially CA3 and CA4, are vulnerable to TBI in rats [2]. Therefore, we can speculate that the expression levels of adiponectin in the brain may act to reduce apoptosis after TBI.

Based on these findings, we hypothesize that adiponectin might participate in cerebroprotective mechanisms through its anti-inflammatory and/or anti-apoptotic actions after TBI. In addition, we consider that the accumulation (recruitment) of adiponectin in the brain might contribute to the decrease in the plasma adiponectin levels. The relationship between adiponectin and its signal after TBI, and the effects of adiponectin administration after TBI should be the subject of future investigations.

Acknowledgments This study was supported by a research grant from The General Insurance Association of Japan.

Conflict of Interest We declare that we have no conflict of interest.

References

1. Conti AC, Raghupathi R, Trojanowski JQ, McIntosh TK (1998) Experimental brain injury induces regionally distinct apoptosis during the acute and delayed post-traumatic period. J Neurosci 18:5663–5672
2. Dietrich WD, Alonso O, Busto R, Globus MY, Ginsberg MD (1994) Post-traumatic brain hypothermia reduces histopathological damage following concussive brain injury in the rat. Acta Neuropathol 87:250–258
3. Gil-Campos M, Cañete RR, Gil A (2004) Adiponectin, the missing link in insulin resistance and obesity. Clin Nutr 23:963–974
4. Hickman IJ, Whitehead JP, Prins JB, Macdonald GA (2007) Raised alanine transaminase and decreased adiponectin are features of the metabolic syndrome in patients with type 2 diabetes. Diabetes Obes Metab 9:438–440
5. Marousi S, Theodorou G, Karakantza M, Papathanasopoulos P, Ellul J (2010) Serum adiponectin acutely after an ischemic stroke: implications for a long-lasting, suppressed anti-inflammatory role. Acta Neurol Scand 121:277–284
6. Matsushita Y, Shima K, Nawashiro H, Wada K (2000) Real-time monitoring of glutamate following fluid percussion brain injury with hypoxia in the rat. J Neurotrauma 17:143–153
7. Nishimura M, Izumiya Y, Higuchi A, Shibata R, Qiu J, Kudo C, Shin HK, Moskowitz MA, Ouchi N (2008) Adiponectin prevents cerebral ischemic injury through endothelial nitric oxide synthase dependent mechanisms. Circulation 117:216–223
8. Thundyil J, Tang SC, Okun E, Shah K, Karamyan VT, Li YI, Woodruff TM, Taylor SM, Jo DG, Mattson MP, Arumugam TV (2010) Evidence that adiponectin receptor 1 activation exacerbates ischemic neuronal death. Exp Transl Stroke Med 2:15
9. Venkatesh B, Hickman I, Nisbet J, Cohen J, Prins J (2009) Changes in serum adiponectin concentrations in critical illness: a preliminary investigation. Crit Care 13:R105
10. Whitehead JP, Richards AA, Hickman IJ, Macdonald GA, Prins JB (2006) Adiponectin – a key adipokine in the metabolic syndrome. Diabetes Obes Metab 8:264–280
11. Yamauchi T, Kamon J, Minokoshi Y, Ito Y, Waki H, Uchida S, Yamashita S, Noda M, Kita S, Ueki K, Eto K, Akanuma Y, Froguel P, Foufelle F, Ferre P, Carling D, Kimura S, Nagai R, Kahn BB, Kadowaki T (2002) Adiponectin stimulates glucose utilization and fatty-acid oxidation by activating AMP-activated protein kinase. Nat Med 8:1288–1295
12. Yatomi K, Miyamoto N, Komine-Kobayashi M, Liu M, Oishi H, Arai H, Hattori N, Urabe T (2009) Pathophysiological dual action of adiponectin after transient focal ischemia in mouse brain. Brain Res 1297:169–176

Metabolomic Analysis of Cerebral Spinal Fluid from Patients with Severe Brain Injury

Thomas C. Glenn, Daniel Hirt, Gustavo Mendez, David L. McArthur, Rachael Sturtevant, Stephanie Wolahan, Farbod Fazlollahi, Matthew Ordon, Arzu Bilgin-Freiert, Ben Ellingson, Paul Vespa, David A. Hovda, and Neil A. Martin

Abstract Proton nuclear magnetic resonance (H-NMR) spectroscopic analysis of cerebral spinal fluid provides a quick, non-invasive modality for evaluating the metabolic activity of brain-injured patients. In a prospective study, we compared the CSF of 44 TBI patients and 13 non-injured control subjects. CSF was screened for ten parameters: β-glucose (Glu), lactate (Lac), propylene glycol (PG), glutamine (Gln), alanine (Ala), α-glucose (A-Glu), pyruvate (PYR), creatine (Cr), creatinine (Crt), and acetate (Ace). Using mixed effects measures, we discovered statistically significant differences between control and trauma concentrations (mM). TBI patients had significantly higher concentrations of PG, while statistical trends existed for lactate, glutamine, and creatine. TBI patients had a significantly decreased concentration of total creatinine. There were no significant differences between TBI patients and non-injured controls regarding β- or α-glucose, alanine, pyruvate or acetate. Correlational analysis between metabolites revealed that the strongest significant correlations in non-injured subjects were between β- and α-glucose ($r=0.74$), creatinine and pyruvate ($r=0.74$), alanine and creatine ($r=0.62$), and glutamine and α-glucose ($r=0.60$). For TBI patients, the strongest significant correlations were between lactate and α-glucose ($r=0.54$), lactate and alanine ($r=0.53$), and α-glucose and alanine ($r=0.48$). The GLM and multimodel inference indicated that the combined metabolites of PG, glutamine, α-glucose, and creatinine were the strongest predictors for $CMRO_2$, ICP, and GOSe. By analyzing the CSF of patients with TBI, our goal was to create a metabolomic fingerprint for brain injury.

T.C. Glenn (✉) D. Hirt, G. Mendez, D.L. McArthur, R. Sturtevant, S. Wolahan, F. Fazlollahi, M. Ordon, A. Bilgin-Freiert, P. Vespa, D.A. Hovda, and N.A. Martin
Department of Neurosurgery,
David Geffen School of Medicine at UCLA,
10833 Le Conte Ave, Los Angeles, CA 90095-7039, USA
e-mail: tglenn@mednet.ucla.edu

B. Ellingson
UCLA Radiological Sciences, 924 Westwood Blvd Ste 615,
Los Angeles, CA 90095-7319, USA

Keywords Cerebral metabolism • Traumatic brain injury • Intracranial pressure • Glucose • Lactate • Propylene glycol • Polyols • Nuclear magnetic resonance spectroscopy

Introduction

Over the past few years, the systematic study of the metabolome has occurred in many clinical fields. Metabolomics is defined as the group of metabolites synthesized by biological and physiological systems and is the phenotypic expression of the genome and proteome [6, 13]. With regard to the brain, cerebral spinal fluid (CSF) offers a potentially rich source for analysis. Methods for studying CSF include high performance liquid chromatography (HPLC), gas chromatography and mass spectroscopy (GCMS), and nuclear magnetic resonance spectroscopy (NMR), all of which may include complex component analyses [9, 11, 16, 20].

Cerebral spinal fluid has been a source of interest for understanding the neurochemistry and pathophysiology caused by TBI for decades. Early notable changes in CSF included increased concentrations of lactate, glucose, acetate, and pyruvate during the first 24 h of admission to the ICU [2, 4, 5, 17, 19]. Given that CSF is one window into the pathophysiology of TBI, the purpose of this paper is to use the metabolomics approach to analyze CSF samples from patients with severe traumatic brain injury (TBI) and compare those findings with CSF samples from a cohort of non-injured subjects.

Materials and Methods

Patient Population

The University of California at Los Angeles (UCLA) Medical Institutional Review Board for human research approved this

Y. Katayama et al. (eds.), *Brain Edema XV*, Acta Neurochirurgica Supplement, Vol. 118,
DOI 10.1007/978-3-7091-1434-6_20, © Springer-Verlag Wien 2013

study. Eligible patients included all mechanically ventilated moderately or severely head-injured patients, ages 14 years and older, who were admitted to the UCLA Medical Center within 24 h of injury. Severe head injury was defined as closed or penetrating injury, including gunshot and stab wounds, with a post-resuscitation Glasgow Coma Scale (GCS) of less than or equal to eight, or deterioration to a GCS of less than or equal to eight within 24 h of admission. Patients required mechanical ventilation, ventriculostomy, and intracranial pressure (ICP) monitoring as part of the American Association of Neurological Surgeons' (AANS) standard of care. Exclusion criteria included the following: (1) Terminal illness (e.g., advanced cancer, AIDS) (2) Severe pre-existing neurological illness (e.g., advanced Parkinson's disease, multiple sclerosis, Alzheimer's dementia, disabling cerebrovascular events, mental retardation) (3) Acute complete spinal cord injury

The non-injured cohort included consenting subjects with normal-pressure hydrocephalus (NPH), as previously described by Bergsneider et al. [1], or subjects with unruptured aneurysms.

General Management Protocol of TBI Patients

Patients were admitted to the neurological intensive care unit (NICU) after initial stabilization or surgical evacuation of an intracranial hematoma and were treated in accordance with the level I Trauma Center protocol, as previously described by Vespa et al. [18]. Briefly, management goals included the maintenance of ICP less than 20 mmHg, CPP above 70 mmHg, and hematocrit between 30 and 34 %, in accordance with AANS guidelines for the management of severe head injury. All patients had a jugular bulb catheter inserted as soon as possible following admission.

CSF Sampling and Specimen Analysis

Cerebrospinal fluid samples were drawn from the ventriculostomy (EVD) of TBI patients and by lumbar puncture or EVD in non-injured controls. Samples were then centrifuged, frozen, and stored at −80 °C until the day of sample preparation and analysis. CSF was thawed on ice. Eight percent perchloric acid was added to an aliquot of 600 μL, and samples were then centrifuged to clear all protein particles. The supernatant pH was adjusted to 6.00–6.50, the precipitated salt removed by centrifugation, and the samples were then lyophilized (FreeZone 4.5 L Console Freeze Dry System, Labconco, Kansas City, MO, USA). Prior to spectroscopy, samples were reconstituted in 600 μL of 99.9 % D_2O containing 0.05 weight percent 3-(trimethylsilyl) propionic-2,2,3,3-d4 sodium salt (TSP) (Sigma-Aldrich), and the pH was adjusted to neutral (7.00–7.20).

Proton nuclear magnetic resonance (H-NMR) spectra were obtained on a Bruker AM 360 or AV 600 spectrometer equipped with a 5-mm triple broadband inverse probe, utilizing Topspin 2.1. The raw data were acquired using a 70° excitation pulse with presaturation of the solvent peak at room temperature with 80 acquisition scans, a 2-s relaxation delay, and a 7-μs pulse width.

Chemical shifts of relevant peaks were assigned relative to TSP and by comparison with previously published values [3, 14]. Peak analysis of the NMR spectra was performed by manually integrating the area under each peak using the baseline flattening feature and Lorentzian fit of the Acorn NMR Incorporated NUTS 1.0.0.1 software. After integration, the amount of ^1H incorporated into the resonance of each metabolite was quantified using TSP as an internal standard [8] and normalized to the initial sample volume. Peaks of many metabolites found in CSF spectra overlap and cause complicated splitting patterns, presenting a limitation inherent to CSF H-NMR spectrum analysis. Peaks were identified based on the published literature [7, 10, 12, 15] and the specificity of the assignment was further investigated by comparing the CSF spectrum with that of the pure compounds of interest. Peaks that were integrated are shown in Fig. 1. The remaining peaks of these metabolites were not integrated because of the limitations mentioned above, and hence only relative concentrations were recorded for comparison analyses.

Data Analysis

Univariate and multivariate statistical analyses, mixed effects, and multimodel inferences were performed using both R, version 2.11.1 (R Development Core Team, 2010) and Stata 12. In addition, the output provided information on the correlations and variances in the data. Model fit comparisons were made using the AIC and BIC.

Results

Forty-four TBI subjects and 13 non-injured control patients were enrolled into the CSF H-NMR study as part of the UCLA Brain Injury Program project (Table 1). The TBI subjects had a mean admission GCS of 6.9 ± 4.2, range 3–15, and a mean age of 38.0 ± 15.2 years, range 17–79. At 6 months,

Table 1 Demographics of the study groups

	Age	Gender	Admin GCS	Study GCS	ISS
TBI	38.0 ± 15.2	19.4 % female	6 (range 3–14)	5.7 ± 2.8 (range 3–14)	30.2 ± 8.4
Non-injured	69.5 ± 16.8	29.1 % female	NA	NA	NA

Forty-four traumatic brain injury (TBI) patients and 13 non-injured subjects were studied
NA not applicable

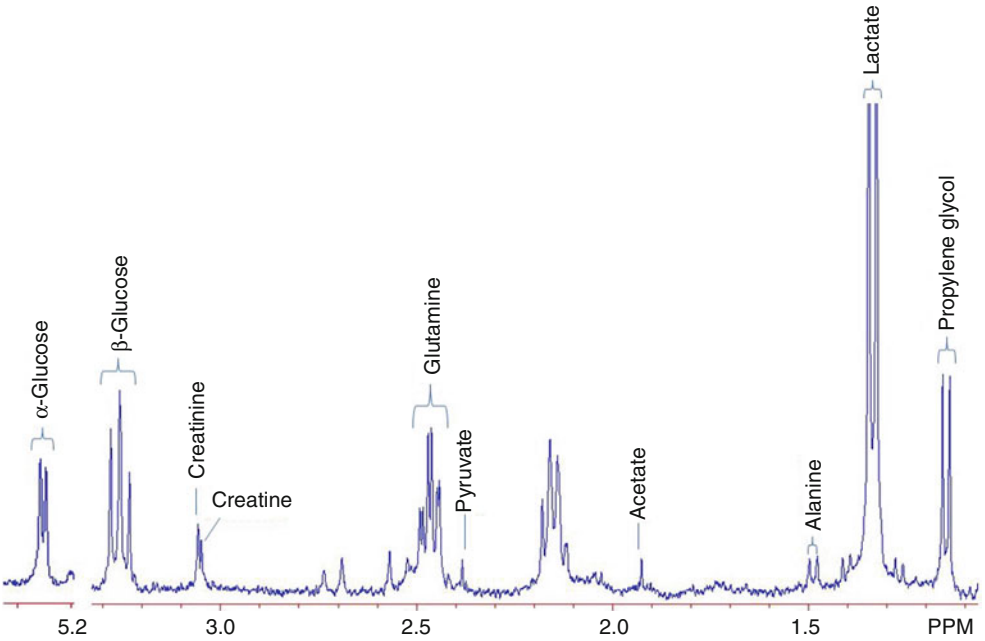

Fig. 1 A representative nuclear magnetic resonance (NMR) spectrum of human cerebrospinal fluid (CSF). Ten metabolites were reliably identified as being determined by comparisons with known standards for each. Metabolite resonance peaks are shown as parts per million (PPM). Chemical shifts of relevant peaks were assigned relative to 3-(trimethylsilyl) propionic-2,2,3,3-d4 sodium salt (TSP)

mean GOSe scores were 4.2 ± 1.9, range 1–8. A total of 176 trauma CSF samples were analyzed from TBI patients. The non-injured controls had a mean age of 69.5 ± 16.8 years, range 17–82. A total of 30 non-injured CSF samples were collected and analyzed.

The Human CSF Metabolome: Differences Between Injured and Non-injured CSF

Analysis of the H-NMR spectra revealed identifiable peaks for lactate, acetate, β-glucose, total creatine, pyruvate, glutamine, alanine, creatinine, α-glucose, and a previously undescribed doublet propylene glycol (Fig. 1; Table 2). Using mixed effects models, TBI patients had significantly higher concentrations of PG while statistical trends existed for lactate, glutamine, and creatine. TBI patients had a significantly decreased concentration of total creatinine. There were no significant differences between TBI patients and non-injured controls with regard to β- or α-glucose, alanine, pyruvate or acetate.

Correlational analysis between metabolites revealed that the strongest significant correlations in non-injured subjects were between β- and α-glucose ($r = 0.74$), creatinine and pyruvate ($r = 0.74$), alanine and creatine ($r = 0.62$), and glutamine and α-glucose ($r = 0.60$). For TBI patients, the strongest significant correlations were between lactate and α-glucose ($r = 0.54$), lactate and alanine ($r = 0.53$), and α-glucose and alanine ($r = 0.48$).

Discovery of Propylene Glycol in CSF of TBI Patients

During the analysis of the lactate peak, a doublet signal at 1.13 ppm to the right of the lactate doublet was noticed in the TBI population. As mentioned in the "Materials and methods" section, the doublet peak was identified as propylene glycol (PG) following a review of the published literature [10, 12, 15]. The specificity of the assignment of PG was further investigated by comparing the CSF spectrum with that of the pure compound PG. CSF PG within the TBI population ranged from 0 to 5.06 mM. PG was not consistently present in non-injured subject samples. In a preliminary analysis utilizing MRI and ADC algorithms, higher PG levels were associated with a larger volume of brain edema.

Table 2 Concentrations (mM) of the ten identified metabolites from non-injured and TBI subjects

Metabolite (mM)	β-glucose	Lactate	PG	Glutamine	Alanine	α-glucose	Pyruvate	Creatine	Creatinine	Acetate
Non-injured $n=13$	1.70±0.34	1.34±1.1	0.01±0.23	0.23±0.11	0.03±0.02	0.91±0.19	0.06±0.03	0.03±0.01	0.10±0.04	0.03±0.05
TBI $n=44$	2.00±0.18 $p=0.11$	2.50±0.50 $p=0.06$	0.25±0.10 $p=0.05$	0.35±0.06 $p=0.07$	0.04±0.01 $p=0.33$	0.92±0.10 $p=0.95$	0.04±0.01 $p=0.21$	0.02±0.01 $p=0.07$	0.03±0.02 $p=0.01$	0.04±0.02 $p=0.50$

p values and means calculated with mixed effects models

Metabolomic Predictors of Metabolism, ICP, Outcome

Using univariate, generalized linear models (GLM) and multimodel inferences, the concentrations of the TBI metabolites were investigated in relation to CMRO2, ICP, and GOSe at 6 months. By univariate analysis, lactate ($r=-0.42$) and PG ($r=-0.51$) were the strongest predictors for CMRO2, PG ($r=0.30$) for ICP, and lactate ($r=-0.43$), PG ($r=-0.45$), and α-glucose for GOSe. The GLM and multimodel inference indicated that the combined metabolites of PG, glutamine, α-glucose, and creatinine were the strongest subset of predictors for CMRO2, ICP, and GOSe.

Limitations

The primary limitation of this project was that this was a small global observational study. CSF draws were not matched to specific clinical parameters such as an increase in intracranial pressure, radiographic findings, or jugular desaturation. There was also a pronounced age disparity between the patients in the TBI pool and the older, non-injured group. The effects of this age difference are unclear, but will be addressed in future studies.

Also of note is the difference in sampling technique, where the majority of non-injured samples were collected via lumbar drain, whereas TBI samples were collected via ventriculostomy. This will be difficult to control even in future studies, given the invasiveness of ventriculostomy. Nevertheless, non-injured samples collected via ventriculostomy in this study yielded similar results to the non-injured samples collected via lumbar puncture, especially with regard to PG concentrations (PG was universally low or non-existent). Furthermore, the fact that cranial CSF is in continuous flux with spinal CSF suggests that either sampling method might be suitable.

As mentioned previously, the resolution in the H-NMR of CSF was limited and presented difficulties during the manual analysis of the spectra. Improvements in the resolution of spectra could be accomplished by the use of 2D-NMR and the addition of other chromatographic techniques such as gas chromatography mass spectroscopy.

Conclusion

This study revealed that NMR analysis of CSF metabolites from TBI patients was uniquely different that of non-injured subjects. The concentration of several metabolites, such as lactate, PG, and glutamine, were higher after TBI. Additionally, the correlation between the concentrations of many of the metabolites was different in non-injured and TBI subjects. For example, lactate correlated negatively with glutamine in non-injured subjects, while it correlated positively following TBI.

Unique findings were observed for the glucose metabolites. Glucose can naturally exist in two anomeric forms (alpha and beta), with β-glucose as the predominant form. β- and α-glucose correlated strongly in non-injured subjects, while exhibiting a weaker correlation in TBI patients. Furthermore, α-glucose, but not β-glucose, was shown to be a stronger predictor of ICP, GOSe, and $CMRO_2$. These findings, taken in conjunction with the presence of PG after TBI, suggest alterations in glucose metabolism following injury. PG can be produced from the methylglyoxal pathway, which can be produced by altered glucose metabolism and hyperglycemia.

Metabolomic analysis of CSF from TBI patients offers a unique window into the pathophysiology of this disease and leads to the discovery of novel biomarkers. The analysis of inter-relationships among the various metabolites is potentially a new way of metabolically diagnosing TBI.

Acknowledgments The authors would like to acknowledge and thank the ICU staff of the Ronald Reagan UCLA Medical Center. Financial support was provided from the University of California Neurotrauma Initiative, the UCLA Brain Injury Research Center, The MacDonald Family Grant, The Baskin and Bronson Family Foundation, Evelyn Freed, and NINDS: PO1NS058489, 1R21NS055902, 1R21NS057252.

Conflict of Interest We declare that we have no conflict of interest.

References

1. Bergsneider M, Yang I, Hu X, Mcarthur DL, Cook SW, Boscardin WJ (2004) Relationship between valve opening pressure, body position, and intracranial pressure in normal pressure hydrocephalus: paradigm for selection of programmable valve pressure setting. Neurosurgery 55(4):851–859
2. Cold GE, Jensen FT, Malmros R (1977) The cerebrovascular CO_2 reactivity during the acute phase of brain injury. Acta Anaesthesiol Scand 21:222–231
3. Cruz F, Cerdan S (1999) Quantitative 13C NMR studies of metabolic compartmentation in the adult mammalian brain. NMR Biomed 12(7):451–462
4. De Salle AA, Muizelaar JP, Young HF (1987) Hyperglycemia, cerebrospinal fluid lactic acidosis, and cerebral blood flow in severely head-injured patients. Neurosurgery 21(1):45–50
5. Enevoldsen EM, Jensen FT (1977) Cerebrospinal fluid lactate and pH in patients with acute severe head injury. Clin Neurol Neurosurg 80(4):213–225
6. Fiehn O (2002) Metabolomics- the link between genotypes and phenotypes. Plant Mol Biol 48:155–171
7. Govindaraju V, Young K, Maudsley AA (2000) Proton NMR chemical shifts and coupling constants for brain metabolites. NMR Biomed 13:129–153
8. Keeler J (2005) Understanding NMR spectroscopy. Wiley, New York
9. Lutz NW, Viola A, Malikova I, Confort-gouny S, Audoin B, Ranjeva JP, Pelletier J, Cozzone PJ (2007) Inflammatory multiple-sclerosis plaques generate characteristic metabolic profiles in cerebrospinal fluid. PLoS One 2(7):e595
10. Morshed KM, Jain SK, McMartin KE (1994) Acute toxicity of propylene glycol: an assessment using cultured proximal tubule cells of human origin. Fundam Appl Toxicol 23(1): 38–43
11. Myint KT, Aoshima K, Tanaka S, Nakamura T, Oda Y (2009) Quantitative profiling of polar cationic metabolites in human cerebrospinal fluid by reversed-phase nanoliquid chromatography/mass spectrometry. Anal Chem 81(3):1121–1129
12. Nagae-Poetscher LM, McMahon M, Braverman N (2004) Metabolites in ventricular cerebrospinal fluid detected by proton magnetic resonance spectroscopic imaging. J Magn Reson Imaging 20(3):496–500
13. Oliver SG, Winson MK, Kell DB, Baganz F (1998) Systematic functional analysis of the yeast genome. Trends Biotechnol 16(9):373–378
14. Preece NE, Cerdan S (1996) Metabolic precursors and compartmentation of cerebral GABA in vigabatrin-treated rats. J Neurochem 67(4):1718–1725
15. Satoh E, Murakami K, Nishimura M (2004) Propylene glycol releases calcium from mitochondrial stores in rat cerebrocortical synaptosomes. Int J Neurosci 114(9):1111–1118
16. Sinclair AJ, Viant MR, Ball AK, Burdon MA, Walker EA, Stewart PM, Rauz S, Young SP (2010) NMR-based metabolomic analysis of cerebrospinal fluid and serum in neurological diseases – a diagnostic tool? NMR Biomed 23(2):123–132
17. Toczylowska B, Chalimoniuk M, Wodowska M, Mayzner-Zawadzk E (2006) Changes in concentration of cerebrospinal fluid components in patients with traumatic brain injury. Brain Res 1104(1):183–189
18. Vespa P, Bergsneider M, Hattori N (2005) Metabolic crisis without brain ischemia is common after traumatic brain injury: a combined microdialysis and positron emission tomography study. J Cereb Blood Flow Metab 25(6):763–774
19. Wagner W, Koch D (2005) Mechanisms of failure after endoscopic third ventriculostomy in young infants. J Neurosurg 103(1 Suppl): 43–49
20. Wishart DS, Lewis MJ, Morissey JA, Flegel MD, Jeronick K, Xiong Y, Cheng D, Eisner R, Gautam B, Tzur D, Sawhney S, Bamforth F, Greiner R, Li L (2008) The human cerebrospinal fluid metabolome. J Chromatogr B Analyt Technol Biomed Life Sci 871(2):164–173

Cortical Damage Following Traumatic Brain Injury Evaluated by Iomazenil SPECT and In Vivo Microdialysis

Hiroyasu Koizumi, Hirosuke Fujisawa, Eiichi Suehiro, Hideyuki Iwanaga, Jyoji Nakagawara, and Michiyasu Suzuki

Abstract [^{123}I] iomazenil (IMZ) single photon emission computed tomography (SPECT) has been reported to be a useful marker of neuronal integrity. We evaluated cortical damage following traumatic brain injury (TBI) with IMZ SPECT at the acute stage. After conventional therapy for a cranial trauma, an IMZ SPECT re-evaluation was performed at the chronic stage. A reduction in IMZ uptake in the location of cerebral contusions was observed during the TBI acute phase; however, images of IMZ SPECT obtained during the chronic phase showed that areas with decreased IMZ distribution were remarkably reduced compared with those obtained during the acute phase. As a result of in vivo microdialysis study, the extracellular levels of glutamate in the cortex, where decreased IMZ distribution was shown during the acute phase, were increased during the 168-h monitoring period. During the chronic phase, IMZ uptake in the region with the microdialysis probes was recovered. The results suggest that this reduction in IMZ uptake might not be a sign of irreversible tissue damage in TBI.

Keywords Iomazenil SPECT • In vivo microdialysis • Traumatic brain injury • Neuronal integrity

H. Koizumi (✉), H. Fujisawa, E. Suehiro, and M. Suzuki
Department of Neurosurgery,
Yamaguchi University School of Medicine,
Minami-Kogushi, Ube, Yamaguchi 755-8505, Japan
e-mail: hiroyasu@yamaguchi-u.ac.jp

H. Iwanaga
Department of Radiology,
Yamaguchi University School of Medicine,
Ube, Yamaguchi, Japan

J. Nakagawara
Department of Neurosurgery and Nuclear Medicine/Radiology,
Nakamura Memorial Hospital,
Chuo-ku, Sapporo, Japan

Introduction

[^{123}I] iomazenil (IMZ) has been developed as a tracer for single photon emission computed tomography (SPECT). Specific radioligands for the central benzodiazepine receptor, such as IMZ and ^{11}C-flumazenil (FMZ), which had been developed as a tracer for positron emission tomography (PET), are highly sensitive to damage of the neuronal membrane and are favored as ideal markers of neuronal integrity. A number of studies have reported the usefulness of IMZ SPECT and FMZ PET in detecting incomplete cerebral infarction at the acute stage [1–3]; however, the reduced binding potentials of these radioligands for the central benzodiazepine receptor are considered to be irreversible reactions [1]. We evaluated cortical damage following traumatic brain injury (TBI) with IMZ SPECT and a 168-h period of in vivo microdialysis monitoring was performed for the patient to investigate the extracellular levels of glutamate in the cortex where reduced IMZ uptake was shown at the acute stage. The results were notable; therefore, we discussed neuronal viability in damaged cortex following TBI with reference to the literature.

Materials and Methods

Patient

The patient is a 56-year-old woman who sustained a TBI by falling off a moving bicycle. An acute subdural hematoma on the left side and left temporal lobe contusion and 5-mm midline shift from the left to the right were observed on initial CT images (Fig. 1). A decompressive hemicraniectomy was performed on the day of the injury. During the surgery, dual microdialysis probes were placed into the left temporal and frontal lobe cortices for a 168-h period of monitoring (Fig. 1).

Y. Katayama et al. (eds.), *Brain Edema XV*, Acta Neurochirurgica Supplement, Vol. 118,
DOI 10.1007/978-3-7091-1434-6_21,

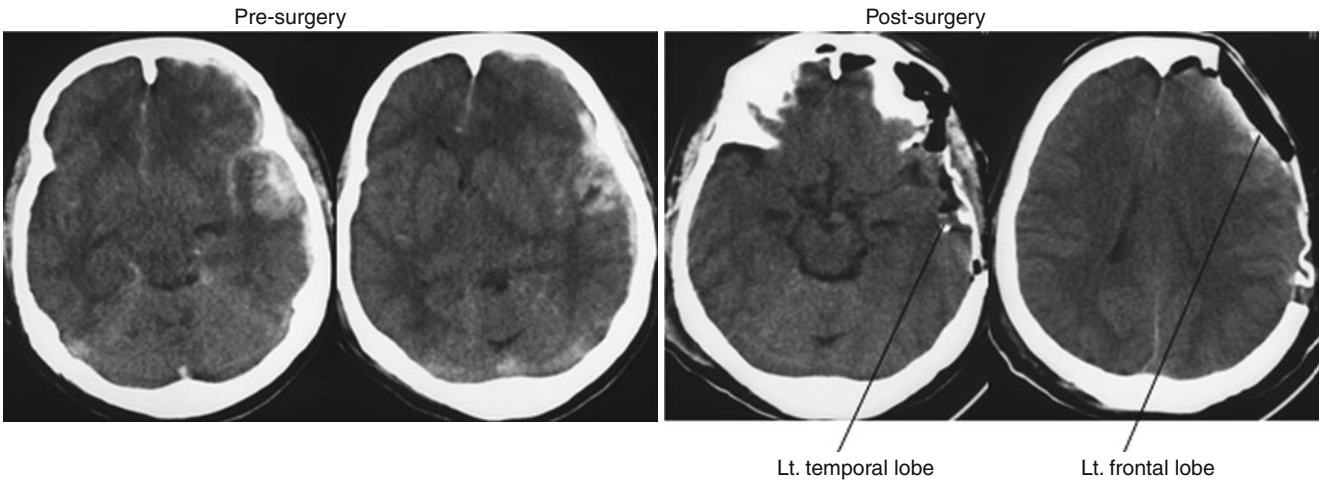

Fig. 1 *Left*: Acute subdural hematoma on the left-hand side and a left temporal lobe contusion and midline shift from the left to the right were observed on cranial CT images. *Right*: Decompressive hemicraniectomy was performed on the day of the injury and dual microdialysis probes were placed in the left frontal lobe and temporal lobe cortices

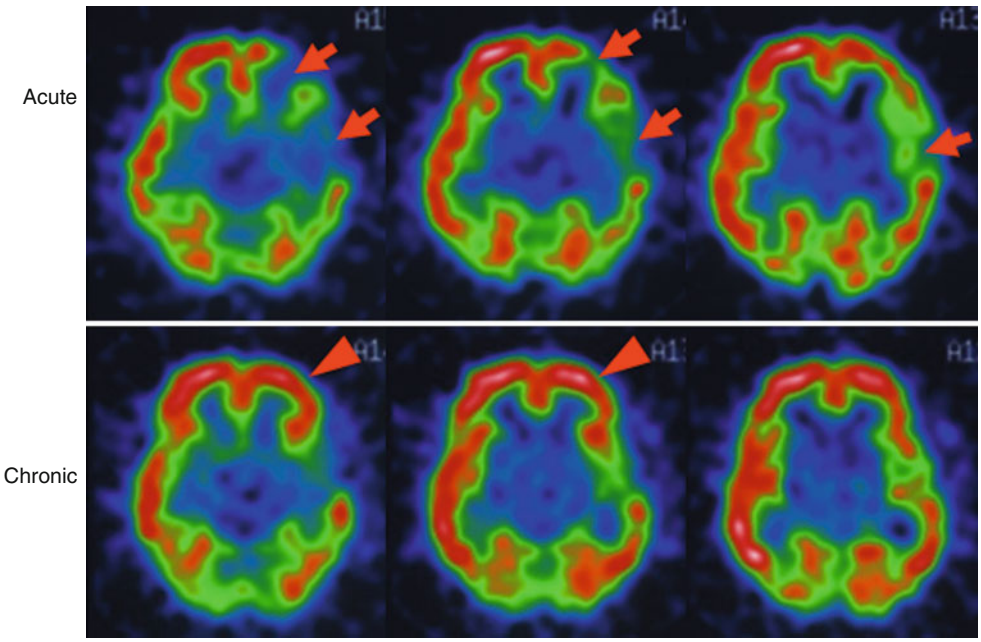

Fig. 2 [^{123}I] iomazenil (IMZ) single photon emission computed tomography (SPECT) acquired at the acute stage after trauma (*top*). Decreased uptake can be seen in part of the left frontal lobe and temporal lobe (*arrows*). IMZ SPECT acquired 2 months after the trauma (*bottom*). Marked recovery of uptake can been seen at the sites of the reduced uptake in the left frontal lobe, which are indicated by *arrowheads*

Iodine-123-Iomazenil SPECT

In this case, IMZ SPECT study was performed at the acute stage 4 days after onset. The patient was injected with a 222-MBq bolus dose of IMZ, and images were obtained 15 and 180 min after the injection. After the conventional treatment for TBI, an IMZ re-evaluation was performed 2 months later. Finally, changes in the areas of decreased IMZ uptake between the acute and chronic stages were investigated.

In Vivo Microdialysis Study

Dual microdialysis probes (CMA 70; CMA Microdialysis, Stockholm, Sweden) placed into the target regions were perfused with Ringer's solution at a flow rate of 0.3 μL/min, and the dialysates were collected every 8 h. Finally, during a 168-h period of monitoring, extracellular levels of glutamate were analyzed using conventional enzymatic techniques (ISCUS; CMA Microdialysis).

Results

On the delayed images of IMZ SPECT acquired at the acute stage after trauma, areas showing decreased accumulation of IMZ were observed in part of the left frontal lobe and temporal lobe (Fig. 2). The regions where dual microdialysis probes were placed happened to coincide with the areas showing reduced IMZ uptake on the images of IMZ SPECT at the acute stage.

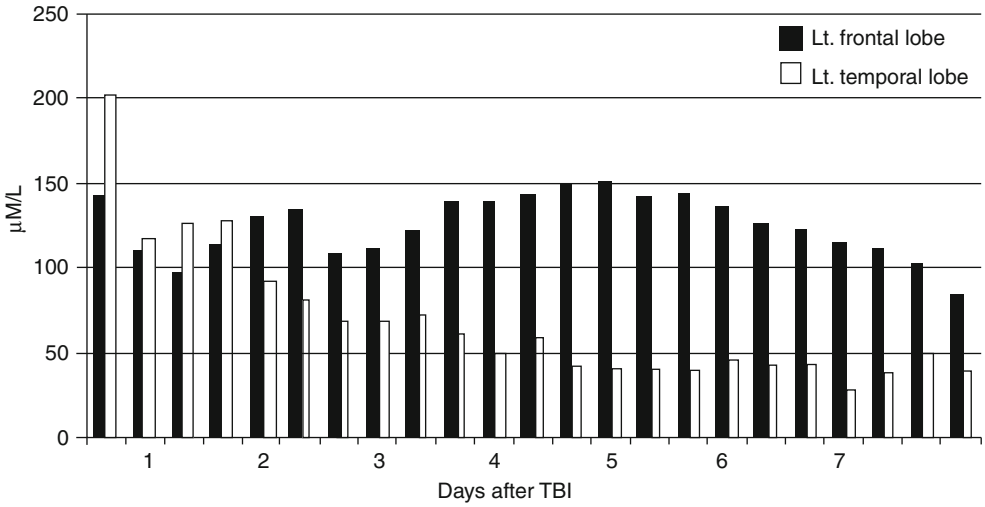

Fig. 3 The changes in extracellular levels of glutamate were higher in the left frontal lobe cortex, where marked recovery of IMZ uptake can be seen at the chronic stage

An IMZ SPECT re-evaluation performed 2 months later showed marked recovery of the decreased IMZ uptake in the left frontal lobe cortex, while IMZ accumulation remained reduced in the left temporal lobe cortex (Fig. 2).

As a result, analysis of dialysates obtained from in vivo microdialysis monitoring showed that the changes in extracellular levels of glutamate were higher in the left frontal lobe cortex than in the temporal lobe cortex during a 168-h period (Fig. 3).

Conclusion

In a previous study, we demonstrated that reduced binding potentials of IMZ can be reversible in patients with TBI [4]. A number of studies with radioligands for the central benzodiazepine receptor have reported that a reduction in the accumulation of the ligand suggests that neuronal loss might predict irreversible functional damage in ischemic stroke [1–3]. No reports have shown that the binding potentials of these radioligands for the central benzodiazepine receptor recovered during the chronic phase after a remarkable reduction in accumulation of the ligands at the acute stage of brain damage. At present, the mechanisms by which TBI is different from ischemic stroke are unknown. Shiga et al. recruited patients with TBI who underwent FMZ PET to investigate the relationship between the distribution of central benzodiazepine receptor and cerebral metabolism [5]. In their study, some of the lesions with abnormally low $CMRO_2$ showed reduced binding potentials of FMZ without abnormalities on MRI. Taking their report into consideration, we supposed that a lesion with metabolic abnormalities exists at the acute stage, and in this lesion reduced IMZ accumulation may be due to reduced affinity of the central benzodiazepine receptor; however, affinity of the receptor may recover in some of the lesions where metabolic abnormalities were normalized at the chronic stage. To prove the hypothesis, further investigation is required to evaluate the regional cerebral metabolism at the acute and chronic stages.

Conflict of Interest We declare that we have no conflict of interest.

References

1. Hatazawa J, Satoh T, Shimosegawa E, Okudera T, Inugami A, Ogawa T, Fujita H, Noguchi K, Kanno I, Miura S, Murakami M, Iida H, Miura Y, Uemura K (1995) Evaluation of cerebral infarction with Iodine-123-iomazenil SPECT. J Nucl Med 36: 2154–2161
2. Heiss WD, Grond M, Thiel A, Ghaemi M, Sobesky J, Rudolf J, Bauer B, Wienhard K (1998) Permanent cortical damage detected by flumazenil positron emission tomography in acute stroke. Stroke 29:454–461
3. Heiss WD, Kracht L, Grond M, Rudolf J, Bauer B, Wienhard K, Pawlik G (2000) Early [^{11}C]Flumazenil/H_2O positron emission tomography predicts irreversible ischemic cortical damage in stroke patients receiving acute thrombolytic therapy. Stroke 31:366–369
4. Koizumi H, Fujisawa H, Kurokawa T, Sueiro E, Iwanaga H, Nakagawara J, Suzuki M (2010) Recovered neuronal viability revealed by Iodine-123-iomazenil SPECT following traumatic brain injury. J Cereb Blood Flow Metab 30:1673–1681
5. Shiga T, Ikoma K, Katoh C, Isoyama H, Matsuyama T, Kuge Y, Kageyama H, Kohno T, Terae S, Tamaki N (2006) Loss of neuronal integrity: a cause of hypometabolism in patients with traumatic brain injury without MRI abnormality in the chronic stage. Eur J Nucl Med Mol Imaging 33:817–822

Decompressive Craniectomy in Trauma: When to Perform, What Can Be Achieved

Piotr Jasielski, Mariusz Głowacki, and Zbigniew Czernicki

Abstract *Subject*: The goal of the study was to evaluate the effectiveness of the decompressive craniectomy (DC) concerning its various parameters.

Material and Methods: Forty-five patients were studied (6 female, 39 male, mean age 53 years). All patients were treated because of severe traumatic brain injury. CT was performed before surgery and on the 1st to 3rd days postoperatively, and was evaluated using specific software. Parameters such as diameter of DC, volume of the additional intradural space obtained, and the shift of the midline were measured.

Results: In the group of patients treated with unilateral DC, the 11-cm craniectomy resulted in an average of 69 mL of additional space. The best score on the Extended Glasgow Outcome Scale (GOS-E) after DC was in patients younger than 35 years old.

Conclusion: In our opinion DC is a suitable method of treatment for patients after severe traumatic brain injury. The best results were achieved in a group of patients aged <50 years, in particular <35 years old. DC gives extra additional space for damaged and edematous brain. DC should be performed early enough and should be large enough. Parameters of the DC obtained positive results with regard to patient status, but there are also other factors such as age and initial Glasgow Coma Scale (GCS) score, which can affect outcome.

Keywords Decompressive craniectomy • Traumatic brain injury • Brain edema • Outcome

P. Jasielski (✉) and M. Głowacki
Department of Neurosurgery,
Mossakowski's Medical Research Centre, PAS,
ul. Cegłowska 80, 01-809 Warsaw, Poland
e-mail: petruspaulus@interia.pl

Z. Czernicki
Department of Neurosurgery,
Mossakowski's Medical Research Centre, PAS,
ul. Cegłowska 80, 01-809 Warsaw, Poland

Department of Neurosurgery,
Warsaw Medical University, Warsaw, Poland

Introduction

Traumatic brain injury (TBI) is a considerable public health problem around the world. According to Polish data, 200–300/100,000 people annually suffer from TBI, traumatic spinal column injury or traumatic spinal cord injury, and 15 % of these injuries are severe [7]. TBI coexists with injuries of other organs in 50 % [7]. In road accidents 55 % of victims suffer from TBI, traumatic spinal column injury or traumatic spinal cord injury [7]. In 2009 in Poland, as a result of 44,196 road accidents, 5,029 resulted in death and 48,952 resulted in injury [20, 22]. According to US statistics, approximately 60 % of patients hospitalized after severe TBI either survive with severe disability or die [18]. Falls are the most frequent cause of TBI [6]. The worst outcome is found in children aged up to 4 years and in adults 65 years or older [6]. The rate of TBI is higher in male subjects than in female subjects in every age group [6]. The hospitalization and death rate after TBI is highest in patients aged 75 years or older [6]. The leading cause of TBI-related death is motor vehicle traffic accidents [6]. The annual burden of TBI in the United States is more than $US 60 billion [8].

The goal of the treatment after severe TBI is a decrease in secondary brain lesions as a result of brain edema and increased intracranial pressure [2]. The surgical treatment of patients after severe TBI that is accepted worldwide is the decompressive craniectomy (DC) [21]. DC is a surgical procedure, in which part of the skull is removed to create additional space for the swollen brain [21]. Decompression is intended to treat increased intracranial pressure and to prevent secondary brain damage [17]. Early DC may be used in the treatment of a patient undergoing emergency surgery (epidural hematoma, subdural hematoma, intracerebral hematoma) [10], when the intracranial volume reserve is exhausted as a result of an increase in intracranial pressure, and when the neurological status of the patient after TBI is quickly deteriorating. There are many different methods of DC after TBI: subtemporal

Y. Katayama et al. (eds.), *Brain Edema XV*, Acta Neurochirurgica Supplement, Vol. 118,
DOI 10.1007/978-3-7091-1434-6_22, © Springer-Verlag Wien 2013

decompression, circular decompression, fronto- or temporoparietal, large fronto-temporoparietal, hemisphere craniectomy, and bifrontal [1, 12–14, 16, 19]. The goal of the surgery is also removing the additional mass from the intracranial space, i.e., hematoma, simultaneous lobectomy, or internal decompression [3, 15].

The aim of this study was to evaluate the effectiveness of DC with regard to its various parameters.

Materials and Methods

Patients

From April 2009 to October 2011 in the Department of Neurosurgery, Mossakowski Medical Research Centre, Polish Academy of Sciences, surgery was performed in 237 patients who suffered from traumatic brain injury. Mortality in this group was 32.91 %. The study involved 45 patients (6 female, 39 male) with severe TBI, who underwent craniectomy. The mean age of the patients was 53 years. Patients were divided into four groups. The first group consisted of 8 patients, 35 years old or younger, the second group 9 patients, aged between 35 and 50 years, the third group 9 patients aged between 51 and 70 years, the fourth group 7 patients above the age of 70 years. In the study group the cause of the injury was mainly falling (Table 1).

Indications and Operative Technique

Patients qualified for surgical treatment after CT examination and clinical assessment, i.e., dynamic changes in the symptoms, intracranial reserve exhaustion, or mass effect. Patients were treated with DC, as a standard large curved dural incision was performed. After removal of the hematoma a large duraplasty was performed using a flap of pericranium. The standard treatment for the brain edema was administered to all patients. On the 1st to 3rd days postoperatively control CTs were performed in all patients. Calculations of the additional volume gained by DC, the parameters of DC, and midline shift were made using the software Praezis Plus (PRECISIS, Heidelberg, Germany).

Results

Forty-three unilateral craniectomies were performed in the study group, bifrontal DC was performed in two patients. Figure 1 shows the relationship between mean craniectomy diameter and additional intracranial space (AIS). In the

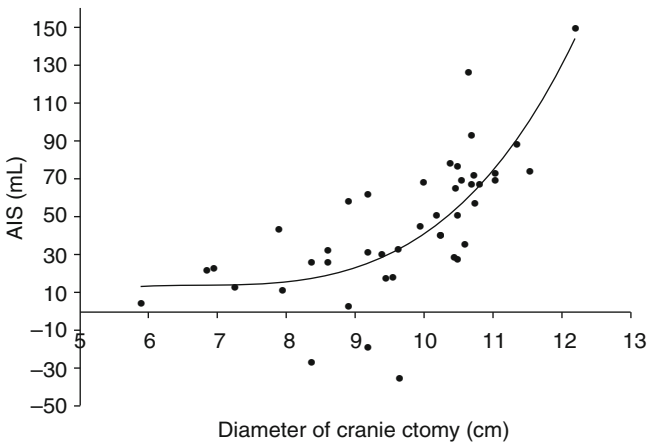

Fig. 1 Additional intradural space (*AIS*) after unilateral craniectomy ($r=0.68$)

Table 1 Clinical information

	Group 1 ($n=8$)	Group 2 ($n=9$)	Group 3 ($n=21$)	Group 4 ($n=7$)
Age (years)	<35	35–50	51–70	>70
Male subjects (%)	8 (100)	7 (77.8)	18 (85.7)	6 (85.7)
GCS at admission				
Arithmetical mean	9.5	7.6	6.5	8.6
Median	9.5	7	4	8
SD	2.5	3.2	3.9	3.2
ASDH	4	5	16	6
ASDH + contusion		1	1	1
Contusion	4	2	1	
ICH			2	
ASDH + ICH		1		
Contusion + ICH + EDH + ASDH			1	

GCS Glasgow Coma Scale, *ASDH* acute subdural hematoma, *EDH* epidural hematoma, *ICH* intracerebral hemorrhage

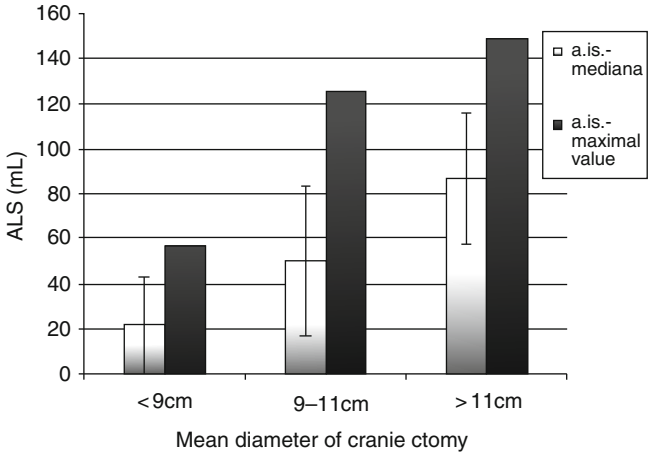

Fig. 2 Additional intradural space (*AIS*) depending on craniectomy diameter (median, SD, maximal value)

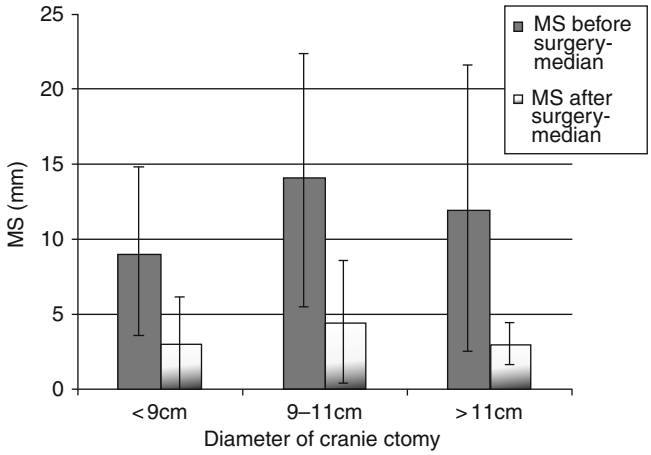

Fig. 3 Midline shift (*MS*) before and after surgery depending on craniectomy diameter (median, SD)

group of patients treated with unilateral DC, the 11-cm craniectomy results in average AIS of 69 mL. The largest unilateral craniectomy had a diagonal measurement of 12.2 cm and resulted in AIS of 148.9 mL. The smallest craniectomy had a diagonal measurement of 5.9 cm and resulted in AIS of 4 mL. There is a statistically significant correlation between AIS after unilateral craniectomy and the diameter of the craniectomy ($r=0.68$).

Patients were divided into three groups according to craniectomy diameter. AIS volume and midline shift were analyzed [9]. The diameter of the craniectomy (cm) in group A was <9 cm, group B 9–11 cm, and in group C>11 cm. The mean AIS in group A was 18.8 mL, in group B 47.6 mL, and in group C 93.4 mL. The largest measurement in group A was 56.8 mL, in group B 125.8 mL, and in group C 148.9 mL. There was a statistically significant correlation between midline shift pre- and postoperatively ($p<0.01$). The results are shown in Figs. 2 and 3.

Table 2 Additional intradural space (AIS) after unilateral craniectomy of similar diameter in various patient age groups (mean, SD, maximal value), $N=25$

	Group 1 ($n=4$)	Group 2 ($n=5$)	Group 3 ($n=10$)	Group 4 ($n=6$)
Age (years)	<35	35–50	51–70	>70
Diameter of craniectomy (mean) cm	9.3	8.9	9.2	9.3
SD	1.6	1.1	1.3	0.7
Additional intradural space (mL)				
Mean	49.6	41.8	33.7	35.6
Median	44.7	56.8	37.5	31.15
SD	36.4	32.9	14.1	14.5
Maximum volume	92.3	77.3	50.5	64.8

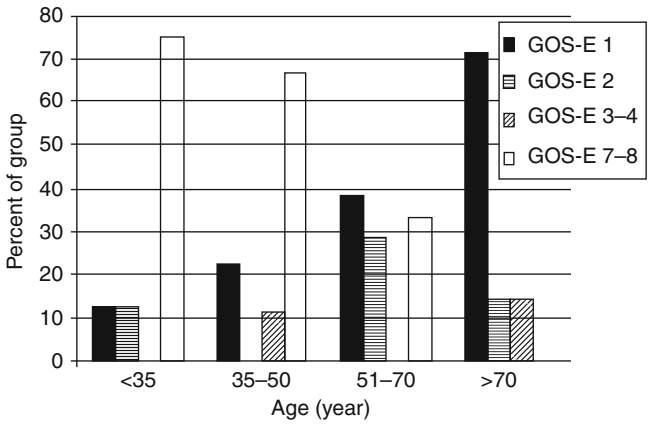

Fig. 4 Outcome at discharge in various age groups of patients (Extended Glasgow Outcome Scale – *GOS-E*)

Patients with similar craniectomy diameters were selected (8.9–9.3 cm). The largest additional intradural space was obtained in the group of patients younger than 35 years old. The results are shown in Table 2.

Figure 4 shows the results of the assessment of patients at discharge according to the Extended Glasgow Outcome Scale (GOS-E). The best GOS-E score was in patients younger than 35 years; fairly good results were achieved in patients younger than 50 years. Death rates and bad outcome were highest in the age group 71 years or older.

Conclusion

In our experience DC is an suitable procedure for the treatment of patients after TBI. Patients with coagulation disorders must be carefully evaluated for DC. Complications after DC rarely occur [5]. Former studies have not drawn satisfactory conclusions as to whether or not DC improves outcome after severe TBI [5, 11].

Our study showed that DC has a significant impact on the results of the treatment of TBI patients. DC should be performed early enough and should be large enough (minimal mean diameter 11 cm). The best outcome after DC for TBI was in a group of patients aged <50 years old, in particular in those <35 years old. Parameters of the DC have obvious results on patient status, but many other factors such as age, initial GCS, and systemic diseases can affect outcome.

A very important factor is the timing of the DC, which may determine the true effect of surgery [4]. Analysis of the timing of the DC should be the subject of the future studies. DC gives the damaged brain an extra chance, because it creates additional space. Very important for its effectiveness is the shape of the dural opening and duraplasty. Gaining space does not mean saving the patient's life in all cases; the severity of the brain damage is what determines whether or not the outcome is bad.

Decompressive craniectomy as a method of treatment for TBI has been widely known for many years, but its effectiveness is still under discussion; thus, there is a need for further detailed studies.

Conflict of Interest We declare that we have no conflict of interest.

References

1. Aarabi B, Hesdorffer DC, Ahn ES et al (2006) Outcome following decompressive craniectomy for malignant swelling due to severe head injury. J Neurosurg 104:469–479
2. Bullock AR, Chesnut R, Ghajar J et al (2006) Introduction: surgical management of traumatic brain injury. Neurosurgery 58(Suppl 3): S2-1–S2-3
3. Caroli M, Locatelli M, Campanella R et al (2001) Multiple intracranial lesions in head injury: clinical considerations, prognostic factors, management and results in 95 patients. Surg Neurol 56:82–88
4. Çavuşoğlu H, Kaya R (2010) Value of early unilateral decompressive craniectomy in patients with severe traumatic brain injury. Ulus Travma Acil Cerrahi Derg 16(2):119–124
5. Cooper DJ, Rosenfeld JV, Murray L et al (2011) Decompressive craniectomy in diffuse traumatic brain injury. N Engl J Med 364(16):1493–1502
6. Faul M, Xu L, Wald MM, Coronado V (2010) Traumatic brain injury in the United States: emergency department visits, hospitalizations and deaths, 2002–2006. Atlanta: Centers for Disease Control and Prevention, National Center for Injury Prevention and Control
7. Fibak J, Michalska E, Widłak-Piernikowa T (2002) Surgery, 2nd edn. PZWL, Warsaw, p 635
8. Finkelstein EA, Corso PS, Miller TR et al (2006) The incidence and economic burden of injuries in the United States. Oxford University Press, New York
9. Głowacki M, Budohoski K, Marszałek P, Walecki J, Czernicki Z (2010) A non-invasive assessment of intracranial volume reserve by measuring cerebrospinal fluid volume with the aid of CT imaging. Acta Neurochir Suppl 106:199–202
10. Holland M, Nakaji P (2004) Craniectomy: surgical indication and technique. Oper Tech Neurosurg 7(1):10–15
11. Huang X, Wen L (2010) Technical considerations in decompressive craniectomy in the treatment of traumatic brain injury. Int J Med Sci 7:385–390
12. Jiang JY, Xu W, Li WP et al (2005) Efficacy of standard trauma craniectomy for refractory intracranial hypertension with severe traumatic brain injury: a multicenter, prospective, randomized controlled study. J Neurotrauma 22:623–628
13. Joint Section on Neurotrauma and Critical Care, The Brain Trauma Foundation, The American Association of Neurological Surgeons (2000) The management and prognosis of severe traumatic brain injury, part 1: guidelines for the management of severe traumatic brain injury. J Neurotrauma 17:451–533
14. Kessler LA, Novelli PM, Reigel DH (1998) Surgical treatment of benign intracranial hypertension-subtemporal decompression revisited. Surg Neurol 50:73–76
15. Kohta M, Minami H, Tanaka K et al (2007) Delayed onset massive edema and deterioration in traumatic brain injury. J Clin Neurosci 14:167–170
16. Maas AI, Dearden M, Teasdale GM et al (1997) EBIC-guidelines for management of severe head injury in adults. European Brain Injury Consortium. Acta Neurochir (Wien) 139:286–294
17. Mracek J, Choc M, Mork J, Vacek P (2011) Osteoplastic decompressive craniotomy – an alternative to decompressive craniectomy. Acta Neurochir 153(11):2259–2263
18. Murray GD, Teasdale GM, Braakman R et al (1999) The European Brain Injury Consortium survey of head injuries. Acta Neurochir (Wien) 141:223–236
19. Polin RS, Shaffrey ME, Bogaev CA et al (1997) Decompressive bifrontal craniectomy in the treatment of refractory posttraumatic cerebral edema. Neurosurgery 41:84–92
20. Symon E, Fidos M (2010) Road accidents in Poland in 2009. The National Police Headquarters
21. Timofeev I, Hutchinson PJ (2006) Outcome after surgical decompression of severe traumatic brain injury. Injury 37:1125–1132
22. Witkowksi J, Dmochowska H (2011) Demographic year book of Poland 2011. Central Statistical Office, Warsaw

Surgical Brain Injury and Edema Prevention

Prativa Sherchan, Cherine H. Kim, and John H. Zhang

Abstract Neurosurgical procedures, carried out routinely in health institutions, present postoperative complications that result from unavoidable brain injury inflicted by surgical maneuvers. These maneuvers, which include incisions, electrocauterization, and retraction, place brain tissue at the margins of the operative site at risk of injury. Brain edema is a major complication that develops subsequent to this surgically induced brain injury. In the present review, we will discuss type of injury as well as the animal model available to study it. In addition, we will discuss potential mediators, including vascular endothelial growth factor, metalloproteinases, and cyclooxygenases, which have been tested in in vivo experimental studies and have been shown to be potential targets for the development of clinical therapies for neuroprotection against brain edema.

Keywords Surgical brain injury • Brain edema • Neurosurgery • Neuroprotection

Introduction

The unique nature of brain tissue poses considerable challenges for neurosurgery. Under the rigid and tough protection of the skull and meninges, the brain is extremely vulnerable to the mechanical insults produced by neurosurgical maneuvers, such as direct incisions, electrocauterization, and retraction. Healthy tissues at the margins of the operative target are inevitably subjected to this surgical brain injury (SBI). Brain edema and hemorrhage are major complications that develop following SBI in neurosurgeries [3]. The blood–brain barrier (BBB), comprising the vascular endothelium, pericyte, and astrocytic processes, prevents the leakage of plasma proteins from the vascular bed into the brain tissue [25]. Vasogenic edema results from the passage of water along with the plasma proteins into the brain tissue because of damage to the capillary endothelium and the interendothelial tight junctions of the BBB, whereas cellular swelling of the injured brain cells results in cytotoxic edema. Both result in increased intracranial pressure, which may lead to further brain injury from cell death or hypoperfusion [3]. Currently, SBI is clinically addressed by nonspecific postoperative care; however, it has become possible to study potential therapies in the preclinical laboratory setting with the recent development of a rodent model for SBI. This review discusses the SBI rodent model and various molecules implicated in the pathogenesis of brain edema as well as treatments that have been applied to reduce brain edema in this model.

P. Sherchan, C.H. Kim, and J.H. Zhang (✉)
Departments of Neurosurgery, Anesthesiology,
Physiology and Pharmacology, Pathology and Human Anatomy,
Loma Linda University School of Medicine,
Loma Linda, CA 92350, USA
e-mail: jhzhang@llu.edu

Surgical Brain Injury Animal Model

An in vivo rodent model was recently developed to study SBI pathophysiology as well as potential therapeutic targets [14, 16, 23]. This model was designed to mimic the injuries sustained from neurosurgical manipulation of brain tissue. The rodent brain is exposed through a small cranial window through which tissue resection is performed. The margins of the resection are designated in relation to the bregma, as shown in Fig. 1. The model provides consistently measureable brain edema using the brain water content (Fig. 2) in the perisurgical site at 24 h. Studies have shown that brain edema in the perisurgical site peaked 24 h after inducing SBI, was significantly higher up to day 3 post-injury, and had subsided by day 7; SBI was associated with neurobehavior deficits that had dissipated by day 7 [16, 23, 34]. Brain edema was assessed using brain water content measurement, Evans blue dye, and IgG extravasation, and by measuring the apparent diffusion coefficient (ADC) values (Table 1).

Y. Katayama et al. (eds.), *Brain Edema XV*, Acta Neurochirurgica Supplement, Vol. 118,
DOI 10.1007/978-3-7091-1434-6_23,

Vascular Endothelial Growth Factor

Vascular endothelial growth factors (VEGFs) are a large family of proteins designated VEGF-A through VEGF-E and are expressed in the choroid plexus and neurons in the normal brain [24]. A well-known growth factor with angiogenic, mitogenic, and permeability-inducing effects, VEGF has also been shown to contribute to SBI-induced brain edema. VEGF-A has a potent hyperpermeability-inducing effect on the microvascular endothelium that is mediated through its receptor VEGF receptor-2 (VEGF-2, kdr) [24]. VEGF-2, a transmembrane tyrosine kinase present in the endothelium of the brain vessels, activates MAPK signaling [19]. An upregulation in VEGF has also been reported in models of TBI predominantly due to the infiltrating neutrophils [5]. VEGF administration and overexpression with viral vectors have both been associated with compromised integrity of the BBB in the rodent brain [29]. A potential mechanism by which VEGF-A might increase BBB permeability involves downregulating the expression of occludin, a tight junction protein; this would disrupt the organization of occludin and ZO-1, another junctional protein, leading to tight junction disassembly [25, 28]. Although VEGF may have potentially reparative actions during later phases after an injury, early inhibition of VEGF or its upstream mediator Src tyrosine kinase have been shown to reduce brain edema in various stroke models [16, 19, 24].

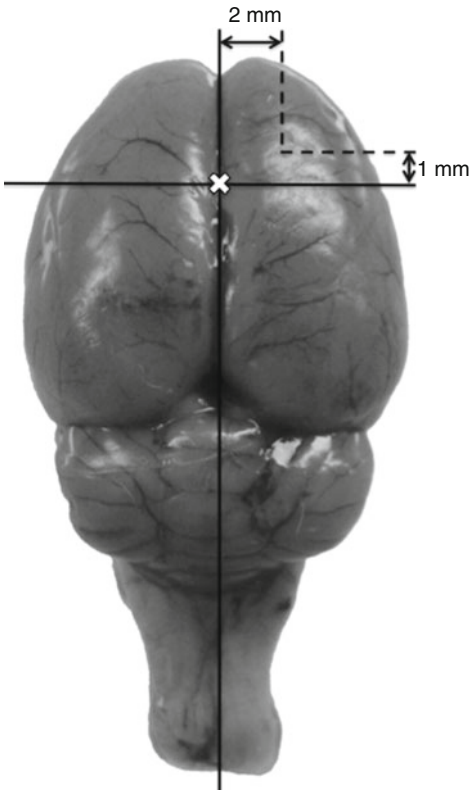

Fig. 1 Partial right frontal lobectomy. Two incisions (*dashed lines*) are made leading away from the bregma (*white X*) along the sagittal and coronal planes, 2 mm lateral to sagittal and 1 mm rostral to coronal respectively

The expression of VEGF was increased at 24 h after SBI in the ipsilateral frontal region surrounding the surgical resection site [16]. The Src family is implicated in VEGF-dependent hyperpermeability [25] and has been shown to be involved in SBI-induced BBB disruption and subsequent brain edema in rodents [16]. An increase in expression of VEGF and p-ERK 1/2 as well as a corresponding decrease in the tight junction protein ZO-1 were reversed when rats were pretreated with PP1, an Src tyrosine kinase inhibitor, prior to inducing SBI [16]. In addition, VEGF was shown to play a possible role in the erythropoietin-induced increase in brain edema during the early phase in a SBI rodent model. Erythropoietin administration led to significantly increased

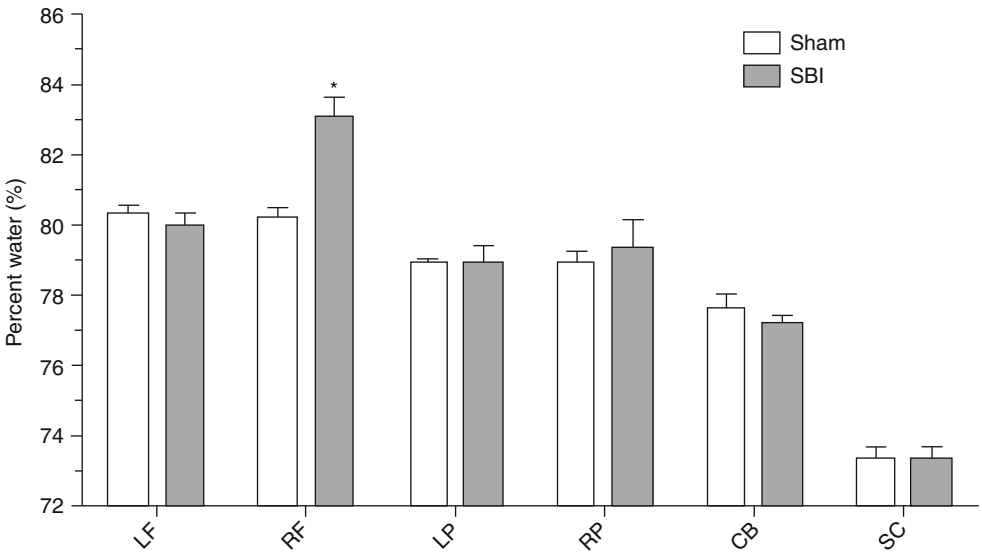

Fig. 2 Twenty-four-hour brain water content. The figure shows marked edema in the right frontal region (bordering the surgical injury) of the brain compared with the sham control group 24 h after the surgical brain injury (SBI). The other brain regions did not differ statistically from each other after the injury. $n=6$. $p<0.05$ for * versus sham. Data are expressed as mean ± SEM. Statistical significance was verified using Student's t test

Table 1 Experimental rodent studies of therapeutic agents for surgical brain injury

Reference	Treatment	SBI findings Treatment outcomes
[23]	Erythropoietin pretreatment	SBI: ↑ brain water content (BWC) Treatment (Tx): harmful, ↑↑ BWC
[22]	NADPH oxidase KO or apocynin pretreatment	SBI: ↑ BWC, ↓neurological score (NS) KO: ↑NS Tx: no effect
[15]	PP1 pretreatment	SBI: ↑VEGF, ↑p-ERK1/2, ↓ZO-1, ↑BWC Treatment: ↓VEGF, ↓p-ERK1/2, ↑ZO-1, ↓BWC
[34]	MMP inhibitor-1 pretreatment	SBI findings: ↑BWC, ↓NS Tx: ↓BWC
[21]	Simvastin pretreatment	SBI: ↑BWC, ↓NS Tx: no effect
[20]	Melatonin pretreatment	SBI: ↑BWC, ↓NS, ↑lipid peroxidation (LPO) Tx (low dose): ↓BWC, ↑NS, ↓LPO Tx (high dose): ↑↑BWC, ↓↓NS, ↑↑LPO
[2]	L-histidine and thioperamide post-treatment	SBI: ↑BWC, ↓NS Tx: ↑↑BWC
[13]	Rosiglitazone pretreatment	SBI: ↑BWC, ↓NS, ↑myeloperoxidase activity (MPO), TNF-α, ↑IL-1β Tx: ↓MPO, ↓TNF-α, ↓IL-1β
[7]	Aminoguanidine post-treatment	SBI: ↑BWC, ↓NS, ↑TNF-α, ↑NF-κB
[12]	Aminoguanidine post-treatment	SBI: ↑malondialdehyde (MDA), ↓glutathione (GSH), aquaporin-4 (AQ-4) Tx (150 mg/kg): ↓BWC, ↓MDA, ↑GSH, ↓AQ-4
[17]	Hyperbaric oxygen preconditioning	SBI: ↑BWC, ↓NS, ↑cyclooxgenase-2 (COX-2), ↑hypoxia-inducible factor-1α (HIF-1α) Tx: ↓BWC, ↑NS, ↓COX-2, ↓HIF-1 α

brain water content in the perisurgical region at 24 h and was associated with increased expression of VEGF [23]. Thus, VEGF-A and its upstream Src tyrosine kinase present potential therapeutic targets for preserving the BBB and reducing brain edema following neurosurgical procedures.

VEGF-B, another member of the VEGF family expressed in the CNS, mediates its effects through the VEGF receptor-1 (VEGF-1, flt-1); VEGF-B is likely responsible for maintaining the BBB in a steady state [25]. Furthermore, when bound to the soluble extracellular portion of VEGFR-1, VEGF is inactive, sequestered, and unable to bind to VEGF receptors [24]. The role of VEGF-B and its receptors in brain edema development following SBI remains to be elucidated.

Matrix Metalloproteinases

Matrix metalloproteinases (MMPs), zinc-dependent endopeptidases involved in tissue remodeling and repair, have been implicated in the SBI-induced destruction of the extracellular matrix proteins of the neurovascular unit. The target substrates of MMPs include collagen IV, fibronectin, and laminin, all of which are critical to maintaining the integrity of the BBB [28]. MMP-2 (gelatinase A) and MMP-9 (gelatinase B) degrade the basal lamina and tight junction proteins of the BBB and promote BBB injury that leads to vasogenic edema during the acute stage in experimental models of brain injury and stroke [9, 28]. Upregulation of MMPs has been demonstrated following subarachnoid hemorrhage, cerebral ischemia, traumatic brain injury (TBI), and intracerebral hemorrhage, and has been shown to contribute to BBB disruption during the early stage of injury [8, 30, 31, 33]. Additionally, MMP-9 knockout mice had improved functional outcomes, lowered BBB permeability, and reduced lesion volume after transient focal cerebral ischemia and TBI [1, 32].

Similarly, the role of MMPs in mediating BBB disruption and brain edema after SBI was demonstrated by Yamaguchi and colleagues [34]. An upregulation of MMP-2 and MMP-9 was temporally associated with BBB disruption after SBI in rats. A significant increase in MMP activity, particularly that of MMP-9, compared with presurgery levels was detected at days 1–14 after SBI, with highest MMP activities observed at days 1 and 3 coinciding with peak values in brain edema; MMP inhibitor, reversed these effects, preserving the BBB integrity and reducing SBI-induced brain edema as early as 3 h post-injury [34]. Evidence of the role of MMPs in the development

of brain edema in the early stages after stroke and in SBI models supports the potential use of MMP inhibition to prevent brain edema following neurosurgical procedures.

Cyclooxygenase-2

Various inflammatory mediators have been implicated in BBB disruption and brain edema after stroke and brain injury [25, 27]. The role of cyclooxygenases, enzymes that catalyze the conversion of arachidonic acid to prostaglandins and thromboxanes [6], in mediating brain edema development has been extensively studied. The upregulation of cyclooxygenase-2 (COX-2), expressed in various cell types including neurons, astrocytes, endothelial cells, macrophages, and microglia in the CNS, has been demonstrated following focal and global cerebral ischemia, neonatal hypoxia–ischemia, and intracerebral hemorrhage [4, 6, 10, 11]. Selective inhibition of COX-2 provided protection after ICH by reducing prostaglandin E_2 production, thereby decreasing inflammation, brain edema, and cell death, which translated into improved functional recovery [6]. Further, the role of COX-2 in mediating preconditioning-induced protection has been suggested. COX-2 has been shown to mediate ischemic preconditioning in vitro [18]. Studies from our laboratory have determined COX-2 to be a potential mediator of hyperbaric oxygen preconditioning (HBO-PC) in SBI and global ischemia rodent models; animals preconditioned for 1 h daily for 5 days with HBO prior to inducing injury had significantly improved neurological function and brain edema [4, 17].

Cyclooxygenase-2 has been shown to play a part in SBI pathophysiology as well. An increase in COX-2 expression was detected 24 h after SBI in mice, and HBO-PC significantly attenuated the increase in COX-2 possibly through suppression of HIF-1α, the upstream regulator of COX-2 [17, 26]. The study showed that HBO-PC increased COX-2 level twofold in comparison to the four-fold increase by the SBI, which suggested that protection conferred by HBO-PC might have involved brain preconditioning by increasing COX-2 to subinjurious levels. Furthermore, the protective effects of HBO-PC were reversed in the presence of selective COX-2 inhibitor. These studies demonstrate HBO-PC or COX-2 inhibition to be promising therapies in attenuating brain edema following neurosurgical procedures.

Conclusion

The SBI rodent model mimics injuries caused by neurosurgical procedures and produces postoperative brain edema. It allows for the study of the cellular signaling pathways and the identification of key molecular targets for neuroprotective pretreatment before neurosurgical intervention. To date, VEGF, MMPs, and COXs have been revealed to be potential targets for therapy. As clinically applicable therapeutic intervention for SBI is likely to result in significant benefits for patients and healthcare organizations, further preclinical and clinical studies are necessary to explore the applicability of these targets.

Conflict of Interest We declare that we have no conflict of interest.

References

1. Asahi M, Wang X, Mori T, Sumii T, Jung JC, Moskowitz MA, Fini ME, Lo EH (2001) Effects of matrix metalloproteinase-9 gene knock-out on the proteolysis of blood-brain barrier and white matter components after cerebral ischemia. J Neurosci 21:7724–7732
2. Bravo TP, Matchett GA, Jadhav V, Martin RD, Jourdain A, Colohan A, Zhang JH, Tang J (2008) Role of histamine in brain protection in surgical brain injury in mice. Brain Res 1205:100–107
3. Bruder N, Ravussin P (1999) Recovery from anesthesia and postoperative extubation of neurosurgical patients: a review. J Neurosurg Anesthesiol 11:282–293
4. Cheng O, Ostrowski RP, Wu B, Liu W, Chen C, Zhang JH (2011) Cyclooxygenase-2 mediates hyperbaric oxygen preconditioning in the rat model of transient global cerebral ischemia. Stroke 42:484–490
5. Chodobski A, Chung I, Kozniewska E, Ivanenko T, Chang W, Harrington JF, Duncan JA, Szymdynger-Chodobska J (2003) Early neutrophilic expression of vascular endothelial growth factor after traumatic brain injury. Neuroscience 122:853–867
6. Chu K, Jeong SW, Jung KH, Han SY, Lee ST, Kim M, Roh JK (2004) Celecoxib induces functional recovery after intracerebral hemorrhage with reduction of brain edema and perihematomal cell death. J Cereb Blood Flow Metab 24:926–933
7. Di F, Yan-Ting G, Hui L, Tao T, Zai-Hua X, Xue-Ying S, Hong-Li X, Yun-Jie W (2008) Role of aminoguanidine in brain protection in surgical brain injury in rat. Neurosci Lett 448:204–207
8. Ding JY, Kreipke CW, Schafer P, Schafer S, Speirs SL, Rafols JA (2009) Synapse loss regulated by matrix metalloproteinases in traumatic brain injury is associated with hypoxia inducible factor-1 alpha expression. Brain Res 1268:125–134
9. Donkin JJ, Vink R (2010) Mechanisms of cerebral edema in traumatic brain injury: therapeutic developments. Curr Opin Neurol 23:293–299
10. Fathali N, Ostrowski RP, Lekic T, Jadhav V, Tong W, Tang J, Zhang JH (2010) Cyclooxygenase-2 inhibition provides lasting protection against neonatal hypoxic-ischemic brain injury. Crit Care Med 38:572–578
11. Graham SH, Hickey RW (2003) Cyclooxygenases in central nervous system diseases: a special role for cyclooxygenase 2 in neuronal cell death. Arch Neurol 60:628–630
12. Hao W, Wu X, Xu R (2009) The molecular mechanism of aminoguanidine-mediated reduction on the brain edema after surgical brain injury in rats. Brain Res 1282:156–161
13. Hyong A, Jadhav V, Lee S, Tong W, Rowe J, Zhang JH, Tang J (2008) Rosiglitazone, a PPAR gamma agonist, attenuates inflammation after surgical brain injury in rodents. Brain Res 1215:218–224
14. Jadhav V, Zhang JH (2007) Surgical brain injury: prevention is better than cure. Front Biosci 13:3793–3797
15. Jadhav V, Matchett G, Hsu FPK, Zhang JH (2007) Inhibition of Src tyrosine kinase and effect on outcomes in a new in vivo model of surgically induced brain injury. J Neurosurg 106:680–686

16. Jadhav V, Solaroglu I, Obenaus A, Zhang JH (2007) Neuroprotection against surgically induced brain injury. Surg Neurol 67:15–20
17. Jadhav V, Ostrowski RP, Tong W, Matus B, Jesunathadas R, Zhang JH (2009) Cyclo-oxygenase-2 mediates hyperbaric oxygen preconditioning-induced neuroprotection in the mouse model of surgical brain injury. Stroke 40:3139–3142
18. Kim E, Raval AP, Defazio RA, Perez-Pinzon MA (2007) Ischemic preconditioning via epsilon protein kinase C activation requires cyclooxygenase-2 activation in vitro. Neuroscience 145:931–941
19. Kusaka G, Ishikawa M, Nanda A, Granger DN, Zhang JH (2004) Signaling pathways for early brain injury after subarachnoid hemorrhage. J Cereb Blood Flow Metab 24:916–925
20. Lee S, Jadhav V, Ayer R, Rojas H, Hyong A, Lekic T, Stier G, Martin R, Zhang JH (2008) The antioxidant effects of melatonin in surgical brain injury in rats. Acta Neurochir Suppl 102: 367–371
21. Lee S, Jadhav V, Lekic T, Hyong A, Allard M, Stier G, Martin R, Zhang J (2008) Simvastatin treatment in surgically induced brain injury in rats. Acta Neurochir Suppl 102:401–404
22. Lo W, Bravo T, Jadhav V, Titova E, Zhang JH, Tang H (2007) NADPH oxidase inhibition improves neurological outcomes in surgically-induced brain injury. Neurosci Lett 414:228–232
23. Matchett G, Hahn J, Obeanus A, Zhang JH (2006) Surgically induced brain injury in rats: the effect of erythropoietin. J Neurosci Methods 158:234–241
24. Merrill MJ, Oldfield EH (2005) A reassessment of vascular endothelial growth factor in central nervous system pathology. J Neurosurg 103:853–868
25. Nag S, Manias JL, Stewart DJ (2009) Pathology and new players in the pathogenesis of brain edema. Acta Neuropathol 118:197–217
26. Ostrowski RP, Colohan AR, Zhang JH (2006) Molecular mechanisms of early brain injury after subarachnoid hemorrhage. Neurol Res 4:399–414
27. Ostrowski RP, Colohan ART, Zhang JH (2005) Mechanisms of hyperbaric oxygen-induced neuroprotection in a rat model of subarachnoid hemorrhage. J Cereb Blood Flow Metab 25:554–571
28. Petty MA, Lo EH (2002) Junctional complexes of the blood–brain barrier: permeability changes in neuroinflammation. Prog Neurobiol 68:311–323
29. Proescholdt MA, Heiss JD, Walbridge S, Muhlhauser J, Capogrossi MC, Oldfield EH, Merrill MJ (1999) Vascular endothelial growth factor (VEGF) modulates vascular permeability and inflammation in rat brain. J Neuropathol Exp Neurol 58:613–627
30. Rosenberg GA, Yang Y (2007) Vasogenic edema due to tight junction disruption by matrix metalloproteinases in cerebral ischemia. Neurosurg Focus 22(5):E4
31. Sehba FA, Mostafa G, Knopman J, Friedrich V Jr, Bederson JB (2004) Acute alterations in microvascular basal lamina after subarachnoid hemorrhage. J Neurosurg 101:633–640
32. Wang X, Jung J, Asahi M, Chwang W, Russo L, Moskowitz MA, Dixon CE, Fini ME, Lo EH (2000) Effects of matrix metalloproteinase-9 gene knock-out on morphological and motor outcomes after traumatic brain injury. J Neurosci 20:7037–7042
33. Wu H, Zhang Z, Zhao R, Li H, Song Y, Qi J, Wang J (2010) Time course of upregulation of inflammatory mediators in the hemorrhagic brain in rats: correlation with brain edema. Neurochem Int 57:248–253
34. Yamaguchi M, Jadhav V, Obeanus A, Colohan A, Zhang JH (2007) Matrix metalloproteinase inhibition attenuates brain edema in an in vivo model of surgically-induced brain injury. Neurosurgery 61:1067–1076

Traumatic Hematoma of the Posterior Fossa

Satoru Takeuchi, Kojiro Wada, Yoshio Takasato, Hiroyuki Masaoka, Takanori Hayakawa, Hiroshi Yatsushige, Keigo Shigeta, Toshiya Momose, Naoki Otani, Hiroshi Nawashiro, and Katsuji Shima

Abstract Posterior fossa injury is rare, occurring in less than 3 % of head injuries. We retrospectively reviewed patients' clinical and radiological findings, management, and outcomes. The aim of the present study was to investigate the features of posterior fossa hematoma, including posterior fossa epidural hematoma (EDH), posterior fossa subdural hematoma (SDH), and intracerebellar hematoma. From January 1995 to January 2009, 4,315 patients with head trauma were hospitalized at our institution. The present study focused on 41 patients (1.0 %) with traumatic hematomas of the posterior fossa. Eighteen patients had EDH, 10 patients had SDH, and 17 patients had intracerebellar hematomas. In each type of injury, occipital bone fractures were seen in many patients, and hematoma enlargement was often observed within a few days of the injury. In addition, a high frequency of associated lesions and a high poor outcome rate were features of intracerebellar hematomas and posterior fossa SDH. The present study suggests that repeat CT imaging and careful management are necessary until the lesion is stabilized, and patients showing lesions with mass effects should therefore be immediately treated with surgery.

Keywords Head trauma • Posterior fossa • Epidural hematoma • Subdural hematoma • Intracerebellar hematoma

S. Takeuchi (✉), K. Wada, N. Otani, H. Nawashiro, and K. Shima
Department of Neurosurgery,
National Defense Medical College, 3-2 Namiki,
Tokorozawa, Saitama 359-8513, Japan
e-mail: s.takeuchi@room.ocn.ne.jp

Y. Takasato, H. Masaoka, T. Hayakawa, H. Yatsushige,
K. Shigeta, and T. Momose
Department of Neurosurgery,
National Hospital Organization Disaster Medical Center,
3256 Midori-cho, Tachikawa, Tokyo 190-0014, Japan

Introduction

Traumatic posterior fossa hematomas are rare, occurring in less than 3 % of head injuries [3, 12]. Because of their rarity, individual neurosurgeons do not gain much experience in their management. Traumatic posterior fossa hematomas are divided into epidural hematoma (EDH), subdural hematoma (SDH), and intracerebellar hematoma [1–13]. During a 14-year period, we treated 41 patients with traumatic posterior fossa hematoma, including posterior fossa epidural hematoma (PFEDH), intracerebellar hematoma, and posterior fossa subdural hematoma (PFSDH), and have retrospectively investigated the clinicoradiological features in these patients.

Materials and Methods

From January 1995 to January 2009, 4,315 patients with head trauma were admitted to our hospital. We gathered information from the electronic medical records of 41 patients (1.0 % of head traumas) with traumatic posterior fossa hematoma. Only those patients with clear evidence of trauma as the primary etiology were included in this study. We retrospectively reviewed the patient's data with regard to age, sex, mechanism of injury, the presence of skull fractures, hematoma size, the presence of hematoma enlargement, the presence of associated intracranial lesions, management, and outcomes. The level of consciousness and outcome in each patient was assessed using the Glasgow Coma Scale (GCS) score at admission and the Glasgow Outcome Scale (GOS) score at discharge. The GOS scores were classified into favorable (good recovery and moderate disability) or poor outcomes (severe disability, vegetative state, or death). We excluded hematomas that were located only in the clivus, tentorium, or brainstem.

Y. Katayama et al. (eds.), *Brain Edema XV*, Acta Neurochirurgica Supplement, Vol. 118,
DOI 10.1007/978-3-7091-1434-6_24, © Springer-Verlag Wien 2013

Results

Eighteen patients had PFEDH, 10 patients had PFSDH, and 17 patients had intracerebellar hematomas. Four patients had intracerebellar hematomas associated with PFEDH or PFSDH. The clinical and radiological findings, treatments, and outcomes of these patients are summarized in Table 1.

PFEDH

Of the 18 patients, 14 were male and 4 were female, with an age range from 1 to 92 years (mean, 40.0 years). The causes of injury were traffic accidents in 6 patients and falls in 12 patients. The mean admission GCS score was 8.3. The sites of impact were the occipital area in 17 patients (unknown in 1 patient). Skull fractures were revealed in 17 patients (94 %). The hematoma sizes ranged from 0.2 to 3.0 cm (mean, 1.1 cm). Hematoma enlargement was observed in 6 patients (33 %). Eight patients presented with isolated PFEDHs, and 10 patients presented with associated intracranial lesions. The associated intracranial lesions were intracerebellar hematomas in 1 patient, supratentorial contusions in 6 patients, supratentorial SDHs in 2 patients, and subarachnoid hemorrhages (SAHs) in 7 patients. Four patients underwent surgery for PFEDHs within 24 h of injury. The outcomes were a good recovery in 13 patients, moderate disability in 3 patients, severe disability in 1 patient, and death in 1 patient. The poor outcome rate was 11 % and the mortality rate was 5.6 %.

PFSDH (Unpublished Data)

Of the 10 patients, 7 were male and 3 were female, with an age range from 3 to 97 years (mean, 57.5 years). The causes of injury were traffic accidents in 3 patients, falls in 6 patients, and being hit by an iron plate in 1 patient. The mean admission GCS score was 8.3. The sites of impact were the occipital area in 3 patients, the parietal area in 3 patients, both the occipital and frontal areas in 2 patients, and the frontal area in 1 patient (unknown in 1 patient). Skull fractures were revealed in 6 patients (60 %). The hematoma sizes ranged from 0.5 to 2.0 cm (mean, 0.8 cm). Hematoma enlargement was observed in 1 patient (10 %). Two patients presented

Table 1 A summary of characteristics of patients with traumatic posterior fossa hematoma ($n=41$)[a]

Characteristics	PFEDH ($n=18$)	PFSDH ($n=10$)	Intracerebellar hematoma ($n=17$)
Age, years	40.0 ± 25.0	57.5 ± 31.2	56.8 ± 20.5
Sex, *n* (%)			
Male	14 (78)	7 (70)	9 (53)
Female	4 (22)	3 (30)	8 (47)
Mechanism, *n* (%)			
Traffic accident	6 (33)	3 (30)	10 (59)
Fall	12 (67)	6 (90)	7 (41)
Other	0 (0)	1 (10)	0 (0)
Glasgow Coma Scale score	12.0 ± 3.4	8.3 ± 4.3	10.1 ± 4.7
Skull fracture, *n* (%)	17 (94)	6 (60)	13 (77)
Hematoma size, cm	1.1 ± 0.8	0.8 ± 0.5	2.4 ± 1.3
Hematoma enlargement, *n* (%)	6 (33)	1 (10)	2 (12)
Associated intracranial lesion, *n* (%)			
Supratentorial contusion	6 (33)	5 (50)	6 (35)
Supratentorial subdural hematoma	2 (11)	7 (70)	7 (41)
Supratentorial epidural hematoma	0 (0)	0 (0)	2 (12)
Subarachnoid hemorrhage	7 (39)	6 (60)	12 (71)
Intraventricular hemorrhage	0 (0)	0 (0)	2 (12)
Diffuse axonal injury	0 (0)	0 (0)	3 (18)
Surgery, *n* (%)	4 (22)	1 (10)	3 (18)
Outcome, *n* (%)			
Favorable	16 (89)	1 (10)	7 (41)
Poor	2 (11)	9 (90)	10 (59)
Mortality, %	5.6	50.0	41.2

PFEDH posterior fossa epidural hematoma, *PFSDH* posterior fossa subdural hematoma
[a]Four patients had intracerebellar hematoma associated with PFEDH or PFSDH

with isolated PFSDHs, and 8 patients presented with associated intracranial lesions. The associated intracranial lesions were intracerebellar hematoma in 3 patients, supratentorial contusions in 5 patients, supratentorial SDHs in 7 patients, and SAHs in 6 patients. Only 1 patient was treated surgically for PFSDHs associated with intracerebellar hematoma 2 days after injury. Three patients underwent burr hole surgery for supratentorial SDHs. The outcomes were a good recovery in 1 patient, severe disability in 1 patient, a vegetative state in 2 patients, and death in 5 patients. The poor outcome rate was 90 %, with a mortality rate of 50 %.

Intracerebellar Hematoma

We have previously reported our series of intracerebellar hematomas [13]. Briefly, of the 17 patients, 9 were male and 8 were female, with an age range from 16 to 84 years (mean, 56.8 years). The causes of injury were traffic accidents in 10 patients and falls in 7 patients. The sites of impact were the occipital area in 11 patients, the frontal area in 2 patients, the temporal area in 3 patients, and both the occipital and frontal areas in 1 patient. Skull fractures were revealed in 13 patients (76.5 %). The mean admission GCS score was 10.1. The hematoma size ranged from 1.0 to 5.0 cm (mean, 2.4 cm). Hematoma enlargement was observed in 2 patients (12 %). Two patients presented with isolated intracerebellar hematoma, and 15 presented with associated intracranial lesions. The associated intracranial lesions were supratentorial contusions in 6 patients, SDHs in 9 patients, EDHs in 3 patients, SAHs in 12 patients, intraventricular hemorrhage in 2 patients, and diffuse axonal injury in 3 patients. Surgeries for intracerebellar hematomas were performed within 24 h in 2 patients and within 3 days after injury in 1 patient. The outcomes of the 17 patients were a good recovery in 5, moderate disability in 2, severe disability in 1, a vegetative state in 2, and death in 7. The poor outcome rate was 59 % and the mortality rate was 41 %.

Conclusion

PFEDH is the most common type of posterior fossa hematoma [1, 6, 7, 9–11]. The prognosis is favorable if the appropriate management is performed. On the other hand, PFSDH and intracerebellar hematoma are extremely rare, accounting for less than 1 % of head injuries [2–5, 8, 12, 13]. The prognosis is quite poor for both injuries. We consider that the high frequency of associated lesions might contribute to the high poor outcome rate in patients with intracerebellar hematomas or PFSDH.

In our series, occipital bone fractures were seen in many patients with each type of hematoma. Additionally, hematoma enlargement was seen in 33 % of PFEDH patients, 10 % of PFSDH patients, and 12 % of those with intracerebellar hematoma, which was in accordance with previous reports [2–7, 10]. Six patients underwent surgery for posterior fossa hematoma within 24 h, and two patients (25 %) underwent surgery 2 or 3 days after injury because of gradual hematoma enlargement. Therefore, a high level of clinical suspicion, a prolonged period of clinical and radiological observation, and the application of the broadest criteria regarding the indications for CT are necessary, especially when patients have occipital bone fractures.

The optimal criteria for the treatment of posterior fossa hematomas have not yet been established; however, Bullock et al. recommended the following: patients demonstrating a lesion with mass effect on CT or with neurological dysfunction or deterioration referable to the lesion should undergo surgical intervention, where a lesion with mass effect on CT is defined as distortion, dislocation, or obliteration of the fourth ventricle; compression or loss of visualization of the basal cisterns; or the presence of obstructive hydrocephalus [3]. It has been reported that surgery may be recommended for patients with PFEDH more than 15 mm thick, PFSDH larger than 10 mm, or intracerebellar hematoma more than 30 mm in thickness [3–5, 11, 13].

In conclusion, the present study suggests that repeat CT imaging and careful management are necessary for posterior fossa hematomas until such lesions stabilize, and that patients showing a lesion with mass effect should be immediately treated with surgery. Further investigations to elucidate the optimal management of posterior fossa hematomas are needed.

Conflict of Interest We declare that we have no conflict of interest.

References

1. Bor-Seng-Shu E, Aguiar PH, de Almeida Leme RJ, Mandel M, Andrade AF, Marino R Jr (2004) Epidural hematomas of the posterior cranial fossa. Neurosurg Focus 16:ECP1
2. Borzone M, Rivano C, Altomonte M, Baldini M (1995) Acute traumatic posterior fossa subdural haematomas. Acta Neurochir (Wien) 135:32–37
3. Bullock MR, Chesnut R, Ghajar J, Gordon D, Hartl R, Newell DW, Servadei F, Walters BC, Wilberger J, Surgical Management of Traumatic Brain Injury Author Group (2006) Surgical management of posterior fossa mass lesions. Surgical management of posterior fossa mass lesions. Neurosurgery 58:S47–S55
4. d'Avella D, Servadei F, Scerrati M, Tomei G, Brambilla G, Angileri FF, Massaro F, Cristofori L, Tartara F, Pozzati E, Delfini R, Tomasello F (2002) Traumatic intracerebellar hemorrhage: clinico-radiological analysis of 81 patients. Neurosurgery 50:16–25
5. d'Avella D, Servadei F, Scerrati M, Tomei G, Brambilla G, Massaro F, Stefini R, Cristofori L, Conti A, Cardali S, Tomasello F (2003) Traumatic

acute subdural haematomas of the posterior fossa: clinicoradiological analysis of 24 patients. Acta Neurochir (Wien) 145:1037–1044
6. Hayashi T, Kameyama M, Imaizumi S, Kamii H, Onuma T (2007) Acute epidural hematoma of the posterior fossa – cases of acute clinical deterioration. Am J Emerg Med 25:989–995
7. Jang JW, Lee JK, Seo BR, Kim SH (2011) Traumatic epidural haematoma of the posterior cranial fossa. Br J Neurosurg 25:55–61
8. Karasawa H, Furuya H, Naito H, Sugiyama K, Ueno J, Kin H (1997) Acute hydrocephalus in posterior fossa injury. J Neurosurg 86:629–632
9. Karasu A, Sabanci PA, Izgi N, Imer M, Sencer A, Cansever T, Canbolat A (2008) Traumatic epidural hematomas of the posterior cranial fossa. Surg Neurol 69:247–251
10. Malik NK, Makhdoomi R, Indira B, Shankar S, Sastry K (2007) Posterior fossa extradural hematoma: our experience and review of the literature. Surg Neurol 68:155–158
11. Otsuka S, Nakatsu S, Matsumoto S, Sato S, Motozaki T, Ban S, Yamamoto T (1990) Study on cases with posterior fossa epidural hematoma–clinical features and indications for operation. Neurol Med Chir (Tokyo) 30:24–28
12. St John JN, French BN (1986) Traumatic hematomas of the posterior fossa. A clinicopathological spectrum. Surg Neurol 25: 457–466
13. Takeuchi S, Takasato Y, Masaoka H, Hayakawa T (2011) Traumatic intra-cerebellar haematoma: study of 17 cases. Br J Neurosurg 25:62–67

Traumatic Basal Ganglia Hematomas: An Analysis of 20 Cases

Satoru Takeuchi, Yoshio Takasato, Hiroyuki Masaoka, Takanori Hayakawa, Hiroshi Yatsushige, Keigo Shigeta, Naoki Otani, Kojiro Wada, Hiroshi Nawashiro, and Katsuji Shima

Abstract Twenty patients with traumatic basal ganglia hematoma (TBGH) were studied. Of the 20 patients, 16 were male and 4 were female, with an age range of 4–89 years (mean, 54.4 years). The causes of injury were traffic accidents in 12 patients and falls in 8. The mean admission GCS score was 7.5. Skull fractures were revealed in five patients (25 %). The hematoma was found in the putamen in 15 patients (80 %), the thalamus in 4, and the caudate in 1. The mean hematoma volume was 10.7 mL. The CT findings indicated focal contusions in 9 patients, subdural hematoma in 5, intraventricular hemorrhage in 4, subarachnoid hemorrhage in 10, and diffuse axonal injury in 5. Six patients (30 %) underwent surgery. The final outcomes were poor: 7 patients (35 %) died, 1 was in a vegetative state, 4 experienced severe disabilities, and 8 patients (40 %) made a favorable recovery. The statistical analysis identified the GCS score and midline shift as prognostic factors.

Our study revealed interesting characteristics of TBGH, including a high frequency of putaminal involvement, a low frequency of skull fractures, a high frequency of associated intracranial lesions, and a high poor outcome and mortality rate.

Keywords Head trauma • Basal ganglia • Hematoma • Computed tomography

S. Takeuchi (✉), N. Otani, K. Wada, H. Nawashiro, and K. Shima
Department of Neurosurgery, National Defense Medical College,
3-2 Namiki, Tokorozawa, Saitama 359-8513, Japan
e-mail: s.takeuchi@room.ocn.ne.jp

Y. Takasato, H. Masaoka, T. Hayakawa, H. Yatsushige, and K. Shigeta
Department of Neurosurgery,
National Hospital Organization Disaster Medical Center,
3256 Midori-cho, Tachikawa, Tokyo 190-0014, Japan

Introduction

Traumatic basal ganglia hematoma (TBGH) is a rare clinical entity. The incidence of TBGH is reported to be approximately 1–3 % of patients with head injury [2–7]. Because of its rarity, the features and prognostic factors have not been established. We have treated 20 patients with TBGH, and retrospectively investigated the clinicoradiological features of these patients and determined the factors that correlated with outcomes.

Materials and Methods

From April 1996 to December 2008, 4,150 patients with head trauma, including 723 patients with traumatic brain contusions, were hospitalized at our hospital. We gathered information from the patients' electronic medical records, and focused on 20 patients (0.48 % of all head traumas, 2.8 % of all brain contusions) with TBGH. Only those patients with clear evidence of trauma as the primary etiology were included in this study. We retrospectively reviewed the patients' data with regard to age, sex, mechanism of injury, level of consciousness, radiological findings, management, and outcomes. Each patient's level of consciousness and outcome were assessed using the Glasgow Coma Scale (GCS) score at admission and the Glasgow Outcome Scale (GOS) score at discharge. We classified the GOS scores into favorable (good recovery and moderate disability) or poor outcomes (severe disability, vegetative state, or death). The features evaluated on head computed tomography (CT) included the presence of skull fractures, hematoma location, hematoma volume, midline shift, and the presence of associated intracranial lesions.

Y. Katayama et al. (eds.), *Brain Edema XV*, Acta Neurochirurgica Supplement, Vol. 118,
DOI 10.1007/978-3-7091-1434-6_25, © Springer-Verlag Wien 2013

The Mann–Whitney *U* test and Fisher's exact test were used to explore the differences in the clinicoradiological features between the groups. $P<0.05$ was considered to be statistically significant. All statistical analyses were performed using the SPSS version 11.0 software program.

Results

The clinical and radiological findings, treatments, and outcomes are summarized in Table 1. Of the 20 patients, 16 were male and 4 were female, with an age range of 4–89 years (mean, 54.4 years). The cause of injury was traffic accident in 12 patients and a fall in 8. The mean admission GCS score was 7.5. Skull fractures were revealed in five patients (25 %). The hematoma was located in the putamen in 15 patients (80 %), the thalamus in 4, and the caudate in 1. Bilateral hematomas were observed in three patients (15 %). The mean hematoma volume was 10.7 mL. The CT findings indicated focal contusions in 9 patients, subdural hematomas in 5, an epidural hematoma in 1, intraventricular hemorrhage in 4, subarachnoid hemorrhage in 10, and diffuse axonal injuries in 5. Six patients (30 %) underwent surgery: decompressive craniectomy with hematoma evacuation in 4 patients, and CT-guided hematoma evacuation in 2. The outcomes were good recovery in 2 patients, moderate disability in 6, severe disability in 4, vegetative state in 1, and death in 7 patients. The poor outcome rate was 60 % and the mortality was 35 %. The statistical analysis identified the GCS score and midline shift as prognostic factors (both $P<0.05$;Table 2).

Table 1 Summary of the patient characteristics ($n=20$)

Variables	
Age, years	54.4 ± 24.2
Sex, *n* (%)	
Male	16 (80)
Female	4 (20)
Mechanism, *n* (%)	
Traffic accident	12 (60)
Fall	8 (40)
Glasgow Coma Scale score	7.5 ± 3.6
Skull fracture, *n* (%)	5 (25)
Hematoma location, *n* (%)	
Putamen	15 (75)
Thalamus	4 (20)
Caudate	1 (5)
Bilateral hematoma distribution, *n* (%)	3 (15)
Hematoma volume (total), mL	10.7 ± 19.8
Midline shift, *n* (%)	
≥5 mm	7 (35)
<5 mm	13 (65)
Associated intracranial lesion, *n* (%)	
Focal contusion	9 (45)
Subdural hematoma	5 (25)
Epidural hematoma	1 (5)
Intraventricular hemorrhage	4 (20)
Subarachnoid hemorrhage	10 (50)
Diffuse axonal injury	5 (25)
Surgery, *n* (%)	6 (30)
Outcome, *n* (%)	
Favorable	8 (40)
Poor	12 (60)
Mortality, %	35

Representative Case

A 72-year-old man crashed while riding his bicycle and hit his head on the ground. On admission, he was hemiparetic on the right side, with a GCS of 11. A CT showed a left-sided TBGH (volume 41.6 mL), subarachnoid hemorrhage, and intraventricular hemorrhage (Fig. 1a), with a 7-mm midline shift. He underwent CT-guided stereotactic hematoma evacuation. A postoperative CT revealed that the hematoma was subtotally evacuated (Fig. 1b). He was transferred to another hospital with severe disability.

Table 2 The prognostic factors related to outcome

Variables	Favorable outcome group ($n=8$)	Poor outcome group ($n=12$)	*P* value
Age, *n*			
≥60 years	4	6	0.675
<60 years	4	6	
Sex, *n*			
Male	6	10	0.535
Female	2	2	
Mechanism, *n*			
Traffic accident	5	7	0.612
Fall	3	5	

Table 2 (continued)

Variables	Favorable outcome group ($n=8$)	Poor outcome group ($n=12$)	P value
Glasgow Coma Scale score	9.6±3.8	6.0±2.7	0.047
Skull fracture, *n*	1	4	0.296
Hematoma location, *n*			
Putamen	5	10	0.296
Thalamus	2	2	0.535
Caudate	1	0	0.400
Bilateral hematoma distribution, *n*	1	2	0.656
Hematoma volume (total), *n*			
≥10 mL	7	8	0.307
<10 mL	1	4	
Midline shift, *n*			
≥5 mm	0	7	0.010
<5 mm	8	5	
Associated intracranial lesion, *n*			
Focal contusion	4	5	0.535
Subdural hematoma	1	4	0.307
Epidural hematoma	0	1	0.600
Intraventricular hemorrhage	1	3	0.465
Subarachnoid hemorrhage	6	4	0.085
Diffuse axonal injury	2	3	0.693

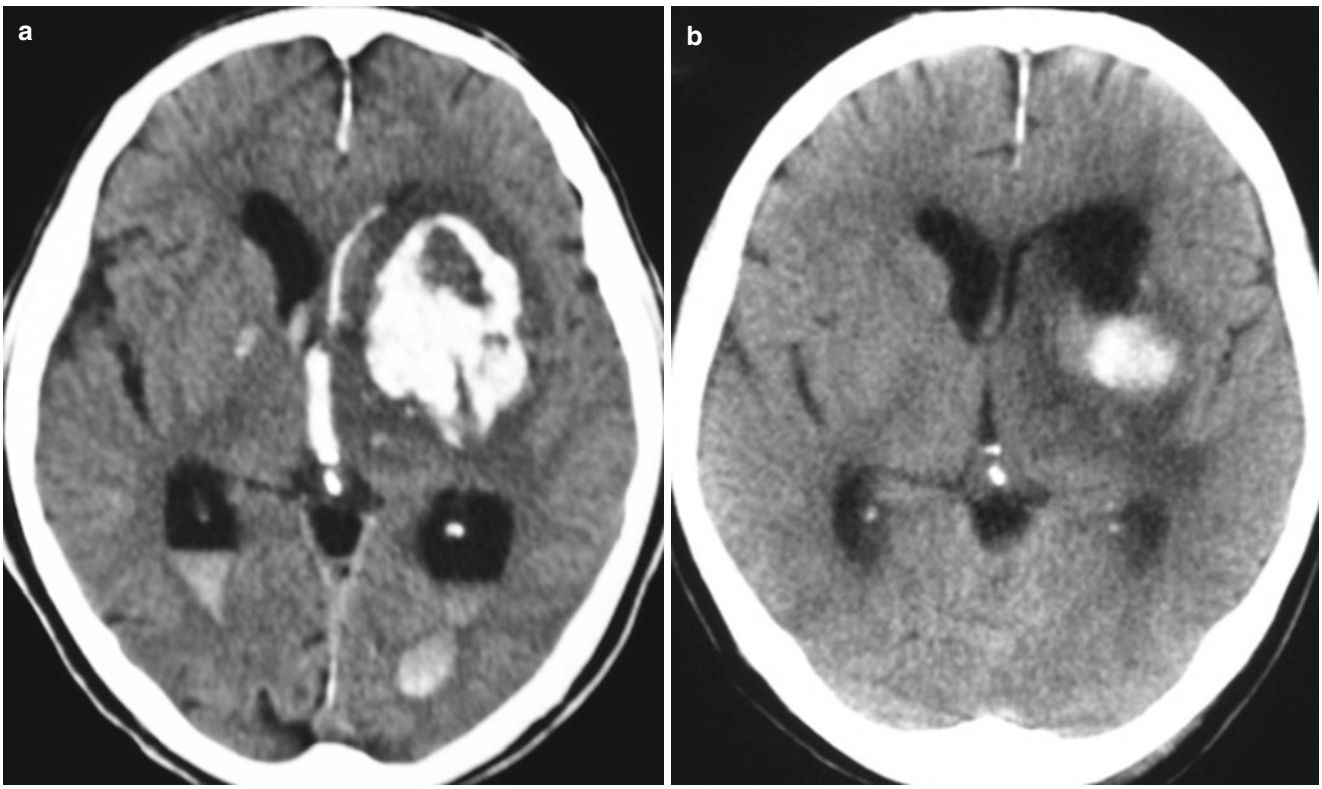

Fig. 1 (**a**) A CT showed a left-sided basal ganglia hematoma (volume: 41.6 mL), subarachnoid hemorrhage, and intraventricular hemorrhage, with a 7-mm midline shift. The patient underwent CT-guided stereotactic hematoma evacuation. (**b**) A postoperative CT revealed that the hematoma was subtotally evacuated

Conclusion

Although the mechanisms responsible for TBGH remain unclear, several pathogenic mechanisms have been proposed. An impact directed toward the tentrium may lead to a shift of the brain through the tentorial notch with pulling and tearing of vessels, which may sometimes occur with enough force to result in the development of TBGH [2, 3]. Shearing injury between the deep nuclei and the perforating vessels may also be one of the mechanisms responsible [2, 3].

In this study, the most frequent location of the hematoma was the putamen, in accordance with past reports [3, 6]. An interesting aspect is the occurrence of bilateral TBGHs [2]. In our series, 3 patients (15 %) had bilateral putaminal hematomas, which correspond to approximately 0.4 % of all brain contusions, which was also in agreement with past reports [1–3, 6]. This seems to be similar to spontaneous intracranial hemorrhage; their bilateral distribution accounts for approximately 0.3 % of all spontaneous hemorrhage [9]. A relatively low frequency of skull fractures and a high frequency of associated intracranial lesions have been reported, as was also the case in the present study [2, 3, 6, 7]. TBGH may be evacuated with open surgery, CT-guided stereotactic surgery, or ultrasound-guided surgery. In our series, 6 patients underwent surgery; however, all of these patients had a poor outcome. Further studies about whether surgery can improve the prognosis of patients with TBGHs are needed.

Some authors have reported that the outcomes of TBGHs are favorable [4, 8, 10], although the incidence of poor outcomes in most past reports was approximately 40–80 % [2, 3, 5, 6], similar to the present study (60 %). We also identified the GCS score and midline shift as prognostic factors. We consider that the poor prognosis might reflect the global nature of injury to the brain, even when the size of the hematoma is small. We also suppose that patients with TBGHs may experience many more severe neurological sequelae because TBGHs are likely to involve the pyramidal tracts in the internal capsule.

In conclusion, the present study revealed interesting characteristics of TBGH, including that it has a high frequency of putaminal involvement, a low frequency of skull fractures, 3a high frequency of associated intracranial lesions, and a high poor outcome and mortality rate. Furthermore, the GCS score and midline shift were identified as prognostic factors.

Conflict of Interest We declare that we have no conflict of interest.

References

1. Adams JH, Doyle D, Graham DI, Lawrence AE, McLellan DR (1986) Deep intracerebral (basal ganglia) haematomas in fatal non-missile head injury in man. J Neurol Neurosurg Psychiatry 49: 1039–1043
2. Boto GR, Lobato RD, Rivas JJ, Gomez PA, de la Lama A, Lagares A (2001) Basal ganglia hematomas in severely head injured patients: clinicoradiological analysis of 37 cases. J Neurosurg 94: 224–232
3. Jayakumar PN, Kolluri VR, Basavakumar DG, Arya BY, Das BS (1989) Prognosis in traumatic basal ganglia haematoma. Acta Neurochir (Wien) 97:114–116
4. Katz DI, Alexander MP, Seliger GM, Bellas DN (1989) Traumatic basal ganglia hemorrhage: clinicopathologic features and outcome. Neurology 39:897–904
5. Kurwale NS, Gupta DK, Mahapatra AK (2010) Outcome of pediatric patients with traumatic basal ganglia hematoma: analysis of 21 cases. Pediatr Neurosurg 46:267–271
6. Lee JP, Wang AD (1991) Post-traumatic basal ganglia hemorrhage: analysis of 52 patients with emphasis on the final outcome. J Trauma 31:376–380
7. Macpherson P, Teasdale E, Dhaker S, Allerdyce G, Galbraith S (1986) The significance of traumatic haematoma in the region of the basal ganglia. J Neurol Neurosurg Psychiatry 49:29–34
8. Sobani ZA, Ali A (2011) Pediatric traumatic putamenal strokes: mechanisms and prognosis. Surg Neurol Int 2:51
9. Takeuchi S, Takasato Y, Masaoka H, Hayakawa T, Yatsushige H, Sugawara T (2011) Simultaneous multiple hypertensive intracranial hemorrhages. J Clin Neurosci 18:1215–1218
10. Yamakawa N, Furuno M, Okada M, Waga S (1995) Traumatic basal ganglia haemorrhage: report of 7 cases. J Clin Neurosci 2:55–58

Subacute Subdural Hematoma

Satoru Takeuchi, Yoshio Takasato, Naoki Otani, Hiroki Miyawaki, Hiroyuki Masaoka, Takanori Hayakawa, Hiroshi Yatsushige, and Keigo Shigeta

Abstract Subacute subdural hematoma (SASDH) is a rare entity. We retrospectively reviewed 8 patients with SASDH. Four patients were male and 4 were female, with an age range of 45–87 years (mean, 67.8 years). The minimal level of deterioration ranged from 8 to 14 (mean, 10.5). The deterioration of neurological symptoms was confirmed 4–20 days after injury (mean, 12.9). The hematoma volume was increased in 6 patients. Seven patients underwent surgeries (burr-hole irrigation in 6, craniotomy in 1). The Glasgow Outcome Scale indicated a good recovery in 4 patients and moderate disability in 4 patients. Increased cerebral blood flow was observed just below the SDH in 1 patient. We consider that the hypoperfused tissue in the acute phase might become hyperperfused during the subacute phase owing to impaired autoregulation, and the hyperperfusion may be responsible for the development of the SASDH, leading to deterioration. Further investigations in a larger series are needed to elucidate the mechanism underlying the development of SASDH.

Keywords Head trauma • Subacute • Subdural hematoma • Surgery

S. Takeuchi (✉) and N. Otani
Department of Neurosurgery, National Defense Medical College,
3-2 Namiki, Tokorozawa, Saitama 359-8513, Japan
e-mail: s.takeuchi@room.ocn.ne.jp

Y. Takasato, H. Masaoka, T. Hayakawa, H. Yatsushige, and K. Shigeta
Department of Neurosurgery,
National Hospital Organization Disaster Medical Center,
3256 Midori-cho, Tachikawa, Tokyo 190-0014, Japan

H. Miyawaki
Department of Traumatology and Critical Care Medicine,
National Defense Medical College,
3-2 Namiki, Tokorozawa, Saitama 359-8513, Japan

Introduction

Subacute subdural hematoma (SASDH) is a rare clinical entity, and has been the focus of only limited investigations because the attention of neurosurgeons has been directed toward acute subdural hematoma (ASDH) and chronic subdural hematoma (CSDH) [2, 3, 7, 8, 10, 11]. Because of their rarity, the features and underlying mechanisms of SASDH have not been established. We have treated eight patients with SASDHs, and retrospectively investigated their features. We herein report these results, and also discuss the potential mechanisms responsible for the development of SASDH from the viewpoint of the cerebral blood flow (CBF).

Materials and Methods

During a period of 12 years, 1,310 patients with a subdural hematoma (SDH) were hospitalized at our hospital. We gathered information from the patients' electronic medical records, and focused on eight patients (0.6 % of all SDHs) with SASDH.

We retrospectively reviewed the patients' clinical and radiological findings, management, and outcomes. We applied the following inclusion criteria for SASDH:

1. ASDH with deteriorating neurological symptoms, such as loss of consciousness, headache during the subacute period (4–20 days after injury) despite the fact that conservative therapy was performed because of a slight neurological deficit on admission.
2. Radiological findings showed no contusion or epidural hematoma.
3. There was no pathological disorder, such as cerebrovascular disease or medications that could cause SDH, except for traumatic brain injury [8].

Y. Katayama et al. (eds.), *Brain Edema XV*, Acta Neurochirurgica Supplement, Vol. 118,
DOI 10.1007/978-3-7091-1434-6_26,

Table 1 A summary of the characteristics of the eight patients

No.	Age/sex (years/old)	Symptoms (other than LOC)	Interval between injury and deterioration	The worst GCS score	Hematoma enlargement	Duration of impaired consciousness	Surgery	Outcome
1	87/F	–	20 days	13	–	21 days	Burr-hole surgery	MD
2	45/M	Pupil abnormality	10 days	8	+	2 days	Burr-hole surgery	MD
3	71/M	Seizure	4 days	14	+	3 days	Burr-hole surgery	GR
4	70/M	Hemiparesis	18 days	14	+	13 days	Burr-hole surgery	GR
5	74/F	–	15 days	13	+	14 days	–	GR
6	59/F	Headache	14 days	6	+	7 days	Craniotomy	GR
7	65/M	Hemiparesis	15 days	10	–	26 days	Burr-hole surgery	MD
8	71/F	Seizure	7 days	6	+	7 days	Burr-hole surgery	MD

GCS Glasgow Coma Scale, *GR* good recovery, *LOC* loss of consciousness, *MD* moderate disability

Results

The clinical findings, treatments, and outcomes of the patients are summarized in Table 1. Four patients were male and 4 were female, with an age range of 45–87 years (mean, 67.8 years). The minimal level of deterioration ranged from 8 to 14 (mean, 10.5). Deterioration of neurological symptoms was confirmed 4–20 days after injury (mean, 12.9). The hematoma volume was increased in 6 patients. Seven patients underwent surgery (burr-hole irrigation in 6, craniotomy in 1). The duration of impaired consciousness ranged from 2 to 26 days (mean, 11.6 days). The outer membrane was observed in all surgical cases, whereas the inner membrane was undetectable. The Glasgow Outcome Scale indicated a good recovery in four patients and moderate disability in four patients.

Representative Case (Case 5)

A 74-year-old woman fell down and hit her head on the ground. Fifteen days after the injury, her consciousness level deteriorated (her GCS score dropped to 13) and she was admitted to our hospital. A CT showed a thin SDH in the left parieto-occipital region (Fig. 1a). She was treated conservatively; however, her impaired consciousness continued. A follow-up CT 9 days after admission revealed a slight increase in the SDH (Fig. 1b). MR fusion ^{99m}Tc-ECD-SPECT images showed an increase in the CBF in the left parieto-occipital lobe (Fig. 1c). Thereafter, she became gradually more alert. A CT demonstrated complete resolution of the SDH 23 days after admission (Fig. 1d), and she was subsequently discharged without neurological deficit.

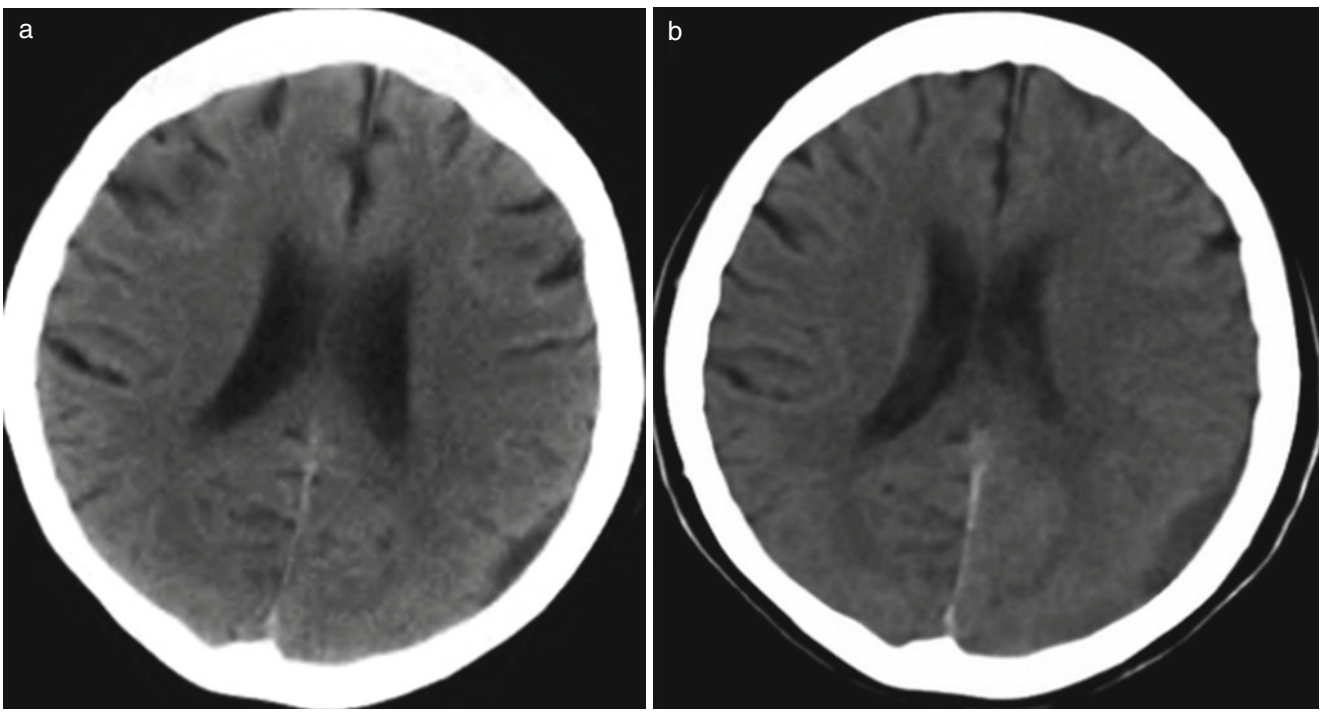

Fig. 1 (**a**) CT on admission showed a thin subdural hematoma in the left parieto-occipital region. (**b**) A follow-up CT 9 days after admission revealed a slight increase in the hematoma. (**c**) MR fusion ^{99m}Tc-ECD-SPECT images showed hyperperfusion in the left parieto-occipital lobe. (**d**) A CT 23 days after admission demonstrated a complete resolution of the hematoma

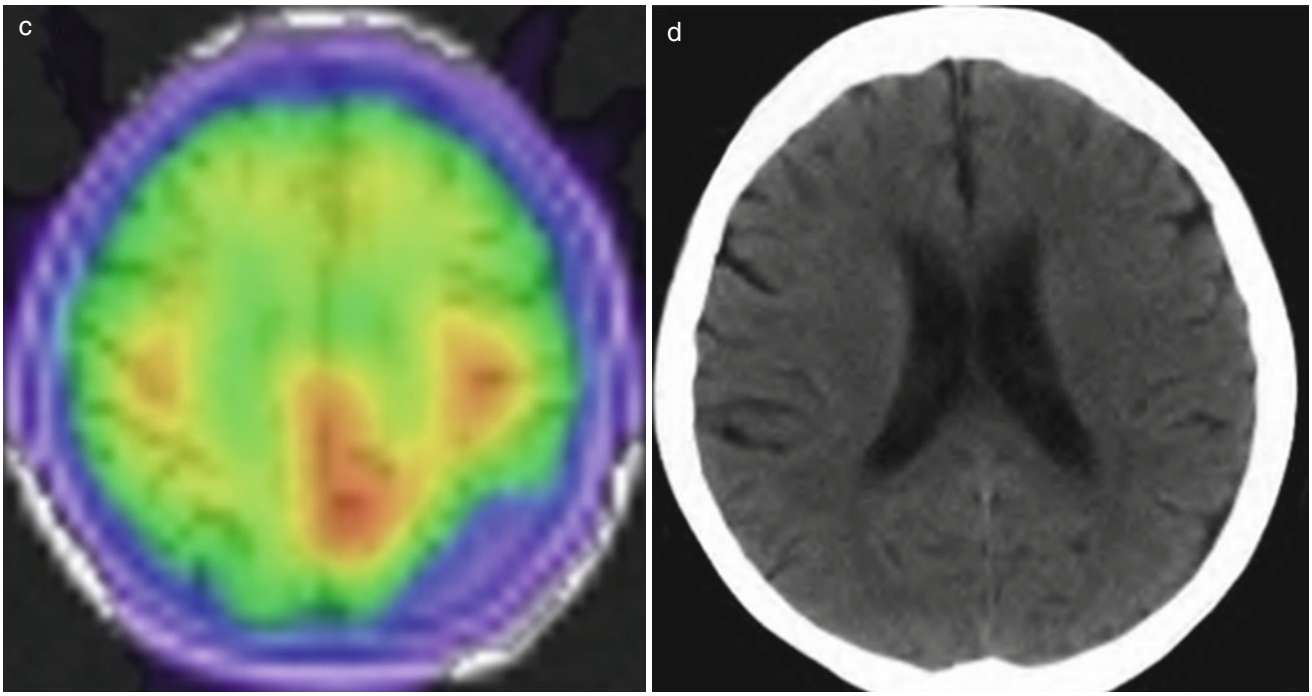

Fig. 1 (continued)

Conclusion

There have been no large series of SASDH, because ASDH patients tend to be managed surgically. The most frequent interval between injury and SASDH development has been reported to be approximately 10–14 days [2, 3, 8, 10], in accordance with our results. Furthermore, the present study showed a high frequency of hematoma enlargement, a relatively long duration of impaired consciousness, and a favorable prognosis.

The mechanism of SASDH has been reported to be secondary to influx of cerebrospinal fluid (CSF) into the subdural space either by colloid-osmotic pressure differences between the liquid hematoma and CSF [2], or owing to the tearing of the arachnoid membrane [8]. Diffuse hypoperfusion is the most frequent finding in cases of ASDH [1, 13], and it has also been reported that most CSDHs show hypoperfusion in the adjacent cortex [5, 6, 9, 12, 14]. In case 5 in our series, hyperperfusion was observed in the region just below the SDH. We consider that the hypoperfused tissue in the acute phase might have become hyperperfused during the subacute phase owing to impaired autoregulation [4, 15], and hyperperfusion may be the mechanism responsible for the development of SASDH, leading to the deterioration. We also suppose that hyperperfusion might contribute to the long durations of impaired consciousness despite the fact that surgery was performed in our series.

Further investigations, including CBF studies, in larger series are needed to elucidate the mechanism responsible for the development of SASDH.

Conflict of Interest We declare that we have no conflict of interest.

References

1. Abe M, Udono H, Tabuchi K, Uchino A, Yoshikai T, Taki K (2003) Analysis of ischemic brain damage in cases of acute subdural hematomas. Surg Neurol 59:464–472
2. Aoki N, Tsutsumi K (1990) Symptomatic subacute subdural haematoma following spontaneous acute subdural haematoma. Acta Neurochir (Wien) 102:149–151
3. Aoki N, Oikawa A, Sakai T (1996) Symptomatic subacute subdural hematoma associated with cerebral hemispheric swelling and ischemia. Neurol Res 18:145–149
4. Deibler AR, Pollock JM, Kraft RA, Tan H, Burdette JH, Maldjian JA (2008) Arterial spin-labeling in routine clinical practice, part 3: hyperperfusion patterns. AJNR Am J Neuroradiol 29: 1428–1435
5. Ikeda K, Ito H, Yamashita J (1990) Relation of regional cerebral blood flow to hemiparesis in chronic subdural hematoma. Surg Neurol 33:87–95
6. Inao S, Kawai T, Kabeya R, Sugimoto T, Yamamoto M, Hata N, Isobe T, Yoshida J (2001) Relation between brain displacement and local cerebral blood flow in patients with chronic subdural haematoma. J Neurol Neurosurg Psychiatry 71:741–746
7. Izumihara A, Orita T, Tsurutani T, Kajiwara K (1997) Natural course of non-operative cases of acute subdural hematoma: sequential computed tomographic study in the acute and subacute stages. No Shinkei Geka 25:307–314
8. Karasawa H, Naito H, Sugiyama K, Ueno J, Kin H, Oketa R (1995) Traumatic subacute subdural hematoma: possible mechanisms that cause their development. Jpn J Neurosurg 4: 121–127
9. Mitchener A, Wyper DJ, Patterson J, Hadley DM, Wilson JT, Scott LC, Jones M, Teasdale GM (1997) SPECT, CT, and MRI in head injury: acute abnormalities followed up at six months. J Neurol Neurosurg Psychiatry 62:633–636
10. Morinaga K, Matsumoto Y, Hayashi S, Omiya N, Mikami J, Sato H, Inoue Y, Okawara S (1995) Subacute subdural hematoma: findings in CT, MRI and operations and review of onset mechanism. No Shinkei Geka 23:213–216

11. Nishio M, Akagi K, Abekura M, Maeda Y, Matsumoto K (1998) A case of traumatic subacute subdural hematoma presenting symptoms arising from cerebral hemispheric edema. No Shinkei Geka 26:425–429
12. Okuyama T, Saito K, Fukuyama K, Yamamoto K, Morimoto M, Aburano T (2000) Clinical study of cerebral blood flow in unilateral chronic subdural hematoma measured by 99mTc-HMPAO SPECT. No To Shinkei 52:141–147
13. Salvant JB Jr, Muizelaar JP (1993) Changes in cerebral blood flow and metabolism related to the presence of subdural hematoma. Neurosurgery 33:387–393
14. Tanaka A, Yoshinaga S, Kimura M (1990) Xenon-enhanced computed tomographic measurement of cerebral blood flow in patients with chronic subdural hematomas. Neurosurgery 27:554–561
15. Teasdale E, Hadley DM (2005) Imaging the head injury. In: Reilly P, Bullock R (eds) Head injury: pathophysiology and management, 2nd edn. Hodder Educational, London, pp 169–214

A Case of Traumatic Hematoma in the Basal Ganglia That Showed Deterioration After Arrival at the Hospital

Takashi Moriya, Rumi Tagami, Makoto Furukawa, Atsushi Sakurai, Kosaku Kinoshita, and Katsuhisa Tanjoh

Abstract A case of traumatic hematoma in the basal ganglia that showed deterioration after arrival at the hospital was reported. A 65-year-old man crashed into the wall while riding a motorcycle. His Glasgow coma scale was E3V4M6 and showed retrograde amnesia and slight right motor weakness. Because head CT in the secondary trauma survey showed subarachnoid hemorrhage in the right Sylvian fissure and multiple gliding contusions in the left frontal and parietal lobe, he was entered into the intensive care unit for diagnosis of diffuse brain injury. He showed complete muscle weakness of left upper and lower limbs 5 h after the accident. Head CT newly showed hematoma, 2 cm in diameter, in the right basal ganglia. The patient vomited following the CT scan, and so his consciousness suddenly deteriorated into a stupor. We performed head CT again. The hematoma had enlarged to 5 cm at the same lesion and partially expanded into midbrain. The patient died on the 13th day of trauma. Based on retrospective interpretation, we conclude that clinical examinations, follow-up CT scans and blood examinations should be performed frequently as part of ICU management for all TBI patients in the early phase after trauma.

Keywords Talk and deteriorate • Traumatic hematoma • Diffuse brain injury • Basal ganglia

Introduction

Patients who talk after head trauma and subsequently deteriorate into a coma are clinically defined as "talk and deteriorate" [4]. They represent a very small but important subgroup of patients with head injury, because these patients are potentially all salvageable, having suffered seemingly mild head trauma. Early recognition and surgical intervention of "talk and deteriorate" is strongly recommended [7]. We have experienced and reported a rare case that initially showed a type of diffuse brain injury then suddenly deteriorated to show a hematoma in the basal ganglia several hours later.

Case Report

A 65-year-old man crashed into a wall while riding a motorcycle. The emergency medical services judged the man to be in need of "high energy injury" transportation to our critical care center. In the primary trauma survey, we secured patency of airways. The patient showed no abnormality in breathing during the physiological examination. His respiration rate was 18/min and arterial oxygen saturation was 100 % with 10 L/min using a reservoir mask. In circulation, no abnormality was present in the airways, in breathing or in circulation. Even though no dysfunction of central nervous system was noted, the patient's Glasgow coma scale was E3V4M6 and showed retrograde amnesia and slight right motor weakness. Because head CT in the secondary trauma survey showed subarachnoid hemorrhage in the right Sylvian fissure and multiple gliding contusions in the left frontal and parietal lobe, the patient was entered into the intensive care unit for diagnosis of diffuse brain injury (Fig. 1). He progressively showed right motor weakness on the right lower limb 4 h after the accident. He suddenly showed complete muscle weakness of left upper and lower limbs five hours after the accident. His head CT newly showed hematoma, 2 cm in diameter, in the right basal ganglia (Fig. 2). Following the scan in the CT room, the patient vomited and his consciousness suddenly deteriorated into a stupor. After urgent endotracheal intubation, we performed another head CT. The hematoma had enlarged to 5 cm at the same lesion and partially expanded into the midbrain (Fig. 3). Although we

T. Moriya, MD, PhD (✉), R. Tagami, M. Furukawa, A. Sakurai, K. Kinoshita, and K. Tanjoh
Division of Emergency and Critical Care Medicine, Department of Acute Medicine, Nihon University School of Medicine, 30-1 Oyaguchi Kamimachi, Itabashi, Tokyo 173-8610, Japan
e-mail: moriya.takashi@nihon-u.ac.jp

Y. Katayama et al. (eds.), *Brain Edema XV*, Acta Neurochirurgica Supplement, Vol. 118,
DOI 10.1007/978-3-7091-1434-6_27,

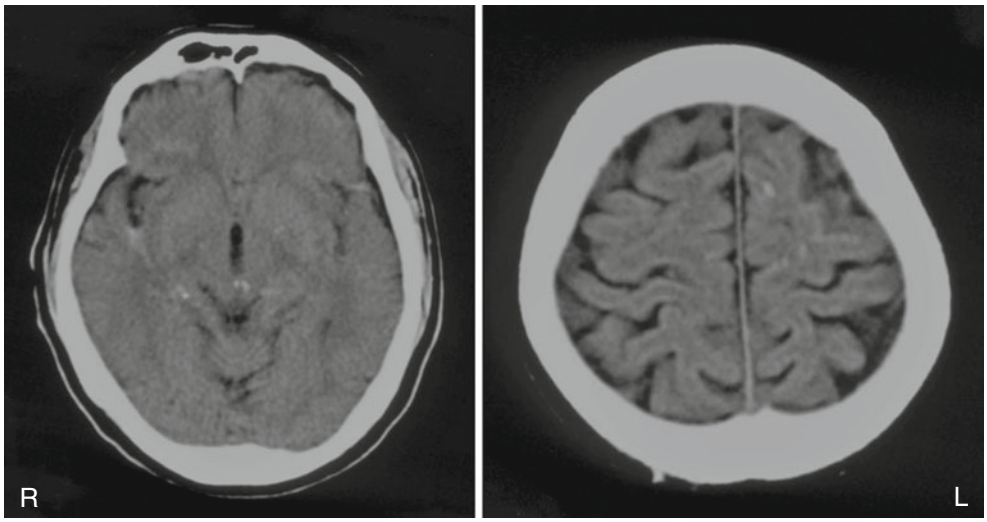

Fig. 1 Computed tomography scan 1 h after the accident (emergency division) showed subarachnoid hemorrhage in the right Sylvian fissure and slight multiple gliding contusions in the left frontal and parietal lobe

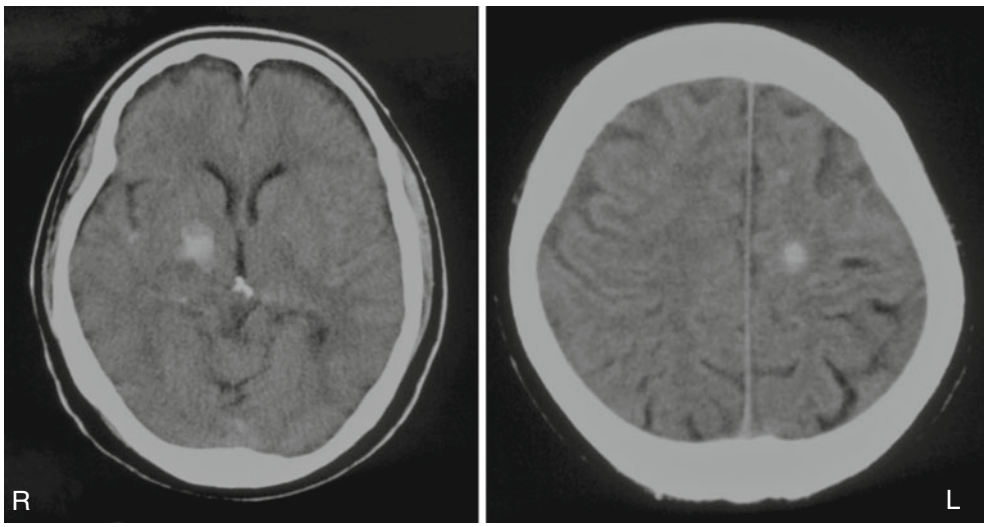

Fig. 2 Computed tomography scan 5 h after the accident furthermore showed hematoma, 2 cm in diameter, in the right basal ganglia

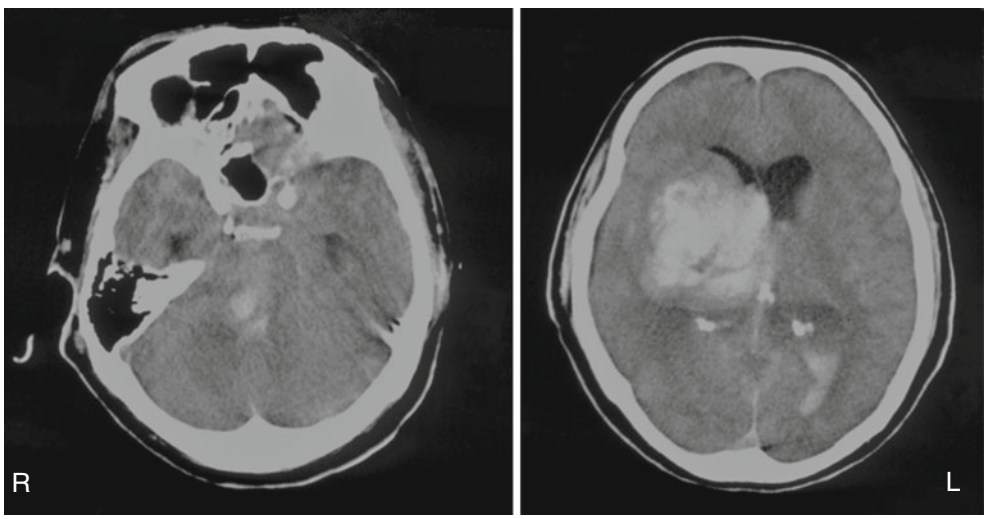

Fig. 3 Computed tomography scan 6 h after the accident showed hematoma enlarged to 5 cm at the same lesion, and partially expanded into the midbrain

considered emergency surgery, his family did not approve. He died on the 13th day of trauma.

Conclusion

The characteristics of clinical pattern for TBI patients who talk and deteriorate have been reported [2, 6]. In this group of patients, it is generally known that the type of injury is focal brain injury, which indicates cerebral contusion or acute subdural/epidural hematoma with no mass effect on initial head CT. However, our rare case shows a type of diffuse brain injury and only subarachnoid hemorrhage and gliding contusion on head CT. Two patients (1.2 %) of 156 cases who showed diffuse brain injury on initial head CT deteriorated [3]. Two patients (2.3 %) of 86 consecutive cases who talk and deteriorate, head CT revealed findings of diffuse brain injury [3].

All TBI patients with altered mental status and hemispheric deficits should undergo CT scanning, especially within a few days after admission. These symptoms of altered mental status and hemispheric deficits are the best predictors of subsequent deterioration or the presence of an operative hematoma [1]. We also performed CT scanning for changes in neurological signs with 6–8 h after admission. However, our case suddenly deteriorated to show new hematoma in the basal ganglia several hours later. We could not induce early operation and consequently resuscitation. The main cause for deterioration in patients who deteriorated within 6 h, the so called "fulminant type" was enlargement of mass lesions [10].

The damaged brain, in proportion to the severity of injury, releases large amount of tissue factor. The increase in fibrinolytic activity at 3 h after trauma correlates with the extent of brain damage regardless of GCS on admission [5]. Takahashi et al have found that following TBI, plasma alpha2-plasmin inhibitor-plasmin complex (PIC) >15 μg/mL, and d-Dimer >5 μg/mL are associated with a poor outcome [8]. We should accurately schedule in not only neurological examination and head CT but also coagulation examination for high risk TBI patients who talk and deteriorate. The assay of fibrinolytic parameters may be especially useful in identifying patients who talk and deteriorate [9].

Conflict of Interest We declare that we have no conflict of interest.

References

1. Andrews BT (1988) Management of delayed posttraumatic intracerebral hemorrhage. Contemp Neurosurg 10:1–6
2. Inoue A, Kohno K, Takeda T, Takechi A, Kohno K, Ishii D, Sasaki U (2005) Eight head trauma patients who talk and die. J Jpn Assoc Acute Med 16:593–599
3. Kawamata T, Katayama Y (2002) Head injured patients who talk and deteriorate: analysis of 86 cases registered on The Japan Neurotrauma Data Bank. Neurotraumatology 25:205–209
4. Marshall LF, Toole BM, Bowers SA (1983) The National Traumatic Coma Data Bank. Part 2: patients who talk and deteriorate: implications for treatment. J Neurosurg 75:285–288
5. Pondaag W (1978) Disseminated intravascular coagulation in head-injured patients. Adv Neurosurg 6:159–163
6. Robato RD, Rivas JJ, Gomez PA, Castafida M, Cafizal JM, Sarabia R, Cabrera A, Murioz MJ (1991) Head-injured patients who talk and deteriorate into coma. Analysis of 211 cases studied with computerized tomography. J Neurosurg 75:256–261
7. Rockswold GL, Pheley PJ (1993) Patients who talk and deteriorate. Ann Emerg Med 22:1004–1007
8. Takahashi H, Urano T, Takeda Y, Nagai N, Takeda A (1997) A fibrinolytic parameters as an admission prognostic marker of head injury in patients who talk and deteriorate. J Neurosurg 86: 367–388
9. Tan JE, Ng I, Lim J, Wong HB, Yeo TT (2004) Patients who talk and deteriorate: a new look at an old problem. Ann Acad Med 33:489–493
10. Yamagami I, Yamaura A, Isobe K (1993) Pathogenesis and management of secondary neural damage in head trauma patients: Analysis of patients who talk and deteriorate "fulminantly". No Shinkeigeka 21:129–133

T2 and T2* Magnetic Resonance Imaging Sequences Predict Brain Injury After Intracerebral Hemorrhage in Rats

Hang Jin, Gang Wu, Shukun Hu, Ya Hua, Richard F. Keep, Jiang Wu, and Guohua Xi

Abstract Magnetic resonance imaging (MRI) has been widely used in intracerebral hemorrhage (ICH) animal models and patients. In the current study, we examined whether MRI can predict at-risk brain tissue during the acute phase and long-term brain tissue loss after ICH. Male Sprague–Dawley rats had an intracaudate injection of autologous whole blood (10, 50 or 100 μL). MRI (T2 and T2*) sequences were performed at days 1, 3, 7, 14, and 28. The volume of brain tissue at risk was calculated as the difference between T2 and T2* lesion volumes. Dopamine- and cAMP-regulated phosphoprotein, Mr 32 kDa (DARPP-32) was used as a neuronal marker in the basal ganglia. Brain swelling at day 3 and brain tissue loss at day 28 after ICH were also measured. We found that the difference in lesion volumes between T2 and T2* measured by MRI coincided well with the difference between the volume of the DARPP-32-negative area and that of the hematoma measured in brain sections. Volumes of brain tissue at risk at day 3 correlated with the brain swelling at day 3 ($p<0.01$) as well as the final brain tissue loss at day 28 ($n=9$, $p<0.05$). The results suggest that the difference between T2 lesions and T2* lesions could be an indicator of at-risk brain tissue and it could be used as a predictor of neuronal loss in ICH patients.

Keywords Magnetic resonance imaging • Intracerebral hemorrhage • Brain swelling • Brain atrophy • DARPP-32

Introduction

Intracerebral hemorrhage (ICH) accounts for 10–15 % of all strokes and is associated with higher mortality and more severe neurological deficits than other stroke subtypes [3, 13]. Perihematomal brain edema develops immediately after ICH and peaks several days later [12]. There is a close temporal relationship between brain edema and neurological deficits [6]. Brain atrophy was found in a rat ICH model [4].

Magnetic resonance imaging (MRI) is an ideal method for characterizing the temporal and spatial evolution of parenchymal alterations following ICH with high sensitivity [1]. T2* gradient-echo imaging has been used in ICH models and patients to evaluate the hematoma size and iron deposition [2, 10]. We hypothesized that a simple MRI examination at an early stage could provide more precise information for predicting brain atrophy. DARPP-32 is a specific marker of GABAergic neurons and is only expressed in the neuronal cell bodies and dendrites in the striatum [9, 15]. The fluorescence-negative area of DARPP-32 can be used as an indicator of damaged brain tissue.

This study examined whether or not early T2- and T2*-weighted MRI imaging can predict at-risk brain tissue during the acute phase and brain tissue loss during the late phase in ICH rats.

H. Jin
Department of Neurosurgery,
University of Michigan, Ann Arbor, MI, USA

Department of Neurology, 1st Affiliated Hospital,
Jilin University, Changchun, China

G. Wu, S. Hu, Y. Hua, and R.F. Keep
Department of Neurosurgery,
University of Michigan, Ann Arbor, MI, USA

J. Wu
Department of Neurology, 1st Affiliated Hospital,
Jilin University, Changchun, China

G. Xi, MD (✉)
Department of Neurosurgery,
University of Michigan, Ann Arbor, MI, USA

Department of Neurosurgery,
University of Michigan, R5018 BSRB, 109 Zina Pitcher Place,
Ann Arbor, MI 48109-2200, USA
e-mail: guohuaxi@umich.edu

Y. Katayama et al. (eds.), *Brain Edema XV*, Acta Neurochirurgica Supplement, Vol. 118,
DOI 10.1007/978-3-7091-1434-6_28, © Springer-Verlag Wien 2013

Materials and Methods

Animal Preparation and Intracerebral Infusion

Animal use protocols were approved by the University of Michigan Committee on the Use and Care of Animals. A total 39 male Sprague–Dawley rats (Charles River Laboratories, Portage, MI, USA), weighing 250–350 g, were used in this study. Rats were anesthetized with pentobarbital (50 mg/kg, i.p.). The right femoral artery was catheterized for continuous blood pressure monitoring and blood sampling. Blood was obtained from the catheter for analysis of blood pH, PaO_2, $PaCO_2$, hematocrit, and blood glucose. Core temperature was maintained at 37 °C. Rats were positioned in a stereotactic frame (Kopf Instruments), and a cranial burr hole (1 mm) was drilled on the right coronal suture 3.5 mm lateral to the midline. A 26-gauge needle was inserted stereotactically into the right basal ganglia (0.2 mm anterior, 5.5 mm ventral, 3.5 mm lateral to the bregma). Autologous whole blood at a volume of 10 μL ($n=4$), 50 μL ($n=5$), and 100 μL ($n=30$) was injected using a microinfusion pump [11]. The rats that had 100 μL of blood injected were euthanized at days 1, 3, 7, 14, and 28 ($n=6$ each time point) and the others were euthanized at day 28 after ICH.

Magnetic Resonance Imaging

Serial MRI, T2-weighted, and T2* gradient-echo imaging (GRE) were performed with a 7.0 T 183 cm Horizontal Bore (Unity Inova, Varian Inc.) imaging spectrometer at days 1, 3, 7, 14, and 28 after ICH. Fifteen 0.5-mm-thick slices were scanned (FOV = 35 × 35mm^2, matrix = 256 × 256, slice gap = 0, flip angle = 25, TR/TE = 4,000 ms/60 ms and 200 ms/5 ms for T2 and T2* imaging respectively). Images were analyzed using NIH Image J. The entire lesion volume was measured on the T2-weighted images and the hematoma volume was measured on the T2*-weighted images. The measurements were as follows:

1. At-risk brain tissue: lesion areas on T2 and T2* weighted images were combined separately and multiplied by section thickness (0.5 mm). At-risk brain tissue volume was obtained by the difference between T2 and T2* lesion volume [8].
2. Brain tissue loss volume: bilateral hemispheres were outlined separately and the areas were measured excluding bilateral ventricle areas on T2-weighted images at day 28 after ICH. Bilateral brain tissue volume was obtained by combining the outlined areas over all slices. Brain tissue loss volume was obtained by the difference in volume between the contralateral and the ipsilateral hemisphere.
3. Brain swelling volume: bilateral hemispheres excluding bilateral ventricles were outlined and measured on T2-weighted images on day 3 after ICH. Brain swelling volume was acquired using the difference in volume between the ipsilateral and the contralateral hemisphere.

Immunofluorescent Staining

Immunofluorescent staining was performed as described previously [14]. The primary antibody was anti-dopamine-and cAMP-regulated phosphoprotein of 32-kDa (DARPP-32) antibody (Cell Signaling Technology, 1:800 dilution). Alexa Fluro 488-conjugated donkey anti-rabbit antibodies (Invitrogen, 1:500 dilution) were used as the secondary antibody.

Results

DARPP-32, a specific marker of GABAergic neurons in basal ganglia [15] was expressed in the neuronal cell bodies and dendrites. At-risk brain tissue area was obtained by two measurements: the difference between the DARPP-32 negative area (Fig. 1a) and the hematoma area (H&E, Fig. 1b), and the difference between T2 (Fig. 1c) and T2* (Fig. 1d) lesions. On day 1 and day 3 after ICH, the difference between T2 and T2* lesion areas on the MRI images was 5.5 ± 1.9 mm^2 on day 1 and 6.7 ± 0.7 mm^2 on day 3 after a 100-μL blood injection. These correlated well with the difference between the DARPP-32-negative area and the hematoma area (4.6 ± 1.0 mm^2 on day 1, and 6.0 ± 0.8 mm^2 on day 3) measured in the brain sections with DARPP-32 immunofluorescent staining. The results indicate that at-risk brain tissue areas measured by MRI reflect the histological measurements (Fig. 1e).

The volume of brain swelling measured on MR images on day 3 (39.7 ± 10.7 mm^3) after rats had a 100-μL blood injection was significantly increased compared with other time points (20.4 ± 7.9 mm^3 on day 1 and 8.4 ± 3.3 mm^3

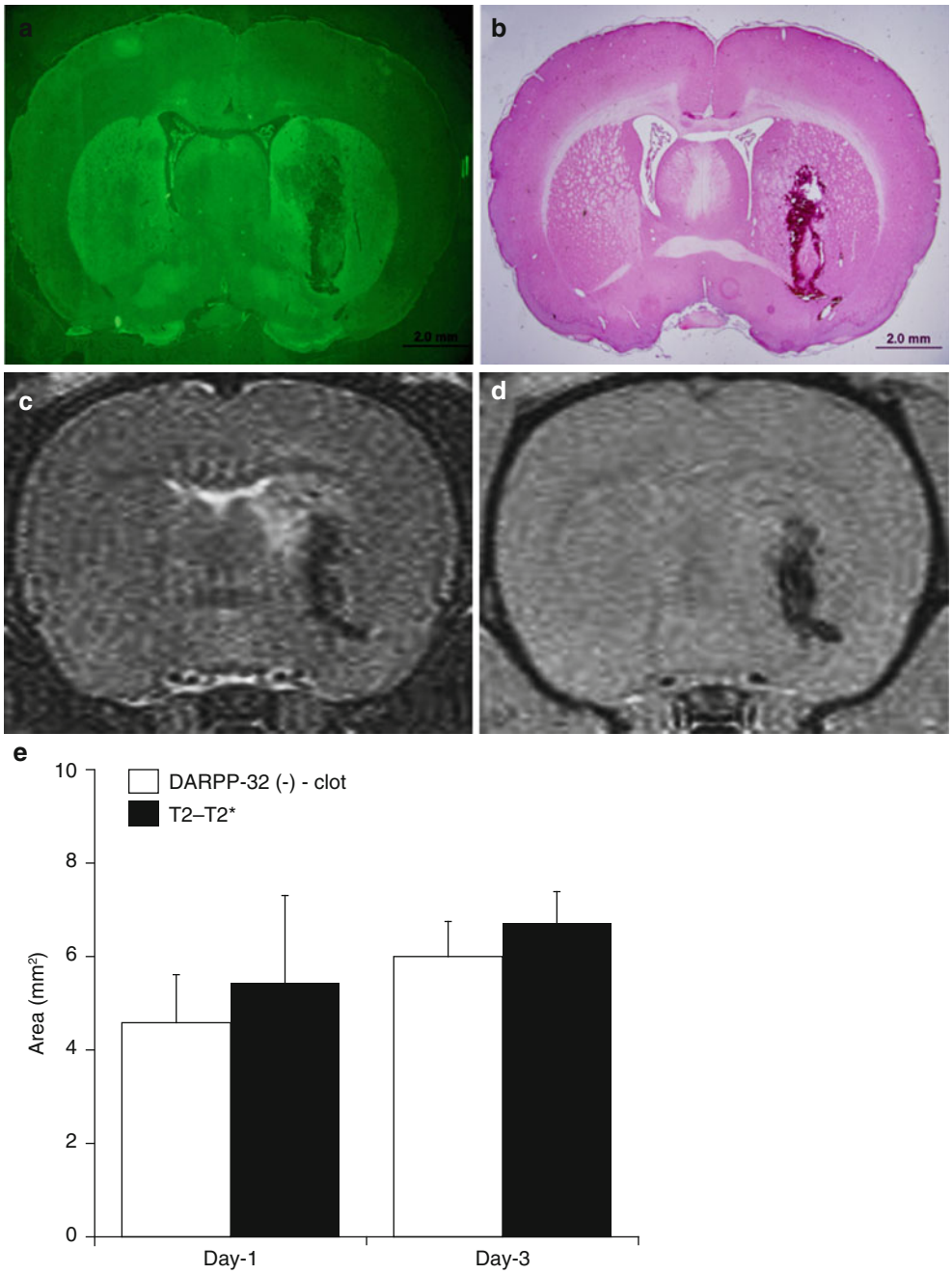

Fig. 1 (**a**) DARPP-32-negative area showing acute neuronal death in the basal ganglia. (**b**) Hematoxylin and eosin stain showing hematoma size. Scale bar = 2 mm; (**c**, **d**) T2 and T2* MR images on day 3 after intracerebral hemorrhage (ICH). (**e**) At-risk brain tissue volumes 1 and 3 days after ICH were determined by the difference between the DARPP-32-negative area and clot size and that between T2 lesions and T2* lesions

on day 7, $p < 0.01$). Volumes of at-risk brain tissue calculated as (T2–T2*) lesion volumes were significantly higher on day 3 (42.5 ± 8.2 mm^3) after ICH compared with other time points (26.9 ± 4.9 mm^3 at day 1 and 6.6 ± 2.8 mm^3 at day 7, $p < 0.01$). Brain swelling volumes on day 3 in rats that had different volumes (10, 50, and 100 μL) of blood injection coincided well with the volume of at risk tissue ($n = 15$, $r = 0.857$, $p < 0.01$, Fig. 2a). Volume of at-risk brain on day 3 after a 10- or 50-μL blood injection also correlated with the final brain tissue loss measured on day 28 ($n = 9$, $r = 0.678$, $p < 0.05$, Fig. 2b). At-risk brain tissue volume measured on MRI images on day 3 could be a desired indicator for predicting long-term brain atrophy (Fig. 3).

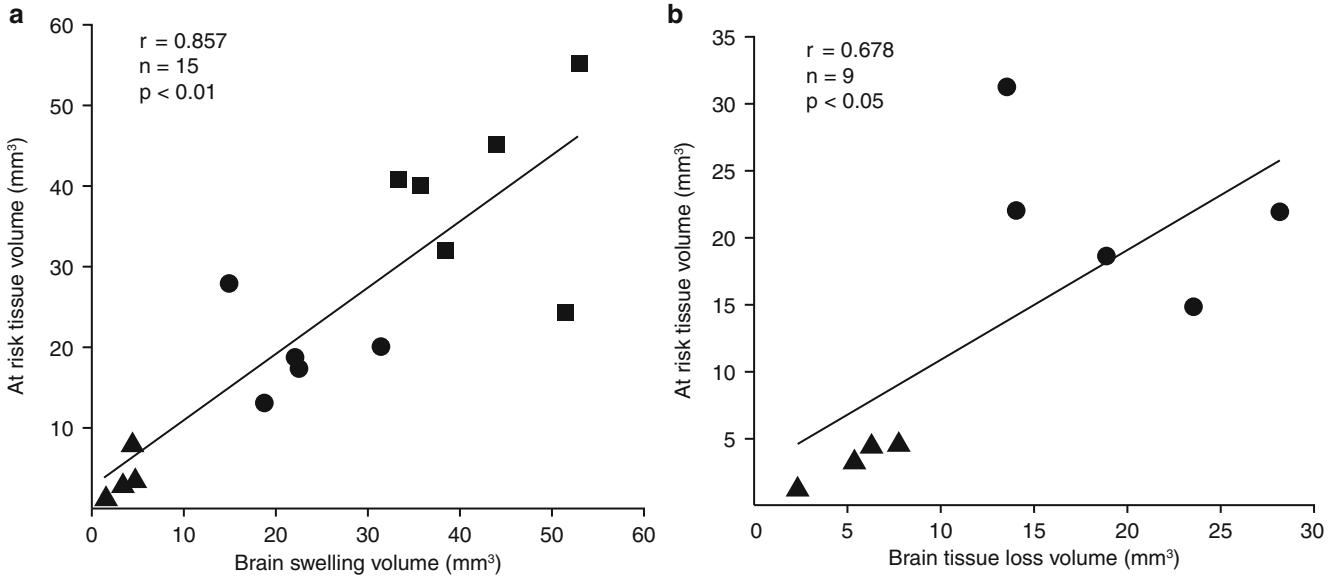

Fig. 2 At-risk tissue volumes correlated well with brain swelling volumes on day 3 (**a**) and with brain tissue loss on day 28 (**b**) after 10, 50 or 100 μL of blood injected into the right caudate of rats. *Triangles* refer to animals with a 10-μL autologous blood injection, *circles* to 50 μL, and *small squares* to 100 μL

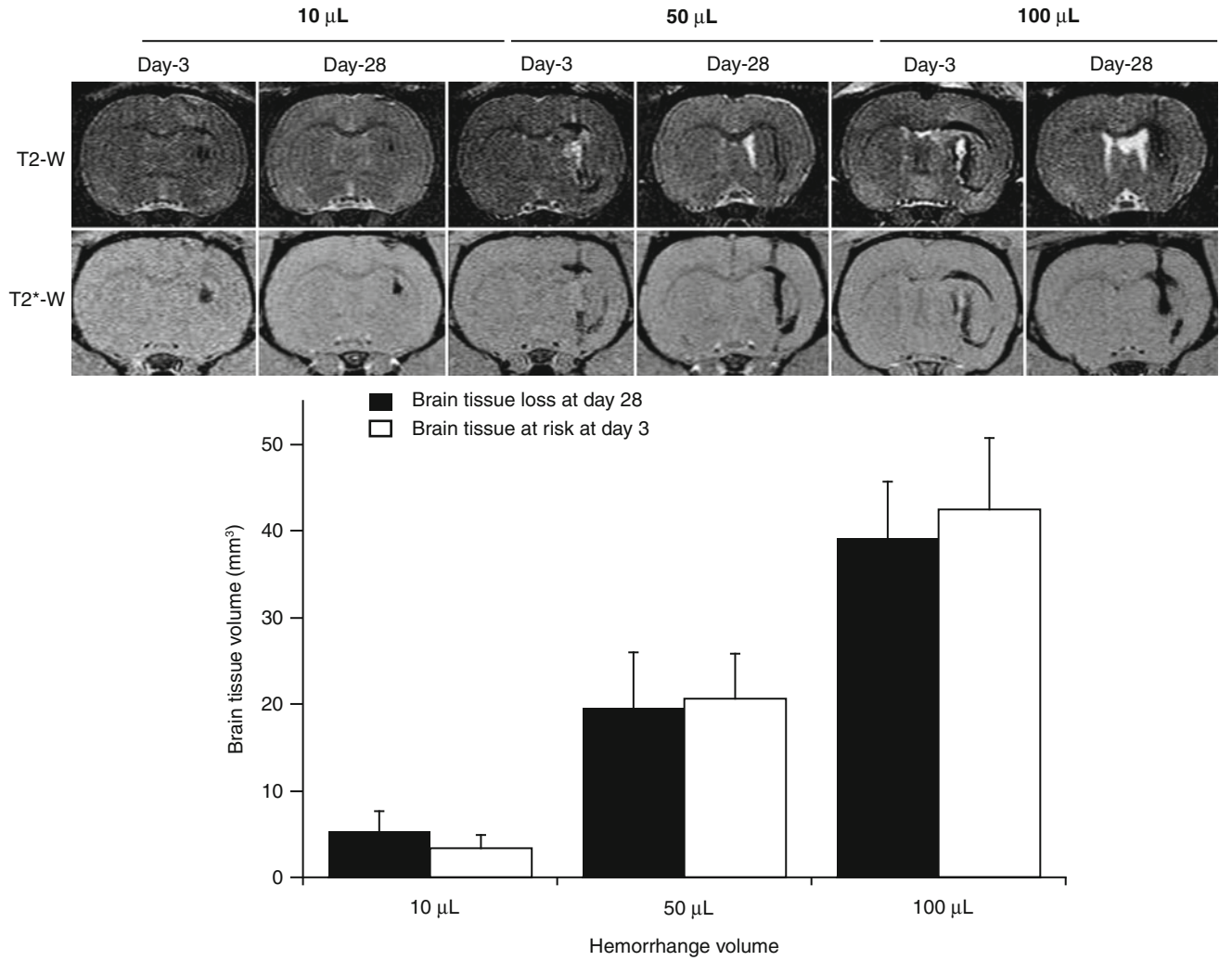

Fig. 3 MRI measurement showing that brain tissue at-risk on day 3 after ICH is a predictor of long-term brain tissue loss

Conclusion

The major findings in this study are: first, at-risk brain tissue areas measured on MRI images correlated well with lesions showing as DARPP-32 immunoreactivity loss during the first several days after ICH; second, at-risk tissue volumes measured at day 3 after ICH correlated not only with the brain swelling volumes on day 3, but also with brain tissue loss measured on day 28.

DARPP-32, a specific marker of GABAergic neurons, is located in the basal ganglia, and was used to confirm brain injury morphologically. T2- and T2*-weighted MR images are non-invasive measurements that can provide important information regarding hematoma, brain edema, as well as brain tissue damage. T2 relaxation times are considered to relate to the dynamic state of water at microscopic tissue levels and are sensitive to water binding [7]. We consider it to be the whole extent of at-risk tissue. T2* sequences are usually obtained to detect small areas of heme deposition. Recent research also demonstrated that it likely represents ferric iron deposition within the brain parenchyma [10]. In this study, T2*-weighted images were used to confirm the existence and evaluate hematoma size during the early phase of ICH [8]. Through the comparison of T2/T2* lesions with DARPP-32 negative/hematoma areas, we found that at-risk tissue areas determined on MR images correlated well with that shown in histological sections at different time points after ICH. This indicates that at-risk brain tissue areas can be determined by the T2/T2* MR images.

It is important to develop a measurement that can be used to estimate acute brain injury. The measurement can then be used to predict ICH patient brain tissue loss and assess the effectiveness of therapies. Brain atrophy after ICH develops gradually and peaks between 1 and 2 months in rats [5]. Our current results showed that at-risk brain tissue volumes measured on day 3 after ICH correlated well with brain tissue loss on day 28. At-risk brain tissue volumes measured by MRI could be an indicator for predicting long-term brain atrophy. In addition, the fact that at-risk brain tissue areas induced by 100 μL of autologous whole blood were much larger than those induced by a 50- or 10-μL blood injection indicates that the key factor affecting ICH outcome is hemorrhagic volume [13].

Our previous studies found a correlation between acute edema formation and ICH-induced neurological deficits during the acute phase [6]. It is not clear whether or not there is connection between edema and the brain tissue at risk measured on MR images. According to the current study, the degree of brain swelling on day 3 after ICH did correlate with volume of at-risk brain tissue on day 3 measured on T2/T2* images.

In summary, the present study shows for the first time to our knowledge the utility of using MRI (T2, T2*) as a tool in evaluating early brain injury and predicting long-term brain tissue loss after ICH.

Acknowledgements This study was supported by grants NS-017760, NS-039866, and NS-057539 from the National Institutes of Health (NIH) and 0840016N from the American Heart Association (AHA). The content is solely the responsibility of the authors and does not necessarily represent the official views of the NIH and AHA.

Conflict of Interest We declare that we have no conflict of interest.

References

1. Allkemper T, Tombach B, Schwindt W, Kugel H, Schilling M, Debus O, Mollmann F, Heindel W (2004) Acute and subacute intracerebral hemorrhages: comparison of MR imaging at 1.5 and 3.0 T–initial experience. Radiology 232:874–881
2. Belayev L, Obenaus A, Zhao W, Saul I, Busto R, Wu C, Vigdorchik A, Lin B, Ginsberg MD (2007) Experimental intracerebral hematoma in the rat: characterization by sequential magnetic resonance imaging, behavior, and histopathology. Effect of albumin therapy. Brain Res 1157:146–155
3. Broderick JP, Adams HP Jr, Barsan W, Feinberg W, Feldmann E, Grotta J, Kase C, Krieger D, Mayberg M, Tilley B, Zabramski JM, Zuccarello M (1999) Guidelines for the management of spontaneous intracerebral hemorrhage: a statement for healthcare professionals from a special writing group of the Stroke Council, American Heart Association. Stroke 30:905–915
4. Felberg RA, Grotta JC, Shirzadi AL, Strong R, Narayana P, Hill-Felberg SJ, Aronowski J (2002) Cell death in experimental intracerebral hemorrhage: the "black hole" model of hemorrhagic damage. Ann Neurol 51:517–524
5. Hua Y, Nakamura T, Keep RF, Wu J, Schallert T, Hoff JT, Xi G (2006) Long-term effects of experimental intracerebral hemorrhage: the role of iron. J Neurosurg 104:305–312
6. Hua Y, Schallert T, Keep RF, Wu J, Hoff JT, Xi G (2002) Behavioral tests after intracerebral hemorrhage in the rat. Stroke 33:2478–2484
7. Jadhav V, Sugawara T, Zhang J, Jacobson P, Obenaus A (2008) Magnetic resonance imaging detects and predicts early brain injury after subarachnoid hemorrhage in a canine experimental model. J Neurotrauma 25:1099–1106
8. Kharatishvili I, Sierra A, Immonen RJ, Grohn OH, Pitkanen A (2009) Quantitative T2 mapping as a potential marker for the initial assessment of the severity of damage after traumatic brain injury in rat. Exp Neurol 217:154–164
9. Svenningsson P, Nishi A, Fisone G, Girault JA, Nairn AC, Greengard P (2004) DARPP-32: an integrator of neurotransmission. Annu Rev Pharmacol Toxicol 44:269–296
10. Wu G, Xi G, Hua Y, Sagher O (2010) T2* magnetic resonance imaging sequences reflect brain tissue iron deposition following intracerebral hemorrhage. Transl Stroke Res 1:31–34
11. Wu J, Hua Y, Keep RF, Nakamura T, Hoff JT, Xi G (2003) Iron and iron-handling proteins in the brain after intracerebral hemorrhage. Stroke 34:2964–2969
12. Xi G, Hua Y, Bhasin RR, Ennis SR, Keep RF, Hoff JT (2001) Mechanisms of edema formation after intracerebral hemorrhage: effects of extravasated red blood cells on blood flow and blood-brain barrier integrity. Stroke 32:2932–2938
13. Xi G, Keep RF, Hoff JT (2006) Mechanisms of brain injury after intracerebral haemorrhage. Lancet Neurol 5:53–63
14. Xi G, Keep RF, Hua Y, Xiang J, Hoff JT (1999) Attenuation of thrombin-induced brain edema by cerebral thrombin preconditioning. Stroke 30:1247–1255
15. Yoshioka H, Niizuma K, Katsu M, Okami N, Sakata H, Kim GS, Narasimhan P, Chan PH (2011) NADPH oxidase mediates striatal neuronal injury after transient global cerebral ischemia. J Cereb Blood Flow Metab 31:868–880

Brain Edema Formation and Complement Activation in a Rat Model of Subarachnoid Hemorrhage

Chao Zhang, Jin-Yul Lee, Richard F. Keep, Aditya Pandey, Neeraj Chaudhary, Ya Hua, and Guohua Xi

Abstract Previous studies have demonstrated that erythrocyte lysis and brain iron overload contribute to early brain injury after subarachnoid hemorrhage (SAH). Activation of the complement system and formation of the membrane attack complex can result in erythrocyte lysis and might, therefore, participate in such injury. This study, therefore, examined complement activation, blood–brain barrier (BBB) disruption, and brain edema in a rat SAH model.

Subarachnoid hemorrhage was induced using a modified endovascular perforation technique. Brain complement activation was determined by Western blotting and immunohistochemistry. Brain edema was measured by dry/wet weight and BBB permeability assessed by measuring brain albumin levels.

We found that there was expression of the membrane attack complex and clusterin in the frontal basal cortex and clot after SAH. The protein levels of the membrane attack complex were much higher in the frontal basal cortex at 72 h after SAH than those in sham ($p<0.01$). We also found that brain water content was increased (81.9 ± 1.4 vs. 79.1 ± 0.2 % in sham, $p<0.05$) and BBB was disrupted (albumin content: 10,695 ± 865 vs. 4,935 ± 3,121 pixels in sham, $p<0.01$) 24 h after SAH.

Our results suggest that complement activation after SAH might contribute to brain edema formation and BBB disruption after SAH.

Keywords Brain edema • Clusterin • Complement • Subarachnoid hemorrhage

C. Zhang
Department of Neurosurgery, University of Michigan, Ann Arbor, MI, USA

Department of Neurosurgery, Huashan Hospital, Fudan University, Shanghai, China

J.-Y. Lee, R.F. Keep, A. Pandey, and Y. Hua
Department of Neurosurgery, University of Michigan, Ann Arbor, MI, USA

N. Chaudhary
Department of Radiology and Neurosurgery, University of Michigan, Ann Arbor, MI, USA

G. Xi, MD (✉)
Department of Neurosurgery, University of Michigan, R5018 BSRB, 109 Zina Pitcher Place, Ann Arbor 48109-2200, MI, USA
e-mail: guohuaxi@umich.edu

Introduction

Acute brain injury after subarachnoid hemorrhage (SAH) is a multifactorial process and in recent years, there has been increasing interest in investigating early brain injury after SAH to clarify the mechanism and in therapy [4, 8, 13]. It is well known that the amount of blood released during SAH correlates with neurological deficits and poor clinical outcome [2]. The clots forms immediately after blood is released into the subarachnoid space and disappears within 3 days via clot lysis, which starts early after SAH [16]. Previous studies have demonstrated that oxidative injury because of erythrocyte lysis, excessive hemoglobin, and iron overload contribute to brain damage after SAH [10, 21]. One potential mediator of erythrocyte lysis is the complement system, which consists of at least 30 proteins involved in many immune reactions, including cell lysis and inflammatory responses. Complement-mediated cell lysis and brain injury may be caused by the formation of membrane attack complex (MAC) and the inflammatory response that ensues. MAC consists of C5b-9 assembled after complement activation [5]. Previous studies indicated that activation of the complement system and formation of MAC resulted in erythrocyte lysis and contributed to perihematomal edema formation and brain damage after intracerebral hemorrhage [6, 19, 22]. This study, therefore, expanded this to SAH and examined MAC formation, blood–brain barrier disruption and brain edema in a rat SAH model.

Y. Katayama et al. (eds.), *Brain Edema XV*, Acta Neurochirurgica Supplement, Vol. 118,
DOI 10.1007/978-3-7091-1434-6_29,

Materials and Methods

Animal Preparation and Subarachnoid Hemorrhage Model

The protocols for animal using were approved by the University of Michigan Committee on the Use and Care of Animals at the University of Michigan. A total of 33 adult male Sprague–Dawley rats weighing between 275 and 325 g were used. General anesthesia was induced with 5 % isoflurane (Aerrane; Baxter Healthcare, Deerfield, IL, USA). Blood was obtained from the catheter for analysis of pH, PaO_2, $PaCO_2$, hematocrit, and blood glucose. Body temperature was maintained at 37 °C, with use of a feedback-controlled heating pad.

In supine position and after a left paramedian incision of the ventral neck, the left external carotid artery was identified under a surgical microscope, transected distally, and reflected caudally in line with the internal carotid artery. A 3-0 nylon monofilament suture with a rounded tip to prevent endothelial injury was inserted into the stump of the external carotid artery, past the common carotid artery bifurcation, and into the internal carotid artery. The external carotid artery was tightened around the suture to prevent blood loss. The filament was advanced distally into the intracranial internal carotid artery and carefully perforated. The suture was then withdrawn, producing hemorrhage. The common carotid artery was temporarily occluded for 2 min to limit the hemorrhage volume. Sham-operated control rats underwent an identical procedure except that the suture was not advanced beyond the point of resistance.

Rats were divided into sham and SAH groups, and were killed 24 and 72 h later. The brains were used for brain water content determination, Western blotting, and immunohistochemical analysis.

Brain Water Content Measurement

Rats were re-anesthetized (pentobarbital 60 mg/kg, i.p.) and decapitated 24 h after SAH for brain water content measurement. The brains were removed immediately and divided into bilateral hemisphere, brainstem, and cerebellum. After weighing, samples were dried for 48 h in a gravity oven. The water content was determined as [(wet weight – dry weight)/wet weight]×100 %. The values of the brainstem and cerebellum served as controls.

Immunohistochemistry

Rats underwent intracardiac perfusion with 4 % paraformaldehyde in 0.1 mol/L PBS (pH 7.4). Brains were removed and kept in 4 % paraformaldehyde for 12 h, then immersed in 30 % sucrose for 3 days at 4 °C. Brains were then placed in an optimal cutting temperature compound (Sakura Finetek USA, Torrance, CA, USA) and sectioned (18 μm) on a cryostat. Immunohistochemical staining was performed using the avidin–biotin complex technique. Primary antibodies were polyclonal sheep anti-rat albumin (Bethyl; 1:10,000 dilution), polyclonal rabbit anti-rat clusterin (1:400 dilution), and monoclonal mouse anti-rat C5b-9 (Abcam; 1:800 dilution).

Western Blot Analysis

Rats were anesthetized and underwent intracardiac perfusion with 0.1 mol/L PBS (pH 7.4). Brains were removed and the ipsilateral frontobasal cortex separated. Western blot analysis was performed as described previously [9]. Primary antibodies were polyclonal sheep anti-rat albumin (Bethyl; 1:20,000 dilution) and monoclonal mouse anti-rat C5b-9 (Abcam; 1:1,000 dilution).

Statistical Analysis

Data are presented as mean ± SD. Data from water content and Western blot analysis were analyzed using Student's *t* test or analysis of variance (ANOVA), followed by Scheffe's post hoc test for multiple comparisons. Significance levels were measured at $p<0.05$.

Results

All physiological variables were measured before SAH induction. The mean values of mean arterial blood pressure, blood pH, blood gases, hematocrit, and blood glucose were controlled within normal ranges.

Following complement activation, MAC is assembled. Clusterin is a putative complement inhibitor that impedes MAC-induced cell lysis [1]. MAC- and clusterin-positive cells are in the deep layer of the frontobasal cortex and clot after SAH (Fig. 1a). Western blot showed that the protein levels of MAC were obviously higher in the ipsilateral frontobasal cortex of SAH rats (4,615 ± 196 vs. 413 ± 200 pixels in sham, $p<0.01$) at 72 h (Fig. 1b).

Brain water content increased significantly after SAH induction in the ipsilateral hemisphere (81.9 ± 1.4 % vs. 79.1 ± 0.2 % in sham, $p<0.01$) and the contralateral hemisphere (80.9 ± 1.5 % vs. 79.2 ± 0.3 % in sham, $p<0.05$,

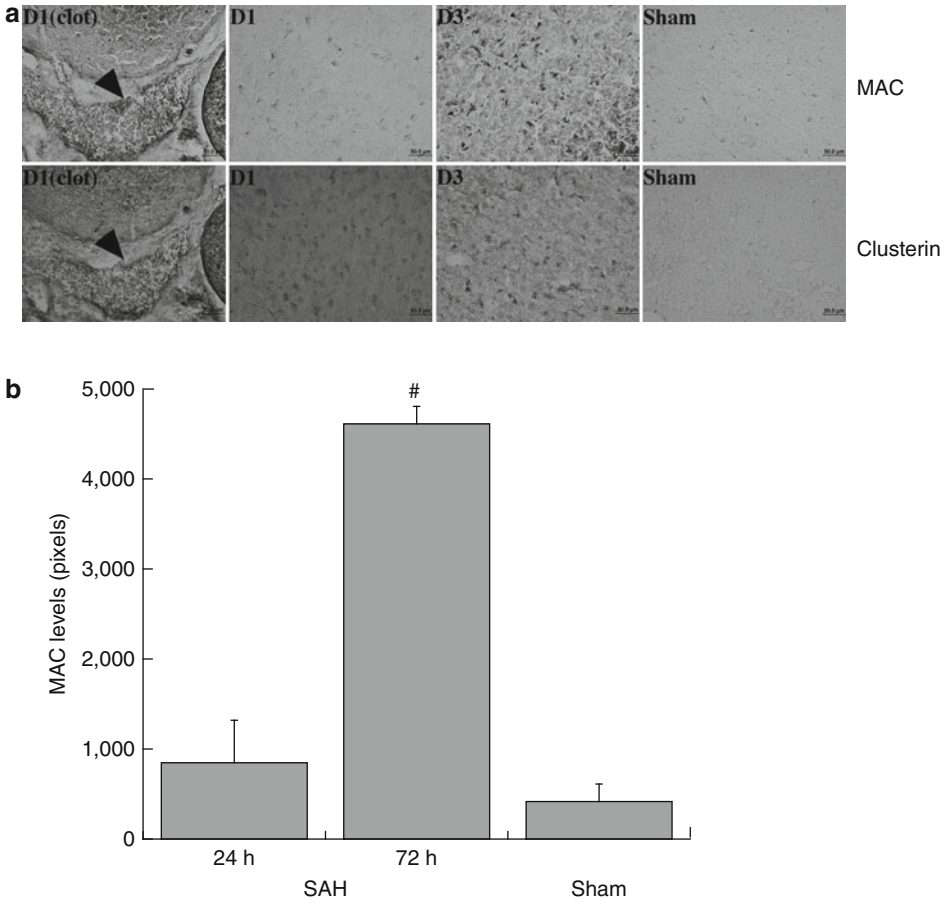

Fig. 1 (**a**) Membrane attack complex (*MAC*)- and clusterin-positive cells in a clot of the subarachnoid space (*black arrowhead*) and the deep layers of the ipsilateral frontobasal cortex 24 (*D1*) and 72 (*D3*) h following subarachnoid hemorrhage (SAH) or sham operation. Scale bar = 50 μm. (**b**) Protein levels of MAC in the ipsilateral frontobasal cortex 24 h and 72 h after SAH or sham operation. Values are mean ± SD, $n = 3$, #$p < 0.01$ versus sham

Fig. 2a). There was no difference in the water content of the brainstem and cerebellum between the SAH and sham-operated control groups.

Blood–brain barrier permeability was determined by measuring brain albumin levels. Albumin immunoreactivity was found in the ipsilateral frontobasal area 24 and 72 h after SAH, but not in sham-operated rats. Western blot showed that the protein levels of albumin in the ipsilateral frontobasal cortex were increased 24 h after SAH induction (10,695 ± 865 vs. 4,935 ± 3,121 pixels in sham, $p < 0.05$) and 72 (10,441 ± 915 vs. 4,935 ± 3,121 pixels in sham, $p < 0.05$; Fig. 2b).

Conclusion

Complement-mediated brain injury has been found in many central nervous system diseases, including ischemic stroke [3, 15], intracerebral hemorrhage [6, 22], aneurysmal SAH [7, 12], and age-related macular degeneration [23]. In this study we provide the evidence for activation of the complement system, formation of MAC, BBB disruption, and brain edema in the rat SAH model.

The complement cascade, a principal effector of erythrocyte hemolysis and activator of inflammatory mediators, has been implicated in the pathogenesis of cerebrovascular disease [11, 18]. After complement cascade activation, complement factors C5b, C6, C7, C8, and C9 form the MAC, which is able to attach to the cell membrane and form a pore, leading to erythrocyte lysis. Clusterin is a complement inhibitor that inhibits MAC-induced cell lysis by the high affinity of the clusterin–MAC interaction [14]. In the present study, the MAC- and clusterin-positive red blood cells of the clot in the subarachnoid space 24 h after SAH induction provided full evidence of activation of the complement system and formation of MAC, which should contribute to erythrocyte lysis.

Complement is normally excluded from the brain parenchyma by the BBB, but entry can occur after SAH as part of the extravasated blood or later because of BBB disruption. Park et al. [17] reported that complement activation by aged red blood cells could result in MAC insertion into bystander smooth-muscle cell membranes. Through the bystander effect, MAC insertion may occur in neurons, causing neuronal death, and may account for BBB leakage by damaging endothelial cells. Our current study found numerous MAC- and clusterin-positive cells in the deep layers of the ipsilateral frontobasal cortex 24 h and 72 h following SAH induction

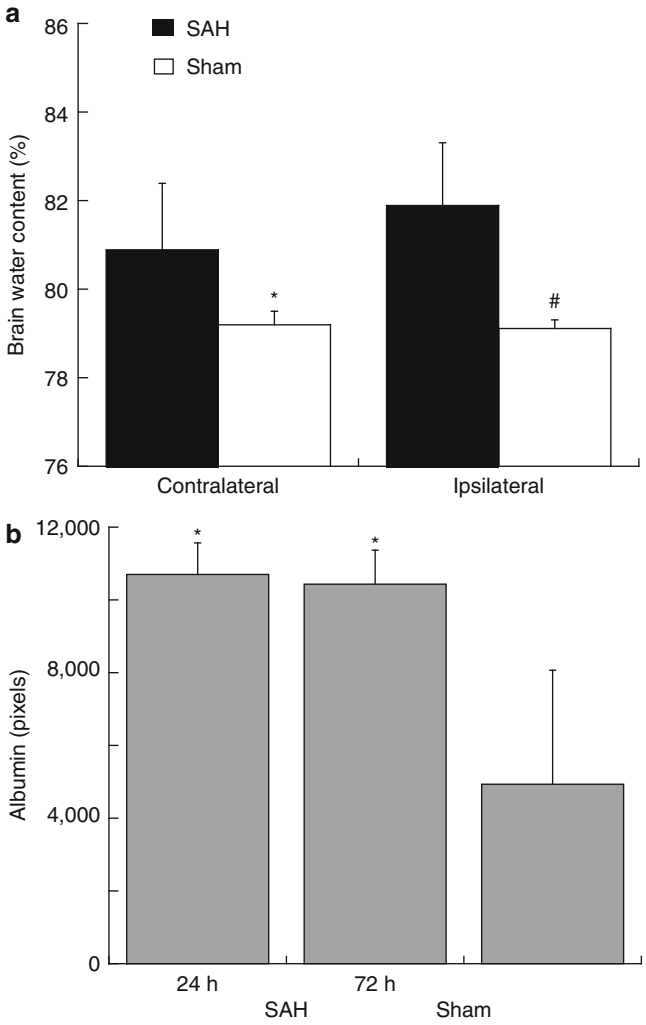

Fig. 2 (**a**) Brain water content in the contra- and ipsilateral hemispheres 24 h after SAH or sham operation. Values are mean ± SD, $n=5–8$, $^*p<0.05$, $\#p<0.01$ versus sham. (**b**) Albumin levels in the ipsilateral frontobasal cortex 24 h and 72 h after SAH or sham operation determined by Western blotting. Values are mean ± SD, $n=3$, $^*p<0.05$ versus sham

and a higher MAC content in the left frontobasal cortex. This suggests that MAC might not only cause erythrocyte lysis, but also directly lead to brain injury, which may induce further BBB disruption and complement extravasation. The BBB leakage was demonstrated by increased albumin content in the brain after SAH.

Previous studies demonstrated that complement activation after ICH is involved in brain edema formation through an inflammatory response or MAC formation [6, 19–22]. Reduced brain edema may be via inhibiting inflammation or inhibiting MAC-mediated erythrocyte lysis and brain injury. Our results revealed remarkable bilateral brain edema following SAH and it could be related to complement activation, MAC formation, and BBB leakage. Future studies should determine whether inhibition of MAC formation can improve BBB permeability and reduce brain edema.

In summary, complement activation and MAC formation arise in the early phase of SAH and are associated with BBB disruption and brain edema.

Acknowledgements This study was supported by grants NS-017760, NS-039866, and NS-057539 from the National Institutes of Health (NIH) and 0840016N from American Heart Association (AHA). The content is solely the responsibility of the authors and does not necessarily represent the official views of the NIH and AHA.

Conflict of Interest We declare that we have no conflict of interest.

References

1. Bellander BM, von Holst H, Fredman P, Svensson M (1996) Activation of the complement cascade and increase of clusterin in the brain following a cortical contusion in the adult rat. J Neurosurg 85:468–475
2. Brouwers PJ, Dippel DW, Vermeulen M, Lindsay KW, Hasan D, van Gijn J (1993) Amount of blood on computed tomography as an independent predictor after aneurysm rupture. Stroke 24:809–814
3. Ducruet AF, Hassid BG, Mack WJ, Sosunov SA, Otten ML, Fusco DJ, Hickman ZL, Kim GH, Komotar RJ, Mocco J, Connolly ES (2008) C3a receptor modulation of granulocyte infiltration after murine focal cerebral ischemia is reperfusion dependent. J Cereb Blood Flow Metab 28:1048–1058
4. Endo H, Nito C, Kamada H, Yu F, Chan PH (2007) Reduction in oxidative stress by superoxide dismutase overexpression attenuates acute brain injury after subarachnoid hemorrhage via activation of Akt/glycogen synthase kinase-3beta survival signaling. J Cereb Blood Flow Metab 27:975–982
5. Esser AF (1991) Big MAC attack: complement proteins cause leaky patches. Immunol Today 12:316–318; discussion 321
6. Hua Y, Xi G, Keep RF, Hoff JT (2000) Complement activation in the brain after experimental intracerebral hemorrhage. J Neurosurg 92:1016–1022
7. Kasuya H, Shimizu T (1989) Activated complement components C3a and C4a in cerebrospinal fluid and plasma following subarachnoid hemorrhage. J Neurosurg 71:741–746
8. Kusaka G, Ishikawa M, Nanda A, Granger DN, Zhang JH (2004) Signaling pathways for early brain injury after subarachnoid hemorrhage. J Cereb Blood Flow Metab 24:916–925
9. Lee JY, He Y, Sagher O, Keep R, Hua Y, Xi G (2009) Activated autophagy pathway in experimental subarachnoid hemorrhage. Brain Res 1287:126–135
10. Lee JY, Keep RF, He Y, Sagher O, Hua Y, Xi G (2010) Hemoglobin and iron handling in brain after subarachnoid hemorrhage and the effect of deferoxamine on early brain injury. J Cereb Blood Flow Metab 30:1793–1803
11. Lindsberg PJ, Ohman J, Lehto T, Karjalainen-Lindsberg ML, Paetau A, Wuorimaa T, Carpen O, Kaste M, Meri S (1996) Complement activation in the central nervous system following blood-brain barrier damage in man. Ann Neurol 40:587–596
12. Mack WJ, Ducruet AF, Hickman ZL, Garrett MC, Albert EJ, Kellner CP, Mocco J, Connolly ES Jr (2007) Early plasma complement C3a levels correlate with functional outcome after aneurysmal subarachnoid hemorrhage. Neurosurgery 61:255–260; discussion 260–261
13. Matz P, Turner C, Weinstein PR, Massa SM, Panter SS, Sharp FR (1996) Heme-oxygenase-1 induction in glia throughout rat brain following experimental subarachnoid hemorrhage. Brain Res 713: 211–222

14. McDonald JF, Nelsestuen GL (1997) Potent inhibition of terminal complement assembly by clusterin: characterization of its impact on C9 polymerization. Biochemistry 36:7464–7473
15. Mocco J, Mack WJ, Ducruet AF, Sosunov SA, Sughrue ME, Hassid BG, Nair MN, Laufer I, Komotar RJ, Claire M, Holland H, Pinsky DJ, Connolly ES Jr (2006) Complement component C3 mediates inflammatory injury following focal cerebral ischemia. Circ Res 99:209–217
16. Nina P, Schisano G, Chiappetta F, Luisa Papa M, Maddaloni E, Brunori A, Capasso F, Corpetti MG, Demurtas F (2001) A study of blood coagulation and fibrinolytic system in spontaneous subarachnoid hemorrhage. Correlation with hunt-hess grade and outcome. Surg Neurol 55:197–203
17. Park CC, Shin ML, Simard JM (1997) The complement membrane attack complex and the bystander effect in cerebral vasospasm. J Neurosurg 87:294–300
18. Sercombe R, Dinh YR, Gomis P (2002) Cerebrovascular inflammation following subarachnoid hemorrhage. Jpn J Pharmacol 88:227–249
19. Xi G, Hua Y, Keep RF, Younger JG, Hoff JT (2001) Systemic complement depletion diminishes perihematomal brain edema in rats. Stroke 32:162–167
20. Xi G, Hua Y, Keep RF, Younger JG, Hoff JT (2002) Brain edema after intracerebral hemorrhage: the effects of systemic complement depletion. Acta Neurochir Suppl 81:253–256
21. Xi G, Keep RF, Hoff JT (2006) Mechanisms of brain injury after intracerebral haemorrhage. Lancet Neurol 5:53–63
22. Yang S, Nakamura T, Hua Y, Keep RF, Younger JG, He Y, Hoff JT, Xi G (2006) The role of complement C3 in intracerebral hemorrhage-induced brain injury. J Cereb Blood Flow Metab 26: 1490–1495
23. Yates JR, Sepp T, Matharu BK, Khan JC, Thurlby DA, Shahid H, Clayton DG, Hayward C, Morgan J, Wright AF, Armbrecht AM, Dhillon B, Deary IJ, Redmond E, Bird AC, Moore AT (2007) Complement C3 variant and the risk of age-related macular degeneration. N Engl J Med 357:553–561

Early Changes in GMRP1 After Intracerebral Hemorrhage: Involvement in Brain Damage and Cell Apoptosis

Xuanchun Wang, Ye Gong, Mingzhe Zheng, Qing Xie, Hailiang Tang, Daijun Wang, and Xiancheng Chen

Abstract Glucose metabolism-related protein 1 (GMRP1), also known as BTBD10, has been reported to inhibit apoptosis of neuronal and islet beta cells via the Akt pathway. The present study attempted to investigate whether GMRP1 and its mediated Akt pathway were involved in brain injury of rats after intracerebral hemorrhage (ICH). Rat models of ICH had been established successfully. Western blotting was used to investigate the levels of GMRP1 protein in the caudate nuclei tissues of the hemorrhagic and contralateral sides at 6 h, day 1, day 3, day 5, and day 7 after ICH. Phosphorylations of Akt was determined in caudate nuclei mentioned above. TUNEL assay was used to measure the cell apoptosis. GMRP1 protein levels, as well as phosphorylations of Akt, significantly decreased in caudate nuclei of the hemorrhagic side, compared with those of the contralateral side on day 1 and day 3 after ICH. Enhanced cell apoptosis was observed on the hemorrhagic side using TUNEL assay. We presented here evidence that a decreased GMRP1-mediated Akt pathway contributed to cell apoptosis on the hemorrhagic side, suggesting that GMRP1 plays an important role in brain damage after ICH.

Keywords GMRP1 • BTBD10 • Intracerebral hemorrhage Apoptosis • Akt

X. Wang
Department of Endocrinology,
Huashan Hospital, Fudan University,
Shanghai, China

Y. Gong (✉), M. Zheng, Q. Xie, H. Tang, D. Wang, and X. Chen
Department of Neurosurgery,
Huashan Hospital, Fudan University,
12 Middle Wurumuqi Road, Shanghai, China
e-mail: yyeegong@yahoo.com.cn

Introduction

Intracerebral hemorrhage (ICH)-triggered cascade of brain injury can cause tragic outcome. A large number of pathophysiological procedures are involved in the progress. Both necrosis and apoptosis are involved in the ICH-induced brain damage. Some investigations have shown that apoptosis is an important mechanism of ICH-induced brain injury [3, 7, 10].

Glucose metabolism-related protein 1 (GMRP1), also known as BTBD10, which is a novel member of BTB/POZ (Broad complex, Tramtrack, Bric-à-brac/Poxvirus and zinc fingers) domain contained protein family, has been reported to have the ability to inhibit apoptosis of neuronal and islet beta cells via Akt pathway [1, 9, 12]. But whether the protein and its mediated Akt pathway could contribute to alleviate brain cell apoptosis is still unknown.

The present study attempted to preliminarily investigate the role of GMRP1 in ICH induced brain damage and cell apoptosis.

Materials and Methods

ICH Model

Animal use protocols were approved by Fudan University. Male Sprague–Dawley rats (300–350 g, Experimental Animal Center of Fudan University) were used in the present study. The rats were anesthetized with pentobarbital (45 mg/kg i.p.). The right femoral artery was catheterized for continuous blood pressure monitoring and blood sampling. All rats received an injection of 100 μL autologous whole blood (obtained from the femoral artery catheter) into the caudate nucleus within 8 min, through a 26-gauge needle (coordinates: 0.2 mm anterior, 5.5 mm ventral, and 3.5 mm lateral to the bregma) with a microinfusion pump.

Y. Katayama et al. (eds.), *Brain Edema XV*, Acta Neurochirurgica Supplement, Vol. 118,
DOI 10.1007/978-3-7091-1434-6_30,

Experimental Groups

These experiments were divided into three parts. In the first part, one control group (needle insertion only) and five ICH groups of rats ($n=4$) were killed 6 h, 1, 3, 5, and 7 days after blood injection for a Western blotting test of GMRP1 and pAkt/Akt. In the second part, one control group and 5 ICH groups of rats ($n=3$) were killed 6 h, and on days 1, 3, 5, and 7 after blood injection for GMRP1 immunohistochemistry analysis. In the third part, TUNEL assay (a different section from the same sample of GMRP1 staining) was performed.

Western Blotting

Western blotting was performed as described previously [2]. Briefly, total protein was extracted from caudate nucleus tissue with Tissue Protein Extraction Reagent (Pierce). Protein concentration was estimated using a BCA Protein Assay Kit (Pierce, Rockford, IL, USA). Samples were run on a polyacrylamide gel and then transferred to a pure nitrocellulose membrane. Membranes were probed with 1: 1,000 dilution of goat anti-GMRP1 polyclonal antibody (generated by our laboratory) and rabbit anti-Akt/pAkt polyclonal antibody (Santa Cruz Biotechnology, Santa Cruz, CA, USA), followed by a secondary antibody (peroxidase-conjugated rabbit anti-goat antibody; Santa Cruz). Protein bands were visualized by chemiluminescence with an ECL Luminescence Kit (Pierce) and exposed to X-ray film.

Immunohistochemistry

The immunohistochemistry method has been described previously [2]. Briefly, the rats were reanesthetized and perfused with 4 % paraformaldehyde. Brains were removed and kept in 4 % paraformaldehyde for 6 h, immersed in 25 % sucrose for 3 days at 4 °C, then dehydrated, embedded in paraffin, and sectioned. The antibodies were described above.

TUNEL Assay

The TUNEL staining was carried out using a DNA fragmentation detection kit (FragEL; Merck, Darmstadt, Germany) according to the manufacturer's instructions. Cells were counted under five high-power fields (×400) to gain the average data.

Statistical Analysis

Values are listed as mean ± SD. One-way ANOVA was used with SPSS12.0 software to determine statistical significance, which is set at $p<0.05$.

Results

Physiological parameters, including mean arterial pressure, blood pH, arterial oxygen and carbon dioxide tensions, hematocrit, and blood glucose, were recorded and controlled within normal ranges.

According to the data from Western blotting, GMRP1 represented a remarkable decline from 6 h (70 % vs. control, $p>0.05$), to the lowest level on day 1 (21 % vs. control, $p<0.05$) and days 3 and 5 ($p>0.05$, vs. day 1), followed by an escalation on day 7 (2.7-fold vs. day 5, $p<0.05$). The protein levels of GMRP1 in the ipsilateral caudate were also lower than those on the contralateral side on days 1, 3, and 5 (Fig. 1).

It was shown by immunohistochemistry analysis that the staining density of GMRP1 was lowest on day 3 after ICH establishment (Fig. 1). The staining was mainly located at the cytoplasm, and not at the nucleus.

Phosphorylation of Akt (pAkt/Akt) was downregulated on day 1 (15 % vs. contralateral, $p<0.05$) and day 3 (20 % vs. contralateral, $p<0.05$; Fig. 2). TUNEL-positive cells could be seen 6 h after ICH establishment, but were very scarce. A remarkable increase in TUNEL-positive cells was observed on day 3 (13.2-fold vs. 6 h, $p<0.05$) to day 7 (6.6-fold vs. 6 h, $p<0.05$; Fig. 3).

Conclusion

The present study demonstrated that hemorrhage-induced downregulation of GMRP1 and its mediated Akt pathway during the early stage of ICH could contribute to an increase in brain cell apoptosis from 12 h to day 3, which was alleviated after day 5.

The BTB/POZ domain-contained proteins have been proven to be able to modulate some important cellular procedures, such as transcription, proliferation, cell morphology maintenance, angiogenesis, and apoptosis [4, 6, 8, 11]. They can bind other proteins or self-bind to form homodimers or heterodimers, and then bind to DNA with their zinc finger region, to participate in the function procedure mentioned above. GMRP1, a novel BTB/POZ family member, also known as BTBD10, was first cloned by Chen et al., and

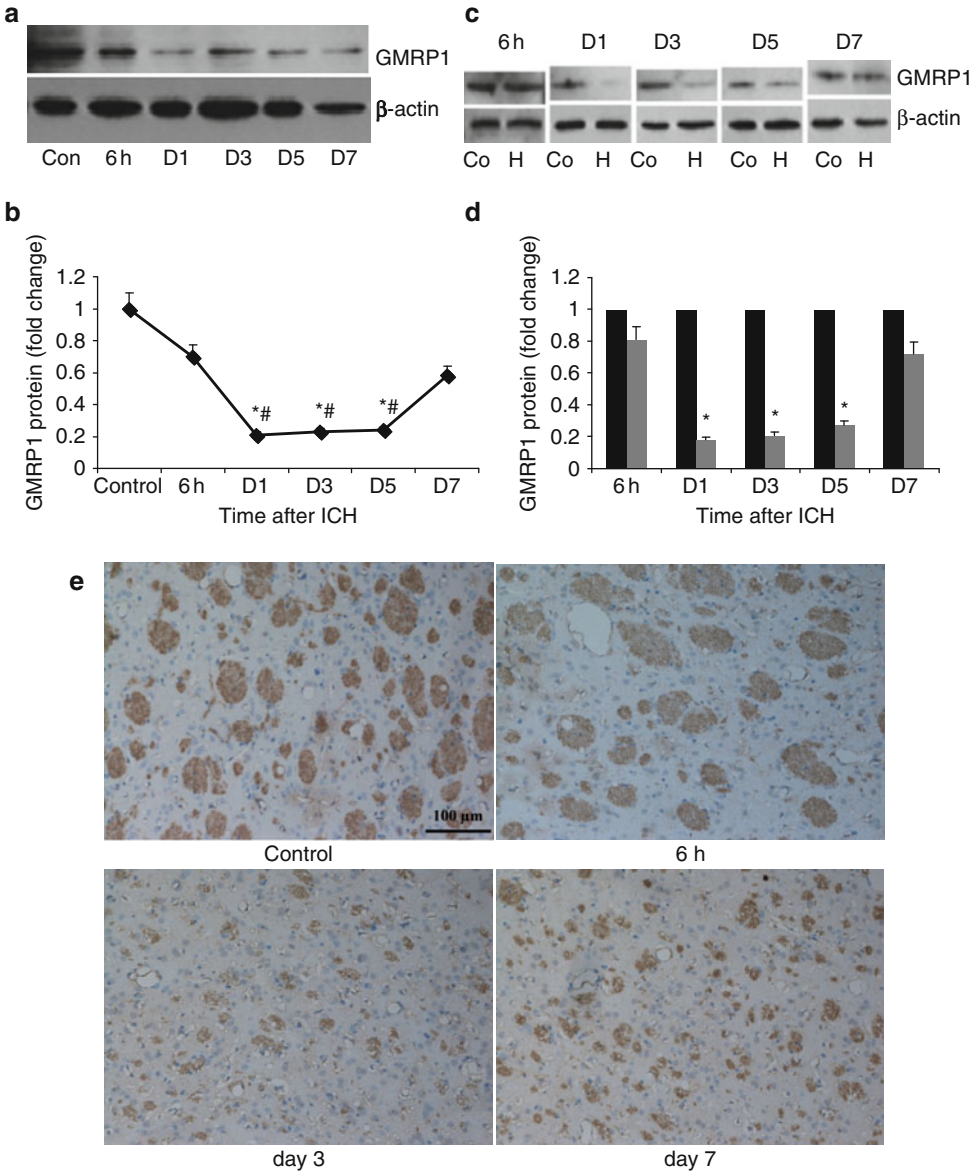

Fig. 1 Glucose metabolism-related protein 1 (GMRP1) protein level after intracranial hemorrhage (ICH). (**a**, **c**) Image recorded of Western blotting, (**b**, **d**) time course of expression. $*p<0.05$ versus control group, $\#p<0.05$ versus 6 h (**e**) Immunohistochemistry analysis showed lower and sparse density of *GMRP1* staining on day 3

proved to be downregulated in gliomas. Moreover, the protein was found to be able to suppress neuronal cell death via its positive regulation of the Akt pathway [1]. The activation of the Akt pathway by GMRP1 on pancreatic beta cell proliferation is another piece of evidence [12]. In our study, we observed remarkable downregulation of GMRP1 protein after ICH, and a low ratio of pAkt/Akt, which decreased to extreme levels on day 3, indicating the repression of cell proliferation maintenance during that period. The mild increase in GMRP1 and pAkt/Akt after day 5 suggested recovery of cell proliferation.

In COS7 cells and NSC34 cells, BTBD10 was found to present a unique filamentous cytoplasmic distribution around the nucleus [9], in an overexpressed pattern or in an endogenous pattern. It was also observed in our study that BTBD10 was localized in the same manner in the cytoplasm of neurons in the nucleus region of Sprague–Dawley rats. For NAC-1, another noted BTB/POZ protein, early research clarified the restricted existence of the protein in nuclei [4]. However, later research also detected diffuse distribution in both nuclei and cytoplasm of NAC-1 in PC12 and Neuro2A cells, implying the complex transcriptional and non-transcriptional role of BTB/POZ proteins [5]. Multiple methods of localization study should be applied. In the present study, we found that GMRP1 was mainly located in the cytoplasm, and not in the nucleus.

Apoptosis is programmed cell death. ICH-induced cell apoptosis has been well investigated. Our data showed that TUNEL-positive cells were observed at 6 h, then increased remarkably, peaked at the top level on day 3, followed by a decline during days 5–7. This time course of apoptosis development after ICH is in good accordance with results from previous investigations [3, 7].

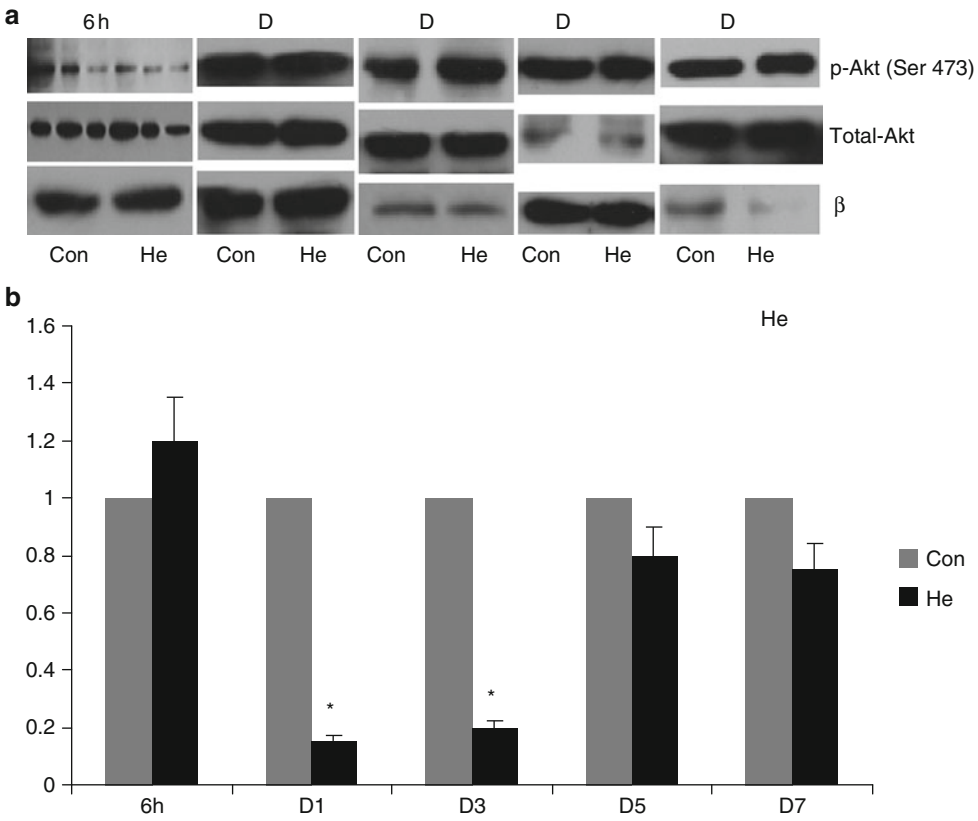

Fig. 2 Phosphorylation of Akt (pAkt/Akt) after ICH. (**a**) Image recorded of Western blotting, (**b**) time course of expression, *$p<0.05$ versus the contralateral side

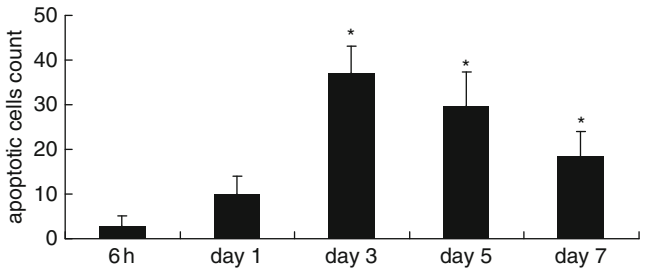

Fig. 3 Apoptotic cell count after ICH establishment. *$p<0.05$ versus 6 h

In summary, we preliminarily presented some evidence that decreased GMRP1-mediated Akt pathway contributed to brain cell apoptosis in the perihemorrhagic region, suggesting that GMRP1 might play an important role in injury after ICH. This finding may provide a new insight into the mechanism of ICH-induced brain damage.

Acknowledgments This study was supported by Grant No. 08411965100 from the Science and Technology Commission of the Shanghai Municipality, and Grant Nos. 30872675 and 30901549 from the National Natural Science Foundation of China.

Conflict of Interest We declare that we have no conflict of interest.

References

1. Chen J, Xu J, Ying K et al (2004) Molecular cloning and characterization of a novel human BTB domain-containing gene, BTBD10, which is down-regulated in glioma. Gene 340(1):61–69
2. Gong Y, Xi GH et al (2008) Increase in brain thrombin activity after experimental intracerebral hemorrhage. Acta Neurochir Suppl 105:47–50
3. Han N, Ding SJ, Wu T et al (2008) Correlation of free radical level and apoptosis after intracerebral hemorrhage in rats. Neurosci Bull 24(6):351–358
4. Ishibashi M, Nakayama K, Yeasmin S et al (2009) Expression of a BTB/POZ protein, NAC1, is essential for the proliferation of normal cyclic endometrial glandular cells and is up-regulated by estrogen. Clin Cancer Res 15(3):804–811
5. Korutla L, Champtiaux N, Shen HW et al (2005) Activity-dependent subcellular localization of NAC1. Eur J Neurosci 22(2):397–403
6. Mackler SA, Korutla L, Cha XY et al (2000) NAC-1 is a brain POZ/BTB protein that can prevent cocaine-induced sensitization in the rat. J Neurosci 20(16):6210–6217
7. Matsushita K, Meng W, Wang X et al (2000) Evidence for apoptosis after intracerebral hemorrhage in rat striatum. J Cereb Blood Flow Metab 20:396–404
8. Nacak TG, Leptien K, Fellner D et al (2006) The BTB-kelch protein LZTR-1 is a novel Golgi protein that is degraded upon induction of apoptosis. J Biol Chem 281(8):5065–5071
9. Nawa M, Kanekura K, Hashimoto Y et al (2008) A novel Akt/PKB-interacting protein promotes cell adhesion and inhibits familial amyotrophic lateral sclerosis-linked mutant SOD1-induced neuronal death via inhibition of PP2A-mediated dephosphorylation of Akt/PKB. Cell Signal 20(3):493–505

10. Qureshi AK, Suri MF, Ostrow PT et al (2003) Apoptosis as a form of cell death in intracerebral hemorrhage. Neurosurgery 52(5):1041–1047
11. Shim K, Blake KJ, Jack J et al (2001) The Drosophila ribbon gene encodes a nuclear BTB domain protein that promotes epithelial migration and morphogenesis. Development 128(23):4923–4933
12. Wang X, Liu Y, Yang Z et al (2011) Glucose metabolism-related protein 1 (GMRP1) regulates pancreatic beta cell proliferation and apoptosis via activation of Akt signalling pathway in rats and mice. Diabetologia 54(4):852–863

Alteration of Intracellular Calcium and Its Modulator SLC24A6 After Experimental Intracerebral Hemorrhage

Mingzhe Zheng, Ye Gong, Xuanchun Wang, Qing Xie, Hailiang Tang, Daijun Wang, and Xiancheng Chen

Abstract Intracerebral hemorrhage (ICH) can lead to tragic disability and mortality. Accumulating evidence has shown that sodium calcium exchanger (NCX) may contribute to the secondary injury of a stroke. Recently, a novel member of NCX, SLC24A6, was discovered with knowledge of its abundant distribution in brain. In the present study, we examined the time course of expression of SLC24A6 and its mediated intracellular calcium concentration ($[Ca^{2+}]i$) to investigate its potential roles in brain damage after ICH. An ICH model was established as previously reported. Real-time PCR and Western blotting were used to test the mRNA and protein levels of SLC24A6 on the hemorrhagic side and on the contralateral side caudate nucleus tissues at 6 h, and on days 1, 3, 5, and 7 after ICH. Immunohistochemistry was used to analyze the morphological changes. Fura-2/AM loaded, dual wavelength spectrophotofluorometry was used to test $[Ca^{2+}]i$. The data presented a remarkable decrease in SLC24A6 early after ICH, along with a comparable increase in $[Ca^{2+}]i$. Our results indicated that SLC24A6 presents specific and remarkable alterations in both mRNA and protein levels after ICH. Decreases in SLC24A6 level were correlated with $[Ca^{2+}]i$ elevation. These data suggest that SLC24A6-mediated calcium overload plays an important role in brain damage after ICH.

Keywords SLC24A6 • Intracerebral hemorrhage • Calcium • Sodium calcium exchanger

M. Zheng, Y. Gong (✉), Q. Xie, H. Tang, D. Wang, and X. Chen
Department of Neurosurgery,
Huashan Hospital, Fudan University,
12 Middle Wurumuqi Road, Shanghai, China
e-mail: yyeegong@yahoo.com.cn

X. Wang
Department of Endocrinology,
Huashan Hospital, Fudan University,
Shanghai, China

Introduction

Intracerebral hemorrhage (ICH) is a devastating event, which accounts for 15–30 % of all stroke hospital admissions [1]. Accumulating evidence has shown that a number of secondary injuries were associated with aggravation of ICH-induced brain damage, such as large hematoma volumes [10], hemoglobin and iron [6, 9], and inflammation [5, 11].

Calcium overload play a pivotal and terminal role in cell injury. Sodium calcium exchanger (NCX), which can modulate intracellular calcium concentration ($[Ca^{2+}]i$), is attracting increasing research [2, 4, 7]. There are two branches of the sodium calcium exchanger family, the potassium-independent members NCX1-3, and the potassium-dependent members NCKX (NCKX1-5). Both branches can catalyze electrogenic transportation of Na^+ and Ca^{2+}.

Recently, a new member of NCX was discovered, the transcript of *SLC24A6* [3], which is abundantly distributed in brain. The similarity of its sequence to previously discovered NCX in the α-repeat regions was 62 %. But whether the short isoform or full-length isoform is functional, and whether it is potassium-dependent is doubtful [8].

In the present study, SLC24A6 protein and mRNA levels, as well as $[Ca^{2+}]i$, were examined in a rat ICH model.

Materials and Methods

ICH Model

Animal use protocol was approved by Fudan University. Male Sprague–Dawley rats (300–350 g, Experimental Animal Center of Fudan University) were used in this study. The rats were anesthetized with pentobarbital (45 mg/kg i.p.). The right femoral artery was catheterized for continuous blood pressure monitoring and blood sampling. All rats

Y. Katayama et al. (eds.), *Brain Edema XV*, Acta Neurochirurgica Supplement, Vol. 118,
DOI 10.1007/978-3-7091-1434-6_31, © Springer-Verlag Wien 2013

received an injection of 100 μL of autologous whole blood (obtained via a femoral artery catheter) into the caudate nucleus within 8 min, through a 26-gauge needle (coordinates: 0.2 mm anterior, 5.5 mm ventral, and 3.5 mm lateral to the bregma) with a microinfusion pump.

Experimental Groups

These experiments were divided into four parts. In the first part, one control group (needle insertion only) and five ICH groups of rats ($n=4$) were killed 6 h, and on days 1, 3, 5, and 7, after blood injection for *SLC24A6* mRNA determination. In the second part, one control group and five ICH groups of rats ($n=4$) were killed 6 h, and on days 1, 3, 5, and 7, after blood injection for Western blotting examination. In the third part, control and ICH rat brains were sampled 6 h, and on days 3 and 7, after ICH for immunohistochemistry analysis ($n=3$). In the fourth part, control group (normal) and five ICH groups of rats ($n=4$, the same rats as in the second part) were killed 6 h, and on days 1, 3, 5, and 7, after blood injection for $[Ca^{2+}]i$ measurements.

Real-Time PCR

Total RNA was extracted with TRIzol Reagent (Invitrogen), and then mRNA was reverse transcripted to cDNA using an Omniscript RT Kit (Qiagen). The primer of *SLC24A6* mRNA was designed with PrimerExpress 1.0 and synthesized. Its upstream primer was 5′-CGTTCTCAGATTTCACGCTGG, and the downstream primer was 5′-GGATATTGAAGATGATGCCGC. QuantiFast SYBR Green PCR kit (Qiagen) was used for real-time PCR amplification according to its guidance.

Western Blotting

Western blotting was performed as described previously [6]. In brief, total protein was extracted from caudate nucleus tissue with tissue protein extraction reagent (Pierce). Protein concentration was estimated using a BCA Protein Assay Kit (Pierce). Samples (50 μg) were run on a polyacrylamide gel and then transferred to pure nitrocellulose membrane. Membranes were probed with 1: 1,000 dilution of goat anti-SLC24A6 polyclonal antibody (Santa Cruz, Santa Cruz, CA, USA), followed by a 1: 1,000 dilution of the secondary antibody (peroxidase-conjugated rabbit anti-goat antibody; Santa Cruz). Protein bands were visualized by chemiluminescence with an ECL Luminescence Kit (Pierce) and exposed to X-ray film.

Immunohistochemistry

The immunohistochemistry method has been described previously [5]. Briefly, the rats were reanesthetized and perfused with 4 % paraformaldehyde. Brains were removed and kept in 4 % paraformaldehyde for 6 h, immersed in 25 % sucrose for 3 days at 4 °C, then dehydrated, embedded in paraffin and sectioned. The antibodies were described above.

$[Ca^{2+}]i$ Measurement

Brain slice preparation was as listed above. The brain tissue was moved and set into cold Hanks salt solution with rinsing. Filtering with a 200-well filter was performed, and 2×10^6 single-cell suspension was then prepared with DMEM. Fura-2/AM was loaded; the terminal concentration was 5 μmol/L. After swaying for 50 min and centrifuging for 5 min at 3,000 rpm, the single-cell suspension was moved from supernatant, and rinsed twice with Hanks. The cell concentration was adjusted. Two milliliters of 0.1 % triton X-100 was added. F_{max} was gained by ultraviolet spectrophotometer (HITACHI F-3000); meanwhile, Fb2 at 380 nm was measured. After 0.5 mL of 4 mmol/L EGTA was added, F_{min} and Ff2 at 380 nm were gained: $[Ca^{2+}]i = kd\times(F-F_{min})/(F_{max}-F)\times Ff2/Fb2$, $kd = 224$ nm.

Statistical Analysis

One-way ANOVA was used with SPSS12.0 software to determine statistical significance. Values are listed as mean ± SD. Statistical significance was set at $p<0.05$.

Results

Mean arterial pressure, blood pH, arterial oxygen and carbon dioxide tensions, hematocrit, and blood glucose were recorded and controlled within normal ranges.

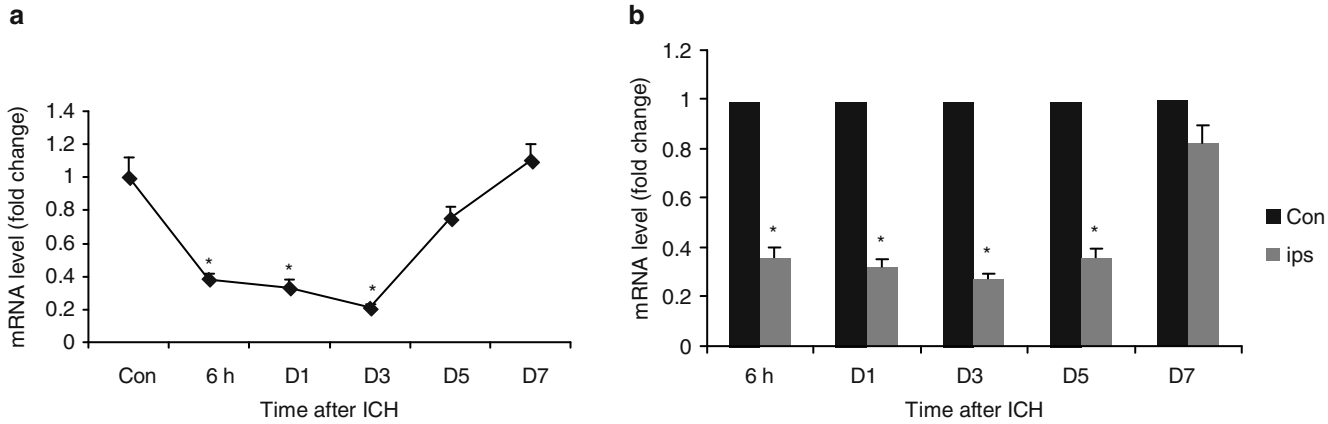

Fig. 1 *SLC24A6* mRNA level after intracerebral hemorrhage (ICH). (**a**) Time course, *$p<0.05$ versus control group. (**b**) Expression of the ipsilateral and the contralateral side, *$p<0.05$ versus contralateral side

After ICH, *SLC24A6* mRNA levels decreased at 6 h (38 %, $p<0.05$) and down to the lowest on day 3 (21 %, $p<0.05$), then back to the normal level on day 7 (1.1-fold, $p>0.05$). The mRNA levels of *SLC24A6* in the ipsilateral caudate nucleus were lower than those in the contralateral side after ICH (Fig. 1).

Western blotting data were in accordance with the data from real-time PCR. The time course of SLC24A6 protein level after ICH was similar. It represented a remarkable decline from 6 h to day 3 (40 and 15 %, $p<0.05$), followed by an escalation on days 5–7 (80 % and 1.3-fold vs. 1.00 ± 0.15, $p>0.05$). The protein levels of SLC24A6 in the ipsilateral caudate were also lower than those on the contralateral side at each time point.

Immunohistochemistry analysis showed lower and sparse density in caudate nucleus tissues of the ipsilateral side rather than the contralateral side at each time point. The staining density of SLC24A6 was lowest 6 h after ICH (Fig. 2).

The data obtained from Fura-2 loaded, dual wavelength spectrophotofluorometry demonstrated that the tested $[Ca^{2+}]i$ in brain tissues of the ipsilateral caudate nucleus was 277.1 ± 22.0 nmol/L within normal conditions. Then, $[Ca^{2+}]i$ elevated to the highest level of 887.5 ± 52.2 nmol/L on day 3 after establishment of ICH, followed by a remarkable decrease on days 5 and 7 (Fig. 3).

Conclusion

According to the data from the present study, *SLC24A6* mRNA and SLC24A6 protein levels decreased early after ICH, exhibiting a special time course, as opposed to that of $[Ca^{2+}]i$. The findings implicate the potential roles of SLC24A6 in hemorrhage-induced brain injury.

In pMCAO model rats, NCX1-3 expression was downregulated, and the infarction area was enlarged when treated with antisense ODNs. Still, in pMCAO model rats, NCKX2 expression also decreased, and gene silencing amplified brain damage. This evidence suggested their protective roles in brain injury [2, 4]. On the contrary, SEA0400, an agonist of the reverse mode of NCX, was able to alleviate brain damage, indicating a negative role [7]. According to the two opposite functions, its bidirectional mode of calcium transportation could be a concern. The similarity of the time course of SLC24A6 and $[Ca^{2+}]i$ presented in the present study, along with the structural and functional comparability of NCKX2 [3], implied that SLC24A6 has a protective effect.

The correlation of SLC24A6 and $[Ca^{2+}]i$ was due to the complex allocation of all the sodium calcium exchanger family members, and the underlying feedback mechanism. It has been shown that calpastatin might prevent NCX3 cleavage by calpain [1], and that calpeptin might reverse the downregulation of NCKX2 after ischemia [4]. This could be a way of achieving feedback. Also, $[Ca^{2+}]i$ is regulated not only by the level of SLC24A6, but also by other involved NCX members and different types of channels of calcium transportation. Thus, individual electrophysiological investigation of SLC24A6 needs to be carried out to clarify how SLC24A6 works and its patency of transportation of Ca^{2+}.

In summary, SLC24A6, a newly discovered member of the NCX family, which can modulate $[Ca^{2+}]i$, presents specific and remarkable alterations to both mRNA and the protein level in caudate nucleus tissues after intracerebral

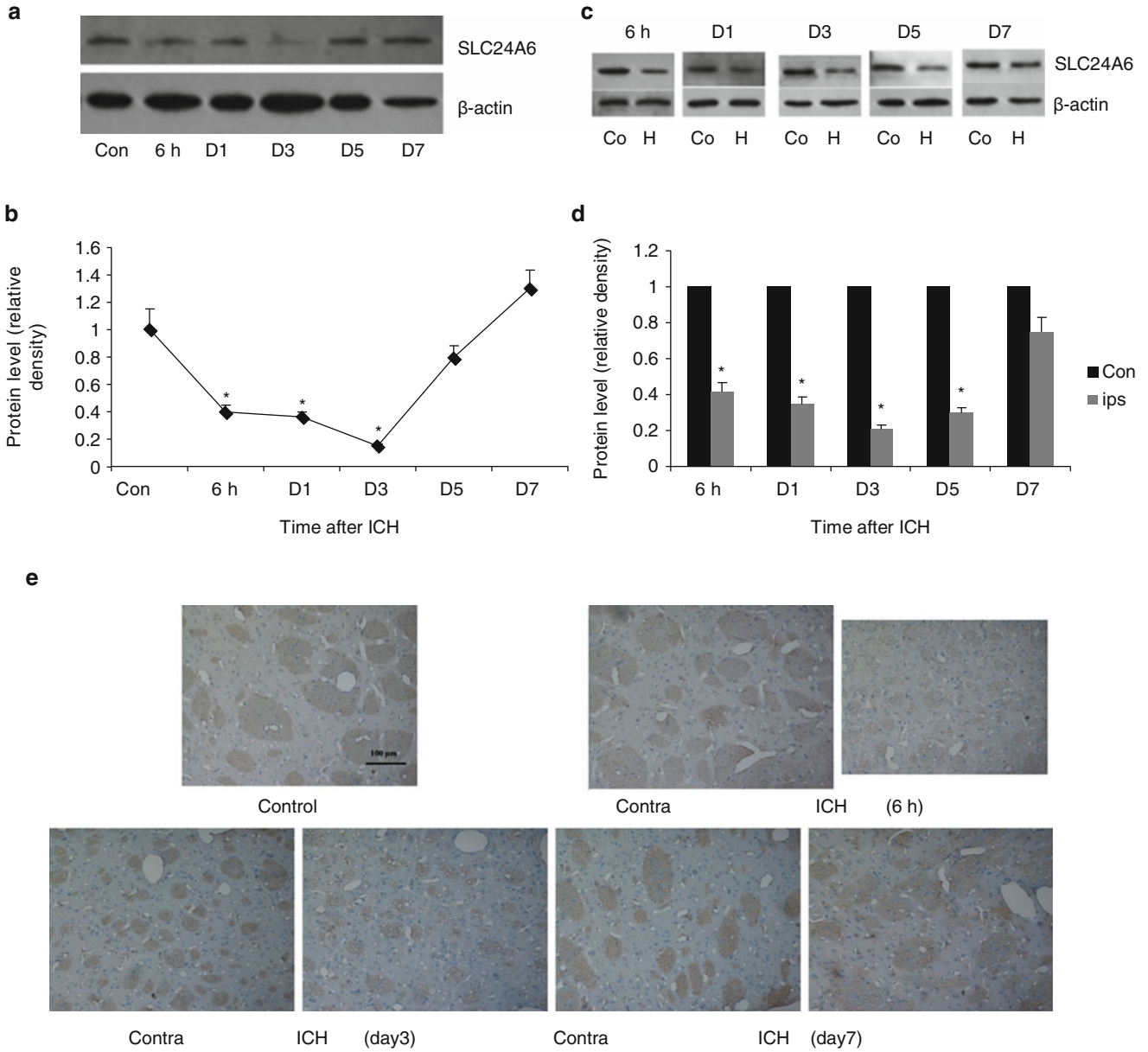

Fig. 2 SLC24A6 protein level after ICH. (**a**, **c**) Image recorded of Western blotting (**b**, **d**) time course of expression, $*p<0.05$ versus control group. (**e**) Immunohistochemistry analysis showed lower and sparse density of the ipsilateral side (*ICH*) rather than the contralateral side (*contra*) at each time point examined

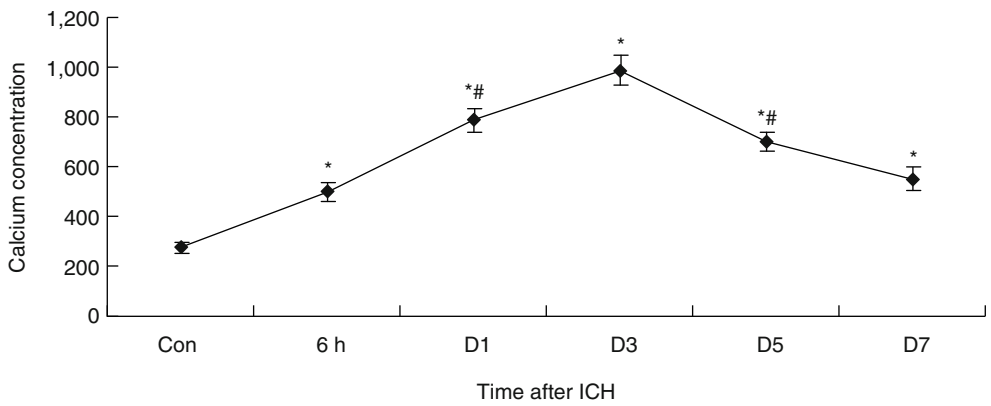

Fig. 3 $[Ca^{2+}]i$ value after ICH. $*p<0.01$ versus control, $\#p<0.01$ versus day 3

hemorrhage. Its decreased level correlated with $[Ca^{2+}]i$ elevation early after ICH establishment. Our results suggest that SLC24A6-mediated $[Ca^{2+}]i$ overload might play a role in brain damage after ICH, although further interventional research should be performed. The potential roles of SLC24A6 in brain injury may contribute new methods of ICH therapy.

Acknowledgments This study was supported by Grant No. 08411965100 from the Science and Technology Commission of Shanghai Municipality, and Grant Nos. 30872675 and 30901549 from the National Natural Science Foundation of China.

Conflict of Interest We declare that we have no conflict of interest.

References

1. Bano D, Young KW, Guerin CJ et al (2005) Cleavage of the plasma membrane Na/Ca^{2+} exchanger in excitotoxicity. Cell 120:275–285
2. Bano D, Nicotera P (2007) Ca^{2+} signals and neuronal death in brain ischemia. Stroke 38(2 Suppl):674–676
3. Cai XJ, Lytton J (2004) Molecular cloning of a sixth member of the K^+-dependent Na^+/Ca^{2+} exchanger gene family, NCKX6. J Biol Chem 279(7):5867–5876, 1999, 30(2):1167–1173
4. Cuomo O, Gala R, Pignataro G et al (2008) A critical role for the potassium-dependent sodium-calcium exchanger NCKX2 in protection against focal ischemic brain damage. J Neurosci 28(9): 2053–2063
5. Gong Y, Xi GH, Keep RF et al (2005) Complement inhibition attenuates brain edema and neurological deficits induced by thrombin. Acta Neurochir Suppl 95:389–392
6. Gong Y, Xi GH et al (2008) Increase in brain thrombin activity after experimental intracerebral hemorrhage. Acta Neurochir Suppl 105:47–50
7. Matsuda T, Arakawa N, Takuma K et al (2001) SEA0400, a novel and selective inhibitor of the Na^+–Ca^{2+} exchanger, attenuates reperfusion injury in the in vitro and in vivo cerebral ischemic models. J Pharmacol Exp Ther 298(1):249–256
8. Palty R, Ohana E, Hershfinkel M et al (2004) Lithium-calcium exchange is mediated by a distinct potassium-independent sodium-calcium exchanger. J Biol Chem 279(24):25234–25240
9. Xi G, Hua Y, Bhasin RR (2001) Mechanisms of edema formation after intracerebral hemorrhage, effects of extravasated red blood cells on blood flow and blood-brain barrier integrity. Stroke 32(12):2932–2938
10. Zazulia AR, Diringer MN, Derdeny CP et al (1999) Progression of mass effect after intracerebral hemorrhage. Stroke 30(6):1167–1173
11. Zhang X, Li H, Hu S et al (2006) Brain edema after intracerebral hemorrhage in rats: the role of inflammation. Neurol India 54(4):402–407

Usefulness of Intraoperative Computed Tomography for the Evacuation of Lobar Hemorrhage

Mutsuo Fujisawa, Shiro Yamashita, and Ryosuke Katagi

Abstract There is a lot of debate on the treatment method for spontaneous intracerebral hemorrhage (ICH). Intraoperative computed tomography (iCT) provides excellent images of cerebrovascular lesions. In this paper, we describe the surgical procedure and the efficacy of iCT during lobar hemorrhage evacuations and subsequent patient outcomes. Fifty-eight patients with lobar hemorrhage were treated using iCT. We performed preoperative cerebral angiography and/or three-dimensional (3D) CT angiography to detect abnormal vessels and identify the spatial relationships between the cerebrovascular structures and the hematoma. After administration of local anesthesia, an enlarged burr-hole was created just above the hematoma. Microsurgical evacuation of the hematoma was performed, and an iCT image was obtained to assess real-time 3D information on residual hematoma or unexpected rebleeding. Mean hematoma volume, evacuation rate, and duration of the surgery were 42 mL, 93 %, and 89 min respectively. Postoperative rebleeding occurred in 1 case. The median Glasgow Coma Scale score upon admission was 12. At discharge, most patients (60 %) had good functional outcomes defined by modified Rankin Scale scores of 0–3. Postoperative neurological findings and consciousness levels showed early improvement. Safe, accurate, and effective evacuation of lobar hemorrhage was possible with iCT as an image-guided intraoperative navigation tool.

Keywords Intraoperative computed tomography • Lobar hemorrhage • Minimally invasive surgery • Microsurgical evacuation • Fusion image

M. Fujisawa, S. Yamashita, and R. Katagi (✉)
Department of Neurosurgery, Katagi Neurosurgical Hospital, 274 Betsumyo, Imabari, Ehime 794-0065, Japan
e-mail: katagihp@katagihosp.com

Introduction

Spontaneous intracerebral hemorrhage (ICH) is one of the most serious types of stroke. Mortality and severe morbidity is higher after primary ICH than after other subtypes of stroke [1]. The treatment of ICH continues to remain a matter of debate [6, 9, 12, 17]. Although conventional craniotomies allow immediate and complete evacuations, these can be associated with poor patient stability and additional brain injury. Minimally invasive surgery, such as stereotactic aspiration, endoscopic evacuation, and keyhole evacuation, are employed in order to improve the surgical results by reducing surgical tissue trauma [2–4, 8, 10, 17].

The recent development of image-guided navigation has enabled safe and accurate neurosurgical operations [5, 14]. Intraoperative computed tomography (iCT) provides excellent diagnostic images for the visualization of cerebrovascular lesions [13, 15]. In this paper, we describe the surgical procedure involved in an enlarged burr-hole hematoma evacuation, the surgical outcomes of the patients, and the efficacy of iCT for the surgical treatment of lobar hemorrhage.

Materials and Methods

Between January 2000 and July 2011, 58 patients with lobar hemorrhage were treated using iCT at our hospital. Preoperative cerebral angiography and/or three-dimensional (3D) CT angiography were performed in order to detect any abnormal vessels and to identify the spatial relationships between the cerebrovascular structures and the hematoma. We included patients who had supratentorial lobar hemorrhage diagnosed using CT and a hematoma volume of more than 10 mL, with a focal neurological deficit. Patients with hemorrhage from brain tumors or cerebral aneurysms or arteriovenous malformations were excluded. After March 2008, preoperative 3D simulation was performed using

Y. Katayama et al. (eds.), *Brain Edema XV*, Acta Neurochirurgica Supplement, Vol. 118,
DOI 10.1007/978-3-7091-1434-6_32,

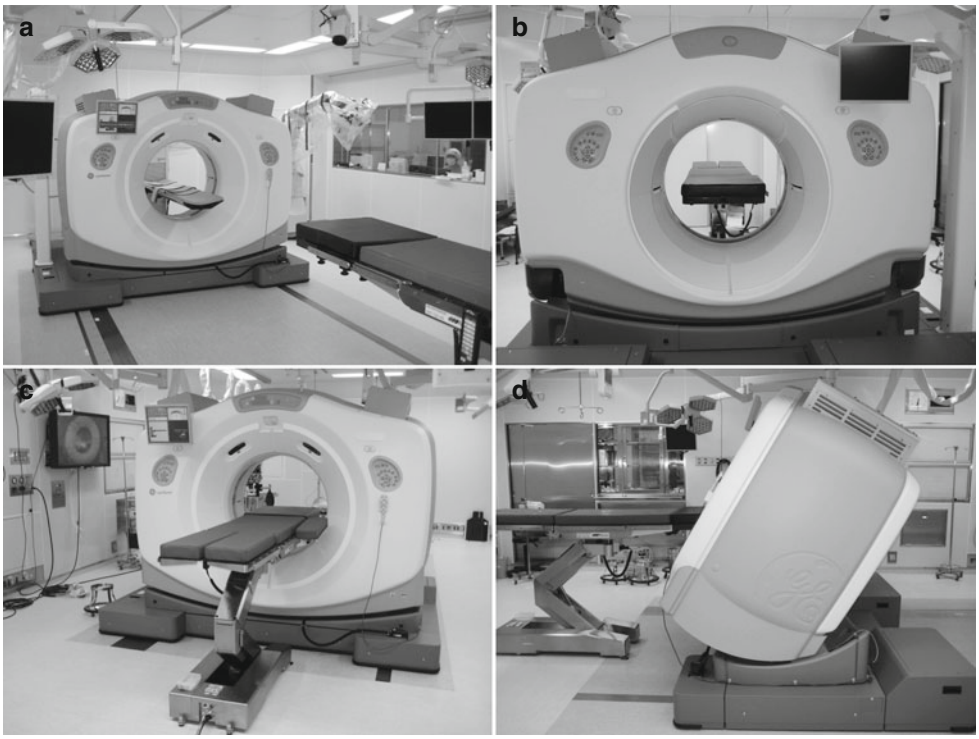

Fig. 1 Photographs of the intraoperative computed tomography (iCT) imaging system. A 16-multislice CT system is installed in the operating room (**a**). A sliding gantry with an 80-cm bore diameter (**b**) is installed on rails, enabling better access to the patients (**c**). Gantry tilt for imaging is possible (**d**)

3D-CT, magnetic resonance imaging (MRI), magnetic resonance angiography (MRA), and magnetic resonance venography (MRV) (3D-CT/MRI/MRA/MRV) fusion images. With the fusion images, the most superficial point in the hematoma and the area just under an avascular region of the cortex was chosen as the target point, which was the area where the effective and safe evacuation of the lobar hemorrhage was possible (see Fig. 2). The volume of the hematoma was measured according to the bedside method for measuring CT hematoma volume. The formula ABC/2 was used, where A is the greatest hemorrhage diameter determined by CT, B is the diameter that is 90° to A, and C is the approximate number of 10-mm CT slices of the hemorrhage [7]. Neurological status was assessed using the following: Glasgow Coma Scale (GCS) upon admission and on day 7, the National Institutes of Health Stroke Scale (NIHSS) upon admission and on day 7, and the modified Rankin Scale (mRS) score at discharge.

In an operating room, a sliding-gantry 16-multislice CT system (Light Speed RT Smart Gantry; GE Healthcare, Tokyo, Japan) with an 80-cm bore diameter was installed on rails. A radiolucent, adjustable, and flexible operating table was fixed. Gantry-tilt imaging was possible to avoid head pin artifacts. During iCT imaging, all staff moved into an adjoining control room where the workstation was installed (Fig. 1). We put a mark on the patient's scalp just above the target point. Preoperative CT was performed in order to confirm the position of the mark (Fig. 2).

After the patients were administered local anesthesia, a 4-cm-long linear skin incision and an enlarged burr-hole (diameter, 20 mm) was created just above the target point, which is the most superficial point of the hematoma. After the dura mater was opened, a 1-cm-long cortical incision was made in an avascular region of the cortex. Microsurgical evacuation of the hematoma was performed with a suction device. Tumor forceps were sometimes used to break down clots for suction. An iCT image was obtained in order to assess real-time 3D information about any residual hematoma or unexpected rebleeding during the operation (Fig. 2).

Results

The mean age of the patients treated was 70 years (range, 40–90 years), and there were 31 men and 27 women. The mean hematoma volume, evacuation rate, and surgery duration were 42 mL (range, 12–144 mL), 93 % (range, 53–100 %), and 89 min (range, 35–145 min) respectively. Postoperative rebleeding was noted in only 1 case (2 %). This patient took an antiplatelet drug before the onset of hemorrhage. Neurological findings and consciousness levels tended to improve early in the postoperative period. The median GCS scores were 12 (range, 5–15) upon admission and 15 (range, 5–15) on the seventh postoperative day. The mean NIHSS scores were 12.7 (range, 1–37) upon admission and 10.1 (range, 0–38) on the seventh postoperative day. A total of 54 patients (93 %) survived and were discharged, and 35 of them (60 %) had good functional outcomes, which was defined as an mRS score of 0–3 at discharge. At discharge,

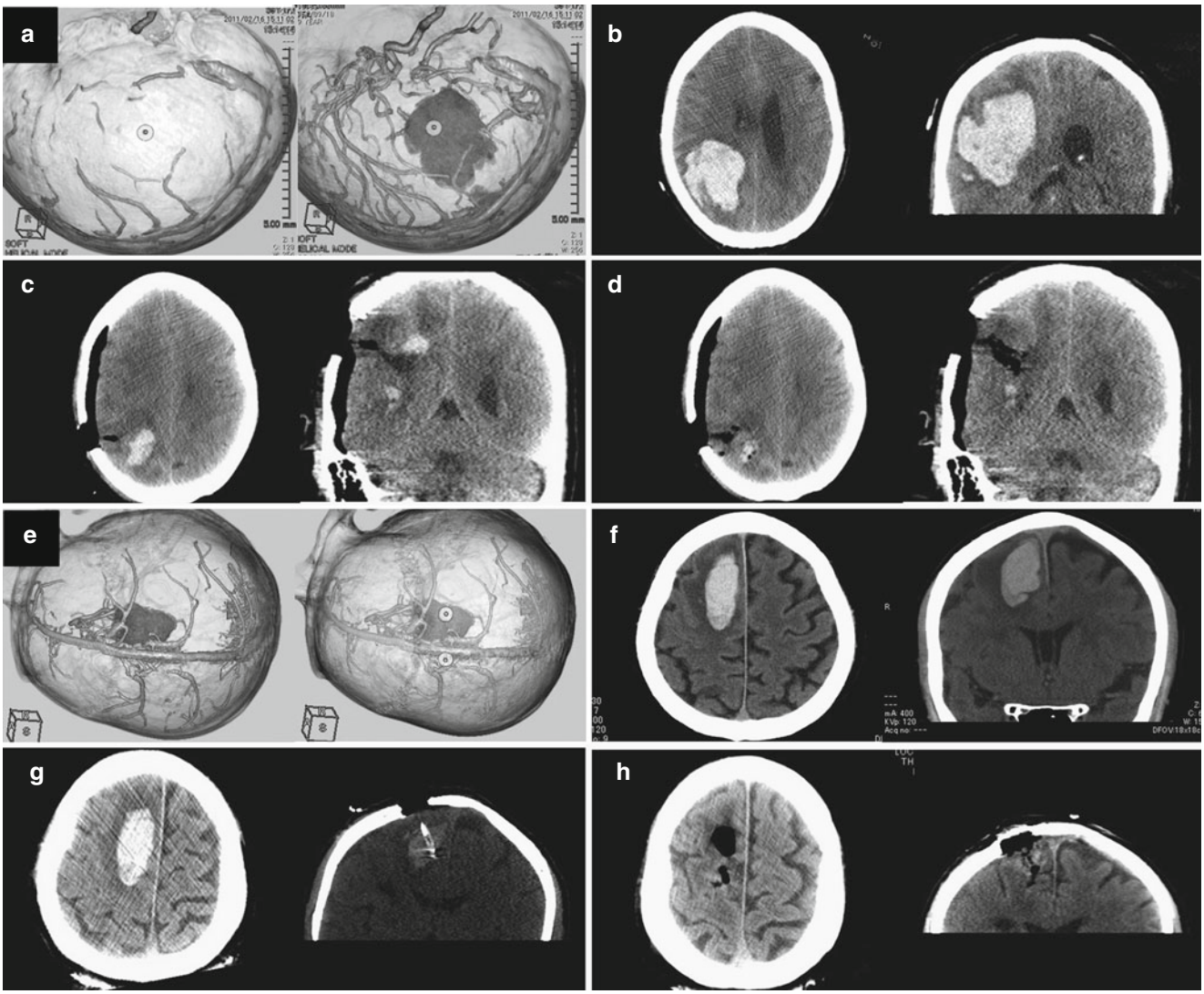

Fig. 2 Preoperative three-dimensional (3D) simulation using 3D-CT, magnetic resonance imaging (MRI), magnetic resonance angiography, and magnetic resonance venography (MRV) fusion images (**a**, **e**) and iCT images (**b–d**, **f–h**) in representative patients with lobar hemorrhage. The patients with right parietal lobar hemorrhage underwent an enlarged burr-hole evacuation with a microscope. The first iCT showed residual hematoma (**c**) and, finally, an almost complete hematoma evacuation was performed (**d**). The patient with a right frontal lobar hemorrhage was operated on by using iCT. The first iCT scan showed an inserted drainage tube in the residual hematoma cavity (**g**). Complete hematoma evacuation was performed using a microscope (**h**)

28 (80 %) of the 35 patients with ages less than 75 years showed good functional outcomes. At discharge, 29 (76 %) of 38 patients with hematoma volumes that were smaller than 50 mL also had good functional outcomes (Fig. 3)

Conclusion

Although the results of the Surgical Trial in Intracerebral Hematoma showed that there were no significant differences in survival or functional outcomes between patients in the surgical and medical treatment groups, a subgroup analysis identified that surgery might be helpful in treating patients with hematomas that are within 1 cm of the cortical surface [9]. Surgical evacuations of lobar hemorrhages were usually performed through craniotomies, which were more invasive than burr-hole operations [11]. Minimally invasive surgeries, such as stereotactic aspiration and endoscopic evacuation of ICH, can be performed after the administration of local anesthesia, and these procedures minimize surgical trauma to the brain. In addition, minimally invasive surgeries show a trend toward better results [2–4, 8, 10, 17]. The main purpose of surgery for ICH is to reduce the mass effect, which can cause secondary brain damage by compressing the adjacent brain tissue and brain edema formation due to the toxic effects of blood degradation products [16]. Microsurgical evacuations of lobar hemorrhages through enlarged burr-holes using iCT provided immediate and

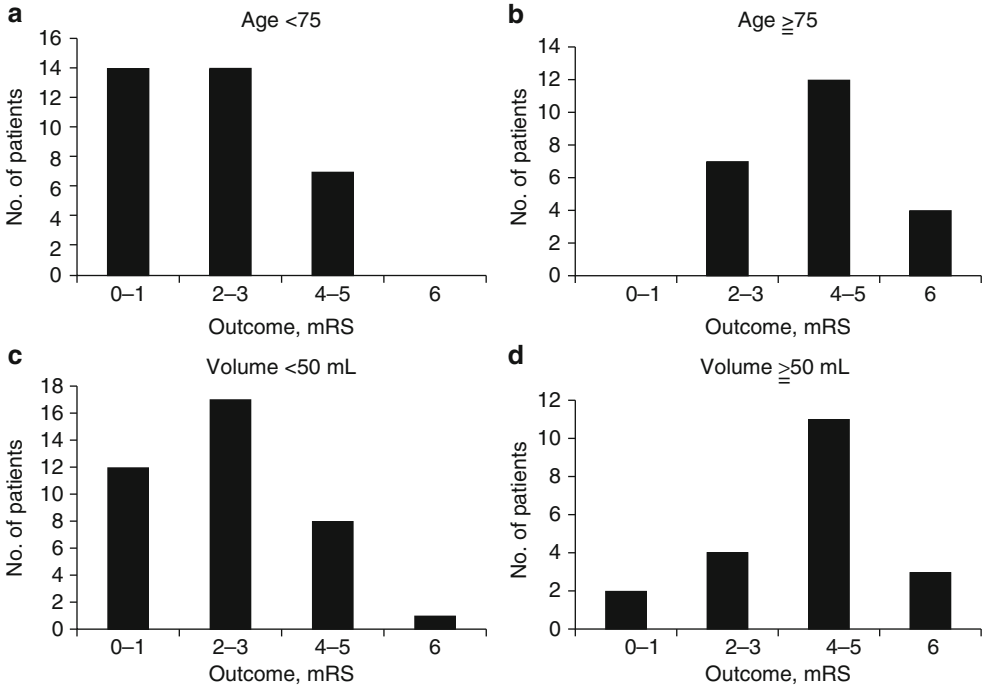

Fig. 3 Comparison of patients less than 75 years of age or 75 years of age or older (**a**, **b**) with a hematoma volume less than 50 mL or 50 mL or more (**c**, **d**) on the basis of their modified Rankin scale scores at discharge. The outcome of patients younger than 75 years of age with a hematoma smaller than 50 mL who showed better functional recovery (**a**, **c**)

almost complete evacuation, which can lessen secondary brain damage. Moreover, the enlarged burr-hole evacuation technique facilitates hemostasis through the use of bipolar forceps and minimizes surgical tissue trauma, allowing safer and minimally invasive surgery.

Recent advances in the technology of image-guided navigation have enabled neurosurgeons to visualize anatomic structures more accurately during neurosurgical operations. The utility of iCT for image-guided navigation in vascular, brain tumor, and spinal surgery has previously been reported [5, 13–15]. iCT can provide real-time information about vascular lesions and bony structures during an operation with very short imaging acquisition times [13, 15]. The intraoperative examination time, including preparation and imaging, was 5 min in this study. An iCT system with a large bore diameter of 80 cm can be used in all operative positions except sitting and enables better access to the patient. An iCT system brings the CT gantry to the patient during surgery without moving the patient. This lessens the risk of complications. iCT has the advantage of precisely verifying the extent of hematoma removal during an operation. In addition, iCT provides a multi-planar reformatting image, which can increase the understanding of real-time 3D information about the hematoma. This real-time information using iCT contributes to improving the orientation of the neurosurgeon during the operation. Moreover, we have been using preoperative 3D-CT/MRI/MRA/MRV fusion images for 3D simulations of surgery. Preoperative fusion images provide good visualization of the spatial relationship between the hematoma, the cerebrovascular structures, and the cranial bones. iCT, in combination with preoperative fusion images, enables surgery to be performed more safely and accurately.

In summary, an enlarged burr-hole evacuation procedure using iCT resulted in good functional recovery, especially in patients younger than 75 years of age and with hematomas smaller than 50 mL and a very low rate of complications, such as postoperative rebleeding. Safe and effective evacuation of lobar hematoma was possible by using iCT as an image-guided intraoperative navigation tool. Enlarged burr-hole evacuation using iCT is a safer, more accurate, and minimally invasive surgery for the treatment of lobar hemorrhage.

Conflict of Interest We declare that we have no conflict of interest.

References

1. Aguilar MI, Freeman WD (2010) Spontaneous intracerebral hemorrhage. Semin Neurol 30:555–564
2. Auer LM, Deinsberger W, Niederkorn K, Gell G, Kleinert R, Schneider G, Holzer P, Bone G, Mokry M, Körner E et al (1989) Endoscopic surgery versus medical treatment for spontaneous intracerebral hematoma: a randomized study. J Neurosurg 70: 530–535
3. Barlas O, Karadereler S, Bahar S, Yesilot N, Krespi Y, Solmaz B, Bayindir O (2009) Image-guided keyhole evacuation of spontaneous supratentorial intracerebral hemorrhage. Minim Invasive Neurosurg 52:62–68
4. Hattori N, Katayama Y, Maya Y, Gatherer A (2004) Impact of stereotactic hematoma evacuation on activities of daily living during the chronic period following spontaneous putaminal hemorrhage: a randomized study. J Neurosurg 101:417–420

5. Hosoda T, Takeuchi H, Hashimoto N, Kitai R, Arishima H, Kodera T, Higashino Y, Sato K, Kikuta K (2011) Usefulness of intraoperative computed tomography in surgery for low-grade gliomas: a comparative study between two series without and with intraoperative computed tomography. Neurol Med Chir (Tokyo) 51: 490–495
6. Juvela S, Heiskanen O, Poranen A, Valtonen S, Kuurne T, Kaste M, Troupp H (1989) The treatment of spontaneous intracerebral hemorrhage. A prospective randomized trial of surgical and conservative treatment. J Neurosurg 70:755–758
7. Kothari RU, Brott T, Broderick JP, Barsan WG, Sauerbeck LR, Zuccarello M, Khoury J (1996) The ABCs of measuring intracerebral hemorrhage volumes. Stroke 27:1304–1305
8. Lee JI, Nam DH, Kim JS, Hong SC, Shin HJ, Park K, Eoh W, Kim JH (2003) Stereotactic aspiration of intracerebral haematoma: significance of surgical timing and haematoma volume reduction. J Clin Neurosci 10:439–443
9. Mendelow AD, Gregson BA, Fernandes HM, Murray GD, Teasdale GM, Hope DT, Karimi A, Shaw MD, Barer DH (2005) Early surgery versus initial conservative treatment in patients with spontaneous supratentorial intracerebral haematomas in the International Surgical Trial in Intracerebral Haemorrhage (STICH): a randomised trial. Lancet 365:387–397
10. Montes JM, Wong JH, Fayad PB, Awad IA (2000) Stereotactic computed tomographic-guided aspiration and thrombolysis of intracerebral hematoma: protocol and preliminary experience. Stroke 31: 834–840
11. Morgenstern LB, Demchuk AM, Kim DH, Frankowski RF, Grotta JC (2001) Rebleeding leads to poor outcome in ultra-early craniotomy for intracerebral hemorrhage. Neurology 56:1294–1299
12. Pantazis G, Tsitsopoulos P, Mihas C, Katsiva V, Stavrianos V, Zymaris S (2006) Early surgical treatment vs conservative management for spontaneous supratentorial intracerebral hematomas: a prospective randomized study. Surg Neurol 66:492–502
13. Schichor C, Rachinger W, Morhard D, Zausinger S, Heigl TJ, Reiser M, Tonn JC (2010) Intraoperative computed tomography angiography with computed tomography perfusion imaging in vascular neurosurgery: feasibility of a new concept. J Neurosurg 112:722–728
14. Senft C, Seifert V, Hermann E, Franz K, Gasser T (2008) Usefulness of intraoperative ultra low-field magnetic resonance imaging in glioma surgery. Neurosurgery 63:257–267
15. Tonn JC, Schichor C, Schnell O, Zausinger S, Uhl E, Morhard D, Reiser M (2011) Intraoperative computed tomography. Acta Neurochir Suppl 109:163–167
16. Xi G, Keep RF, Hoff JT (2006) Mechanisms of brain injury after intracerebral haemorrhage. Lancet Neurol 5:53–63
17. Zuccarello M, Brott T, Derex L, Kothari R, Sauerbeck L, Tew J, Van Loveren H, Yeh HS, Tomsick T, Pancioli A, Khoury J, Broderick J (1999) Early surgical treatment for supratentorial intracerebral hemorrhage: a randomized feasibility study. Stroke 30:1833–1839

Early CT Signs of Hypoxia in Patients with Subarachnoid Hemorrhage Presenting with Cardiac Arrest: Early CT Signs in SAH Patients Presenting with CA

Joji Inamasu, Masashi Nakatsukasa, Takuro Hayashi, Yoko Kato, and Yuichi Hirose

Abstract *Background*: For cardiac arrest (CA) victims, brain computed tomography (CT) may serve as a prognosticator. Loss of gray–white matter discrimination (GWMD) and sulcal edema/effacement are reliable CT signs of hypoxia, and a time window may exist for development of these signs. Most data are derived from CA victims of cardiac etiology, however, and CT signs have rarely been evaluated in victims of CA secondary to subarachnoid hemorrhage (SAH).

Methods: A retrospective study was conducted to clarify the incidence, temporal profile, and prognostic significance of early CT signs in resuscitated SAH-CA patients.

Results: During a 6-year period, 35 SAH-CA patients were identified. CT signs were observed in 94 %: loss of GWMD was observed in 94 %, whereas sulcal edema/effacement was observed in 77 %. In 29 patients, the interval between CA and the return of spontaneous circulation (ROSC) was estimated. CT signs developed almost invariably when the CA-ROSC interval exceeded 10 min. Loss of GWMD always preceded sulcal edema/effacement. None of the 35 patients achieved long-term survival, regardless of the presence of the CT signs.

Conclusion: CT signs may develop earlier in patients with SAH-CA than CA of cardiac origin. Because of a poor prognosis, early CT signs are not useful prognosticators in that population.

Keywords Cardiac arrest • CT sign • Gray–white matter discrimination • Return of spontaneous circulation • Subarachnoid hemorrhage • Sulcal edema

Introduction

Recently, the role and importance of imaging studies in the treatment of cardiac arrest (CA) victims has been recognized [1–5, 8, 9]. Brain computed tomography (CT) may be the imaging modality of choice for evaluation of hypoxic/ischemic brain damage in CA victims shortly after resuscitation [1–5, 8, 9]. Loss of gray–white matter differentiation (GWMD) and sulcal edema/effacement are the early CT signs that develop relatively reproducibly when the interval between CA and the return of spontaneous circulation (ROSC) is prolonged, and the presence of such CT signs almost invariably predicts a poor outcome [1, 4, 9]. In CA victims of cardiac etiology, those with CA-ROSC >20 min reliably develop early CT signs, suggesting that a time window may exist for the development of CT signs [4, 7]. However, such CT signs have rarely been studied in victims of CA secondary to subarachnoid hemorrhage (SAH). In victims of SAH-CA, the brain has already sustained irreversible brain damage at the time of aneurysmal rupture, and the temporal profile of early CT signs may differ substantially from that of CA of cardiac etiology [2, 3, 5]. A retrospective study was conducted to clarify the incidence and temporal profile of early CT signs in resuscitated victims of SAH-CA.

Materials and Methods

This study was conducted between July 2003 and June 2009 in a single institution. Cardiopulmonary resuscitation (CPR) for CA victims was performed following the latest advanced

J. Inamasu, MD (✉)
Department of Neurosurgery, Saiseikai Utsunomiya Hospital, Utsunomiya, Japan

Department of Neurosurgery, Fujita Health University, 1-98 Dengakugakubo, Toyoake 470-1192, Japan
e-mail: ginamasu@aol.com

M. Nakatsukasa
Department of Neurosurgery, Saiseikai Utsunomiya Hospital, Utsunomiya, Japan

T. Hayashi, Y. Kato, and Y. Hirose
Department of Neurosurgery, Fujita Health University, 1-98 Dengakugakubo, Toyoake 470-1192, Japan

Y. Katayama et al. (eds.), *Brain Edema XV*, Acta Neurochirurgica Supplement, Vol. 118,
DOI 10.1007/978-3-7091-1434-6_33, © Springer-Verlag Wien 2013

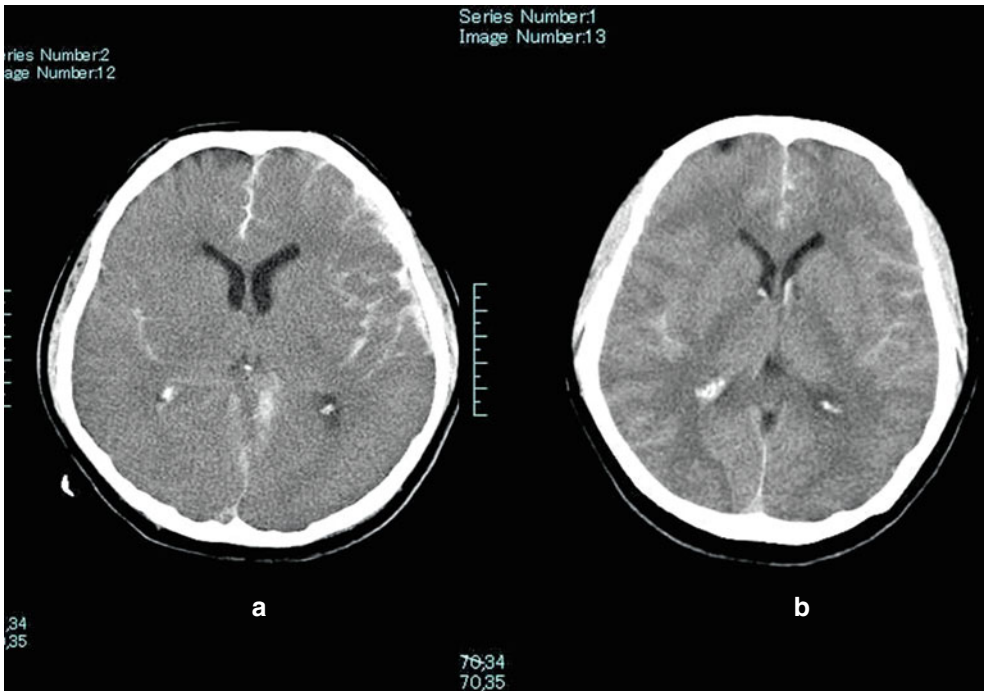

Fig. 1 Representative cases with (**a**) and without (**b**) loss of gray–white matter discrimination at the basal ganglia. Note that the contrast between gray and white matter is lost only in **a**

cardiac life support guidelines [6]. After arrival in the emergency department (ED), the temporal sequence of the resuscitative events was recorded on a minute-by-minute basis by emergency medicine residents. Those who achieved ROSC in the ED after resuscitation were routinely brought to a CT suite adjacent to the ED immediately after resuscitation. The CT suite was equipped with a General Electric Light-Speed 16-detector row CT system, and contiguous non-helical 5-mm slices of the brain were obtained. During the 5-year period, a total of 35 victims of SAH-CA achieved ROSC and underwent brain CT immediately after resuscitation. The incidence and temporal profile of two early CT signs of hypoxia, i.e., loss of GWMD and sulcal edema/effacement, were evaluated. A board-certified radiologist read all the films, but was not notified of the patient's status. They evaluated the loss of GWMD signs at the level of the basal ganglia and sulcal edema/effacement at the level of the parietal cortex in each patient. The 2×2 table analyses, including the Chi-squared test, were performed using Statview 5.0, and a $p<0.05$ was considered significant.

Results

The age of the 35 resuscitated SAH-CPA patients ranged from 33 to 91 years (mean: 62.0±5.2 years), and the male:female ratio was 1:2.2. Brain CTs of a patient with and without early CT signs are shown in Fig. 1. Loss of GWMD was observed in 33 (94 %), whereas sulcal edema/effacement was observed in 27 (77 %). Two patients exhibited neither of the CT signs. None of the patients achieved long-term survival, however. The length of survival ranged from 1 to 15 days (mean: 3.5±0.7 days, median: 1 day).

In 29 patients with witnessed collapse (83 %), the time of collapse had been recorded and the CA-ROSC interval was estimated. The estimated CA-ROSC interval ranged from 8 to 60 min (mean: 28.2±2.5 min). Distribution of the 29 SAH-CA patients in relation to the CA-ROSC interval was illustrated as a histogram, with the interval on the *x*-axis and the number of cases on the *y*-axis (Fig. 2). Those who were positive only for the loss of GWMD sign were shown in gray, whereas those who were positive for both the loss of GWMD and sulcal edema/effacement were shown in black. There were no patients who were positive only for the sulcal edema/effacement. The number of patients with positive CT signs seemed to increase substantially when the interval exceeded 10 min, and loss of GWMD developed either concomitantly with, or earlier than, sulcal edema/effacement (Fig. 2).

Conclusion

The CT signs of brain hypoxia in CA victims have been known for years [1, 4, 8, 9]. Loss of GWMD and sulcal edema/effacement are the radiographic signs most frequently documented in the literature [1, 4, 8, 9]. The presence of these CT signs is associated with poor outcome in victims of CA of cardiac etiology: we previously reported that a positive

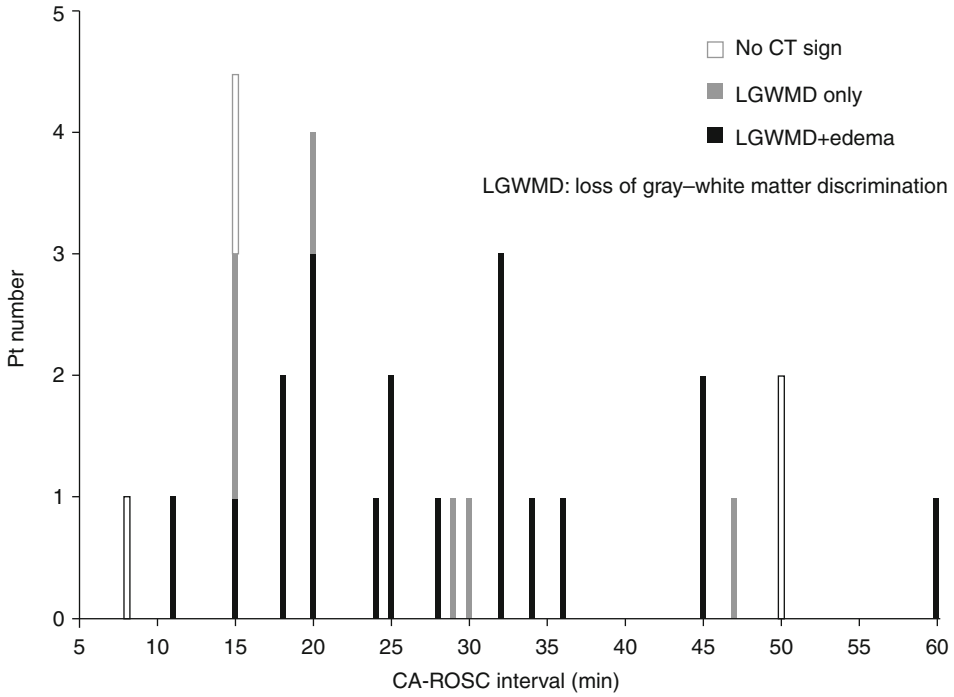

Fig. 2 A histogram showing the distribution of the 29 resuscitated SAH-CA patients in relation to the CA-ROSC interval. Those who exhibited intact brain CT are indicated by the *white bar*, whereas those who exhibited loss of gray–white matter discrimination (LGWMD) are indicated by the *gray bar*, and those exhibited both LGWMD and sulcal edema/effacement are indicated by the *black bar*

GWMD sign in resuscitated CA victims of cardiac etiology was predictive of unfavorable outcome (either vegetative state or death) with 81 % sensitivity and 92 % specificity [4]. Furthermore, a positive sulcal edema/effacement sign was predictive of unfavorable outcome with 32 % sensitivity and 100 % specificity [4]. Following these results, we concluded that brain CT obtained immediately after resuscitation might have prognostic value [4]. However, little has been known about early CT signs in resuscitated victims of SAH-CA. This study is one of the first to investigate the incidence and temporal profile of CT signs in that population.

In resuscitated victims of CA of cardiac etiology, early CT signs develop reproducibly when the CA-ROSC interval exceeds 20 min [4, 7], and loss of GWMD signs develops earlier and more frequently than sulcal edema/effacement [4]. By contrast, in resuscitated SAH-CA victims, loss of GWMD sign seemed to develop reproducibly when CA-ROSC interval exceeded 10 min (Fig. 2), indicating that the time window for development of early CT signs was narrower in that subgroup. The pathophysiological mechanism of hypoxic brain injury differs substantially between CA of cardiac etiology and SAH-CA: in the former, brain oxygen deprivation begins with CA [1, 4, 7, 9]. By contrast, in the latter, a sudden rise in the intracranial pressure after aneurysmal bleeding results in either transient or persistent arrest of the cerebral blood flow (CBF) before CA occurs [2–5]. Therefore, the narrower time window may be attributable to the combined detrimental effect of SAH-induced CBF reduction and cessation of systemic circulation. The outcomes of resuscitated SAH-CA patients were extremely poor in this study: regardless of the presence of early CT signs, none achieved long-term survival. In this context, brain CT obtained immediately after resuscitation may not be useful as a prognosticator in this population.

The limitations of this study need to be mentioned. First, the accuracy of the CA-ROSC interval may be hard to verify because information regarding the time at which the victim collapsed was solely reliant on the memory of witnesses. Second, the CA-ROSC interval of 10 min as a time window is arbitrary because of the small number of patients. The accuracy of the interval needs to be verified with studies with larger sample sizes. Finally, the possibility that a few CPA-SAH patients might have sustained pseudo-SAH, i.e., hypoxia-induced high attenuation areas along the basal cisterns mimicking SAH [10], cannot be denied.

Conflict of Interest We declare that we have no conflict interest.

References

1. Choi SP, Park HK, Park KN et al (2008) The density ratio of grey to white matter on computed tomography as an early predictor of vegetative state or death after cardiac arrest. Emerg Med J 25: 666–669
2. Inamasu J, Saito R, Nakamura Y et al (2001) Survival of a subarachnoid hemorrhage patient who presented with prehospital cardiopulmonary arrest: case report and review of the literature. Resuscitation 51:207–211
3. Inamasu J, Miyatake S, Tomioka H et al (2009) Headache, cardiac arrest, and intracranial hemorrhage. J Headache Pain 10:357–360

4. Inamasu J, Miyatake S, Suzuki M et al (2010) Early CT signs in out-of-hospital cardiac arrest survivors: temporal profile and prognostic significance. Resuscitation 81:534–538
5. Inamasu J, Nakagawa Y, Kuramae T et al (2011) Subarachnoid hemorrhage causing cardiopulmonary arrest: resuscitation profiles and outcomes. Neurol Med Chir (Tokyo) 51:619–623
6. International Liaison Committee on Resuscitation (2005) 2005 International consensus on cardiopulmonary resuscitation and emergency cardiovascular care science with treatment recommendations. Part 4: advanced life support. Resuscitation 67: 213–247
7. Oddo M, Ribordy V, Feihl F et al (2008) Early predictors of outcome in comatose survivors of ventricular fibrillation and non-ventricular fibrillation cardiac arrest treated with hypothermia: a prospective study. Crit Care Med 36:2296–2301
8. Szold O, Reider-Groswasser II, Ben Abraham R et al (2002) Gray-white matter discrimination: a possible marker for brain damage in heat stroke? Eur J Radiol 43:1–5
9. Torbey MT, Selim M, Knorr J, Bigelow C, Recht L (2000) Quantitative analysis of the loss of distinction between gray and white matter in comatose patients after cardiac arrest. Stroke 31: 2163–2167
10. Yuzawa H, Higano S, Mugikura S et al (2008) Pseudo-subarachnoid hemorrhage found in patients with postresuscitation encephalopathy: characteristics of CT findings and clinical importance. AJNR Am J Neuroradiol 29:1544–1549

Decrease in the Apparent Diffusion Coefficient in Peritumoral Edema for the Assessment of Recurrent Glioblastoma Treated by Bevacizumab

Shingo Takano, Hidehiro Kimu, Kyoji Tsuda, Satoru Osuka, Kei Nakai, Tetsuya Yamamoto, Eiichi Ishikawa, Hiroyoshi Akutsu, Masahide Matsuda, and Akira Matsumura

Abstract *Purposes*: Anti-edema effect of bevacizumab was evaluated using the apparent diffusion coefficient (ADC) of peritumoral edema associated with regional cerebral blood flow (rCBV) of the tumor.

Materials and Methods: Nine patients with recurrent glioblastoma were treated using bevacizumab for 4 ~ 36 months (average 12 months). MRI was performed every 2 months. For each MRI, ADC value, Gd-enhanced area on T1 imaging, area of peritumoral edema on T2 imaging, and rCBV on perfusion imaging were measured. ADC and rCBV values were determined by the use of regions of interest positioned in areas of high signal intensity, as seen on T2-weighted images and ADC maps.

Results: After 2 months of bevacizumab treatment, ADC values and rCBV decreased 49 and 32 % respectively, associated with marked diminishment of the Gd-enhanced area compared with pretreatment. After 6 months, in 5 of the 9 cases, the Gd-enhanced area appeared again with no change in the ADC value and rCBV. In the other four cases, the Gd-enhanced area as well as the ADC value and rCBV returned to the initial status.

Conclusion: The anti-edema effect of bevacizumab for treatment of recurrent glioblastoma that was demonstrated by decreased ADC values and rCBV was dramatic and prolonged at 6 months even with tumor progression.

Keywords Bevacizumab • Glioblastoma • Recurrence • ADC • rCBV

S. Takano, MD, PhD (✉), H. Kimu, K. Tsuda, S. Osuka, K. Nakai, T. Yamamoto, E. Ishikawa, H. Akutsu, M. Matsuda, and A. Matsumura
Department of Neurosurgery, Institute of Clinical Medicine, University of Tsukuba,
1-1-1Tennoudai, Tsukuba city, Ibaraki 305-8575, Japan
e-mail: shingo4@md.tsukuba.ac.jp

Introduction

The apparent diffusion coefficient (ADC) has been intensively investigated in glioma biology. Minimum ADC values have been found to be prognostic of outcomes in gliomas [5]. For up-front bevacizumab-treated patients, lower ADC was associated with significantly longer progression-free survival and tended toward longer overall survival [7]. Lower ADC is associated with the tumor MGMT promoter methylation, which may account for the favorable outcome associated with low ADC tumors [7]. The ADC of non-enhancing lesions progressively decreases in progressors after bevacizumab treatment, suggesting that ADC may be used as an additional imaging biomarker for early treatment response [6]. These papers mentioned the significance of the ADC on the tumor cell itself. The ADC is lowered by increased cell attenuation, but increased in association with vasogenic edema and necrosis [3]. Investigation into ADC measurement on peritumoral edema is limited. The ADC in peritumoral edema has been reported to be higher in glioblastoma than in low-grade gliomas [4]. We evaluated the significance of ADC measurement on peritumoral edema as well as tumoral blood flow, which was demonstrated by rCBV on perfusion MRI after bevacizumab treatment for recurrent glioblastoma.

Materials and Methods

All patients ($N=9$) who met the following criteria were selected: (1) Pathology confirmed GBM with recurrence following chemotherapy and radiation therapy (RT). (2) No surgical resection for the duration of the study. All signed institutional review board consent. They were treated every 2 weeks per

Y. Katayama et al. (eds.), *Brain Edema XV*, Acta Neurochirurgica Supplement, Vol. 118,
DOI 10.1007/978-3-7091-1434-6_34,

cycle with bevacizumab (5–10 mg/kg body weight) alone for 4 ~ 36 months (average 12 months). MRI was performed every 2 months. On each MRI, ADC value, Gd-enhanced area on T1 imaging, area of peritumoral edema on T2 imaging, and rCBV on perfusion imaging were measured. Gd-enhanced area was evaluated using the Macdonald criteria (largest diameter × perpendicular diameter). A peritumoral T2 high-intensity area was evaluated using RECIST criteria (maximal diameter). ADC and rCBV values were determined by the use of regions of interest positioned in areas of high signal intensity, as seen on T2-weighted images and ADC maps.

Results

Nine patients with recurrent glioblastoma were treated by bevacizumab with measurement of MRI parameters. Figure 1 shows a representative patient who has been well controlled for a long time. Figure 2 shows a representative patient who had progression during the treatment. The degree of change in each parameter was compared with the baseline. The T1-Gd-enhanced lesion decreased 48.1 ± 33.4 % at 2 months, but increased 123 ± 78 % at 6 months. The T2 high-intensity area decreased 72.1 ± 15.0 % at 2 months and 84.2 ± 19.2 % at

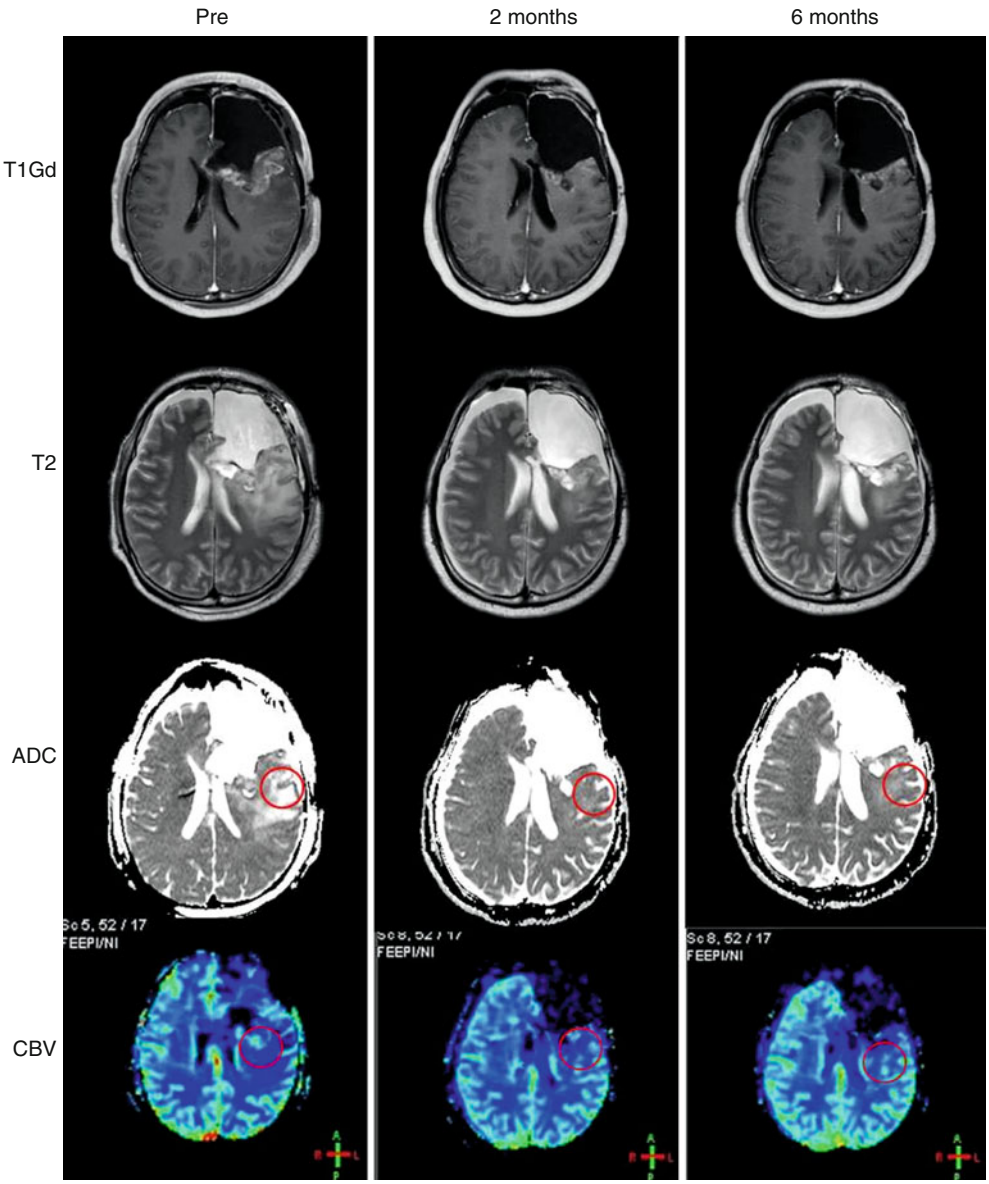

Fig. 1 Case 2, serial change with bevacizumab treatment at baseline and at 2 and 6 months. Please note that even at 6 months, there is no tumor progression associated with a decrease in ADC and rCBV values at the peritumoral lesion (*red circle*)

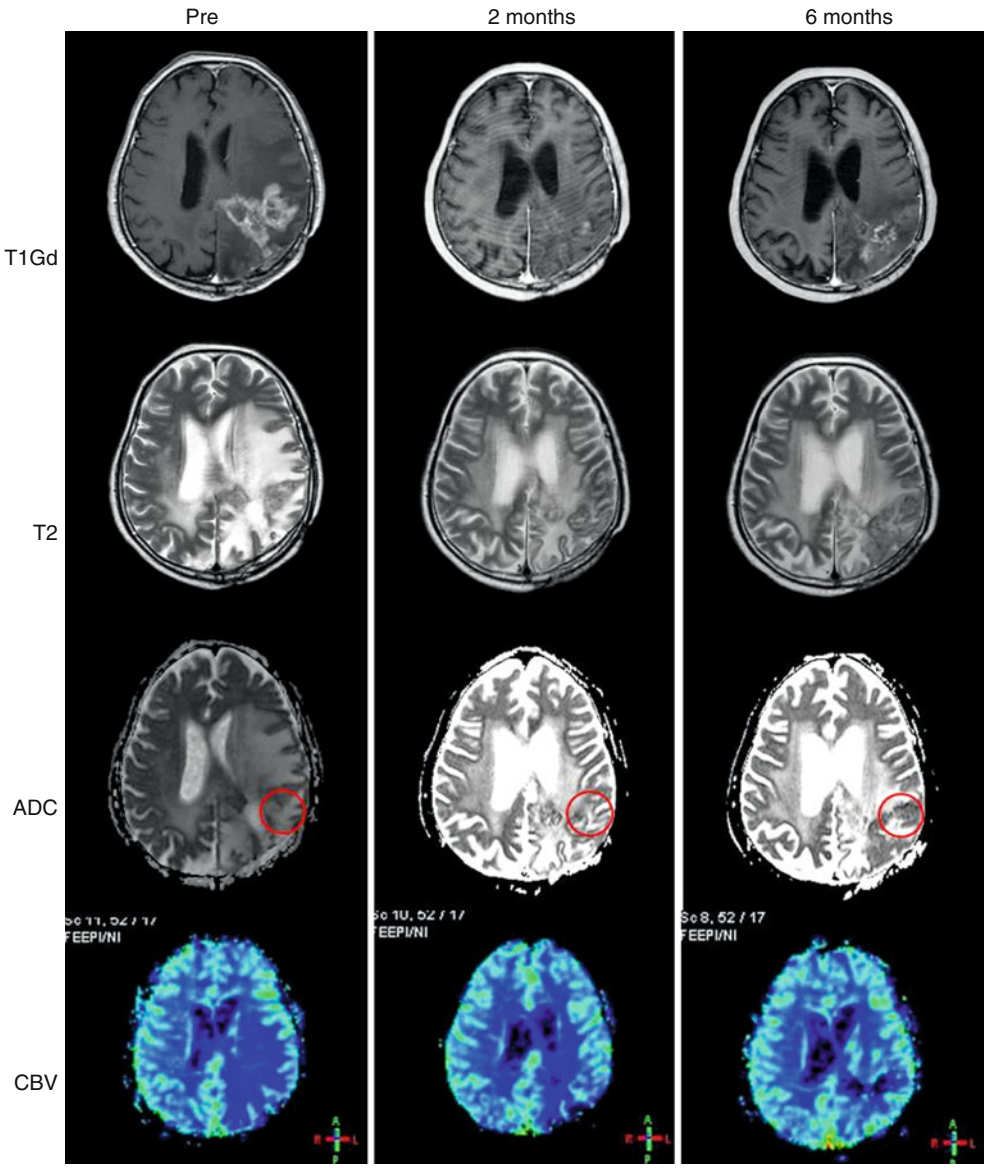

Fig. 2 Case 7, serial change with bevacizumab treatment at baseline and at 2 and 6 months. Please note that at 6 months, a decrease in ADC and rCBV values remains low, even if there is tumor progression

6 months. There was a decrease in ADC values of 49.8 ± 14.1 % at 2 months and 66.3 ± 25.2 % at 6 months and a decrease in rCBV values of 32 % at 2 months and 32 % at 6 months. After 6 months, in 5 of the 9 cases the Gd-enhanced area appeared again with no change in ADC values and rCBV. In the other four cases, the Gd-enhanced area as well as the ADC values and rCBV returned to their initial status (Fig. 3).

From these results, it can be seen that ADC and rCBV values are sensitive to measuring the anti-edema effect with bevacizumab, even if the tumor reveals progression.

Conclusion

In order to determine the radiographic response to bevacizumab regimen treatment, we measured the volume of the tumor (T1-Gd-enhanced lesion), peritumoral edema, and rCBV for each patient at each follow-up scan.

A response can occur quickly; a reduction in tumor volume has been documented within 6 weeks of therapy initiation. In addition to diminished tumor size, bevacizumab

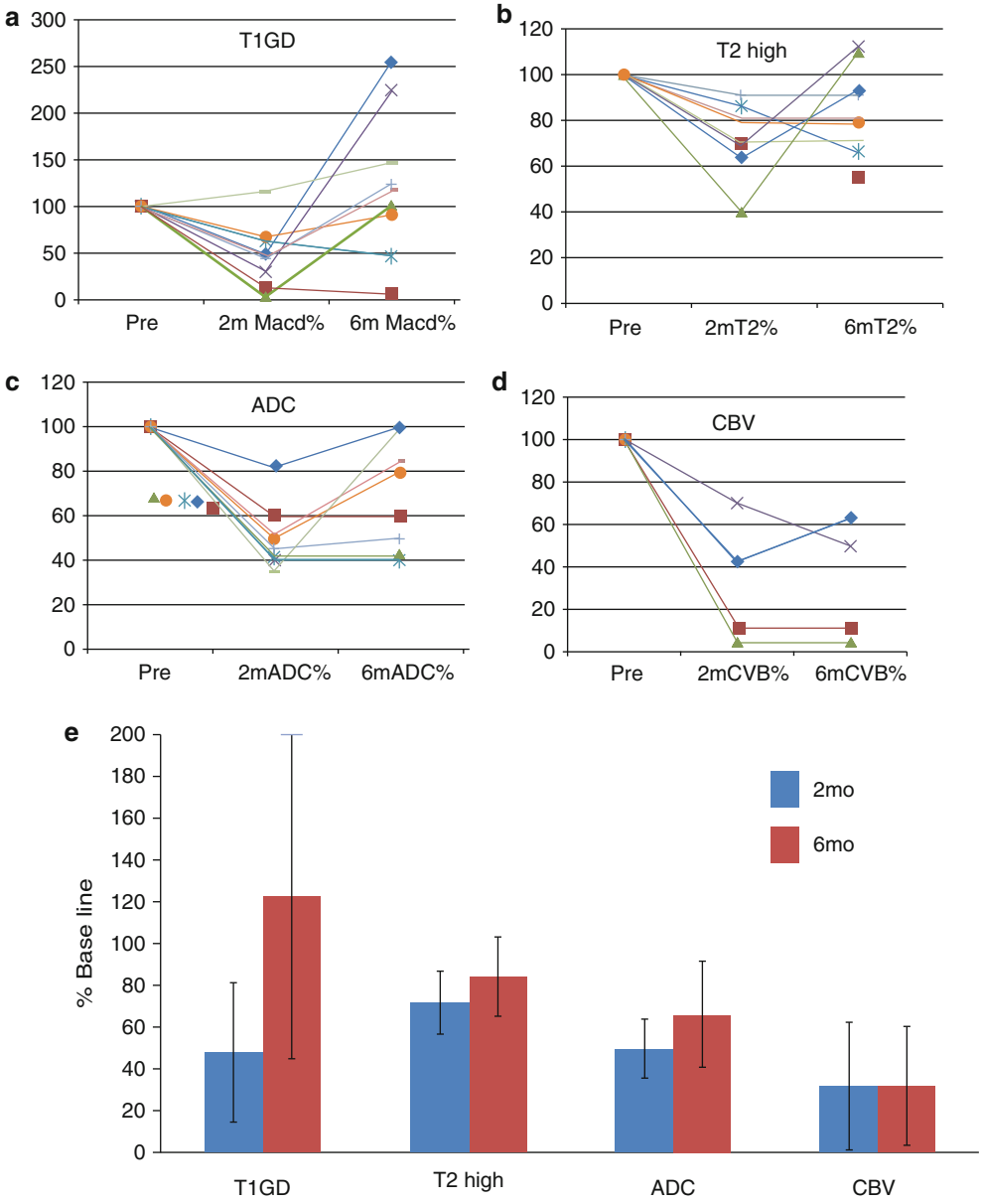

Fig. 3 Serial MRI parameters change in each case. (**a**) T1-Gd-enhanced lesion, (**b**) T2 high-intensity area, (**c**) ADC value at ROI, (**d**) rCBV value at ROI. (**e**) Each MRI parameter (mean ± SD) at 2 and 6 months after bevacizumab treatment

regimen treatment can also result in a dramatic reduction in edema [1]. We showed a rapid and significant median reduction of tumor and edema volumes from the baseline in patients by the first (approximately 2 month) follow-up scan, in agreement with a previous nonquantitative report. The rate of tumor progression was also similar to that observed for patients in prior studies. The evaluation of peritumoral edema is difficult because of the irregular shape of edema, such as a finger-like shape. We first evaluated edema by measuring the maximal diameter of the T2 high intensity area using RECIST criteria. The decrease rate of T2 high intensity was less than 72 % after 2 months' treatment. By contrast, the decrease rate of ADC values was 50 %, suggesting its greater sensitivity compared with T2 high-intensity measurement. Also, in 5 of the 9 patients who demonstrated tumor progression, ADC values remained low, suggesting the superiority of the detection of the bevacizumab-specific response [1].

Glioma angiogenesis is also an important biological process of which bevacizumab is a strong inhibitor. Because rCBV has been reported to predict astrocytic tumor progression and tumor vascular density [2], rCBV should be useful in evaluating the bevacizumab effect on glioma. We demonstrated that rCBV as well ADC values remain low even if there is tumor progression. This sustained angiosuppressive action of bevacizumab with tumor progression is another specific response of bevacizumab and rCBV measurement is a suitable method for evaluating this action. We characterized the extent and time course of these bevacizumab-specific

changes, which may provide a benchmark that is useful in judging an individual patient's response to bevacizumab regimen therapy.

In conclusion, the anti-edema effect of bevacizumab for recurrent glioblastoma that was demonstrated by decreased ADC values and rCBV was dramatic and prolonged at 6 months even with tumor progression.

Conflict of Interest We declare that we have no conflict of interest.

References

1. Ananthnarayan S, Bahng J, Roring J, Nghiemphu P, Lai A, Cloughesy T, Pope WB (2008) Time course of imaging changes of GBM during extended bevacizumab treatment. J Neurooncol 88:339–347
2. Bisdas S, Kirkpatrick M, Giqlio P, Welsh C, Spampinato MV, Rumboldt Z (2009) Cerebral blood volume measurements by perfusion-weighted MR imaging in gliomas: ready for prime time in predicting short-term outcome and recurrent disease? AJNR Am J Neuroradiol 30:681–688
3. Ellingson BM, Malkin MG, Rand SD, Connelly JM, Quinsey C, LaViolette PS, Bedekar DP, Schmainda KM (2010) Validation of functional diffusion maps (fDMs) as a biomarker for human glioma cellularity. J Magn Reson Imaging 31:538–548
4. Guzman R, Altrichter S, El-Koussy M, Gralla J, Weis J, Barth A, Seiler RW, Schroth G, Lovblad KO (2008) Contribution of the apparent diffusion coefficient in perilesional edema for the assessment of brain tumors. J Neuroradiol 35:224–229
5. Higano S, Yun X, Kumabe T, Watanabe M, Mujikawa S, Umetsu A, Saito A, Yamada T, Takahashi S (2006) Malignant atsrocytic tumors: clinical importance of apparent diffusion coefficient in production of grade and progression. Radiology 241:839–846
6. Jain R, Scarpace LM, Ellika S, Torcuator R, Schultz LR, Hearshen D, Mikkelsen T (2010) Imaging response criteria for recurrent gliomas treated with bevacizumab: role of diffusion weighted imaging as an imaging biomarker. J Neurooncol 96: 423–431
7. Pope WB, Lai A, Mehta R, Kim HJ, Qiao J, Young JR, Xue X, Goldin J, Brown MS, Nghiemphu PL, Tran A, Cloughesy TF (2011) Apparent diffusion coefficient histogram analysis stratifies progression-free survival in newly diagnosed bevacizumab-treated glioblastoma. AJNR Am J Neuroradiol 32:882–889

Protease Activated Receptor-1 and Brain Edema Formation in Glioma Models

Qing Xie, Guohua Xi, Ye Gong, Richard Keep, Karin Muraszko, and Ya Hua

Abstract *Objective*: Our previous studies showed that thrombin contributes to brain edema in gliomas. The present study investigated the role of a thrombin receptor, protease activated receptor-1 (PAR-1), in edema formation in glioma models.

Methods: These experiments were performed in Fischer 344 rats, PAR-1 knockout mice, and wild-type C57BL/6 mice controls. F98 glioma cells were infused into the right caudate. Animals were euthanized and the brains were used for measurements of brain edema and PAR-1 expression.

Results: In rats, implantation of glioma cells resulted in significant brain edema in the ipsilateral hemisphere (82.6 ± 1.4 vs. 78.1 ± 0.9 % in the contralateral hemisphere, $p < 0.01$). By Western blot analysis and RT-PCR, we found that both protein and mRNA levels of PAR-1 were upregulated in the glioma ($p < 0.01$). In mice, implantation of glioma cells also caused brain edema in the ipsilateral hemisphere ($p < 0.05$). Glioma-induced brain edema was less in PAR-1 knockout mice (day 12: 79.4 ± 1.3 vs. 81.5 ± 1.1 % in the wild-type mice, $p < 0.05$).

Conclusion: PAR-1 plays a role in glioma-induced brain edema. Clarification of the role of PAR-1 in edema formation should help to develop new therapeutic strategies for gliomas.

Keywords Brain edema • Gliomas • Protease activated receptor-1 • Thrombin

Q. Xie and Y. Gong
Department of Neurosurgery, University of Michigan,
R5018 BSRB, 109 Zina Pitcher Place,
Ann Arbor, MI 48109-2200, USA

Department of Neurosurgery, Huashan Hospital,
Fudan University, Shanghai, China

G. Xi, R. Keep, K. Muraszko, and Y. Hua, MD (✉)
Department of Neurosurgery, University of Michigan,
R5018 BSRB, 109 Zina Pitcher Place,
Ann Arbor, MI 48109-2200, USA
e-mail: yahua@umich.edu

Introduction

Recent studies indicate that thrombin contributes to tumor proliferation, invasion, angiogenesis, and metastasis [6, 13, 14, 17–19]. In our previous studies, we found that thrombin causes edema formation in and around gliomas. Thrombin has been detected in several tumors [24] and in our rat glioma models [8]. Argatroban, an inhibitor of thrombin, reduces brain edema, tumor mass, and neurological deficits in glioma models [7, 9].

The effects of thrombin may be via activation of protease-activated receptors (PARs). Thrombin receptors are activated by proteolytic cleavage rather than by ligand binding and thrombin receptor-activated peptides are able to mimic many cellular activities of thrombin [4, 20]. PAR-1 has been found in many types of tumor cells [11, 16, 17]. Activation of PAR-1 is associated with tumor cell invasion [5] and angiogenesis [3]. PAR-1 activation by thrombin receptor-activating peptide (TRAP) results in angiogenesis [12, 14].

F98 glioma cells have been used previously in our studies on rats and the median survival time after tumor cell implantation was only 14 days [8, 9]. It has also been reported that an intracerebral inoculum of as few as 100 cells is lethal [1]. In this study, we examined the role of PAR-1 in F98 glioma cells and glioma models.

Materials and Methods

Experimental Groups

There were two parts in this study. First, Fischer rats (weight 200–250 g, Charles River Laboratories) were used in this study. Rats (5–6 for each group) received an intracerebral injection of F98 glioma cells (1×10^6) or a needle (sham) injection and they were euthanized on day 9. Brains were used for water content ($n = 5$–6), Western blot analysis ($n = 4$), and RT-PCR assays ($n = 4$). In the second part, wild-type and

Y. Katayama et al. (eds.), *Brain Edema XV*, Acta Neurochirurgica Supplement, Vol. 118,
DOI 10.1007/978-3-7091-1434-6_35, © Springer-Verlag Wien 2013

PAR-1 knockout mice had 10-μL injection of F98 glioma cells (2×10^6) into the right caudate. Mice were sacrificed to measure tumor mass on day 7 or 12 ($n=5$). Brain water content was determined on day 12 ($n=8$).

Animal Preparation and Injection

Animal use protocols were approved by the University of Michigan Committee on the Use and Care of Animals. Rats were anesthetized with pentobarbital (45 mg/kg i.p.) and had a cranial burr-hole (0.5 mm) drilled on the right coronal suture 3.5 mm lateral to the midline. F98 cells (1×10^6) suspended in 10 μL of saline were infused into the right caudate nucleus (coordinates: 0.2 mm anterior, 5.5 mm ventral and 3.5 mm lateral to the bregma) at a rate of 1 μL/min using a 10-μL syringe (Hamilton) [8]. Sham controls only underwent needle insertion.

Mice were anesthetized by a mixture of ketamine (50 mg/kg, i.p.) and xylazine (5 mg/kg, i.p.) and a cranial burr-hole (1 mm) was drilled on the right coronal suture 2.5 mm lateral to the midline. A microsyringe was inserted stereotactically into the right caudate (coordinates: 0.2 mm anterior, 3.5 mm ventral, 2.5 mm lateral to the bregma). F98 cells (2×10^5/μL, 10 μL) in saline were infused at a rate of 1 μL/min.

Brain Water Content

Rats were sacrificed by decapitation under deep pentobarbital anesthesia. The brains were removed immediately. For rats, brain samples were then divided in the ipsilateral or the contralateral hemisphere. For mice, the brains were cut in to four parts: front (ipsilateral and contralateral) and rear (ipsilateral and contralateral) parts. The brain water content was measured using the wet/dry method [23].

Western Blot Analysis

Western blot analysis was performed as described previously [22]. Rabbit anti PAR-1 antibody (Santa Cruz Biotechnology, Santa Cruz, CA, USA; 1:2,000 dilution) was used.

Reverse Transcription-Polymerase Chain Reaction (RT-PCR) Analysis

The rat PAR-1 primers (NIH genBank database) corresponded to nucleotides 900–924 (Sense primer 5′-ACTATTTCTCCG-CCTTCTCCGCCAT-3′) and 1,148–1,172 (anti-sense primer 5′-TCACGCAGACGCAGAGGAGG-3′). Rat GAPDH primers (5′-CTCAGTTAGCCCAGGATGC-3′,5′-ACCACC-ATGGAGAAGGCTGG-3′) were used to amplify GAPDH mRNA, a housekeeping gene used as a control. Amplification was performed in a DNA thermal cycler (MJ Research, Watertown, MA, USA). Samples were subjected to 35 cycles (94 °C, 1 min; 57 °C, 1 min; and 72 °C, 2 min). PCR products were electrophoretically separated in a 1 % agarose gel, stained with ethidium bromide, visualized under UV light, and photographed. PCR products were normalized to the respective GAPDH PCR products. Data were expressed as pixels [10].

Statistics

The results are reported as mean ± SD. Data were analyzed by analysis of variance (ANOVA) followed by Scheffe's post hoc test, Student's t test, Mann–Whitney U rank test. Differences were considered significant at the $p<0.05$ level.

Results

PAR-1 mRNA and Protein Levels Upregulated in Rat F98 Glioma

PAR-1 mRNA levels were significantly upregulated in the rats on day 9 after F98 cells were implanted into the right caudate (2,668 ± 121 vs. 510 ± 15 pixels in sham, $p<0.01$, Fig. 1). The protein levels of PAR-1 were also upregulated on day 9 (3,618 ± 542 vs. 542 ± 478 in sham, $p<0.01$, Fig. 2).

Brain Edema Formation and Tumor Growth

In rats, brain water content was significantly higher in the ipsilateral basal ganglia of rats 9 days after F98 glioma cell (1×10^6 cells) implantation (82.6 ± 1.4 vs. 78.1 ± 0.9 % in the contralateral basal ganglia, $p<0.01$). In mice, the implantation of F 98 glioma cells also caused brain edema in the ipsilateral hemisphere (80.8 ±1.33 vs. 78.5 ± 0.2 in contralateral hemisphere, $p<0.01$) on day 12 and glioma-induced brain edema was less in PAR-1 knockout mice (79.4 ± 1.3 vs. 81.5 ± 1.1 % in the wild-type mice, $p<0.05$). Brain tumor mass increased over time in wild-type mice from an average of 18.9 mg on day 7 to 43.4 mg on day 12 after F98 cell implantation, and the brain tumor was smaller in PAR-1 knockout mice (11.3 ± 23.2 vs. 43.4 ± 27.8 mg in wild-type mice on day 12, $p<0.05$).

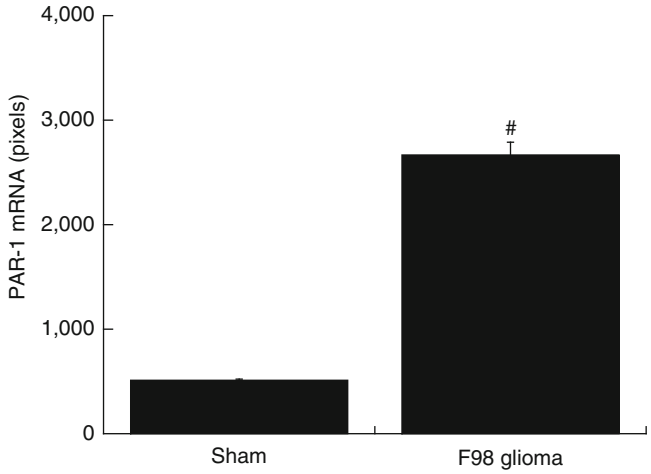

Fig. 1 PAR-1 messenger RNA levels in the right caudate of rat brain 9 days after a needle injection, or 1×10^6 of F98 cell implantation into the right caudate. Values are mean ± SD, $n = 3$, #$p < 0.01$ versus sham

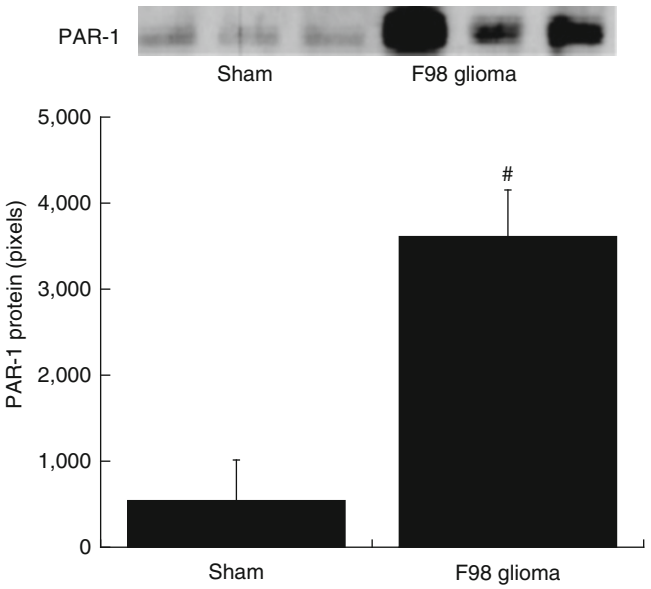

Fig. 2 PAR-1 protein levels in the ipsilateral caudate 9 days after a needle injection, or 1×10^6 of F98 cell implantation into the right caudate. Values are mean ± SD, $n = 3$, #$p < 0.01$ versus sham

Conclusion

In the current study, we found PAR-1 expression in F98 gliomas. F98 glioma growth was slower and tumor-induced brain edema was less in PAR-1 knockout mice. These results suggest that PAR-1 might play a role in glioma growth and peri-glioma edema formation.

Thrombin is a key factor for activation of the coagulation system in the malignancy [6, 8, 24]. In addition, thrombin may act as a growth factor for tumor cells [2] and induce a proliferative response in tumor cells [15]. Thrombin has been detected in several tumors [24]. Although the primary role of thrombin in homeostasis is through cleaving fibrinogen to fibrin, other important cellular activities of thrombin may be related to receptor activation [24]. The current study showed that PAR-1 plays a role in glioma growth. Thrombin receptor has been found in many types of tumor cells [16, 21]. Activation of PAR-1 is associated with tumor cell invasion [5]. Our findings are supported by other investigations. For example, Zain et al. found that thrombin has a bimodal effect on tumor cells via PAR-1, enhanced growth at low concentrations, impaired growth/apoptosis at higher concentrations [25]. Moreover, PAR-1 activation by thrombin receptor-activating peptide results in angiogenesis [12, 14].

The impact of PAR-1 on edema, tumor growth, and angiogenesis may reflect the multiple actions of thrombin on different cell types (e.g., glioma cells and endothelial cells). Alternatively, the broad effects of thrombin/PAR-1 may reflect one action that has multiple down-stream effects (e.g., a change in angiogenesis altering tumor growth, vascular permeability and edema). There is evidence of thrombin/PAR effects on multiple cell types, but the development of cell-type-specific PAR-1 KO mice would help to elucidate the importance of the different cellular effects in vivo.

In summary, PAR-1 plays a role in glioma growth and glioma-induced brain edema formation. Clarification of the role of PAR-1 in glioma growth should help to develop new therapeutic strategies for gliomas.

Acknowledgments This study was supported by grants NS-017760, NS-039866, and NS-057539 from the National Institutes of Health (NIH) and 0840016 N from the American Heart Association (AHA). The content is solely the responsibility of the authors and does not necessarily represent the official views of the NIH and AHA. Drs. Xie and Gong were supported by NSFC-30901549 and NSFC-30872675 from the China National Natural Science Foundation.

Conflict of Interest We declare that we have no conflict of interest.

References

1. Chang EF, Meeker M, Holland MC (2006) Acute traumatic intraparenchymal hemorrhage: risk factors for progression in the early post-injury period. Neurosurgery 58:647–656; discussion 647–656
2. Chinni C, de Niese MR, Tew DJ, Jenkins AL, Bottomley SP, Mackie EJ (1999) Thrombin, a survival factor for cultured myoblasts. J Biol Chem 274:9169–9174
3. Christensen EN, Mendelsohn ME (2006) Cyclic GMP-dependent protein kinase Ialpha inhibits thrombin receptor-mediated calcium mobilization in vascular smooth muscle cells. J Biol Chem 281(13): 8409–8416
4. Debeir T, Benavides J, Vige X (1996) Dual effects of thrombin and a 14-amino acid peptide agonist of the thrombin receptor on septal cholinergic neurons. Brain Res 708:159–166
5. Even-Ram SC, Maoz M, Pokroy E, Reich R, Katz BZ, Gutwein P, Altevogt P, Bar-Shavit R (2001) Tumor cell invasion is promoted by activation of protease activated receptor-1 in cooperation with the alpha vbeta 5 integrin. J Biol Chem 276:10952–10962

6. Hu L, Lee M, Campbell W, Perez-Soler R, Karpatkin S (2004) Role of endogenous thrombin in tumor implantation, seeding, and spontaneous metastasis. Blood 104:2746–2751
7. Hua Y, Keep RF, Schallert T, Hoff JT, Xi G (2003) A thrombin inhibitor reduces brain edema, glioma mass and neurological deficits in a rat glioma model. Acta Neurochir Suppl 86:503–506
8. Hua Y, Tang L, Keep RF, Schallert T, Fewel M, Muraszko K, Hoff JT, Xi G (2005) The role of thrombin in gliomas. J Thromb Haemost 3:1–7
9. Hua Y, Tang LL, Fewel ME, Keep RF, Schallert T, Muraszko KM, Hoff JT, Xi GH (2005) Systemic use of argatroban reduces tumor mass, attenuates neurological deficits and prolongs survival time in rat glioma models. Acta Neurochir Suppl 95:403–406
10. Hua Y, Xi G, Keep RF, Wu J, Jiang Y, Hoff JT (2002) Plasminogen activator inhibitor-1 induction after experimental intracerebral hemorrhage. J Cereb Blood Flow Metab 22:55–61
11. Kaushal V, Kohli M, Dennis RA, Siegel ER, Chiles WW, Mukunyadzi P (2006) Thrombin receptor expression is upregulated in prostate cancer. Prostate 66:273–282
12. Maragoudakis ME, Tsopanoglou NE (2000) On the mechanism(s) of thrombin induced angiogenesis. Adv Exp Med Biol 476:47–55
13. Maragoudakis ME, Tsopanoglou NE (2004) Role of thrombin in angiogenesis: a rebuttal. J Thromb Haemost 2:841–842
14. Maragoudakis ME, Tsopanoglou NE, Andriopoulou P, Maragoudakis MM (2000) Effects of thrombin/thrombosis in angiogenesis and tumour progression. Matrix Biol 19:345–351 [Review]
15. Medrano EE, Cafferata EG, Larcher F (1987) Role of thrombin in the proliferative response of T-47D mammary tumor cells. Mitogenic action and pleiotropic modifications induced together with epidermal growth factor and insulin. Exp Cell Res 172:354–364
16. Nierodzik ML, Bain RM, Liu LX, Shivji M, Takeshita K, Karpatkin S (1996) Presence of the seven transmembrane thrombin receptor on human tumour cells: effect of activation on tumour adhesion to platelets and tumor tyrosine phosphorylation. Br J Haematol 92: 452–457
17. Nierodzik ML, Chen K, Takeshita K, Li JJ, Huang YQ, Feng XS, D'Andrea MR, Andrade-Gordon P, Karpatkin S (1998) Protease-activated receptor 1 (PAR-1) is required and rate-limiting for thrombin-enhanced experimental pulmonary metastasis. Blood 92: 3694–3700
18. Nierodzik ML, Kajumo F, Karpatkin S (1992) Effect of thrombin treatment of tumor cells on adhesion of tumor cells to platelets in vitro and tumor metastasis in vivo. Cancer Res 52:3267–3272
19. Nierodzik ML, Plotkin A, Kajumo F, Karpatkin S (1991) Thrombin stimulates tumor-platelet adhesion in vitro and metastasis in vivo. J Clin Invest 87:229–236
20. Suidan HS, Stone SR, Hemmings BA, Monard D (1992) Thrombin causes neurite retraction in neuronal cells through activation of cell surface receptors. Neuron 8:363–375
21. Wojtukiewicz MZ, Tang DG, Ben-Josef E, Renaud C, Walz DA, Honn KV (1995) Solid tumor cells express functional "tethered ligand" thrombin receptor. Cancer Res 55:698–704
22. Xi G, Hua Y, Keep RF, Hoff JT (2000) Induction of colligin may attenuate brain edema following intracerebral hemorrhage. Acta Neurochir Suppl 76:501–505
23. Xi G, Keep RF, Hoff JT (1998) Erythrocytes and delayed brain edema formation following intracerebral hemorrhage in rats. J Neurosurg 89:991–996
24. Zacharski LR, Memoli VA, Morain WD, Schlaeppi JM, Rousseau SM (1995) Cellular localization of enzymatically active thrombin in intact human tissues by hirudin binding. Thromb Haemost 73:793–797
25. Zain J, Huang YQ, Feng X, Nierodzik ML, Li JJ, Karpatkin S (2000) Concentration-dependent dual effect of thrombin on impaired growth/apoptosis or mitogenesis in tumor cells. Blood 95: 3133–3138

An Analysis of T2 Mapping on Brain Tumors

Kanji Nakai, Hiroshi Nawashiro, Katsuji Shima, and Tatsumi Kaji

Abstract *Purpose*: Vasogenic edema on glioblastoma multiforme (GBM) or a metastatic brain tumor (METS) may have different T2 relaxation time values because it involves an increased water component. In this study, we assessed the diagnostic utility of T2 mapping techniques in distinguishing GBM from METS.

Materials and Methods: We studied a glioblastoma (GBM) patient and a metastatic brain tumor (METS) patient who had not undergone previous surgery or treatment. All MR imaging was carried out using a 3.0-T whole-body unit, and axial T2 maps were generated with five TEs (TE = 20, 40, 60, 80, and 100 ms). Data were analyzed by using image processing and analysis software.

Results: The T2 map of a GBM case showed that the peritumoral area at a T2 relaxation time of 120–160 ms is prominent compared with the area at 210–240 ms. In contrast, the peritumoral area at 210–240 ms was prominent compared with the area at 120–160 ms in a METS case.

Conclusion: The distribution of T2 relaxation time in the peritumoral area shows different patterns in glioblastomas and metastatic brain tumors.

Keywords T2 relaxation time • T2 mapping • Glioblastoma multiforme • Metastatic brain tumor

K. Nakai (✉)
Department of Neurosurgery, Fukuoka University Chikushi Hospital, 1-1-1 Zokumyoin, Chikushino, Fukuoka 818-8502, Japan
e-mail: neuroivr@gmail.com

H. Nawashiro, K. Shima, and T. Kaji
Department of Radiology, National Defense Medical College, 3-2 Namiki, Tokorozawa, Saitama 359-8513, Japan

Introduction

Conventional radiological characteristics that are thought to favor cerebral lesions being metastatic as opposed to primary brain cancer include a peripheral location, spherical shape, ring enhancement, and multiple lesions [1]. Gliomas may, however, be multifocal (showing gross or microscopic continuity or evidence of cerebrospinal fluid spread and/or local metastases) or multicentric (no macroscopic or microscopic connection) and are therefore potentially indistinguishable on conventional imaging from metastatic disease with multiple enhancing lesions [2].

Currently, conventional MRI consists of a combination of proton density-, T1-, and T2-weighted sequences. T2-weighted imaging is sensitive to the identification of pathological change, and T2 relaxation is governed by both the total amount of water and the ratio of free to bound water, which is itself dependent on the macromolecular environment. A disturbance to this environment, such as neuronal loss or demyelination, results in an increase in free water, with a longer T2 relaxation time and greater signal intensity on a T2-weighted image. Quantitative evaluation of T2-weighted images is more sensitive and objective than visual assessment for the identification of subtle cerebral pathology. Quantitative T2 mapping has been applied to cerebral neoplasia [3], neurodegenerative conditions [4], ischemia [5], head injury [6], encephalitis [7], and, most frequently, multiple sclerosis (MS) [8], where increased T2 signal has been observed within lesions as well as in cerebral tissue that appeared normal on conventional MRI.

Most of the new MRI techniques, with reported use in distinguishing glioma from metastatic disease, rely on detecting differences in the peritumoral region. In metastases, this area consists of vasogenic edema, whereas in glioma, neoplastic cells may also be present. As a result, a relative reduction in the peritumoral T2-weighted fluid-attenuated inversion recovery (FLAIR) hyperintense signal is expected in glioma, in contrast to cerebral metastases. Many exciting new developments in MR imaging techniques have been used to differen-

Y. Katayama et al. (eds.), *Brain Edema XV*, Acta Neurochirurgica Supplement, Vol. 118,
DOI 10.1007/978-3-7091-1434-6_36,

tiate between a solitary metastasis and a high-grade glioma in the peritumoral region, including the use of spectroscopy, diffusion and perfusion imaging, and absolute apparent diffusion coefficient (ADC) measurements. Magnetic resonance spectroscopy alone has been shown to allow discrimination between metastases and glioblastomas [9, 10]. Diffusion tensor imaging has also shown promise in this distinction [11, 12]. Tang et al. suggested that non-enhancing adjacent cortical signal abnormality detected by FLAIR has the potential to differentiate between solitary gliomas and metastases [13]. These studies have all involved differentiating solitary cerebral lesions. No study to date has specifically assessed the T2 relaxation time and the detection of non-enhancing adjacent cortical signal abnormality for differentiating between multicentric and/or multifocal gliomas and other cerebral tumors with multiple enhancing foci.

The key to making the distinction between these two entities appears to lie in detecting the changes within the peritumoral area, the area beyond the enhancing margin on imaging. In metastases, this consists essentially of vasogenic edema, while in glioma, this may also contain neoplastic cells. Our hypothesis is that vasogenic edema on glioblastoma multiforme (GBM) and that on a metastatic brain tumor (METS) should show different T2 relaxation time values because it involves an increased water component. In this study, we investigated the diagnostic utility of T2 mapping in assessing non-enhancing signal intensity abnormality to distinguish GBM from METS. To the best of our knowledge, no previous similar studies have considered the implications of these findings.

Materials and Methods

Subjects

We studied a patient with glioblastoma (GBM) and a patient with metastatic brain tumor (METS) who had not undergone any previous surgery or treatment. Diagnosis was confirmed by histological examination.

Magnetic Resonance Imaging

All MR imaging was carried out using a 3.0-T whole-body unit (Achieva3T; Philips, Eindhoven, The Netherlands) with a SENSE-head-8 coil.

Axial T2 maps with fat saturation were generated by using a multishot GRASE protocol with 5 TEs (TE = 20, 40, 60, 80, and 100 ms). Other sequence parameters were TR = 3,705 ms (shortest); field of view (FOV), 230 × 183 mm; section thickness, 2 mm; section gap, 0 mm. and number of acquisitions = 1.

Image Interpretation

Data were analyzed sequentially by one author (Kanji Nakai) using image processing and analysis software (Image J, version 1.45n, available at http://imagej.nih.gov/ij/index.html; MRI Analysis Calculator plugin, available at http://imagej.nih.gov/ij/plugins/mri-analysis.html). T2 maps were calculated on a pixel-by-pixel basis in the transverse plane. The ROI was obtained by the primary author (K.Nakai) by manually tracing the outline of the peritumoral area where T2/FLAIR was hyperintense. The tumoral area, where the borderline was obvious with contrast enhancement and compatible with the tumor margin seen by a T2/FLAIR image, was excluded from the ROI. Addition to the ROI of the whole slices including perifocal edema on the T2 map generated a histogram of T2 distribution for each case. As patients can have different edema volumes, the histogram was normalized according to each ROI.

Results

Normalized percentage of pixels of T2 relaxation time showed a marked peak at around 80 ms in both tumors. In the GBM case, it decreased with prolongation of the T2 relaxation time, whereas in the METS case, it decreased to around 160 ms and then increased to a second small peak at 190 ms, indicating that the profile of normalized pixels had a bimodal distribution (Fig. 1). The T2 map of the GBM case showed that the peritumoral area at T2 relaxation time of 120–160 ms is prominent compared with the area at 210–240 ms (Fig. 2). In contrast, the peritumoral area at 210–240 ms was prominent compared with the area at 120–160 ms in the METS case (Fig. 3). The ratio of 160–230 ms at T2 relaxation time of the GBM case was higher than that of the METS case (Table 1).

Conclusion

In our study, the T2 mapping technique showed that there was a significant difference in the distribution of T2 relaxation time in the peritumoral area between the GBM group and the METS group.

The key to differentiating between the two neoplasm types appears to lie in the peritumoral area. In a glioblastoma, the

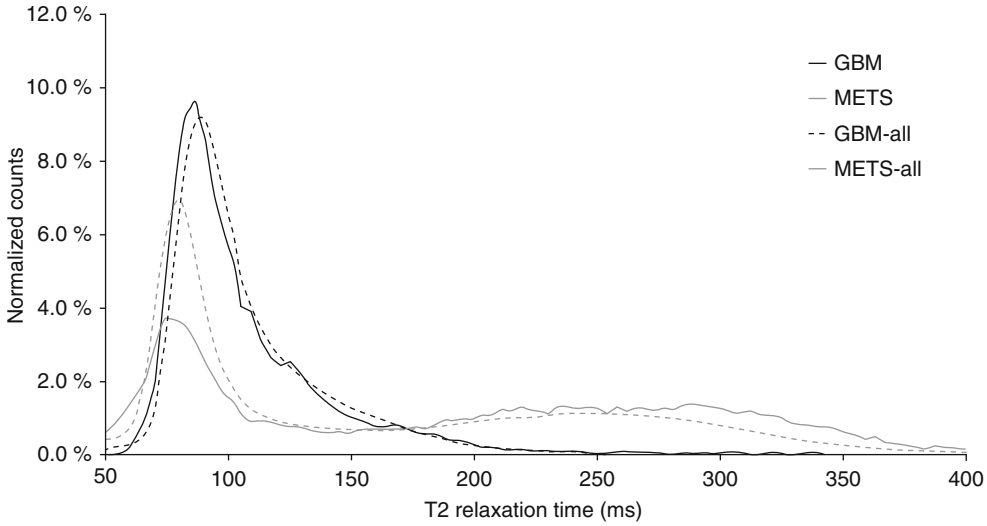

Fig. 1 Histogram of normalized T2 relaxation time. In a glioblastoma multiforme (*GBM*) case, it decreased with prolongation of T2 relaxation time, whereas in a metastatic brain tumor (*METS*) case, it showed a mild bimodal distribution

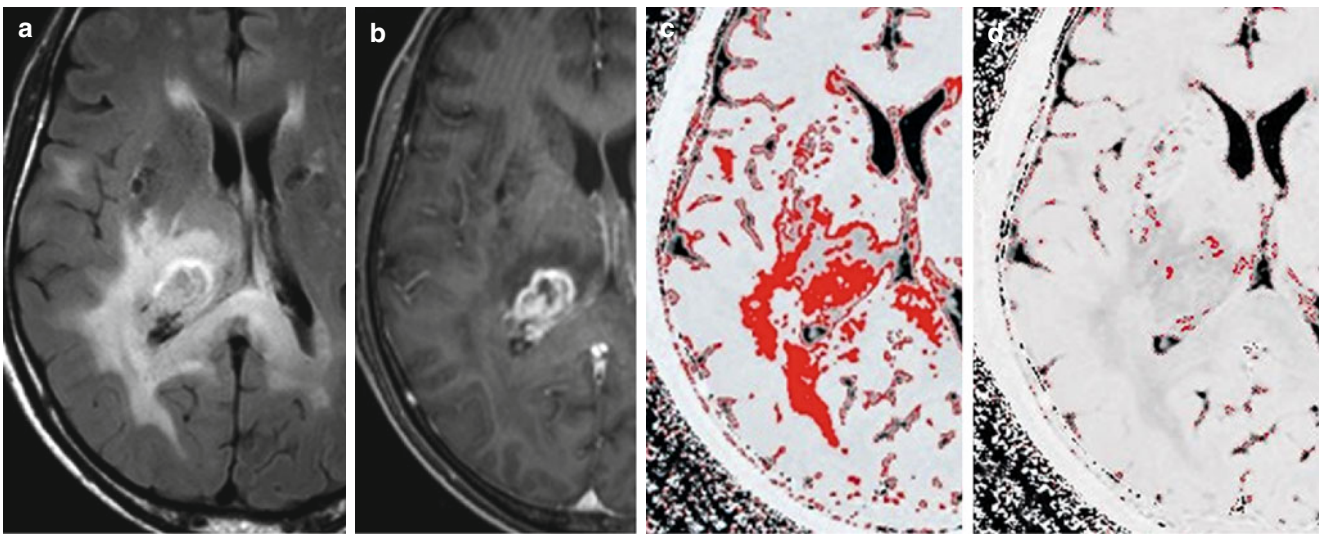

Fig. 2 A 70-year-old man with surgically confirmed glioblastoma multiforme. (**a**) Axial fluid attenuated inversion recovery (FLAIR) image shows a hyperintense mass surrounded by a moderate degree of edema. (**b**) Axial post-contrast T1-weighted image shows enhancement of the solid part. (**c**), (**d**) T2 maps show a larger area at 120–160 ms (**c**) than at 210–240 ms (**d**)

peritumoral region may be infiltrated by malignant cells in addition to vasogenic edema [14], whereas in a metastatic deposit, the surrounding peritumoral area comprises predominantly vasogenic edema. By appearance alone, these peritumoral changes cannot generally be used to differentiate glioma from metastatic disease; however, vasogenic edema involves an increased water component. Using diffusion tensor imaging (DTI), Lu et al. demonstrated that there are clear differences in the diffusion characteristics of the vasogenic edema surrounding brain tumors compared with those of normal-appearing white matter [12].

Tang et al., who examined solitary enhancing cerebral lesions using FLAIR to detect non-enhancing adjacent cortical signal abnormality, reported a sensitivity of 44 % in distinguishing glioma [13], whereas Stuckey et al. reported that this sign was present in all multicentric/multifocal glioma patients presenting with more than one cerebral enhancing lesion [15]. Thus, it appears that non-enhancing adjacent cortical FLAIR signal abnormality is more common in multicentric/multifocal disease; however, this is not entirely unexpected as, by definition, these patients have more than one enhancing lesion to evaluate for the presence of this sign. In a larger series, 100 % sensitivity would presumably not be maintained. In contrast, the positive predictive values in the studies by Stuckey et al. and Tang et al. were 67 and 84 % respectively [13, 15]. The presence of this sign is not necessarily as good a predictor of multicentric/multifocal glioma when multiple enhancing lesions are present as it is for

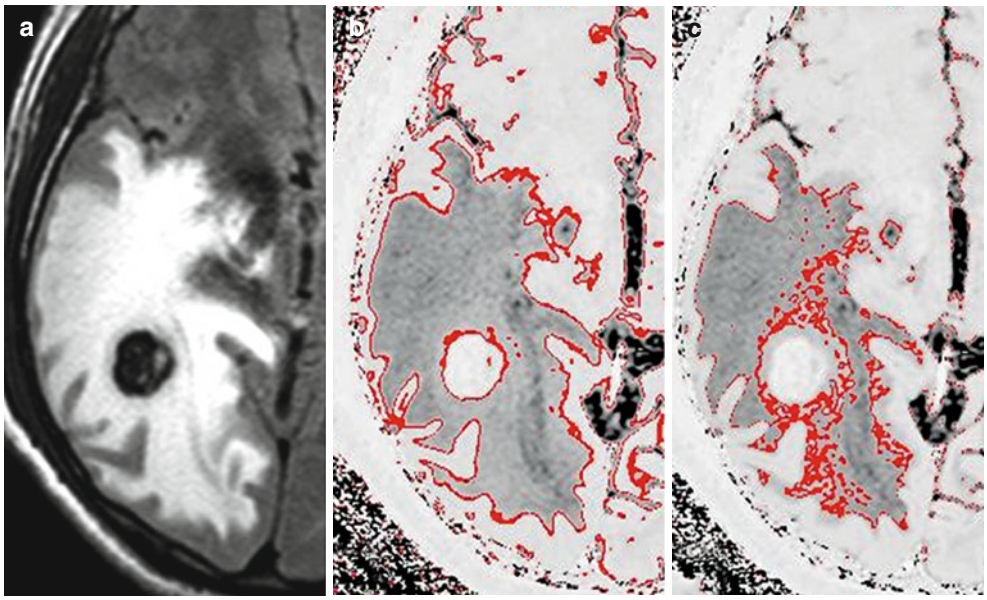

Fig. 3 A 59-year-old man with surgically confirmed metastatic renal cell carcinoma. (**a**) Axial FLAIR image shows a low intense mass surrounded by edema. (**b**), (**c**) T2 maps show a smaller area at 120–160 ms (**b**) than at 210–240 ms (**c**)

Table 1 Ratios of 160–230 ms at T2 relaxation time in glioblastoma multiforme (GBM) and metastatic brain tumor (METS) cases

	GBM		METS	
	One slice	All slices	One slice	All slices
160 ms/230 ms	8.56	12.95	0.60	0.63

One slice means counts of the slice shown in Figs. 2 and 3, and all slices mean the sum of counts of all slices including the hyperintensive peritumoral area in the same cases. The ratio of the GBM case is higher than that of the METS case

glioma when a solitary lesion is present. The difference is presumably due to the assumption made by the treating doctors that multicentric/multifocal cerebral lesions (in the context of proven malignancy at other sites) reflect metastatic disease, lessening the perceived clinical need for a histological diagnosis.

In conclusion, the distribution of T2 relaxation time in the peritumoral area shows different patterns in glioblastoma and metastatic brain tumors. T2 mapping may be useful for differentiating glioblastoma from metastasis in patients.

Conflict of Interest We declare that we have no conflict of interest.

References

1. Soffietti R, Ruda R, Mutani R (2002) Management of brain metastases. J Neurol 249:1357–1369. doi:10.1007/s00415-002-0870-6
2. Prather JL, Long JM, van Heertum R, Hardman J (1975) Multicentric and isolated multifocal glioblastoma multiforme simulating metastatic disease. Br J Radiol 48:10–15
3. Kurki T, Lundbom N, Valtonen S (1995) Tissue characterisation of intracranial tumours: the value of magnetisation transfer and conventional MRI. Neuroradiology 37:515–521
4. Laakso MP, Partanen K, Soininen H, Lehtovirta M, Hallikainen M, Hanninen T, Helkala EL, Vainio P, Riekkinen PJ Sr (1996) MR T2 relaxometry in Alzheimer's disease and age-associated memory impairment. Neurobiol Aging 17:535–540
5. Jacobs MA, Mitsias P, Soltanian-Zadeh H, Santhakumar S, Ghanei A, Hammond R, Peck DJ, Chopp M, Patel S (2001) Multiparametric MRI tissue characterization in clinical stroke with correlation to clinical outcome: part 2. Stroke 32:950–957
6. Yanagawa Y, Tsushima Y, Tokumaru A, Un-no Y, Sakamoto T, Okada Y, Nawashiro H, Shima K (2000) A quantitative analysis of head injury using T2*-weighted gradient-echo imaging. J Trauma 49:272–277
7. Thurnher MM, Thurnher SA, Fleischmann D, Steuer A, Rieger A, Helbich T, Trattnig S, Schindler E, Hittmair K (1997) Comparison of T2-weighted and fluid-attenuated inversion-recovery fast spin-echo MR sequences in intracerebral AIDS-associated disease. AJNR Am J Neuroradiol 18:1601–1609
8. Stevenson VL, Parker GJ, Barker GJ, Birnie K, Tofts PS, Miller DH, Thompson AJ (2000) Variations in T1 and T2 relaxation times of normal appearing white matter and lesions in multiple sclerosis. J Neurol Sci 178:81–87
9. Opstad KS, Murphy MM, Wilkins PR, Bell BA, Griffiths JR, Howe FA (2004) Differentiation of metastases from high-grade gliomas using short echo time 1H spectroscopy. J Magn Reson Imaging 20:187–192. doi:10.1002/jmri.20093
10. Ishimaru H, Morikawa M, Iwanaga S, Kaminogo M, Ochi M, Hayashi K (2001) Differentiation between high-grade glioma and metastatic brain tumor using single-voxel proton MR spectroscopy. Eur Radiol 11:1784–1791
11. Tsuchiya K, Fujikawa A, Nakajima M, Honya K (2005) Differentiation between solitary brain metastasis and high-grade glioma by dif-

fusion tensor imaging. Br J Radiol 78:533–537. doi:10.1259/bjr/68749637
12. Lu S, Ahn D, Johnson G, Cha S (2003) Peritumoral diffusion tensor imaging of high-grade gliomas and metastatic brain tumors. AJNR Am J Neuroradiol 24:937–941
13. Tang YM, Ngai S, Stuckey S (2006) The solitary enhancing cerebral lesion: can FLAIR aid the differentiation between glioma and metastasis? AJNR Am J Neuroradiol 27:609–611. doi:27/3/609[pii]
14. Kelly PJ, Daumas-Duport C, Kispert DB, Kall BA, Scheithauer BW, Illig JJ (1987) Imaging-based stereotaxic serial biopsies in untreated intracranial glial neoplasms. J Neurosurg 66:865–874. doi:10.3171/jns.1987.66.6.0865
15. Stuckey SL, Wijedeera R (2008) Multicentric/multifocal cerebral lesions: can fluid-attenuated inversion recovery aid the differentiation between glioma and metastases? J Med Imaging Radiat Oncol 52:134–139. doi:ARA1931[pii]10.1111/j.1440-1673.2008.01931.x

Substance P Antagonists as a Novel Intervention for Brain Edema and Raised Intracranial Pressure

Levon Gabrielian, Stephen C. Helps, Emma Thornton, Renée J. Turner, Anna V. Leonard, and Robert Vink

Abstract Increased intracranial pressure (ICP) following acute brain injury requires the accumulation of additional water in the intracranial vault. One source of such water is the vasculature, although the mechanisms associated with control of blood–brain barrier permeability are unclear. We have recently shown that acute brain injury, such as neurotrauma and stroke, results in perivascular accumulation of the neuropeptide, substance P. This accumulation is associated with increased blood–brain barrier permeability and formation of vasogenic edema. Administration of a substance P antagonist targeting the tachykinin NK1 receptor profoundly reduced the increased blood–brain barrier permeability and edema formation, and in small animal models of acute brain injury, improved functional outcome. In a large, ovine model of experimental traumatic brain injury, trauma resulted in a significant increase in ICP. Administration of an NK1 antagonist caused a profound reduction in post-traumatic ICP, with levels returning to normal within 4 h of drug administration. Substance P NK1 antagonists offer a novel therapeutic approach to the treatment of acute brain injury.

Keywords Neurotrauma • Neurokinins • Tachykinins • Neurogenic inflammation • Rat • Sheep

L. Gabrielian, S.C. Helps, E. Thornton, R.J. Turner, and A.V. Leonard
Adelaide Centre for Neuroscience Research, School of Medical Sciences, University of Adelaide, Adelaide, SA, Australia

R. Vink (✉)
Adelaide Centre for Neuroscience Research, Discipline of Anatomy and Pathology, School of Medical Sciences, University of Adelaide, Adelaide, SA, Australia

School of Medical Sciences, University of Adelaide, Adelaide, SA 5005, Australia
e-mail: robert.vink@adelaide.edu.au

Introduction

Worldwide, traumatic brain injury is considered the biggest killer of individuals under 45 years of age, with most neurotrauma occurring as a result of motor vehicle accidents. Survivors can be left with permanent neurological deficits caused by a secondary injury cascade that is initiated at the time of the traumatic event, and continues for a number of days to weeks thereafter. While a number of different secondary injury factors have been identified [1], edema has been recognized as the one factor that is responsible for up to as much as half of all the associated mortality and morbidity [2, 3]. In large part, this is because edema is the major contributor to raised intracranial pressure (ICP), which can have deleterious consequences on brain perfusion and oxygenation, and for this reason, has become one of the primary endpoints for clinical management of TBI patients. Indeed, a number of clinical studies have confirmed that raised ICP is associated with worse outcome [4, 5]. Despite this realization, little progress has been made over the last 50 years with respect to understanding the mechanisms associated with edema formation, and how to effectively intervene in its development. In this review, we highlight recent findings describing the potentially critical role of the neuropeptide, substance P, in the pathogenesis of edema formation and the development of increased ICP following acute brain injury.

Neurogenic Inflammation

Studies of peripheral tissues have established that the stimulation of neuronal, sensory C-fibers results in a process known as neurogenic inflammation, encompassing vasodilation, protein extravasation, and tissue swelling [6]. This inflammatory reaction is mediated by the release of neuropeptides, and while several have been implicated, it is generally accepted that substance P (SP) increases microvascular permeability,

Y. Katayama et al. (eds.), *Brain Edema XV*, Acta Neurochirurgica Supplement, Vol. 118,
DOI 10.1007/978-3-7091-1434-6_37, © Springer-Verlag Wien 2013

leading to edema formation, whilst calcitonin gene-related peptide (CGRP) is an extremely potent vasodilator [7]. Substance P also results in leukocyte activation and mast cell degranulation [8], thus supporting an additional role in both innate and specific immune responses. While sensory nerve fibers that contain both CGRP and SP surround essentially all blood vessels, cerebral blood vessels, in particular, appear to receive a dense supply of these nerve fibers.

Following experimental TBI, there is a generalized increase in brain SP immunoreactivity, which is particularly apparent around the vasculature [9], and within pyramidal neurones. Maximum immunoreactivity was present after 5 h and persisted for 24 h before gradually declining. Nonetheless, 3 days after TBI, mRNA for SP was still elevated [10]. Increased SP immunoreactivity has also been detected following experimental stroke [11], and has been recently described in human post-mortem tissue following TBI [12]. In the human tissue, perivascular SP immunoreactivity was often co-localized with positive APP immunoreactivity, suggesting that mechanical disruption of perivascular neurones might be associated with neuropeptide release. The increase in serum SP detected in the first 30 min after experimental TBI supports this view [9], although serum SP levels declined rapidly thereafter, presumably due to rapid proteolysis by nonspecific serum proteases. Notably, inhibition of brain SP breakdown using the angiotensin-converting enzyme inhibitor, captopril, increased SP immunoreactivity [13].

The Blood–Brain Barrier and Edema

Increased perivascular SP immunoreactivity after TBI was associated with increased extravasation of Evans blue as assessed by confocal microscopy [9], suggesting that SP release as part of neurogenic inflammation might be linked to increased blood–brain barrier (BBB) permeability. This was confirmed by studies demonstrating that pre-injury depletion of sensory neuropeptides using capsaicin, which would prevent neurogenic inflammation, resulted in a profound attenuation of BBB disruption after experimental TBI [14]. Subsequent studies have shown that post-injury administration of a SP NK1 receptor antagonist, n-acetyl-tryptophan (NAT), attenuated BBB permeability after both TBI [9] and stroke [11]. Indeed, the ability of NAT to attenuate BBB dysfunction after TBI was used to establish a dose-response relationship and identify the optimal dose for administration [9].

Disruption of the BBB was associated with the development of edema, which again was significantly attenuated by pre-injury depletion of sensory neuropeptides using capsaicin [14], or by administration of an NK1 receptor antagonist

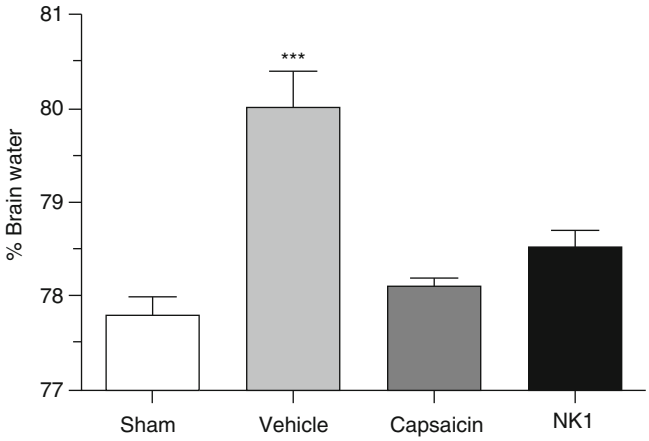

Fig. 1 Brain water content 5 h after traumatic brain injury in rats (mean ± SEM; $n=6$/group). Injury results in an increase in brain water content that is significantly attenuated ($p<0.001$) by neuropeptide depletion prior to injury (capsaicin pre-treatment) or by treatment with an NK1 receptor antagonist (2.5 mg/kg i.v. n-acetyl-tryptophan [NAT]) at 30 min after injury. ***$p<0.001$ compared with sham

[9] administered at 30 min after the traumatic event (Fig. 1). Given the presence of the disrupted BBB, edema at the 5-h time point was assumed to be vasogenic in nature, which was confirmed using diffusion-weighted MRI [9, 14]. Nonetheless, early administration of the NK1 antagonist also significantly attenuated subsequent edema formation, which by 24 h has been shown to be predominantly cytotoxic in nature [3, 5]. This is consistent with the view that vasogenic edema is permissive for the development of cytotoxic edema [5].

Attenuation of increased BBB permeability and edema formation after TBI with administration of the NK1 antagonist was associated with significant improvements in both motor and cognitive outcome in rats [9]. In contrast, inhibition of SP breakdown using captopril exacerbated both the histological damage and functional deficits after TBI [13]. The improvements in neurological outcome with administration of NK1 antagonists could be observed even when the compounds were administered up to 4 h after onset of ischemic stroke [15], and up to 12 h after TBI [16]. This improvement in functional outcome was shown to be a class effect of the NK1 receptor antagonists rather than a drug-specific effect [16], thus confirming that the observed changes were dependent on activation of the SP NK1 receptor. A similar improvement in functional outcome to that observed with the NK1 antagonists was noted with pre-injury depletion of the sensory neuropeptides using capsaicin [14], supporting the view that neurogenic inflammation plays a central role in the pathophysiology of TBI, and, more specifically, that attenuation of the induced BBB disruption and edema formation is associated with improvements in functional outcome after acute brain injury.

Effects on ICP

Given that SP was integrally involved in edema formation, we subsequently set out to examine the effects of the NK1 antagonists on ICP following TBI. While previous studies of SP in BBB permeability, edema formation, and functional outcome were conducted in rats, we have recently shown that rat models of either diffuse or focal TBI produce inconsistent increases in ICP depending on the presence or absence of mass lesions and/or hypoxia [17]. Thus, an interventional study examining the effects of NK1 antagonists on ICP was unlikely to be successful in the rat models. Accordingly, we chose to use the ovine, captive-bolt model of injury, which produces more consistent changes in ICP that are temporally similar to those observed in human TBI [18].

The model uses a humane stunner to accelerate the head of a sheep to induce an impact-acceleration type of injury. Briefly, castrated male Merino sheep (45–55 kg) are anesthetized and placed into a prone sphinx position, their body restrained to the table, but leaving the neck and head mobile relative to the body. A captive-bolt stunner armed with a number 17 red charge (model KML; Karl Schermer, Ettlingen, Germany) is then used to induce an impact injury at the midpoint between the left supraorbital process and the left external auditory meatus [18]. After injury, a calibrated Codman Microsensor ICP transducer was placed through a 2.5-mm burr-hole made at a point 15 mm lateral to the sagittal midline on the ipsilateral side, just in front of the coronal suture. After being inserted into the parenchyma to a depth of 1.5 cm, the probe was attached to a Codman ICP Express monitoring system (Codman and Shurtleff, Raynham, MA, USA), which was linked to an AD Instruments PowerLab® system where the data were post-processed. The burr-hole was sealed using bone wax to prevent CSF leakage and the sheep monitored for 4 h. Sham animals were surgically prepared and ICP monitoring initiated in the absence of any induced brain injury.

Figure 2 summarizes the ICP 4 h after injury. In sham animals, ICP was typically to the order of 10 mmHg. After injury, there was a marked increase in ICP that by 4 h, was above 30 mmHg. While early increases in ICP (<30 min) may be associated with reactive vasodilatation, the gradual increase in ICP over the ensuing hours is thought to reflect vasogenic edema formation [19]. The appearance of albumin immunostaining in the sheep brain parenchyma after injury confirms that BBB disruption had occurred at these early time points [19], thus supporting the likely presence of vasogenic edema. In contrast to vehicle-treated animals, administration of the NK1 antagonist 30 min after injury resulted in an immediate reduction in ICP, achieving levels that were not significantly different from sham animals at the 4-h time point.

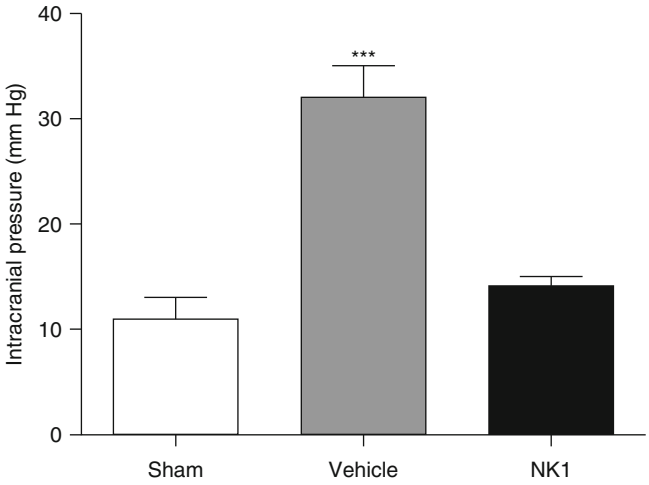

Fig. 2 Intracranial pressure in sheep 4 h after traumatic brain injury (mean ± SEM; $n=6$/group). Injury results in an increase in ICP that is significantly attenuated ($p<0.001$) by administration of an *NK1* receptor antagonist (2.5 mg/kg iv NAT) 30 min after injury. ***$p<0.001$ compared with sham

Conclusion

The series of experiments summarized herein have shown that increased perivascular SP immunoreactivity after TBI is associated with opening of the BBB and facilitation of vasogenic edema formation. Inhibiting the neurogenic inflammation initiated by the SP release, using either capsaicin to deplete sensory neuropeptides prior to injury or an NK1 receptor antagonist administered after injury, attenuates BBB permeability and edema formation and results in a significant improvement in functional outcome. In a large animal model of TBI, administration of the NK1 antagonist 30 min after injury caused a profound reduction in ICP such that it had returned to normal levels within 4 h of drug administration. While the mechanisms associated with the edema resolution and lowering of ICP are unknown, the reduction in brain water content induced by the NK1 antagonist suggests that water is actively leaving the brain tissue. Whether this effect is mediated through aquaporin channels located on perivascular, astrocytic end foot processes is unknown and requires further investigation. Substance P NK1 receptor antagonists represent a novel, mechanistic-based approach to managing increased ICP after acute brain injury.

Acknowledgment Supported, in part, by the National Health and Medical Research Council (Australia) and the Neurosurgical Research Foundation.

Conflict of Interest We declare that we have no conflict of interest.

References

1. Vink R, Nimmo AJ (2009) Multifunctional drugs for head injury. Neurotherapeutics 6:28–42
2. Feickert HJ, Drommer S, Heyer R (1999) Severe head injury in children: impact of risk factors on outcome. J Trauma 47:33–38
3. Marmarou A (2003) Pathophysiology of traumatic brain edema: current concepts. Acta Neurochir Suppl 86:7–10
4. American Association of Neurological Surgeons (2000) The joint section on neurotrauma and critical care: initial management. J Neurotrauma 17:463–469
5. Marmarou A (2007) A review of progress in understanding the pathophysiology and treatment of brain edema. Neurosurg Focus 22:E1
6. Brain SD, Williams TJ (1989) Interactions between the tachykinins and calcitonin gene-related peptide lead to the modulation of oedema formation and blood flow in rat skin. Br J Pharmacol 97:77–82
7. Baluk P (1997) Neurogenic inflammation in skin and airways. J Investig Dermatol Symp Proc 2:76–81
8. Bost KL (2004) Tachykinin-mediated modulation of the immune response. Front Biosci 9:3331–3332
9. Donkin JJ, Nimmo AJ, Cernak I, Blumbergs PC, Vink R (2009) Substance P is associated with the development of brain edema and functional deficits after traumatic brain injury. J Cereb Blood Flow Metab 29:1388–1398
10. Cook NL, Vink R, Donkin JJ, van den Heuvel C (2009) Validation of reference genes for normalization of real-time quantitative RT-PCR data in traumatic brain injury. J Neurosci Res 87:34–41
11. Turner RJ, Blumbergs PC, Sims NR, Helps SC, Rodgers KM, Vink R (2006) Increased substance P immunoreactivity and edema formation following reversible ischemic stroke. Acta Neurochir Suppl 96:263–266
12. Zacest AC, Vink R, Manavis J, Sarvestani GT, Blumbergs PC (2010) Substance P immunoreactivity increases following human traumatic brain injury. Acta Neurochir Suppl 106:211–216
13. Harford-Wright E, Thornton E, Vink R (2010) Angiotensin-converting enzyme (ACE) inhibitors exacerbate histological damage and motor deficits after experimental traumatic brain injury. Neurosci Lett 481:26–29
14. Nimmo AJ, Cernak I, Heath DL, Hu X, Bennett CJ, Vink R (2004) Neurogenic inflammation is associated with development of edema and functional deficits following traumatic brain injury in rats. Neuropeptides 38:40–47
15. Turner RJ, Helps SC, Thornton E, Vink R (2011) A substance P antagonist improves outcome when administered 4 h after onset of ischemic stroke. Brain Res 1393:84–90
16. Donkin JJ, Cernak I, Blumberg PC, Vink R (2011) A substance P antagonist reduces axonal injury and improves neurologic outcome when administered up to 12 hours after traumatic brain injury. J Neurotrauma 28:218–224
17. Gabrielian L, Willshire LW, Helps SC, van den Heuvel C, Mathias JL, Vink R (2011) Intracranial pressure changes following traumatic brain injury in rats: lack of significant change in the absence of mass lesions or hypoxia. J Neurotrauma 28:2103–2111
18. Vink R, Bhatia KD, Reilly PL (2008) The relationship between intracranial pressure and brain oxygenation following traumatic brain injury in sheep. Acta Neurochir Suppl 102:189–192
19. Byard RW, Bhatia KD, Reilly PL, Vink R (2009) How rapidly does cerebral swelling follow trauma? Observations using an animal model and possible implications in infancy. Leg Med (Tokyo) 11(Suppl 1):S128–S131

Microvascular Shunts in the Pathogenesis of High Intracranial Pressure

Edwin M. Nemoto, Denis Bragin, Martina Stippler, Suguna Pappu, Jessica Kraynik, Tracey Berlin, and Howard Yonas

Abstract Hyperemia in the infarcted brain has been suggested for years by "red veins" reported by neurosurgeons, shunt peaks in radioactive blood flow clearance curves, and quantitative cerebral blood flow using stable xenon CT. Histological characterization of infarcted brain revealed capillary rarefaction with prominent microvascular shunts (MVS). Despite abundant histological evidence, the presence of cerebrovascular shunts have been largely ignored, perhaps because of a lack of physiological evidence demonstrating the transition from capillary flow to MVS flow. Our studies have shown that high intracranial pressure induces a transition from capillary to microvascular shunt flow resulting in cerebral hypoperfusion, tissue hypoxia and brain edema, which could be delayed by increasing cerebral perfusion pressure. The transition from capillary to microvascular shunt flow provides for the first time a physiological basis for evaluating the optimal cerebral perfusion pressure with increased intracranial pressure. It also provides a physiological basis for evaluating the effectiveness of various drugs and therapies in reducing intracranial pressure and the development of brain edema and tissue hypoxia after brain injury and ischemia. In summary, the clear-cut demonstration of the transition from capillary to MVS flow provides an important method for evaluating various therapies for the treatment of brain edema and loss of autoregulation.

Keywords Brain edema • Cerebrovascular shunts • Cerebral perfusion pressure • Intracranial pressure • Microvascular shunts • Rats

Introduction

Determination of the critical cerebral perfusion pressure (CPP) to maintain adequate cerebral blood flow (CBF) has been historically defined by definition of the CBF autoregulation curve by progressive reduction of CPP by phlebotomy to decrease arterial pressure [1, 2]. Thus defined, the critical CPP was determined to be approximately 60 mmHg. However, clinically, compromised CPP is often due to an increase in intracranial pressure (ICP) rather than a decrease in arterial pressure. Hence, the question arises as to whether the critical CPP measured by decreasing arterial pressure is equivalent to that obtained by increasing ICP. Comparisons were made between the two methods in the CBF autoregulation curve, which showed that the critical CPP determined by increasing ICP was actually lower and about 50 % lower at 30 mmHg compared with 60 mmHg [1, 2]. The lower critical CPP suggests that CBF autoregulation was better preserved when CPP was decreased by increasing ICP. However, we hypothesized that the higher CBF maintained at a lower CPP with increasing ICP was caused by pathologically maintained CBF due to microvascular shunting, resulting in an apparently lower critical CPP.

To test the hypothesis, we measured flow velocity in capillaries (3–8 μm in diameter) and larger microvessels (9–45 μm), NADH (hypoxia), Doppler flow, and water content with decreasing CPP by either increasing ICP or decreasing arterial pressure [3].

Materials and Methods

The procedures used in these studies have been previously described [3]. Briefly, male Sprague–Dawley (SD) rats weighing between 300 and 350 g were intubated and mechanically ventilated on 2 % isoflurane/30 % oxygen/70 % nitrous oxide. Measured variables were: microvascular red blood

E.M. Nemoto, PhD (✉), D. Bragin, PhD, M. Stippler, MD, PhD, S. Pappu, MD, PhD, J. Kraynik, BS, T. Berlin, BSN, CNRN, and H. Yonas, MD
Department of Neurosurgery, University of New Mexico, 1, MSC 10 5615, Albuquerque, NM 87131, USA
e-mail: enemoto@salud.unm.edu

Y. Katayama et al. (eds.), *Brain Edema XV*, Acta Neurochirurgica Supplement, Vol. 118,
DOI 10.1007/978-3-7091-1434-6_38,

Table 1 Distribution (mean ± SEM) of low (<1 mm/s) and high (>1 mm/s) flow velocity capillaries (CAP) and microvascular shunts (MVS), CAP/MVS ratio, average volume flow per microvessel (μL/s) and normalized Doppler flux in rat cerebral cortex

	ICP group (%) $n=10$					MAP group (%) $n=10$					
CPP mmHg	CAP <1 mm/s	TFC >1 mm/s	CAP/MVS Ratio	MVS flow μL/s	Doppler flux	CAP <1 mm/s	TFC >1 mm/s	CAP/MVS ratio	MVS flow μL/s	Doppler flux	$p<$
70	70±5	30±2	2.3±0.7	39±2	1.0±0.1	65±6	35 ±4	2.1±0.7	40±2	1.0±0.1	0.145
50	58±5	41±3	1.4±0.5	68±6	0.9±0.1	71±6	29±4	2.4±0.8	33±2	0.8±0.1	0.001
30	49±5	51±5	1.0±0.1	135±8	0.7±0.1	86±7	14±3	6.2±1.5	21±1	0.5±0.1	0.001

p values refer to comparisons of the distribution between the groups at each cerebral perfusion pressure (CPP). Note the increase in MVS shunt in the ICP group as CPP was reduced compared with the reverse in the mean arterial pressure (MAP) group

cell (RBC) flow velocity; nicotinamide adenine dinucleotide (NADH) fluorescence as an indicator of tissue oxygenation; cortical Doppler flux and cortical water content. Rectal and temporal muscle temperatures, arterial pressure, and intracranial pressure were continuously monitored.

Velocity of RBC flow was measured using in vivo two-photon laser scanning microscopy (2PLSM) of microvessels in the parietal cortex. Blood plasma was labeled with fluorescein isothiocyanate dextran (20 kDa) in physiological saline (5 % wt/vol). The selection of capillary microvessels was based on tortuosity, degree of branching, and diameters ranging from 3 to 8 μm. Multiple recordings were made from the same vessel and mean microvessel RBC velocity and SEM were determined. Approximately 100 microvessels were scanned at each CPP and the diameter of each scanned vessel was measured. Tissue NADH autofluoresence was measured by 2PLSM imaging at each CPP level. Cortical Doppler flux was performed using a single-fiber surface Doppler probe measuring 0.8 mm in diameter (DRT4; Moor Instruments, Axminster, UK). Parietal cortex water content was measured by wet/dry weight.

Results

Reduction of CPP by a progressive increase in ICP caused a shift in MVS flow relative to CAP flow, whereas decreasing CPP by decreasing mean arterial pressure did not (Table 1). Decreasing CPP by increasing ICP decreased the percentage of capillaries (<1.0 mm/s), whereas the percentage of microvessels (>1.0 mm/s) increased with decreasing arterial pressure. The ratio of CAP/MVS also decreased with increasing ICP, whereas the opposite was true with decreasing arterial pressure. These results suggest that the reduction in the critical CPP when ICP was increased in the CBF autoregulation curve was due to a pathologically maintained elevated CBF as a result of microvascular shunting. The distribution of microvascular diameter with increasing ICP versus decreasing mean arterial pressure (MAP) to reduce CPP also verifies the fact that the increase in flow velocities with increasing ICP is attributable to flow through larger "shunts" or arterioles and not capillaries measuring 3–7 μm in diameter (Fig. 1).

The increase in MVS with increasing ICP raises another question, which is whether an increase in CPP at a given elevated ICP could prevent or delay the transition from CAP to MVS flow (Fig. 1). We have also shown that this increase in MVS flow with increasing ICP can be prevented by increasing CPP (unpublished results) [4]. The increase in MVS flow with increasing ICP is accompanied by increased tissue hypoxia, i.e., increased tissue NADH, and decreased cortical Doppler flow, which is less marked in the MAP as opposed to the ICP group (Fig. 2). The increase in brain tissue water also occurred in the ICP group, but not in the MAP group. These results clearly show the detrimental effects of increasing ICP and its relation to the shift from CAP to MVS flow. The interaction between ICP and CPP in relation to MVS flow could lead to better understanding in the management of high ICP in patients.

Conclusion

Our demonstration of the transition from CAP to MVS flow with increasing ICP provides for the first time, to our knowledge, documentation of this process. Up to now, MVS flow has been observed in infarcted brain [5] combined with capillary rarefaction, but only described as two different states. Without documentation of the transition process, the existence of cerebrovascular shunts was ignored except for a small group of investigators [5]. Now that we have observed and documented this transition between the two states, we now have a measureable and quantitative basis for evaluating the interaction between CPP and ICP and thereby the optimal CPP for a given ICP. We recently showed that MVS can be circumvented at high ICP by increasing CPP. We have also shown that the CPP required to reduce ICP depends upon the degree of elevated ICP (unpublished).

The Brain Trauma Guidelines based on level III evidence suggests that CPP be kept between 50 and 70 mmHg without aggressive measures to increase CPP above 70 mmHg using vasopressors and fluid loading [6]. There is also an ongoing debate on the methods of managing patients with high ICP based upon the recommendations of the "Lund concept" for

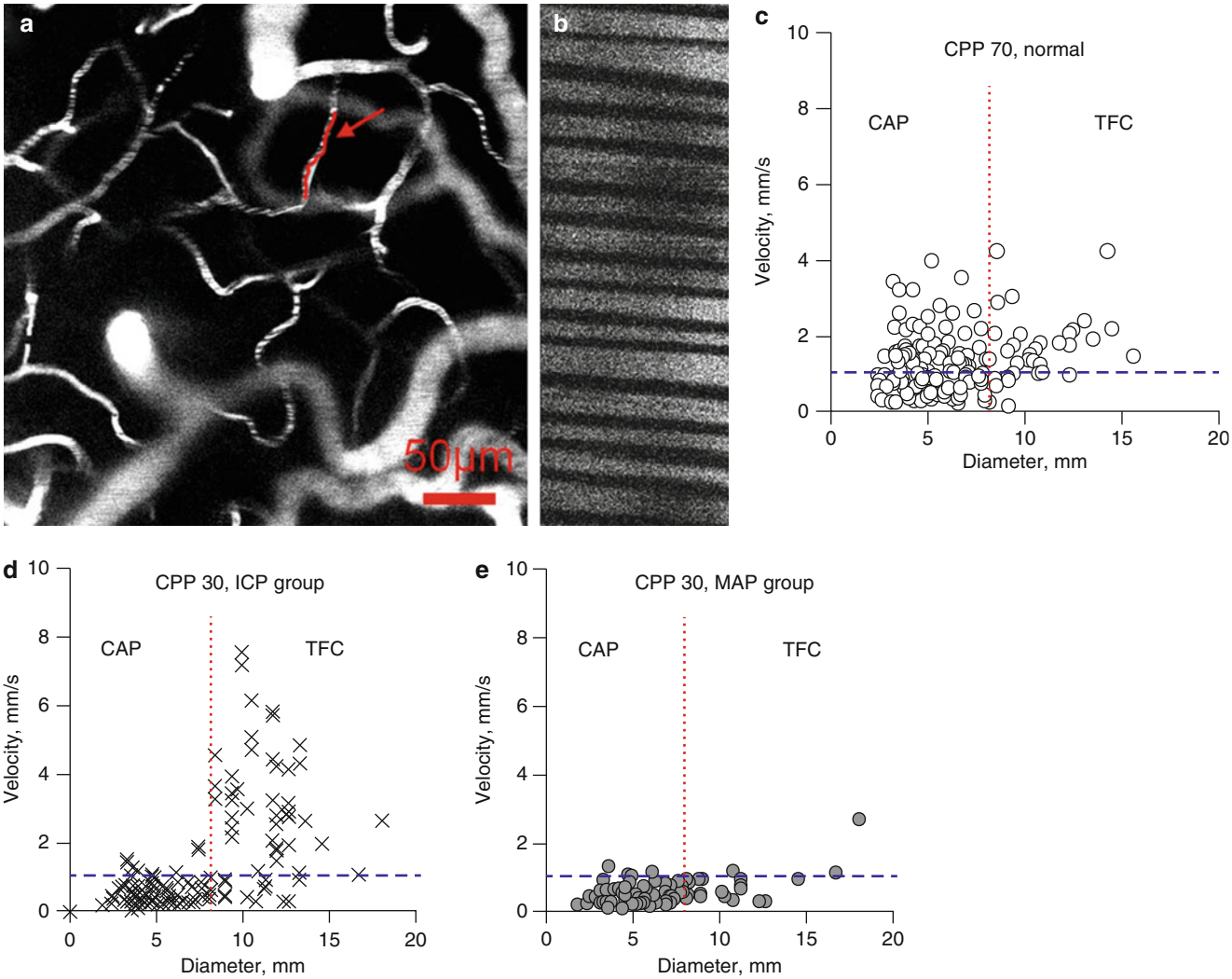

Fig. 1 (**a**) 2-photon laser scanning micrograph showing a region from which microvascular flow was recorded. (**b**) Line-scan data for red blood cell (RBC) flow velocity in the microvessel shown in **a** (*arrow*). (**c**) Distribution of flow velocity versus vessel diameter in cortical microvessels at normal cerebral perfusion pressure (CPP; 70 mmHg, $n=10$ rats). *CAP* capillary, *TFC* thoroughfare channel. (**d**) Decrease in CPP to 30 mmHg by increasing intracranial pressure (ICP) reduces capillary (3–6 μm in diameter) and increases thoroughfare channel (8–15 μm in diameter) flow velocities ($n=10$ rats). (**e**). Decrease in mean arterial pressure (MAP) to reduce the CPP to 30 mmHg reduces the velocity of all microvessels in the rat parietal cortex ($n=10$ rats). *Blue dashed line* indicates a velocity of 1.0 mm/s. *Red dotted line* indicates a diameter of 8 μm (Reprinted with permission from the *Journal of Neurotrauma*)

ICP-targeted therapy, largely by the use of various drugs, as opposed to CPP-targeted therapy [4, 7]. Thus, clinicians, lacking a standard of care (SOC) are left to manage their patients with high ICP using methods based largely on individual bias.

What light can be shed on the problems confronting clinicians with responsibility for caring for these severely brain injured patients suffering from high ICP and resolve the debate regarding ICP versus CPP targeted therapy according to our observations? Based on the hypothesis that in traumatic brain injury (TBI) where high ICP and thereby brain edema is an issue, is characterized by MVS. Thus, in an animal model of TBI resulting in elevated ICP with documentation of MVS, the efficacy of various clinical therapies prescribed by the Lund concept such as beta blockade, sedation with benzodiazepines, and barbiturates while maintaining CPP at 50–60 mmHg can be studied. The dose response and in reducing or counteracting MVS can also be tested. The same can be done in evaluating the effectiveness of increasing CPP on MVS in the brain after TBI. We have already shown in the brain injured with artificially elevated ICP that MVS can be reduced or prevented by increasing CPP (unpublished data). It is important to note that historically, the determination of the critical CPP based on CBF autoregulation curves was carried out in animals with normal brains and was translated to clinical use. Later studies in humans seem to indicate that patients with CBF autoregulation do better with a higher CPP of 60–70 mmHg, whereas if there is no CBF autoregulation patients do better with lower

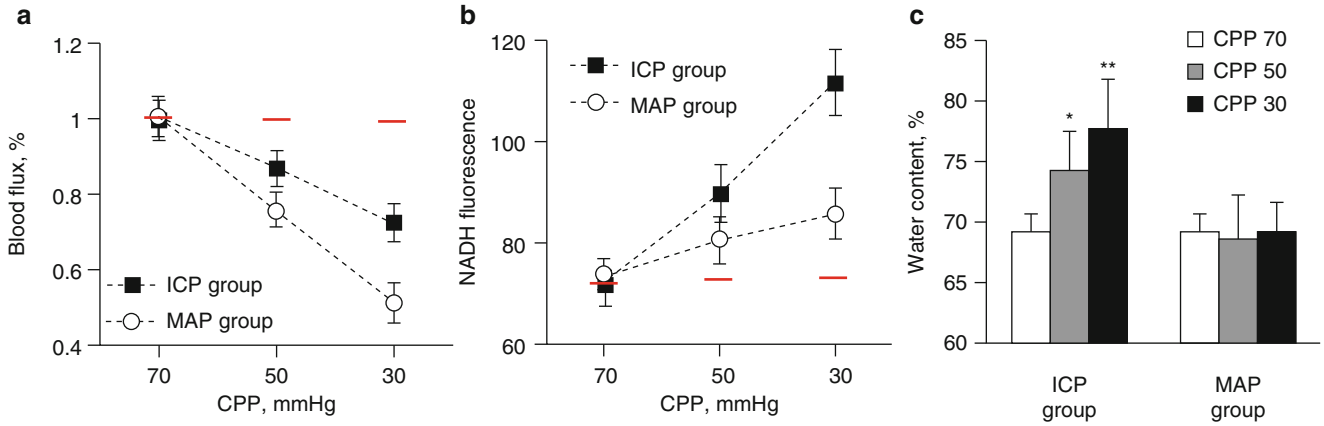

Fig. 2 (**a**) Hemispheric Doppler flow flux when *CPP* is reduced by increasing *ICP* ($n=10$) or decreasing *MAP* ($n=10$). (**b**) *NADH* reduction during reduction in CPP by increasing ICP ($n=10$) or decreasing MAP ($n=10$). *Red dashes* show levels in the control group at appropriate time points. (**c**) CPP decrease by elevation of ICP causes an increase in cortical water content. In the MAP group cortical water content was not different from controls ($n=3$ for each, mean ± SEM, $*p<0.05$, $**p<0.01$). Cortical tissue water content obtained by rapidly scooping the cortex out of the craniotomy yields a water content consistently lower, 73.52 ± 0.45 % (mean ± SD, $n=2$) than that obtained by decapitating the rat, removing the brain, and sampling the cortex, which yields values of 79.91 ± 0.40 % (mean ± SD, $n=2$), significantly different ($p=0.0262$) according to the Shapiro–Wilk test (Reprinted with permission from the *Journal of Neurotrauma*)

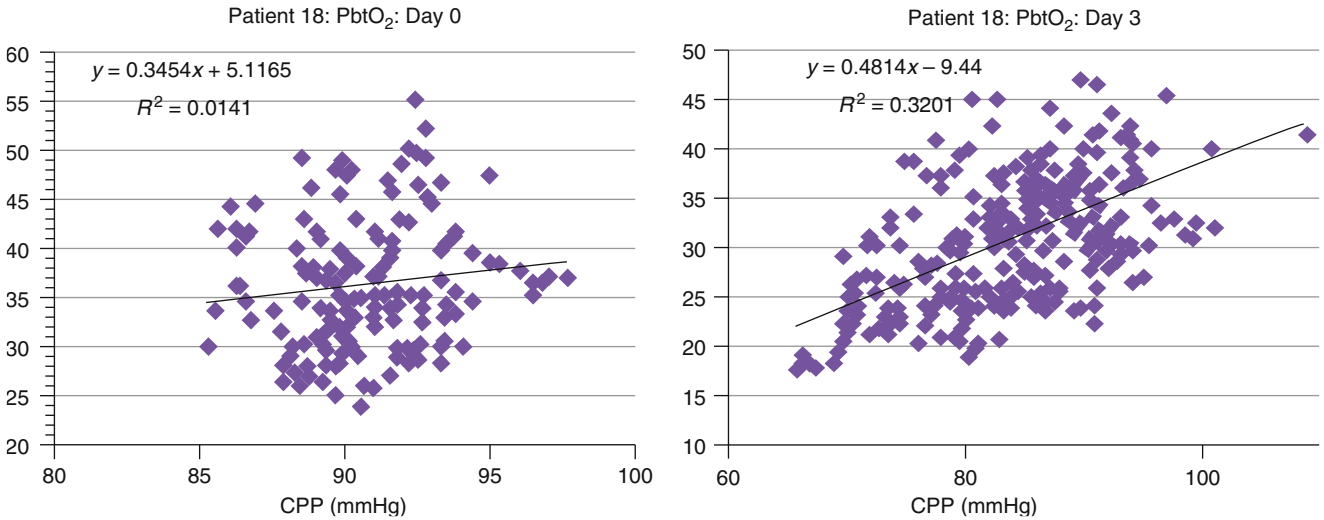

Fig. 3 Brain tissue $PbtO_2$ (Licox probe) versus *CPP* in the white matter of the contralateral hemisphere on days 0 and 3 after traumatic brain injury. Note the absence of correlation between $PbtO_2$ versus CPP on day 0 as opposed to the linear correlation on day 3, suggesting delayed loss of autoregulation on day 3

CPP within the range 50–60 mmHg, as promoted by the Lund concept [6]. However, other studies have suggested that higher CPP of 70–80 mmHg improves outcome after TBI [8–11]. The above-mentioned are all animal studies that can be carried out to address clinical problems encountered by clinicians in managing patients with high ICP after brain injury.

There is already substantial evidence suggesting that patients without CBF autoregulation might fare better if maintained at a lower CPP within the range of 50–60 mmHg [6], whereas those with CBF autoregulation fare better at high CPP [8–11]. It is also notable that with the advent of multimodal neuromonitoring, the presence or absence of CBF autoregulation, whether based on CBF measurements or brain tissue PO_2 (Licox; Fig. 3) varies in each patient from day to day. These data suggest that therapy in these patients might need to be tailored on a daily basis, depending upon their status on any given day rather than standardized therapeutic intervention protocols. Thus, the patient suffering from high ICP with evidence of no CBF autoregulation may be better maintained at a lower CPP of 50–60 mmHg, whereas patients with high ICP and with CBF autoregulation may respond better with high CPP within the range

70–80 mmHg. Whether this is the case, remains to be determined in future randomized clinical trials.

Conflict of Interest We declare that we have no conflict of interest.

References

1. Miller JD, Stanek A, Langfitt TW (1972) Concepts of cerebral perfusion pressure and vascular compression during intracranial hypertension. Prog Brain Res 35:411–432
2. Grubb RL Jr, Raichle MD, Phelps ME, Ratcheson RA (1975) Effects of increased intracranial pressure on cerebral blood volume, blood flow, and oxygen utilization in monkeys. J Neurosurg 43(4):385–398
3. Bragin D, Bush R, Nemoto EM (2011) High intracranial pressure effects on cerebral cortical microvascular flow in rats. J Neurotrauma 28:775–785
4. Nordstrom CH (2003) Assessment of critical thresholds for cerebral perfusion pressure by performing bedside monitoring of cerebral energy metabolism. Neurosurg Focus 15:1–8
5. Tomita M (1988) Significance of cerebral blood volume. In: Tomita M, Sawada T, Naritomi H, Heiss WD (eds) Cerebral hyperemia and ischemia: from the standpoint of cerebral blood volume. Excerta Medica, Amsterdam, pp 3–31
6. Bratton SL, Chestnut RM, Ghajar J, McConnell Hammond FF, Harris OA, Hartl R, Manley GT, Nemecek A, Newell DW, Rosenthal G, Schouten J, Shutter L, Timmons SD, Ullman JS, Videtta W, Wilberger JE, Wright DW (2007) Guidelines for the management of severe traumatic brain injury. IX. Cerebral perfusion thresholds. J Neurotrauma 24(Suppl 1):S59–S64
7. Grande PO, Asgiersson B, Nordstrom CH (2002) Volume targeted therapy of increased intracranial pressure: the Lund concept unifies surgical and non-surgical treatments. Acta Anaesthesiol Scan 46:929–941
8. Balestreri M, Czosnyka M, Hutchinson P, Steiner LA, Hiler M, Smielewski P, Pickard JD (2006) Impact of intracranial pressure and cerebral perfusion pressure on severe disability and mortality after head injury. Neurocrit Care 4:8–13
9. Lin JW, Tsai JT, Lin CM, Lee LM, Hung KS, Huang SJ, Hsiao SH, Chung WY, Tsai MD, Hsia CC, Hung CC, Chiu WT (2008) Evaluation of optimal cerebral perfusion pressure in severe traumatic brain injury. Acta Neurochir Suppl 101:131–136
10. Rosner MJ, Daughton S (1990) Cerebral perfusion pressure management in head injury. J Trauma 30:933–940
11. McGraw CP (1989) A cerebral perfusion pressure greater that 80 mmHg is more beneficial. In: Hoff JT, Betz AL (eds) ICP VII. Springer, Berlin, pp 839–841

The Frontal and Temporal Horn Ratio to Assess Dimension of Paediatric Hydrocephalus: A Comparative Volumetric Study

Sebastian Antes, Melanie Welsch, Michael Kiefer, Mareike Gläser, Heiko Körner, and Regina Eymann

Abstract Magnetic resonance imaging and cranial ultrasound are the most frequently implemented imaging methods for investigating the infantile hydrocephalic brain. A general and reliable measurement index that can be equally applied in both imaging methods to assess dimension of ventricular dilatation is currently not available. For this purpose, a new parameter called the frontal and temporal horn ratio – determinable in coronal slices of the brain – was developed and evaluated in a comparative volumetric retrospective study: Statistical analyses of 118 MRIs of 46 different shunt-treated pediatric patients revealed a good linear correlation between the new index and the actual ventricular volume.

Keywords Hydrocephalus • Ventricular size • Volumetric analysis • Volumetry • Frontal and temporal horn ratio Linear measurement

Introduction

Regular examinations of the brain and ventricular system in pediatric hydrocephalus patients, especially in cases of shunt treatment, are indispensable [1, 2, 7, 12, 14]. As well as clinical evaluation of a child's condition, imaging methods such as cranial ultrasound (cUS) and magnetic resonance imaging (MRI) are the preferred diagnostics for appreciating the extent of hydrocephalus and for controlling therapy success [4, 5, 10–12, 15, 16, 18]. Size and configuration of the ventricular system are usually estimated either by subjective assessment [9, 12], two-dimensional measurement [3, 8–11, 13, 14, 17] of ventricular width (e.g. Evan's index, frontal and occipital horn ratio, etc.) or in very rare cases by the most precise volumetric analysis [1, 4, 9, 12, 14, 19]. Consecutively reported findings of several follow-up examinations are often not comparable, leading to incorrect conclusions. For these reasons, a general, valid, and efficient diagnostic tool for analogical measurements of the ventricular system – regardless of the imaging method used – has been developed.

Materials and Methods

One hundred and eighteen MRIs (Siemens Sonata, 1.5 T, axial and coronal T1 sequences) of 46 different VP-shunted hydrocephalus patients (24 male, 22 female) aged 0–12 years (average: 3.0 years ± 3.4) were analyzed. Irrespective of age and hydrocephalus etiology (Chiari II malformation, 35 %; intraventricular hemorrhage, 22 %; congenital complex cerebral malformations including different syndromes, 20 %; congenital aqueductal stenosis, 15 %; occlusive tumors, 4 %; post-inflammatory diseases, 4 %) images were divided into two categories depending on ventricular configuration. Group A included 92 MRIs with dilated ventricles, group B included 26 MRIs with slit or slit-deformed ventricles resulting from shunt overdrainage. Supratentorial ventricular system (without Sylvian aqueduct) of each MRI was sized using a volumetric technique (Mac OS X Osirix v.9.3.1.). By using the complete axial imaging series, ventricle borders were manually outlined, subsumed, and multiplied by slice thickness for volume calculation. In a second step, three different linear parameters were determined. The Evan's index (EI) as well as the frontal and occipital horn ratio (FOHR) were measured

S. Antes, MD (✉), M. Kiefer,
M. Gläser, and R. Eymann
Department of Neurosurgery, Saarland University, Medical School,
Kirrberger Strasse, Building 90.5, 66421 Homburg/Saar, Germany
e-mail: sebastian.antes@uks.eu

M. Welsch
University Hospital Mannheim, University of Heidelberg,
Theodor-Kutzer-Ufer 1-3, 68167 Mannheim, Germany

H. Körner
Department of Diagnostic and Interventional Neuroradiology,
Saarland University Hospital,
66421 Homburg, Germany

Y. Katayama et al. (eds.), *Brain Edema XV*, Acta Neurochirurgica Supplement, Vol. 118,
DOI 10.1007/978-3-7091-1434-6_39, © Springer-Verlag Wien 2013

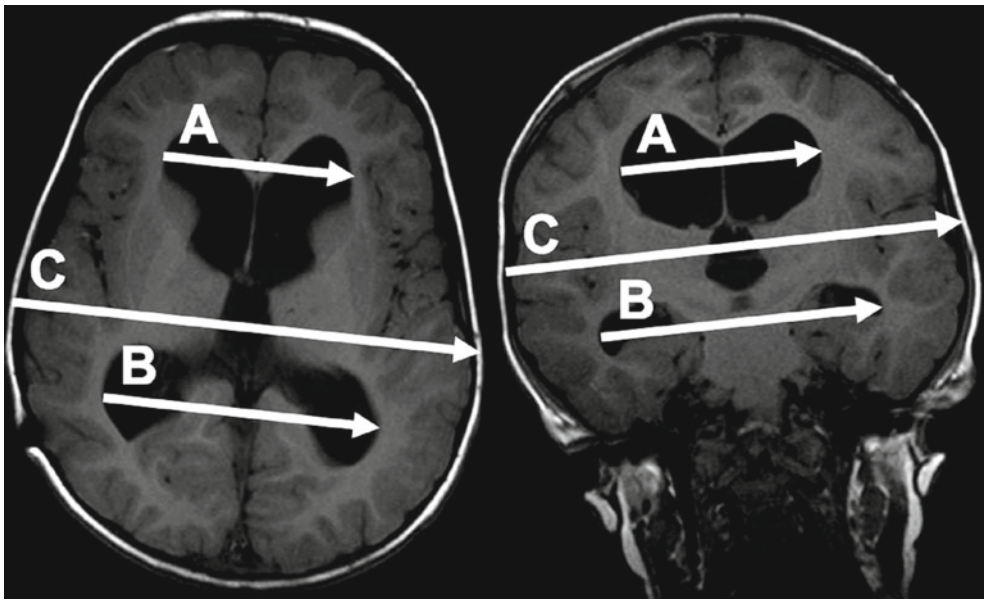

Fig. 1 Illustration of frontal and occipital horn ratio (FOHR) (*left*) and frontal and temporal horn ratio (FTHR; *right*) measurement on axial and coronal T1-weighted MRIs of the same imaging series. Parameters are analogously calculated as follows: $(A+B)/(2\times C)$

Table 1 Spearman's correlation coefficients

	Frontal and occipital horn ratio	Frontal and temporal horn ratio	Evan's index
Ventricular volume (all images)	0.868	0.850	0.530
Ventricular volume group A	0.800	0.773	0.453
Ventricular volume group B	0.544	0.466	0.205

on axial MRI planes as usual, whereas the third quotient – the new frontal and temporal horn ratio (FTHR) – was determined on coronal slices. The frontal and temporal horn ratio is defined as half of the sum of the frontal and temporal horn width divided by the broadest skull diameter at the level of the foramen of Monro (Fig. 1). Finally, all two-dimensional parameters (EI, FOHR, and FTHR) were statistically compared with actual ventricular volume (VOL) using Spearman's correlation coefficients (Rho).

Results

Regarding all 118 MRI measurements, the following mean values were calculated: EI = 0.32 ± 0.07 (range: 0.15–0.58), FOHR = 0.44 ± 0.10 (range: 0.23–0.71), FTHR = 0.48 ± 0.12 (range: 0.26–0.73) and VOL = 190.0 ± 214.2 mL (range: 3.1–830.5 mL). Correlation analysis revealed strong and linear coherences between VOL and FOHR (Rho = 0.868, $p = 0.000$) and between VOL and FTHR (Rho = 0.850, $p = 0.000$). On the contrary, EI correlated less well with actual volume (Rho = 0.530, $p = 0.000$).

Distinguishing ventricular configuration, significant differences could be detected. Ventricular volume of group A (mean VOL = 236.2 ± 221.5 mL) highly correlated with the FOHR (Rho = 0.800, $p = 0.000$) and the FTHR (Rho = 0.773, $p = 0.000$). By contrast, in slit-ventricle group B (mean VOL = 26.2 ± 18.9 mL) much lower correlations were seen between VOL and FOHR (Rho = 0.544, $p = 0.004$) and between VOL and FTHR (Rho = 0.466, $p = 0.017$). Additionally, in both groups, likewise, low statistical coherence concerning VOL and EI was revealed (group A: Rho = 0.453, $p = 0.000$; group B: Rho = 0.205, $p = 0.316$). Spearman's correlation coefficients of ventricular measurements are clearly listed in Table 1.

Conclusion

The results obtained prove the new frontal and temporal horn ratio to be a valid and reliable linear measurement index for estimating ventricular size in pediatric hydrocephalus patients, especially in cases of dilated ventricles. Similar to previous studies [8, 9, 12, 14], the frontal and occipital horn ratio was also demonstrated to be an adequate alternative to precise [1, 4, 9, 12, 14, 19], but time-consuming [9, 12, 19] volumetry. On the other hand, the widely used Evan's index seems to be less suitable for this purpose [1, 8, 14].

Interestingly, none of the two-dimensional parameters tested could really assess the size of slit or slit-deformed ventricles (due to shunt-overdrainage). A similar result has

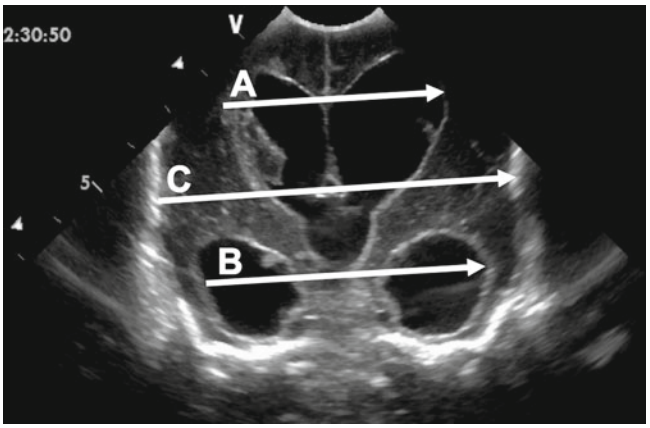

Fig. 2 Coronal ultrasound (Vivid S5 ultrasound system; GE Healthcare) of a 5-week-old child suffering from intraventricular hemorrhage. All structures to determine the FTHR at the level of the foramen of Monro are clearly identifiable

already been published in the past; authors suggested therefore individual axial measurements of both frontal and occipital horns to generate an appropriate quotient [8]. The same procedure is equally as conceivable with frontal and temporal horns in coronal imaging slices.

Nevertheless, the crux with commonly used tomography parameters (such as Evan's index or the frontal and occipital horn ratio) is that axial slices of the brain are required. That issue limits the parameters' application in cUS; previous efforts have shown that compliant perspective axial views are difficult to render [2]. Therefore, the frontal and temporal horn ratio seems to be a solution to circumventing the perspective problem. By using the anterior fontanel, the ultrasound depiction of a coronal brain slice at the level of the foramen of Monro is simply practicable (Fig. 2).

There still remains the question of whether or not ultrasound and MRI views, even when appearing visually equal, are actually congruent. In the literature, some authors have found inconsistencies between the two imaging methods in measuring the size of the ventricular system [10, 13]; others have shown good accordance [6, 11]. Aside from that, it is difficult to imagine whether (minor) changes in the perspective view can wield significant influence on linear measurements leading to relevant changes in a parameter's value.

However, the preliminary findings of this retrospective study presume reliable and stable characteristics of the new index concerning the assessment of hydrocephalic dimension. Moreover, owing to its applicability to MR and ultrasound images, the frontal and temporal horn ratio could be a very useful and efficient universal follow-up parameter in pediatrics.

Conflict of Interest We declare that we have no conflict of interest.

References

1. Ambarki K, Israelsson H, Wahlin A, Birgander R, Eklund A, Malm J (2010) Brain ventricular size in healthy elderly: comparison between Evans index and volume measurement. Neurosurgery 67:94–99
2. Antes S, Kiefer M, Schmitt M, Lechtenfeld M, Geipel M, Eymann R (2012) Frontal and temporal horn ratio – a valid and reliable index to determine ventricular size in paediatric hydrocephalus patients? Acta Neurochir Suppl 114:227–230
3. Evans W (1942) An encephalographic ratio for estimating ventricular enlargement and cerebral atrophy. Arch Neurol Psychatry 47:931–937
4. Gilmore JH, Gerig G, Specter B, Charles HC, Wilber JS, Hertzberg BS, Kliewer MA (2001) Infant cerebral ventricle volume: a comparison of 3-D ultrasound and magnetic resonance imaging. Ultrasound Med Biol 27:1143–1146
5. Hoon AH Jr, Melhem ER (2000) Neuroimaging: applications in disorders of early brain development. J Dev Behav Pediatr 21:291–302
6. Horsch S, Bengtsson J, Nordell A, Langercrantz H, Adén U, Blennow M (2009) Lateral ventricular size in extremely premature infants: 3D MRI confirms 2D ultrasound measurements. Ultrasound Med Biol 35:360–366
7. Iova A, Garmashov A, Androutchenko N, Kehrer M, Berg D, Becker G, Garmashov Y (2004) Evaluation of the ventricular system in children using transcranial ultrasound: reference values for routine diagnostics. Ultrasound Med Biol 30:745–751
8. Jamous M, Sood S, Kumar R, Ham S (2003) Frontal and occipital horn width ratio for the evaluation of small and asymmetrical ventricles. Pediatr Neurosurg 39:17–21
9. Kulkarni AV, Drake JM, Armstrong DC, Dirks PB (1999) Measurement of ventricular size: reliability of the frontal and occipital horn ratio compared to subjective assessment. Pediatr Neurosurg 31:65–70
10. Leijser LM, Srinivasan L, Rutherford MA, Counsell SJ, Allsop JM, Cowan FM (2007) Structural linear measurement in the newborn brain: accuracy of cranial ultrasound compared to MRI. Peadiatr Radiol 37:640–648
11. Leijser LM, de Bruine FT, Steggerda SJ, van der Grond J, Walther FJ, van Wezel-Meijler G (2009) Brain imaging findings in very preterm infants throughout the neonatal period: part I. Incidences and evolution of lesions, comparison between ultrasound and MRI. Early Hum Dev 85:101–109
12. Mann SA, Wilkinson JS, Fourney DR, Stoneham GW (2009) Comparison of computed tomography 3-dimensional volumetric analysis of ventricular size to visual radiological assessment. J Comput Assist Tomogr 33:789–794
13. Maunu J, Parkkola R, Rikalainen H, Lehtonen L, Haataja L, Lapinleimu H (2009) Brain and ventricles in very low birth weight infants at term: a comparison among head circumference, ultrasound, and magnetic resonance imaging. Pediatrics 123:617–626
14. O'Hayon BB, Drake JM, Ossip MG, Tuli S, Clarke M (1998) Frontal and occipital horn ratio: a linear estimate of ventricular size for multiple imaging modalities in pediatric hydrocephalus. Pediatr Neurosurg 29:245–249
15. Ouahba J, Luton D, Vuillard E, Garel C, Gressens P, Blanc N, Elmaleh M, Evrard P, Oury JF (2006) Prenatal isolated mild ventriculomegaly: outcome in 167 cases. BJOG 113:1072–1079
16. Patel TR, Bannister CM, Thorne J (2003) A study of prenatal ultrasound and postnatal magnetic imaging in the diagnosis of central nervous system abnormalities. Eur J Pediatr Surg 13:18–22

17. Poland RL, Slovis TL, Shankaran S (1985) Normal values for ventricular size as determined by real time sonographic techniques. Pediatr Radiol 15:12–14
18. Senapati GM, Levine D, Smith C, Estroff JA, Barnewolt CE, Robertson RL, Poussaint TY, Mehta TS, Werdich XQ, Pier D, Feldman HA, Robson CD (2010) Frequency and cause of disagreements in imaging diagnosis in children with ventriculomegaly diagnosed prenatally. Ultrasound Obstet Gynecol 36:582–595
19. von Bezing H, Andronikou S, van Toorn R, Douglas T (2012) Are linear measurements and computerized volumetric ratios determined from axial MRI useful for diagnosing hydrocephalus in children with Tuberculous meningitis? Childs Nerv Syst 28(1):79–85

Cerebrospinal Fluid Congestion in the Perioptic Space

Satoru Takeuchi, Hiroshi Nawashiro, Kojiro Wada, Hideo Osada, Naoki Otani, Kimihiro Nagatani, Hiroaki Kobayashi, Takamoto Suzuki, and Katsuji Shima

Abstract Recent attention has been paid to the cerebrospinal fluid (CSF) dynamics between the intracranial subarachnoid space (SAS) and the SAS around the optic nerve (ON-SAS). We experienced three patients who had an expanded ON-SAS associated with mass lesions extending into the optic canal, and studied their MRI findings after decompressive surgery. In all three patients, decompressive surgery of the optic canal resulted not only in the disappearance of the expanded ON-SAS, but also in improvement of the visual function. The present study may indicate that normalization of the ON-SAS can be considered to be the achievement of "effective" decompression. Therefore, we suggest that, in patients with an expanded ON-SAS associated with mass lesions, the state of the ON-SAS should be evaluated by pre- and postoperative MRI, in addition to the degree of tumor resection.

Keywords Cerebrospinal fluid • Magnetic resonance imaging • Optic nerve • Subarachnoid space

Introduction

The cerebrospinal fluid (CSF) circulation has been studied for a long time; however, its dynamics have not yet been explored [14]. Among several related topics, recent attention has been paid to the cerebrospinal fluid (CSF) dynamics between the intracranial and the subarachnoid space (SAS) of the optic nerve (ON) (ON-SAS) [3, 5–10].

The expansion of the ON-SAS, which is known as an optic nerve meningocele, optic hydrops, or perioptic hygroma, has been reported to be caused by various neoplastic and non-neoplastic conditions [1, 2, 4, 5, 11–13]. MRI is a useful tool for objectively evaluating the ON-SAS [12].

We experienced three patients with an expanded ON-SAS associated with mass lesions that extended into the optic canal, and studied their MRI findings after decompressive surgery. We herein report these cases and discuss the CSF dynamics of the ON-SAS.

Materials and Methods

We experienced three patients who met the inclusion criteria as follows: (1) Preoperative MRI demonstrated an expanded ON-SAS associated with mass lesions extending into the optic canal. (2) ON decompression had been performed. (3) Postoperative MRI was performed to observe the ON-SAS. We investigated the pre-and postoperative MRI findings and visual functions of these patients.

Results

Case 1

A 53-year-old man was admitted with vision loss in the left eye. Magnetic resonance imaging (MRI) showed a tumor of the tuberculum sellae, which extended into the left optic canal (Fig. 1a). MRI also demonstrated an expanded SAS of the left ON (Fig. 1b, c). Tumor resection with optic canal decompression was performed. A histological examination revealed meningothelial meningioma. After surgery, the patient's visual acuity showed improvement. MRI obtained 7 days after surgery demonstrated complete tumor resection and a subtotal disappearance of the expanded SAS of the left ON (Fig. 1d, e).

S. Takeuchi (✉), H. Nawashiro, K. Wada, H. Osada, N. Otani, K. Nagatani, H. Kobayashi, T. Suzuki, and K. Shima
Department of Neurosurgery, National Defense Medical College, 3-2 Namiki, Tokorozawa, Saitama 359-8513, Japan
e-mail: s.takeuchi@room.ocn.ne.jp

Y. Katayama et al. (eds.), *Brain Edema XV*, Acta Neurochirurgica Supplement, Vol. 118,
DOI 10.1007/978-3-7091-1434-6_40,

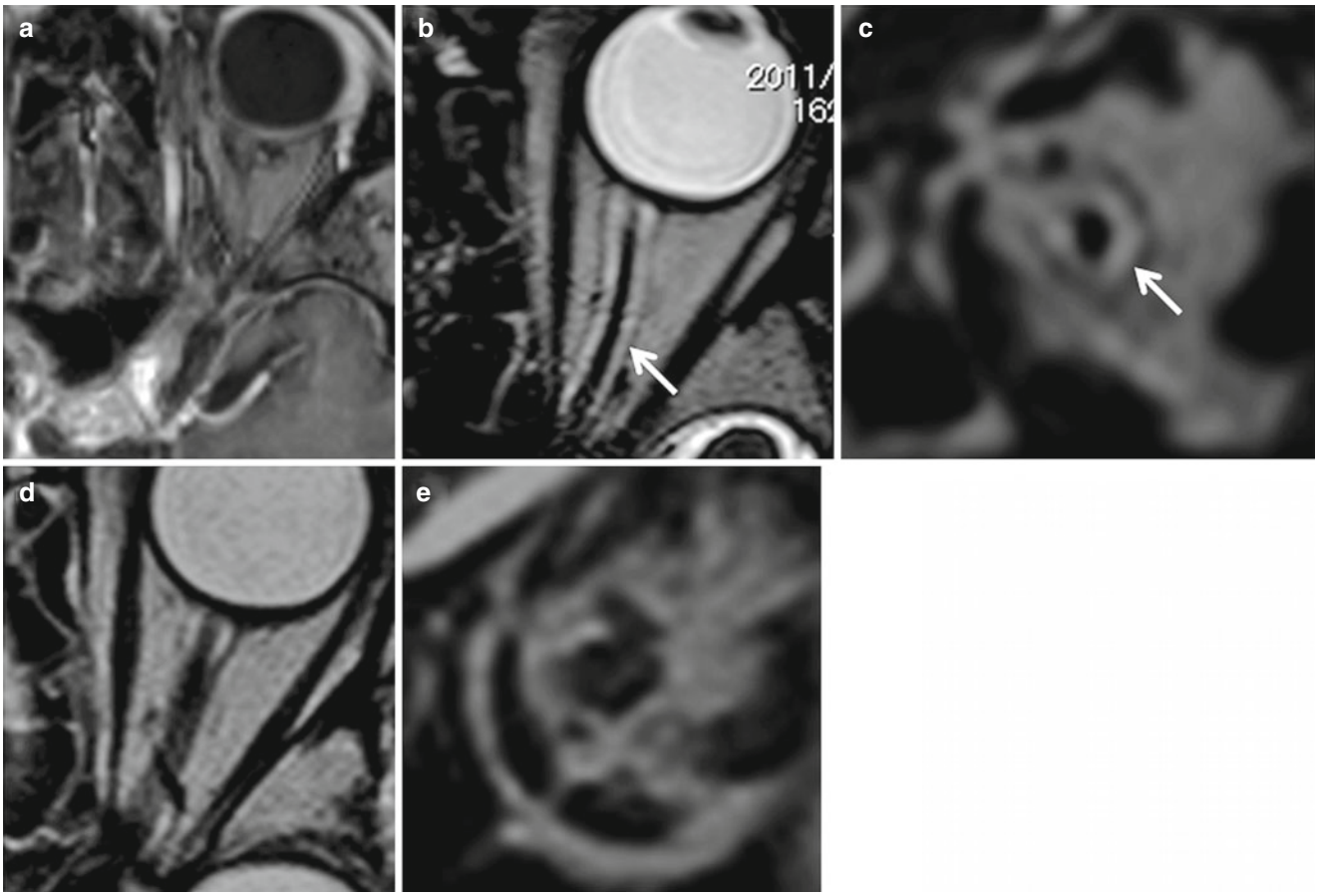

Fig. 1 The preoperative gadolinium-enhanced T1-weighted MR images of case 2 (**a**) showed a mass lesion of the tuberculum sellae, which extended into the left optic canal. The same patient's preoperative T2-weighted MR images (**b**: axial, **c**: coronal) demonstrated the expanded subarachnoid space in the left optic nerve (*arrow*). The postoperative T2-weighted MR images (**d**: axial, **e**: coronal) demonstrated a subtotal disappearance of the abnormality

Case 2

A 57-year-old man was admitted with vision loss in the left eye. MRI showed a tumor of the tuberculum sellae, which extended into the left optic canal. MRI also demonstrated an expanded SAS of the left ON. Tumor resection with optic canal decompression was performed. A histological examination revealed meningothelial meningioma. After surgery, the patient's visual acuity showed improvement. MRI obtained 3 months after the surgery demonstrated subtotal tumor resection and a subtotal disappearance of the expanded SAS of the left ON.

Case 3 (Unpublished Data)

An 88-year-old man presented with vision loss and limited abduction of the left eye. A brain CT showed a mass lesion in the left frontal and temporal bone, which extended into the optic canal. CISS-MRI demonstrated an expanded SAS of the left ON. Tumor resection with optic canal decompression was performed. A histological examination revealed metastatic adenocarcinoma of the prostate. After surgery, the patient's visual acuity showed improvement, and the eye movement recovered. A postoperative CT demonstrated a decompressed optic nerve canal. MRI obtained 9 days after surgery showed the complete disappearance of the expanded SAS of the left ON.

Conclusion

In our cases, decompressive surgeries of the optic canal resulted in not only the disappearance of the expanded ON-SAS, but also improvement of the visual function. The present study may indicate that normalization of the

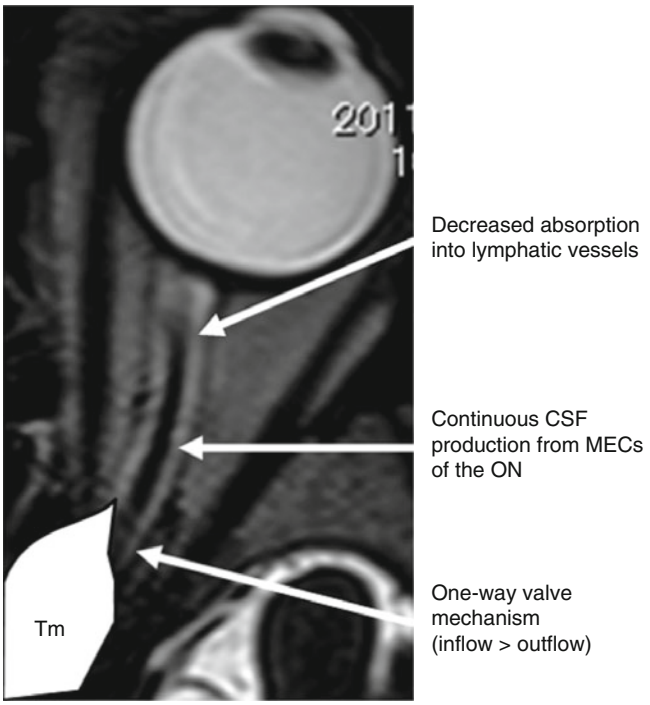

Fig. 2 The three possible mechanisms underlying the CSF congestion of the subarachnoid space of the optic nerve due to the mass lesions (*Tm*) that extended into the optic canal

ON-SAS can be considered to reflect the achievement of "effective" decompression. Therefore, we suggest that, in patients with an expanded ON-SAS associated with mass lesions, the state of the ON-SAS should be evaluated by pre- and postoperative MRI, in addition to the degree of tumor resection.

The CSF dynamics between the intracranial SAS and the ON-SAS are complex and poorly understood. Recent evidence suggests that the flow of CSF between the intracranial SAS and the ON-SAS is neither continuous nor bidirectional [8, 10]. CSF is produced primarily by the choroid plexus epithelium, but also by the meningoepithelial cells (MECs) that line the surface of the SAS [14]. MECs are seen at the surface of the ON-SAS, as well as of the brain. MECs have been reported to participate in the production of CSF-related proteins [15, 16], whereas it remains unclear whether CSF is produced in the ON-SAS. Furthermore, the drainage mechanisms of the CSF in the ON-SAS are not well understood. Among the candidate outflow routes from the ON-SAS, drainage via lymphatic vessels has been reported to be a powerful new concept that has demonstrated a great capacity for CSF outflow from the CNS [8, 9]. In addition, it has been reported that the anatomy and the arrangement of the trabeculae and septae in the ON-SAS offer the possibility of a one-way valve mechanism [7, 9].

In our cases, CSF congestion in the ON-SAS was observed, while the CSF influx into the ON-SAS from the intracranial SAS should have been blocked. Therefore, we consider there to be three possible mechanisms responsible for the CSF congestion observed in our cases (Fig. 2):

1. There may be a one-way valve mechanism that causes local CSF entrapment, as well as a reduced influx of CSF into the ON-SAS, and/or
2. The tumors may have blocked the transmission of pulsatile CSF waveforms, leading to decreased CSF absorption at the lymphatic vessels, and/or
3. Continuous CSF production from the MECs in the ON-SAS was present.

Further investigations into the ON-SAS may provide further insights into CSF dynamics.

Conflict of Interest We declare that we have no conflict of interest.

References

1. Garrity JA, Trautmann JC, Bartley GB, Forbes G, Bullock JD, Jones TW Jr, Waller RR (1990) Optic nerve sheath meningoceles. Clinical and radiographic features in 13 cases with a review of the literature. Ophthalmology 97:1519–1531
2. Geeraerts T, Newcombe VF, Coles JP, Abate MG, Perkes IE, Hutchinson PJ, Outtrim JG, Chatfield DA, Menon DK (2008) Use of T2-weighted magnetic resonance imaging of the optic nerve sheath to detect raised intracranial pressure. Crit Care 12:R114
3. Jaggi GP, Harlev M, Ziegler U, Dotan S, Miller NR, Killer HE (2010) Cerebrospinal fluid segregation optic neuropathy: an experimental model and a hypothesis. Br J Ophthalmol 94:1088–1093
4. Jinkins JR (1987) Optic hydrops: isolated nerve sheath dilation demonstrated by CT. AJNR Am J Neuroradiol 8:867–870
5. Killer HE, Mironov A, Flammer J (2003) Optic neuritis with marked distension of the optic nerve sheath due to local fluid congestion. Br J Ophthalmol 87:249
6. Killer HE, Laeng HR, Flammer J, Groscurth P (2003) Architecture of arachnoid trabeculae, pillars, and septa in the subarachnoid space of the human optic nerve: anatomy and clinical considerations. Br J Ophthalmol 87:777–781
7. Killer HE, Jaggi GP, Flammer J, Miller NR, Huber AR (2006) The optic nerve: a new window into cerebrospinal fluid composition? Brain 129:1027–1030
8. Killer HE, Jaggi GP, Flammer J, Miller NR, Huber AR, Mironov A (2007) Cerebrospinal fluid dynamics between the intracranial and the subarachnoid space of the optic nerve. Is it always bidirectional? Brain 130:514–520
9. Killer HE, Jaggi GP, Miller NR, Flammer J, Meyer P (2008) Does immunohistochemistry allow easy detection of lymphatics in the optic nerve sheath? J Histochem Cytochem 56:1087–1092
10. Killer HE, Jaggi GP, Miller NR, Huber AR, Landolt H, Mironov A, Meyer P, Remonda L (2011) Cerebrospinal fluid dynamics between the basal cisterns and the subarachnoid space of the optic nerve in patients with papilloedema. Br J Ophthalmol 95:822–827
11. Lunardi P, Farah JO, Ruggeri A, Nardacci B, Ferrante L, Puzzilli F (1997) Surgically verified case of optic sheath nerve meningocele: case report with review of the literature. Neurosurg Rev 20:201–205

12. Mashima Y, Oshitari K, Imamura Y, Momoshima S, Shiga H, Oguchi Y (1996) High-resolution magnetic resonance imaging of the intraorbital optic nerve and subarachnoid space in patients with papilledema and optic atrophy. Arch Ophthalmol 114:1197–1203
13. Mesa-Gutiérrez JC, Quiñones SM, Ginebreda JA (2008) Optic nerve sheath meningocele. Clin Ophthalmol 2:661–668
14. Pollay M (2010) The function and structure of the cerebrospinal fluid outflow system. Cerebrospinal Fluid Res 7:9
15. Urade Y, Kitahama K, Ohishi H, Kaneko T, Mizuno N, Hayaishi O (1993) Dominant expression of mRNA for prostaglandin D synthase in leptomeninges, choroid plexus, and oligodendrocytes of the adult rat brain. Proc Natl Acad Sci U S A 90: 9070–9074
16. Xin X, Fan B, Flammer J, Miller NR, Jaggi GP, Killer HE, Meyer P, Neutzner A (2011) Meningothelial cells react to elevated pressure and oxidative stress. PLoS One 6:e20142

Assessment of Brain Compliance Using ICP Waveform Analysis in Water Intoxication Rat Model

Kotaro Oshio, Hidetaka Onodera, Masashi Uchida, Yuichiro Tanaka, and Takuo Hashimoto

Abstract Intracranial pressure (ICP) monitoring has been used widely for patients with intracranial hypertension. However, the data of mean ICP do not reflect various brain conditions correctly. Therefore, we performed ICP waveform analysis to assess brain compliance. Data for ICP waveform analysis were obtained by stereotactic intraventricle puncture. ICP waveform is expressed as a three-phase wave. Analyzed differential waveforms in a water intoxication model and continuous infusion models were evaluated respectively. In the water intoxication models, the second wave (P2) known to reflect compliance is elevated. ICP waveform analysis will be valuable for the assessment of the pathological condition of the brain.

Keywords Intracranial pressure waveform • Compliance • Water intoxication

Presentation The 15th International Symposium of Brain Edema and Cellular Injury, October 22–24, 2011, Tokyo, Japan

Introduction

Intracranial pressure (ICP) monitoring is useful for the treatment of patients with intracranial hypertension. It is important, especially in patients with severe head injury. However, we cannot estimate the pathophysiology of intracranial hypertension only with mean ICP. Therefore, we have to perform a variety of other monitoring and radiological imaging procedures to understand the pathophysiology. Intracranial hypertension involves not only the intracranial space-occupying lesion, but also several types of brain edema. Cerebral edema can be divided into intracellular edema (cytotoxic and osmotic) and extracellular edema (vasogenic and interstitial). If we could correctly diagnose the type of cerebral edema, we would be able to choose the appropriate treatment. We hypothesized that intracranial compliance might reflect the type of brain edema. ICP waveform (ICPWF) analysis has been well studied, but has not been used in clinical practice. ICPWF has three fairly consistent components. The initial components of the pulse wave (P1) originate at the choroid plexus and large intracranial conductive vessels, while the second component (P2) is known to reflect variations in cerebral bulk compliance [1, 2, 5, 7]. In this study, we tried to assess the intracranial compliance using ICPWF analysis in a water intoxication rat model.

K. Oshio, MD, PhD (✉), H. Onodera, MD, M. Uchida, MD, Y. Tanaka, MD, PhD, and T. Hashimoto, MD, PhD
Department of Neurosurgery, St. Marianna University School of Medicine, Higashi-Bldg. 2F 2-16-1 Sugao Miyamae-ku, Kawasaki, Kanagawa 216-8511, Japan
e-mail: koshio@marianna-u.ac.jp

Materials and Methods

Materials

Eight male Sprague–Dawley rats were used at 60 weeks old (weight range: 880–1,040 g).

All experiments were performed on male wild-type and AQP1-deficient littermates. All protocols were approved by St. Marianna University School of Medicine, Committee on Animal Research.

Intracranial Pressure Measurement and Continuous Infusion Method

The constant-rate infusion method using rats originally described by Davson et al. [3] was used. Rats were anaesthetized with 2,2,2-tribromoethanol (0.5 mg/g body weight i.p.; Aldrich, Milwaukee, WI, USA) and immobilized in the prone

Y. Katayama et al. (eds.), *Brain Edema XV*, Acta Neurochirurgica Supplement, Vol. 118,
DOI 10.1007/978-3-7091-1434-6_41,

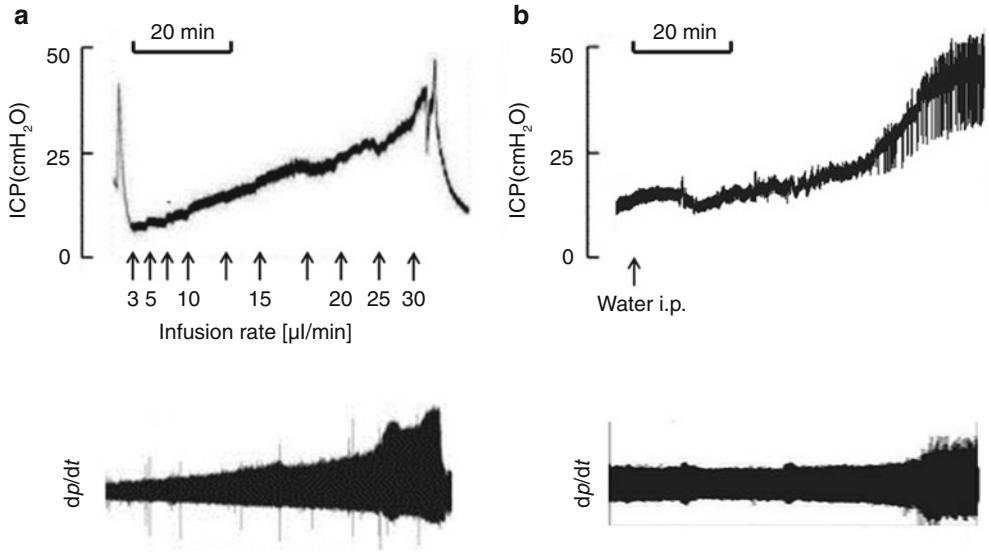

Fig. 1 Continuously infused rats (**a**) and water-intoxicated rats (**b**) were compared in terms of intracranial pressure (ICP; *top*) and differential analysis of the intracranial pressure waveform (ICPWF; d*p*/d*t*; *bottom*). The infusion rate was transiently increased to 30 μL/min (*arrows*) resulting in a step-wise increase in ICP. The d*p*/d*t* data at higher ICPs demonstrate an increase in a continuous infused rat and a stable response in a water-intoxicated rat. Low and high ICP points are indicated (*arrows*) in the figure

position in a stereotaxic device (Natsume, Tokyo, Japan). Body temperature was monitored and maintained at 38 °C using a warming pad. A dorsal midline incision was made over the skull and the upper cervical spine and the cranial sutures were exposed. A burr-hole 1-mm in diameter was drilled into the right parietal bone above the right lateral ventricle, using coordinates 1.5 mm lateral and 0.8 mm caudal to the bregma. The 27-gauge needle was connected using short noncompliant tubing to a pressure transducer (TSD104A; Biopac Systems, Santa Barbara, CA, USA) interfaced to a recording system (model MP100; Biopac Systems). This circuit also permits the introduction of artificial CSF, Artcereb® (Otsuka Pharmacenntical, Tokushima, Japan) using a Harvard syringe pump (KD Scientific, New Hope, PA, USA) driving a gas-tight glass Hamilton syringe. The needle was introduced into the lateral ventricle using a stereotaxic manipulator in order to obtain consistent ICP measurements according to a procedure described previously [6]. During the left lateral ventricle perfusion with CSF, the ICP wave was monitored continuously. The infusion rate was transiently increased from 5 to 30 μL/min. The ICP gradually increased and reached a steady-state (Fig. 1a).

Water Intoxication Model

Water intoxication was induced in age and weight-matched SD rats ($n=4$) by intraperitoneal infusion of distilled water (40 mL). Following water loading, water-intoxicated rat showed a gradual increase in ICP to nearly 50 mmHg. ICP waveform was recorded until a steady-state was achieved.

Intracranial Pressure Waveform Analysis

Intracranial elastance is represented by d*p*/d*v*. The differential (d*p*/d*t*=*E*·d*v*/d*t*) curve of ICP was calculated by a pressure processor (AcqKnowledge software; Biopac Systems) and originally described by Hashimoto et al. [4]. Three positive peaks (U1, U2, U3) were shown in the d*p*/d*t* curve corresponding to three ICP-pulse wave peaks. Each d*p*/d*t* represents the maximum rate of change in the ICP pulse pressure in one cardiac cycle (Fig. 2a).

Results

Figure 1a shows an ICP waveform and d*p*/d*t* recording in a continuous infused rat. ICP increased with the increasing infusion rate. With an increase in ICP, the d*p*/d*t* also increased gradually. Figure 2b, which is from a water intoxicated rat, also shows that the ICP increased gradually after the injection of distilled water. As the ICP rose above 25 cmH_2O, b-waves were observed frequently. The d*p*/d*t* of the water intoxication model did not show an increase accompanied by an increased ICP until b-waves appeared. Figure 2 demonstrates a detail of the ICP pulse waveform (top), ECG (electrocardiogram) (middle), and d*p*/d*t* curve (bottom). Water-intoxicated rats (b) showed an increase in the U2 pulse compared with continuously infused rats (a). This was dependent on ICP magnitude.

Conclusion

The aim of this experiment was to examine whether or not the ICPWF analysis was able to assess intracranial compliance. We compared the water intoxication model (intracellular edema) and continuous infusion model (extracellular edema). The result revealed differences in ICPWF between the two models.

The water intoxication model causes osmotic edema known as intracellular edema. In this model, P2 and U2 had

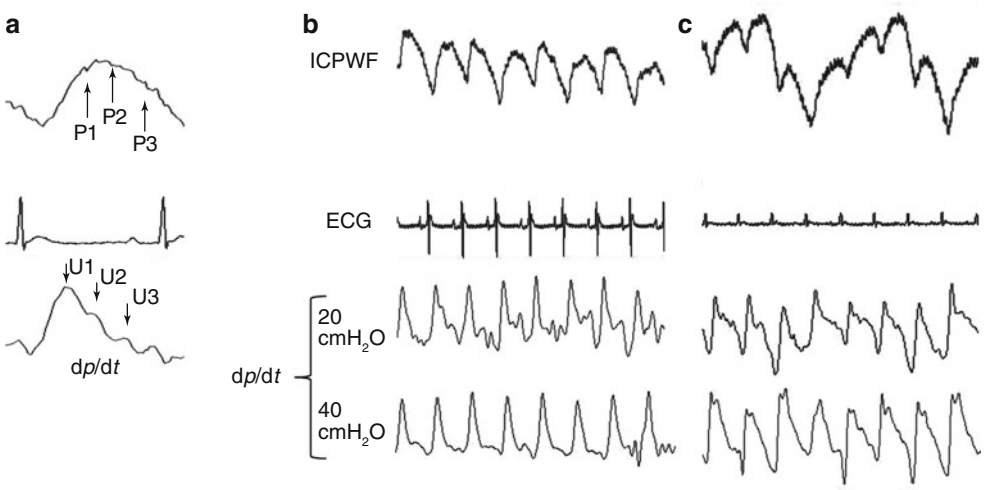

Fig. 2 The ICP pulse waveforms and d*p*/d*t* curves generated at the low ICP and high ICP were compared in continuously infused rats (**b**) and water-intoxicated (**c**) rats. (**a**) Graphs demonstrating the interrelationship of the ICP pulse waveform (*top*), electrocardiogram (*ECG*; *middle*), and *dp/dt* curve (*bottom*). A water-intoxicated rat (**c**) showed an increase in the U2 pulse compared with continuously infused rat (**b**). This was dependent on ICP magnitude

increased clearly as expected. As has been previously reported [1, 2, 5, 7], P2 reflects variations in the cerebral bulk compliance, including brain substance, cerebrospinal fluid, and the cerebrovascular capacity. The water intoxication model has shown that water moves into cells by osmotic pressure gradient, which causes cell swelling. Therefore, these results indicate that intracranial compliance decreased because of the cellular edema. On the other hand, P1 and U1 were elevated, but P2 and U2 were not in the infusion model.

These results suggest that ICPWF might contain information for the estimation of the compliance of the brain. Furthermore, there is the potential that ICPWF analysis will be a new monitoring method for diagnose and selection of the appropriate treatment for cerebral edema. We need to understand more about ICPWF in another type of brain edema.

In summary, the difference in ICPWFs was observed between the two edematous brain conditions, osmotic edema and interstitial edema, even under equivalent ICP. These results indicate that ICPWF analysis will provide us with more useful information on intracranial pathological conditions.

Acknowledgments This study was supported in part by the Research Committee of Normal Pressure Hydrocephalus and Related Disorders, Study on the Etiology, Pathogenesis and Therapy from the Ministry of Health, Labor and Welfare of Japan.

Conflict of Interest We declare that we have no conflict of interest.

References

1. Avezaat CJ, van Eijndhoven JHM (1986) Clinical observations on the relationship between cerebrospinal fluid pulse pressure and intracranial pressure. Acta Neurochir (Wien) 79:13–29
2. Cardoso ER, Rowan JO, Galbraith S (1983) Analysis of the cerebrospinal fluid pulse wave in intracranial pressure. J Neurosurg 59: 817–821
3. Davson H, Hollingsworth G, Segal M (1970) The mechanism of drainage of the cerebrospinal fluid. Brain 93:665–678
4. Hashimoto M, Higashi S, Kogure Y, Fujii H, Tokuda K, Ito H, Yamamoto S (1988) Intracranial pressure pulse waveform and its dp/dt analysis of plateau waves. Intracranial pressure VII. Springer, Berlin/Heidelberg/New York, pp 367–371
5. Hashimoto M, Higashi S, Tokuda K, Yamamoto Y, Yamashita J (1991) Changes of intracranial pressure and pulse wave form induced by various mechanical stresses upon intracranial hemodynamics. Intracranial pressure VIII. Springer, Berlin/Heidelberg/New York, pp 367–371
6. Oshio K, Watanabe H, Song Y, Verkman AS, Manley GT (2005) Reduced cerebrospinal fluid production and intracranial pressure in mice lacking choroid plexus water channel Aquaporin-1. FASEB J 19:76–78
7. Portnoy HD, Chopp M, Branch C, Shannon MB (1982) Cerebrospinal fluid pulse wave form as an indicator of cerebral autoregulation. J Neurosurg 56:666–678

Neuromonitoring with Microdialysis in Severe Traumatic Brain Injury Patients

Jose J. Sanchez, Carlos J. Bidot, Kristine O'Phelan, Shyam Gajavelli, Shoji Yokobori, Stephen Olvey, Jonathan Jagid, Jose Alberto Garcia, Zsuzsanna Nemeth, and Ross Bullock

Abstract *Background*: Neuromonitoring with microdialysis has the potential for early detection of metabolic derangements associated with TBI. *Methods*: 1,260 microdialysis samples from 12 TBI patients were analyzed for glucose, lactate, pyruvate, lactate/pyruvate ratio (LPR), and lactate/glucose ratio (LGR). Analytes were correlated with the Glasgow Coma Scale (GCS) before surgery and with the Glasgow Outcome Scale (GOS) at the time of discharge. The patients were divided into two groups for GCS: 3–6 and 7–9, and for GOS 1–3 and 4–5. Chi-squared test was performed for correlations. *Results*: Glucose, lactate levels, and LGR were high in TBI patients with GCS 3–6 ($p<0.0001$). Pyruvate level was lower in patients with GCS 7–9 ($p<0.001$). LPR was higher in patients with GCS 3–6 ($p<0.05$). High glucose, lactate level ($p<0.001$), and LPR ($p<0.01$) was observed in patients with GOS 1–3. Pyruvate level was low in patients with GOS 1–3 ($p<0.001$). LGR was higher in patient with better outcome (GOS 4–5). *Conclusion*: After craniotomy extracellular glucose and lactate were good "biomarkers" of cerebral damage in TBI patients. We consider that high extracellular lactate and low glucose is an indicator of severe neurological damage and poor outcome, because of impaired brain metabolism.

Abbreviations

GCS	Glasgow Coma Scale
GOS	Glasgow Outcome Scale
HIE	Hypoxic ischemic encephalopathy
LGR	Lactate/glucose ratio
LPI	Lactate/pyruvate index
LPR	Lactate/pyruvate ratio
PET	Positron emission tomography
SDs	Spreading depolarizations
TBI	Traumatic brain injury

J.J. Sanchez, C.J. Bidot, K. O'Phelan, S. Gajavelli, S. Yokobori, S. Olvey, J. Jagid, J.A. Garcia, Z. Nemeth, and R. Bullock, MD, PhD (✉)
Neurointensive Care Unit, Jackson Memorial Hospital, University of Miami Miller School of Medicine, 1095 NW 14th Terrace, LPLC D4-6, Miami, FL 33136, USA
e-mail: rbullock@med.miami.edu

Introduction

Traumatic brain injury is a major cause of long-term disability with significant social and economic consequences. It is known that outcome following a severe TBI is related to the initial characteristics of injury, reflecting its severity, such as the Glasgow Coma Scale. Outcomes are also related to ongoing patho-physiological processes and secondary insults. The detection of these secondary events remains a major target of neuromonitoring and an area of ongoing research. Monitoring of cerebral extracellular chemistry with microdialysis has the potential for early detection of metabolic derangements associated with such events.

Materials and Methods

Prospectively collected observational neuromonitoring data from 12 TBI patients were analyzed. Monitoring included microdialysis markers: glucose, lactate, pyruvate, and lactate–pyruvate ratio. Outcome was assessed using the Glasgow Outcome Scale (GOS) at discharge. We collected in total 1,260 microdialysis samples from these patients.

Correlation of these metabolites was performed with the Glasgow Coma Scale (GCS) before surgery and the Glasgow Outcome Scale (GOS) at the time of discharge. For the statistical analyses the patients were divided into two groups: patients with GCS 3–6 and 7–9, and for GOS 1–3 and 4–5. Chi-Squared test was performed for correlations.

Y. Katayama et al. (eds.), *Brain Edema XV*, Acta Neurochirurgica Supplement, Vol. 118,
DOI 10.1007/978-3-7091-1434-6_42,

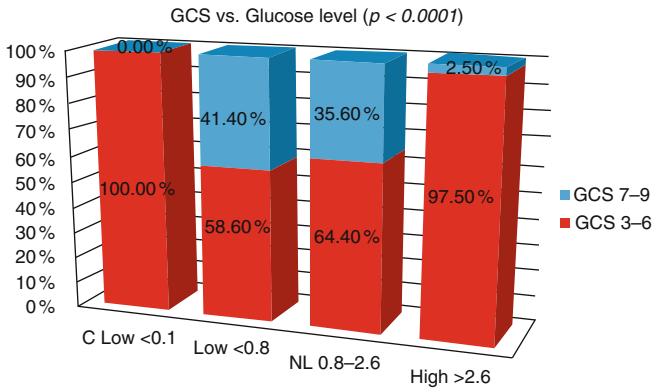

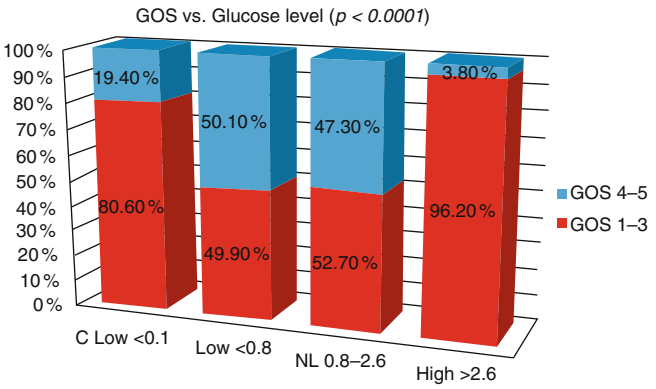

Fig. 1 Relative frequencies of extracellular brain glucose microdialysis sample levels during the first week after decompressive craniectomy categorized as critically low, low, normal, and high levels versus patients' Glasgow Coma Scale (*GCS*) score before surgery and Glasgow Outcome Scale (*GOS*) score at the moment of discharge from hospital

Biomarkers reference levels were as follows:

Glucose: *C* Low <0.1, Low <0.8, NL 0.8–2.6 and High >2.6.
Lactate: NL <4, High ≥ 4 and C High ≥ 8.9.
Pyruvate: *C* Low < 31, Low <120, NL ≥ 120.
LPR: NL < 25, High > 25, *C* High > 45.
LGR: NL < 10, High > 10.

Results

Of 12 patients, there were 2 female and 10 male, the median age was 38 (range 18–70). 58.4 % had a bad outcome (BO) at discharge and 41.6 % had a good outcome.

Glucose, lactate levels, and LGR were high in TBI patients with GCS 3–6 ($p < 0.0001$) (Figs. 1 and 2). Pyruvate level was lower in patients with GCS 7–9 ($p < 0.001$). LPR was high in patients with GCS 3–6 ($p < 0.05$).

When we compared the biochemical markers between patients with good versus bad outcome we found that: high glucose, lactate level ($p < 0.001$), and LPR ($p < 0.01$) were observed in patients with GOS 1–3 (Fig. 1) and the pyruvate level was low in patients with GOS 1–3 ($p < 0.001$). LGR was higher in patients with a better outcome (GOS 4–5; Fig. 2).

Discussion

Glucose Metabolism (Glucose and LGR)

The metabolic state of the traumatically injured brain should be defined differentially in terms of *glucose* and *oxygen* metabolism. Glucose is the predominant cerebral energetic compound, fueling both neurons and astrocytes [1].

The majority of low glucose values are related primarily to the brain trauma rather than substrate limitation or ischemia.

Lower extracellular cerebral glucose appears not to be related to hypoglycemia. There was a low incidence of hypoglycemia in this data set, minimizing the frequency of episodes and the potential impact of reduced cerebral glucose on outcome.

In TBI patients, it is documented that glucose is metabolized to both lactate and pyruvate without signs of anaerobic metabolism, which is reflected by unchanged LPR [5] The calculated LGR is a marker of increased glycolysis.

Low glucose concentrations are associated with increased hyperglycolysis in ongoing cellular injury (*penumbra*, Fig. 3) despite the absence of ischemia (defined by decreased CBF measurements and increases in the LPR).

Regional and global hyperglycolysis during the initial 5 days post-injury has been documented [6]. The initial intent of measuring extracellular glucose in a continuous fashion has been to use this as a surrogate marker for glucose utilization.

Another explanation for low extracellular glucose is increased glycolysis, i.e., glucose utilization and lactate production in astrocytes [7].

Low Glucose (≥0.2 mM and 1.5 nM) Versus Extremely Low Glucose (<0.2 mM)

Using a glucose threshold of less than 0.2 mmol, Vespa et al. [4] found that the majority of episodes of low glucose levels occur *independently* of overt secondary clinical insults (i.e., ischemia or cerebral hypoxia) and independent of changes in systemic glucose levels. Persistent extreme

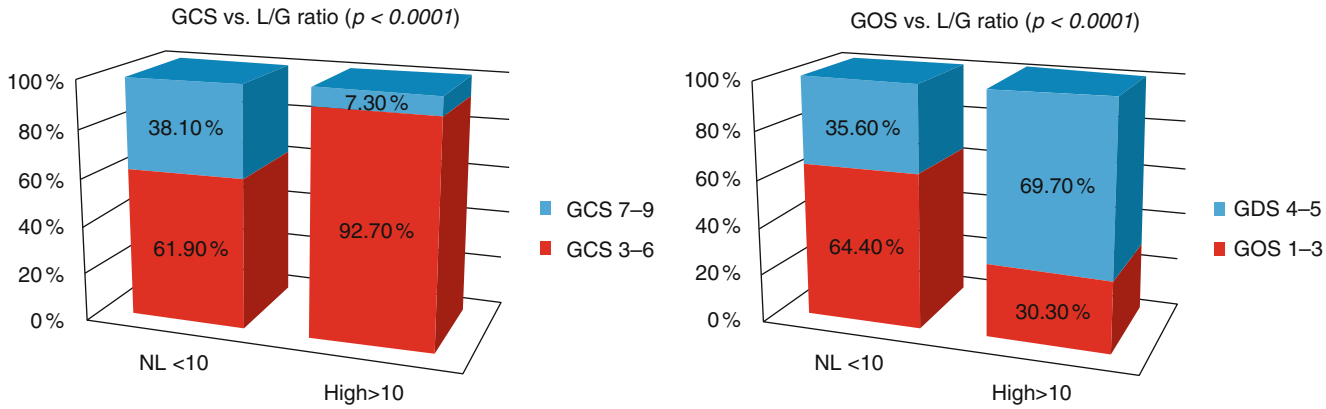

Fig. 2 Microdialysis sample levels during the first week after decompressive craniectomy. Relative frequencies of normal and high lactate/glucose ratio versus patients' GCS score before surgery and GOS score at the moment of discharge from hospital

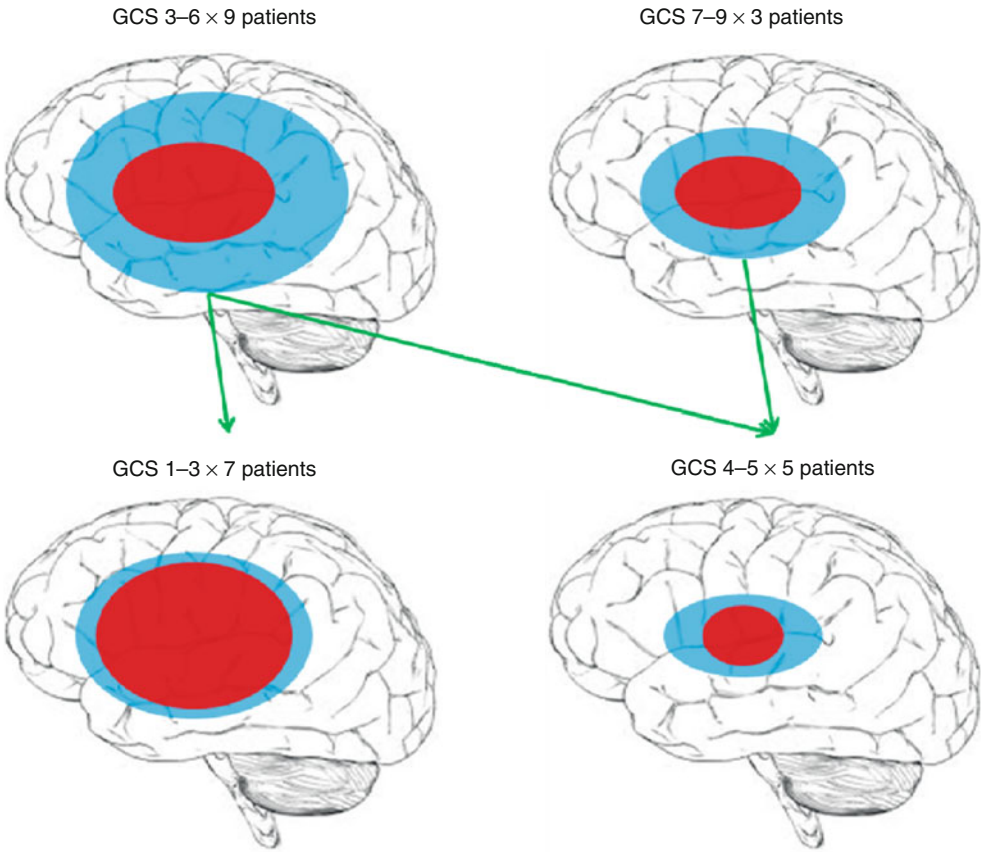

Fig. 3 Hypothetical relationships between the areas of damage (core vs. penumbra) in severe TBI. Core related to high extracellular glucose and penumbra with a high lactate/glucose ratio

low extracellular glucose levels (<0.2 mmol/L for greater than 20 % of the time) correlated independently with a poor outcome at 6 months. This finding may suggest an effect of the duration of low glucose levels on later brain function and not simply the severity of the primary injury alone. Given the relationship between regional glucose utilization and glucose values below the 0.2-mmol/L threshold, these data may also suggest an increase in glucose utilization during the acute post-injury period. The high concurrence of elevated glutamate with low glucose levels and the uniform reduction in oxidative metabolism are suggestive of hyperglycolysis. The occurrence of very low glucose level and elevated lactate/pyruvate ratio) was infrequent in this study. Given that low levels of glucose are uniformly

associated with increased glycolysis, that low glucose values do occur in conjunction with all cases of documented hyperglycolysis in this series of patients, and that low glucose is simultaneously associated with increased glutamate over 90 % of the time, it is tempting to speculate that continued hyperglycolysis is responsible for the majority of the low microdialysis glucose values reported herein.

Persistent very low levels of glucose (<0.1 mmol/L) appear to be a function of limited glucose supply caused by ischemia in only a few patients with herniation syndrome in: terminal events or the first 48 h after decompressive craniectomy. Substrate (e.g., glucose) limitation occurs with herniation syndrome events that correlated with patients with more severe brain damage and poor outcome (Fig. 1).

Oxygen Metabolism (Lactate, Pyruvate, and LPR)

Increased lactate and LPR were frequent findings after decompressive craniotomy in severe acute TBI.

Lactate and the LPR are two hypoxia markers widely used to detect brain tissue hypoxia/ischemia. These two markers have a more complex behavior than expected as they can be abnormally high in circumstances with no detectable brain hypoxia in patients with acute traumatic brain injury. This condition must be considered in the differential diagnosis because it also reflects an alteration of brain energy metabolism. For this reason a hypoxia/ischemia event needs confirmation by other means, e.g., $PbtO_2$ and Hemedex (CBF).

The lactate/pyruvate ratio reflects the equilibrium of the lactate dehydrogenase (LDH) reaction. During ischemia and hypoxia there is a rapid shift in the LDH equilibrium and the ratio increases to very high levels because of either:

1. A simultaneous increase in lactate and a decrease in pyruvate (ischemia, hypoxia with relative ischemia) or
2. A pronounced increase in lactate and a moderate increase in pyruvate (pure hypoxia)

Lactate alone is insufficient as a marker of brain hypoxia/ischemia. Increased extracellular lactate resulting from:

1. Exaggerated substrate supply, i.e., hyperglycemia [8],
2. Impaired enzymatic function, or structural and functional mitochondrial damage with a subsequent shift from oxidative/aerobic to non-oxidative
3. Hypoxia/ischemia events inducing anaerobic glycolysis [9].

Vespa et al. [10], comparing the LPR with PET for metabolism of glucose and oxygen, concluded that TBI leads to a state of persistent metabolic crisis as reflected by an abnormal increase in cerebral microdialysis LPR that is not related to hypoxia/ischemia.

Merino et al. [11] found increased lactate and LPR in most cases of TBI and they were not related to episodes of brain tissue hypoxia. Furthermore, the concordance between the two biomarkers to classify metabolic dysfunction was weak. They recommend that LPR and lactate should not be used alone in everyday clinical practice because of the weak correlation between these two markers, the difficulty in their interpretation, and the heterogeneous and complex nature of the pathophysiology. Other differential diagnoses apart from tissue hypoxia should always be considered when high lactate and/or LPR are detected in the acute injured brain.

The LGR appears to be a marker of brain tissue at risk of progressing to permanent cell loss, but which is still viable and able to metabolize glucose to lactate (*penumbra* area; Fig. 3).

Conclusion

In summary, glucose and LGR seem to be a more sensitive indicator of change, specifically in TBI as opposed to secondary ischemia. These biomarker measurements may be of more value in the neuro-intensive care unit, specifically in the trauma patient as opposed to the ischemia patient.

After craniotomy extracellular glucose appears to be a good “biomarker” for monitoring brain tissue integrity. LGR seems to be related to brain metabolism of the viable tissue able to metabolize glucose to lactate (penumbra).

Conflict of Interest We declare that we have no conflict of interest.

References

1. Zielke HR, Zielke CL, Baab PJ (2009) Direct measurement of oxidative metabolism in the living brain by microdialysis: a review. J Neurochem 109(Suppl 1):24–29
2. Goodman JC, Valadka AB, Gopinath SP, Uzura M, Robertson CS (1999) Extracellular lactate and glucose alterations in the brain after head injury measured by microdialysis. Crit Care Med 27(9):1965–1973
3. Goodman JC, Valadka AB, Gopinath SP, Uzura M, Robertson CS (1999) Extracellular lactate and glucose alterations in the brain after head injury measured by microdialysis. Crit Care Med 27(9):1965–1973
4. Vespa PM, McArthur D, O’Phelan K, Glenn T, Etchepare M, Kelly D et al (2003) Persistently low extracellular glucose correlates with poor outcome 6 months after human traumatic brain injury despite a lack of increased lactate: a microdialysis study. J Cereb Blood Flow Metab 23(7):865–877
5. Hutchinson PJ, O’Connell MT, Seal A, Nortje J, Timofeev I, Al-Rawi PG et al (2009) A combined microdialysis and FDG-PET

study of glucose metabolism in head injury. Acta Neurochir (Wien) 51(1):51–61; discussion 61. Epub 2008 Dec 20
6. Bergsneider M, Hovda DA, Shalmon E, Kelly DF, Vespa PM, Martin NA et al (1997) Cerebral hyperglycolysis following severe traumatic brain injury in humans: a positron emission tomography study. J Neurosurg 86(2):241–251
7. Pellerin L, Magistretti PJ (1994) Glutamate uptake into astrocytes stimulates aerobic glycolysis: a mechanism coupling neuronal activity to glucose utilization. Proc Natl Acad Sci USA 91(22):10625–10629
8. Diaz-Parejo P, Stahl N, Xu W, Reinstrup P, Ungerstedt U, Nordstrom CH (2003) Cerebral energy metabolism during transient hyperglycemia in patients with severe brain trauma. Intensive Care Med 29(4):544–550
9. Hlatky R, Valadka AB, Goodman JC, Contant CF, Robertson CS (2004) Patterns of energy substrates during ischemia measured in the brain by microdialysis. J Neurotrauma 21(7):894–906
10. Vespa P, Bergsneider M, Hattori N, Wu HM, Huang SC, Martin NA et al (2005) Metabolic crisis without brain ischemia is common after traumatic brain injury: a combined microdialysis and positron emission tomography study. J Cereb Blood Flow Metab 25(6):763–774
11. Merino MA, Sahuquillo J, Borrull A, Poca MA, Riveiro M, Exposito L (2010) Is lactate a good indicator of brain tissue hypoxia in the acute phase of traumatic brain injury? Results of a pilot study in 21 patients. Neurocirugia (Astur) 21(4):289–301

Monitoring of Brain Tissue Perfusion Utilizing a Transducer Holder for Transcranial Color Duplex Sonography

Toshiyuki Shiogai, Mari Koyama, Mayumi Yamamoto, Hifumi Hashimoto, Kenji Yoshikawa, and Masanori Nakagawa

Abstract *Objective*: We have improved a transducer holder for transcranial color duplex sonography (TCDS) monitoring via both the temporal and foraminal windows (TW/FW). The objective is to clarify the clinical usefulness of and identify problems with TCDS monitoring in the evaluation of brain tissue perfusion.

Methods: Brain tissue perfusion was monitored in 11 patients (ages 31–94, mean 66). After an intravenous bolus, power modulation imaging (PMI) in all cases and second harmonic imaging (SHI) in two cases were evaluated at the diencephalic horizontal plain via bilateral (6 cases) and unilateral (5 cases) TWs. After a transducer was installed into the holder, acetazolamide (ACZ) cerebral vasoreactivity utilizing PMI was evaluated in ten cases.

Results: PMI proved superior to SHI in the quantitative evaluation of the bilateral hemispheres via the unilateral TWs. Brain tissue perfusion could be precisely quantified before/after ACZ in the same regions of interest (ROI). All patients could be monitored continuously by one examiner. Fixed-probe shifts during monitoring were easily readjustable. Owing to re-fixation for contra-lateral TW monitoring, it was not possible to evaluate precisely in the same ROIs.

Conclusion: TCDS monitoring succeeds in continuously and quantitatively evaluating precise and reproducible intracranial hemodynamics in the brain tissue.

T. Shiogai, MD, PhD (✉), M. Koyama, M. Yamamoto, and H. Hashimoto
Department of Clinical Neurosciences, Kyoto Takeda Hospital, Minamikinuta-cho 11, Nishinanajo, Shimogyo-ku, Kyoto 600-8884, Japan
e-mail: shiogait@pop11.odn.ne.jp

K. Yoshikawa, MD, PhD
Department of Stroke Medicine, Hoshigaoka Kouseinenkin Hospital, Kyoto, Japan
e-mail: byg10777@nifty.com

M. Nakagawa, MD, PhD
Department of Neurology, Kyoto Prefectural University of Medicine, Kyoto, Japan
e-mail: mnakagaw@koto.kpu-m.ac.jp

Keywords Transcranial color duplex sonography • Transducer holder • Brain tissue perfusion • Acetazolamide vasoreactivity • Second harmonic imaging • Power modulation imaging

Introduction

Compared with conventional transcranial Doppler sonography (TCD), transcranial color Duplex sonography (TCDS) is able to measure much more accurately on the basis of angle-collected velocities in the intracranial major vessels. Furthermore, TCDS is able to visualize intracranial lesions in stroke [11], severe head injury [14], and other neurological disorder cases [20]. Utilizing ultrasound contrast agents (UCA), TCDS has been able to evaluate brain tissue perfusion non-invasively, particularly in ischemic stroke patient investigations [8, 13]. Possibilities of quantitative measurements have been evaluated in an identical way to neuroradiological perfusion imaging, based on the bolus dye-dilution principle. However, quantitative reliability has not yet been established, owing to problems of skull- and depth-dependent ultrasound attenuation, shadowing effects, bubble saturation, and low data reproducibility (the latter due to UCA administration methods, transducer fixation, data analysis, etc.) [7, 13].

Transducer holders or probe fixation devices for conventional TCD monitoring have been introduced into clinical settings [1, 5–7]. However, a transducer holder for TCDS has yet to be clinically introduced. We have developed such a transducer holder (Sonopod) for TCDS monitoring via both windows (Fig. 1).

To overcome the inherent problems and establish the clinical significance of transcranial ultrasound perfusion imaging, we have introduced clinically the Sonopod for TCDS monitoring [16, 19] and evaluated acetazolamide (ACZ) vasoreactivity [15, 18]. The objective of this study is to clarify the clinical usefulness of and identify problems with TCDS-Sonopod monitoring in the evaluation of brain tissue perfusion.

Y. Katayama et al. (eds.), *Brain Edema XV*, Acta Neurochirurgica Supplement, Vol. 118,
DOI 10.1007/978-3-7091-1434-6_43, © Springer-Verlag Wien 2013

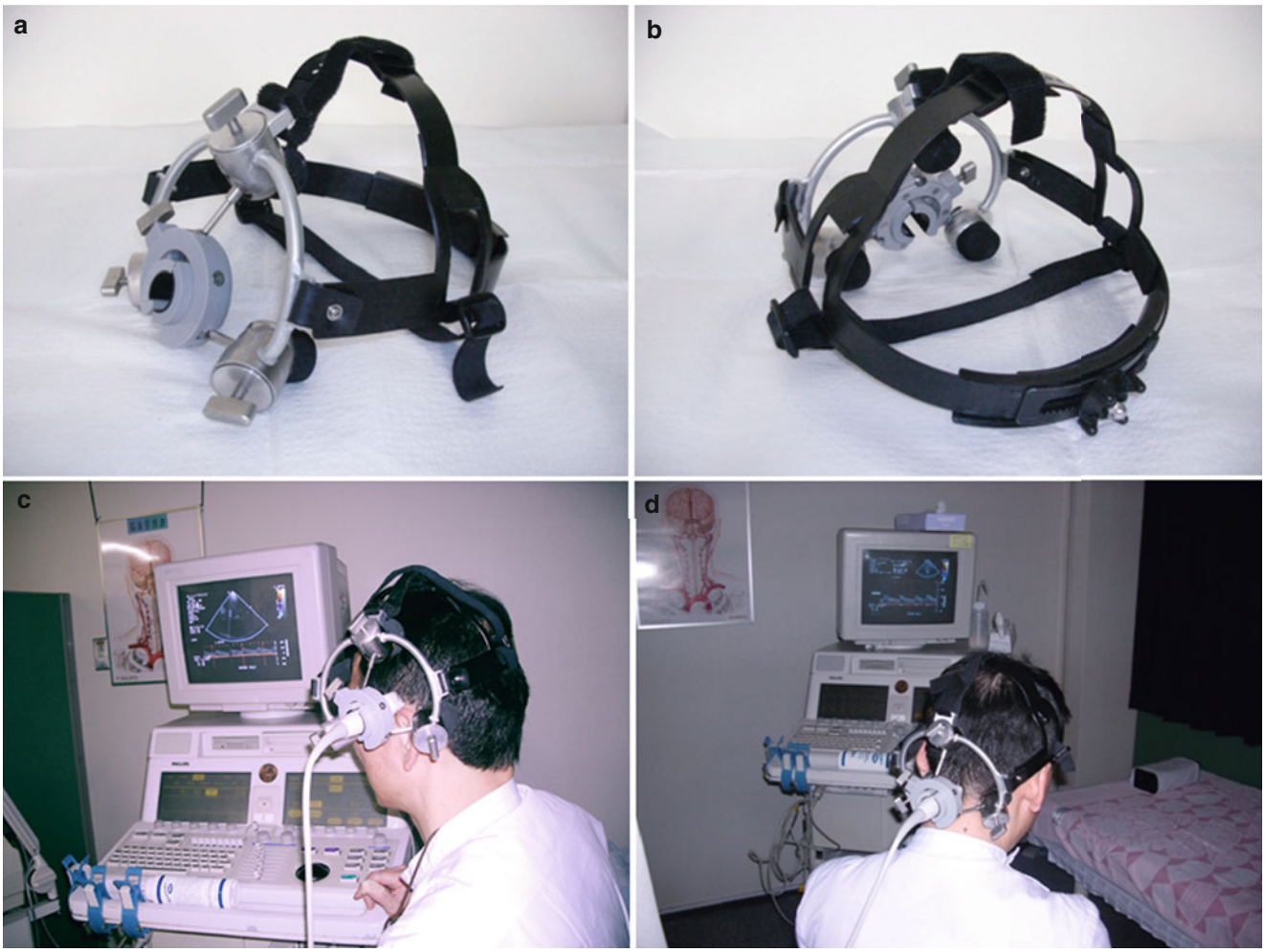

Fig. 1 We have developed and improved the transducer holder (Sonopod) for transcranial color duplex sonography (TCDS) monitoring. (**a**, **b**) via both the temporal window (TW; **c**) and the foraminal window (FW; **d**)

Materials and Methods

Brain tissue perfusion monitoring was evaluated in 11 patients (ages 31–94, mean 66). Details of patients' demographics are shown in Table 1. After injection of a 5-mL bolus of Levovist® (2.5 g, 400 mg/mL) via the antecubital vein, power modulation imaging (PMI) in all cases and second harmonic imaging (SHI) in the initial two cases were evaluated in the supine position via bilateral (6 cases) and unilateral (5 cases) temporal windows (TWs). Both imaging types were visualized by an integrated backscatter method. The transmitting and receiving frequencies of PMI and SHI were 1.7/1.7 MHz and 1.3/2.6 MHz respectively. The investigation depth was 16 cm with a focus of 8 cm. Settings were mechanical index 1.6, system gain 75, and compression 70. ACZ cerebral vasoreactivity, before and after 500 mg Diamox® intravenous injection, was evaluated in ten cases utilizing a SONOS5500 S3 transducer installed in the Sonopod. Time–intensity curves

Table 1 Patient demographics

Total patients	$N=11$
Causes of brain injury	
Cerebral infarction	8 (atherothrombotic 5, lacunar 2, embolic 1)
Hypertensive putaminal hemorrhage	1
Ruptured anterior communicating aneurysm	1
Chronic subdural hematoma	1
Age	31–94 years (mean 66)
Gender	Male 9, female 2
Monitoring (via temporal window)	Bilateral 6, unilateral 5
Perfusion imaging	
Power modulation imaging only	9
Second harmonic imaging and power modulation imaging	2
Acetazolamide vasoreactivity test	10 (30 TIC analyses)
TIC base-line drift during monitoring	4 (7 TIC analyses)

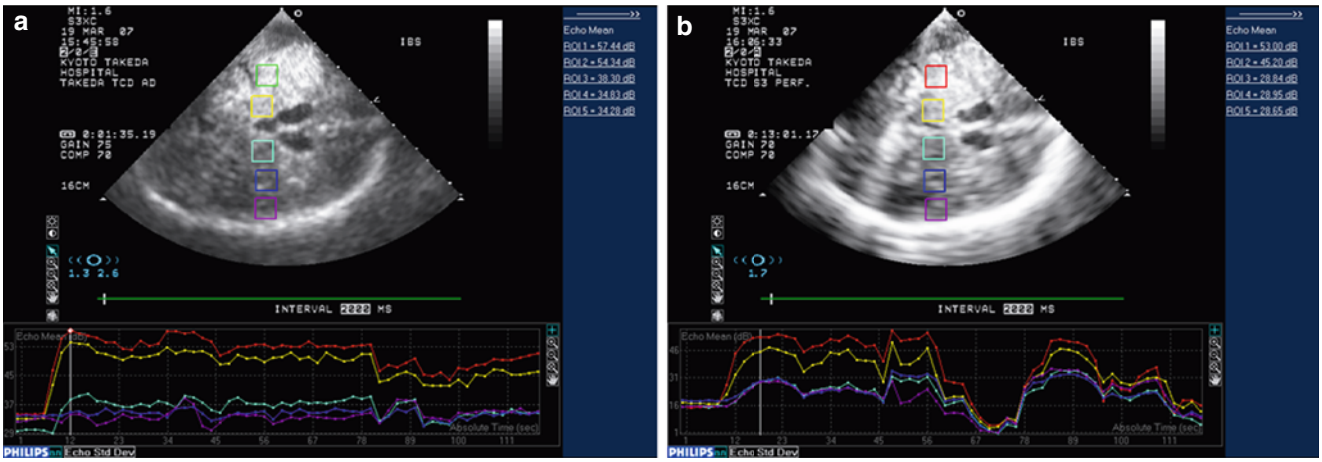

Fig. 2 Hand-held monitoring of brain tissue perfusion via the left TWs utilizing second harmonic imaging (SHI; **a**) and power modulation imaging (PMI; **b**) are depicted in a post-operative patient with an anterior communicating artery aneurysm. Time–intensity curves (TICs) derived from the five ROIs, placed in the bilateral basal ganglia (BG) and thalamus (Th), and contra-lateral TL, are shown in the *lower panels*. TICs drifted from the base-line and were unstable because of the patient's movements

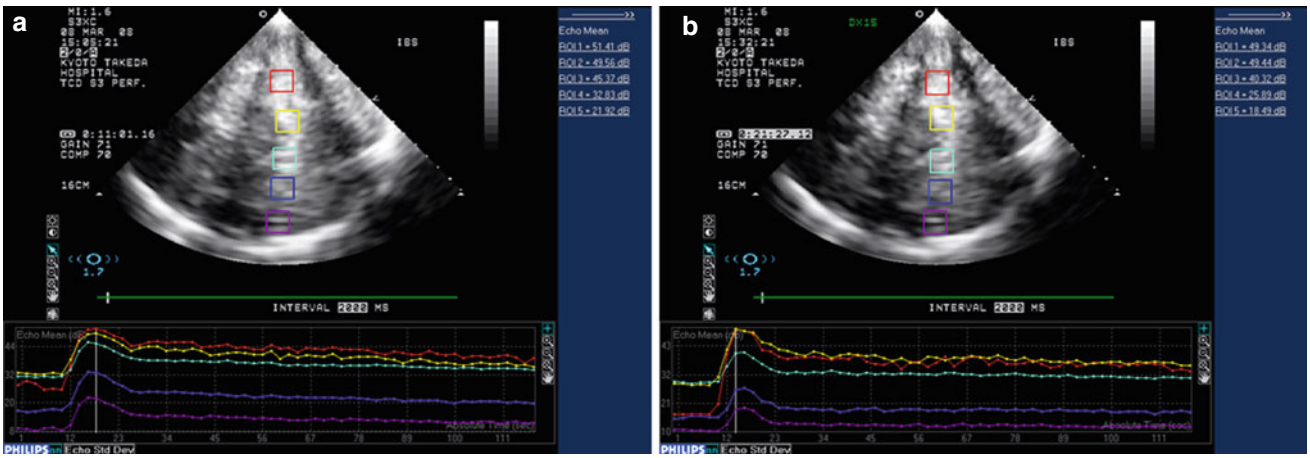

Fig. 3 Sonopod acetazolamide (ACZ) vasoreactivity test utilizing PMI. Sonopod monitoring of brain tissue perfusion via the right TWs utilizing PMI before (**a**) and after (**b**) ACZ administration is demonstrated in a post-operative patient with chronic subdural hematoma. TICs were stable during 10 min of monitoring

(TICs) on the diencephalic horizontal plain were evaluated before and after ACZ in five regions of interest (ROI): the bilateral basal ganglia (BG) and thalamus (Th), and the contra-lateral temporal lobe (TL). A total of 30 TICs with a duration of 10 min were analyzed before and after ACZ.

Results

Hand-Held Monitoring Utilizing PMI and SHI

Conventional SHI and PMI utilizing hand-held monitoring were compared in two cases. In the visualization of the contra-lateral hemispheres via the unilateral TWs, PMI was superior to SHI, as shown in the upper panels of Fig. 2. As shown in the lower panels of the quantitative TIC evaluations in both PMI and SHI, peak intensity (PI) in the contra-lateral hemisphere ROIs was lower than in the ipsilateral hemisphere ROIs. During hand-held monitoring, TICs were not always stable and drifted from the baseline owing to patients' movements, as shown in the lower panels of Fig. 2.

Sonopod ACZ Monitoring Utilizing PMI

All patients were fitted and monitored continuously by one examiner. Brain tissue perfusion could be precisely quantified before/after ACZ in the same ROI as shown in Fig. 3.

Mainly because of the patient's movements, drifts from the baseline were observed in the TICs of 4 (7 TIC analyses) out of 10 (30 TIC analyses) patients. However, fixed-probe shifts due to patients' movements during monitoring were easily readjustable and the TICs were returned to the baseline in all patients. Regarding contra-lateral TW monitoring in the five bilaterally ACZ examined patients, it was not possible to evaluate precisely in the same ROI locations because of Sonopod re-fixation.

Conclusion

Transducer Holder for TCD and TCDS

Transducer holders or probe fixation devices for conventional TCD monitoring have been introduced into clinical settings. Formerly, for use in newborns, a hood-like probe fixation device via the transfontanellar window was investigated [9]. Trials in adult patients have focused not only on the middle cerebral artery (MCA) via the TWs [4, 5], but also on the vertebrobasilar arteries via the foraminal window (FW) for high-intensity transient signals (HITS) monitoring [21]. More recently, a commercially available head-frame (Marc 600; Spencer Technologies, Seattle, WA, USA) for monitoring via the TWs has been used for detection of recanalization in the MCA during tissue plasminogen activator studies [1]. Furthermore, a long-term ambulatory TCD monitoring device placed on a spectacle frame has been introduced for HITS detection in the MCAs via the TWs [7]. A modified head-frame combining two Spencer Technologies' head-frames for both the TWs and FW has been tried for vasoreactivity tests [6].

Our TCDS transducer fixation device Sonopod is able to monitor not only via the TWs, but also via the FW (Fig. 1). A further important advantage is the long, stable TCDS monitoring that implies accurate quantitative measurements in the major cerebral arteries and brain tissue. However, our prototype of this transducer, the Sonopod, is still so heavy that long-time TW monitoring in the sitting position will probably result in fatigue of the neck muscles. This problem will be improved in changing materials from heavy stainless steel to light weight aluminum, titanium, or similar. For FW monitoring, the Sonopod cannot be applied in a supine position; therefore, patients should be instructed to lie down semilaterally. It is necessary to tighten four screws during the set-up of the Sonopod and this may prove a slightly time-consuming drawback while searching for the appropriate location of vessels or anatomical places. In our experience, however, we were usually ready for monitoring in around 5–10 min.

Comparison of SHI and PMI

Since the clinical introduction of transcranial ultrasound perfusion imaging of brain tissue, depth-dependent ultrasound attenuation has been the toughest problem for qualitative and quantitative evaluation [10, 12]. In our study, significant depth-dependent PI attenuation on the TICs was observed in both image types, particularly in the contralateral hemisphere. In the pioneering work utilizing SHI with Levovist® by Postert et al. [10], not only PI, but also the area under the TIC showed a significantly larger ROI in the BG and white matter than in the Th. Furthermore, SHI utilizing an alternative UCA (Optison) showed a significantly larger Th ROI in the ipsilateral hemisphere than in the contra-lateral hemisphere [12]. More recent studies utilizing phase-inversion harmonic imaging (PIHI) utilizing Optison and SonoVue [2] showed typical depth-dependent PI attenuation in the contralateral hemisphere rather than the ipsilateral hemisphere using bilateral or unilateral (ipsilateral) approaches. A bilateral approach utilizing PIHI [2, 3] has been suggested for evaluating contra-lateral hemispheres. Our previous study of ultrasound perfusion imaging also showed that PMI utilizing transient response high-power images is superior to conventional SHI in the evaluation of the contra-lateral cerebral hemisphere [17]. This study reconfirmed that result. However, limitations of the contra-lateral approach, e.g., shadowing [3], have been pointed out [13].

ACZ Vasoreactivity Utilizing PMI

In order to overcome problems in quantifying brain tissue perfusion, e.g., depth-dependent ultrasound attenuation, we have applied transcranial ultrasound perfusion imaging to the ACZ vasoreactivity test [15, 18]. In ACZ vasoreactivity tests, the same ROI placements before and after ACZ are very important for accurate quantification. From this point of view, the Sonopod is very useful for the precise quantification of brain tissue perfusion.

Summary

Transcranial color duplex sonography Sonopod monitoring succeeds in continuously and quantitatively evaluating precise and reproducible intracranial hemodynamics in the major cerebral arteries and brain tissue.

Conflict of Interest We declare that we have no conflict of interest.

References

1. Alexandrov AV, Demchuk AM, Felberg RA, Christou I, Barber PA, Burgin WS, Malkoff M, Wojner AW, Grotta JC (2000) High rate of complete recanalization and dramatic clinical recovery during tPA infusion when continuously monitored with 2-MHz transcranial Doppler monitoring. Stroke 31:610–614
2. Eyding J, Krogias C, Wilkening W, Meves S, Ermert H, Postert T (2003) Parameters of cerebral perfusion in phase-inversion harmonic imaging (PIHI) ultrasound examinations. Ultrasound Med Biol 29:1379–1385
3. Eyding J, Krogias C, Wilkening W, Postert T (2004) Detection of cerebral perfusion abnormalities in acute stroke using phase inversion harmonic imaging (PIHI): preliminary results. J Neurol Neurosurg Psychiatry 75:926–929
4. Gehring H, Meyer zu Westrup L, Berndt S, Joubert-Hübner E, Eleftheriadis S, Schmucker P (1997) A new probe holding device for continuous bilateral measurements of blood flow velocity in basal brain vessels. Anasthesiol Intensivmed Notfallmed Schmerzther 32:355–359
5. Giller CA, Giller AM (1997) A new method for fixation of probes for transcranial Doppler ultrasound. J Neuroimaging 7:103–105
6. Hong JM, Joo IS, Huh K, Sheen SS (2010) Simultaneous vasomotor reactivity testing in the middle cerebral and basilar artery with suboccipital probe fixation device. J Neuroimaging 20:83–86
7. Mackinnon AD, Aaslid R, Markus HS (2004) Long-term ambulatory monitoring for cerebral emboli using transcranial Doppler ultrasound. Stroke 35:73–78
8. Martina AD, Meyer-Wiethe K, Allemann E, Seidel G (2005) Ultrasound contrast agents for brain perfusion imaging and ischemic stroke therapy. J Neuroimaging 15:217–232
9. Michel E, Zernikow B, Rabe H, Jorch G (1993) Adaptive multipurpose probe fixation device for use on newborns. Ultrasound Med Biol 19:581–586
10. Postert T, Muhs A, Meves S, Federlein J, Przuntek H, Buttner T (1998) Transient response harmonic imaging: an ultrasound technique related to brain perfusion. Stroke 29:1901–1907
11. Seidel G, Kaps M, Dorndorf W (1993) Transcranial color-coded duplex sonography of intracerebral hematomas in adults. Stroke 24:1519–1527
12. Seidel G, Algermissen C, Christoph A, Claassen L, Vidal-Langwasser M, Katzer T (2000) Harmonic imaging of the human brain. Visualization of brain perfusion with ultrasound. Stroke 31: 151–154
13. Seidel G, Meyer-Wiethe K (2006) Acute stroke: perfusion imaging. Front Neurol Neurosci 21:127–139
14. Shiogai T, Nagayama K, Damrinjap G, Saruta K, Hara M, Saito I (1998) Morphological and hemodynamic evaluations by means of transcranial power Doppler imaging in patients with severe head injury. Acta Neurochir Suppl 71:94–100
15. Shiogai T, Ikeda K, Morisaka A, Nagakane Y, Mizuno T, Nakagawa M, Furuhata H (2008) Acetazolamide vasoreactivity evaluated by transcranial power harmonic imaging and Doppler sonography. Acta Neurochir Suppl 102:177–183
16. Shiogai T, Matsumoto M, Ikeda K, Morisaka A, Yoshikawa K, Nagakane Y, Mizuno T, Nakagawa M (2008) Continuous monitoring in the vertebrobasilar artery utilizing a newly developed transducer holder (Sonopod) for transcranial color duplex sonography. Cerebrovasc Dis 25(Suppl 1):36, Abstract
17. Shiogai T, Ikeda K, Matsumoto M, Morisaka A, Mizuno T, Nakagawa M, Furuhata H (2009) Comparison of quantitative parameters in transcranial brain tissue perfusion images between power modulation imaging and second harmonic imaging. Cerebrovasc Dis 27(Suppl 5):20, Abstract
18. Shiogai T, Koyama M, Mizuno T, Nakagawa M, Furuhata H (2010) Cerebral vasoreactivity in the brain tissue and the major cerebral arteries evaluated by transcranial power modulation imaging and color duplex sonography. Cerebrovasc Dis 29(Suppl 1): 23–24, Abstract
19. Shiogai T, Koyama M, Yamamoto M, Yoshikawa K, Mizuno T, Nakagawa M (2011) Monitoring of brain tissue perfusion utilizing Sonopod for transcranial color duplex sonography. Cerebrovasc Dis 31(Suppl 1):18, Abstract
20. Tsai CF, Wu RM, Huang YW, Chen LL, Yip PK, Jeng JS (2007) Transcranial color-coded sonography helps differentiation between idiopathic Parkinson's disease and vascular parkinsonism. J Neurol 254:501–507
21. Woodtli M, Müller HR (1994) A head and transducer holding technique for TCD monitoring of the vertebrobasilar circulation. Ultraschall Med 15:293–295

Computed Tomography After Decompressive Craniectomy for Head Injury

Satoru Takeuchi, Yoshio Takasato, Go Suzuki, Takuya Maeda, Hiroyuki Masaoka, Takanori Hayakawa, Naoki Otani, Hiroshi Yatsushige, Keigo Shigeta, and Toshiya Momose

Abstract New findings (NF) on postoperative CTs are occasionally found in patients who undergo surgery for traumatic brain injury (TBI). We conducted a retrospective registry-based review of the care of 102 patients who underwent decompressive craniectomy (DC) for TBI to investigate the prognostic factors of new findings on CT early after surgery. Of the 102 patients, the mean age was 50 years and 69.6 % were male. The overall survival was 72.5 %. The primary indication for DC included subdural hematoma in 72 (70.6 %), epidural hematoma in 17 (16.7 %), and intraparenchymal contusion in 13 (12.7 %). New findings on postoperative CTs were observed in 26 patients (25.5 %). The univariate analysis showed that a GCS score ≤8 ($P=0.012$) and the absence of a basal cistern ($P=0.012$) were significantly associated with NF on postoperative CT. The logistic regression analysis demonstrated that the GCS score ≤8 ($P=0.041$; OR, 3.0; 95 % CI, 1.048–8.517) was the only significant factor. TBI patients with a low GCS score who underwent DC should undergo additional CT evaluations immediately after surgery.

Keywords Traumatic brain injury • Computed tomography • New findings • Decompressive craniectomy • Surgery

S. Takeuchi (✉) and N. Otani
Department of Neurosurgery, National Defense Medical College,
3-2 Namiki, Tokorozawa, Saitama 359-8513, Japan
e-mail: s.takeuchi@room.ocn.ne.jp

Y. Takasato, T. Maeda, H. Masaoka, T. Hayakawa, H. Yatsushige, K. Shigeta, and T. Momose
Department of Neurosurgery,
National Hospital Organization Disaster Medical Center,
3256 Midori-cho, Tachikawa, Tokyo 190-0014, Japan

G. Suzuki
Department of Emergency and Critical Care Medicine,
Nippon Medical School,
1-1-5 Sendagi, Bunkyo-ku, Tokyo 113-8613, Japan

Introduction

Considerable efforts and resources have been devoted to preserving life in patients with severe traumatic brain injury (TBI). However, TBI remains a major cause of death and disability among young individuals, and its incidence is increasing among the elderly [6, 13].

Decompressive craniectomy (DC) has been reported to be an important method in the management of refractory intracranial hypertension after TBI. The rationale for this treatment consists of opening the skull and removing a bone flap to allow the edematous brain to swell outward, thereby preventing intracranial tissue shifts and life-threatening downward herniation.

Several intracranial hemorrhagic lesions have been reported to emerge after DC, including subdural hematomas [8] or epidural hematomas [3, 4], at the site contra-lateral to the craniectomy, or hemorrhagic contusion at the ipsilateral site [1, 5].

In this study, we investigated the prognostic factors of the new findings (NF) on computed tomography (CT) early after DC.

Materials and Methods

During a period of 7 years, 111 patients underwent DC as an initial surgical procedure for TBI at our institution. We gathered the information from patients' medical charts for this study, and focused on 102 patients who underwent pre- and post-operative CTs.

We retrospectively reviewed the patients' data, with regard to age, sex, level of consciousness, the presence of light reflex, mechanism, the admission platelet counts, the admission international normalized ratio (INR), the interval from injury to last preoperative CT, the last preoperative and postoperative CT findings, and outcome at discharge. Each

Y. Katayama et al. (eds.), *Brain Edema XV*, Acta Neurochirurgica Supplement, Vol. 118,
DOI 10.1007/978-3-7091-1434-6_44,

patient's level of consciousness was assessed using the Glasgow Coma Scale (GCS) score at admission. The patient's outcomes were recorded as good recovery, moderate disability, severe disability, vegetative state, or death. The features evaluated on the last preoperative CT included the primary indication for surgery, midline shift, and the state of the basal cistern. NFs were defined as any massive intracranial hemorrhagic or ischemic lesions that were found on a postoperative CT obtained within 24 h of surgery and that were entirely absent on the last preoperative CT. Then, according to the postoperative CT findings, the patients were classified into two groups: an NF group or a non-NF group.

Surgical Technique

DC was performed via standard unilateral frontoparietotemporal craniectomy, except for two patients. These two patients underwent craniotomy as the initial surgical procedure (unilateral frontoparietal in one patient and unilateral frontal in the other) for an epidural hematoma, but their bone flaps were removed owing to exacerbated brain swelling. In patients who underwent standard DC, their anteroposterior diameter was at least 12 cm, and a subtemporal craniectomy reaching the middle cranial fossa was included. The dura was widely opened in a stellate fashion to the extent of bone decompression, and a duraplasty was performed using a synthetic graft (Gore-tex graft) to increase the available volume before closure.

Statistical Analysis

The univariate and multivariate analyses were performed to investigate the factors related to NF on postoperative CT. Quantitative data were analyzed using Student's *t* test. Categorical data were assessed using the Chi-squared test. However, Fisher's exact test was used if any of the expected cell frequencies were less than five. All variables with a significance level of $P < 0.15$ in the univariate analysis were included as independent variables in a logistic regression analysis. Only those variables with $P < 0.15$ in two-tailed tests were retained within the model. The odds ratios (OR) and 95 % confidence intervals (CI) were reported. $P < 0.05$ was considered to be statistically significant. All statistical analyses were performed using the Statistical Package for the Social Sciences software program version 11.0 for Windows (SPSS; Chicago, IL, USA).

Results

Of the 102 patients, 71 (69.6 %) were male and 31 (30.4 %) were female, with an age range of 7–95 years (mean, 50.3 years). The median admission GCS score was 7.5 (25th–75th percentile, 4–11). Fifty-six (54.9 %) patients had a GCS score ≤ 8. The mechanism of injury included falls in 50 patients (49.0 %), traffic accidents in 45 (44.1 %), and other causes in 1 (1.0 %), while the cause was unknown in 6 patients (5.9 %). The mean admission platelet counts and INR were $17.9 \times 10^4/\mu L$ and 1.2 respectively. The interval from injury to the last preoperative CT was ≤2 h in 72 patients (76.6 %). The primary indication for DC was a subdural hematoma in 72 patients (70.6 %), epidural hematoma in 17 (16.7 %), and contusion in 13 (12.7 %).

The mean midline shift was 8.0 mm (range, 0–27 mm). An absence of a basal cistern was observed in 61 patients (59.8 %). Twenty-six patients (25.5 %) had NF on the postoperative CT findings. The outcomes were a good recovery in 20 patients (19.6 %), moderate disability in 21 (20.6 %), severe disability in 19 (18.6 %), vegetative state in 14 (13.7 %), and death in 28 (27.5 %).

We performed the univariate and multivariate analyses to investigate the prognostic factors related to NFs on postoperative CT. In patients with NFs on postoperative CT, 20 patients (76.9 %) had a GCS score ≤8; the primary indication for DC was a subdural hematoma in 21 (80.7 %) patients, an epidural hematoma in 3 (11.5 %), and contusion in 2 (7.7 %); the mean midline shift was 9.5 mm (range, 0–22 mm). The absence of a basal cistern was observed in 21 patients (80.8 %). The univariate analysis showed that a GCS score ≤8 ($P = 0.012$) and the absence of a basal cistern ($P = 0.012$) were significantly associated with NF on postoperative CT. The logistic regression analysis demonstrated that the GCS score ≤8 ($P = 0.041$; OR, 3.0; 95 % CI, 1.048–8.517) was the only significant factor.

NFs were detected on the first postoperative CTs obtained within 24 h of surgery in all 26 of the patients with NF on postoperative CTs: ≤1 h after surgery in 18 patients (69.2 %), 1 h < and ≤ 12 h in 3 (11.5 %), and >12 h in 5 (19.2 %). A total of 26 NFs were detected on postoperative CT: contralateral subdural hematomas in 8 patients (29.6 %), ipsilateral contusions in 8 (29.6 %), contra-lateral epidural hematomas in 5 (18.5 %), whole brain ischemia in 3 (11.1 %), contralateral contusions in 2 (7.4 %), and an ipsilateral subdural hematoma in 1 (3.7 %).

Conclusion

Our results indicate that a low GCS score are independent factors related to the occurrence of NFs on early CT after DC. We also found that NFs occurred more often on the contra-lateral side, and especially within 1 h of DC.

DC is usually considered to be technically simple; however, several complications have been reported. Among these complications, the development of intracranial hemorrhagic lesions can be directly fatal to TBI patients [1, 5, 14].

Several intracranial hemorrhagic lesions have been reported to emerge after DC, including subdural hematomas [8] or epidural hematomas [3, 4] at the site contra-lateral to the craniectomy, or hemorrhagic contusion at the ipsilateral site [1, 5]. In our series, hemorrhagic lesions at the contralateral site were more common than at the ipsilateral site.

It can be hypothesized that a brain shift is responsible for remote bleeding after DC [3]. Furthermore, we also consider that it is possible that some postoperative hemorrhagic lesions could simply be lesions that have developed during the natural course of injury, which the initial CT could not detect, especially when the interval between the injury and the initial CT was short [2, 9, 10, 12]. In particular, the latter mechanism may be most likely in some cases of brain contusions as NFs on postoperative CTs, because they are difficult to detect on acute phase preoperative CTs [7]. However, with regard to the timing of the initial CT, we found that the interval between the injury and the initial CT was not related to NFs. Paci et al. reported that subdural hematoma as an indication for surgery was the only variable associated with unexpected findings, which were defined as NFs, or unexpected worsening, which was assigned when the worsening was not within reasonable expectations on the postoperative CT [11]. In our study, subdural hematoma as an indication for surgery was not a factor associated with NFs. The discrepancy between the results of Paci et al. and our present results may be due to the differences in subjects and comparisons.

Additionally, our results may suggest that early postoperative CT after DC might be required for patients with a low GCS score. Routine immediate CTs after surgery in patients with a low GCS score may be preferable because it is difficult to judge neurological worsening in patients with a low GCS score, regardless of sedation.

The retrospective analysis performed in our study was subject to observation and assessment bias.

In summary, the present study showed that a low GCS score was an independent factor related to the occurrence of NFs on early CTs after DC. TBI patients with a low GCS score who underwent DC should undergo additional CT evaluation immediately after surgery.

Conflict of Interest We declare that we have no conflict of interest.

References

1. Aarabi B, Hesdorffer DC, Ahn ES, Aresco C, Scalea TM, Eisenberg HM (2006) Outcome following decompressive craniectomy for malignant swelling due to severe head injury. J Neurosurg 104: 469–479
2. Alahmadi H, Vachhrajani S, Cusimano MD (2010) The natural history of brain contusion: an analysis of radiological and clinical progression. J Neurosurg 112:1139–1145
3. Cohen JE, Rajz G, Itshayek E, Umansky F (2004) Bilateral acute epidural hematoma after evacuation of acute subdural hematoma: brain shift and the dynamics of extraaxial collections. Neurol Res 26:763–766
4. Feuerman T, Wackym PA, Gade GF, Lanman T, Becker D (1988) Intraoperative development of contralateral epidural hematoma during evacuation of traumatic extraaxial hematoma. Neurosurgery 23:480–484
5. Flint AC, Manley GT, Gean AD, Hemphill JC 3rd, Rosenthal G (2008) Post-operative expansion of hemorrhagic contusions after unilateral decompressive hemicraniectomy in severe traumatic brain injury. J Neurotrauma 25:503–512
6. Kannus P, Palvanen M, Niemi S (2001) Time trends in severe head injuries among elderly Finns. JAMA 286:673–674
7. Laalo JP, Kurki TJ, Sonninen PH, Tenovuo OS (2009) Reliability of diagnosis of traumatic brain injury by computed tomography in the acute phase. J Neurotrauma 26:2169–2178
8. Matsuno A, Katayama H, Wada H, Morikawa K, Tanaka K, Tanaka H, Murakami M, Fuke N, Nagashima T (2003) Significance of consecutive bilateral surgeries for patients with acute subdural hematoma who develop contralateral acute epi- or subdural hematoma. Surg Neurol 60:23–30
9. Narayan RK, Maas AI, Servadei F, Skolnick BE, Tillinger MN, Marshall LF, Traumatic Intracerebral Hemorrhage Study Group (2008) Progression of traumatic intracerebral hemorrhage: a prospective observational study. J Neurotrauma 25:629–639
10. Oertel M, Kelly DF, McArthur D, Boscardin WJ, Glenn TC, Lee JH, Gravori T, Obukhov D, McBride DQ, Martin NA (2002) Progressive hemorrhage after head trauma: predictors and consequences of the evolving injury. J Neurosurg 96:109–116
11. Paci GM, Sise MJ, Sise CB, Sack DI, Swanson SM, Holbrook TL, Hunstock AM, Altenau LL, Carver TW (2008) The need for immediate computed tomography scan after emergency craniotomy for head injury. J Trauma 64:326–333
12. Servadei F, Nanni A, Nasi MT, Zappi D, Vergoni G, Giuliani G, Arista A (1995) Evolving brain lesions in the first 12 hours after head injury: analysis of 37 comatose patients. Neurosurgery 37:899–906
13. Stein SC, Georgoff P, Meghan S, Mizra K, Sonnad SS (2010) 150 Years of treating severe traumatic brain injury: a systematic review of progress in mortality. J Neurotrauma 27:1343–1353
14. Yang XF, Wen L, Shen F, Li G, Lou R, Liu WG, Zhan RY (2008) Surgical complications secondary to decompressive craniectomy in patients with a head injury: a series of 108 consecutive cases. Acta Neurochir (Wien) 150:1241–1247

Use of Preoperative 3D CT/MR Fusion Images and Intraoperative CT to Detect Lesions That Spread onto the Brain Surface

Shiro Yamashita, Mutsuo Fujisawa, Kazuaki Kodama, Motonori Ishikawa, and Ryosuke Katagi

Abstract *Objective*: Preoperative 3D CT/MR fusion images were prepared for preoperative evaluations and intraoperative assistance for the following lesions: arteriovenous malformations (AVMs), meningiomas, and metastatic tumors that spread onto the brain surface.

Method: We prepared 3D CT/MR fusion images for 4 AVMs, 13 meningiomas, and 7 metastatic tumors, and demonstrate representative cases. Data acquired from 16-slice multidetector CT and 1.5-T MRI were used. The volume rendering technique was used. During operations, mobile 16-slice multidetector CT was used to update information.

Results: Even after opening the dura mater, the relationship between a brain surface lesion and the surrounding structures on the preoperative 3D fusion images corresponded to the patient's operation field. Updated information via intraoperative CT was useful because operation fields might change owing to the brain shift. These images made extirpations of lesions easier and less invasive.

Conclusion: Not only the preoperative 3D information, but also intraoperative CT information are beneficial for smooth and safe operations.

Keywords Preoperative 3D CT/MR fusion image • Intraoperative mobile CT • Brain surface • Arteriovenous malformation • Meningioma • Metastatic tumor

S. Yamashita (✉), M. Fujisawa, and R. Katagi
Department of Neurological Surgery,
Katagi Neurosurgical Hospital, 274 Betsumyo,
Imabari, Ehime 794-0065, Japan
e-mail: shiro@kms.ac.jp

K. Kodama and M. Ishikawa
Section of Radiology, Katagi Neurosurgical
Hospital, Ehime, Japan

Introduction

The recent development of imaging devices and workstations has resulted in more detailed and finer three-dimensional (3D) images than before. For operative cases, 3D images are helpful for surgical simulation [3–5] and as a reference during operations. However, a brain shift following cerebrospinal fluid leakage due to opening of the dura mater is well known and indicates that preoperative images do not necessarily correspond to the operation fields.

To address this issue, we contemplated that in cases of lesions that spread onto the brain surface, even though the brain shift might occur, the relationship between a lesion of the brain surface and surrounding structures would not change widely. Here, we present operated lesions that spread onto the brain surface, assisted by both preoperative 3D CT/MR fusion images and intraoperative mobile CT.

Patients and Methods

Patient Groups

In our hospital, preoperative 3D CT/MR fusion images have been made for arteriovenous malformations (AVMs), meningiomas, and metastatic tumors that spread onto the brain surface for 2.5 years, since April 2008. Images were prepared for 4 patients with AVMs (average age: 51.3 years; 3 male and 1 female; Spetzler–Martin grade I: 1, II: 1, III: 2; location: 3 supratentorial and 1 infratentorial), 13 patients with meningiomas (average age: 70.5 years; 3 male and 10 female; location: 12 supratentorial and 1 infratentorial), and 7 patients metastatic tumors (average age: 61.4 years; 2 male and 5 female; location: 5 supratentorial and 2 infratentorial).

Y. Katayama et al. (eds.), *Brain Edema XV*, Acta Neurochirurgica Supplement, Vol. 118,
DOI 10.1007/978-3-7091-1434-6_45,

Imaging Preparation

Preoperative 3D CT/MR images were prepared as previously reported [3]. Briefly, data were acquired from 16-slice multidetector CT (BrightSpeed Elite Pro; GE Healthcare, Waukesha, WI, USA) and 1.5 T MRI (Intera Achieva 1.5T; Phillips, Amsterdam, The Netherlands). MR angiography (MRA) was performed with a time-of-flight sequence. MR venography (MRV) was performed with a phase-contrast sequence. Three dimensional CT/MR fusion image data were acquired using image analysis software (AZE Virtual Place WS-AD21; AZE, Tokyo, Japan) and the volume rendering technique was used. To discriminate between arteries and veins, angiographic information was used. Angiography was conducted with a biplane and rotational digital subtraction equipment (Innova3131IQ; GE Healthcare).

Intraoperative CT

During operations, updated information was obtained by using a mobile 16-slice multidetector CT (Light Speed RT SmartGantry; GE Healthcare), which was developed in co-operation with GE Healthcare. This CT was installed in our operating room in April 2008. Its gantry runs on two rails and tilts smoothly like conventional CT. It provides us with not only the 2D information, but also 3D images, including CT angiography (CTA) [8].

Use of Information During Operations

Mobile parallel monitors hanging from the ceiling were prepared beside the operative field. Both preoperative and intraoperative information was shown on the monitors from the manipulation room next to the operating room. Most of the 3D images were available to be seen stereographically.

Results

Based on the preoperative CT/MR images, operative approaches were decided. After opening the dura mater, the relationship between the brain surface lesion and the surrounding structures on the preoperative 3D fusion images corresponded to the patient's actual operative field. Updated information via intraoperative CT was useful because structures were changing as the operation progressed. In patients with AVM, total resections were accomplished without any new neurological deficits. In patients with meningiomas, 8 were totally removed, but 4 were not because they involved sinuses and subsequently received additional radiosurgery. In patients with metastatic tumors, all lesions were totally removed except in two patients owing to invasion into superior sagittal sinuses and involvement of the motor cortex.

Illustrative Cases

Case 1

A 34-year-old woman with an AVM (Spetzler–Martin grade III) partially on the left precentral gyrus (Fig. 1a–c). Left fronto-temporal craniotomy was performed. After opening the dura mater, we could see the operative field (Fig. 1d) as well as the preoperative image (Fig. 1e). We used two small forceps, whose tips were very sharp, in both hands. We tore the pia mater without injuring the cortex itself. Then the feeder appeared (Fig. 1f), as on the preoperative image (Fig. 1g). Before extirpating the AVM, intraoperative enhanced CT (Fig. 1h) and 3DCTA (Fig. 1i) were performed. The AVM was taken without injuring the cortex (Fig. 1j). Postoperative CT (Fig. 1k) and angiography (Fig. 1l) showed neither unexpected hemorrhage nor residual AVM.

Case 2

A 66-year-old woman with a left cerebellar meningioma (Fig. 2a–d). A left lower occipital craniectomy was performed. To confirm the maximum bone window, intraoperative 3DCT was fused with preoperative sinus images (Fig. 2e). During the operation, we confirmed the process (Fig. 2f) and the final stage (Fig. 2g) by enhanced CT. To avoid injuring the sinuses, we intentionally left the tumor around the sinuses as planned. Postoperative T1W1-Gd MRI showed a residual tumor involving the left transverse and sigmoid sinuses (Fig. 2h–j).

Case 3

A 57-year-old woman with right temporal metastatic tumor (Fig. 3a–c). Left temporal craniotomy was performed. After opening of the dura, cortical veins including the vein of Labbé in the operative field (Fig. 3d) corresponded to the preoperative image (Fig. 3e). Moreover, to confirm that the

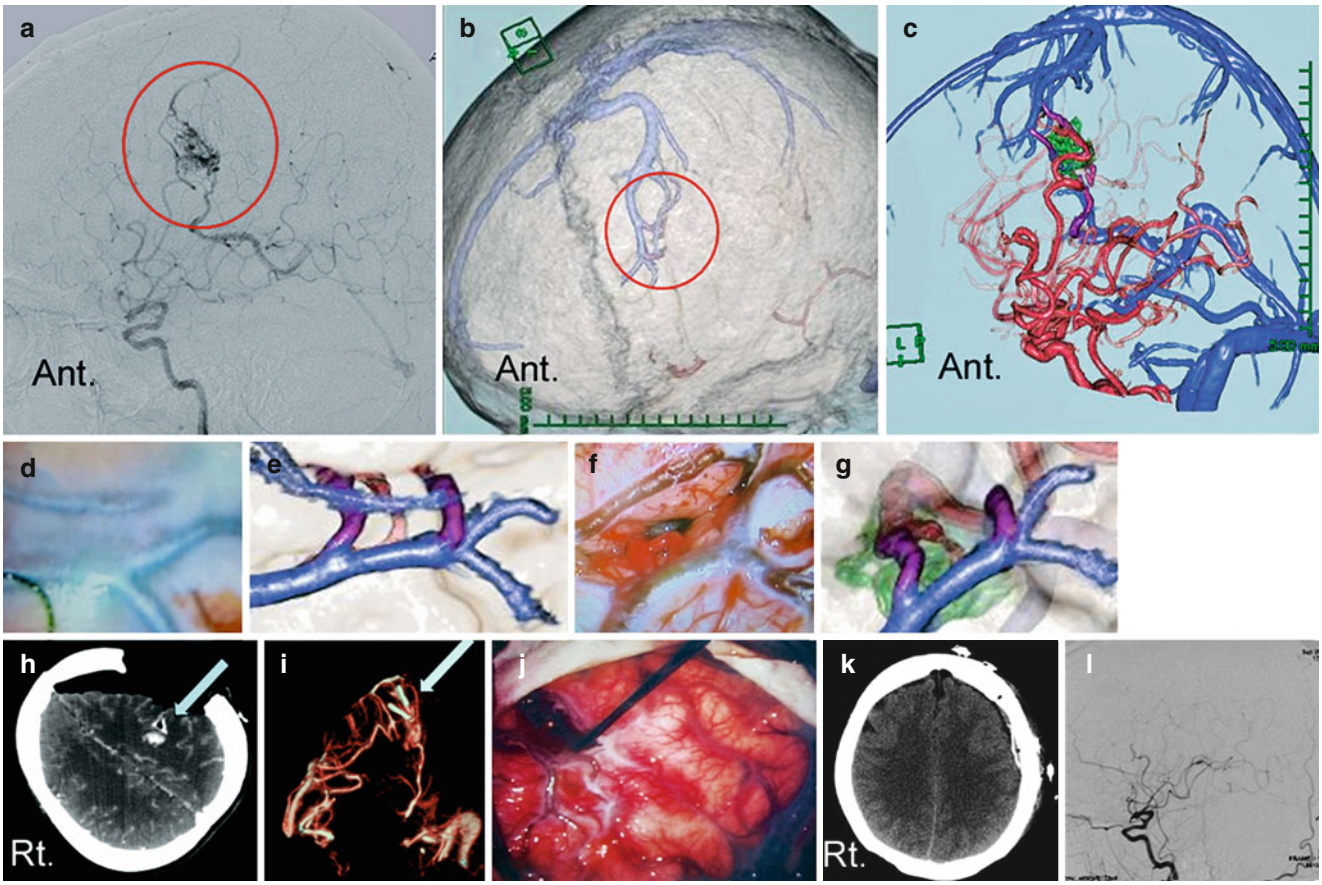

Fig. 1 Angiogram of the left internal carotid artery (**a**), three-dimensional (3D) CT/MRI/MRA/MRV fusion image (**b**), and 3D MRA/MRV fusion image (**c**) show an arteriovenous malformation (AVM) on the left precentral gyrus (Spetzler–Martin grade III). Cortical vein on the operative field (**d**) and the preoperative image (**e**) before tearing the pia mater. Cortical vein and feeder on the operative field (**f**) and the preoperative image (**g**). Intraoperative enhanced CT (**h**) and 3DCTA (**i**) show the relationship between the nidus and small sheets. Intact cortex (**j**) after extirpation of the AVM. CT (**k**) after the operation shows no unexpected hemorrhage. Angiogram of the left internal carotid artery (**l**) after the operation shows no residual nidus. *Circles* indicate the location of the AVM and *arrows* indicate the small sheets

region in which we were going to make an incision was the lesion itself, an intraoperative CT was taken, which showed that there were small sheets directly above the tumor (Fig. 3f). Then, we incised the tumor beside the vein of Labbé. Total resection of the tumor was confirmed by intraoperative enhanced CT (Fig. 3g). Postoperative T1W1-Gd MRI showed no residual tumor (Fig. 3h–j).

Conclusion

Many reports of preoperative 3D CT/MR fusion images for surgical simulations have already been documented [3, 5]. These images, unlike 2D images, assist us to immediately understand the relationships between lesions and surrounding structures. In our hospital, 3D CT/MR fusion images for neurosurgical cases have been prepared routinely since April 2006 [3]. In terms of accuracy, it is possible that the fusion technique might cause a deviation of 0.1–0.5 mm [3]. Even though a deviation is caused, those images seem to be more accurate than images that we have in our heads.

The importance of preoperative simulation has been reported, especially for superficial AVMs [4, 7]. However, when operations progress, simulated images do not completely correspond to the operative fields because of the structural changes. That is why we have installed mobile intraoperative CT to generate images during the operations. The importance of the intraoperative images has been emphasized [1, 2, 6, 8, 9]. Intraoperative CT provides information without losing time, and information from CT is very familiar to neurosurgeons, even though additional radiation exposure for patients is unavoidable [9].

This time, we used 3D CT/MR fusion images to decide approaches and simulate operations. After the dura opening,

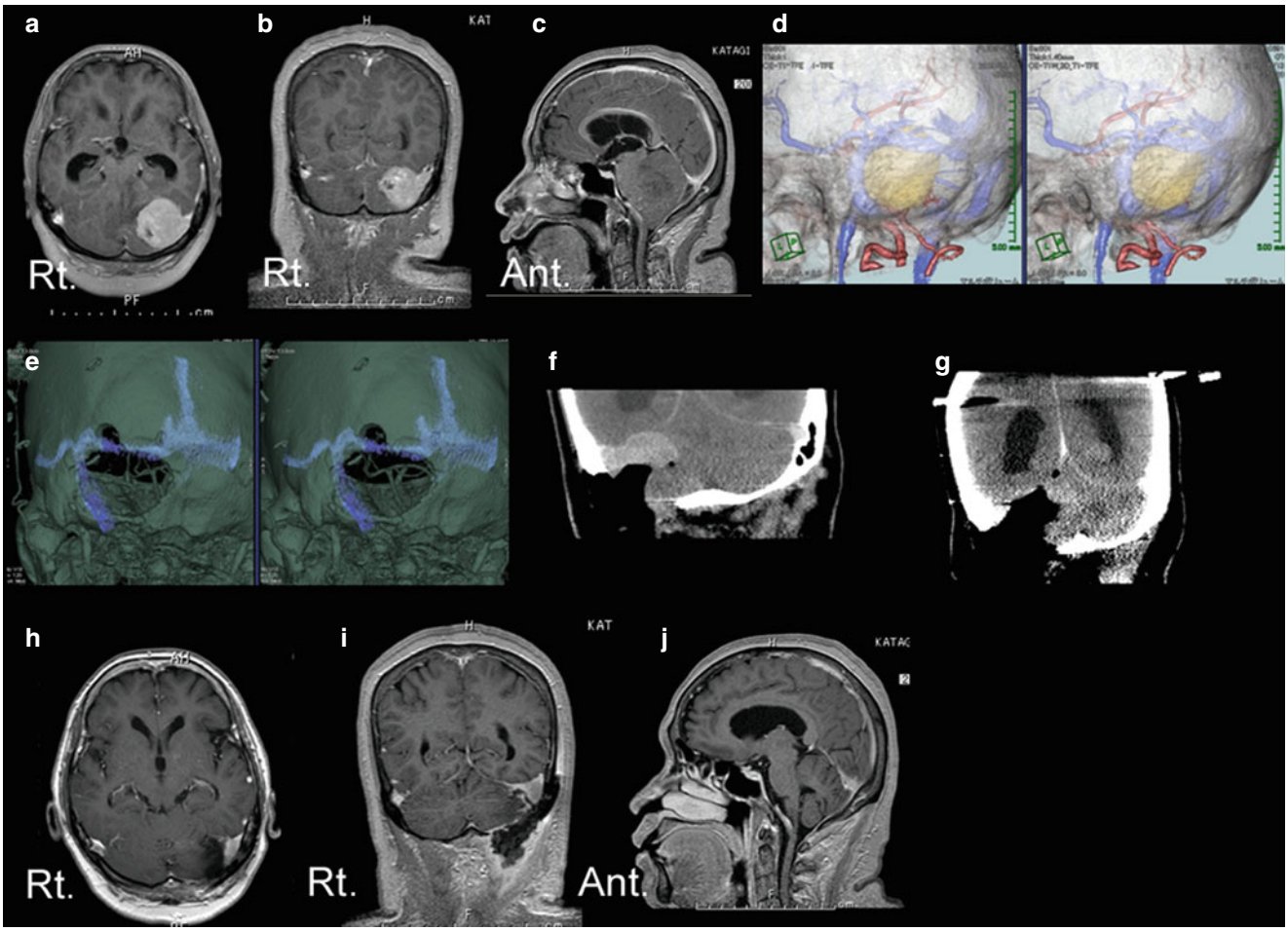

Fig. 2 T1-weighted MR contrast-enhanced images (axial **a**, coronal **b**, and sagittal **c** views), and stereo 3D CT/MRI/MRA/MRV fusion images (**d**) show the left cerebellar meningioma. 3D CT fused with preoperative venous images after craniectomy (**e**). Intraoperative enhanced CT show residual meningioma (**f** and **g**). Postoperative T1-weighted MR contrast-enhanced images (axial **h**, coronal **i**, and sagittal **j** views)

to incise the lesion without injuring normal cortex is not easy even in a simple case. Cortex on the MR fusion images corresponded to the operative field. Preoperative views of the brain surface in all patients on whom we operated were very similar to real operative fields. However, as seen in case 3, even though the structural relationship was the same as the real patient's operative field, it was difficult to discriminate between the lesion and normal brain (Fig. 3d). The intraoperative CT information that small sheets were directly above the tumor (Fig. 3f) improved surgeons' confidence. It enabled us to incise the lesions without injuring normal cortex. Intraoperative CT information including 3DCTA led us to continue and execute operations more safely and more easily.

In summary, use of both preoperative CT/MR fusion images and intraoperative CT contributes to making the neurosurgical procedure for lesions that have spread onto the brain surface easier and safer.

Conflict of Interest We declare that we have no conflict of interest.

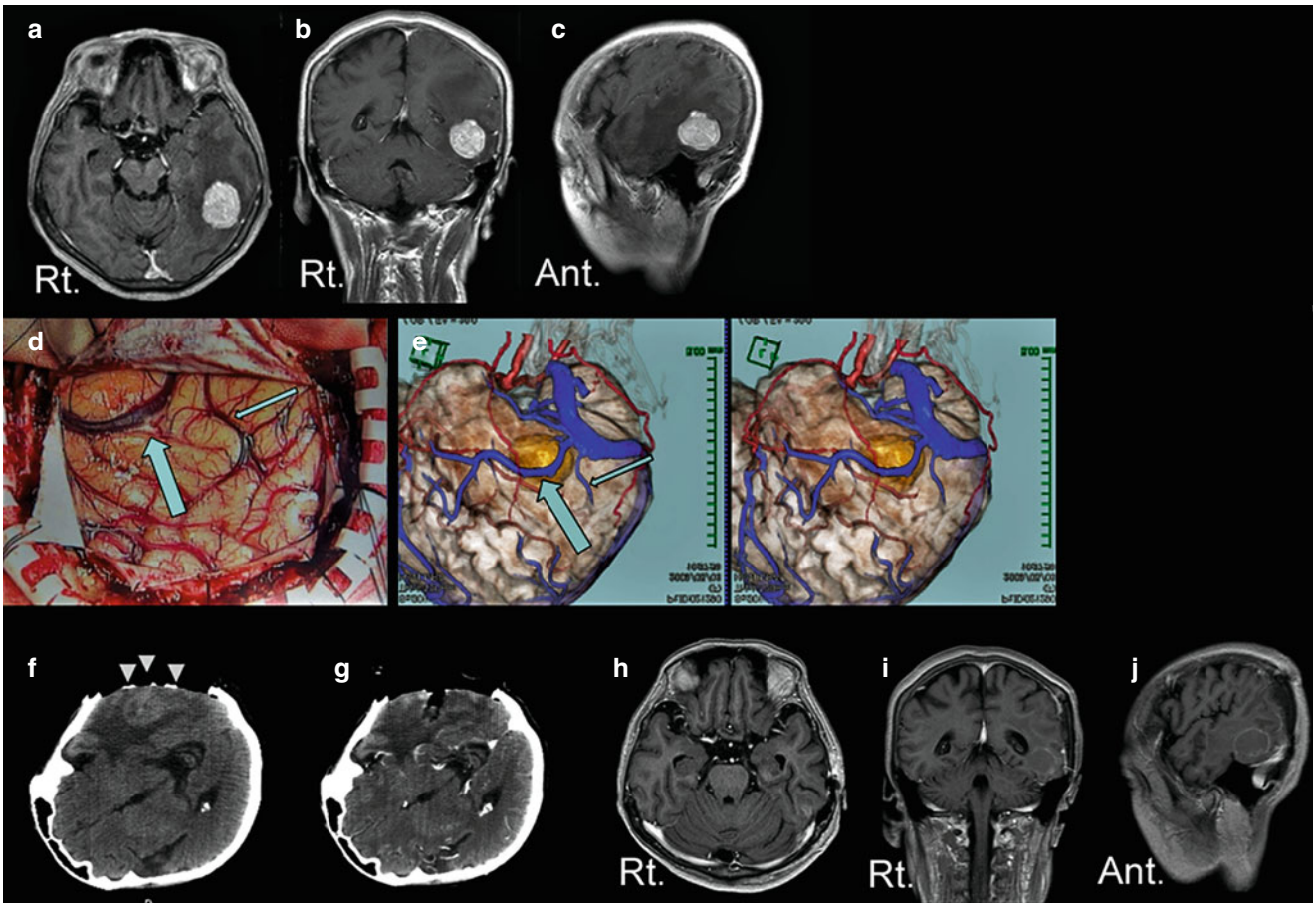

Fig. 3 T1-weighted MR contrast-enhanced images (axial **a**, coronal **b**, and sagittal **c** views) show enhanced mass with edema in the left temporal lobe. Operative field (**d**) corresponds to stereo 3D MRI/MRA/MRV fusion images (**e**). Intraoperative CT shows the relationship between the tumor and small sheets (**f**). Intraoperative enhanced CT (**g**) shows neither residual tumor nor unexpected hemorrhage. Postoperative T1-weighted MR contrast-enhanced images (axial **h**, coronal **i**, and sagittal **j** views) show no residual tumor. *Arrows* in the **d** indicate the same *arrows* as in **e**. *Arrowhead*s indicate small sheets

References

1. Kabuto M, Kubota T, Kobayashi H, Handa Y, Sato K, Ishii H, Takeuchi H, Uno H, Arishima H, Ido K, Ueda Y, Adachi M, Ishida M, Hasegawa Y, Yanagimoto M, Goto Y (1998) Intraoperative CT imaging system using a mobile CT scanner gantry mounted on floor-embedded rails for neurosurgery. Brain Nerve 50:1003–1008, In Japanese
2. Kuhnt D, Ganslandt O, Schlaffer SM, Buchfelder M, Nimsky C (2011) Quantification of glioma removal by intraoperative high-field magnetic resonance imaging: an update. Neurosurgery 69: 852–863
3. Morisaki K, Fujisawa M, Katagi R (2008) Utility of three-dimensional MR volume rendering images for neurosurgical treatment. Progr CI 30:143–149, In Japanese
4. Murata T, Horiuchi T, Rahmah NN, Sakai K, Hongo K (2011) Three-dimensional magnetic resonance imaging based on time-of-flight magnetic resonance angiography for superficial cerebral arteriovenous malformation –technical note-. Neurol Med Chir (Tokyo) 51:163–167
5. Oishi M, Fukuda M, Ishida G, Saito A, Hiraishi T, Fujii Y (2011) Prediction of the microsurgical window for skull-base tumors by advanced three-dimensional multi-fusion volumetric imaging. Neurol Med Chir (Tokyo) 51:201–207
6. Senft C, Seifert V, Hermann E, Franz K, Gasser T (2008) Usefulness of intraoperative ultra low-field magnetic resonance imaging in glioma surgery. Neurosurgery 63:257–267
7. Wong GK, Zhu CX, Ahuja AT, Poon WS (2009) Stereoscopic virtual reality simulation for microsurgical excision of cerebral arteriovenous malformation: case illustrations. Surg Neurol 72:69–73
8. Yamashita S, Fujisawa M, Katagi R (2011) Intra-operative mobile 16 slice multi-detector CT for cerebrovascular disease. Int J Comput Assist Radiol Surg 6(Suppl):S253–S254
9. Yamashita S, Fujisawa M, Katagi R, Kodama K, Ishikawa M (2009) Use of intraoperative mobile helical CT in our hospital. Progr CI 31:113–118, In Japanese

Cortical Neuron Loss in Post-Traumatic Higher Brain Dysfunction Using ^{123}I-Iomazenil SPECT

Jyoji Nakagawara, Kenji Kamiyama, Masaaki Takahashi, and Hirohiko Nakamura

Abstract In patients with higher brain dysfunction (HBD) after mild traumatic brain injury (MTBI), diagnostic imaging of cortical neuron loss in the frontal lobes was studied using SPECT with ^{123}I-iomazenil (IMZ), as a radioligand for central benzodiazepine receptor (BZR). Statistical imaging analysis using three-dimensional stereotactic surface projections (3D-SSP) for ^{123}I-IMZ SPECT was performed in 17 patients. In all patients with HBD defined by neuropsychological tests, cortical neuron loss was indicated in the bilateral medial frontal lobes in 14 patients (83 %). A comparison between the group of 17 patients and the normal database demonstrated common areas of cortical neuron loss in the bilateral medial frontal lobes involving the medial frontal gyrus (MFG) and the anterior cingulate gyrus (ACG). In an assessment of cortical neuron loss in the frontal medial cortex using the stereotactic extraction estimation (SEE) method (level 3), significant cortical neuron loss was observed within bilateral MFG in 9 patients and unilateral MFG in 4, and bilateral ACG in 12 and unilateral ACG in 3. Fourteen patients showed significant cortical neuron loss in bilateral MFG or ACG. In patients with MTBI, HBD seemed to correlate with selective cortical neuron loss within the bilateral MFG or ACG where the responsible lesion could be. 3D-SSP and SEE level 3 analysis for ^{123}I-IMZ SPECT could be valuable for diagnostic imaging of HBD after MTBI.

Keywords Post-traumatic higher brain dysfunction • Cortical neuron loss • I-iomazenil (IMZ) SPECT • 3D stereotactic surface projections • Stereotactic extraction estimation

J. Nakagawara (✉), K. Kamiyama, M. Takahashi, and H. Nakamura
Department of Neurosurgery,
Nakamura Memorial Hospital,
South-1, West-14, Chuo-ku, Sapporo 060-8570, Japan
e-mail: nakagawara.joji.hp@mail.ncvc.go.jp;
ikamirin@med.nmh.or.jp; spect777@nmh.or.jp;
hirohiko@med.nmh.or.jp

Introduction

It is still unknown that post-traumatic higher brain dysfunction (HBD) [1] could be induced by mild traumatic brain injury (MTBI) associated with no or mild unconsciousness (Japan Coma Scale [JCS] 1–3) at the time of brain injury [2]. Structural neuroimaging such as CT or MRI could be insufficient for obtaining significant findings concerning HBD. However, the recent development of diffusion tensor imaging could show diffuse axonal injury (DAI) in white matter such as the corpus callosum or internal capsule in patients with MTBI [3], defined as unconsciousness within 0–20 min and mild Glasgow Coma Scale (GCS) score (13–15) [4]. Traumatic injury of the corpus callosum could be assumed to be the main cause of post-traumatic HBD; the presence of unconsciousness at the time of brain injury might not be a necessary factor in certifying the diagnosis of post-traumatic HBD.

We then investigated a focal lesion using ^{123}I-iomazenil (IMZ) SPECT, which provides an indicator of cortical neuron damage in patients with post-traumatic HBD after MTBI and consists of cognitive impairment such as memory, attention, performance, and social behavioral disturbances evaluated by neuropsychological tests [5].

Materials and Methods

Seventeen patients (6 male, 11 female with a mean age of 49 ± 21 years) were subjected to this study. Mean duration from brain injury to detailed examination was 89 ± 81 (9–240) months. Post-traumatic HBD after MTBI in these patients was confirmed by neuropsychological tests such as an intelligence test (WAIS-R or WAIS-III), a memory test (WMS-R), frontal lobe function tests (trail-making test parts A and B, verbal fluency test, "Kana" letter pick-up test, and the Wisconsin Cards Sorting Test), and Behavioral Assessment

Y. Katayama et al. (eds.), *Brain Edema XV*, Acta Neurochirurgica Supplement, Vol. 118,
DOI 10.1007/978-3-7091-1434-6_46, © Springer-Verlag Wien 2013

of the Dysexecutive Syndrome (BADS) test. All patients were also evaluated using several MRI sequences (T2WI, T1WI, PDI, T2*WI, susceptibility weighted imaging [SWI]) and MRA, only one patient showed low signal spots (minimal contusion areas) in the corpus callosum on T2*WI and SWI.

^{123}I-IMZ-SPECT was able to practically provide an indicator of the intactness of cortical neurons. ^{123}I-IMZ is a specific radioligand (RI tracer) for central benzodiazepine receptor (BZR), which distributes to cerebral cortex in proportion to inhibitory cortical neurons. Focal reduction of BZR density indicated that a decrease in ^{123}I-IMZ could be a marker of cortical neuron loss. Projection data of ^{123}I-IMZ-SPECT were obtained within 3 h of intravenous tracer injection, and the ^{123}I-IMZ-3 h image was reconstructed. In that time, distribution of RI tracer and BZR could be in a state of pseudo-equilibrium. ^{123}I-IMZ-3 h imaging can be estimated by statistical imaging analysis such as three-dimensional stereotactic surface projections (3D-SPP) [6]. In 3D-SSP analysis, axial images of ^{123}I-IMZ-3 h from subjects are transformed to the Talairach standard brain frame of reference pixel by pixel, and then the relative tracer distribution of the cortex is compared with the normal database in which every pixel has a mean count value and standard deviation (SD), which are normalized by the count value of the whole cerebral cortex. Differences between one subject's data and the normal database in each pixel are converted to a Z-score as a multiple of SD, then the cluster of pixels that have a significant difference (Z-score >2) could be identified as the specific area with cortical neuron loss on the stereotactic surface projections (a total of eight directions).

On assessment of cortical neuron loss in the frontal lobes, areas of cortical neuron loss around the medial frontal gyrus (MFG) and anterior cingulate gyrus (ACG) were focused on the medial frontal lobe, and areas of cortical neuron loss around the superior frontal gyrus and middle frontal gyrus were focused on the lateral frontal lobe by visual assessment. A cluster of pixels that indicated a significant reduction of BZR on 3D-SSP (Z score >2) was defined as significant cortical neuron loss, and assessed as follows: ++, cortical neuron loss in multiple areas; +, cortical neuron loss in a single area; −, no areas of cortical neuron loss. Group comparison was carried out between the normal database and the group of 17 patients to estimate common areas of significant cortical neuron loss in the frontal lobes.

Cortical neuron loss in the frontal medial cortex was analyzed using the stereotactic extraction estimation (SEE) method (level 3: gyrus level analysis) [7, 8] for 3D-SSP images of ^{123}I-IMZ SPECT (Z-score >2). Extent (%) of pixels with a significant reduction of BZR density within the target gyrus was calculated on 3D-SSP images. Extent of such pixels of more than10 % in the target gyrus (bilateral MFG and ACG) was defined as significant cortical neuron loss, and 1–10 % as mild cortical neuron loss, on a scattering of the normal database.

Results

On assessment of cortical neuron loss in the medial frontal lobes, areas of cortical neuron loss were observed bilaterally in 14 patients (83 %) and unilaterally in 3 patients (17 %). On the other hand, in the lateral frontal lobes, areas of cortical neuron loss were not observed bilaterally in any cases and only unilaterally in 8 patients (47 %). In a group comparison between the normal database and the group of 17 patients, common areas of significant cortical neuron loss were demonstrated in the bilateral medial frontal lobes, especially around the bilateral MFG and ACG, under a Z-score >2 (Fig. 1).

On assessment of significant neuron loss in the bilateral medial frontal cortex, significant neuron loss was observed at the bilateral MFG in 9 patients (53 %), and unilateral MFG in 4 patients (24 %), mild neuron loss was observed at the bilateral MFG in 3 patients (17 %), and no neuron loss was indicated in 1 patient (6 %; Fig. 2, Table 1). Mean extent of abnormal pixels that indicated a reduction of BZR was 16.5 ± 11.9 % in the left MFG, and 17.9 ± 13.7 % in the right MFG (Table 1). Significant cortical neuron loss was also observed at bilateral ACG in 12 patients (71 %), and unilateral ACG in 3 patients (17 %); and mild cortical neuron loss was observed at bilateral ACG in 2 patients (12 %; Fig. 2). Mean extent of abnormal pixels that indicated a reduction of BZR was 22.9 ± 20.9 % in the left ACG, and 22.1 ± 16.7 % in the right ACG (Table 1).

Fourteen of the 17 patients (83 %) demonstrated a significant loss of cortical neurons in bilateral MFG or ACG, and in these patients, cortical neuron loss in bilateral ACG (12 patients) was more frequent than that in bilateral MFG (9 patients; Fig. 2).

Conclusion

Localization of the lesion in patients with HBD after MTBI has to be discussed in view of IMZ-SPECT findings. ^{123}I-IMZ-SPECT could provide an indicator of the intactness of cortical neurons [9]. In epilepsy surgery, ^{123}I-IMZ-SPECT was already established as a diagnostic tool for cortical neuron loss around the focus in patients with uncontrolled epilepsy

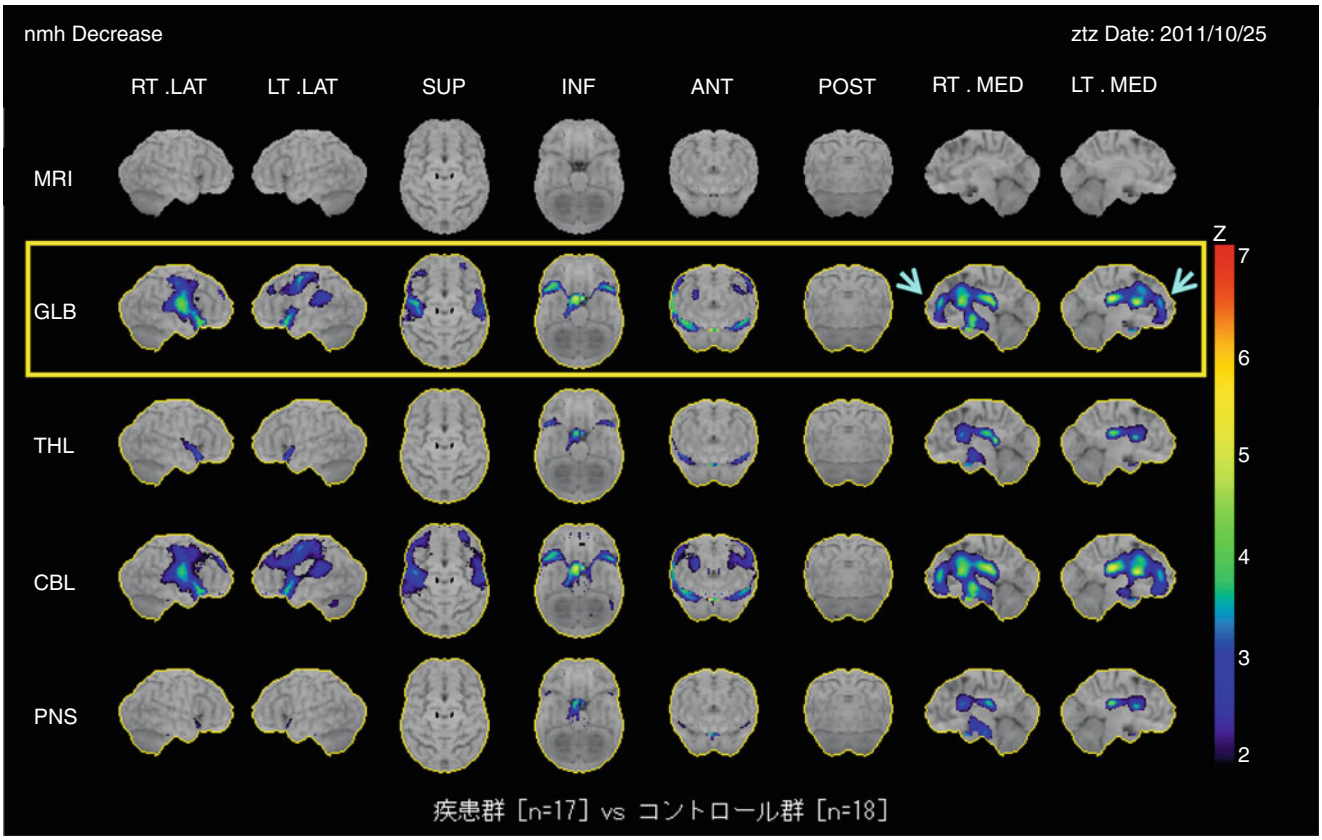

Fig. 1 Comparison between the normal database and the group of 17 patients (Z-score >2). *Upper law*: MRI;magnetic resonance imaging(reference image) standardized brain surface (eight directions). *2nd law*: GLB;global tissue 3D-SSP analysis using standardized counts of global tissue. *3rd law*: THL;thalamus three-dimensional stereotactic surface projection (3D-SSP) analysis using standardized counts of the thalamus. *4th law*: CBL; cerebellum 3D-SSP analysis using standardized counts of the cerebellum. *5th law*: PNS: pons 3D-SSP analysis using standardized counts of the pons. *Right bar*: *rainbow color* shows cluster of pixels (Z-score >2). On the 2nd law, 3D-SSP analysis shows a common area of significant cortical neuron loss in the bilateral medial frontal lobes, especially around the bilateral medial frontal gyrus (MFG) and the anterior cingulate gyrus (ACG)

who should be managed with surgery. ^{123}I-IMZ-SPECT could also be useful as an indicator of cortical neuron loss after focal cerebral ischemia. The reduction of BZR density in reperfused cortex that remained structurally intact is likely to be the result of injury to only a limited number of neurons (i.e., incomplete brain infarction) [10, 11]. The study of permanent or transient ischemia (lasting 3–6 h) in baboons by Sette et al. [12], who used ^{18}F-flumazenil (FMZ) as a BZR radioligand and PET, has a more direct relevance to the study of the incomplete brain infarction in reperfused cortex using ^{123}I-IMZ-SPECT. They observed a decrease in BZR binding, not only in the infarcted area, but also, albeit to a lesser degree, in the CT-intact opercular cortex overlying the hypodense area. Incomplete brain infarction defined by the reduction of central BZR density using ^{123}I-IMZ-SPECT had been observed within ischemic penumbra salvaged by restored CBF in acute stroke and could have occurred within long-term hemodynamic cerebral ischemia such as misery perfusion in chronic stroke. More recently, the relationship between long-term hemodynamic ischemia and the occurrence of incomplete brain infarction in patients with moyamoya disease was estimated to establish diagnostic neuroimaging for the HBD using ^{123}I-IMZ-SPECT [13].

Recently, in patients with HBD after MTBI, ^{123}I-IMZ-SPECT study demonstrated areas of cortical neuron loss in bilateral medial frontal lobes [14]. In the present study, a group comparison between the normal database and the group of 17 patients clearly showed that common areas of significant cortical neuron loss were demonstrated in bilateral medial frontal lobes, especially around bilateral MFG and ACG, under a Z-score >2. In the assessment of cortical neuron loss at the gyrus level, 14 of the 17 patients (83 %) demonstrated significant loss of cortical neurons in bilateral MFG or ACG. Cortical neuron loss in the bilateral medial frontal lobes was also demonstrated using ^{11}C-FMZ

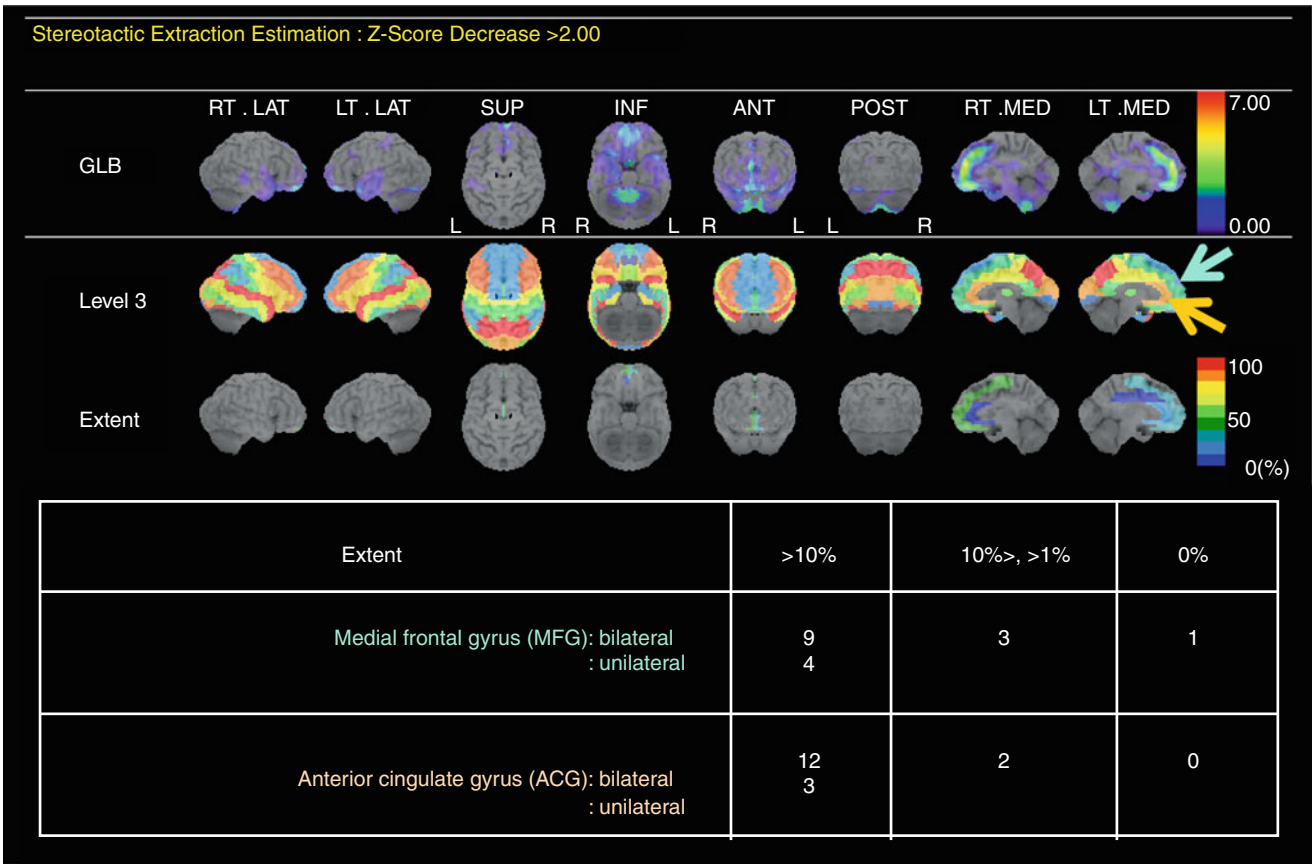

Extent	>10%	10%>, >1%	0%
Medial frontal gyrus (MFG): bilateral : unilateral	9 4	3	1
Anterior cingulate gyrus (ACG): bilateral : unilateral	12 3	2	0

Fig. 2 Stereotactic extraction estimation (SEE) level 3 analysis for the assessment of cortical neuron loss in the bilateral frontal medial cortex. *1st law*: 3D-SSP analysis using standardized counts of global tissue (Z-score>0). *2nd law*: each gyrus was represented by a different color. *3rd law*: extent (%) of abnormal pixels in each gyrus was shown by a different color. *Lower table*: number of patients with significant cortical neuron loss in the bilateral and unilateral MFG and ACG. The lower table shows the summary of SEE level 3 analysis. In 17 patients, significant cortical neuron loss was observed in the bilateral MFG in 9 patients and unilateral MFG in 4 patients, and in the bilateral ACG in 12 patients and unilateral ACG in 3 patients

Table 1 Summary of 17 patients and degree of cortical neuron loss in bilateral frontal lobes and the extent (%) of abnormal pixels indicated a reduction of benzodiazepine receptor (BZR) in the bilateral frontal medial cortex

			Frontal lobe				Frontal medial cortex (%)			
			MFL		LFL		MFG		ACG	
Case	Age/sex	Duration to examinations (months)	Leftt	Right	Left	Right	Left	Right	Left	Right
1	64/M	82	+	++	–	+	26.7	36.8	5.6	10.6
2	61/M	47	++	++	–	–	17.8	17.6	18.9	23.9
3	67/F	207	+	+	+	–	24.5	16.2	8.3	8.9
4	27/F	132	++	+	+	–	15.0	7.7	25.6	25.0
5	29/F	146	++	++	++	–	43.1	34.4	32.8	32.2
6	67/F	14	++	++	–	+	21.9	35.0	22.2	25.0
7	17/F	138	–	+	–	–	0.2	5.9	6.1	10.0
8	57/F	15	++	+	–	–	14.0	4.9	92.2	71.7
9	19/M	34	++	++	–	–	36.8	45.7	23.9	14.4
10	40/F	109	++	+	–	–	15.0	9.5	26.7	16.7
11	21/F	22	+	–	–	–	0.0	0.0	11.7	7.8
12	70/M	36	++	++	–	–	12.6	15.6	45.6	45.0
13	63/M	31	++	++	–	–	13.8	16.8	18.3	27.2
14	71/F	238	+	+	–	+	7.5	4.9	13.3	13.3
15	27/F	9	–	+	–	+	9.3	24.9	1.1	1.7
16	68/M	240	+	+	+	–	2.0	3.2	18.3	27.2
17	68/F	17	++	++	–	–	20.9	24.3	17.8	14.4
平均	49±21	89±81					16.5±11.9	17.9±13.7	22.9±20.9	22.1±16.7

++ cortical neuron loss in multiple area, + cortical neuron loss in single area, – no area of cortical neuron loss
MFL medial frontal lobe, *LFL* lateral frontal lobe, *MFG* medial frontal gyrus, *ACG* anterior cingulate gyrus

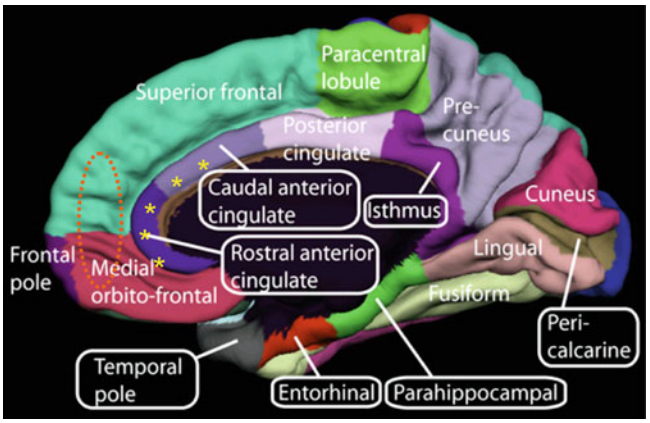

Fig. 3 Injury of the anterior corpus callosum (*asterisk*) assumed by cortical neuron loss in the bilateral MFG and ACG. In patients with higher brain dysfunctions, selective cortical neuron loss within the bilateral MFG and ACG could be caused by Wallerian degeneration as a secondary phenomenon after DAI within the anterior corpus callosum

PET in patients with HBD after diffuse TBI [15]. In addition, reduction of glucose metabolism in bilateral medial frontal lobes was reported in patients with post-traumatic HBD using ^{18}F-glucose PET [16]. From these findings, in patients with MTBI, HBD seems to correlate with cortical neuron loss within bilateral MFG or ACG where the lesions responsible for HBD could be, which consist of cognitive impairments such as memory, attention, performance, and social behavioral disturbances.

The mechanism of cortical neuron loss in the bilateral medial frontal lobe has to be discussed in relation to diffuse axonal injury (DAI) in MTBI. Initially, DAI had been reported to be a pathophysiological process of severe head injury associated with consciousness disturbance without intracranial occupying lesions [17]. Lesions of DAI were generally produced in the upper brain stem, the corpus callosum, and the cerebral white matter. However, recent study using diffusion tensor imaging showed that DAI could be produced in patients with MTBI [4, 18]. The concept of DAI can provide an important interpretation of the mechanism of post-traumatic HBD [19, 20]. DAI could easily occur in cases of traffic accidents with a rotational acceleration or deceleration force within intracranial structures [21]. Recently, a three-dimensional digital voxel or finite element human-head model showed that rotational accelerated head injury could produce DAI in specific structures of the brain such as the corpus callosum neighboring the edge of the falx or the upper brain stem neighboring the edge of the tentorium [22, 23]. High shear strain around the edge of the falx and the edge of the tentorium could be generated by a difference in mobility dural tissue and brain tissue at the time of rotational accelerated head injury. In patients with higher brain dysfunction, selective cortical neuron loss within bilateral MFG and ACG could be mainly caused by Wallerian degeneration [24] as a secondary phenomenon after DAI within an anterior corpus callosum (Fig. 3). Consciousness disturbance at the time of head injury seems to be produced by DAI in the upper brain stem, but in patients with post-traumatic HBD after MTBI, DAI in the upper brain stem could be less severe than that in the anterior corpus callosum. From this speculation, DAI in anterior corpus callosum could be assumed to be the main cause of post-traumatic HBD, and the presence of unconsciousness at the time of brain injury might not be a necessary factor in certifying a diagnosis of post-traumatic HBD.

In summary, in patients with MTBI, HBD seems to correlate with cortical neuron loss within the bilateral MFG or ACG, which could be the lesion responsible, and mainly caused by Wallerian degeneration as a secondary phenomenon after DAI within the anterior corpus callosum. Statistical imaging analysis using 3D-SSP and SEE level 3 for ^{123}I-IMZ SPECT could be valuable for the diagnostic imaging of post-traumatic HBD after MTBI. Multicenter study should be performed to confirm the clinical significance of ^{123}I-IMZ SPECT for the diagnosis of post-traumatic HBD.

Conflict of Interest This study was supported by research funds from the general insurance association of Japan.
We declare that we have no conflict of interest.

References

1. Masuzawa H, Hirakawa K, Tomita H et al (2004) Higher brain dysfunction due to traumatic brain injury through traffic accident. Jpn J Neurosurg (Tokyo) 13:104–110
2. Holm L, Cassidy JD, Carroll LJ et al (2005) Summary of the WHO collaborating centre for neurotrauma task force on mild traumatic brain injury. J Rehabil Med 37:137–141
3. Inglese M, Makani S, Johnson G et al (2005) Diffuse axonal injury in mild traumatic brain injury: a diffusion tensor imaging study. J Neurosurg 103:298–303
4. Esselman PC, Uomoto JM (1995) Classification of the spectrum of mild traumatic brain injury. Brain Inj 9:417–424
5. Nakjima Y, Terashima A (eds) (2006) Hand book of higher brain dysfunction. Igaku-shoin, Tokyo
6. Minoshima S, Frey KA, Koeppe RA et al (1995) A diagnostic approach in Alzheimer's disease using three-dimensional stereotactic surface projections of fluorine-18-FDG PET. J Nucl Med 36:1238–1248
7. Mizumura S, Kumita S, Cho K et al (2003) Development of quantitative analysis method for stereotactic brain image: assessment of reduced accumulation in extent and severity using anatomical segmentation. Ann Nucl Med 17:289–295
8. Mizumura S, Nakagawara J, Takahashi M et al (2004) Three-dimensional display in staging hemodynamic brain ischemia for JET study: objective evaluation using SEE analysis and 3D-SSP display. Ann Nucl Med 18:13–21
9. Hatazawa J, Satoh T, Shimosegawa E et al (1995) Evaluation of cerebral infarction with iodine-123-iomazenil SPECT. J Nucl Med 36:2154–2161
10. Garcia JH, Lassen NA, Weiller C et al (1996) Ischemic stroke and incomplete infarction. Stroke 27:761–765
11. Nakagawara J, Sperling B, Lassen NA (1997) Incomplete brain infarction may be quantitated with iomazenil. Stroke 28:124–132
12. Sette G, Baron JC, Young AR et al (1993) In vivo mapping of brain benzodiazepine receptor changes by positron emission tomography after focal ischemia in the anesthetized baboon. Stroke 24:2046–2058

13. Nakagawara J (2010) Iomazenil SPECT (BZR-receptor). In: Cho B-K, Tominaga T (eds) Moyamoya disease update. Springer, Tokyo, pp 189–196
14. Nakagawara J, Kamiyama K, Takahashi M et al (2010) Neuroimaging of post-traumatic higher brain dysfunction using ^{123}I-iomazenil (IMZ) SPECT. Neurotraumatology 33:165–172
15. Kawai N, Okauchi M, Kawakita K et al (2010) Focal neuronal los in patients with neuropsychological impairment following traumatic brain injury: evaluation of central benzodiazepine receptor using ^{11}C-flumazenil positron emission tomography. Neurotraumatology 33:173–179
16. Kato T, Nakayama N, Yasokawa Y et al (2007) Statistical image analysis of cerebral glucose metabolism in patients with cognitive impairment following diffuse traumatic brain injury. J Neurotrauma 24:919–926
17. Gennarelli TA, Thibault LE, Adams JH et al (1982) Diffuse axonal injury and traumatic coma in the primate. Ann Neurol 12: 564–574
18. Niogi SN, Mukherjee P, Ghajar J et al (2008) Extent of microstructural white matter injury in postconcussive syndrome correlates with impaired cognitive reaction time: a 3T diffusion tensor imaging study of mild traumatic brain injury. AJNR Am J Neuroradiol 29:967–973
19. Fork M, Bartels C, Ebert AD et al (2005) Neuropsychological sequelae of diffuse traumatic brain injury. Brain Inj 19:101–108
20. Scheid R, Walther K, Guthke T et al (2006) Cognitive sequelae of diffuse axonal injury. Arch Neurol 63:418–424
21. Kawamata T, Katayama Y (2008) Diffuse axonal injury. In: Oota T, Matsutani M (eds) Neurosurgery. Kinpodo, Kyoto, pp 1272–1278
22. Watanabe D, Yuge K, Nishimoto T et al (2008) Head impact analysis related to the mechanism of diffuse axonal injury. Student papers from FISITA 2008. International Federation of Automotive Engineering Societies, 2008. Available from online. http://www.fisita.com/education/congress/sc08papers/f2008sc044.pdf. Accessed 27 Oct 2011
23. Kleiven S (2006) Evaluation of head injury criteria using a finite element model validated against experiments on localized brain motion, intracerebral acceleration, and intracranial pressure. Int J Crashworthiness 11(1):65–79
24. Kelley BJ, Farkas O, Lifshitz J et al (2006) Traumatic axonal injury in the perisomatic domain triggers ultrarapid secondary axotomy and Wallerian degeneration. Exp Neurol 198:350–360

PET Molecular Imaging to Investigate Higher Brain Dysfunction in Patients with Neurotrauma

Tadashi Nariai, Motoki Inaji, Yoji Tanaka, Mikio Hiura, Chihiro Hosoda, Kenji Ishii, and Kikuo Ohno

Abstract *Introduction*: Many neurotrauma patients suffer from higher brain dysfunction even when focal brain damage is not detected with MRI. We performed functional imaging with positron emission tomography (PET) to clarify the relationship between the functional deficit and symptoms of such patients. *Methods*: Patients who complain of higher brain dysfunction without apparent morphological cortical damage were recruited. Thirteen patients underwent PET study to image glucose metabolism by ^{18}F-FDG, and central benzodiazepine receptor (cBZD-R) by ^{11}C-flumazenil, together with measurement of cognition. *Results*: Diffuse axonal injury (DAI) patients have a significant decrease in glucose metabolism and cBZD-R distribution in the cingulated cortex than normal controls. Score of cognition test was variable among patients. The degree of decreased glucose metabolism and cBZD-R in the dominant hemisphere corresponded well to the severity of cognitive disturbance. Patients with a milder type of diffuse brain injury (i.e., cerebral concussion) also showed abnormal glucose metabolism and cBZD-R distribution when they suffered from cognitive deficit. *Conclusion*: PET molecular imaging was useful for depicting the cortical dysfunction of neurotrauma patients even when morphological change was not apparent. This method may be promising in clarifying the pathophysiology of higher brain dysfunction of patients with neurotrauma, but without morphological abnormality.

Keywords Diffuse brain injury • Cerebral concussion • PET • FDG • Flumazenil • Brain cognition

Introduction

Higher brain dysfunction is a major problem for patients who have recovered from neurotrauma as it prevents them from returning to their previous social life. Many patients with diffuse brain injury such as diffuse axonal injury, cerebral concussion, and chronic traumatic encephalopathy (CTE) [1, 2] do not have their focal brain damage detected with morphological imaging. In such cases, the lack of concrete evidence to connect symptoms and focal brain lesions often causes medical and social problems.

Positron emission tomography (PET) is a powerful tool for depicting the abnormal pathology of the brain using various molecular probes. In the clinical study of cognitive disorders such as Alzheimer's disease, functional or pathological changes are known to be detected in the early stages when there is no brain atrophy and the cognitive deficit is only mild [3, 4]. We considered that the use of PET molecular imaging is also useful in depicting the cognitive deficit of patients with diffuse brain injury, even when they do not have apparent morphological damages. We also hypothesized that the high sensitivity of PET imaging might also be utilized to analyze mild cognitive change in cerebral concussion patients. We focused on studying the correlation between PET-measured focal brain dysfunction and the score of various cognition tests using a statistical image analysis technique.

T. Nariai (✉), M. Inaji, Y. Tanaka, and K. Ohno
Department of Neurosurgery, Tokyo Medical and Dental University, Bunkyo-ku, Tokyo, Japan
e-mail: nariai.nsrg@tmd.ac.jp

M. Hiura
Faculty of Sports and Health Science, Hosei University, Tokyo, Japan

C. Hosoda
Department of Cortical Function Disorders, National Center of Neurology and Psychiatry, Kodaira, Tokyo, Japan

K. Ishii
Positron Medical Center, Tokyo Metropolitan Institute of Gerontology, Itabashi-ku, Tokyo, Japan

Y. Katayama et al. (eds.), *Brain Edema XV*, Acta Neurochirurgica Supplement, Vol. 118,
DOI 10.1007/978-3-7091-1434-6_47,

Patients and Methods

Patients who complained of higher brain dysfunction without apparent morphological cortical damage were recruited for this study. Thirteen patients with diffuse axonal injury (DAI), cerebral concussion, or acute epidural or subdural hematoma without brain contusion were included.

They were subjected to PET study in order to image the glucose metabolism by ^{18}F-FDG, and the central benzodiazepine receptor (cBZD-R; a neuronal body marker) using ^{11}C-flumazenil. PET study was carried out using a Headtome-V scanner (Shimadzu Corporation, Kyoto, Japan). In both studies, static images after bolus injection of radiopharmaceuticals (150 MBq of t^{18}F-FDG and 300 MBq of ^{11}C-flumazenil) were obtained depending on our former validation study [5]. The database of normal controls that was established in the Positron Medical Center, at the Tokyo Metropolitan Institute of Gerontology, was used to perform statistical analysis by comparing age-matched controls with patients. In selected subjects, diffusion-weighted MR imaging was performed to examine the regional fractional anisotropy (FA) value.

All subjects underwent measurement of cognition using the Wechsler Adult Intelligence Scale (WAIS-R), the Wechsler Memory Scale (WMS-R), and at least one of the tests that evaluate executive function such as the Wisconsin Card Sorting Test (WCST). PET data of the patients were analyzed using the SPM2 program working on a personal computer [6].

The local ethics committee of the Tokyo Metropolitan Institute of Gerontology approved the study protocol.

Results

Eight patients had a history of diffuse axonal injury with prolonged loss of consciousness after injury. Some of them had minor subcortical lesions detectable with MRI such as petechial hemorrhage or white matter lesions, but none of them had apparent focal cortical lesions. Statistical analysis of PET images of patients' group in comparison to the age-matched normal volunteers was performed for FDG and FMZ studies. Area with a significantly reduced FDG uptake (upper row) and flumazenil (FMZ) binding (lower row) of the group of patients in comparison to normal controls were displayed in Fig. 1. FDG uptake was significantly reduced in the cerebellum, bilateral thalamus, and cingulate cortex. FMZ binding was significantly reduced in the whole of the cingulate gyrus and left medial temporal lobe. As FMZ binding is considered to represent neuronal integrity and FDG uptake represents brain function, the cingulate gyrus may be the initially damaged area in DAI and dysfunction of the thalamus and cerebellum may represent a remote effect (diaschisis) of the cerebral functional deficit.

In this group analysis, the characteristic functional deficit of DAI may be attributed to the initial damage of the cingulate cortex. The degree of the cognitive deficit, however, is highly variable among patients. Also, the higher brain function of humans has been described as the functional deficit of the neocortex rather than the archicortex. Statistical analysis of PET images of each patient in comparison to normal controls, therefore, must be performed. In Fig. 2, SPM analyses of flumazenil (FMZ) binding of two patients with DAI were displayed. Case 1 is a 24 year-old man who had a disturbed intelligent quotient (verbal IQ = 69) and memory. Reduced FMZ binding was noted in the left temporal lobe in addition to the cingulate cortex. Case 2 is a 37-year-old man whose WAIS and WMS scores were within the normal range. Deficit of executive function was observed in cognitive tests and he has failed to return to his previous occupation. Reduced FMZ binding was noted in the right frontal lobe in addition to the cingulate cortex. As these case presentations suggest, the functional deficit of the dominant hemisphere caused major cognitive deficit, but that of the non-dominant hemisphere seemed to cause minor deficit such as executive dysfunction.

Some of patients enrolled into the present study did not have a history of prolonged consciousness disturbance, but still have cognitive deficit. PET images of such a category of patients are displayed in Fig. 3. In this patient, routine MRI examination was normal. We performed statistical analysis of diffusion MRI data to examine the change in the fractional anisotropy (FA) value of this patient in comparison to a normal control. Although routine MR examination failed to detect morphological focal brain damage, an area with significantly reduced FMZ binding was noted in the right frontal and temporal cortex (arrows). An area with a significantly reduced FA value was more prominently noted in the right hemisphere and partly corresponded to the area with reduced FMZ binding (arrows).

Conclusion

In the present study, using PET molecular imaging for the analysis of cognitive deficits of patients with diffuse brain injury such as DAI or cerebral concussion, we demonstrated that statistical analysis of FDG-PET and FMZ-PET depicts well the dysfunction of the cerebral cortex among the group of patients and also in each patient.

When cortical damage was not detected by a morphological image, the functional deficit should be attributable to axonal injury. In previous reports from our group, we demonstrated that irreversible cortical dysfunction elicited by axonal injury decreased both glucose metabolism and central benzodiazepine receptor. On the other hand, decreased glucose metabolism at the area of preserved central benzodiazepine receptor recovered well, together with recovery of neurological

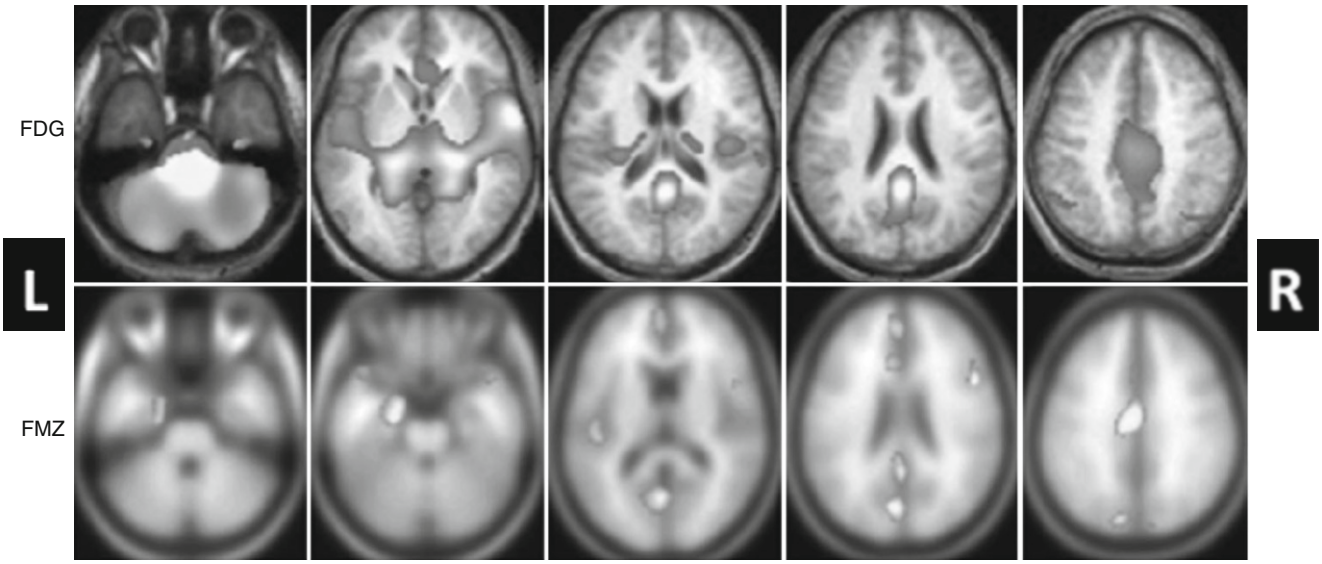

Fig. 1 Statistical analysis of PET images of the group of patients with diffuse axonal injury. Area with significantly reduced *FDG* uptake (*upper row*) and flumazenil (*FMZ*) binding (*lower row*) of the group of patient in comparison to normal controls were depicted by using SPM2 and were displayed on axial standardized brain slices. FDG uptake was significantly reduced in the cerebellum, bilateral thalamus, and posterior cingulate cortex. FMZ binding was significantly reduced in the whole of the cingulate gyrus and left medial temporal lobe

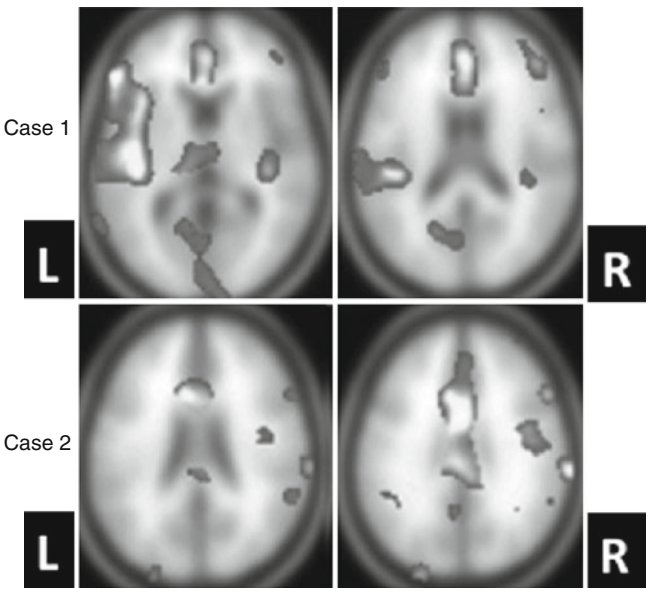

Fig. 2 Statistical analysis of FMZ binding of a single patient with diffuse axonal injury. Area with significantly reduced FMZ of the single patient in comparison to the normal control group was depicted by using SPM2 and was displayed on axial standardized brain slices. Case 1 is a 24-year-old man who has a disturbed intelligent quotient (verbal IQ = 69) and memory. Reduced FMZ binding was noted in the left temporal lobe in addition to the cingulate cortex. Case 2 is a 37-year-old man whose WAIS and WMS score was within the normal range. Only the executive function was disturbed. Reduce FMZ binding was noted in the right frontal lobe in addition to the cingulate cortex

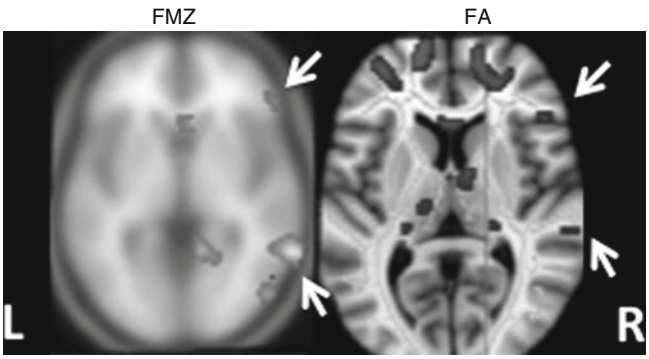

Fig. 3 Statistical analysis of PET FMZ binding and magnetic resonance diffusion fractional anisotropy (*FA*) map of a patient who presented higher brain dysfunction after cerebral concussion. Routine MR examination failed to detect morphological focal brain damage. Area with significantly reduced FMZ was noted in the right frontal and temporal cortex (*arrows*). Area with significantly reduced FA was more prominently noted in the right hemisphere and partly corresponded to the area with reduced FMZ binding (*arrows*)

symptoms [7]. Depending on this finding, we hypothesized that the combined measurement of cerebral glucose metabolism with ^{18}F-FDG and central benzodiazepine receptor using PET may be useful to analyze the correlation between axonal injury and cortical dysfunction. Binding of central benzodiazepine receptor is considered to represent the distribution of neurons in chronic conditions and can be measured by ^{11}C-flumazenil with PET and by ^{123}I-iomazenil with SPECT, although another interpretation must be made during the acute stage of ischemia, epilepsy, and neurotrauma [8–10].

Blood flow, metabolism, and benzodiazepine receptor distribution of the group of DAI patients have been investigated in several groups in Japan, and all of them, including our present study, depicted the cingulate gyrus as being one site of primary damage [11–13]. As this point is quite consistent among the studies, it may be recognized as a common finding. Higher brain dysfunction, however, has been described as the functional

deficit of the neo-cortex rather than the archicortex. Therefore, further analysis to examine the variation in cortical metabolism and receptor is necessary. By now, we demonstrated that the dysfunction of the dominant hemisphere correlated well with the severity of the higher brain dysfunction. Further accumulation of data is necessary to perform statistical correlation analysis [14], especially in order to analyze the correlation between focal brain dysfunction and the scores of various tests.

At present, higher brain dysfunction induced by mild head injury has been of interest. Of these cases, cerebral concussion patients have been included in our study. In our previous work [15], we examined the cerebral blood flow of concussion patients at the acute stage, and reported that a hyperemic condition in the mesial temporal lobe or frontal cortex was induced by disturbed auto-regulation of cerebral vessels. In the present work, we found that abnormal metabolism and receptor distribution existed when patients had a cognitive deficit, even when their initial consciousness disturbance was rather mild. As cerebral concussion often occurs in younger generations, especially in relation to sports injury, accumulation of clinical data is extremely important to protect athletes from chronic traumatic encephalopathy [16–19].

In our present report, we used diffusion-weighted MRI to depict the axonal damage as a pilot study (Fig. 3). Location of significant fractional anisotropy values [20, 21] in the subcortical white matter and decreased FMZ binding cortex corresponded well. This combined use of PET and MRI must be the next step to be performed.

In summary, PET molecular imaging was useful in depicting the cortical dysfunction of neurotrauma patients, even when morphological change was not apparent. This method may be promising in clarifying the pathophysiology of higher brain dysfunction of patients with neurotrauma but without morphological abnormality. Further accumulation of various types of patients is necessary to clarify the correlation between abnormality according to the cognitive tests and focal cortical damage.

Acknowledgment This study was supported by a research grant from The General Insurance Association of Japan.

Conflict of Interest We declare that we have no conflict of interest.

References

1. Omalu BI, Fitzsimmons RP, Hammers J, Bailes J (2010) Chronic traumatic encephalopathy in a professional American wrestler. J Forensic Nurs 6:130–136
2. Omalu BI, DeKosky ST, Minster RL, Kamboh MI, Hamilton RL, Wecht CH (2005) Chronic traumatic encephalopathy in a National Football League player. Neurosurgery 57:128–134; discussion 128–134
3. Minoshima S, Frey KA, Koeppe RA, Foster NL, Kuhl DE (1995) A diagnostic approach in Alzheimer's disease using three-dimensional stereotactic surface projections of fluorine-18-FDG PET. J Nucl Med 36:1238–1248
4. Klunk WE, Engler H, Nordberg A, Wang Y, Blomqvist G, Holt DP, Bergstrom M, Savitcheva I, Huang GF, Estrada S, Ausen B, Debnath ML, Barletta J, Price JC, Sandell J, Lopresti BJ, Wall A, Koivisto P, Antoni G, Mathis CA, Langstrom B (2004) Imaging brain amyloid in Alzheimer's disease with Pittsburgh Compound-B. Ann Neurol 55:306–319
5. Mishina M, Senda M, Kimura Y, Toyama H, Ishiwata K, Ohyama M, Nariai T, Ishii K, Oda K, Sasaki T, Kitamura S, Katayama Y (2000) Intrasubject correlation between static scan and distribution volume images for [11C]flumazenil PET. Ann Nucl Med 14:193–198
6. Friston KJ (1996) Statistical parametric mapping and other analyses of functional imaging data. In: Toga AW, Mazziotta JC (eds) Brain mapping the methods. Academic, San Diego, pp 363–386
7. Suzuki Y, Horie C, Kiyosawa M, Nariai T, Mochizuki M, Oda K, Kimura Y, Ishiwata K, Ishii K (2008) Measurement of the (11) C-flumazenil binding in the visual cortex predicts the prognosis of hemianopia. J Neurol Sci 268:102–107
8. Koizumi H, Fujisawa H, Kurokawa T, Suehiro E, Iwanaga H, Nakagawara J, Suzuki M (2010) Recovered neuronal viability revealed by iodine-123-iomazenil SPECT following traumatic brain injury. J Cereb Blood Flow Metab 30:1673–1681
9. Nakagawara J, Sperling B, Lassen NA (1997) Incomplete brain infarction of reperfused cortex may be quantitated with iomazenil. Stroke 28:124–132
10. Amemiya S, Hamamoto M, Mishina M, Ueda M, Kumagai T, Nishiyama Y, Katayama Y (2008) Short-term plasticity of central benzodiazepine receptors in status epilepticus: case report. Acta Neurol Scand 117:285–288
11. Kawai N, Maeda Y, Kudomi N, Yamamoto Y, Nishiyama Y, Tamiya T (2010) Focal neuronal damage in patients with neuropsychological impairment after diffuse traumatic brain injury: evaluation using ^{11}C-flumazenil positron emission tomography with statistical image analysis. J Neurotrauma 27:2131–2138
12. Okamoto T, Hashimoto K, Aoki S, Ohashi M (2007) Cerebral blood flow in patients with diffuse axonal injury – examination of the easy Z-score imaging system utility. Eur J Neurol 14:540–547
13. Nakashima T, Nakayama N, Miwa K, Okumura A, Soeda A, Iwama T (2007) Focal brain glucose hypometabolism in patients with neuropsychologic deficits after diffuse axonal injury. AJNR Am J Neuroradiol 28:236–242
14. Hosoda C, Nariai T, Ishiwata K, Ishii K, Matsushima Y, Ohno K (2010) Correlation between focal brain metabolism and higher brain function in patients with Moyamoya disease. Int J Stroke 5:367–373
15. Nariai T, Suzuki R, Ohta Y, Ohno K, Hirakawa K (2001) Focal cerebral hyperemia in postconcussive amnesia. J Neurotrauma 18: 1323–1332
16. McCrory P, Zazryn T, Cameron P (2007) The evidence for chronic traumatic encephalopathy in boxing. Sports Med 37:467–476
17. Omalu B, Bailes J, Hamilton RL, Kamboh MI, Hammers J, Case M, Fitzsimmons RJ (2011) Emerging histomorphologic phenotypes of chronic traumatic encephalopathy in American athletes. Neurosurgery 69:173–183
18. Johnson VE, Stewart W, Smith DH (2011) Widespread Tau and amyloid-beta pathology many years after a single traumatic brain injury in humans. Brain Pathol. doi:10.1111/j.1750-3639.2011.00513.x
19. McKee AC, Cantu RC, Nowinski CJ, Hedley-Whyte ET, Gavett BE, Budson AE, Santini VE, Lee HS, Kubilus CA, Stern RA (2009) Chronic traumatic encephalopathy in athletes: progressive tauopathy after repetitive head injury. J Neuropathol Exp Neurol 68:709–735
20. Kang X, Herron TJ, Woods DL (2010) Validation of the anisotropy index ellipsoidal area ratio in diffusion tensor imaging. Magn Reson Imaging 28:546–556
21. Xu J, Rasmussen IA, Lagopoulos J, Haberg A (2007) Diffuse axonal injury in severe traumatic brain injury visualized using high-resolution diffusion tensor imaging. J Neurotrauma 24:753–765

Evaluation of Cerebral Function Using Iomazenil SPECT for Patients with Traumatic Brain Injury

Yasushi Shibata and Kiyoshi Endo

Abstract Traumatic brain injuries demonstrate various symptoms, including the disturbance of higher brain function, which is not visualized as a morphological lesion on magnetic resonance (MR) imaging. We examined the use of iomazenil single photon emission computed tomography (SPECT) for patients with traumatic brain injury and evaluated its diagnostic value. The study population included patients who were admitted to our hospital for traumatic brain injuries. All patients survived and were discharged from our hospital. MR imaging and iomazenil SPECT were examined during the acute and/or chronic phases. MR images were acquired using a 1.5-T clinical instrument. The T1- and T2-weighted and fluid-attenuated inversion recovery (FLAIR) axial images were evaluated. SPECT images were acquired using a multi-detector SPECT machine 3 h after the intravenous injection of 740 MBq of iomazenil. Axial, statistically analyzed images and stereotactic extraction estimation images were reconstructed and evaluated statistically based on the Z-score for each cerebral cortex. Iomazenil SPECT showed various lesions that were not demonstrated by MR imaging. Some clinical symptoms correlated with the iomazenil SPECT findings. Iomazenil SPECT is thus considered to be valuable for evaluating both brain lesions and the brain function after traumatic brain injury.

Keywords Cerebral contusion • Concussion • Subarachnoid hemorrhage • Diffuse axonal injury • Acute epidural hematoma • Acute subdural hematoma • Magnetic resonance imaging • Single photon emission computed tomography • Iomazenil • Traumatic brain injury

Y. Shibata, MD, PhD (✉) and K. Endo, MD, PhD
Department of Neurosurgery, Mito Medical Center,
Mito Kyodo General Hospital, University of Tsukuba,
Miyamachi 3-2-7, Mito, Ibaraki, 310-0015, Japan
e-mail: yasushishibatamd@yahoo.co.jp

Introduction

Traumatic brain injury demonstrates various symptoms, including the disturbance of higher brain function, which is not revealed as a morphological lesion by magnetic resonance (MR) imaging. Iomazenil single photon emission computed tomography (SPECT) is a functional imaging method used to evaluate the cortical benzodiazepine receptor density [1, 8]. Iomazenil SPECT is valuable in evaluating the neuronal injury caused by ischemia, hematoma, and reperfusion injury [4–7]. We examined iomazenil SPECT for patients with traumatic brain injury during the acute and chronic phases and evaluated its diagnostic value compared with MRI findings.

Patients and Methods

The study population included patients who were admitted to our hospital for traumatic brain injury. The clinical and MRI diagnoses were concussion, traumatic subarachnoid hemorrhage (SAH), cerebral contusion, diffuse axonal injury (DAI), acute epidural hematoma (AEDH), and acute subdural hematoma (ASDH). All patients survived and were discharged from our hospital.

Magnetic resonance imaging and SPECT were performed during the acute and/or chronic phases. MR images were acquired using a 1.5-T clinical machine (Symphony, Siemens). T1- and T2-weighted and fluid attenuated inversion recovery (FLAIR) axial images were evaluated for MRI. For SPECT, images were acquired using a multi-detector SPECT machine (E.CAM, Siemens) 3 h after the intravenous injection of 740 MBq of iomazenil. Axial and stereotactic extraction estimation (SEE) images were reconstructed, and brain surface projection images were evaluated by calculating the Z-score for each cerebral cortex.

Y. Katayama et al. (eds.), *Brain Edema XV*, Acta Neurochirurgica Supplement, Vol. 118,
DOI 10.1007/978-3-7091-1434-6_48,

Results

Case 1

Magnetic resonance imaging of a 17-year-old boy with cerebral concussion did not show any high T2 intensity lesions (Fig. 1). However, the iomazenil SPECT demonstrated decreased iomazenil uptake at the temporal lobe. During the chronic phase, the area of decreased iomazenil uptake shrunk, but still remained, and a crossed cerebellar diaschisis was observed.

Case 2

In a 48-year-old man with traumatic SAH, focal low iomazenil uptake was observed at bilateral peripheral areas of the middle cerebral arteries (Fig. 2). These findings may be related to the vasospasms caused by traumatic SAH. However, these low uptake areas were observed during both the acute and chronic phases. In cases of DAI, focal low cortical uptake of iomazenil was observed, and this finding was not related to the MRI findings of both FLAIR and T2* lesions. Iomazenil SPECT may therefore reveal cortical or subcortical dysfunction not revealed by MRI.

In cases of cerebral contusion, focal low cortical uptake of iomazenil was observed. Generally, the lesion sizes indicated by iomazenil SPECT were larger than those indicated by MR FLAIR imaging. Most low iomazenil uptake areas correlated with the area of the MRI lesions; however, some areas were not correlated. Small contusional lesions often shrunk or disappeared during the chronic phase, as determined by both MRI and iomazenil SPECT. Large contusions showed decreased high T2 areas and atrophy in the chronic phase. In iomazenil SPECT, some decreases in the low uptake area were observed; however, large low uptake areas were still observed during the chronic phase.

In cases of AEDH and ASDH, iomazenil SPECT showed decreased uptake of iomazenil at the site of the lesion, even though the MR imaging showed no abnormality. These decreases in iomazenil uptake during the acute phase returned to normal during the chronic phase.

Case 3

In a 72-year-old man with interhemispheric ASDH, MRI showed unilateral lesions; however, iomazenil SPECT demonstrated a bilateral decrease in iomazenil uptake (Fig. 3). In comatose patients, even though MR imaging showed no abnormalities, decreased iomazenil uptake at the thalamus or

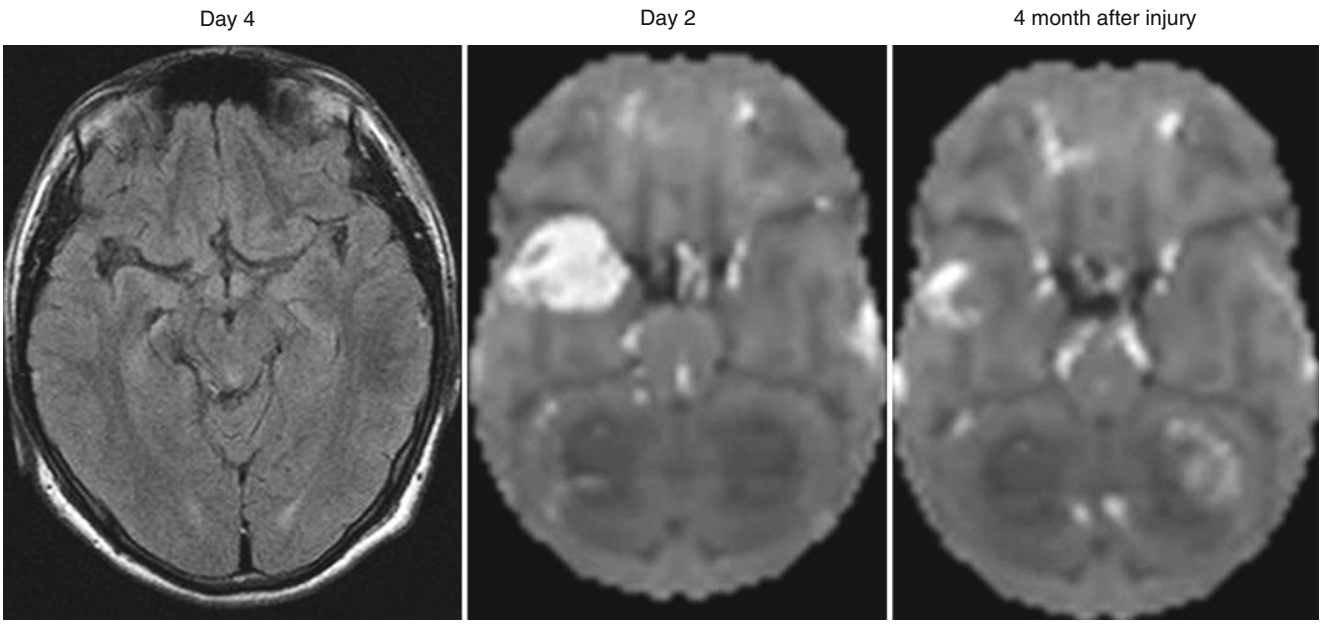

Fig. 1 A 17-year-old boy with cerebral concussion. He had transient loss of consciousness. MRI showed no abnormalities. Iomazenil single photon emission computed tomography (SPECT) demonstrated low uptake at the right temporal lobe during the acute phase. The size of this abnormality decreased during the chronic phase

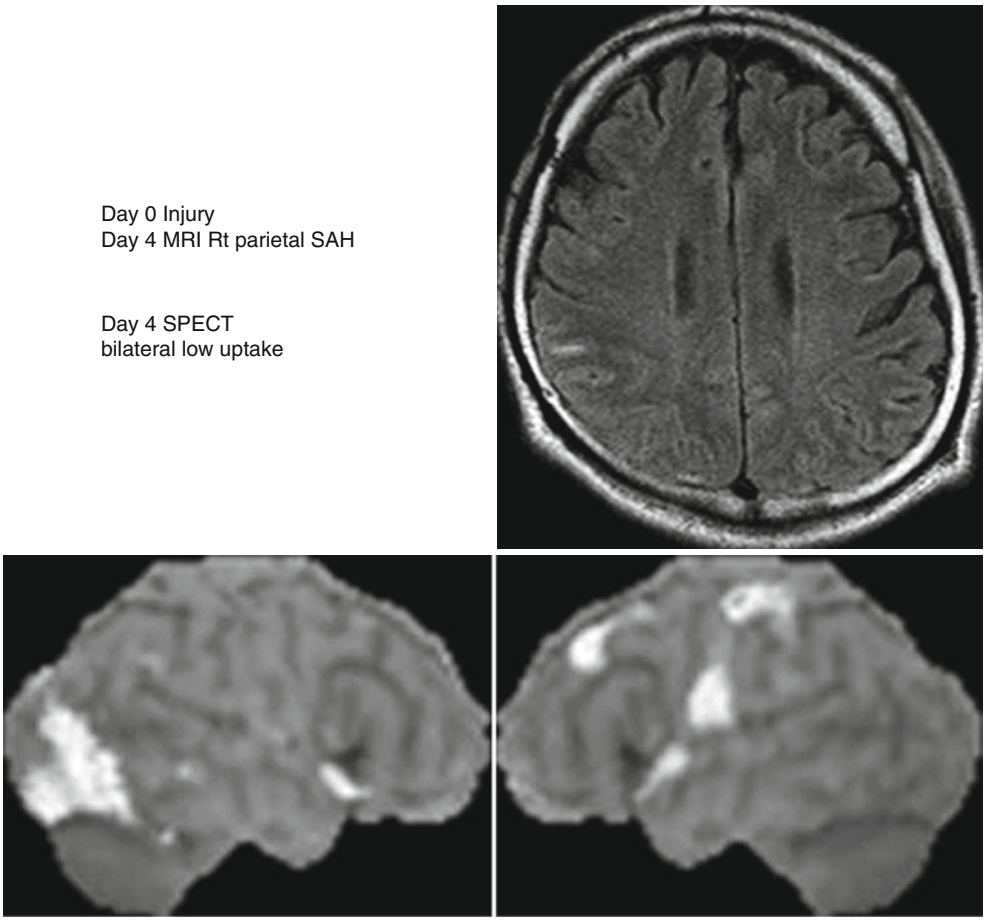

Fig. 2 A 48-year-old man with traumatic subarachnoid hemorrhage (SAH). MRI showed a right parietal traumatic SAH. Iomazenil SPECT revealed bilateral low cortical uptake, and these locations did not correspond with the location of the traumatic SAH

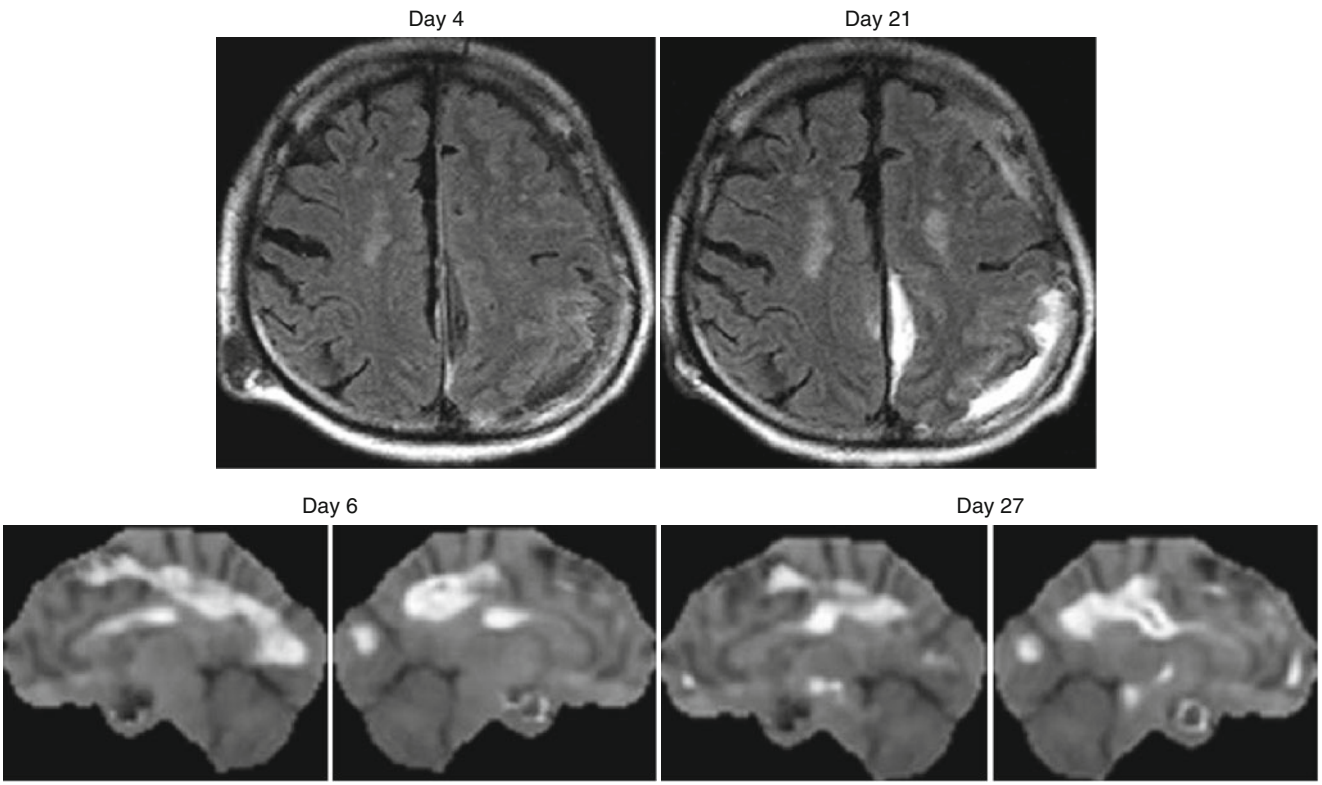

Fig. 3 A 72-year-old man with interhemispheric acute subdural hematoma (ASDH). MR imaging showed left-sided ASDH. Iomazenil SPECT demonstrated bilateral medial frontal low uptake. The low uptake at the temporal tip seems to be an artifact

limbic system were demonstrated during the acute phase. As the patients' consciousness returned to normal, the iomazenil SPECT findings also returned to normal.

Conclusion

Cerebral perfusion SPECT was reported to be valuable in evaluating the cerebral function and metabolism in traumatic brain injury [1, 2]. However, perfusion and metabolism are not always coupled. Only a few small series of iomazenil SPECT studies for traumatic brain injury have been reported [3, 6].

In our study, there were some discrepancies between the MRI and iomazenil SPECT findings. Some plausible reasons for these discrepancies are the different image resolutions, different imaging targets, and image reconstruction methods. MR imaging provides good spatial resolution. Because the spatial resolution of SPECT is poor, tiny lesions are not demonstrated by SPECT. MRI demonstrates the proton density and relaxation time values; thus, tomographic MR images show both the cortical and subcortical lesions. Iomazenil SPECT demonstrates the density of the benzodiazepine receptor, which is essentially located on the brain cortex. The Z-score and SEE images demonstrate only the cortical iomazenil uptake. It is reasonable to consider that subcortical lesions may also influence the apparent cortical iomazenil uptake. To understand the effect of subcortical lesions on the cortical iomazenil uptake, more clinical experience or a basic study will be necessary. Statistical image analysis is a useful method for easily evaluating raw data. However, because statistically analyzed images contain statistical artifacts that can interfere with the evaluation of data, it is necessary to evaluate the analyzed images carefully. The recovery of abnormal findings of both MRI and iomazenil SPECT was observed. The locations of the abnormality on MRI and iomazenil SPECT did not always correspond. Moreover, iomazenil SPECT was useful for evaluating neuronal function and metabolism, which are not revealed by MR imaging. In this study, we evaluated only the imaging findings. It will be necessary to compare our image findings with the clinical and neurological functions, especially higher-level functions like memory and cognitive function.

In summary, iomazenil SPECT showed various lesions that were not demonstrated by MR imaging. Some of the clinical symptoms correlated with the iomazenil SPECT findings. Iomazenil SPECT is therefore valuable in evaluating brain function after traumatic brain injury. Statistical image analysis is a useful method for easily evaluating raw data. However, because statistically analyzed images contain artifacts that can interfere with the evaluation of data, the analyzed images should be assessed carefully.

Conflict of Interest This study was partially supported by a Research Grant for the authors from ZENKYOREN (National Mutual Insurance Federation of Agricultural Cooperatives).

We declare that we have no conflict of interest.

References

1. Abi-Dargham A, Laruelle M, Seibyl J, Rattner Z, Baldwin RM, Zoghbi SS et al (1994) SPECT measurement of benzodiazepine receptors in human brain with iodine-123-iomazenil: kinetic and equilibrium paradigms. J Nucl Med 35:228–238
2. Gowda NK, Agrawal D, Bal C, Chandrashekar N, Tripati M, Bandopadhyaya GP et al (2006) Technetium Tc-99m ethyl cysteinate dimer brain single-photon emission CT in mild traumatic brain injury: a prospective study. AJNR Am J Neuroradiol 27: 447–451
3. Hashimoto K, Abo M (2009) Abnormal regional benzodiazepine receptor uptake in the prefrontal cortex in patients with mild traumatic brain injury. J Rehabil Med 41:661–665
4. Hatazawa J, Satoh T, Shimosegawa E, Okudera T, Inugami A, Ogawa T et al (1995) Evaluation of cerebral infarction with iodine 123-iomazenil SPECT. J Nucl Med 36:2154–2161
5. Hatazawa J, Shimosegawa E, Satoh T, Kanno I, Uemura K (1995) Central benzodiazepine receptor distribution after subcortical hemorrhage evaluated by means of [^{123}I]iomazenil and SPECT. Stroke 26:2267–2271
6. Koizumi H, Fujisawa H, Kurokawa T, Suehiro E, Iwanaga H, Nakagawara J et al (2010) Recovered neuronal viability revealed by iodine-123-iomazenil SPECT following traumatic brain injury. J Cereb Blood Flow Metab 30:1673–1681
7. Nakagawara J, Sperling B, Lassen NA (1997) Incomplete brain infarction of reperfused cortex may be quantitated with iomazenil. Stroke 28:124–132
8. Savic I, Roland P, Sedvall GR, Persson A, Pauli S, Widen L (1988) In-vivo demonstration of reduced benzodiazepine receptor binding in human epileptic foci. Lancet 332:863–866

Early Cerebral Circulation Disturbance in Patients Suffering from Different Types of Severe Traumatic Brain Injury: A Xenon CT and Perfusion CT Study

Mitsuru Honda, Shigeru Sase, Kyosuke Yokota, Ryo Ichibayashi, Katsunori Yoshihara, Hiroyuki Masuda, Hiroyuki Uekusa, Jun Nomoto, Nobuo Sugo, Taichi Kishi, and Yoshikatsu Seiki

Abstract *Introduction*: Traumatic brain injury (TBI) is widely known to cause dynamic changes in cerebral blood flow (CBF). In particular, secondary brain insults have been reported to decrease CBF. The purpose of this study was to clarify the cerebral circulation in different types of TBI.

Methods: Sixty-nine patients with TBI were divided into four groups, the subdural hematoma group, the contusion/intracerebral hematoma group, the diffuse axonal injury group, and the diffuse brain swelling group. In these patients, we simultaneously performed Xe-CT and perfusion CT to evaluate the cerebral circulation on post-injury days 1–3. We measured CBF using Xe-CT and mean transit time using perfusion CT and calculated the cerebral blood volume using the AZ-7000 W98 computer system.

Results: There were no significant differences in the Glasgow Coma Scale score on arrival or the Glasgow Outcome Scale score between the groups. The patients who had suffered focal TBI displayed more significant cerebral circulation disturbances than those that had suffered diffuse TBI. We were able to evaluate the cerebral circulation of TBI patients using these parameters.

Conclusion: Moderate hypothermia therapy, which decreases CBF, the cerebral metabolic rate oxygen consumption ($CMRO_2$), and intracranial pressure might be effective against the types of TBI accompanied by cerebral circulation disturbance. We have to use all possible measures including hypothermia therapy to treat severe TBI patients according to the type of TBI that they have suffered.

Keywords Severe brain injury • Acute cerebral circulation disturbance • Xenon CT • Perfusion CT

M. Honda, MD, PhD (✉), K. Yokota,
R. Ichibayashi, and K. Yoshihara
Department of Critical Care Center, Toho University
Medical Center Omori Hospital,
6-11-1 Omori-Nishi Ota-ku, Tokyo 143-8541, Japan
e-mail: mhonda@toho-u.ac.jp

S. Sase
R&D Division, Anzai Medical Co., Ltd,
3-9-15 Nishi-Shinagawa, Shinagawa-ku, Tokyo 141-0033, Japan

H. Masuda, H. Uekusa, J. Nomoto, N. Sugo, and Y. Seiki
Department of Neurosurgery, Toho University
Medical Center Omori Hospital,
Tokyo, Japan

T. Kishi
Department of Education Planning and Development,
Faculty of Medicine, School of Medicine, Toho University,
Tokyo, Japan

Introduction

Traumatic brain injury (TBI) is widely known to cause dynamic changes in cerebral blood flow (CBF). These hemodynamic changes play a key role in the pathophysiology of TBI. In particular, secondary brain insults have been reported to cause decreases in CBF. Ischemia is one of the major risk factors contributing to death and disability in TBI patients. In fact, several clinical TBI studies have linked low CBF to poor outcome [2, 9, 11]. Several factors can cause a decrease in CBF: intracranial hypertension, systemic arterial hypotension, cerebral edema, focal tissue compression by hematomas, and microvascular circulation disturbance. However, severe TBI induces heterogeneous hemodynamic changes, and different types of TBI induce different hemodynamic changes.

Positron emission tomography (PET), single-photon emission computed tomography (SPECT), and xenon-enhanced computed tomography (Xe-CT) are used to evaluate cerebral circulation and metabolism in the early phase of severe TBI. Recently, there has been interest in using CT perfusion imaging to assess patients with stroke and delayed cerebral vasospasm (CVS) after subarachnoid hemorrhaging [15, 16]. A number of hemodynamic parameters are available

Y. Katayama et al. (eds.), *Brain Edema XV*, Acta Neurochirurgica Supplement, Vol. 118,
DOI 10.1007/978-3-7091-1434-6_49,

for CT perfusion imaging. However, few investigations have attempted to explain the circulatory disturbances induced by TBI using perfusion CT [13, 14].

The purpose of this study was to clarify the effects of different types of TBI on the cerebral circulation with regard to hemodynamic parameters, neurological grade on admission, and patient outcome in the early phase (post-injury days 1–3). We measured the mean transit time (MTT), CBF, and cerebral blood volume (CBV) using CT perfusion and Xe-CT and evaluated the early circulatory disturbances induced by different types of TBI.

Patients and Methods

Patients

Sixty-nine patients who were admitted to our hospital with severe TBI were prospectively enrolled. The TBI of all patients was verified by CT on admission. Patients who were admitted to the intensive care unit (ICU) with TBI that was sufficiently severe to justify mechanical ventilation and a Glasgow Coma Scale (GCS) score of 8 or less at the time of admission to the ICU were included in this study. The exclusion criteria for the present study were patients with epidural hematoma, patients who suffered brain herniation prior to the cerebral circulation examination, and patients who were in a state of cardiopulmonary arrest on arrival. The clinical status of the patients according to the GCS was recorded on admission. Written informed consent for the study was obtained from the patients' family members, and the study protocol was approved by the ethics committee of our institute.

Management Protocol

All patients were admitted to the ICU from the emergency room after initial stabilization and brain CT, as well as surgery for those who required craniotomy to evacuate an intracranial mass. The management protocol included mechanical ventilation, sedation induced by the continuous infusion of sedative agents, and the administration of analgesic agents as clinically required for ventilation purposes and intracranial pressure (ICP) control. The therapeutic end point was defined as the maintenance of an ICP of less than 20 mmHg. To achieve this, mild hyperventilation (reduction in $PaCO_2$ to 35–40 mmHg), mild hypothermia (reduction of body temperature to 35–36 °C), and the administration of boluses of 20 % mannitol and/or vasopressors were implemented according to the patient's clinical condition. A fluid regimen was employed to maintain a mean arterial pressure of 95–100 mmHg.

Outcome was assessed at 3 months after onset according to the Glasgow Outcome Scale (GOS). For statistical purposes, a simplified GOS scoring system was used.

Statistical Analysis

All parameters are presented as the mean ± standard deviation. The value of each parameter was averaged using regions of interest in both hemispheres at the basal ganglia level. The *t* test, analysis of variance, and multiple comparisons analysis were used to assess the differences among the groups. All statistical calculations were performed with a personal computer using a statistical software package (SPSS, version 12.0; SPSS Japan, Tokyo, Japan).

Imaging Technique

After a standard CT study, Xe-CT and perfusion CT were performed continuously using an X Vigor scanner (Toshiba, Tokyo, Japan). As measuring CBF using perfusion CT is not a quantitative method, we measured CBF using Xe-CT. We measured MTT by perfusion CT and calculated the CBV using an AZ-7000 W98 computer system (Anzai Medical, Tokyo, Japan). CBV maps were produced by multiplying CBF and MTT according to the central volume principle: $CBV = CBF \times MTT$ [8]. The CBF, MTT, and CBV maps were created at the level of the basal ganglia.

During Xe-CT, the patients inhaled 30 % stable xenon for 4 min (wash-in), followed by 5 min of desaturation (wash-out), using a xenon gas inhalation system (AZ-725; Anzai Medical). Perfusion CT was performed just after the plain CT and Xe-CT. Twenty dynamic conventional scans were obtained in a 50-mm plane above the orbito-meatal orientation, which included the basal ganglia and the thalamus. Thirty milliliters of non-ionic contrast material (Iomeron 300; Eisai, Tokyo, Japan) were injected into the central vein through a 16-gauge cannula. CTs were performed at intervals of 2 s for 30 s, and subsequently, at 6-s intervals for 30 s. The resultant CT images were used to calculate MTT. On a pixel-by-pixel basis, the time-course of the changes in CT enhancement (time–density curve) was fitted to the gamma variate using the Gauss–Newton method, while the width between two inflection points (maximum upward slope and maximum downward slope) was calculated as the MTT value [10].

Results

We recruited 69 patients (11 women) who ranged in age from 11 to 86 years (mean: 45.5 years). The 69 patients with TBI were divided into four groups, the subdural hematoma (SDH) group (group A), the contusion/intracerebral hematoma (ICH) group (group B), the diffuse axonal injury (DAI) group (group C), and the diffuse brain-swelling group (TCDB III–IV; group D).

Of the 69 patients, 34 (49 %) did not undergo treatment for a mass lesion or decompression. The remaining patients underwent surgical craniotomy for a mass lesion or decompression.

A comparison of the focal injury (group A + group B) and diffuse injury groups (group C + group D) with regard to age, GCS score on admission, GOS score, and the hemodynamic parameters CBF, MTT, and CBV was performed. The patients in the focal injury group were significantly older (53.5 ± 20.9 years) than those in the diffuse injury group (34.9 ± 22.7 years, $p < 0.01$). Neither the GCS score on admission nor the GOS score differed significantly between the focal injury group and the diffuse injury group. The CBF value was significantly higher in the diffuse injury group (34.3 ± 14.2 mL/100 g/min) than in the focal injury group (26.4 ± 8.7 mL/100 g/min, $p < 0.01$). The MTT value was significantly higher in the focal injury group (7.0 ± 1.4 s) than in the diffuse injury group (6.3 ± 1.3 s, $p < 0.05$). The CBV was significantly higher in the diffuse injury group (3.4 ± 0.9 mL/100 g) than in the focal injury group (2.9 ± 0.7 mL/100 g, $p < 0.05$; Table 1).

The relationship among the four groups with regard to age, GCS score on admission, GOS score, and the hemodynamic parameters CBF, MTT, and CBV was assessed. The mean ages of groups A, B, C, and D were 54.7 ± 22.1, 51.1 ± 18.7, 35.4 ± 23.7, and 34.1 ± 22.2 years old respectively. The mean age of group A was significantly higher than that of group C ($p < 0.05$) and group D ($p < 0.05$). The GCS scores on admission of groups A, B, C, and D were 5.7 ± 2.6, 7.7 ± 3.8, 5.9 ± 3.1, and 5.5 ± 2.4 respectively. There were no significant differences among the four groups. The GOS scores of groups A, B, C, and D were 2.6 ± 1.4, 3.5 ± 1.3, 3.4 ± 1.2, and 3.2 ± 1.8 respectively. There were no significant differences among the four groups (Fig. 1). The CBF values of groups A, B, C, and D were 26.1 ± 8.7, 27.0 ± 8.9, 36.2 ± 13.2, and 31.5 ± 13.2 mL/100 g/min respectively. The CBF value of group C was significantly higher than that of group A ($p < 0.05$). The MTT values of groups A, B, C, and D were 7.3 ± 1.5, 6.6 ± 1.1, 6.1 ± 1.2, and 6.7 ± 1.3 s respectively. The MTT value of group A was significantly higher than that of group C ($p < 0.05$). The CBV values of groups A, B, C, and D were 2.9 ± 0.7, 2.8 ± 0.8, 3.3 ± 0.8, and 3.4 ± 1.0 mL/100 g respectively. There were no significant differences among the four groups (Fig. 2).

Table 1 Comparison between focal and diffuse injuries

	Focal injury	Diffuse injury	*p* value
Age	53.5 ± 20.9	34.9 ± 22.7	$p < 0.01$
Male/female	34/8	24/3	0.38
GCS on admission	6.4 ± 3.2	5.8 ± 2.8	0.44
GOS	2.9 ± 1.4	3.3 ± 1.5	0.23
CBF (mL/100 g/min)	26.4 ± 8.7	34.3 ± 14.2	$p < 0.01$
MTT (s)	7.0 ± 1.4	6.3 ± 1.3	$p < 0.05$
CBV (mL/100 g)	2.9 ± 0.7	3.4 ± 0.9	$p < 0.05$

GCS Glasgow Coma Scale, *GOS* Glasgow Outcome Scale, *CBF* cerebral blood flow, *MTT* mean transit time, *CBV* cerebral blood volume

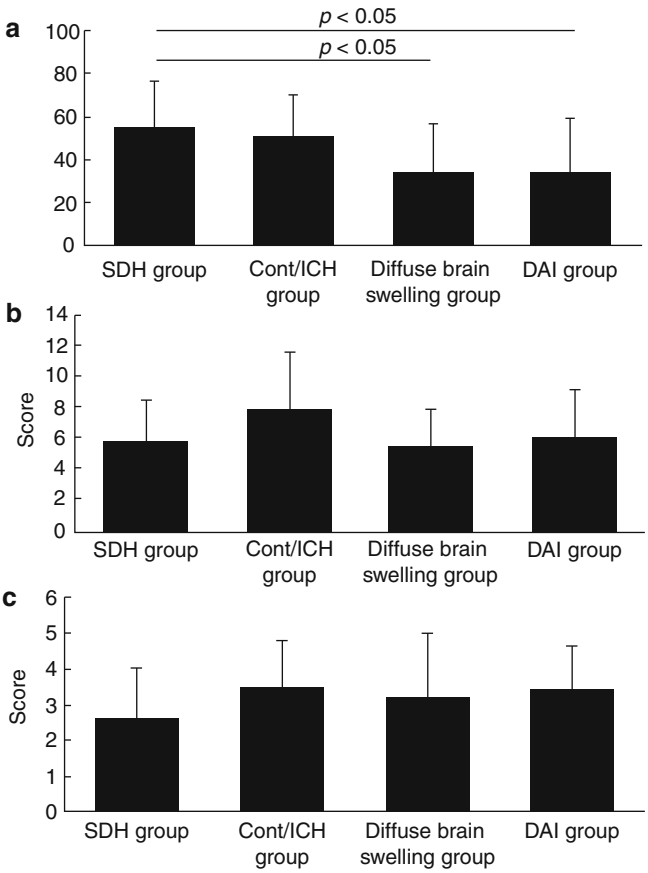

Fig. 1 (**a**) The ages of patients with subdural hematoma (*SDH*), contusion/intracerebral hematoma (*Cont/ICH*), diffuse axonal injury (*DAI*), and diffuse brain swelling were compared. Multiple comparisons analysis of age showed significant differences between the SDH and DAI patients, and between the SDH and diffuse brain swelling patients. (**b**) The Glasgow Coma Scale (GCS) scores on admission of patients with SDH, contusion/intracerebral hematoma, DAI, and diffuse brain swelling were compared. There were no significant differences among the groups. (**c**) The Glasgow Outcome Scale (GOS) scores of patients with SDH, contusion/intracerebral hematoma, DAI, and diffuse brain swelling were compared. There were no significant differences among the groups

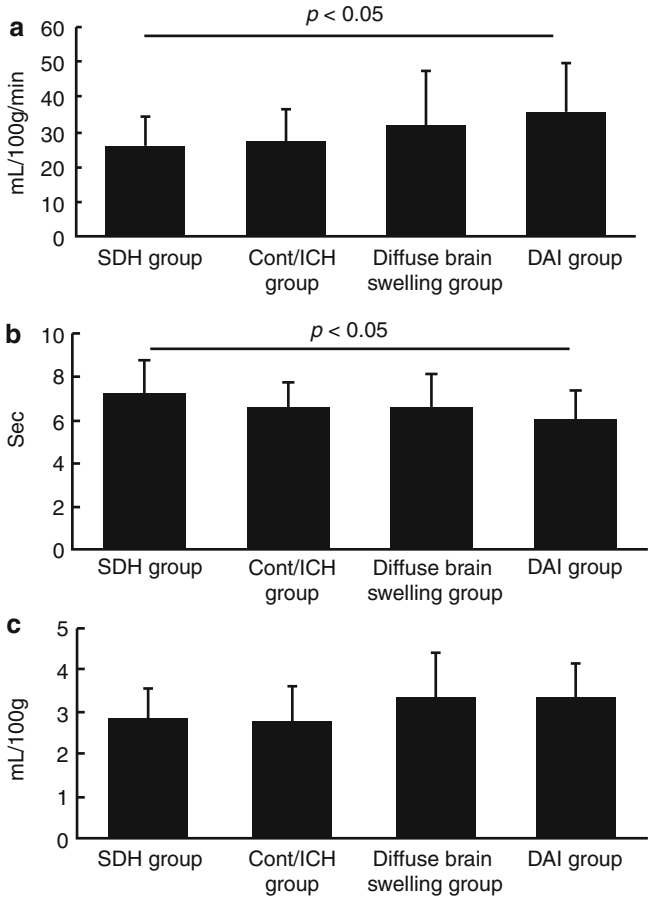

Fig. 2 (**a**) The cerebral blood flow (CBF) values of patients with *SDH*, contusion/intracerebral hematoma, *DAI*, and diffuse brain swelling were compared. Multiple comparisons analysis of age showed significant differences between the SDH and DAI patients, and between the SDH and diffuse brain swelling patients. (**b**) The mean transit times (MTT) of the patients with SDH, contusion/intracerebral hematoma, DAI, and diffuse brain swelling were compared. Multiple comparisons analysis of age showed a significant difference between the SDH and DAI patients. (**c**) The cerebral blood flow (CBV) values of the patients with SDH, contusion/intracerebral hematoma, DAI, and diffuse brain swelling were compared. There were no significant differences between the groups

Discussion

As it is important to understand the cerebral circulation dynamics induced in the early phase of TBI in order to determine its pathogenesis, develop appropriate treatment plans, evaluate treatment results, and predict outcomes, many studies have examined this topic. It has been reported that there are three distinct hemodynamic phases: I, hypoperfusion, which occurs during the first 24 h (post-injury day 0); II, hyperemia, which occurs on post-injury days 1–3; and III, vasospasm, which occurs on post-injury days 4–14 [6]. The hypoperfusion phase that occurs during the first 24 h after a head injury is followed by progressively increasing CBF, and CBF reaches its maximum between 48 and 72 h after the injury. Obrist et al. [9], Overgaard and Tweed [11], and others [4] have described a similar time course for the post-traumatic hemodynamic phase. However, severe TBI are heterogeneous pathophysiological conditions, and different types of TBI induce different hemodynamic changes after TBI.

We confirmed that CBF was decreased in the focal types of TBI on days 1–3. However, decreased CBF does not represent ischemia. CBF is markedly influenced by the cerebral metabolic rate of oxygen consumption ($CMRO_2$), body temperature, $PaCO_2$, and ICP, etc. Therefore, in the present study, we used both Xe-CT and perfusion CT. As CT is routinely used for the follow-up of TBI, Xe-CT and perfusion CT are convenient because they can be performed successively after plain CT examinations. PET, SPECT, and Xe-CT have been used to evaluate cerebral circulation and metabolism in the acute phase after TBI. Recent studies have reported the utility of perfusion CT for subarachnoid hemorrhaging and stroke [15, 16]. In particular, MTT values obtained from this modality are believed to be much more sensitive than other parameters for evaluating cerebral vasospasm [15]. However, the CBF values obtained from perfusion CT are not quantitative, although they do correlate with those obtained from Xe-CT [12]. Based on these reports, we performed Xe-CT and perfusion CT simultaneously and evaluated the cerebral circulation of TBI patients using the CBF, CBV, and MTT values obtained with these methods.

In the present study, we detected significant decreases in CBF and significant increases in MTT in focal injury patients during the hyperemic phase. It has been reported that the finding of MTT prolongation on perfusion CT is suggestive of a disturbance in the cerebral circulation [1]. Thus, it has become clear that there are significant differences in cerebral circulation between focal and diffuse injuries, and focal injuries display significant cerebral circulatory disturbances compared with diffuse injuries. We also detected decreases in CBV in focal injuries. It appears that, in occlusive cerebrovascular disease, the cerebral perfusion pressure decreases, the CBV increases because of the compensatory dilatation of the cerebral blood vessels, and the MTT is prolonged. However, in the acute phase after focal injury, the CBV and CBF decrease owing to ICP elevation. The MTT is also prolonged. Indeed, in this study, the CBV values of the patients with focal injuries were decreased compared with those of the patients with diffuse injuries.

It has been reported that patients who have had hematomas surgically removed are at a higher risk of increased intracranial pressure [7], and in experimental models it was found that the ischemic brain tissue adjacent to subdural hematomas was not reperfused after clot evacuation, and brain swelling after hematoma is more likely to be due to progressive edema rather than hyperemia [5]. Moderate hypothermia therapy, which decreases CBF, $CMRO_2$, and

ICP, might be effective against the types of TBI associated with disturbances in the cerebral circulation. We have to take all possible measures including hypothermia therapy to prevent the exacerbation of severe TBI associated with cerebral circulatory disturbance. Indeed, Clifton reported that the very early induction of hypothermia is effective for 16 to 45–year-old patients who have undergone surgery to remove an intracranial hematoma [3].

The main limitation of this study is its size. There were no significant differences between the patients with SDH and those with diffuse brain swelling, or between the patients with contusion/ICH and those with diffuse injuries (the DAI group and the diffuse brain swelling group). Thus, we need to evaluate the cerebral circulatory parameters of patients belonging to these four groups using a greater number of patients.

Conflict of Interest We declare that we have no conflict of interest.

References

1. Araki Y, Furuichi M, Nokura H, Sakai N (2002) Evaluation of cerebral hemodynamics with perfusion CT. No To Shinkei 54:581–588
2. Bouma GJ, Muizelaar JP (1993) Evaluation of regional cerebral blood flow in acute head injury by stable xenon-enhanced computerized tomography. Acta Neurochir Suppl (Wien) 59:34–40
3. Clifton GL, Valadka A, Zygun D, Coffey CS, Drever P, Fourwinds S, Janis LS, Wilde E, Taylor P, Harshman K, Conley A, Puccio A, Levin HS, McCauley SR, Bucholz RD, Smith KR, Schmidt JH, Scott JN, Yonas H, Okonkwo DO (2011) Very early hypothermia induction in patients with severe brain injury (the National Acute Brain Injury Study: Hypothermia II): a randomised trial. Lancet Neurol 10:131–139
4. Enevoldsen EM, Cold G, Jensen FT, Malmros R (1976) Dynamic changes in regional CBF, intraventricular pressure, CSF pH and lactate levels during the acute phase of head injury. J Neurosurg 44:191–214
5. Kuroda Y, Bullock R (1992) Local cerebral blood flow mapping before and after removal of acute subdural hematoma in the rat. Neurosurgery 30:687–691
6. Martin NA, Patwardhan RV, Alexander MJ, Africk CZ, Lee JH, Shalmon E, Hovda DA, Becker DP (1997) Characterization of cerebral hemodynamic phase following severe head trauma: hypoperfusion, hyperemia, and vasospasm. J Neurosurg 87:9–19
7. Miller JD, Becker DP, Ward JD, Sullivan HG, Adams WE, Rosner MJ (1977) Significance of intracranial hypertension in severe head injury. J Neurosurg 47:503–516
8. Muizelaar JP, Fatouros PP, Schroder ML (1997) A new method for quantitative regional cerebral blood volume measurements using computed tomography. Stroke 28:1998–2005
9. Obrist WD, Gennarelli TA, Segawa H, Dolinskas CA, Langfitt TW (1979) Relation of cerebral blood flow to neurological status and outcome in head-injured patients. J Neurosurg 51:292–300
10. Oldendorf WH, Kitano M (1967) Radioisotope measurement of brain blood turnover time as a clinical index of brain circulation. J Nucl Med 8:570–587
11. Overgaard J, Tweed WA (1974) Cerebral circulation after head injury. 1. Cerebral blood flow and its regulation after closed head injury with emphasis on clinical correlations. J Neurosurg 41: 531–541
12. Sase S, Honda M, Machida K, Seiki Y (2005) Comparison of cerebral blood flow between computed tomography and xenon-enhanced computed tomography for normal subjects: territorial analysis. J Comput Assist Tomogr 29:270–277
13. Soustiel JF, Mahamid E, Goldsher D, Zaaroor M (2008) Perfusion-CT for early assessment of traumatic cerebral contusions. Neuroradiology 50:189–196
14. Wintermark M, Chioléro R, van Melle G, Revelly JP, Porchet F, Regli L, Meuli R, Schnyder P, Maeder P (2004) Relationship between brain perfusion computed tomography variables and cerebral perfusion pressure in severe head trauma patients. Crit Care Med 32:1579–1587
15. Wintermark M, Ko NU, Smith WS, Liu S, Higashida RT, Dillon WP (2006) Vasospasm after subarachnoid hemorrhage: utility of perfusion CT and CT angiography on diagnosis and management. AJNR Am J Neuroradiol 27:26–34
16. Yamada M, Yoshimura S, Kaku Y, Iwama T, Watarai H, Andoh T, Sakai N (2004) Prediction of neurologic deterioration in patients with lacunar infarction in the territory of the lenticulostriate artery using perfusion CT. AJNR Am J Neuroradiol 25:402–408

Application of Transcranial Color-Coded Sonography in Severe Brain Injury

Radovan Turek, Petr Linzer, Michal Filip, Filip Šámal, and Patrik Jurek

Abstract Transcranial color-coded sonography (TCCS) monitoring of severe brain injury patients may reveal various pathological hemodynamic changes. According to changes in flow velocities in basal brain arteries, the presence of brain hyperemia, vasospasms, and oligemia can be detected. The study included a group of 20 patients with severe brain injury. TCCS measured flow velocities and ICP values were monitored on a daily basis in the course of a week after injury. In nearly 50 % of patients significant hemodynamic changes occurred. The most frequent pathological finding was hyperemia (31.8 %), followed by vasospasm (10.9 %) and oligemia (9.1 %). In 42.7 % of patients increased flow velocities were registered and only 9.1 % of records were within the normal range of values. The most substantial elevation in time-averaged mean velocity occurred from the second to the sixth day after injury. In a subgroup of patients with raised intracranial pressure 41.6 % of flow velocity (FV) measuring met the TCCS criteria for hyperemia compared with 26 % in a subgroup of patients without intracranial pressure (ICP) elevation. The study showed that hemodynamic changes after severe brain injury are relatively common findings and that TCCS is a useful bed-side tool for the monitoring of intracranial hemodynamic changes.

Keywords Transcranial color-coded sonography • Brain injury • Brain hyperemia • Vasospasms • Intracranial pressure

Introduction

Brain ischemia is one of the most important components of secondary brain injury. A fundamental mechanism of brain ischemia is the lowering of cerebral blood flow (CBF) below a critical level. Among factors contributing to CBF decline are intracranial hypertension, hypotension, microvascular damage, and compression by hematomas. The current therapeutic strategy is based on the control of intracranial pressure and maintenance of adequate cerebral perfusion pressure (CPP). In cases of severe brain injury disturbances of autoregulation may occur. CPP-oriented therapy may worsen intracranial hypertension owing to increased cerebral blood volume. On the other hand, in patients with post-traumatic vasospasms, adequate CPP is higher than in the presence of hyperemia. The knowledge of a patient's hemodynamic status – hyperemia or vasospasm – may help in choosing the proper therapeutic strategy. A linear correlation between blood flow velocity and CBF makes it possible to determine CBF with the use of transcranial color-coded sonography (TCCS) [1]. The calculation of the Lindegaard index distinguishes brain hyperemia from vasospasm.

Materials and Methods

Twenty subjects with severe brain injury were included in the study. Inclusion criteria were GCS score 3–8 on admission to hospital, time since injury <24 h, surgical evacuation of space-occupying lesion (hematomas, contusions), decompressive craniectomy at the surgeon's discretion, ICP monitoring (intraparenchymal ICP sensor CODMAN), and CPP monitoring. The patients received full conservative treatment. TCCS equipped with a transcranial ultrasound probe 2.0 MHz was used to measure blood flow velocity in the middle cerebral artery bilaterally through the transtemporal bone window. The ICA flow velocities in the cervical region

R. Turek, MD (✉)
Department of Anaesthesiology, T. Bata Regional Hospital, Zlín, Czech Republic
e-mail: turek.radovan@seznam.cz

P. Linzer, M. Filip, F. Šámal, and P. Jurek
Department of Neurosurgery, T. Bata Regional Hospital, Zlín, Czech Republic

Y. Katayama et al. (eds.), *Brain Edema XV*, Acta Neurochirurgica Supplement, Vol. 118,
DOI 10.1007/978-3-7091-1434-6_50,

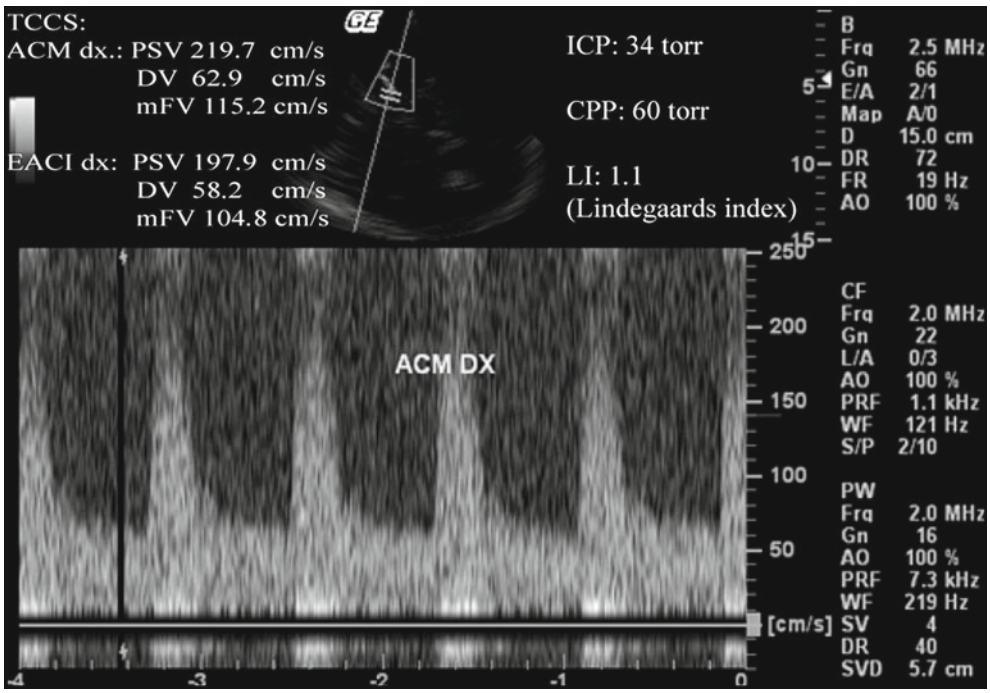

Fig. 1 Transcranial color-coded sonography (TCCS) record of hyperemia – third day after injury (ACM dx. mFV 115.2 cm/s, ACI mFV 104.8 cm/s, LI: 1.1, ICP: 34 Torr, CPP: 60 Torr)

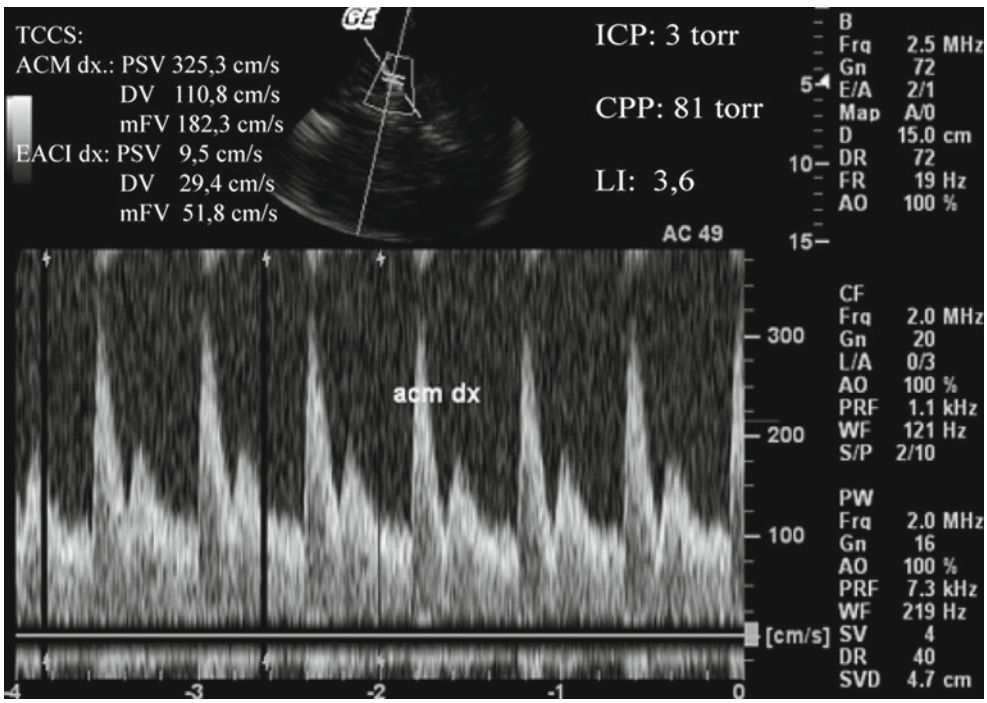

Fig. 2 The TCCS record of vasospasm – second day after injury (ACM dx. mFV 182.3 cm/s, ACI mFV 51.8 cm/s, LI: 3.6, ICP: 3 Torr, CPP: 81 Torr)

were recorded too. After ACM identification and a correction of an insonation angle the peak systolic velocity (PSV), end-diastolic velocity (DV), and time-averaged mean velocity (TAMEAN) were registered. Pulsatile index (PI), resistance index (RI), and the Lindegaard index (LI) were calculated. Increased flow velocity (FV) was considered when FV exceeded 1 SD above the reference data of normal blood-flow parameters matched by sex and age. TCCS examination was performed once daily and the duration of the study was 7 days. At the time of the investigations the patients received full conservative treatment, were hemodynamically stable with arterial pCO_2 pressure within a normal range of values. ICP and CPP values were recorded simultaneously. When mean flow velocity (mFV) exceeded 100 cm/s, the LI was used to distinguish between hyperemia (LI < 3) and vasospasms (LI > 3) [3, 4]. We analyzed a time course of time-averaged mean velocities in the whole group of patients (Figs. 1 and 2).

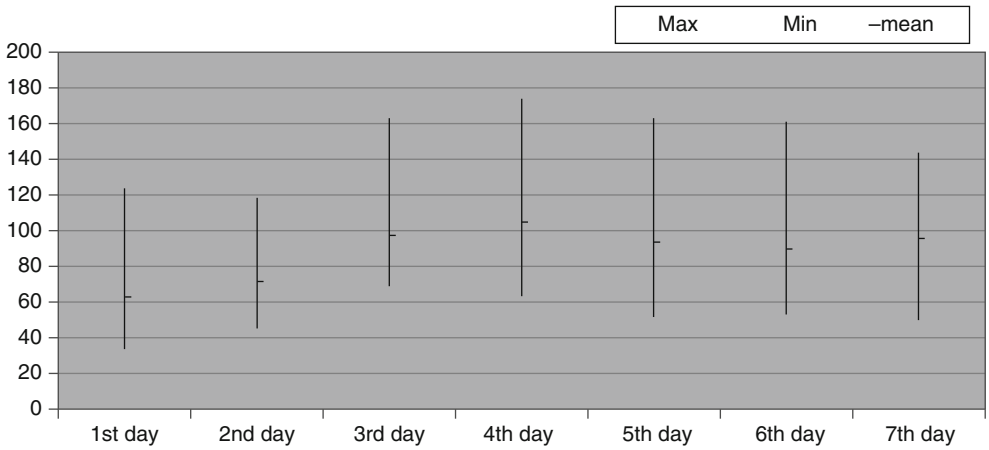

Fig. 3 The time course of TAMEAN values

Results

Interhemispheric differences in TAMEAN were insignificant. Fifty percent of patients showed a significant hemodynamic change during 1 week of the follow-up. The most frequent pathological finding was hyperemia (31.8 %), followed by vasospasm (10.9 %) and oligemia (9.1 %). In 42.7 % of patients increased flow velocities were registered, but did not reach pathological values and only 9.1 % of records were within the normal range of values. The most significant elevation of the time-averaged mean flow velocity occurred between the second and sixth day after injury (Fig. 3). In the subgroup of patients with raised intracranial pressure (ICP >20 Torr), 41.6 % of FV measuring met TCCS criteria of hyperemia compared with 26 % in a subgroup of patients without ICP elevation. The presence of vasospasms was detected in two patients (10.9 % of all measurements) with an average duration of 2.8 days. Vasospasms occurred even in cases when subarachnoid hemorrhage was absent.

Conclusion

In more than 90 % of patients increased FV values were detected in course of the study. In the period between the second and sixth days after injury these changes are most likely to occur. In 42.7 % of patients the TCCS criteria of hyperemia or vasospasm were fulfilled. The distinction between hyperemia and vasospasms in these patients may influence further therapeutic strategy. The testing of cerebrovascular autoregulation may be appropriate in cases of hyperemia. The development of vasospasm may require pharmacological intervention and maintenance of CPP at higher levels. TCCS examination may provide valuable information about intracranial hemodynamics [2], but there are also some limitations to the method. The quality of the temporal bone window influences signal quality and measurement accuracy. Furthermore, the measurement of FV changes in ACM may not necessarily reflect the situation on the periphery.

Conflict of Interest We declare that we have no conflict of interest.

References

1. Aaslid R (1986) The Doppler principle applied to measurement of blood flow velocity in cerebral arteries. In: Aaslid R (ed) Transcranial Doppler sonography. Springer, Vienna/New York
2. Kochanowicz J, Krejza J, Mariak Z, Bilello M, Lyson T, Lewko J (2006) Detection and monitoring of cerebral hemodynamic disturbances with transcranial color-coded duplex sonography in patients after head injury. Neuroradiology 48(1):31–36
3. Romner B, Bellner J, Kongstad P, Sjöholm H (1996) Elevated transcranial Doppler flow velocities after severe head injury: cerebral vasospasm or hyperemia? J Neurosurg 85(1):90–97
4. White H, Venkatesh B (2006) Applications of transcranial Doppler in the ICU: a review. Intensive Care Med 32(7):981–994

Surgical Results After Primary Decompressive Craniectomy in Poor-Grade Aneurysmal Subarachnoid Hemorrhage

Naoki Otani, Hiroshi Nawashiro, Kojiro Wada, Kimihiro Nagatani, Satoru Takeuchi, Hiroaki Kobayashi, Hideo Osada, Takamoto Suzuki, and Katsuji Shima

Abstract It is well known that patients with poor-grade aneurysmal subarachnoid hemorrhage (SAH) have poor outcomes owing to significant mass effect and brain stem compression. On the other hand, decompressive craniectomy (DC) has shown efficacy in reducing morbidity and mortality in patients with intracranial hypertension. Here, we study the efficacy of DC in poor-grade SAH with attention to surgical outcome. A total of 38 consecutive patients with poor-grade SAH was treated in our hospital between 1 August 2005 and 30 July 2010. Among these 38 patients, we involved 15 patients with DC in the present study. We retrospectively reviewed medical charts and radiological findings. Glasgow Outcome Scale score on discharge showed good response in 1 (6.7 %), moderate disability in 6 (40.0 %), severe disability in 4 (28.1 %), vegetative state in 2 (1.3 %), and death in 2 (13.3 %). In particular, 3 grade IV patients (50.0 %) had a favorable outcome. Recent several experimental studies also indicated that DC significantly improves outcome owing to increased perfusion pressure or reduced intracranial pressure. We suggest that the DC provided the efficacy in reducing mortality in poor-grade SAH patients.

Keywords Brain stem compression • Massive ischemic infarction • Subarachnoid hemorrhage • Cerebral angiography • Intracranial hypertension • Intracerebral hematoma

N. Otani, MD (✉), H. Nawashiro, K. Wada, K. Nagatani, S. Takeuchi, H. Kobayashi, H. Osada, T. Suzuki, and K. Shima
Department of Neurosurgery,
National Defense Medical College,
3-2 Namiki, Tokorozawa, Saitama 359-8513, Japan
e-mail: naotani@ndmc.ac.jp

Introduction

The outcomes of patients with poor-grade aneurysmal subarachnoid hemorrhage (SAH) are poor because of the significant brain stem compression following mass effect. On the other hand, decompressive craniectomy (DC) can reduce morbidity and mortality in critically ill patients with massive ischemic infarction [9] and severe head injury [4]. However, the role of DC in poor-grade SAH remains obscure. DC could be an effective strategy for poor-grade SAH in patients with ICH [3, 11, 12]. The present study examines the clinical outcome of DC in poor-grade SAH patients.

Patients and Methods

A total of 38 consecutive patients with poor-grade SAH (H&K grades IV or V, and Fisher grade 4) were treated in our hospital between 1 August 2005 and 30 July 2010. Among these 38 patients, we involved 15 patients who had undergone DC in the study. We retrospectively reviewed medical charts, radiological findings, operative notes, and video records. Patient outcome was assessed on discharge using the Glasgow Outcome Scale (GOS) score, which comprises five levels: recovery (GR), moderate disability (MD), severe disability (SD), vegetative state (VS), and death (D). The GOS describes good recovery and moderate disability as favorable outcomes, whereas severe disability, vegetative state, and death constitute unfavorable outcomes.

All patents were managed in the same fashion, as follows. Aggressive resuscitation such as tracheal intubation and adequate ventilation using sedation was performed in the emergency room. The diagnosis of SAH was confirmed by computed tomography (CT). To prevent aneurysmal rebleeding during the acute stage, the systolic blood pressure was actively lowered to <120 mmHg. All patients immediately underwent cerebral angiography after stabilization.

Y. Katayama et al. (eds.), *Brain Edema XV*, Acta Neurochirurgica Supplement, Vol. 118,
DOI 10.1007/978-3-7091-1434-6_51, © Springer-Verlag Wien 2013

Table 1 Clinical characteristics in 15 patients who underwent decompressive craniectomy (DC) for poor-grade subarachnoid hemorrhage (SAH)

Patient no.	Age/sex	GCS on admission	GCS preoperatively	Site	Aneurysmal location	WFNS grade	Onset to operation (h)	Follow-up period (month)	GOS
1	59/F	7	5	Left	MCA	IV	84	38	VS
2	70/M	14	6	Right	MCA	V	264	52	VS
3	51/F	6	7	Right	ICA	IV	60	72	SD
4	66/M	4	4	Left	MCA	V	5	0.2	D
5	57/F	6	6	Right	IC-PC	V	9	62	MD
6	63/M	14	13	Right	MCA	IV	148	54	MD
7	34/M	12	11	Left	ICA	IV	13	50	GR
8	64/F	3	3	Left	MCA	V	15	45	MD
9	55/M	6	6	Left	IC-PC	V	16	45	MD
10	63/F	4	4	Left	IC-PC	V	12	12	SD
11	57/M	3	3	Left	IC-Achol	V	18	34	SD
12	54/F	4	4	Left	MCA	V	6	30	MD
13	51/F	4	4	Left	ICA	V	16	0.7	D
14	66/F	9	8	Right	MCA	IV	6	13	MD
15	64/M	9	6	Left	MCA	IV	12	24	SD

GCS Glasgow Coma Scale, *GOS* Glasgow Outcome Scale, *MCA* middle carotid artery, *ICA* internal carotid artery, *IC-PC* internal carotid-posterior communicating artery, *IC-Achol* internal carotid-anterior choroidal artery aneurysm, *GR* good recovery, *MD* moderate disability, *SD* severe disability, *VS* vegetative state, *D* dead

All patients underwent DC and standard microscopic techniques to obliterate the aneurysm. The surgical procedure consisted of the following. A generous craniotomy flap was removed via a large reversed question mark scalp incision with the following margins: anteriorly, frontal to the floor of the anterior cranial fossa; superiorly, within 2 cm of the superior sagittal sinus; posteriorly, within 1 cm of the asterion, and inferiorly, to the floor of the middle fossa. The dura was opened in a semicircular fashion with additional dural incisions for decompression. Patients were aggressively treated post-operatively in the neurological intensive care unit to avoid intracranial hypertension and vasospasm with ICP monitoring. CSF drainage was performed to decrease the ICP caused by hydrocephalus. To prevent cerebral vasospasm, the prophylactic hypervolemic hyperdynamic therapy was introduced for at least 2 weeks after surgery. The cranial bone flap was replaced 1–2 months after the initial surgery.

Results

We summarized the clinical characteristics in 15 patients who had undergone DC for poor-grade SAH (Table 1). In these 15 patients (mean age 65, male 7, female 8), 6 were classified as H&K grade IV and 9 as grade V. Radiological findings revealed that ruptured aneurysms were located at the internal carotid artery (ICA) in 7, and the middle cerebral artery (MCA) in 8 patients. Three aneurysms were small, 12 were of medium size. Re-rupture was confirmed in 1 (6.7 %) preoperatively. Glasgow Outcome Scale score on discharge showed good recovery in 1 (6.7 %), moderate disability in 6 (40.0 %), severe disability in 4 (28.1 %), vegetative state in 2 (1.3 %), and death in 2 (13.3 %). In particular, 3 (50.0 %) showed a favorable outcome, 3 (50.0 %) showed a poor outcome, and there were no deaths in grade IV patients. We present here case 9 (Fig. 1). The patient was a 55-year-old man, who suffered sudden onset headache with loss of consciousness loss. The CT on admission showed a diffuse SAH with intracerebral hematoma (Fig. 1a, b). The cerebral angiography revealed the internal carotid–posterior communicating artery (IC-PC) aneurysm, left (Fig. 1c). The patients underwent a clipping operation with primary decompressive craniectomy (Fig. 1d). Two months after operation, the cranioplasty was performed (Fig. 1e). The patients recovered with a GOS score of moderate disability.

Conclusion

Several authors have proposed that early, aggressive surgery and intensive care for SAH patients in poor clinical condition can improve the mortality and morbidity [1]. Despite recent advances in the treatment of poor-grade SAH, surgical outcome in many patients remains unfavorable because of uncontrollable intracranial hypertension. Increased ICP has been associated with several detrimental effects such as cerebral ischemia following reduced perfusion pressure [5]. Several investigators have reported that intractable intracranial hypertension is associated with a poor outcome among poor-grade patients with aneurysmal SAH [8].

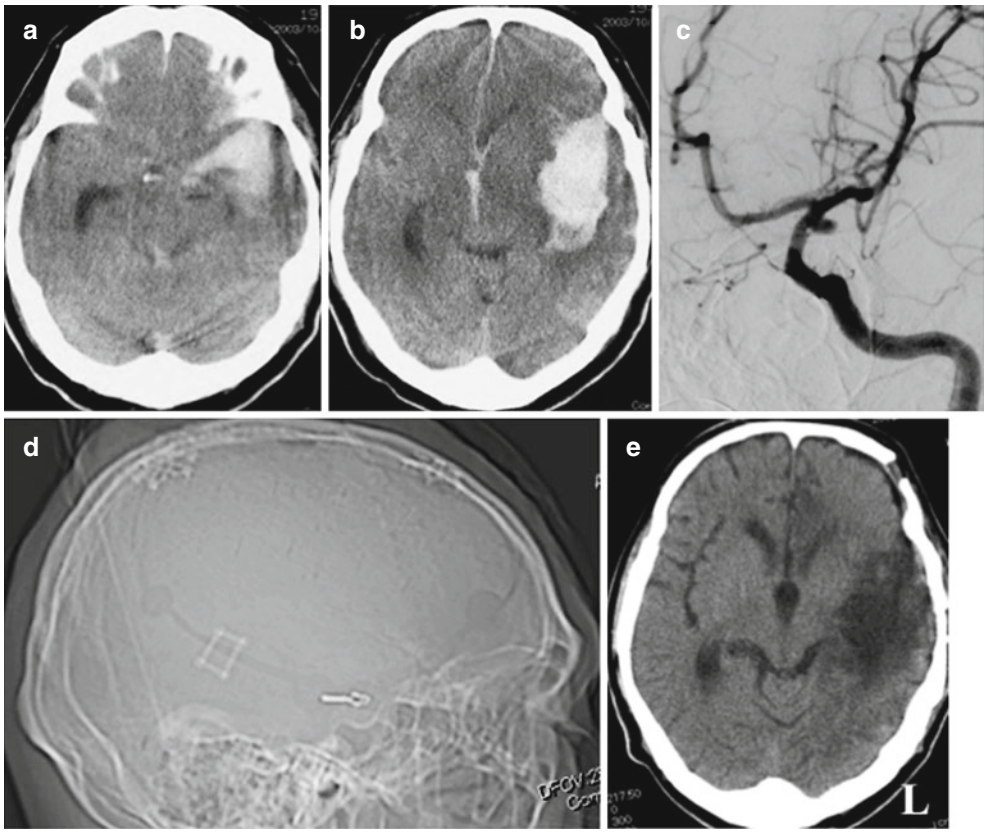

Fig. 1 Case 9: the patient was a 55-year-old man who suffered sudden onset headache with loss of consciousness. CT on admission showed a diffuse subarachnoid hemorrhage (SAH) with intracerebral hematoma (**a**, **b**). The cerebral angiography revealed the internal carotid-posterior communicating artery (IC-PC) aneurysm, *left* (**c**). The patients underwent a clipping operation with primary decompressive craniectomy (**d**). Two months after operation, the cranioplasty was performed (**e**). The patients recovered with a GOS score indicating moderate disability

Intracranial hypertension in patients with SAH can be associated with deleterious changes, which could have a profound impact on outcome [13]. The authors of these studies recommend aggressive clot evacuation and aneurysm obliteration. Rapid control of ICP has been associated with improved outcome, indicating that early control of ICP and cerebral blood flow is important for improving outcome or to counteract deterioration. Recent clinical findings suggest that DC might reduce ICP [7, 10]. Craniectomy and enlarged dural plasty has induced a significant decrease in ICP and an increase in cerebral tissue oxygenation [10]. Others suggest that DC significantly increases cerebral tissue oxygenation [7]. In addition, experimental studies have suggested that DC significantly elevates cerebral mean blood flow velocity and that MCA pulsatility indices significantly decrease after surgery, indicating reduced cerebrovascular resistance in most patients with traumatic brain swelling [2]. Thus, DC can induce an immediate ICP reduction and control the ICP elevation that occurs several days after SAH. Surgical outcome improves once ICP is controlled by DC, compared with that when ICP is not controlled [6]. In particular, delayed swelling can induce elevated ICP, which can be confused with symptoms of vasospasm. Thus, early DC would be useful to avoid this clinical dilemma.

Recent clinical studies have found that DC can improve the surgical outcome of patients with poor grade SAH and massive ICH [3, 11, 12]. Smith et al. [12] suggested that the surgical outcome was improved by ICP control in a series of eight patients with poor-grade MCA aneurysmal SAH and Sylvian hematoma treated with external decompression. They reported a favorable outcome rate of 62.5 % compared with a poor outcome rate of 37.5 %. Shimoda et al. [11] reported a favorable outcome rate of 33 % in grade IV, and 40 % in grade V patients with Sylvian hematoma treated with external decompression. Although DC has prolonged the short-term survival of patients with poor-grade SAH and intracerebral hematoma, the overall quality of life experienced by survivors remains poor [9]. Further investigation is required to clarify long-term outcome with particular focus upon higher cerebral function, in particular compared with a valid control group.

Conflict of Interest We declare that we have no conflict of interest.

References

1. Bailes JE, Spetzler RF, Hadley MN, Balwin HZ, Baldwin HZ (1990) Management morbidity and mortality of poor grade aneurysm patients. J Neurosurg 72:559–566
2. Bor-Seng-Shu E, Hirsch R, Teixeira MJ, De Andrade AF, Marino R Jr (2006) Cerebral hemodynamic changes gauged by transcranial

Doppler ultrasonography in patients with posttraumatic brain swelling treated by surgical decompression. J Neurosurg 104:93–100
3. D'Ambrosio AL, Sughrue ME, Yorgason JG, Mocco JD, Kreiter KT, Mayer SA, McKhann GM, Connolly ES (2005) Decompressive hemicraniectomy for poor-grade aneurysmal subarachnoid hemorrhage patients with associated intracerebral hemorrhage: clinical outcome and quality of life assessment. Neurosurgery 56:12–20
4. Guerra WK, Gaab MR, Dietz H, Muellaer JU, Piek J, Fritsch MJ (1999) Surgical decompression for traumatic brain swelling: indications and results. Neurosurgery 90(2):187–196
5. Hayashi M, Kobayashi H, Kawano H, Yamamoto S, Maeda T (1984) Cerebral blood flow and ICP patterns in patients with communicating hydrocephalus after aneurysm rupture. J Neurosurg 61:30–36
6. Heuer G, Smith M, Elliott J, Winn H, Leroux P (2004) Relationship between intracranial pressure and other clinical variables in patients with aneurismal subarachnoid hemorrhage. J Neurosurg 101:408–416
7. Jaeger M, Soehle M, Meixensberger J (2003) Effects of decompressive craniotomy on brain tissue oxygen in patients with intracranial hypertension. J Neurol Neurosurg Psychiatry 74:513–515
8. Kaye AH, Brownbill D (1981) Postoperative intracranial pressure in patients operated on for cerebral aneurysms following subarachnoid hemorrhage. J Neurosurg 54:726–732
9. Kondziolka D, Fazl M (1988) Functional recovery after decompressive craniectomy for cerebral infarction. Neurosurgery 23(2): 143–147
10. Reithmeier T, Lohr M, Rakos P, Ketter G, Ernestus RL (2005) Relevance of ICP and ptiO_2 for indication and timing of decompressive craniectomy in patients with malignant brain edema. Acta Neurochir (Wien) 147:947–952
11. Shimoda M, Oda S, Mamata Y, Tsugane R, Sato O (1997) Surgical indications in patients with an intracerebral hemorrhage due to ruptured middle cerebral artery aneurysm. J Neurosurg 87:170–175
12. Smith ER, Carter BS, Ogilvy CS (2002) Proposed use of prophylactic decompressive craniectomy in poor-grade aneurysmal subarachnoid hemorrhage patients presenting with associated large sylvian hematomas. Neurosurgery 51:117–124
13. Yoshimoto Y, Wakai S, Satoh A, Hirose Y (1999) Intraparenchymal and intrasylvian haematomas secondary to ruptured middle cerebral artery aneurysms: prognostic factors and therapeutic considerations. Br J Neurosurg 13:18–24

Endovascular Treatment for Ruptured Vertebral Artery Dissecting Aneurysms at the Acute Stage

Takeshi Suma, Tadashi Shibuya, Nobuo Kutsuna, Yoshiyuki Takada, Toshinori Matsuzaki, Shin Nakamura, Teruyasu Hirayama, and Yoichi Katayama

Abstract *Objective*: Ruptured vertebral artery dissecting aneurysms (VADA) should be treated promptly because of the high risk of rebleeding. However, it is difficult to treat dissecting aneurysm during the acute stage using microsurgery because of high intracranial pressure or brain edema. Therefore, endovascular treatment of the ruptured VADA may be a better technique. We retrospectively studied the efficacy and outcome of endovascular treatment of ruptured VADA at the acute stage.

Methods: Ten patients with ruptured VADA received endovascular treatment at the acute stage. Eight patients who had dissecting aneurysms were treated by internal trapping of the dissected segment. We performed stent-assisted coiling (SAC) for a case of VADA in contralateral hypoplastic VA and a case of bilateral dissections, ruptured VADA of the right VA and VA dissection of the left VA.

Results: Four patients had good recovery, 3 patients had moderate disability, 2 patients had severe disability, and 1 patient died from initial severe SAH. There was no rebleeding or procedure-related complication. However, one patient who was treated by SAC had ischemic complications post-treatment.

Conclusion: Endovascular treatment of ruptured VADA in the acute stage appears to be safe and effective.

Keywords Endovascular treatment • Ruptured dissecting vertebral aneurysms • Acute stage

Introduction

When vertebral artery dissecting aneurysms (VADA) occur with subarachnoid hemorrhage (SAH), the risk of recurrent hemorrhage is extremely high. In a study by Yamada et al. of 24 conservatively treated patients with ruptured VADA, 14 (58 %) experienced a total of 35 re-bleeding episodes. Of these 14 patients, 13 died and 11 of these deaths were directly attributable to rebleeding [11]. Therefore, it is recommended that ruptured VADA should be treated within 24 h because of the high risk of re-bleeding and high morbidity and mortality. Nevertheless, it is difficult to treat VADA during the acute stage using craniotomy because of high intracranial pressure or brain edema.

In recent years, endovascular treatment of VADA has evolved as an alternative to surgical treatment and may consist of proximal vertebral occlusion, internal coil trapping, stent-assisted coiling, or stent placement as the only therapy [1, 5, 6, 12].

We retrospectively studied the efficacy and outcome of endovascular treatment of ruptured VADA at the acute stage.

Materials and Methods

Between 2004 and 2011, we treated 10 patients with ruptured VADA using the endovascular technique at the acute stage at our institute and affiliated hospital. They were 7 men and 3 women ranging in age from 38 to 70 years (mean 50.6 years). SAH was diagnosed on the basis of findings from computed tomography of the brain. Identification of dissecting aneurysms was based primarily on angiographic

T. Suma (✉), N. Kutsuna, Y. Takada, T. Matsuzaki, S. Nakamura, T. Hirayama, and Y. Katayama
Division of Neurosurgery, Department of Neurological Surgery, Nihon University School of Medicine, 30-1 Ohyaguchikamicho, Itabashi-ku, Tokyo 173-8610, Japan
e-mail: suma.takeshi@nihon-u.ac.jp

T. Shibuya
Division of Neurosurgery, Department of Neurological Surgery, Nihon University School of Medicine, 30-1 Ohyaguchikamicho, Itabashi-ku, Tokyo 173-8610, Japan

Department of Neuroendovascular Therapy, Sagamihara Kyodo Hospital, Sagamihara, Kanagawa, Japan

Y. Katayama et al. (eds.), *Brain Edema XV*, Acta Neurochirurgica Supplement, Vol. 118,
DOI 10.1007/978-3-7091-1434-6_52, © Springer-Verlag Wien 2013

criteria. One patient had dissecting aneurysm involving the origin of the posterior inferior cerebellar artery (PICA; PICA-involved type), 7 patients had VADA occurring at a distal site of the VA from the origin of the PICA (post-PICA type), and 2 patients had no PICA in the ipsilateral vertebral artery with dissecting aneurysm (no PICA type).

Endovascular Procedure

All the patients were placed under general anesthesia or intravenous anesthesia in the angiography room. A 6.0-F or a 5.0-F ultra-long sheath as a guiding catheter was placed in the affected VA at the cervical portion via the right femoral artery. The guiding catheter was perfused continuously with normal saline flush solution containing heparin (5,000 U/L). Another 5.0-F catheter was used to obtain an angiogram of the contralateral VA during the procedure.

Postoperative Management

Post-procedurally, all patients underwent close neurological monitoring in our intensive care unit. Antiplatelet therapy with clopidogrel, cilostazol or aspirin was maintained for at least 3 months after treatment. Serial follow-up angiographic examinations were performed to ensure complete angiographic healing with occlusion of the dissected segment with conventional DSA or MRA. The patient outcome was assessed according to the Glasgow Outcome Scale at 3 months after onset.

Illustrative Cases

Case 1

An unconscious 39-year-old man (patient 10) was admitted to our hospital. Computed tomography (CT) revealed severe SAH, and his status was estimated as Hunt and Kosnik grade 4. An angiogram demonstrated a dissecting aneurysm of the left VA; the contralateral VA supplied sufficient quantities of blood to the basilar artery and posterior cerebral artery; thus, we performed internal trapping for the left VADA. Postoperative angiography demonstrated that the aneurysm and the parent vessel were completely obliterated (Fig. 1). The patient did not present recurrent hemorrhage or neurological deficits. However, he suffered from visual disturbance due to Terson syndrome. This symptom was improved by ophthalmic surgery.

Case 2

A 54-year-old male (patient 9) was admitted to our hospital complaining of severe headache. Computed tomography (CT) revealed mild SAH in the posterior fossa, and his status was estimated as Hunt and Kosnik grade 2. An angiogram demonstrated bilateral dissections, ruptured VADA of the right VA, and VA dissection of the left VA. It has been reported that patients with bilateral dissections, who are treated with parent artery occlusion on one side, may suffer rupture of the contralateral lesion [7]. Therefore, stent-assisted coiling (SAC) was performed for the ruptured VADA of the right

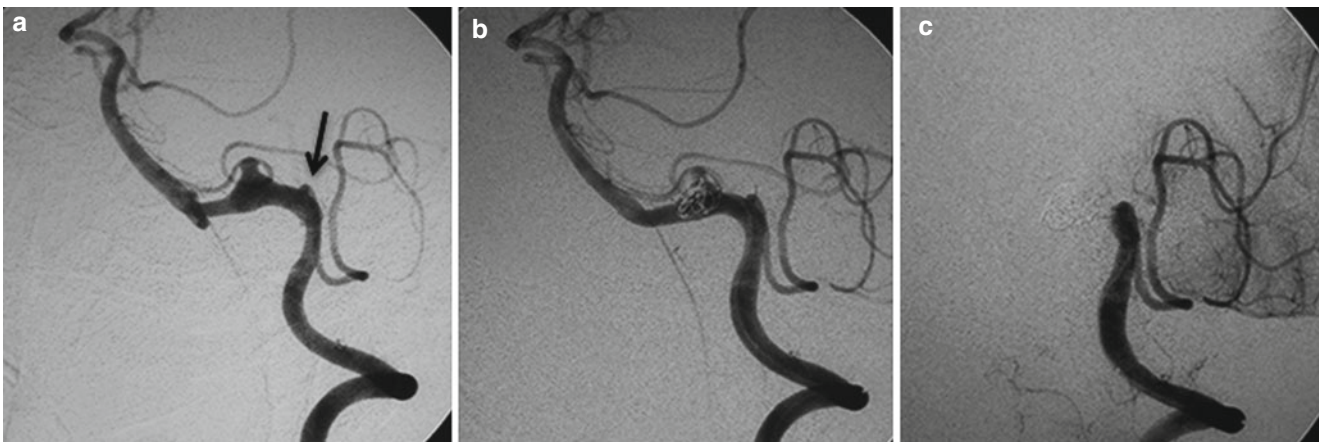

Fig. 1 Working angle of left vertebral artery (VA) angiogram before internal trapping. The vertebral artery dissecting aneurysm (VADA) occurring at a site distal to the VA from the origin of the posterior inferior cerebellar artery (PICA; *arrow*) (**a**). After the first coil was placed in the VADA (**b**). Left VA angiogram after internal trapping by coil embolization (**c**). The VADA was totally occluded with coils and the PICA was well visualized

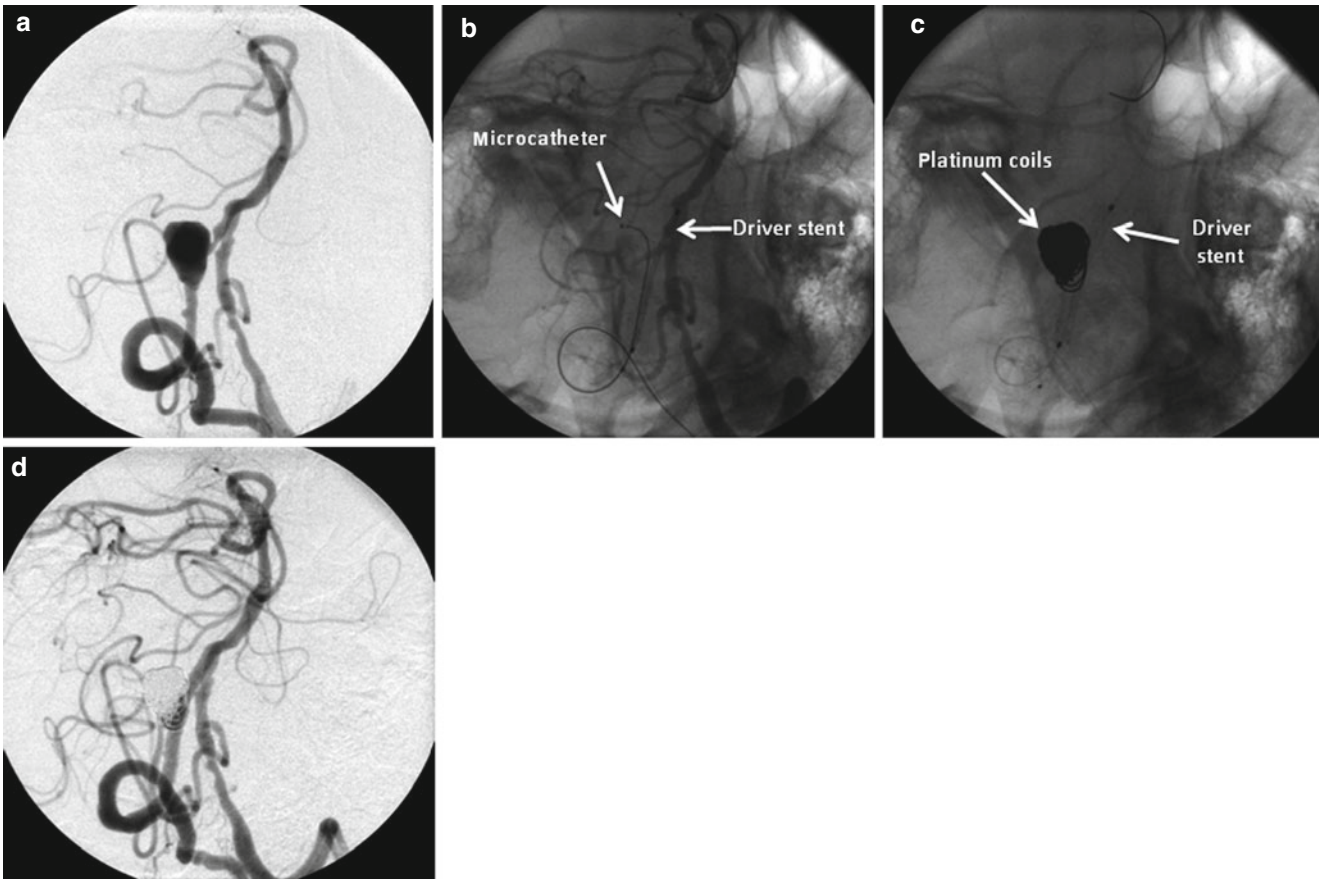

Fig. 2 Working angle of right VA angiogram showing bilateral VA dissections (**a**). Nonsubtracted fluoroscopic image before a balloon-expandable stent was deployed and a microcatheter was placed in the VADA (**b**). After deployment of a balloon-expandable stent across the aneurysm neck and placement of platinum coils in the aneurysm (**c**). Right VA angiogram after coil embolization assisted with the balloon-expandable stent (**d**). The VADA was almost totally occluded with coils

VA without occlusion of the right VA or ischemic complication during endovascular treatment (Fig. 2). The patient did not present recurrent hemorrhage or neurological deficits immediately after the SAC. However, ischemic complications were observed after 14 days and were associated with a change from clopidogrel to aspirin owing to liver dysfunction. MRI-DWI revealed an ischemic lesion in the lateral medulla oblongata following the endovascular treatment.

Results

All the patients received endovascular treatment. Eight patients who had VADA were treated by internal trapping of the dissected segment and parent artery occlusion. We performed stent-assisted coiling (SAC) for 2 cases of VADA, 1 with contralateral hypoplastic VA and 1 with bilateral VADA. Four patients had good recovery (GR), 3 patients had moderate disability (MD), 2 patients had severe disability (SD), and 1 patient who had VADA with involvement of the origin of the PICA died (D) from initial severe SAH. There was no recurrent hemorrhage or procedure-related complications. However, as mentioned above, one patient who was treated by SAC (case 2) presented ischemic complications post-treatment, associated with a change from clopidogrel to aspirin owing to liver dysfunction (Table 1).

Conclusion

The preferred therapy for dissecting artery is trapping. However, it is difficult to perform trapping by craniotomy owing to brain edema and high intracranial pressure. Trapping is especially difficult at the acute stage of SAH if dissecting aneurysms are located near the median part of the brainstem [10]. VADA presenting with subarachnoid hemorrhage (SAH) should be treated promptly because of the high risk of recurrent hemorrhage.

There have been several studies and case reports describing endovascular therapy for the treatment of vertebral dissecting

Table 1 Summary of the ten patients with VA dissecting aneurysms

Patient no.	Age (year)/sex	H&K	Angiographic findings	Procedure	Outcome (GOS)	Complication
1	38/M	4	PICA-involved	Internal trapping	D	None
2	52/M	2	Post-PICA	Internal trapping	GR	None
3	55/M	4	Post-PICA	Internal trapping	MD	None
4	70/F	4	Post-PICA (contralateral hypoplastic VA)	SAC	MD	None
5	43/F	2	Post-PICA	Internal trapping	GR	None
6	65/M	4	No PICA	Internal trapping	GR	None
7	40/M	4	No PICA	Internal trapping	SD	None
8	45/F	5	Post-PICA	Internal trapping	MD	None
9	59/M	2	Post-PICA, bilateral VADA	SAC	MD	Ischemia
10	39/M	4	Post-PICA	Internal trapping	GR	None

VA vertebral artery, *PICA* posterior inferior cerebellar artery, *SAC* stent-assisted coiling, *D* death, *GR* good recovery, *MD* moderate disability, *SD* severe disability

aneurysms [4, 8]. Internal trapping and proximal occlusion of the parent artery with detachable coils, as shown in Fig. 1, can provide a favorable outcome in the majority of patients [2, 4].

Vertebral artery dissecting aneurysms are classified according to the originating portion of the VA and dissecting segment: those occurring at a site distal to the VA from the origin of the PICA are called post-PICA type, those occurring at a site proximal to the VA from the origin of the PICA are called pre-PICA type, and those involving the origin of the PICA are called PICA-involved type. Internal trapping is suitable for VADA of the post- and pre-PICA types. Nevertheless, for patients with VADA involving the origin of the PICA, this approach is rarely indicated because of the risk of ischemic complications in the PICA territory. Also, for patients with contralateral hypoplastic or aplastic VA and patients with bilateral VADA, internal trapping is not suitable because of the risk of ischemic complications and rupture of the contralateral dissected lesion [7]. Several reports have described the use of stent endovascular treatment, such as stent-assisted coiling (SAC), for these patients [1, 3, 8, 9].

Stent-assisted coiling may be used for VADA where internal trapping of the dissected segment of the parent artery at the acute stage is difficult or inappropriate, but ischemic complications are likely to develop. The optimal treatment for dissecting aneurysms of these patients at the acute stage of SAH remains to be established.

In summary, VADA presenting with subarachnoid hemorrhage (SAH) should be treated promptly because of the high risk of recurrent hemorrhage. In our present study, there was no re-bleeding after endovascular treatment and no procedure-related complications. Even if it is difficult to perform trapping by craniotomy for VADA because of brain edema and high intracranial pressure at the acute stage of SAH, endovascular treatment appears to be safe and effective.

Conflict of Interest The authors report no conflict of interest concerning the material or methods used in the study.

References

1. Ahn JY, Han IB, Kim TG, Yoon PH, Lee YJ, Seo SH, Kim DI, Hong CK, Joo JY (2006) Endovascular treatment of intracranial vertebral artery dissections with stent placement or stent assisted coiling. AJNR Am J Neuroradiol 27:1514–1520
2. Albuquerque FC, Fiorella DJ, Han PP, Deshmukh VR, Kim LJ, McDougall CG (2005) Endovascular treatment of intracranial vertebral artery dissecting aneurysms. Neurosurg Focus 18:1–6
3. Chung J, Kim BS, Lee D, Kim TH, Shin YS (2010) Vertebral artery occlusion with vertebral artery-to-posterior inferior cerebellar artery stenting for preservation of the PICA in treating ruptured vertebral artery dissection. Acta Neurochir 153:1489–1492
4. Kai Y, Hamada JI, Morioka M, Todaka T, Mizuno T, Ushio Y (2003) Endovascular coil trapping for ruptured vertebral artery dissecting aneurysms by using double microcathters technique in that acute stage. Acta Neurochir (Wien) 145:447–451
5. Leibowitz R, Do HM, Marcellus ML, Chang SD, Steinberg GK, Marks MP (2003) Parent vessel occlusion for vertebrobasilar fusiform and dissecting aneurysms. AJNR Am J Neuroradiol 24: 902–907
6. Mehta B, Burke T, Kole M, Bydon A, Seyfriend D, Malik G (2003) Stent-within-a-stent technique for the treatment of dissecting vertebral artery aneurysms. AJNR Am J Neuroradiol 24:1814–1818
7. Otawara Y, Ogasawara K, Ogawa A, Kogure T (2002) Dissecting aneurysms of bilateral vertebral arteries with subarachnoid haemorrhage: report of three cases. Neurosurgery 50:1372–1374
8. Peluso JPP, van Rooij WJ, Sluzewski M, Beute GN, Majoie CB (2008) Endovascular treatment of symptomatic intracranial vertebral dissecting aneurysms. AJNR Am J Neuroradiol 29:102–106
9. Suh SH, Kim BM, Park SI, Kim DI, Shin YS, Kim EJ, Chung EC, Koh JS, Shin HC, Choi CS, Won YS (2009) Stent-assited coil embolization followed by a stent-within-a-stent technique for ruptured dissecting aneurysms of the intracranial vertebrobasilar artery. J Neurosurg 111:48–52
10. Uhl E, Schmid-Elsaesser R, Steiger HJ (2003) Ruptued intracranial dissecting aneurysms: management considerations with a focus on surgical and endovascular techniques to preserve arterial continuity. Acta Neurochir (Wien) 145:1073–1084
11. Yamada M, Takao K, Kurata A, Fujii K, Miyasaka Y (2004) Intracranial vertebral artery dissection with subarachnoid hemorrhage: clinical characteristics and outcomes in conservatively treated patients. J Neurosurg 101:25–30
12. Yamaura A, Tani E, Yokota M, Nakano A, Fukami M, Kaba K, Matsumoto T (1999) Endovascular treatment of ruptured dissecting aneurysms aimed at occlusion of the dissected site by using Guglielmi detachable coils. J Neurosurg 90:853–856

Decompressive Craniectomy with Hematoma Evacuation for Large Hemispheric Hypertensive Intracerebral Hemorrhage

Satoru Takeuchi, Yoshio Takasato, Hiroyuki Masaoka, Takanori Hayakawa, Hiroshi Yatsushige, Keigo Shigeta, Kimihiro Nagatani, Naoki Otani, Hiroshi Nawashiro, and Katsuji Shima

Abstract Hemispheric hypertensive intracerebral hemorrhage (ICH) has a high mortality rate. Decompressive craniectomy (DC) has generally been used for the treatment of severe traumatic brain injury, aneurysmal subarachnoid hemorrhage, and hemispheric cerebral infarction. However, the effect of DC on hemispheric hypertensive ICH is not well understood. To investigate the effects of DC for treating hemispheric hypertensive ICH, we retrospectively reviewed the clinical and radiological findings of 21 patients who underwent DC for hemispheric hypertensive ICH. Eleven of the patients were male and 10 were female, with an age range of 22–75 years (mean, 56.6 years). Their preoperative Glasgow Coma Scale scores ranged from 3 to 13 (mean, 6.9). The hematoma volumes ranged from 33.4 to 98.1 mL (mean, 74.2 mL), and the hematoma locations were the basal ganglia in 10 patients and the subcortex in 11 patients. Intraventricular extensions were observed in 11 patients. With regard to the complications after DC, postoperative hydrocephalus developed in ten patients, and meningitis was observed in three patients. Six patients had favorable outcomes and 15 had poor outcomes. The mortality rate was 10 %. A statistical analysis showed that the GCS score at admission was significantly higher in the favorable outcome group than that in the poor outcome group ($P=0.029$). Our results suggest that DC with hematoma evacuation might be a useful surgical procedure for selected patients with large hemispheric hypertensive ICH.

S. Takeuchi (✉), K. Nagatani, N. Otani, H. Nawashiro, and K. Shima
Department of Neurosurgery, National Defense Medical College,
3-2 Namiki, Tokorozawa, Saitama 359-8513, Japan
e-mail: s.takeuchi@room.ocn.ne.jp

Y. Takasato, H. Masaoka, T. Hayakawa, H. Yatsushige,
and K. Shigeta
Department of Neurosurgery, National Hospital
Organization Disaster Medical Center,
3256 Midori-cho, Tachikawa, Tokyo 190-0014, Japan

Keywords Decompressive craniectomy • Intracerebral hemorrhage • Hypertensive • Outcome

Introduction

Hypertensive intracerebral hemorrhage (ICH) accounts for 10–20 % of strokes [2]. The reported 30-day mortality range is approximately 30–50 % [3, 6]. The International Surgical Trial in Intracerebral Haemorrhage (STICH) study, a landmark trial of over 1,000 ICH patients, showed that emergency surgical hematoma evacuation via craniotomy within 72 h of onset failed to improve the outcome compared with a policy of initial medical management [10]. However, patients with large ICH always experience progressive neurological deterioration or cerebral herniation, and this subgroup of patients has been excluded from most of the previous trials. Therefore, the results of such trials cannot be extrapolated to guide the treatment of rapidly deteriorating patients with ICH [13], and for now, the issue of what is the best treatment for patients with ICH remains controversial.

Decompressive craniectomy (DC) is a surgical procedure performed to relieve the malignant elevation of intracranial pressure (ICP), and has been used for the treatment of severe traumatic brain injury (TBI) [1, 12], high-grade aneurysmal subarachnoid hemorrhage [4, 15], and hemispheric cerebral infarction [7, 16]. The application of DC in patients with hemispheric hypertensive ICH has been much less common, although several studies have shown the usefulness of this procedure for large hemispheric hypertensive ICH [5, 11, 14].

Here, we present our experience of this procedure in a subset of 21 patients who were treated with DC for hemispheric hypertensive ICH. We also analyzed the factors related to outcome in these patients.

Y. Katayama et al. (eds.), *Brain Edema XV*, Acta Neurochirurgica Supplement, Vol. 118,
DOI 10.1007/978-3-7091-1434-6_53, © Springer-Verlag Wien 2013

Materials and Methods

Patients

Twenty-one patients who underwent DC for hemispheric hypertensive ICH were studied. The patient charts were retrospectively reviewed, and the following variables were recorded: age, sex, Glasgow Coma Scale (GCS) score just before surgery, the side, location, and volume of the hematoma, the presence of a midline shift, intraventricular hemorrhage (IVH), subarachnoid hemorrhage, or complications after DC, and the outcome. The patient's outcome was assessed using the Glasgow Outcome Scale (GOS) at discharge. We classified GOS scores into favorable (good recovery and moderate disability) or poor (severe disability, vegetative state, or death) outcomes.

Calculation of the Hematoma Volume

The hematoma volume was calculated using the ABC/2 formula where A and B are the perpendicular maximal diameters of the lesion and C is the total length in the vertical plane, using CTs obtained just before DC [9].

Surgical Technique

The decision to proceed with surgery was made by the neurosurgical team when patients exhibited a deteriorating level of consciousness and evidence of a significant mass effect on head CT despite maximal medical therapy, including head elevation, sedation, hyperventilation, and hyperosmolar therapy. DC was performed via standard unilateral frontoparietotemporal craniectomy in all patients. The dura was widely opened in a stellate fashion to the extent of bone decompression, and a duraplasty was performed using a synthetic graft (Gore-tex graft) to increase the available volume before closure.

Statistical Analyses

The Fisher's exact test or Mann–Whitney test was used to explore the factors related to outcomes in patients who underwent DC for hemispheric hypertensive ICH. A value of $P<0.05$ was considered to be statistically significant. All statistical analyses were performed using SPSS version 11.0 software program (SPSS, Chicago, IL, USA).

Results

Eleven of the 21 patients were male and 10 were female, and they had an age range of 22 to 75 years (mean, 56.6 years). Their preoperative Glasgow Coma Scale scores ranged from 3 to 13 (mean, 6.9). The hematoma volumes ranged from 33.4 to 98.1 mL (mean, 74.2 mL). The hematoma locations were the basal ganglia in 10 patients and the subcortex in 11 patients. Intraventricular extensions were observed in 11 patients. With regard to the complications after DC, postoperative hydrocephalus developed in ten patients, and meningitis was observed in three patients. The outcomes included a good recovery in 1 patient, moderate disability in 5 patients, severe disability in 6 patients, vegetative state in 7 patients, and death in 2 patients. The mortality rate was 10 %. The incidence of a favorable outcome was 29 %, and that of a poor outcome was 71 %. The duration of follow-up was at least 54 days for all patients.

The results of the analyses of the prognostic factors in patients who underwent DC for hemispheric hypertensive ICH are shown in Table 1. The GCS score at admission was significantly higher in the favorable outcome group than that in the poor outcome group ($P=0.029$). There were no significant differences in the other variables.

Conclusion

DC has been proposed to be a life-saving intervention for several neurological catastrophes. The rationale for this treatment consists of opening the skull and removing a bone flap to allow the edematous brain to swell outward, thereby preventing intracranial tissue shifts and life-threatening downward herniation. The beneficial effect of DC in reducing ICP has been well documented in several studies, and it also contributes to improvements in cerebral compliance, cerebral oxygen supply, cerebral blood perfusion, and various abnormal CT signs [1, 8]. The application of DC in patients with hemispheric hypertensive ICH has been much less frequent, although several studies have shown the usefulness of this procedure for large hemispheric hypertensive ICH [5, 11, 14].

Dierssen et al. [5] reported a series of 73 patients with spontaneous ICH who were treated by surgical evacuation of the hematoma and DC, and they indicated that the results were much better in acute cases; the mortality of acute cases with DC was 32 % whereas without DC it was 70 %. A case series reported by Murthy et al. [11] revealed that of the 12 patients with spontaneous ICH treated with DC, 11 (92 %) survived at discharge, and 6 of them (55 %) had good functional outcomes (modified Rankin Score 0–3). A similar observational study conducted by Ramnarayan et al. [14]

Table 1 The prognostic factors related to outcome in patients who underwent decompressive craniectomy for hemispheric hypertensive intracerebral hemorrhage

Variable	Favorable outcomes ($n=6$)	Poor outcomes ($n=15$)	P value
Age, years	54.0 ± 13.1	57.6 ± 12.2	0.519
Male gender, *n* (%)	2 (33.3)	9 (60.0)	0.268
GCS score	8.8 ± 2.5	6.1 ± 2.8	0.029
Left-sided hematoma, *n* (%)	1 (16.7)	4 (26.7)	0.550
Hematoma location, *n* (%)			0.633
Basal ganglia	3 (50)	7 (46.7)	
Subcortex	3 (50)	8 (53.3)	
Hematoma volume, mL	69.6 ± 19.0	76.1 ± 14.0	0.677
Midline shift, mm	16.2 ± 3.2	16.5 ± 3.0	0.910
Intraventricular hemorrhage, *n* (%)	1 (16.7)	10 (66.7)	0.055
Subarachnoid hemorrhage, *n* (%)	1 (16.7)	4 (26.7)	0.550
Postoperative meningitis, *n* (%)	1 (16.7)	2 (13.3)	0.658
Postoperative hydrocephalus, *n* (%)	1 (16.7)	9 (60.0)	0.094

GCS Glasgow Coma Scale

also revealed that, of 23 patients who underwent DC for large putaminal hemorrhage, 3 (13 %) died and 13 (57 %) achieved a good outcome (GOS score 5).

In our series, at discharge (at least 54 days), the mortality rate was 10 %, which was consistent with other studies. These results suggest that DC might improve the mortality rate of patients with large hemispheric ICH. However, in our series, only six patients (29 %) had favorable outcomes, and we found that a low GCS score was related to the outcomes in patients after DC. Further studies on the indications for DC are required to investigate whether DC can improve the functional outcomes in patients with large hemispheric ICH, especially taking into consideration their level of consciousness prior to the procedure.

Conflict of Interest We declare that we have no conflict of interest.

References

1. Aarabi B, Hesdorffer DC, Ahn ES, Aresco C, Scalea TM, Eisenberg HM (2006) Outcome following decompressive craniectomy for malignant swelling due to severe head injury. J Neurosurg 104:469–479
2. Bamford J, Sandercock P, Dennis M, Burn J, Warlow C (1990) A prospective study of acute cerebrovascular disease in the community: the Oxfordshire Community Stroke Project–1981–86. Incidence, case fatality rates and overall outcome at one year of cerebral infarction, primary intracerebral and subarachnoid haemorrhage. J Neurol Neurosurg Psychiatry 53:16–22
3. Broderick JP, Brott T, Tomsick T, Huster G, Miller R (1992) The risk of subarachnoid and intracerebral hemorrhages in blacks as compared with whites. N Engl J Med 326:733–736
4. D'Ambrosio AL, Sughrue ME, Yorgason JG, Mocco JD, Kreiter KT, Mayer SA, McKhann GM 2nd, Connolly ES Jr (2005) Decompressive hemicraniectomy for poor-grade aneurysmal subarachnoid hemorrhage patients with associated intracerebral hemorrhage: clinical outcome and quality of life assessment. Neurosurgery 56:12–19
5. Dierssen G, Carda R, Coca JM (1983) The influence of large decompressive craniectomy on the outcome of surgical treatment in spontaneous intracerebral haematomas. Acta Neurochir (Wien) 69:53–60
6. Giroud M, Gras P, Chadan N, Beuriat P, Milan C, Arveux P, Dumas R (1991) Cerebral haemorrhage in a French prospective population study. J Neurol Neurosurg Psychiatry 54:595–598
7. Johnson RD, Maartens NF, Teddy PJ (2011) Decompressive craniectomy for malignant middle cerebral artery infarction: evidence and controversies. J Clin Neurosci 18:1018–1022
8. Kontopoulos V, Foroglou N, Patsalas J, Magras J, Foroglou G, Yiannakou-Pephtoulidou M, Sofianos E, Anastassiou H, Tsaoussi G (2002) Decompressive craniectomy for the management of patients with refractory hypertension: should it be reconsidered? Acta Neurochir (Wien) 144:791–796
9. Kothari RU, Brott T, Broderick JP, Barsan WG, Sauerbeck LR, Zuccarello M, Khoury J (1996) The ABCs of measuring intracerebral hemorrhage volumes. Stroke 27:1304–1305
10. Mendelow AD, Gregson BA, Fernandes HM, Murray GD, Teasdale GM, Hope DT, Karimi A, Shaw MD, Barer DH, STICH investigators (2005) Early surgery versus initial conservative treatment in patients with spontaneous supratentorial intracerebral haematomas in the International Surgical Trial in Intracerebral Haemorrhage (STICH): a randomised trial. Lancet 365:387–397
11. Murthy JM, Chowdary GV, Murthy TV, Bhasha PS, Naryanan TJ (2005) Decompressive craniectomy with clot evacuation in large hemispheric hypertensive intracerebral hemorrhage. Neurocrit Care 2:258–262
12. Olivecrona M, Rodling-Wahlström M, Naredi S, Koskinen LO (2007) Effective ICP reduction by decompressive craniectomy in patients with severe traumatic brain injury treated by an ICP-targeted therapy. J Neurotrauma 24:927–935
13. Rabinstein AA, Atkinson JL, Wijdicks EF (2002) Emergency craniotomy in patients worsening due to expanded cerebral hematoma: to what purpose? Neurology 58:1367–1372
14. Ramnarayan R, Anto D, Anilkumar TV, Nayar R (2009) Decompressive hemicraniectomy in large putaminal hematomas: an Indian experience. J Stroke Cerebrovasc Dis 18:1–10
15. Schirmer CM, Hoit DA, Malek AM (2007) Decompressive hemicraniectomy for the treatment of intractable intracranial hypertension after aneurysmal subarachnoid hemorrhage. Stroke 38:987–992
16. Staykov D, Gupta R (2011) Hemicraniectomy in malignant middle cerebral artery infarction. Stroke 42:513–516

Is Decompressive Craniectomy a Risk Factor for Ventriculomegaly?

Satoru Takeuchi, Kimihiro Nagatani, Kojiro Wada, Hiroshi Nawashiro, Naoki Otani, Hideo Osada, Hiroaki Kobayashi, Takamoto Suzuki, and Katsuji Shima

Abstract *Objective*: Decompressive craniectomy (DC) is an established therapeutic option following severe traumatic brain injury (TBI). However, several delayed complications of DC have been reported, including ventriculomegaly, which can lead to poor patient outcomes. Nevertheless, ventriculomegaly can occur after TBI even without DC. The aim of the present study was to investigate the influence of DC on ventriculomegaly.

Material and Methods: Adult male Sprague–Dawley rats (300–400 g) were subjected to lateral fluid percussion injury using a fluid percussion device. Rats were randomly divided into four groups: sham, craniectomized without trauma (D group), traumatized without DC (FPI group), and craniectomized immediately after trauma (FPI + D group). On day 28 of recovery, ventricular volumes were measured by image analysis.

Results: There was no significant difference in ventricular size between the sham group and the D group animals or between the FPI group and the FPI + D group animals.

Conclusion: These data suggest that DC may not be a risk factor for ventriculomegaly after TBI.

Keywords Ventriculomegaly • Decompressive craniectomy • Traumatic brain injury • Rat

Introduction

Decompressive craniectomy (DC) is an established therapeutic option following severe traumatic brain injury (TBI), and is widely used in the treatment of malignant post-traumatic brain edema [1, 12, 14, 16]. The beneficial effects of DC in reducing intracranial pressure (ICP) are well documented, and DC can also contribute to improvements in cerebral compliance, cerebral oxygen supply, cerebral blood perfusion, and various abnormal computed tomography signs [1, 12, 14, 16]. However, several delayed complications of DC have been reported [2, 4, 5, 7, 15, 20], including ventriculomegaly, which can lead to a poor outcome for the patients [2, 4, 5]. On the other hand, ventriculomegaly can occur after TBI even without DC [3, 6, 9, 13], and clinical studies failed to examine whether DC itself could aggravate ventriculomegaly. The aim of the present study was to investigate the influence of DC on ventriculomegaly.

Materials and Methods

Animals and Experimental Procedures

All experimental procedures were approved by the Animal Care and Use Committee of the National Defense Medical College. Sprague–Dawley (SD) rats (male, 320–390 g; 9–10 weeks of age) were used. The rats were housed in individual cages under controlled environmental conditions (12/12 h light/dark cycle, 20–22 °C; room temperature) with food and water freely available, for 1 week before the experimental surgery. The rats were anesthetized with isofluorane (1.5 %) in a 30 % oxygen to 70 % nitrous oxide gas mixture via a nose cone and were fixed in a stereotaxic frame for the procedure. A 4.8 mm craniotomy was made over the right parietal cortex (3.8 mm posterior and 2.5 mm lateral to the bregma), keeping the underlying dura intact. The bone flaps were cleanly preserved. A plastic Luer-Loc was placed over the opening and secured with dental acrylic cement. The rats were returned to their cages and allowed free access to water overnight. The following day, the rats were anesthetized, intubated, and maintained on a mechanical ventilator after

S. Takeuchi (✉), K. Nagatani, K. Wada, H. Nawashiro, N. Otani, H. Osada, H. Kobayashi, T. Suzuki, and K. Shima
Department of Neurosurgery, National Defense Medical College, 3-2 Namiki, Tokorozawa, Saitama 359-8513, Japan
e-mail: s.takeuchi@room.ocn.ne.jp

Y. Katayama et al. (eds.), *Brain Edema XV*, Acta Neurochirurgica Supplement, Vol. 118,
DOI 10.1007/978-3-7091-1434-6_54,

infusion of pancronium bromide (0.1 mg/kg; tidal volume: 2.5–3.0 mL/kg; respiratory rate: 60/min). The femoral artery was cannulated with a polyethylene catheter. The rats' blood pressure was monitored throughout the procedure, and arterial blood samples were intermittently analyzed ($PaCO_2$ was controlled at 30–40 mmHg). The rectal temperature was measured with a rectal probe and maintained at a constant level of approximately 37.0 °C with a heating pad. Ten rats received fluid percussion injury (FPI) at a moderate severity (2.5–3.0 atm, 16 ms in duration) using a Dragonfly fluid percussion device (model HPD-1700; Dragonfly R&D, Silver Spring, MD, USA), as previously described [10]. FPI animals were further divided into decompressive craniectomy (DC; FPI + D group; $n = 5$) or sham (FPI group; $n = 5$) groups. A further 10 rats were subjected to the same procedures except that the actual insult was not performed, and then received DC without FPI (D group; $n = 5$) or sham ($n = 5$). In rats subjected to DC (the FPI + D group and the D group), the opening of the craniotomy was extended using bone forceps within 20 min of the insult or pseudo-insult. The dura was left intact during the surgical procedure. The craniectomy area was between the anterior coronal suture and the posterior rhomboid suture. The sagittal suture and the superior temporal line formed the medial and lateral borders. In rats without DC (the FPI group and the sham group), the craniotomy opening was glued closed (dental acrylic cement) using the previously removed bone flap. Following these procedures, the scalp was sutured and the rats were returned to their home cages with food and water available ad libitum.

Ventricular Volume Measurement

At day 28 after TBI, the rats were euthanized by decapitation under intraperitoneal anesthesia, and the brains were rapidly removed and immersed in 4 % buffered paraformaldehyde for 12 h. Fixed brains were sectioned coronally at 1-mm intervals (from 2.7 mm anterior to 9.3 mm posterior to the bregma). Ventricular volumes were measured using image analysis software (ImageJ, NIH, USA).

Statistical Analysis

Data are presented as the mean ± SD. Comparisons between the groups were made using one-way analysis of variance followed by Tukey's test. A value of $p < 0.05$ was considered significant. Graphpad Prism 4.0 (San Diego, CA, USA) was used for all statistical tests.

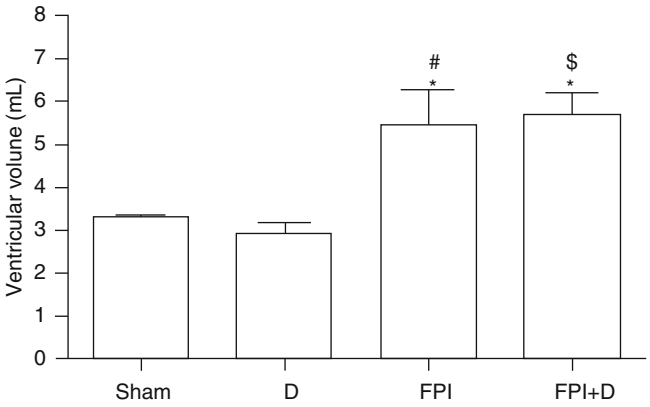

Fig. 1 Ventricular volumes at 28 days after injury. Ventricular volume in the FPI group was larger than that in the sham group and the D group (*$p < 0.05$, #$p < 0.05$ respectively). Ventricular volume in the FPI + D group was larger than that in the sham group and the D group (*$p < 0.05$ and $^{\$}p < 0.01$ respectively)

Results

Physiological Data

There were no significant differences in the physiological data between each group with regard to the mean arterial blood pressure, pH, pCO_2, pO_2, or body temperature (data not shown).

Ventricular Volumes

At day 28, ventricular volume was 3.3 ± 0.2 mL in the sham group, 2.9 ± 0.5 mL in the D group, 5.5 ± 1.7 mL in the FPI group, and 5.7 ± 1.0 mL in the FPI + D group (Fig. 1). Ventricular volume in the FPI group was larger than that in the sham group and the D group ($p < 0.05$, for both), while there was no difference between the FPI group and the FPI + D group (Fig. 1). Ventricular volume in the FPI + D group was larger than that in the sham group and the D group ($p < 0.05$ and $p < 0.01$ respectively), while there was no difference between the sham group and the D group (Fig. 1).

Conclusion

It has been hypothesized that the disruption of pulsatile ICP dynamics secondary to opening of the cranial vault might result in decreased cerebrospinal fluid (CSF) outflow, thus affecting ventricular enlargement [5, 19]. However, our data suggest that DC may not be a risk factor for ventriculomegaly after TBI. Aquaporin (AQP)-4 is one of the main aquaporins

in the central nervous system and acts as a water channel. It is located primarily in astrocytic end-feet, glial limiting membranes, and the basolateral membrane of the ventricular ependymal cells [11]. Several studies have examined the roles of AQP-4 in ventricular enlargement. Li et al. reported that the majority of AQP-4-null mice demonstrated smaller ventricular sizes and reduced cerebrospinal fluid production [8], and Tourdias et al. reported that the degree of hydrocephalus correlated with the upregulation of AQP-4 [18]. Interestingly, our colleagues recently reported that DC after TBI significantly decreased AQP-4 expression [17]. Therefore, combined with the results of the present study, we suggest that DC can both increase and decrease the incidence of ventriculomegaly after TBI, and that DC does not always cause ventricular enlargement. A limitation of our study is that we were unable to determine whether ventriculomegaly was a result of hydrocephalus or atrophy. Further studies are required to fully elucidate the role of DC in hydrocephalus.

Acknowledgments This study was supported by a research grant from The General Insurance Association of Japan.

Conflict of Interest We declare that we have no conflict of interest.

References

1. Aarabi B, Hesdorffer DC, Ahn ES, Aresco C, Scalea TM, Eisenberg HM (2006) Outcome following decompressive craniectomy for malignant swelling due to severe head injury. J Neurosurg 104: 469–479
2. Beauchamp KM, Kashuk J, Moore EE, Bolles G, Rabb C, Seinfeld J, Szentirmai O, Sauaia A (2010) Cranioplasty after post-injury decompressive craniectomy: is timing of the essence? J Trauma69:270–274
3. Beyerl B, Black PM (1984) Posttraumatic hydrocephalus. Neurosurgery 15:257–261
4. Choi I, Park HK, Chang JC, Cho SJ, Choi SK, Byun BJ (2008) Clinical factors for the development of posttraumatic hydrocephalus after decompressive craniectomy. J Korean Neurosurg Soc 43: 227–231
5. De Bonis P, Pompucci A, Mangiola A, Rigante L, Anile C (2010) Post-traumatic hydrocephalus after decompressive craniectomy: an underestimated risk factor. J Neurotrauma 27:1965–1970
6. Guyot LL, Michael DB (2000) Post-traumatic hydrocephalus. Neurol Res 22:25–28
7. Honeybul S (2010) Complications of decompressive craniectomy for head injury. J Clin Neurosci 17:430–435
8. Li X, Kong H, Wu W, Xiao M, Sun X, Hu G (2009) Aquaporin-4 maintains ependymal integrity in adult mice. Neuroscience 162:67–77
9. Marmarou A, Foda MA, Bandoh K, Yoshihara M, Yamamoto T, Tsuji O, Zasler N, Ward JD, Young HF (1996) Posttraumatic ventriculomegaly: hydrocephalus or atrophy? A new approach for diagnosis using CSF dynamics. J Neurosurg 85:1026–1035
10. Matsushita Y, Shima K, Nawashiro H, Wada K (2000) Real-time monitoring of glutamate following fluid percussion brain injury with hypoxia in the rat. J Neurotrauma 17:143–153
11. Owler BK, Pitham T, Wang D (2010) Aquaporins: relevance to cerebrospinal fluid physiology and therapeutic potential in hydrocephalus. Cerebrospinal Fluid Res 7:15
12. Piek J (2002) Decompressive surgery in the treatment of traumatic brain injury. Curr Opin Crit Care 8:134–138
13. Poca MA, Sahuquillo J, Mataró M, Benejam B, Arikan F, Báguena M (2005) Ventricular enlargement after moderate or severe head injury: a frequent and neglected problem. J Neurotrauma 22: 1303–1310
14. Qiu W, Guo C, Shen H, Chen K, Wen L, Huang H, Ding M, Sun L, Jiang Q, Wang W (2009) Effects of unilateral decompressive craniectomy on patients with unilateral acute post-traumatic brain swelling after severe traumatic brain injury. Crit Care 13:R185
15. Stiver SI (2009) Complications of decompressive craniectomy for traumatic brain injury. Neurosurg Focus 26:E7
16. Timofeev I, Czosnyka M, Nortje J, Smielewski P, Kirkpatrick P, Gupta A, Hutchinson P (2008) Effect of decompressive craniectomy on intracranial pressure and cerebrospinal compensation following traumatic brain injury. J Neurosurg 108:66–73
17. Tomura S, Nawashiro H, Otani N, Uozumi Y, Toyooka T, Ohsumi A, Shima K (2011) Effect of decompressive craniectomy on aquaporin-4 expression after lateral fluid percussion injury in rats. J Neurotrauma 28:237–243
18. Tourdias T, Dragonu I, Fushimi Y, Deloire MS, Boiziau C, Brochet B, Moonen C, Petry KG, Dousset V (2009) Aquaporin 4 correlates with apparent diffusion coefficient and hydrocephalus severity in the rat brain: a combined MRI-histological study. Neuroimage 47:659–666
19. Waziri A, Fusco D, Mayer SA, McKhann GM 2nd, Connolly ES Jr (2007) Postoperative hydrocephalus in patients undergoing decompressive hemicraniectomy for ischemic or hemorrhagic stroke. Neurosurgery 61:489–493
20. Yang XF, Wen L, Shen F, Li G, Lou R, Liu WG, Zhan RY (2008) Surgical complications secondary to decompressive craniectomy in patients with a head injury: a series of 108 consecutive cases. Acta Neurochir (Wien) 150:1241–1247

A Suitable Formula for Estimating the Volume Gained by Decompressive Craniectomy in Malignant Hemispheric Infarction

Kimihiro Nagatani, Kojiro Wada, Satoru Takeuchi, Hiroaki Kobayashi, Terushige Toyooka, Naoki Otani, Hideo Osada, Takamoto Suzuki, Hiroshi Nawashiro, and Katsuji Shima

Abstract Decompressive craniectomy (DC) improves the survivability and functional outcome in patients with malignant hemispheric infarction (MHI). The decompressive effect of DC depends on the decompressive volume (DV). The value of the formulas for estimating DV has not been reported to date. We have investigated the value of the formulas to estimate DV in patients with MHI. We analyzed the head CTs of six patients who underwent DC for MHI. We examined 1/2ABC, 1/3ABC, π/6ABC, and 2/3Sh formulas to determine the formula that gives the closest estimation of DV compared with computer-assisted volumetric analysis (gold standard). The mean volume values of the gold standard, 1/2ABC, 1/3ABC, π/6ABC, and 2/3Sh formulas were 100.2, 102.4, 68.3, 105.2, and 109.2 mL respectively. Spearman's correlation coefficient was assessed for DV obtained by each of the four different formulas relative to the gold standard. These were as follows: 1/2ABC = 0.8095 ($p < 0.05$), 1/3ABC = 0.8095 ($p < 0.05$), π/6ABC = 0.7381 ($p < 0.05$), and 2/3Sh = 0.4524 ($p > 0.05$). In conclusion, the 1/2ABC formula is the most useful and the closest estimation of DV in patients with MHI after DC.

Keywords Decompression • Craniectomy • Computed tomography • 1/2ABC • 1/3ABC • π/6ABC • 2/3Sh • Volume • Stroke

K. Nagatani (✉), K. Wada, S. Takeuchi, H. Kobayashi, N. Otani, H. Osada, T. Suzuki, H. Nawashiro, and K. Shima
Department of Neurosurgery, National Defense Medical College, 3-2 Namiki, Tokorozawa, Saitama 359-8513, Japan
e-mail: naval.kimi@gmail.com

T. Toyooka
Department of Neurosurgery, Kuki General Hospital, 418-1 Kamihayami, Kuki, Saitama 346-0021, Japan

Introduction

Randomized trials have suggested that decompressive craniectomy (DC) reduces mortality and improves functional outcome in patients with malignant hemispheric infarction (MHI) [1, 3, 6]. The decompressive effect of DC depends on the volume gained by craniectomy (i.e., decompressive volume [DV]) [7]. However, DV is not simple to assess. There have not yet been any reports on the value of formulas to estimate DV.

There are, however, several techniques to estimate the acute subdural and epidural hematoma volume, including the 1/2ABC, 1/3ABC, π/6ABC, and 2/3Sh methods [2, 4, 5, 8]. Here, we applied these formulas to estimate DV. The aim of the present study was to investigate the value of using formulas to estimate DV in patients with MHI.

Materials and Methods

Patient Population and Operative Therapy

We focused on six patients who underwent DC for MHI between January 2000 and March 2008, and whose volumetric data from head CTs were available. Of the 6 patients, 4 were men and 2 were women, whose age ranged from 46 to 73 years (mean, 61.3 years). The decision to proceed with surgery was made by the neurosurgical team when the patients exhibited a deteriorating level of consciousness, and the head CT showed evidence of a significant mass effect, despite maximal medical therapy. DC was performed via standard unilateral frontoparietotemporal craniectomy in all patients (Fig. 1). Duraplasty was performed using a synthetic graft (Gore-tex graft) to increase the available volume before closure. The bone flap was removed. Internal decompression was not performed in all patients.

Y. Katayama et al. (eds.), *Brain Edema XV*, Acta Neurochirurgica Supplement, Vol. 118,
DOI 10.1007/978-3-7091-1434-6_55, © Springer-Verlag Wien 2013

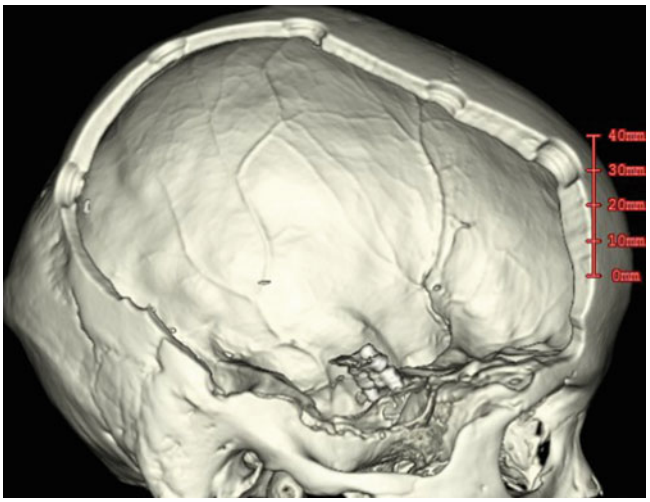

Fig. 1 A representative three-dimensional CT showing an optimal decompressive craniectomy. The craniectomy area is large and performed at the floor of the middle fossa

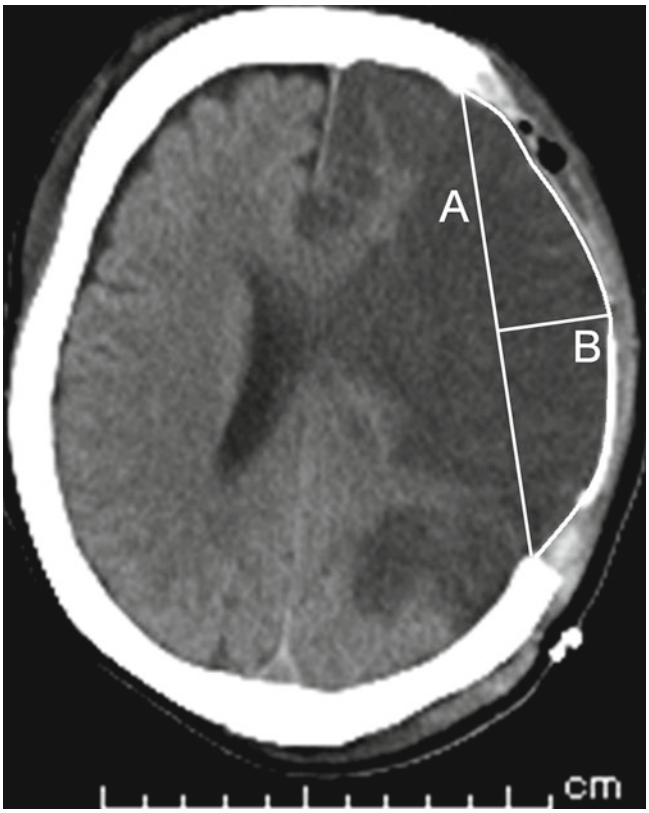

Fig. 2 CT of a brain after craniectomy. (*A*) diameter of the craniectomy; (*B*) perpendicular line of the longest distance from the diameter (*A*) to the dural flap. Margin of the area gained by the craniectomy was hand-traced

Imaging and Estimation Techniques

Pre- and postoperative CTs, performed between 1 and 9 days after surgery, were analyzed. Computer-assisted volumetric analysis was considered the gold standard for comparison. Volumetric analysis was performed using Ziostation analytical software (Ziosoft, Tokyo, Japan) as follows: pre- and postoperative volumes of the whole brain were measured. The preoperative volume was subtracted from the postoperative volume to calculate the gold standard measurement of DV. Moreover, the postoperative CTs were analyzed as follows: the diameter of the craniectomy was measured in centimeters in each CT slice. The CT slice showing the largest diameter (A) was then taken, and a perpendicular line (B) was measured from the horizontal diameter to the dural flap. The number of CT slices of the craniectomy, multiplied by the slice thickness, was the height (C) of DV. Margins of the area that was gained by DC were traced by hand on each CT slice (Fig. 2). The label "S" indicates the largest area value gained by DC, and "h" indicates the height of DV [8]. In the π/6ABC formula, A refers to the largest diameter (at the slice with the largest area), and B indicates the perpendicular line (the longest distance from the horizontal diameter to the dural flap) in the same slice, as described above [5]. Each value was measured using image analysis software (ImageJ, NIH, USA). We examined four different formulas to determine which formula gives the closest estimation of DV relative to the gold standard. The evaluated formulas were 1/2ABC, 1/3ABC, π/6ABC, and 2/3Sh. Spearman's correlation coefficient was used to statistically compare the volumes calculated using each of these four formulas to the gold standard. *P* values less than 0.05 were considered significant. Graphpad Prism 4.0 software (San Diego, CA, USA) was used for all statistical tests.

Results

Compared with the gold standard measurement (100.2 mL), the mean volume values calculated with the 1/2ABC, 1/3ABC, π/6ABC, and 2/3Sh formulas were 102.4, 68.3, 105.2, and 109.2 mL respectively (Table 1). In addition to an underestimation of 31.8 % with the 1/3ABC formula, the DV assessed by the 1/2ABC, π/6ABC, and 2/3Sh formulas gave 2.2%, 5.0%, and 9.0% overestimations, respectively. Spearman's correlation coefficients for the DV obtained by each of the four different formulas relative to the gold standard were as follows: 1/2ABC = 0.8095; 1/3ABC = 0.8095; π/6ABC = 0.7381; and 2/3Sh = 0.4524. Each of the correlation coefficients of 1/2ABC, 1/3ABC, and π/6ABC was significant ($p < 0.05$). However, the correlation coefficient of the 2/3Sh formula was not significant ($p > 0.05$; Fig. 3).

Table 1 Decompressive volumes measured using different techniques

	Decompressive volume (mL)			95 % CI for mean	
Techniques	Mean	Minimum	Maximum	Lower bound	Upper bound
Gold standard	100.2	70.44	136.1	82.36	118.1
1/2ABC	102.4	77.31	145.6	84.97	119.9
1/3ABC	68.3	51.54	97.05	56.65	79.94
π/6ABC	105.2	70.37	156.9	83.14	127.2
2/3Sh	109.2	87.97	139.1	93.82	124.6

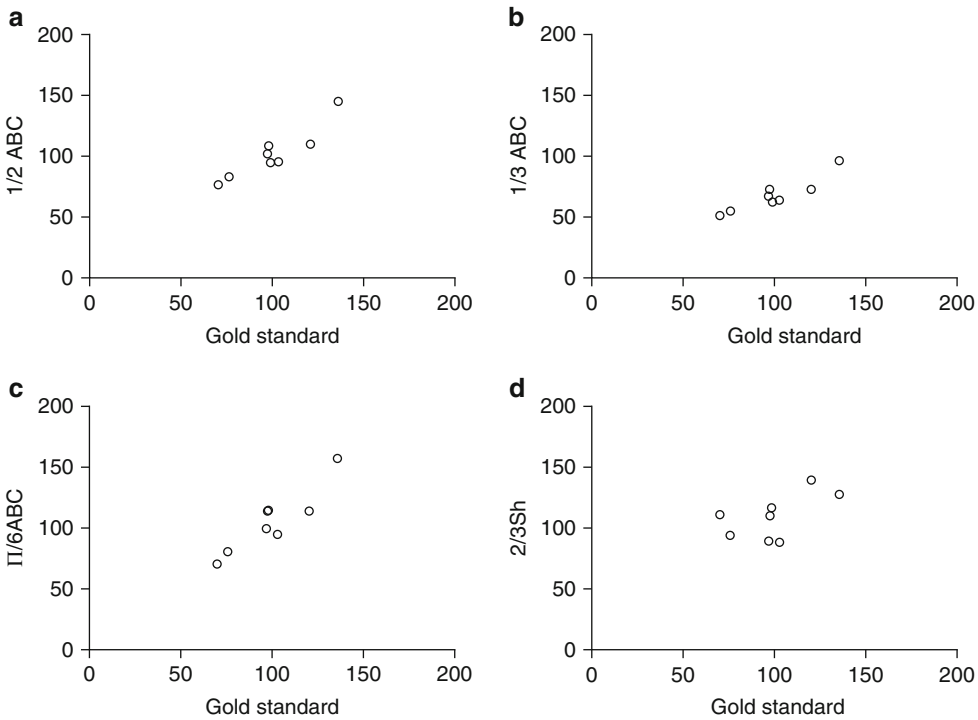

Fig. 3 Comparison of decompressive volumes measured by the 1/2ABC, 1/3ABC, π/6ABC, and 2/3Sh techniques, relative to the gold standard measurement. (**a**) 1/2ABC: $r=0.8095$ ($p<0.05$). (**b**) 1/3ABC: $r=0.8095$ ($p<0.05$). (**c**) π/6ABC: $r=0.7381$ ($p<0.05$). (**d**) 2/3Sh: $r=0.4524$ ($p>0.05$)

Conclusion

All formulas, except 2/3Sh, produced a strong correlation with the gold standard measurement. Overall, the 1/2ABC and 1/3ABC techniques showed the best correlation with the gold standard. Furthermore, the formula 1/2ABC only slightly overestimated DV, by 2.2 %, in comparison with the gold standard. It is evident that the 1/2ABC technique gives the closest estimation of DV gained by DC. Although the 1/3ABC formula also provided the best correlation with the gold standard, it was not useful because it considerably underestimated DV by 31.8 %, in comparison with the gold standard. The formula π/6ABC gave the second best correlation; however, calculating π/6ABC is more troublesome.

Although DC is a surgical procedure for treating the malignant elevation of intracranial pressure (ICP) in patients with MHI and the decompressive effect depends on the DV [1, 3, 6, 7], there are no data on the relationship between DV and ICP. In addition, there are no reports on the relationship between DV and the outcome of patients with MHI after DC, although the infarct volume, midline shift, and craniectomy area have already been examined [1, 3, 6, 7]. We believe that one reason for the lack of these data may be the difficulty in estimating the DV immediately and precisely. To the best of our knowledge, this is the first report measuring DV in patients with MHI using computer-assisted volumetric analysis. However, it is not convenient because of the need for special analytical software. We therefore feel that the simple 1/2ABC technique is a more useful method of estimating DV. This technique may be useful to analyze the effect of DC on the ICP, the incidence of complications (e.g., hydrocephalus), and the outcome of patients with MHI.

The present study has several limitations. A major limitation of this study was the relatively small number of patients

involved. Further studies are required, with a larger number of patients. Furthermore, we did not evaluate ICP in patients with MHI in this study. We hope that further investigations will reveal the relationship between DV and change in ICP. In summary, this study proves the validity of the 1/2ABC technique for estimating the DV gained by DC in patients with MHI.

Acknowledgments This study was supported by a research grant from The General Insurance Association of Japan.

Conflict of Interest We declare that we have no conflict of interest.

References

1. Hofmeijer J, Kappelle LJ, Algra A, Amelink GJ, van Gijn J, van der Worp HB, HAMLET investigators (2009) Surgical decompression for space-occupying cerebral infarction (the Hemicraniectomy After Middle Cerebral Artery infarction with Life-threatening Edema Trial [HAMLET]): a multicentre, open, randomised trial. Lancet Neurol 8:326–333
2. Huttner HB, Steiner T, Hartmann M, Köhrmann M, Juettler E, Mueller S, Wikner J, Meyding-Lamade U, Schramm P, Schwab S, Schellinger PD (2006) Comparison of ABC/2 estimation technique to computer-assisted planimetric analysis in warfarin-related intracerebral parenchymal hemorrhage. Stroke 37:404–408
3. Jüttler E, Schwab S, Schmiedek P, Unterberg A, Hennerici M, Woitzik J, Witte S, Jenetzky E, Hacke W, DESTINY Study Group (2007) Decompressive surgery for the treatment of malignant infarction of the middle cerebral artery (DESTINY): a randomized, controlled trial. Stroke 38:2518–2525
4. Petersen OF, Espersen JO (1984) Extradural hematomas: measurement of size by volume summation on CT scanning. Neuroradiology 26:363–367
5. Tada A, Hisada K, Suzuki T, Kadoya S (1981) Measurement volume of intracranial hematoma by computed tomography (author's transl). No Shinkei Geka 9:251–256
6. Vahedi K, Hofmeijer J, Juettler E, Vicaut E, George B, Algra A, Amelink GJ, Schmiedeck P, Schwab S, Rothwell PM, Bousser MG, van der Worp HB, Hacke W, DECIMAL, DESTINY, and HAMLET investigators (2007) Early decompressive surgery in malignant infarction of the middle cerebral artery: a pooled analysis of three randomised controlled trials. Lancet Neurol 6:215–222
7. Wirtz CR, Steiner T, Aschoff A, Schwab S, Schnippering H, Steiner HH, Hacke W, Kunze S (1997) Hemicraniectomy with dural augmentation in medically uncontrollable hemispheric infarction. Neurosurg Focus 2:E3
8. Zhao KJ, Zhang RY, Sun QF, Wang XQ, Gu XY, Qiang Q, Gao C, Shen JK (2010) Comparisons of 2/3Sh estimation technique to computer-assisted planimetric analysis in epidural, subdural and intracerebral hematomas. Neurol Res 32:910–917

Hydrocephalus Following Decompressive Craniectomy for Ischemic Stroke

Satoru Takeuchi, Yoshio Takasato, Hiroyuki Masaoka, Takanori Hayakawa, Hiroshi Yatsushige, Keigo Shigeta, Kimihiro Nagatani, Naoki Otani, Kojiro Wada, Hiroshi Nawashiro, and Katsuji Shima

Abstract Numerous studies on hydrocephalus after decompressive craniectomy (DC) for severe traumatic brain injury have been reported, whereas there have been only two reports on DC for hemispheric cerebral infarction. Here, we present the clinical details of 23 patients who underwent DC for hemispheric cerebral infarction and the incidence of hydrocephalus following DC. Of the 23 patients, 13 were male and 10 were female, with an age range from 34 to 75 years (mean, 60.8 years). The areas of hemispheric infarctions were those of the middle cerebral arteries in 12 patients and of the internal carotid arteries in 11 patients. The mean preoperative GCS score was 6. Nineteen patients (82.6 %) underwent cranioplasty. Pre-cranioplasty hydrocephalus was observed in 11 (47.8 %) patients. Four patients who had precranioplasty hydrocephalus were transferred or died without cranioplasty, and post-cranioplasty hydrocephalus occurred in 7 (36.8 %). Only one patient underwent a shunt procedure after cranioplasty. We consider that the explanation for the discrepancies between our study and the previous studies might lie in the definition of hydrocephalus and the indications for shunting.

Keywords Decompressive craniectomy • Hydrocephalus • Complication • Stroke

S. Takeuchi (✉), K. Nagatani, N. Otani, K. Wada,
H. Nawashiro, and K. Shima
Department of Neurosurgery, National Defense Medical College,
3-2 Namiki, Tokorozawa, Saitama 359-8513, Japan
e-mail: s.takeuchi@room.ocn.ne.jp

Y. Takasato, H. Masaoka, T. Hayakawa, H. Yatsushige, and K. Shigeta
Department of Neurosurgery,
National Hospital Organization Disaster Medical Center,
3256 Midori-cho, Tachikawa, Tokyo 190-0014, Japan

Introduction

Decompressive craniectomy (DC) is a surgical procedure for treating the malignant elevation of intracranial pressure (ICP), and it has generally been used for the treatment of severe traumatic brain injury (TBI) [1, 6, 13–15], aneurysmal subarachnoid hemorrhage [5, 8, 16, 18] and hemispheric cerebral infarction [9, 10, 19, 20]. The rationale for this treatment modality consists of opening the skull and removing a bone flap to allow the edematous brain to swell outward, thereby preventing intracranial tissue shifts and life-threatening downward herniation.

In patients who had undergone DC for malignant hemispheric cerebral infarction, several randomized controlled trials and meta-analyses showed a significant reduction in mortality in craniectomized patients compared with conservatively treated patients [9, 10, 19, 20]. However, these trials failed to demonstrate a significant benefit of DC when the functional outcome was considered.

Several delayed complications of DC have been reported, and include sinking flap syndrome, extra-axial fluid collections, hydrocephalus, and the development of subdural hematomas [2–4, 7, 21, 22]. Among these, recent attention has been focused on hydrocephalus because it may have an impact on patients' clinical outcomes [3, 4, 7, 21, 22].

Numerous studies on hydrocephalus after DC for severe TBI have been reported [3, 4, 7, 22], whereas there have been only two reports on DC for hemispheric cerebral infarction [17, 21]. Here, we present the clinical details of 23 patients who underwent DC for hemispheric cerebral infarction and report the incidence of hydrocephalus following DC.

Y. Katayama et al. (eds.), *Brain Edema XV*, Acta Neurochirurgica Supplement, Vol. 118,
DOI 10.1007/978-3-7091-1434-6_56,

Materials and Methods

Patients

Twenty-three patients who underwent DC for a malignant hemispheric cerebral infarction were studied. The patient charts were retrospectively reviewed and the following variables were recorded: age, sex, Glasgow Coma Scale (GCS) score at the time of surgery, interval from onset to surgery, timing of cranioplasty, the presence of hydrocephalus pre- and post-cranioplasty, and the duration of follow-up.

Surgical Technique

The decision to proceed with surgery was made by the neurosurgical team when patients exhibited a deteriorating level of consciousness and evidence of a significant mass effect on head CT despite maximal medical therapy, including head elevation, sedation, hyperventilation, and hyperosmolar therapy. DC was performed via standard unilateral frontoparietotemporal craniectomy in all patients (right side, 11 patients; left side, 12 patients). The dura was widely opened in a stellate fashion to the extent of bone decompression, and a duraplasty was performed using a synthetic graft (Gore-tex graft) to increase the available volume before closure. The bone flap was stored under sterile conditions with cryopreservation until cranioplasty.

Definition of Hydrocephalus

For the purposes of this study, hydrocephalus after DC was defined as radiographic evidence of progressive ventricular dilation, with an Evans index >0.3, associated with narrowed cerebrospinal fluid spaces at the convexity on CT. Clinical examination was not included as a defining element in the determination of hydrocephalus given the poor baseline neurological status of most patients in the acute period, secondary to their initial neurological insult, which resulted in an inability to quantify subtle clinical changes possibly referable to hydrocephalus.

Results

Of the 23 patients, 13 were male and 10 were female, with an age range from 34 to 75 years (mean, 60.8 years). The areas of hemispheric infarctions were those of the middle cerebral arteries in 12 patients and of the internal carotid arteries in 11 patients. The interval from onset to surgery ranged from 1 to 8 days (mean, 2.4 days). The mean preoperative GCS score was 6. Nineteen patients (82.6 %) underwent cranioplasty, and the interval from DC to cranioplasty ranged from 22 to 130 days (mean, 57.2 days).

Pre-cranioplasty hydrocephalus was observed in 11 patients (47.8 %). Four patients who had precranioplasty hydrocephalus were transferred or died without cranioplasty, and post-cranioplasty hydrocephalus occurred in 7 (36.8 %). Nevertheless, only 1 patient underwent a shunt procedure after cranioplasty. The mean duration of follow-up was 173 days.

Conclusion

Waziri et al. have hypothesized that DC might play a role in the flattening of the normally dicrotic CSF pulse waveform seen in patients who undergo DC, because of the transmission of the pressure pulse out through the open cranium. It is possible that disruption of the pulsatile ICP dynamics secondary to opening the cranial vault results in decreased CSF outflow, thus leading to ventriculomegaly [21].

Numerous studies about hydrocephalus after DC for severe TBI have been reported [3, 4, 7, 22]. Although the development of hydrocephalus as a result of DC may be a common occurrence [21], there have been only a few studies about the association between hydrocephalus and DC for hemispheric cerebral infarction [17, 21].

In the series of patients reported by Waziri et al., hydrocephalus developed in 15 of the 17 patients (88 %) after DC for hemispheric cerebral infarction, and 5 required shunting after cranioplasty [21]. On the other hand, Rahme et al. reported that significant hydrocephalus did not develop in any of their 17 patients who underwent DC for stroke, including 12 patients with hemispheric cerebral infarction [17]. Therefore, they concluded that hydrocephalus does not frequently occur after DC in stroke patients [17]. Furthermore, Kim et al. also described a 0 % rate of shunting in 23 patients who underwent DC for infarction [11].

In the present study, post-cranioplasty hydrocephalus occurred in 7 of the 19 patients (36.8 %) and a shunt procedure was required in only 1 of these 7 patients (5.3 %) As mentioned by Rahme et al. [17], we also hypothesize that the explanation for the discrepancies between our study and the previous studies might lie in the definition of hydrocephalus and the indications for shunting. As most authors, including ourselves, defined hydrocephalus after DC based only on radiological findings, we failed to clarify whether the ventriculomegaly was attributable to hydrocephalus or cerebral atrophy because of the patients' baseline neurological state.

Therefore, we believe that further studies should be performed to resolve the questions regarding the incidence of hydrocephalus after DC for infarction. CSF dynamic studies may be helpful in differentiating ventriculomegaly due to cerebral atrophy from hydrocephalus [12].

Conflict of Interest We declare that we have no conflict of interest.

References

1. Aarabi B, Hesdorffer DC, Ahn ES, Aresco C, Scalea TM, Eisenberg HM (2006) Outcome following decompressive craniectomy for malignant swelling due to severe head injury. J Neurosurg 104:469–479
2. Akins PT, Guppy KH (2008) Sinking skin flaps, paradoxical herniation, and external brain tamponade: a review of decompressive craniectomy management. Neurocrit Care 9:269–276
3. Ban SP, Son YJ, Yang HJ, Chung YS, Lee SH, Han DH (2010) Analysis of complications following decompressive craniectomy for traumatic brain injury. J Korean Neurosurg Soc 48:244–250
4. Beauchamp KM, Kashuk J, Moore EE, Bolles G, Rabb C, Seinfeld J, Szentirmai O, Sauaia A (2010) Cranioplasty after postinjury decompressive craniectomy: is timing of the essence? J Trauma 69:270–274
5. D'Ambrosio AL, Sughrue ME, Yorgason JG, Mocco JD, Kreiter KT, Mayer SA, McKhann GM 2nd, Connolly ES Jr (2005) Decompressive hemicraniectomy for poor-grade aneurysmal subarachnoid hemorrhage patients with associated intracerebral hemorrhage: clinical outcome and quality of life assessment. Neurosurgery 56:12–19
6. Danish SF, Barone D, Lega BC, Stein SC (2009) Quality of life after hemicraniectomy for traumatic brain injury in adults. A review of the literature. Neurosurg Focus 26:E2
7. De Bonis P, Pompucci A, Mangiola A, Rigante L, Anile C (2010) Post-traumatic hydrocephalus after decompressive craniectomy: an underestimated risk factor. J Neurotrauma 27:1965–1970
8. Güresir E, Raabe A, Setzer M, Vatter H, Gerlach R, Seifert V, Beck J (2009) Decompressive hemicraniectomy in subarachnoid haemorrhage: the influence of infarction, haemorrhage and brain swelling. J Neurol Neurosurg Psychiatry 80:799–801
9. Hofmeijer J, Kappelle LJ, Algra A, Amelink GJ, van Gijn J, van der Worp HB, HAMLET investigators (2009) Surgical decompression for space-occupying cerebral infarction (the Hemicraniectomy After Middle Cerebral Artery infarction with Life-threatening Edema Trial [HAMLET]): a multicentre, open, randomised trial. Lancet Neurol 8:326–333
10. Jüttler E, Schwab S, Schmiedek P, Unterberg A, Hennerici M, Woitzik J, Witte S, Jenetzky E, Hacke W, DESTINY Study Group (2007) Decompressive surgery for the treatment of malignant infarction of the middle cerebral artery (DESTINY): a randomized, controlled trial. Stroke 38:2518–2525
11. Kim KT, Park JK, Kang SG, Cho KS, Yoo DS, Jang DK, Huh PW, Kim DS (2009) Comparison of the effect of decompressive craniectomy on different neurosurgical diseases. Acta Neurochir (Wien) 151:21–30
12. Marmarou A, Foda MA, Bandoh K, Yoshihara M, Yamamoto T, Tsuji O, Zasler N, Ward JD, Young HF (1996) Posttraumatic ventriculomegaly: hydrocephalus or atrophy? A new approach for diagnosis using CSF dynamics. J Neurosurg 85:1026–1035
13. Morgalla MH, Will BE, Roser F, Tatagiba M (2008) Do long-term results justify decompressive craniectomy after severe traumatic brain injury? J Neurosurg 109:685–690
14. Münch E, Horn P, Schürer L, Piepgras A, Paul T, Schmiedek P (2000) Management of severe traumatic brain injury by decompressive craniectomy. Neurosurgery 47:315–322
15. Olivecrona M, Rodling-Wahlström M, Naredi S, Koskinen LO (2007) Effective ICP reduction by decompressive craniectomy in patients with severe traumatic brain injury treated by an ICP-targeted therapy. J Neurotrauma 24:927–935
16. Otani N, Takasato Y, Masaoka H, Hayakawa T, Yoshino Y, Yatsushige H, Miyawaki H, Sumiyoshi K, Chikashi A, Takeuchi S, Suzuki G (2008) Surgical outcome following decompressive craniectomy for poor-grade aneurysmal subarachnoid hemorrhage in patients with associated massive intracerebral or Sylvian hematomas. Cerebrovasc Dis 26:612–617
17. Rahme R, Weil AG, Sabbagh M, Moumdjian R, Bouthillier A, Bojanowski MW (2010) Decompressive craniectomy is not an independent risk factor for communicating hydrocephalus in patients with increased intracranial pressure. Neurosurgery 67:675–678
18. Schirmer CM, Hoit DA, Malek AM (2007) Decompressive hemicraniectomy for the treatment of intractable intracranial hypertension after aneurysmal subarachnoid hemorrhage. Stroke 38:987–992
19. Vahedi K, Vicaut E, Mateo J, Kurtz A, Orabi M, Guichard JP, Boutron C, Couvreur G, Rouanet F, Touzé E, Guillon B, Carpentier A, Yelnik A, George B, Payen D, Bousser MG, Investigators DECIMAL (2007) Sequential-design, multicenter, randomized, controlled trial of early decompressive craniectomy in malignant middle cerebral artery infarction (DECIMAL Trial). Stroke 38:2506–2517
20. Vahedi K, Hofmeijer J, Juettler E, Vicaut E, George B, Algra A, Amelink GJ, Schmiedeck P, Schwab S, Rothwell PM, Bousser MG, van der Worp HB, Hacke W, DECIMAL, DESTINY, and HAMLET investigators (2007) Early decompressive surgery in malignant infarction of the middle cerebral artery: a pooled analysis of three randomised controlled trials. Lancet Neurol 6:215–222
21. Waziri A, Fusco D, Mayer SA, McKhann GM 2nd, Connolly ES Jr (2007) Postoperative hydrocephalus in patients undergoing decompressive hemicraniectomy for ischemic or hemorrhagic stroke. Neurosurgery 61:489–493
22. Yang XF, Wen L, Shen F, Li G, Lou R, Liu WG, Zhan RY (2008) Surgical complications secondary to decompressive craniectomy in patients with a head injury: a series of 108 consecutive cases. Acta Neurochir 150:1241–1247

Treatment of Mild Traumatic Brain Injury by Epidural Saline and Oxygen Injection: Report of Two Cases

Kiyoshi Takagi, Kazuyoshi Kato, and Yoko Kato

Abstract Mild traumatic brain injury (mTBI) is a common complication of minor head injury and a serious problem in the Iraq war returnees. Effective treatment is not yet available. We have treated 23 patients with chronic post-traumatic headache by epidural saline and oxygen injection (ESOI) with efficacy of 96 %. Among them, ten cases were cured. Two out of these cured cases fulfilled the criteria of mTBI and their improvement were objectively demonstrated by a TriIRIS C9000 (Hamamatsu Photonics K.K.) that can monitor the accommodation and convergence function simultaneously. We show the treatment protocol of ESOI and the clinical courses of the two cases in this paper. Both had symptoms somewhat similar to those of spontaneous intracranial hypotension. However, their intracranial pressure was not low and their symptoms were relieved immediately after removal of cerebrospinal fluid (CSF). Although symptoms of mTBI are believed to be attributed to brain damage, some symptoms may not be derived from brain damage itself, but from CSF circulation abnormalities. This is the first report of successfully treated mTBI by ESOI. The effectiveness of the treatment can be verified objectively by monitoring eye function. The outcome suggests that war returnees with mTBI can be treated successfully by ESOI.

K. Takagi (✉)
Department of Neurosurgery, Chiba-Kashiwa Tanaka Hospital, 110 Wakashiba, Kashiwa, Chiba 277-0871, Japan

Department of Neurosurgery, Fujita Health University, Toyoake, Aichi, Japan
e-mail: ktakagi-nsu@umin.ac.jp

K. Kato
Department of Surgery, Kitatama Hospital, Choufu, Tokyo, Japan

Y. Kato
Department of Neurosurgery, Fujita Health University, Toyoake, Aichi, Japan

Keywords Mild traumatic brain injury • mTBI • Chronic post-traumatic headache • CPTH • Treatment • Epidural saline and oxygen injection • Accommodation • Convergence • Intracranial pressure • Cerebrospinal fluid

Introduction

The terms mild traumatic brain injury (mTBI) and chronic post-traumatic headache (CPTH) are used interchangeably [16]. They are common complications of minor head injuries [15] and recently mTBI has been a serious problem in Iraq war returnees [7]. However, effective treatments are not yet available [15, 16]. We have reported that epidural blood patching (EBP) is effective for CPTH, but the effectiveness is limited [22]. In that study, we have found that the chronic headache after minor head and neck injury was orthostatic and sensitive to low atmospheric pressure [22]. Although the symptoms were somewhat similar to those of spontaneous intracranial hypotension (SIH) [20], intracranial pressure (ICP) was normal and brain MRI was negative [22].

Before the era of CT and MRI, pneumoencephalography (PEG) [3] and air epidurography [24] were performed and they were used as a treatment for CPTH [17, 19] or lumbago [12]. We have applied therapeutic PEG to treat CPTH. Although therapeutic PEG is effective, it is accompanied by severe headache until the intracranial air is absorbed (unpublished data). To avoid the severe headache associated with PEG, we developed epidural air injection (EAI), epidural saline and air injection (ESAI), epidural oxygen injection (EOI), and epidural saline and oxygen injection (ESOI) by modifying air epidurography for the treatment of CPTH.

Because patients with CPTH usually complain of eye symptoms such as photophobia and blurred vision [16, 21–23], we monitored accommodation and convergence function simultaneously by means of a TriIRIS C9000

Y. Katayama et al. (eds.), *Brain Edema XV*, Acta Neurochirurgica Supplement, Vol. 118,
DOI 10.1007/978-3-7091-1434-6_57,

instrument (Hamamatsu Photonics, Hamamatsu, Japan) [1] in some of the patients with eye symptoms.

Based upon previous studies [6, 22, 23], we selected the patients with CPTH for epidural injection therapy (EBP, EAI, ESAI, EOI, and ESOI) when they fulfilled all of the following conditions (diagnostic criteria of CPTH for the epidural injection therapy):

1. Headache must be associated with other symptoms such as dizziness, blurred vision, and concentration problems.
2. Headache and other symptoms develop within 7 days of the injury.
3. Headache and other symptoms persist over 3 months after the onset.
4. Headache and other symptoms worsen by staying in upright position and are relieved by lying down.
5. Headache and other symptoms worsen with low atmospheric pressure.
6. The patient has experienced long lasting disability in daily life because of the symptoms.
7. The patient has not experienced such severe annoying symptoms before the injury.
8. The patient has no definite neurological deficits such as motor palsy.
9. Neuroimaging studies do not show any abnormalities compatible with the symptoms.
10. The patient has already received several treatments other than EBP.
11. Although the symptoms resemble those of SIH, the ICP is not low.

Since October 2009, 23 consecutive cases with CPTH have been treated by ESOI under the approval of our IRB. ESOI was effective in 22 patients (96 %) and 10 patients (43 %) were cured almost completely (unpublished data). Among the ten cured patients, two fulfilled the diagnostic criteria for mTBI published by the American Congress of Rehabilitation Medicine [23]. Therefore, the purpose of this paper is to demonstrate the therapeutic protocol for CPTH by ESOI and to report the clinical courses of these two successfully treated patients.

Therapeutic Protocol for CPTH by ESOI

Lumbar puncture is performed to measure the ICP and to examine the cerebrospinal fluid. When the ICP is low (≤60 mmH_2O), the patient is diagnosed with SIH [6] and excluded as a candidate for ESOI. When the ICP is over 60 mmH_2O, the patient maintains bed rest after lumbar puncture for 1–7 days with DIV (1,500–2,000 mL of fluid). ESOI is performed in a sitting position. A lumbar puncture needle is inserted into the epidural space. The position of the needle's tip in the epidural space is confirmed by the loss of resistance method [25]. Saline (10–40 mL) and filtered oxygen (20–100 mL) are injected slowly into the epidural space. We set the limit of total injection volume at 120 mL. The injection is stopped if the patient complains of pain or discomfort. After ESOI, the patient maintains bed rest for 1 week with DIV (1,500–2,000 mL of fluid). After discharge, the patient is asked to rest at home for 1 month. Three months after ESOI, the effect of the ESOI is evaluated. In some patients, accommodation and convergence functions are monitored by TriIRIS C9000 before and 3 months after ESOI.

Report of Two Cases

The first case was a 32-year-old woman. Her complaints were headache, shoulder stiffness, dizziness, blurred vision, photophobia, fatigability, and loss of taste. She had been in a traffic accident 2.5 years earlier. She had an initial short period of loss of consciousness. Her symptoms developed shortly after the accident and were worsened by staying in an upright position and by low atmospheric pressure. Although she consulted several doctors, no definite abnormalities were found. She resigned her job as a nurse because she could not sit or stand for a long time. Two and a half years after the onset of her symptoms, she consulted us.

Her general condition was good, but she looked tired. She had no definite focal neurological deficits such as limb palsy except that she complained of taste loss. Her brain MRI was normal. She fulfilled the criteria of CPTH for ESOI and she accepted the treatment.

Following the protocol, lumbar puncture was performed. The ICP was 150 mmH_2O and 15 mL of watery clear CSF was removed. Immediately after CSF removal, she felt better. She stated that her shoulder stiffness was relieved and her vision became clear and bright. Four days after the lumbar tap, ESOI was performed (40 mL of saline and 60 mL of oxygen). Shortly after ESOI, her headache disappeared and she regained taste. Three months after the treatment, she was symptom free and completely cured.

Before the treatment, TriIRIS C9000 demonstrated that her convergence was disturbed although the pupils were constricted by near vision. Three months after the treatment, her accommodation and convergence were normal supporting her statement that she had no visual disturbances. Complete cure was achieved by only one ESOI.

The second case was a 36-year-old man. His complaints were headache, lumbago, dizziness, blurred vision, photophobia, fatigability, and loss of concentration. He was a professional boxer until the age of19 years when he was knocked out. He lost consciousness for a short period of time.

Although he had no neurological deficits, he resigned boxing because headache and blurred vision developed shortly after the accident and persisted for a long time. Later, new symptoms such as lumbago were added. His symptoms were worsened by staying in an upright position and by low atmospheric pressure. Although he was a company owner, he was not able to go his office sometimes because of these symptoms. He consulted several doctors but no definite abnormalities were found. Seventy years after the onset of his symptoms, he consulted us.

His general condition was good, but he looked tired. He had no definite focal neurological deficits. His brain was slightly atrophic on MRI, which showed no definite abnormalities compatible with his symptoms. He fulfilled the criteria of CPTH for ESOI and he accepted the treatment.

Following the protocol, lumbar puncture was performed. The ICP was 238 mmH_2O and 10 mL of watery clear CSF was removed. Immediately after CSF removal, he felt better. He stated that his mind became sharp and his vision clear. One day after the lumbar tap, ESOI was performed (20 mL of saline and 30 mL of oxygen). Shortly after ESOI, his headache and lumbago disappeared. Three months after the treatment, he was symptom free and worked normally.

Before the treatment, TriIRIS C9000 demonstrated that his accommodation and convergence functions were disturbed. Three months after the treatment, his accommodation and convergence functions were normal, supporting his statement that he had no visual disturbances.

Conclusion

We have reported two patients with mTBI successfully treated by epidural saline and oxygen injection (ESOI), a newly developed therapeutic modality based upon diagnostic air epidurography. This treatment is safe and almost pain-free compared with therapeutic PEG.

Mild traumatic brain injury or CPTH is an old disease. The earliest medical description of this condition can be traced back to at least the late seventeenth century [4]. The incidence increased with the development of steam locomotives [5] and motor vehicles [18]. Although mTBI or CPTH are common complications of minor head injuries [15, 16] and recently mTBI has been a serious problem in Iraq war returnees [7], effective treatments have not been available until now [15, 16]. However, CPTH was once treated successfully by PEG [2, 17, 19]. With the development of CT [9] and MRI [8], PEG has been abandoned and the treatment method for CPTH or mTBI has been lost.

Recently, several studies indicated that chronic headache with many other symptoms such as photophobia and dizziness after a motor vehicle accident resembled that of SIH [13, 20] and was related to CSF leakage and EBP was effective treatment [10, 14]. They reported that EBP was an effective treatment [10, 14]. However, they did not show the intracranial pressure [10, 14]. We have also reported that EBP was effective for CPTH after head and neck injury, but the effectiveness is limited [22]. Although the symptoms were somewhat similar to those of spontaneous intracranial hypotension (SIH) [20], intracranial pressure (ICP) was normal and brain MRI was negative [22]. Therefore, we speculated that CSF leakage into the epidural space might not occur, but that spinal CSF absorption might be over-activated in the patients with CPTH after head and neck injury [22]. The International Headache Society has published the definition of CPTH, which describes the headache as having no typical characteristics [6]. Recent studies indicate that some parts of CPTH are of orthostatic nature and can be relieved or cured by EBP [10, 14].

Although the symptoms of mTBI are believed to be attributed to brain damage and some abnormalities have been demonstrated in white matter by MRI [11], the lesion was not detected in all the patients and the correlation of the lesion and the symptoms was not clear. The improvement in the symptoms occurred shortly after CSF removal and ESOI in the two cases reported in this paper. These observations indicate that at least some part of the symptoms of mTBI might not be attributed to brain damage, but instead to some kind of CSF circulation abnormalities. When blood, gas, and/or saline are injected into the epidural space, epidural pressure goes up temporarily. This rise in epidural pressure may suppress the over-activated spinal CSF absorption. We have proposed hypothetical mechanisms to cause abnormalities of CSF flow by whiplash injury [22].

The underlying mechanisms of ESOI are still unclear. However, the treatment result of these two cases is promising in the treatment of war returnees and victims of traffic accidents with mTBI. Epidural saline and oxygen injection may be a new and safe treatment modality for the long lasting symptoms of mTBI. The effectiveness can be verified objectively by monitoring eye function.

Conflict of Interest We declare that we have no conflict of interest.

References

1. Asakawa K, Ishikawa H, Shoji N (2009) New methods for the assessment of accommodative convergence. J Pediatr Ophthalmol Strabismus 46:273–277
2. Boyd D (1929) Post-traumatic headache treated by spinal insufflation of air. Arch Surg 18:1626–1636
3. Dandy WE (1919) Roentgenography of the brain after injection of air into the spinal canal. Ann Surg 70:397–403
4. De Morsier G (1943) Les Encephalopathies traumatiques. Etude neurologique. Schweiz Arch Neurol Neurochir Psychiatr 50:161

5. Erichsen JE (1866) On concussion of the spine from slight injury. On railway and other injuries of the nervous system. Walton and Moberly, London, pp 44–63
6. Headache Classification Subcommittee of the International Headache Society (2004) The international classification of headache disorders: 2nd edition. Cephalalgia 24(Suppl 1):9–160
7. Hoge CW, McGurk D, Thomas JL, Cox AL, Engel CC, Castro CA (2008) Mild traumatic brain injury in U.S. soldiers returning from Iraq. N Engl J Med 358:453–463
8. Holland GN, Hawkes RC, Moore WS (1980) Nuclear magnetic resonance (NMR) tomography of the brain: coronal and sagittal sections. J Comput Assist Tomogr 4:429–433
9. Hounsfield GN (1973) Computerized transverse axial scanning (tomography). 1. Description of system. Br J Radiol 46: 1016–1022
10. Ishikawa S, Yokoyama M, Mizobuchi S, Hashimoto H, Moriyama E, Morita K (2007) Epidural blood patch therapy for chronic whiplash-associated disorder. Anesth Analg 105:809–814
11. Mac Donald CL, Johnson AM, Cooper D, Nelson EC, Werner NJ, Shimony JS, Snyder AZ, Raichle ME, Witherow JR, Fang R, Flaherty SF, Brody DL (2011) Detection of blast-related traumatic brain injury in U.S. military personnel. N Engl J Med 364:2091–2100
12. Matyas M (1953) Erfolgreiche Behandlung der Kreuzschmerzen durch Luftinjektionen in den Epiduralraum. Zentralbl Gynakol 75:1096–1099
13. Mokri B (1999) Spontaneous cerebrospinal fluid leaks: from intracranial hypotension to cerebrospinal fluid hypovolemia – evolution of a concept. Mayo Clin Proc 74:1113–1123
14. Moriyama E, Ogawa T, Nishida A, Ishikawa S, Beck H (2004) Quantitative analysis of radioisotope cisternography in the diagnosis of intracranial hypotension. J Neurosurg 101:421–426
15. Nampiaparampil DE (2008) Prevalence of chronic pain after traumatic brain injury: a systematic review. JAMA 300:711–719
16. Pardine J, Bailes JE, Maroon JC (2011) Mild traumatic brain injury in adults and concussion in sports. In: Winn HR (ed) Youmans neurological surgery, vol 4. W B Sounders Co., Philadelphia, pp 3380–3389
17. Penfield W (1927) Chronic meningeal headache and its specific treatment by lumbar air insufflation. Surg Gynecol Obstet 45: 747–759
18. Penfield W, Norcross NC (1936) Subdural traction and posttraumatic headache, study of pathology and therapeusis. Arch Neurol Psychiatry 36:75–95
19. Sasabe T, Shindo K, Taneda M, Iwata Y (1968) Considerations on sequels of head injuries and whiplash injuries. Therapeutic oxygen encephalography for a posttraumatic, chronic intracranial hypotension syndrome. No To Shinkei 20:959–963
20. Schievink WI (2006) Spontaneous spinal cerebrospinal fluid leaks and intracranial hypotension. JAMA 295:2286–2296
21. Stovner LJ, Schrader H, Mickeviciene D, Surkiene D, Sand T (2009) Headache after concussion. Eur J Neurol 16:112–120
22. Takagi K, Bolke E, Peiper M, van Griensven M, Orth K, Son JH, Ueno T, Oshima M (2007) Chronic headache after cranio-cervical trauma – hypothetical pathomechanism based upon neuroanatomical considerations. Eur J Med Res 12:249–254
23. The Mild Traumatic Brain Injury Committee of the Head Injury Interdisciplinary Special Interest Group of the American Congress of Rehabilitation Medicine (1993) Definition of mild traumatic brain injury. J Head Trauma Rehabil 8:86–87
24. Weber HM (1941) Epidural air injection: in diagnosis of spinal canal masses. Cal West Med 54:27
25. Williams RA (1975) A syringe for extradural analgesia. Anaesthesia 30:788–790

Blood–Brain Barrier Transport of an Essential Amino Acid After Cerebral Ischemia Reperfusion Injury

Toyofumi Suzuki, Yumiko Miyazaki, Aya Ohmuro, Masaki Watanabe, Takayuki Furuishi, Toshiro Fukami, and Kazuo Tomono

Abstract Under pathophysiological conditions such as cerebral ischemia–reperfusion (IR), damage to cerebrovascular endothelial cells causes alterations in the blood–brain barrier (BBB) function that can exacerbate neuronal cell injury and death. Clarifying changes in BBB transport in the early period of IR is important for understanding BBB function during therapy after cerebral ischemia. The present study was aimed at clarifying changes during IR in the BBB transport of L-phenylalanine (Phe) as a substrate of L-type amino acid transporter 1. An IR model was produced in mice by blood recirculation following occlusion of the middle cerebral artery. Permeability of the BBB to [^{3}H]Phe was measured after IR injury using the brain perfusion method. Confocal microscopy of the IR injury showed no brain penetration of fluorescent tracer, thus confirming BBB integrity during 45 min of ischemia. Tight junction opening was not observed at 30 min after reperfusion following ischemia for 45 min. At the time of IR, [^{3}H]Phe uptake into the brain appeared saturated. The Michaelis constant and maximum transport velocity in the IR group was reduced by 22 % compared with those in controls. These results suggest that the intrinsic transport clearance of Phe is slightly decreased in the early phase of IR.

Keywords Blood-brain barrier • Cerebral ischemia-reperfusion • L-phenylalanine • Middle cerebral artery occlusion • Sodium fluorescein • Evans blue albumin

T. Suzuki, Ph.D. (✉), Y. Miyazaki, A. Ohmuro,
M. Watanabe, T. Fukami, Ph.D., and K. Tomono, Ph.D.
Laboratory of Pharmaceutics, Department of Applied Pharmacy,
Nihon University School of Pharmacy,
7-7-1 Narashinodai, Funabashi,
Chiba 274-8555, Japan
e-mail: suzuki.toyofumi@nihon-u.ac.jp

T. Furuishi, Ph.D.
Department of Physical Chemistry, Hoshi University,
2-4-41 Ebara, Shinagawa 142-8501, Tokyo, Japan

Introduction

Brain tissue is highly susceptible to the effects of ischemia. Subjected to short-term ischemia, the brain rapidly suffers functional damage due to energy depletion. Without the recirculation of cerebral blood flow, irreversible brain damage and ultimately cerebral infarcts result [4]. Even with the recirculation of blood flow following ischemia, the increased production of reactive oxygen species and free radicals that can occur depending on the duration of reperfusion inhibits the repair mechanism of cerebral endothelial cells, advancing cellular injury [4]. This phenomenon is clinically known as stroke–reperfusion injury.

Cerebral endothelial cells are characterized by the formation of tight junctions and the presence of several transport mechanisms, which together comprise the blood–brain barrier (BBB) [12]. Damage to cerebrovascular endothelial cells following cerebral ischemia-reperfusion (IR) causes alterations in BBB function that can exacerbate neuronal cell injury and death. Clarifying changes in BBB transport in the early period following IR is important for understanding BBB function during therapy after cerebral ischemia.

The blood-to-brain influx transporters supply hydrophilic nutrients and other essential molecules such as glucose and amino acids to the brain. Among the amino acid transporter systems, system L is an important factor that provides the cells with large, neutral, branched or aromatic amino acids, including several essential amino acids [5]. System L consists of L-type amino acid transporter 1 (LAT1/SLC7A6) and the heavy chain of the 4 F2 cell-surface antigen (4F2hc). LAT1 is selectively expressed in the brain, specifically in the luminal and abluminal membranes of the BBB in many species [2, 5, 8]. L-phenylalanine (Phe) as a substrate for protein synthesis in the brain is transported from the blood to the brain via a Na^+-independent pathway involving LAT1 at the BBB. Also, several amino acid-mimetic drugs such as L-Dopa, the alkylating agent melphalan (phenylalanine mustard), the antiepileptic drug gabapentin, and the muscle

Y. Katayama et al. (eds.), *Brain Edema XV*, Acta Neurochirurgica Supplement, Vol. 118,
DOI 10.1007/978-3-7091-1434-6_58,

relaxant baclofen are transported across the BBB by system L [1, 6, 8]. Therefore, system L is potentially important for drug delivery to the brain.

The present study aimed to clarify changes during IR in the BBB transport of L-phenylalanine (Phe) as a substrate of LAT1. Specifically, BBB integrity on tight junction opening after ischemia using fluorescent tracers and changes in the LAT1-mediated transport of Phe at the BBB without BBB disruption during I/R were evaluated.

Materials and Methods

Animals and Reversible Focal Cerebral Ischemia

All procedures involving animals were approved by the Nihon University Animal Care and Use Committee (Nihon University, Japan). Adult male ddY mice (20–22 g) were anesthetized by intraperitoneal (*i.p.*) injection of chloral hydrate (300 mg/kg). Rectal temperature was maintained at 37 ± 0.5 °C with a feedback-regulated heating pad during the procedure. Focal cerebral ischemia was induced with the suture occlusion technique as previously described [7].

Measurement of Blood–Brain Barrier Permeability

The *in situ* mouse brain perfusion was performed by the method reported previously [11]. After blood recirculation following ischemia and under re-anesthetization, the left common carotid artery was catheterized. Using an infusion pump, mice were perfused at a constant rate of 1 mL/min with a series of perfusion fluid compositions (described below).

Extravasation of Fluorescent Tracers Following Focal Cerebral Ischemia

Blood–brain barrier permeability following focal cerebral ischemia was evaluated by extravasation of two exogenous fluorescent tracers. A perfusion fluid was prepared consisting of a mixture of 0.1 % sodium fluorescein (SF), 0.1 % Evans blue-tagged albumin (EBA), and 1.8 % bovine serum albumin in Krebs–Henseleit buffer (KHB). To ensure sufficient and reproducible accumulation of tracers in the brain tissue, initially KHB without the tracers was perfused to the injured area for 3 min after withdrawal of the suture. For a positive control, KHB with oxygenated 1.6 M mannitol (Man) was perfused to the targeted area in the sham-operated mice instead of KHB alone. Next, perfusion was switched continuously to the tracers for 1 min using another syringe pump. Finally, the tracers remaining in the brain vessels were removed by perfusion of KHB for 5 min. The brain was then immediately removed, and a left coronal section (4 mm thick) in the infarct area was dissected from the perfused cerebral hemisphere and weighed. The brain section was mechanically homogenized in 1 mL of 50 % (w/v) trichloroacetic acid, and centrifuged at 10,000 G for 10 min. The resulting supernatant was divided into two aliquots. For determination of SF, one aliquot was neutralized with 5 M NaOH (1:0.8) and its fluorescence intensity measured (excitation at 440 nm and emission at 525 nm) with a spectrofluorometer. For determination of EB, the second aliquot was diluted with ethanol (1:4), and its fluorescence determined (excitation at 620 nm and emission at 680 nm).

To visualize localized changes in BBB permeability, fluorescence imaging of microvessels damaged in the infarct area was achieved using confocal microscopy. Instead of SF/EBA tracers, KHB with FITC-gelatin was perfused to the targeted area for 5 min without the prior washout rinse with KHB. A 300-μm thick coronal section was mounted onto slides for visualization on a Zeiss 510 laser scanning confocal microscope with an oil objective (×10).

Effect of Reperfusion Time Following Ischemia on BBB Integrity

To investigate BBB integrity during reperfusion following ischemia for 45 min, the brain intravascular volume in the left hemisphere coronal section (4 mm thick) in the infarct area was estimated from its distribution volume over 1 min using [^{14}C]sucrose. Perfusion fluid flow through this area using [^{3}H]diazepam was calculated based on brain uptake from the perfusion fluid [13].

BBB Transport of Phe Following Ischemic–Reperfusion

To investigate [^{3}H]Phe transport across the BBB, a perfusion fluid containing a tracer concentration of [^{3}H]Phe (0.5 μCi/mL, 4.5 nM) and [^{14}C]sucrose in KHB was used. The perfusion was continued for 1 min. The radioactivity in the perfusion solution and the left coronal section in the infarct area sample were determined according to the method described previously [13].

Data Analysis

The permeability–surface area product (PS_{inf}) value (mL/min/g brain), which represents *in vivo* BBB permeability,

was calculated as described previously [13]. The uptake rate (J; nmol/min/g brain) is given by the following equation: $J = PS_{inf} \times C_{tot}$, where C_{tot} is the total concentration of Phe in the perfusion fluid. Statistical analyses were carried out using unpaired Student's t- test and one-way ANOVA.

Results

Extravasation of Fluorescent Tracers Following Focal Cerebral Ischemia

Sodium fluorescein and EBA permeation into the injured brain following ischemia were comparable with permeation in the control for ischemia lasting up to 45 min (Fig. 1a). In contrast, following 60 min of ischemia, SF permeation increased by approximately four-fold and EBA extravasation increased two-fold. The tight junction opening effect of Man was measured to evaluate the effects of ischemia on SF and EBA permeation into the injured brain. Following the perfusion of Man, SF increased by approximately 13-fold, whereas EBA extravasation increased by approximately four-fold. In agreement with the quantitative permeability, fluorescent tracers remained in blood vessels as in the control following ischemia of up to 45 min (Fig. 1b). In contrast, fluorescent tracer extravasation was observed following 60 min of ischemia. The extravasation observed following the perfusion of Man was more pronounced than that seen after 60 min of ischemia.

Effect of Reperfusion on the Intravascular Volume Space in the Brain Following Ischemia

After 45 min of ischemia, the cerebral intravascular volume of [^{14}C]sucrose following reperfusion of up to 120 min was not significantly different from the control (data not shown). Cerebral intravascular volume, however, was approximately six-fold greater than that in the control after 240 min of reperfusion. On the other hand, the perfusion fluid flow measured using [^{3}H]diazepam was not significantly different from that of the control over the reperfusion time range of 30–240 min.

BBB Transport of Phe After IR

[^{3}H]Phe permeability in the sham-operated mice was higher than that in the IR-treated mice, which underwent 45 min of ischemia followed by 30 min of reperfusion (Fig. 2). BBB permeability to [^{3}H]Phe was kinetically analyzed as a function of the total Phe concentration in the perfusion fluid. The initial brain uptake rate of [^{3}H]Phe (J; nmol/min/g brain) was fitted to a Michaelis–Menten equation. These plots in the sham-operated mice and the IR-treated mice were saturable in a concentration-dependent manner. Each Eadie–Hofstee plot gave a single straight line (Fig. 2, inset). The calculated kinetic parameters (mean ± SE) for the sham-operated mice and the IR-treated mice were the maximum transport velocity (J_{max}) = 8.1 ± 1.0 and 7.2 ± 0.9 nmol/min/g brain, and the Michaelis constant (K_m) = 11.2 ± 2.2 and 12.7 ± 2.4 μM respectively.

Conclusion

In the present study, we demonstrated that the promotion of the transport of small water-soluble molecules, i.e., the opening of tight junctions in the BBB, does not occur during a relatively short ischemia of 45 min. In addition, intravascular volume in the injured brain is maintained during reperfusion for up to 120 min after ischemia of 45 min, which means that leakage of small water-soluble molecules through the BBB does not occur. Koyama et al. reported the vascular permeability of fluorescent tracers in cerebral edema caused by radiofrequency damage [9]. The two-fold increase in SF permeation relative to EB permeation in the sites of damage in the cerebral hemispheres with 60 min of ischemia when SF and EB were injected into the tail veins of rats coincides with our findings.

Man is apparently able to temporarily open the tight junctions of the BBB. Therefore, the increase in brain permeation of SF (MW: 376; 5 Å diameter) with 60 min of ischemia, which was similar to the result with Man, strongly suggests transport via an intercellular route. Although the large molecular weight of EBA (MW: 69,000; 78 Å diameter) normally prevents its passage through the intercellular route, even EBA extravasation in the brain was somewhat increased. This finding suggests that EB not bound to albumin in the perfusion fluid may have permeated into the brain by passing through intercellular tight junctions opened by Man perfusion. Osmotic pressure shock may have also promoted endocytosis for transporting large molecules. The degree of localized BBB breakdown agrees well with the fluorescent tracer quantitative values. These findings indicate that, following ischemia of up to only 45 min, the intercellular route for transport of small water-soluble molecules due to the opening of tight junctions in the BBB does not occur, and the physical barrier function of tight junctions between cells is maintained.

The inhibition of cellular repair and enhanced endothelial cell damage caused by the increased production of reactive oxygen species and free radicals following the resumption of

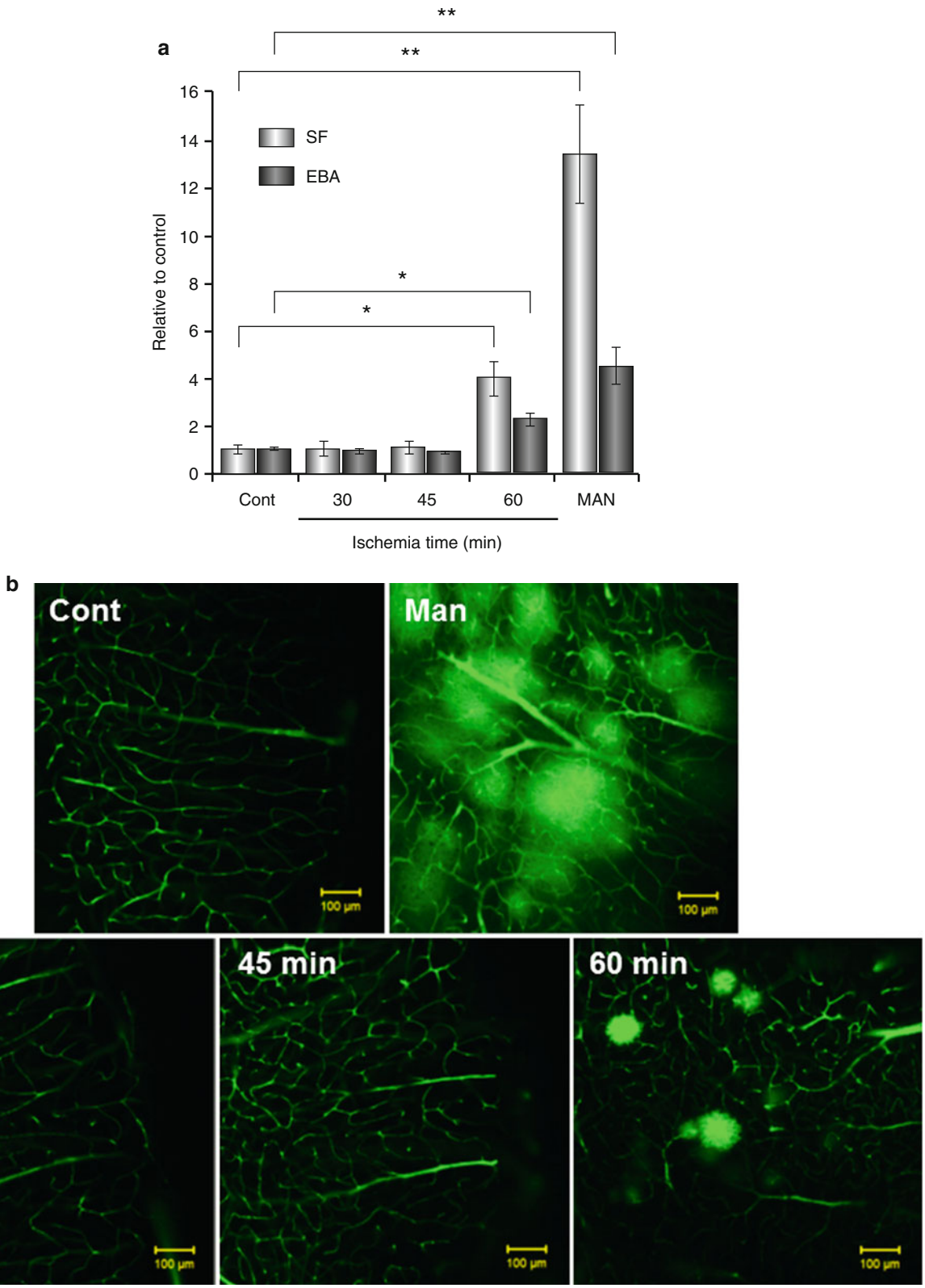

Fig. 1 (**a**) Extravasation of sodium fluorescein (SF) and Evans blue-tagged albumin (EBA) on the ischemic region after different periods of transient MCA occlusion in mouse brains. Each column represents the mean ± SEM ($n = 4$). *$P < 0.05$, **$P < 0.01$, significantly different from the control. (**b**) Fluorescence imaging of cerebral microvascular damage on slices of the ischemic region by confocal microscopy. Scale bar = 100 μm

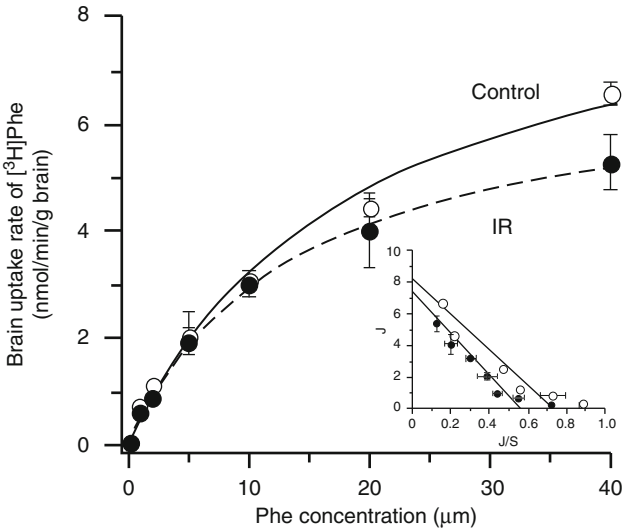

Fig. 2 Concentration dependence of [^{3}H]Phe uptake by the brain and Eadie–Hofstee plot of saturable transport (*inset*) after blood recirculation for 30 min following transient MCA occlusion for 45 min. Each point represents the mean ± SEM (n = 3–5)

blood flow in the ischemic brain is one type of reperfusion injury. [^{14}C]sucrose, like SF, is a small water-soluble molecule that normally does not pass through the BBB. Therefore, we investigated the effects of reperfusion on the opening of tight junctions in the BBB following ischemia using the intravascular volume marker [^{14}C]sucrose. Our findings suggest that BBB damage over this interval is minimal and that BBB integrity is maintained during reperfusion of up to 120 min after ischemia of 45 min. Brown et al. hypothesized that increased levels of intracellular Ca^{2+} following cerebral ischemia modify proteins that make up tight junctions and thereby modify BBB function [3]. The present finding suggests that following relatively short ischemia of 45 min, the production of reactive oxygen species and angiogenic factors and the increase in intracellular Ca^{2+} concentrations are minimized with reperfusion of up to 120 min.

From the above results it can be concluded that, under the conditions described, small water-soluble molecules do not undergo extravasation, and structural damage to vascular endothelial cells does not progress. Therefore, during this period in which tight junctions in the BBB are not found to be open, we have been able to demonstrate in vivo the effects of IR on the BBB transport of Phe. With 45 min of ischemia followed by 30 min of reperfusion, Phe transport involved a LAT1-mediated transport at the BBB and the intercellular route transport had no contribution. The K_m in the control group was comparable with the value reported by Momma et al., who used a rat model of brain perfusion [10]. The K_m and J_{max} in the IR-treated group were each 22 % lower than in the control group. This result suggests that the intrinsic transport efficiency (J_{max}/K_m) of Phe in early IR is slightly lower in comparison to the control.

In summary, use of two fluorescent tracers of different molecular weights allowed us to quantitatively determine and visualize the increase in intracellular route transport and endocytosis in the BBB following ischemia in a mouse model of IR. The BBB after the early phase of IR with 45 min of ischemia followed by 30 min of reperfusion appears to be minimally permeable not only to amino acids, but also to drugs via carrier-mediated transport, during which the opening of tight junctions does not occur. Future investigation of the impact of IR on BBB uptake of other amino acid substrates of LAT1 and the impact of IR on drug transporters should help researchers identify optimal drug therapies that make use of changes in BBB permeability caused by reperfusion injury.

Acknowledgments This work was supported in part by a Grant-in-Aid for Scientific Research (C) (KAKENHI #22590149) to T.S. from the Ministry of Education, Culture, Sports, Science and Technology (MEXT) of Japan, and a grant from the "High-Tech Research Center" Project for Private Universities: matching fund subsidy from MEXT in 2007–2011 (to T.S and T.F.).

Conflict of Interest We declare that we have no conflict of interest.

References

1. Abbott NJ, Romero IA (1996) Transporting therapeutics across the blood-brain barrier. Mol Med Today 2:106–113
2. Boado RJ, Li JY, Nagaya M, Zhang C, Pardridge WM (1999) Selective expression of the large neutral amino acid transporter at the blood-brain barrier. Proc Natl Acad Sci USA 96:12079–12084
3. Brown RC, Davis TP (2002) Calcium modulation of adherens and tight junction function: a potential mechanism for blood-brain barrier disruption after stroke. Stroke 33:1706–1711
4. Candelario-Jalil E (2009) Injury and repair mechanisms in ischemic stroke: considerations for the development of novel neurotherapeutics. Curr Opin Investig Drugs 10:644–654
5. del Amo EM, Urtti A, Yliperttula M (2008) Pharmacokinetic role of L-type amino acid transporters LAT1 and LAT2. Eur J Pharm Sci 35:161–174
6. Gomes P, Soares-da-Silva P (1999) L-DOPA transport properties in an immortalised cell line of rat capillary cerebral endothelial cells, RBE 4. Brain Res 829:143–150
7. Ikeda-Matsuo Y, Ota A, Fukada T, Uematsu S, Akira S, Sasaki Y (2006) Microsomal prostaglandin E synthase-1 is a critical factor of stroke-reperfusion injury. Proc Natl Acad Sci USA 103: 11790–11795
8. Kageyama T, Nakamura M, Matsuo A, Yamasaki Y, Takakura Y, Hashida M, Kanai Y, Naito M, Tsuruo T, Minato N, Shimohama S (2000) The 4F2hc/LAT1 complex transports L-DOPA across the blood-brain barrier. Brain Res 879:115–121
9. Koyama Y, Matsui S, Itoh S, Osakada M, Baba A, Matsuda T (2004) The selective Na^+-Ca^{2+} exchange inhibitor attenuates brain edema after radiofrequency lesion in rats. Eur J Pharmacol 489: 193–196

10. Momma S, Aoyagi M, Rapoport SI, Smith QR (1987) Phenylalanine transport across the blood-brain barrier as studied with the in situ brain perfusion technique. J Neurochem 48:1291–1300
11. Murakami H, Takanaga H, Matsuo H, Ohtani H, Sawada Y (2000) Comparison of blood-brain barrier permeability in mice and rats using in situ brain perfusion technique. Am J Physiol Heart Circ Physiol 279:H1022–H1028
12. Redzic Z (2011) Molecular biology of the blood-brain and the blood-cerebrospinal fluid barriers: similarities and differences. Fluids Barriers CNS 8:3
13. Suzuki T, Oshimi M, Tomono K, Hanano M, Watanabe J (2002) Investigation of transport mechanism of pentazocine across the blood-brain barrier using the in situ rat brain perfusion technique. J Pharm Sci 91:2346–2353

The Effect of an NK1 Receptor Antagonist on Blood Spinal Cord Barrier Permeability Following Balloon Compression-Induced Spinal Cord Injury

Anna V. Leonard and Robert Vink

Abstract The blood spinal cord barrier (BSCB) is disrupted following spinal cord injury (SCI) resulting in vasogenic edema and increased intrathecal pressure (ITP). The neuropeptide substance P (SP) has been implicated in the development of blood–brain barrier (BBB) disruption, edema, and increased intracranial pressure following brain injury, although it has not been investigated in SCI. The balloon compression model of experimental SCI has many advantages in that it replicates the "closed" environment observed clinically. Accordingly, this study characterized whether this model produces an increase in BSCB permeability and edema, and whether a SP, NK1 tachykinin receptor antagonist, N-acetyl-L-tryptophan (NAT) reduces such BSCB disruption and edema formation. At 30 min post-injury, animals were administered 2.5 mg/kg NAT or saline. Subgroups of animals were assessed for BSCB permeability (Evan's Blue) and spinal cord edema (wet weight/dry weight). BSCB permeability and edema were significantly increased in injured groups compared with sham ($p<0.001$). There was no significant difference between vehicle and NAT treatment. We conclude that the balloon compression model of SCI produces significant BSCB disruption although NAT treatment did not attenuate BSCB permeability or edema. Further studies are required to fully elucidate the role of SP following SCI.

Keywords Spinal cord injury • Blood spinal cord barrier permeability • Edema • Substance P • Neurogenic inflammation

A.V. Leonard and R. Vink (✉)
Adelaide Centre for Neuroscience Research,
Discipline of Anatomy and Pathology,
School of Medical Sciences, University of Adelaide,
Adelaide, SA, Australia
e-mail: robert.vink@adelaide.edu.au

Introduction

Spinal cord injury (SCI) is an unexpected event that often results in permanent physical disability. There is currently no widely accepted treatment for SCI and research into improving neurological function and reducing injury is of increasing importance. Many secondary injury processes occur following severe SCI, contributing to tissue damage [7, 10]. Of particular importance is disruption to the blood spinal cord barrier (BSCB) resulting in the development of vasogenic edema and increased intrathecal pressure [4, 6, 8]. Our laboratory has previously shown that the neuropeptide substance P (SP) plays a critical role in blood–brain barrier (BBB) disruption and associated development of vasogenic edema following traumatic brain injury [3] and stroke [12]. Furthermore, inhibition of SP via its receptor, the NK1 tachykinin receptor, attenuated BBB permeability and reduced edema. The role of SP in BSCB disruption and edema formation after SCI has not been previously investigated.

Clinically, SCI occurs in a "closed" environment, whereas many experimental models of SCI involve a laminectomy creating "open" injuries. Such open injuries remove the potential for increased pressure. As such, it is of profound importance that experimental models closely replicate a closed environment to ensure clinical relevance. The balloon compression model is a promising candidate as it provides a closed environment at the injury center. This study, therefore, sought to characterize whether this balloon compression-induced SCI produces an increase in BSCB permeability and edema development, and whether an NK1 tachykinin receptor antagonist, N-acetyl- L-tryptophan (NAT) could attenuate such BSCB disruption and edema genesis.

Y. Katayama et al. (eds.), *Brain Edema XV*, Acta Neurochirurgica Supplement, Vol. 118,
DOI 10.1007/978-3-7091-1434-6_59, © Springer-Verlag Wien 2013

Materials and Methods

Balloon Compression Model of Spinal Cord Injury

Adult male New Zealand White rabbits (3–3.5 kg) were fed and watered ad libitum for 1 week prior to surgery. Anesthesia was induced with a ketamine (2.5 mg/kg) and Domitor (0.25 mg/kg) injection subcutaneously. After a suitable level of anesthesia was induced, a T12 laminectomy was performed, involving retraction of the paraspinal muscles and removal of the spinous process and laminae. An Apex™ Monorail™ 4 × 8 mm balloon catheter was then inserted into the epidural space and advanced 4.5 cm, before being inflated to a pressure of 8 atm for 5 min, then deflated and removed. The muscles were then sutured closed and the wound closed with wound clips (9-mm autoclip wound clips; Becton Dickinson, Franklin Lakes, NJ, USA). Animal temperature throughout all procedures was maintained at 37 °C using a thermostatically controlled heating pad.

N-Acetyl-L-Tryptophan Treatment

Following injury, animals were intravenously administered either 2.5 mg/kg NAT or an equal volume of saline vehicle. Treatment was administered at 30 min post-injury for the 5 and 24 h groups, plus an additional dose of NAT at 24 and 48 h post-injury for the 3-day survival groups. The dosing regimen was based on our previous studies in traumatic brain injury and stroke [3, 12].

BSCB Permeability: Evan's Blue

The extent of BSCB permeability was determined using the Evan's Blue (EB) extravasation method as previously described [13]. Briefly, at 5 h post-injury, animals ($n = 15$) were perfused intracardially with saline having been administered 6 mg/kg intravenous EB 30 min prior to perfusion. Once the saline perfusate ran clear, the spinal cord was rapidly removed and cut into 1-cm segments and weighed. Each sample was then homogenized in 3.75 mL of phosphate buffered saline (PBS) to which 1.25 mL of 100 % TCS was added. Samples were then cooled on ice for 30 min, centrifuged at 1,000 G for 30 min and the supernatant sampled. Absorbance of the sample was read using a spectrometer at 620 nm. The amount of EB extravasation was expressed as μg/mg of spinal cord tissue.

Edema: Spinal Water Content

The water content of the spinal cord was determined using the wet weight/dry weight (ww/dw) method as previously described [13]. Briefly, at 5 h ($n = 6$), 24 h ($n = 5$), or 3 days ($n = 10$) post-injury, animals were killed by a lethal (2-mL) injection of Lethobarb, and their spinal cords rapidly removed. One-centimeter sections were then dissected and weighed to obtain wet weight. The spinal cord sections were then dried at 100 °C for 48 h and reweighed to obtain the dry weight. The percentage of spinal water content was subsequently calculated using the ww/dw formula: $\%\ \text{water} = (\text{ww} - \text{dw}/\text{ww}) \times 100$.

Immunohistochemistry for Albumin

Albumin is a plasma protein normally contained within the vasculature. When the barrier is disrupted, albumin can pass into the spinal cord tissue indicating BSCB disruption. At 5 h, 24 h, and 3 days following SCI or sham surgery, animals were transcardially perfused with 10 % buffered formalin. Spinal cords were then removed, processed and embedded in paraffin wax. Sections (5 μm) were cut and processed for albumin immunoreactivity (goat polyclonal anti-albumin antibody; Cappel #0113-0341).

Results

BSCB Permeability: EB Extravasation

The degree of EB extravasation in sham animals along the entire length of the spinal cord was 6.93 ± 1.25 μg EB/g spinal cord tissue (Fig. 1). Following SCI, there was a significant increase ($p < 0.001$) in BSCB permeability at the injury epicenter of vehicle -treated animals (15.43 ± 3.04 μg/g). There was no significant difference between the vehicle-treated and NAT-treated animals at any region of the spinal cord following injury.

Edema: Spinal Cord Water Content

Spinal cord water content in sham animals along the entire length of the spinal cord was 65.55 ± 0.48 % (Fig. 2a). Following SCI, there was a significant increase at the injury epicentre at 5 h (69.95 ± 1.74 %, $p < 0.01$) 24 h (71.18 ± 1.31 %, $p < 0.001$) and 3 days (77.47 ± 1.00 %, $p < 0.001$). At 3 days

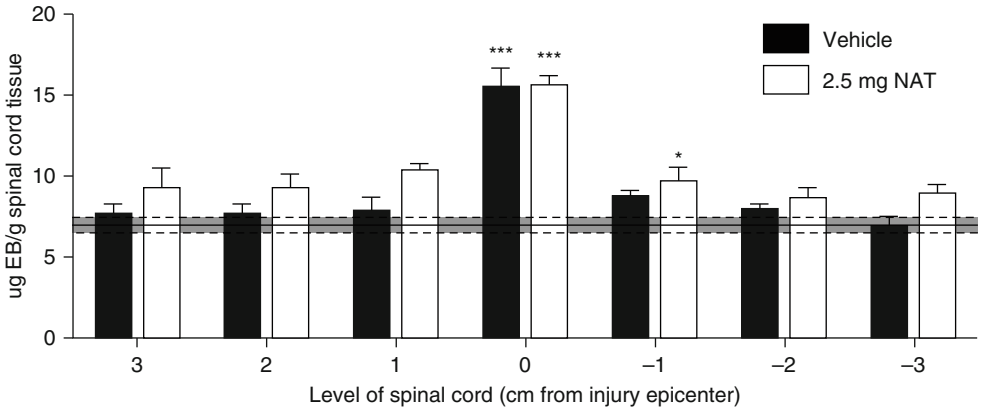

Fig. 1 Blood spinal cord barrier (BSCB) permeability as assessed by Evan's Blue extravasation at 5 h post-injury. *Solid line* represents sham, $n=5$; vehicle, $n=5$; N-acetyl-L-tryptophan (NAT), $n=5$. Results are displayed as mean ± SD. *** denotes $p<0.001$ compared with sham; * denotes $p<0.05$ compared with sham

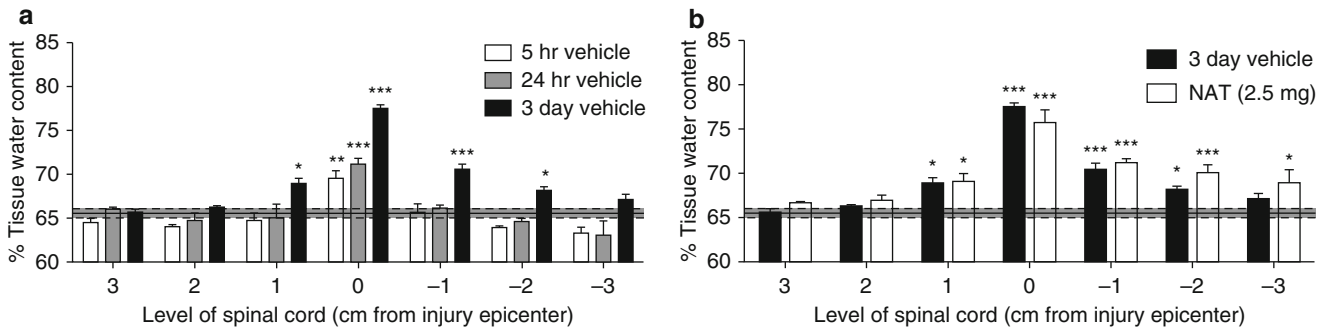

Fig. 2 (**a**) Temporal profile of edema following spinal cord injury (SCI) and (**b**) the effects of NAT treatment on edema measured at 3 days post-injury. Results are displayed as mean ± SD. *** denotes $p<0.001$ compared with sham; ** denotes $p<0.01$ compared with sham; * denotes $p<0.05$ compared with sham. (**a**) *Solid line* represents sham, $n=5$; 5 h, $n=5$; 24 h, $n=4$; 3 days, $n=4$. (**b**) Vehicle, $n=4$; NAT, $n=4$

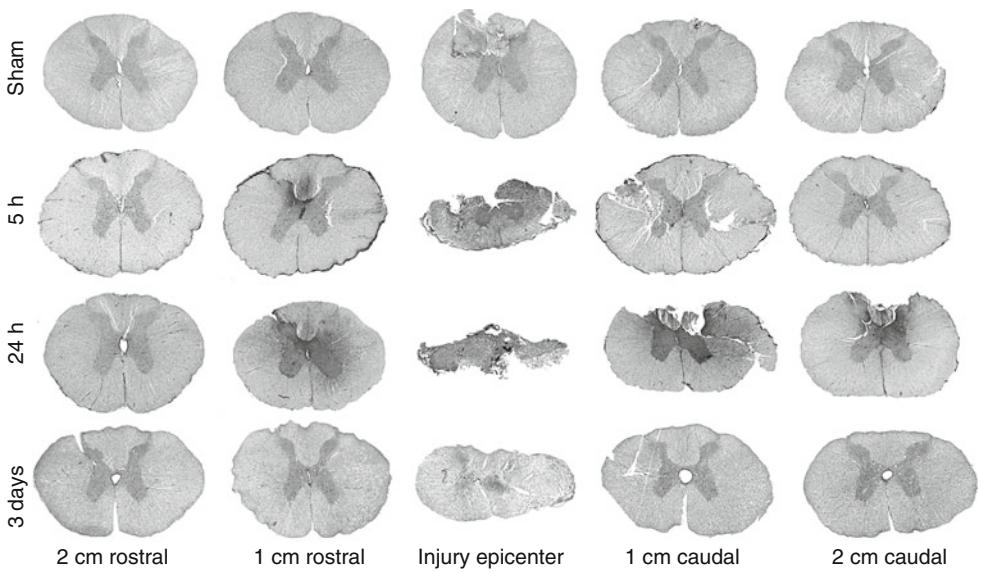

Fig. 3 Albumin immunoreactivity following SCI. Note the increased immunoreactivity at 5 h post-injury in the epicenter. Further immunoreactivity can be seen at 24 h post-injury

post-injury there was a significant increase observed 1 cm rostral (68.82 ± 1.39 %, $p<0.05$) from the injury epicenter and as far as 2 cm caudally (68.08 ± 1.04 %, $p<0.05$). There was no significant difference between the vehicle and NAT-treated animals at any time point or at any region of the spinal cord post-injury (Fig. 2b).

Albumin Immunoreactivity

Increased albumin immunoreactivity was observed at 5 h post-injury within the injury epicenter and 1 cm both rostrally and caudally (Fig. 3). The intensity of staining increased further at 24 h post-injury within the injury epicentre. Increased

immunoreactivity was also observed 1 cm rostral from the injury, and extended to 2 cm caudally. At 3 days post-injury albumin immunoreactivity was similar to sham intensity.

Conclusion

The present study has demonstrated that the balloon compression model of SCI results in disruption of the BSCB and increased edema. In addition, given the associated increase in albumin immunoreactivity, these results demonstrate that the early edema was vasogenic in nature. This is important as, to date, these findings have not been shown within a closed injury model, such as the balloon compression model, where there is potential for an increase in ITP. Most experimental spinal cord injury models require a laminectomy to be performed, creating an open environment, thus preventing a rise in ITP. However clinically, spinal cord injuries occur within a closed environment created by the surrounding vertebrae. Such a setting leads to increased ITP [5], caused by edema genesis [4]. This contributes to the secondary injury process following SCI by reducing vascular perfusion, increasing tissue death and resulting in greatly impaired neurological function. Indeed, Batchelor et al. [2] recently demonstrated that increased intrathecal pressure results in a sharp decline in neurological function. This highlights the need for clinically relevant experimental models of SCI that incorporate all features of the injury development such as the potential for increased ITP.

We have also demonstrated in the present study that administration of an NK1 antagonist after SCI does not significantly reduce barrier disruption or edema genesis. This was in contrast to previous investigations in both TBI [3] and stroke [11], where increased SP expression was associated with increased BBB permeability, increased edema, and reduced neurological function. Indeed, Donkin et al. [3] demonstrated that NAT administration resulted in reduced BBB disruption and edema development and improved neurological function. It should be noted that increases in SP expression at 1 and 2 h post-SCI have been observed, with subsequent decreases at 5 h [9], implying that there may be an immediate release of SP following SCI, followed by depletion of the SP stores. The failure of NAT to have a significant effect in the present study may be due to the severe mechanical disruption of the BSCB following SCI, thus rendering any SP-mediated BSCB disruption less critical. Nonetheless, other neuropeptides such as neurokinin A or calcitonin-gene-related-peptide (CGRP) may still play an important role under such conditions. Indeed, increased CGRP has been reported in human cases of chronic SCI [1], although further investigation is needed to determine such a role in acute SCI.

In summary, this study has demonstrated that the balloon compression model of SCI produces significant disruption of the BSCB and associated increases in edema. This model may represent a more clinically relevant injury model given the closed environment. Whilst this study demonstrated that NAT administration does not attenuate BSCB permeability or edema genesis, further studies are required to fully elucidate the role of SP following traumatic SCI.

Acknowledgment Supported, in part, by the Neil Sachse Foundation.

Conflict of Interest We declare that we have no conflict of interest.

References

1. Ackery AD, Norenberg MD, Krassioukov A (2007) Calcitonin gene-related peptide immunoreactivity in chronic human spinal cord injury. Spinal Cord 45:678–686
2. Batchelor PE, Kerr NF, Gatt AM, Cox SF, Ghasem-Zadeh A, Wills TE, Sidon TK, Howells DW (2011) Intracanal pressure in compressive spinal cord injury: reduction with hypothermia. J Neurotrauma 28:809–820
3. Donkin JJ, Nimmo AJ, Cernak I, Blumbergs PC, Vink R (2009) Substance P is associated with the development of brain edema and functional deficits after traumatic brain injury. J Cereb Blood Flow Metab 29(8):1388–1398
4. Goldsmith HS (2009) Treatment of acute spinal cord injury by omental transposition: a new approach. J Am Coll Surg 208: 289–292
5. Kwon BK, Curt A, Belanger LM, Bernardo A, Chan D, Markez JA, Gorelik S, Slobogean GP, Umedaly H, Giffin M, Nikolakis MA, Street J, Boyd MC, Paquette S, Fisher CG, Dvorak MF (2009) Intrathecal pressure monitoring and cerebrospinal fluid drainage in acute spinal cord injury: a prospective randomized trial. J Neurosurg Spine 10:181–193
6. Popovich PG, Horner PJ, Mullin BB, Stokes BT (1996) A quantitative spatial analysis of the blood-spinal cord barrier. I. Permeability changes after experimental spinal contusion injury. Exp Neurol 142:258–275
7. Sekhon LH, Fehlings MG (2001) Epidemiology, demographics, and pathophysiology of acute spinal cord injury. Spine 26:S2–S12
8. Sharma HS (2005) Pathophysiology of blood-spinal cord barrier in traumatic injury and repair. Curr Pharm Des 11:1353–1389
9. Sharma HS, Nyberg F, Olsson Y, Dey PK (1990) Alteration of substance P after trauma to the spinal cord: an experimental study in the rat. Neuroscience 38:205–212
10. Tator CH, Fehlings MG (1991) Review of the secondary injury theory of acute spinal cord trauma with emphasis on vascular mechanisms. J Neurosurg 75:15–26
11. Turner RJ, Blumbergs PC, Sims NR, Helps SC, Rodgers KM, Vink R (2006) Increased substance P immunoreactivity and edema formation following reversible ischemic stroke. Acta Neurochir Suppl 96:263–266
12. Turner RJ, Helps SC, Thornton E, Vink R (2011) A substance P antagonist improves outcome when administered 4 h after onset of ischaemic stroke. Brain Res 1393:84–90
13. Vink R, Young A, Bennett CJ, Hu X, Connor CO, Cernak I, Nimmo AJ (2003) Neuropeptide release influences brain edema formation after diffuse traumatic brain injury. Acta Neurochir Suppl 86: 257–260

Hypnotic Effect of Volatile Anesthetics Is Mediated by PKC-γ Dynamics

Akiko Takeda, Ayano Okita, Kouki Kaneko, Takeo Nagura, Naoto Iwase, Shusuke Sekine, Takayasu Kakinuma, Masashi Noguchi, and Kiyoshi Hatakeyama

Abstract *Background*: Although protein kinase C-γ (PKC-γ) is a target for the effects of volatile anesthetics, the molecular mechanisms of the kinase function remain unclear. We examined the effects of different types of anesthetics on PKC-γ knockout mice, and investigated the dynamics of the kinase in mouse brain.

Methods: We measured the required number of times for loss of righting reflex (rtfLORR) after administration of isoflurane, sevoflurane, and propofol on PKC-γ knockout mice and compared with those of wild-type mice. We also used immunoblotting to investigate the intracellular distribution of PKC-γ and phosphorylated PKC-γ (p-PKC-γ) in brain of wild-type mice anesthetized by these anesthetics.

Results: Isoflurane and sevoflurane significantly prolonged the rtfLORRs in PKC-γ knockout mice compared with those in wild-type mice, while no significant difference was observed between knockout and wild-type mice treated with propofol. Examination of the cellular fractions showed that PKC-γ was significantly decreased, whereas p-PKC-γ was significantly increased in the synaptic membrane fraction (P2). There was no significant change in the supernatant fraction (S). In propofol-treated mice, PKC-γ and p-PKC-γ showed no significant changes in P2 or S.

Conclusion: Our results provide new evidence to support the possibility of the involvement of PKC-γ in the actions of volatile anesthetics.

Keywords Protein kinase C-γ • Phosphorylated protein kinase C-γ • Volatile anesthetics • Isoflurane • Sevoflurane • Propofol

Introduction

Protein kinase C (PKC) is a serine/threonine kinase that plays an important role in various intracellular processes such as neurotransmitter release, ion channel activity, and neurotransmitter receptor desensitization. Thus, PKC is an attractive molecular target for the synaptic action of general anesthetics [1]. PKC-γ is present in large quantities in the cerebral cortex, particularly post-synaptically [8]. PKC is activated by increases in intracellular calcium, which brings about the translocation of PKC to the plasma membrane and causes the phosphorylation of specific substrates [1]. In particular, this transfer during ischemia is known to be suppressed by volatile anesthetic exposure and hypothermia [2, 5, 8]. However, because experimental evidence regarding the relationship between PKC activities and the effects of volatile anesthetics is contradictory, the participation of PKC dynamics in their actions is not universally accepted. In the present study, we examined the effect of different types of anesthetic agents on PKC-γ knockout mice to ascertain whether the enzyme participates in the process of anesthesia. Furthermore, we investigated the effects of those anesthetics on the translocation of PKC-γ and phosphorylated PKC-γ within brain cells fractionated just after the mice had succumbed to anesthesia.

A. Takeda (✉), A. Okita, K. Kaneko, T. Nagura, N. Iwase, S. Sekine, T. Kakinuma, and M. Noguchi
Department of Anesthesiology, Tokyo Medical University Hospital, 6-7-1 Nishi-shinjuku, Shinjuku-ku, Tokyo 160-0023, Japan
e-mail: a-takeda@tokyo-med.ac.jp

K. Hatakeyama
Department of Anesthesiology, Tokyo Medical University, Tokyo, Japan

Department of Anesthesiology, Toda Chuo General Hospital, Toda, Japan

Department of Anesthesiology, Hachioji Medical Center, Tokyo Medical University, 1163 Tate-machi Hachioji City, Shinjuku, Tokyo 193-0998, Japan

Department of Anesthesiology, Toda Central General Hospital, Tokyo, Japan

Y. Katayama et al. (eds.), *Brain Edema XV*, Acta Neurochirurgica Supplement, Vol. 118,
DOI 10.1007/978-3-7091-1434-6_60,

Materials and Methods

Animal Preparation

Male C57BL/6 N mice, PKC-γ knockout mice (B6;129P2-Prkcc tm1Stl/J) and wild-type mice (B6129PF2/J) were used.

Knockout Mouse Study to Compare the Required Times for LORR

Male knockout mice lacking PKC-γ and male wild-type mice with a mean body weight of 24 g were used. Knockout (KO) and wild-type (W) mice were randomly divided into isoflurane, sevoflurane, and propofol groups of five animals each. The minimum alveolar concentrations (MAC) of isoflurane and sevoflurane are 1.3 and 1.7 % respectively. With 50 % oxygen, mice inhaled 2 MAC of isoflurane and sevoflurane. The other group of mice was given 200 mg/kg i.p. of propofol. Anesthetic induction by isoflurane and sevoflurane was evaluated using loss of righting reflex (LORR). We measured the required times for LORR (rtfLORR) with different anesthetics in the KO groups and compared them with those in the W group.

Examination of the Effects of Anesthetics on the Cellular Distribution of PKC-γ and Phosphorylated PKC-γ

Thirty animals were used and randomly divided into groups. The volatile anesthetic groups were exposed to 1 or 2 MAC of isoflurane or sevoflurane for 10 min ($F_1O_2 = 0.5$). In the control group, mice ($n = 4$) inhaled oxygen without volatile anesthetic. In the intravenous anesthetic group, five animals received 200 mg/kg of propofol intraperitoneally, and five others, as controls, were given the same volume of soybean oil emulsion. In anesthetized groups, the mice were decapitated in a state of LORR, their heads were immediately frozen in liquid nitrogen, and the cerebral cortex was isolated inside a −25 °C.

Sample homogenization and subcellular fractionation were performed as described [6]. The samples (20 μg protein for P2 and S) were subjected to SDS-PAGE, and then incubated overnight with anti-β-actin monoclonal antibody and anti-PKC-γ rabbit polyclonal antibody or anti-p-PKC-γ antibody against phosphorylated threonine 514 at 4 °C. Then, using the ECL Western Blotting System, blots were incubated in secondary antibody conjugated to horseradish peroxidase. Immunoreactivity (IR) was visualized, and the blots were quantified. Quantification of optical densities was performed by obtaining ratios between the densitometric scores for PKC-γ, p-PKC-γ, and β-actin.

Statistical Analysis of Experimental Data

The data are presented as the mean ± SE. A *t* test was employed to compare the differences in rtfLORR between the W and KO groups. To compare the distribution of PKC-γ and p-PKC-γ, the density of the PKC-γ or p-PKC-γ bands was normalized to the density of β-actin (PKC-γ or p- PKC-γ/β-actin) and expressed as the average ± SE. To compare the 1 MAC and 2 MAC, a one-way ANOVA followed by a post-hoc Dunnet's test were used. To compare the changes in PKC-γ and p-PKC-γ in the propofol group, a Mann–Whitney's *U* test was employed. A *p* value of less than 0.05 was considered statistically significant.

Results

Times for LORR Under Volatile and Intravenous Anesthetics in PKC-γ Knockout and Wild-Type Mice

The rtfLORR under isoflurane in the KO mice was significantly prolonged by almost two times that observed in the wild-type mice: 548.5 ± 8.8 s vs. 297.3 ± 8.7 s ($p < 0.01$). The rtfLORR in KO mice given sevoflurane was also significantly prolonged compared with that of wild-type mice:129.8 ± 5.0 s vs 103.2 ± 5.3 s ($p < 0.01$). The effect of propofol on the induction time in the KO mice was almost the same as that in the wild-type mice: 156.8 ± 12.7 s vs 158.0 ± 12.6 s.

Effects of Volatile and Intravenous Anesthetics on the Cellular Distribution of PKC-γ and p-PKC-γ

Total PKC-γ did not change following exposure to isoflurane, sevoflurane, and propofol (data not shown). In the volatile anesthetic groups, all animals were exposed to 1 or 2 MAC of isoflurane or sevoflurane for 10 min ($FIO_2 = 0.5$). In the control group, mice inhaled oxygen without volatile anesthetic.

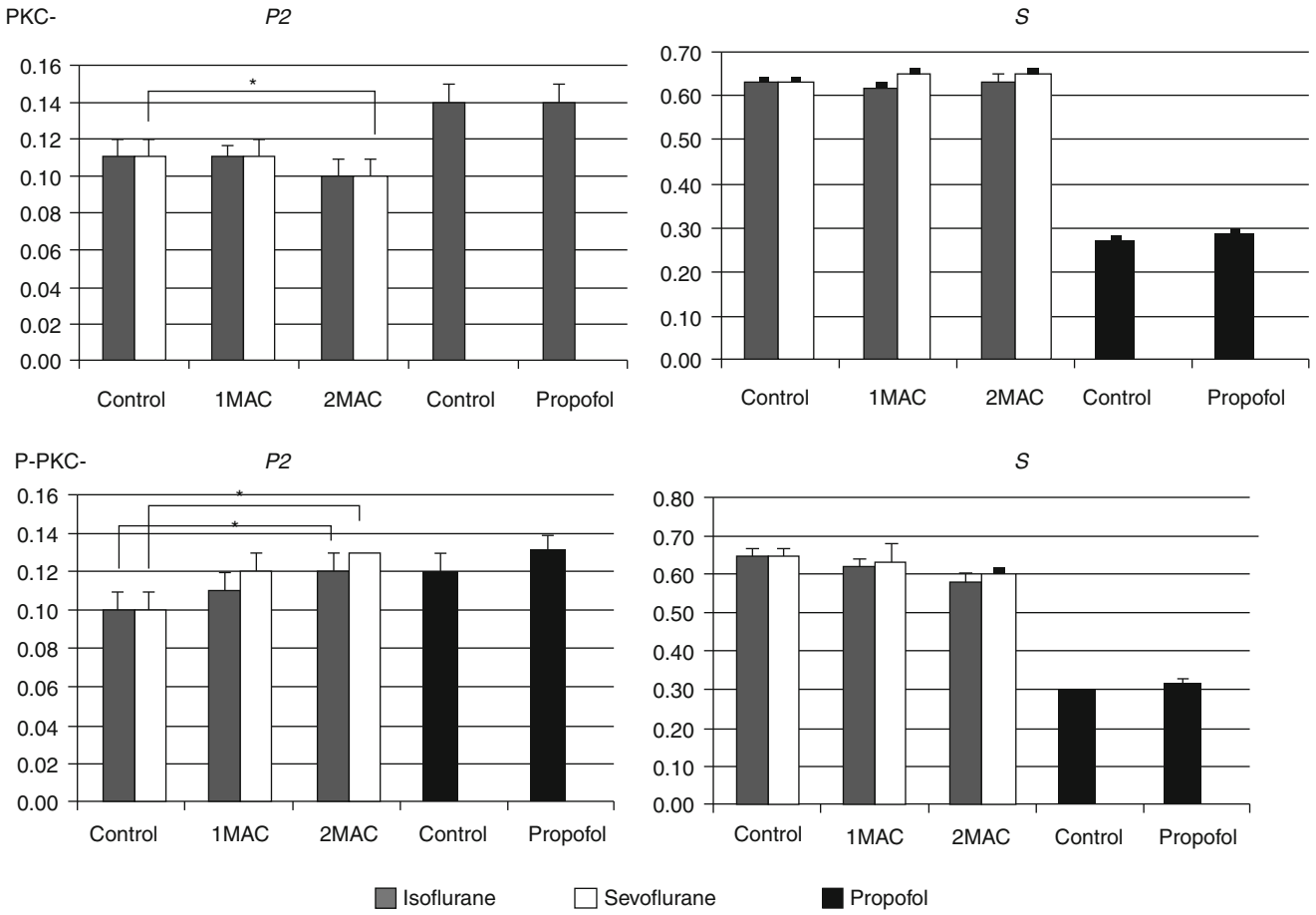

Fig. 1 The cellular distribution of PKC-γ. The *upper part* shows graphs quantitating the immunoreactivity (IR) of PKC-γ in the synaptosomal fraction (*P2*) and the cytosolic fraction (*S*). The *lower part* is the immunoreactivity (IR) of p-PKC-γ. Ordinates indicate the ratio between the densitometric scores for PKC-γ and β-actin. *Statistically significant differences from the control (*$p<0.05$)

Effects of Inhaled Isoflurane, Sevoflurane, and Propofol on the Cellular Distribution of PKC-γ and p*-PKC-γ*

As shown in Fig. 1, PKC-γ in the P2 fraction in isoflurane groups tended to be reduced, but the change was statistically insignificant. In the 2 MAC sevoflurane group, the level of PKC-γ decreased significantly ($p<0.05$). In the S fraction, isoflurane groups tend to increase, sevoflurane had no significant effect on PKC-γ.

Also, p-PKC-γ in the 2 MAC groups increased significantly in the P2 fraction ($p<0.05$). In the S fraction, there was a tendency toward a decrease in 2 MAC groups.

On the other hand, the levels of PKC-γ and p-PKC-γ in the P2 and S fraction did not show any significant changes compared with vehicle controls.

Conclusion

Our experiments showed that the kinase may at least partly participate in the anesthetic effects of the volatile anesthetics. On the other hand, the effects of propofol seemed to have no relationship to the kinase. We employed the rtfLORR as the index for the onset of anesthesia. The rtfLORR of sevoflurane was far shorter than that of isoflurane, when used at 2 MAC. The effects of volatile anesthetics on PKC-γ KO mice may indicate that PKC-γ-dependent processes can participate in a process that enhances the development of anesthesia. Although the rtfLORR of propofol on wild-type mice was no prolongation in rtfLORR in KO mice. This result indicated that PKC-γ may not be involved in propofol-induced anesthesia. In the present study, we found that volatile anesthetics tended to show reduced IR for PKC-γ in the P2 fraction.

However, these anesthetics did not produce any significant changes in the S fraction. We measured the PKC-γ level in the entire tissue prior to fractionation, but there were no significant differences between the volatile anesthetic-treated and control groups. The result suggested that the change in intracellular distribution of PKC-γ might occur during anesthesia from the volatile anesthetic.

Also, we found a significant increase in the p-PKC-γ level in the P2 fraction in volatile anesthetics groups. Although the levels in the S fraction tended to decrease, the differences were not statistically significant. These results suggest that the translocation of PKC-γ from the cytosol to the membrane is facilitated by its phosphorylation. Previous studies show that isoflurane, sevoflurane, and desflurane all attenuated the function of mutant NMDA receptors expressed in oocytes [3, 7]. Furthermore, isoflurane facilitated the opening of the sarcolemmal K_{ATP} channel. p-PKC-γ may contribute to the selective modulation of NMDA receptor or K_{ATP} channel function, which is involved in mediating these anesthetic effects. So, phosphorylation of PKC-γ may be at least partly essential for the anesthetic action of volatile anesthetics. Regarding p-PKC-γ, the actions of phosphoenzymes and dephosphorized oxidase are related, and it is thought that the distribution of p-PKC-γ varies according to the period of anesthesia [4, 9].

To determine whether PKC-γ activation was specific to volatile anesthetics, we compared the effects with an intravenous anesthetic, propofol. Propofol did not change the induction time and distribution of PKC-γ or p-PKC-γ. These results suggest that the mechanism of the anesthetic action of the intravenous drug propofol is different from that of volatile anesthetics, which affected PKC-γ and p-PKC-γ translocation at least during the induction and development of their action.

In summary, our current study suggests that PKC-γ might be involved in the induction and development of the effects of volatile anesthetics, and that the translocation of PKC-γ and/or p- PKC-γ in brain cells might be involved in the expression of their effects. However, the effects of an intravenous anesthetic seemed to be independent of kinase activity, at least during the early stages of the anesthetic effects.

Conflict of Interest We declare that we have no conflict of interest.

References

1. Gomez RS, Guatimosim C (2003) Mechanism of action of volatile anesthetics: involvement of intracellular calcium signaling. Cell Mol Neurobiol 23:877–885
2. Harada K, Maekawa T, Tsuruta R, Kaneko T, Sadamitsu D, Yamashima T, Yoshida Ki K (2002) Hypothermia inhibits translocation of CaM kinase II and PKC-alpha, beta, gamma isoforms and fodrin proteolysis in rat brain synaptosome during ischemia-reperfusion. J Neurosci Res 67:664–669
3. Hollmann MW, Liu HT, Hoenemann CW, Liu WH, Durieux ME (2001) Modulation of NMDA receptor function by ketamine and magnesium. Part II: interactions with volatile anesthetics. Anesth Analg 92:1182–1191
4. Kumar S, Lane BM, Morrow AL, Wu K, Suen PC, Xu JL, Lin SY, Levine ES, Black IB (2006) Differential effects of systemic ethanol administration on protein kinase cepsilon, gamma, and beta isoform expression, membrane translocation, and target phosphorylation: reversal by chronic ethanol exposure. J Pharmacol Exp Ther 319:1366–1375
5. Matsumoto S, Murozono M, Nagaoka D, Matsuoka S, Takeda A, Narita H, Watanabe S, Isshiki A, Watanabe Y (2008) Isoflurane inhibits protein kinase Cgamma and calcium/calmodulin dependent protein kinase ii-alpha translocation to synaptic membranes in ischemic mice brains. Neurochem Res 33:2302–2309
6. Matsumoto S, Shamloo M, Matsumoto E, Isshiki A, Wieloch T (2004) Protein kinase C-gamma and calcium/calmodulin-dependent protein kinase II-alpha are persistently translocated to cell membranes of the rat brain during and after middle cerebral artery occlusion. J Cereb Blood Flow Metab 24:54–61
7. Ogata J, Shiraishi M, Namba T, Smothers CT, Woodward JJ, Harris RA (2006) Effects of anesthetics on mutant N-methyl-D-aspartate receptors expressed in Xenopus oocytes. J Pharmacol Exp Ther 318:434–443
8. Saito N, Shirai Y (2002) Protein kinase C gamma (PKC gamma): function of neuron specific isotype. J Biochem 132:683–687
9. Sanchez-Perez AM, Felipo V, Giordano G, Burgal M, Montoliu C, Costa LG (2005) Serines 890 and 896 of the NMDA receptor subunit NR1 are differentially phosphorylated by protein kinase C isoforms. Neurochem Int 47:84–91

Cyclophilin-D Inhibition in Neuroprotection: Dawn of a New Era of Mitochondrial Medicine

Hiroyuki Uchino, Kiyoshi Hatakeyama, Saori Morota, Tadashi Tanoue, Takahisa Nishiyama, Daiki Usui, Chisato Taguchi, Morika Suzuki, Magnus J. Hansson, and Eskil Elmér

Abstract Traumatic brain injury and ischemia can result in marked neuronal degeneration and residual impairment of cerebral function. However, no effective pharmacological treatment directed at tissues of the central nervous system (CNS) for acute intervention has been developed. The detailed pathophysiological cascade leading to neurodegeneration in these conditions has not been elucidated, but cellular calcium overload and mitochondrial dysfunction have been implicated in a wide range of animal models involving degeneration of the CNS. In particular, activation of the calcium-induced mitochondrial permeability transition (mPT) is considered to be a major cause of cell death inferred by the broad and potent neuroprotective effects of pharmacological inhibitors of mPT, especially modulators of cyclophilin activity and, more specifically, genetic inactivation of the mitochondrial cyclophilin, cyclophilin D. Reviewed are evidence and challenges that could bring on the dawning of mitochondrial medicine aimed at safeguarding energy supply following acute injury to the CNS.

Keywords Mitochondria • Neurodegeneration • Neuroprotection • Permeability transition • Brain • Cyclophilin Cyclosporin

H. Uchino, MD, PhD (✉) and M. Suzuki
Department of Anesthesiology, Tokyo Medical University,
6-7-1 Nishishinjuku, Shinjuku-ku, 160-0023, Tokyo, Japan
e-mail: h-uchi@tokyo-med.ac.jp

K. Hatakeyama
Department of Anesthesiology, Tokyo Medical University,
6-7-1 Nishishinjuku, Shinjuku-ku, 160-0023, Tokyo, Japan

Department of Anesthesiology, Toda Chuo General Hospital,
1-19-3 Honmachi, Toda City, 335-0023, Saitama, Japan

S. Morota, M.J. Hansson, and E. Elmér
Mitochondrial Pathophysiology Unit,
Department of Clinical Sciences, Lund University,
BMC A13, 221 84 Lund, Sweden
e-mail: saori.morota@med.lu.se; magnus.hansson@med.lu.se;
eskil.elmer@med.lu.se

T. Tanoue, D. Usui, C. Taguchi, and T. Nishiyama
Department of Anesthesiology,
Tokyo Medical University,
6-7-1 Nishishinjuku, Shinjuku-ku, 160-0023, Tokyo, Japan

Department of Anesthesiology, Kimura Hospital,
2-39-10 Chidori, Ohta-ku, 146-0083, Tokyo, Japan
e-mail: nishiyat@tokyo-med.ac.jp

Abbreviations

ANT	Adenine nucleotide translocator
BBB	Blood–brain barrier
CRC	Calcium retention capacity
CsA	Cyclosporin A
CypD	Cyclophilin D
MCAO	Middle cerebral artery occlusion
mPT	Mitochondrial permeability transition
PhArs	Phenylarsine oxide
RCR	Respiratory control ratios
TBI	Traumatic brain injury
tBOOH	Tert-butyl hydroperoxide

Y. Katayama et al. (eds.), *Brain Edema XV*, Acta Neurochirurgica Supplement, Vol. 118,
DOI 10.1007/978-3-7091-1434-6_61, © Springer-Verlag Wien 2013

Mitochondria are central to the maintenance and survival of cells of the CNS and have been proposed to participate both directly and indirectly in the pathogenesis of brain damage. A well-described aspect of neurodegeneration is calcium dysregulation. Following cellular calcium overload, a sudden increase in the permeability of the inner mitochondrial membrane can occur, a phenomenon named the mitochondrial permeability transition (mPT). mPT induction results in immediate loss of ion homeostasis and the proton motive force required for ATP synthesis. The mitochondrial matrix protein cyclophilin D (CypD) is a peptidylprolyl cis-trans isomerase that regulates mPT and facilitates its activation by calcium [50].

The most common evidence for mPT as a mediator of cell death and thus its potential as a pharmacological target derives from studies using cyclosporin-A (CsA, cyclosporine). Neuroprotection by CsA treatment can, however, not be taken as proof of an involvement of mPT because the effect of CsA in vivo is not specific to the mitochondria. The target for CsA in mitochondria is the mitochondria-specific cyclophilin D, CypD. However, several other cyclophilins are present in mammalian cells and are involved in protein folding and other functions in different cellular compartments, as well as intercellular communication [47]. CsA is clinically used as an immunosuppressant and this effect is related to binding to the cytoplasmic cyclophilin A, CypA. The CypA-CsA complex in turn binds to the calcineurin enzyme and prevents its phosphatase activity, which conveys inhibition of immune cells. The neuroprotective effect of systemic CsA treatment may therefore be mediated by inhibition of calcineurin and not mPT or, likely, a combination of the two. In order to pinpoint the neuroprotective target for CsA, FK506 (tacrolimus, which inhibits calcineurin, but not mPT), and non-immunosuppressive cyclosporin derivatives (usually amino acid variants, which inhibit mPT but not calcineurin) have been employed in the experimental setting [15, 20, 21, 31, 32, 37, 46]. The derivatives provide significant benefits over native CsA when evaluating the relevant pharmacological target, but they too inhibit the activity of non-mitochondrial cyclophilins. The difference from CsA lies in their inability to bind to calcineurin, which renders them non-immunosuppressive. Specific evidence of an involvement of mPT in brain disease has come from studies using CypD knockout mice (*Ppif*$^{-/-}$) [8, 12, 39].

For an extended time, the existence of mPT in brain mitochondria and relevance to neuronal cell death was debated [1, 3, 4, 9, 23]. Several unique features were suggested for brain mitochondria in relation to more classically examined tissues, e.g., liver mitochondria such as general increased resistance to mPT inducers, the presence of resistant subpopulations and the suggestion that CypD would down-regulate with age – all evidence that raised doubts concerning the pathophysiological role of mPT in the central nervous system. In addition to demonstrating extensive and reversible and CypD-sensitive mPT in rodent brain-derived and spinal cord mitochondria [14–17, 33], we have recently provided evidence of several classical characteristics of the mPT phenomenon following calcium overload in human brain mitochondria (Fig. 1). Brain-derived mitochondria isolated from freshly resected tissue obtained during hemorrhage or tumor surgery displayed increased calcium retention capacity (CRC) by CypD inhibition, thiol-reactive compounds and oxidants sensitized mitochondria to calcium-induced mPT, and the mPT was reversible, i.e., if calcium was removed mitochondria could re-seal the inner membrane (Fig. 1). The conclusion was that adult human brain mitochondria possess an active CypD-sensitive mPT [16]. Validating mPT as a pharmacological target in human brain mitochondria is a crucial translational step toward controlled clinical trials of CypD inhibition in humans.

Cerebral ischemia results in several prominent changes of the cellular bioenergetic status favoring mPT activation – hydrolysis of adenine nucleotides, rise in tissue Pi, increased oxidative stress, release of free fatty acids, and rapid cytoplasmic acidification due to the conversion from aerobic to anaerobic metabolism [6, 11, 48, 49]. Importantly, acidic pH was initially believed to protect cells from mPT-induction but there is now convincing evidence that altered phosphate transport and decreased solubility of stored calcium phosphates in the matrix at low pH will override the direct inhibitory effect of protons on mPT seen under so-called de-energized conditions [22, 36].

In models of global ischemia, the hippocampal CA1 neurons are selectively vulnerable, and CsA dramatically ameliorates cell death both under normo- and hyperglycemic conditions if administered before or early after ischemia in situations where the blood–brain barrier (BBB) has been disrupted, allowing for brain penetration of CsA [7, 25, 35, 43–45]. The non-immunosuppressive cyclosporin derivatives have not been thoroughly studied in global ischemia models, but there is protection demonstrated with high concentrations of a non-immunosuppressive CsA analog in animals with intact BBB [19]. In contrast, delayed CA1 cell death in hippocampal slices exposed to oxygen glucose deprivation is readily prevented by CsA and a non-immunosuppressive CsA analog [38]. Furthermore, CsA has been demonstrated to block early mitochondrial depolarization following global ischemia using in vivo imaging with two-photon microscopy [26]. Additional evidence in vivo is needed in order to definitely conclude that mPT is essential in the pathogenesis of this type of delayed ischemic cell death.

In animal models of transient or permanent focal ischemia, CsA significantly reduces cerebral infarction when administered up to 3 h following reperfusion. The most robust effect has been observed with intracarotid CsA infusion following 5 min of reperfusion after 2 h of middle cerebral artery occlusion (MCAO), where CsA virtually eliminated the

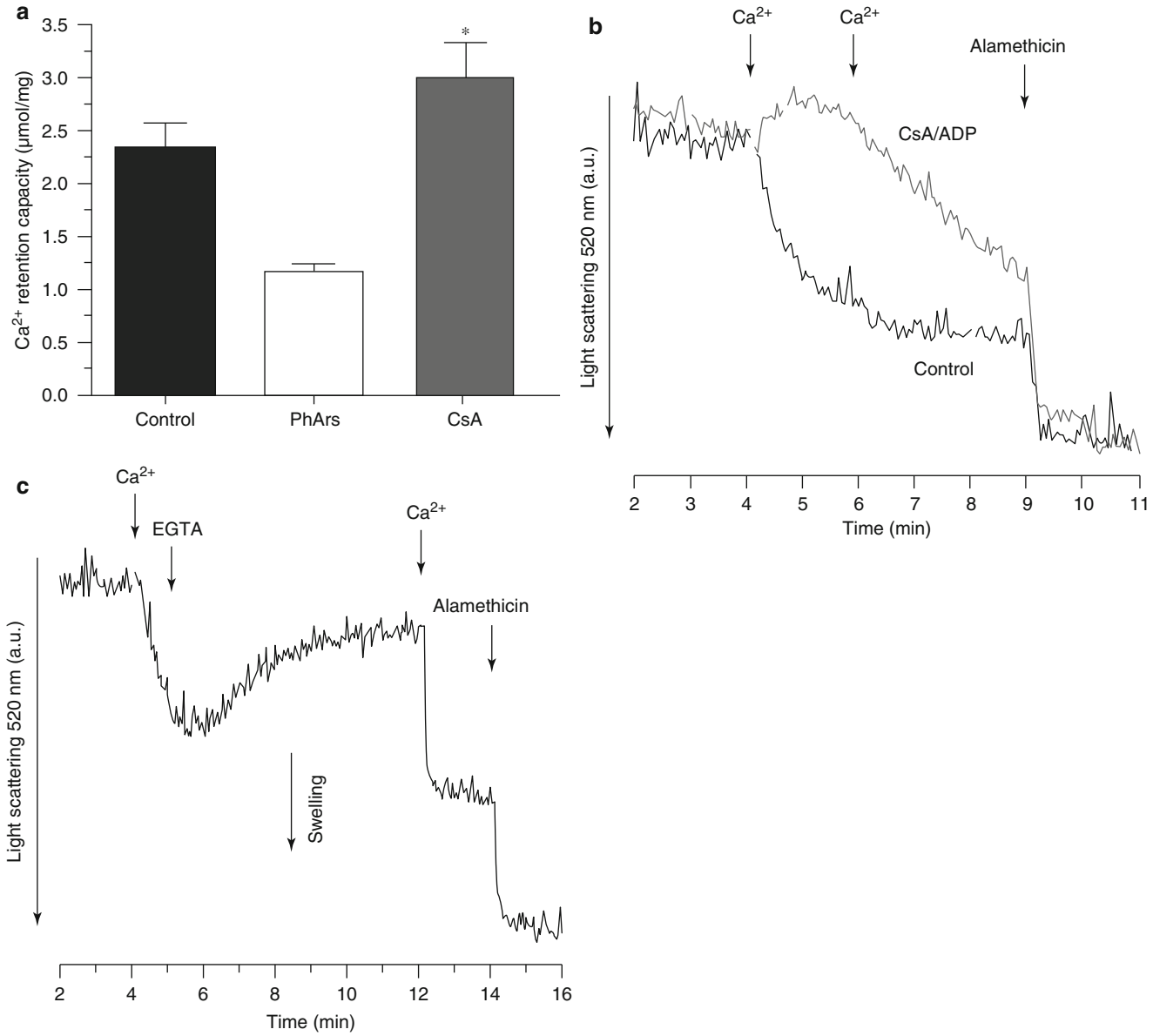

Fig. 1 Characteristics of permeability transition in human brain mitochondria. (**a**) Calcium retention capacity (CRC) of freshly isolated human brain mitochondria. Suspensions of respiring mitochondria were continuously infused with calcium. At onset of permeability transition, calcium retained in mitochondria was released and CRC was calculated with or without the presence of the CypD-inhibitor cyclosporin A (CsA, 1 μM) and the vicinal thiol reagent phenylarsine oxide (PhArs, 1 μM). Values are means ± SEM. (**b**) Representative traces of calcium-induced swelling assayed by 90° light scattering with or without the presence of the endogenous permeability transition inhibitor ADP (100 μM) and CsA (1 μM). Mitochondria were challenged with two additions of 100 μM Ca^{2+} followed by exposure to the unspecific ionophore alamethicin. (**c**) Representative traces of reversible swelling in human brain mitochondria induced by 200 μM Ca^{2+} followed by 400 μM of the Ca^{2+} chelator EGTA. Swelling was induced a second time by Ca^{2+} (1 mM), and mitochondria were then fully permeabilized by alamethicin (Adapted from Hansson et al. [16], with permission)

infarct [51]. On the other hand, equal efficacy of CsA and a non-immunosuppressive CsA analog in transient MCAO have also been demonstrated [28]. Strongly supporting the essential role of CypD in this model of ischemia is the finding that CypD knock-out mice display a dramatic reduction of brain infarct size following MCAO compared with their littermate controls [39], similar to the effect in cardiac ischemia [2, 34].

A major obstacle in evaluating the neuroprotective effects of cyclosporin compounds is their limited penetration across the blood–brain barrier (BBB) [24, 41, 42]. CsA and several other lipophilic compounds are actively extruded into the blood stream by the p-glycoprotein transporter present in the capillary endothelium. Different techniques can be used to overcome this problem. The BBB can be disrupted by physical damage to the tissue (see "Traumatic brain injury" below)

or osmotically through, for example, mannitol injection. The p-glycoprotein can be saturated by using high systemic doses of CsA or by reaching high local concentrations by arterial injection. Alternatively, CsA can be administered directly into the cerebrospinal fluid. It should be noted that only a few experimental studies examine the resulting tissue concentration following CsA administration and in addition, there is a lack of knowledge of the effective concentration range in the CNS. Consequently, a positive outcome of CsA treatment in an animal model cannot be regarded as unequivocal evidence of mPT involvement because of the compound's non-mitochondrial targets. Further, a lack of effect cannot be taken as unequivocal evidence that mPT is not involved, especially if CsA has not penetrated the BBB. A safe and effective way of targeting drugs to the entire brain may be via delivery systems directed at endogenous receptor-mediated uptake mechanisms present at the cerebral capillaries [13]. This or similar approaches may then enable treatment of a number of CNS disorders by CypD inhibitors where the BBB is intact, but mPT has been implicated in the pathogenesis.

There is extensive documentation of the neuroprotective effect of CsA in different models of traumatic brain injury (TBI) [27]. The shear forces will cause an immediate, but also a delayed cell structure injury and a disruption of the BBB, allowing for systemic CsA administration [40]. The promising animal data have led different academic groups to initiate human clinical trials of CsA administration to patients with severe TBI. The initial studies in patients with TBI show, that CsA is well tolerated, enters the central nervous system, and according to the authors demonstrates a dose-related improvement in favorable outcome [5, 10, 18, 29, 30]. These clinical trials in TBI are the first human studies aimed at testing the hypothesis of mPT-mediated injury in human neurological disease (with the reservation of calcineurin inhibition mentioned above). Larger clinical trials with CsA in TBI are currently being planned in the USA and in Europe. If complemented by clinical trials using specific inhibitors of CypD, mitochondrial cyclophilin inhibition will be validated as a feasible pharmaceutical target in neuroprotection, marking the dawn of a new era of mitochondrial medicine.

Conflict of Interest Author EE is co-founder and officer and MJH a stockholder of Maas Biolab, LLC and NeuroVive Pharmaceutical AB (publ), which hold intellectual property rights and develop the use of cyclosporins such as cyclophilin D inhibitors for neurological treatment.

References

1. Andreyev A, Fiskum G (1999) Calcium induced release of mitochondrial cytochrome c by different mechanisms selective for brain versus liver. Cell Death Differ 6:825–832
2. Baines CP, Kaiser RA, Purcell NH, Blair NS, Osinska H, Hambleton MA, Brunskill EW, Sayen MR, Gottlieb RA, Dorn GW, Robbins J, Molkentin JD (2005) Loss of cyclophilin D reveals a critical role for mitochondrial permeability transition in cell death. Nature 434:658–662
3. Berman SB, Watkins SC, Hastings TG (2000) Quantitative biochemical and ultrastructural comparison of mitochondrial permeability transition in isolated brain and liver mitochondria: evidence for reduced sensitivity of brain mitochondria. Exp Neurol 164:415–425
4. Brustovetsky N, Dubinsky JM (2000) Limitations of cyclosporin A inhibition of the permeability transition in CNS mitochondria. J Neurosci 20:8229–8237
5. Cook AM, Whitlow J, Hatton J, Young B (2009) Cyclosporine A for neuroprotection: establishing dosing guidelines for safe and effective use. Expert Opin Drug Saf 8:411–419
6. Crompton M (1999) The mitochondrial permeability transition pore and its role in cell death. Biochem J 341:233–249
7. Domanska-Janik K, Buzanska L, Dluzniewska J, Kozlowska H, Sarnowska A, Zablocka B (2004) Neuroprotection by cyclosporin A following transient brain ischemia correlates with the inhibition of the early efflux of cytochrome C to cytoplasm. Brain Res Mol Brain Res 121:50–59
8. Du H, Guo L, Fang F, Chen D, Sosunov AA, McKhann GM, Yan Y, Wang C, Zhang H, Molkentin JD, Gunn-Moore FJ, Vonsattel JP, Arancio O, Chen JX, Yan SD (2008) Cyclophilin D deficiency attenuates mitochondrial and neuronal perturbation and ameliorates learning and memory in Alzheimer's disease. Nat Med 14:1097–1105
9. Eliseev RA, Filippov G, Velos J, VanWinkle B, Goldman A, Rosier RN, Gunter TE (2007) Role of cyclophilin D in the resistance of brain mitochondria to the permeability transition. Neurobiol Aging 28:1532–1542
10. Empey PE, McNamara PJ, Young B, Rosbolt MB, Hatton J (2006) Cyclosporin A disposition following acute traumatic brain injury. J Neurotrauma 23:109–116
11. Folbergrova J, Minamisawa H, Ekholm A, Siesjo BK (1990) Phosphorylase alpha and labile metabolites during anoxia: correlation to membrane fluxes of K^+ and Ca^{2+}. J Neurochem 55:1690–1696
12. Forte M, Gold BG, Marracci G, Chaudhary P, Basso E, Johnsen D, Yu X, Fowlkes J, Bernardi P, Bourdette D (2007) Cyclophilin D inactivation protects axons in experimental autoimmune encephalomyelitis, an animal model of multiple sclerosis. Proc Natl Acad Sci U S A 104:7558–7563
13. Gaillard PJ, Visser CC, de Boer AG (2005) Targeted delivery across the blood-brain barrier. Expert Opin Drug Deliv 2:299–309
14. Hansson MJ, Mansson R, Mattiasson G, Ohlsson J, Karlsson J, Keep MF, Elmer E (2004) Brain-derived respiring mitochondria exhibit homogeneous, complete and cyclosporin-sensitive permeability transition. J Neurochem 89:715–729
15. Hansson MJ, Mattiasson G, Mansson R, Karlsson J, Keep MF, Waldmeier P, Ruegg UT, Dumont JM, Besseghir K, Elmer E (2004) The nonimmunosuppressive cyclosporin analogs NIM811 and UNIL025 display nanomolar potencies on permeability transition in brain-derived mitochondria. J Bioenerg Biomembr 36:407–413
16. Hansson MJ, Morota S, Chen L, Matsuyama N, Suzuki Y, Nakajima S, Tanoue T, Omi A, Shibasaki F, Shimazu M, Ikeda Y, Uchino H, Elmer E (2011) Cyclophilin D-sensitive mitochondrial permeability transition in adult human brain and liver mitochondria. J Neurotrauma 28:143–153
17. Hansson MJ, Persson T, Friberg H, Keep MF, Rees A, Wieloch T, Elmer E (2003) Powerful cyclosporin inhibition of calcium-induced permeability transition in brain mitochondria. Brain Res 960:99–111
18. Hatton J, Rosbolt B, Empey P, Kryscio R, Young B (2008) Dosing and safety of cyclosporine in patients with severe brain injury. J Neurosurg 109:699–707

19. Hokari M, Kuroda S, Iwasaki Y (2010) Pretreatment with the ciclosporin derivative NIM811 reduces delayed neuronal death in the hippocampus after transient forebrain ischaemia. J Pharm Pharmacol 62:485–490
20. Khaspekov L, Friberg H, Halestrap A, Viktorov I, Wieloch T (1999) Cyclosporin A and its nonimmunosuppressive analogue N-Me-Val-4-cyclosporin A mitigate glucose/oxygen deprivation-induced damage to rat cultured hippocampal neurons. Eur J Neurosci 11: 3194–3198
21. Korde AS, Pettigrew LC, Craddock SD, Pocernich CB, Waldmeier PC, Maragos WF (2007) Protective effects of NIM811 in transient focal cerebral ischemia suggest involvement of the mitochondrial permeability transition. J Neurotrauma 24:895–908
22. Kristian T, Bernardi P, Siesjo BK (2001) Acidosis promotes the permeability transition in energized mitochondria: implications for reperfusion injury. J Neurotrauma 18:1059–1074
23. Kristian T, Weatherby TM, Bates TE, Fiskum G (2002) Heterogeneity of the calcium-induced permeability transition in isolated non-synaptic brain mitochondria. J Neurochem 83: 1297–1308
24. Lemaire M, Bruelisauer A, Guntz P, Sato H (1996) Dose-dependent brain penetration of SDZ PSC 833, a novel multidrug resistance-reversing cyclosporin, in rats. Cancer Chemother Pharmacol 38: 481–486
25. Li PA, Uchino H, Elmer E, Siesjo BK (1997) Amelioration by cyclosporin A of brain damage following 5 or 10 min of ischemia in rats subjected to preischemic hyperglycemia. Brain Res 753: 133–140
26. Liu RR, Murphy TH (2009) Reversible cyclosporin A-sensitive mitochondrial depolarization occurs within minutes of stroke onset in mouse somatosensory cortex in vivo: a two-photon imaging study. J Biol Chem 284:36109–36117
27. Lulic D, Burns J, Bae EC, van Loveren H, Borlongan CV (2011) A review of laboratory and clinical data supporting the safety and efficacy of cyclosporin A in traumatic brain injury. Neurosurgery 68:1172–1185; discussion 1185–1176
28. Matsumoto S, Friberg H, Ferrand-Drake M, Wieloch T (1999) Blockade of the mitochondrial permeability transition pore diminishes infarct size in the rat after transient middle cerebral artery occlusion. J Cereb Blood Flow Metab 19:736–741
29. Mazzeo AT, Alves OL, Gilman CB, Hayes RL, Tolias C, Niki Kunene K, Ross Bullock M (2008) Brain metabolic and hemodynamic effects of cyclosporin A after human severe traumatic brain injury: a microdialysis study. Acta Neurochir (Wien) 150: 1019–1031; discussion 1031
30. Mazzeo AT, Kunene NK, Gilman CB, Hamm RJ, Hafez N, Bullock MR (2006) Severe human traumatic brain injury, but not cyclosporin a treatment, depresses activated T lymphocytes early after injury. J Neurotrauma 23:962–975
31. Mbye LH, Singh IN, Carrico KM, Saatman KE, Hall ED (2009) Comparative neuroprotective effects of cyclosporin A and NIM811, a nonimmunosuppressive cyclosporin A analog, following traumatic brain injury. J Cereb Blood Flow Metab 29:87–97
32. McEwen ML, Sullivan PG, Springer JE (2007) Pretreatment with the cyclosporin derivative, NIM811, improves the function of synaptic mitochondria following spinal cord contusion in rats. J Neurotrauma 24:613–624
33. Morota S, Hansson MJ, Ishii N, Kudo Y, Elmer E, Uchino H (2007) Spinal cord mitochondria display lower calcium retention capacity compared with brain mitochondria without inherent differences in sensitivity to cyclophilin D inhibition. J Neurochem 103: 2066–2076
34. Nakagawa T, Shimizu S, Watanabe T, Yamaguchi O, Otsu K, Yamagata H, Inohara H, Kubo T, Tsujimoto Y (2005) Cyclophilin D-dependent mitochondrial permeability transition regulates some necrotic but not apoptotic cell death. Nature 434:652–658
35. Nakatsuka H, Ohta S, Tanaka J, Toku K, Kumon Y, Maeda N, Sakanaka M, Sakaki S (1999) Release of cytochrome c from mitochondria to cytosol in gerbil hippocampal CA1 neurons after transient forebrain ischemia. Brain Res 849:216–219
36. Nicholls DG, Chalmers S (2004) The integration of mitochondrial calcium transport and storage. J Bioenerg Biomembr 36: 277–281
37. Ravikumar R, McEwen ML, Springer JE (2007) Post-treatment with the cyclosporin derivative, NIM811, reduced indices of cell death and increased the volume of spared tissue in the acute period following spinal cord contusion. J Neurotrauma 24:1618–1630
38. Rytter A, Cardoso CM, Johansson P, Cronberg T, Hansson MJ, Mattiasson G, Elmer E, Wieloch T (2005) The temperature dependence and involvement of mitochondria permeability transition and caspase activation in damage to organotypic hippocampal slices following in vitro ischemia. J Neurochem 95:1108–1117
39. Schinzel AC, Takeuchi O, Huang Z, Fisher JK, Zhou Z, Rubens J, Hetz C, Danial NN, Moskowitz MA, Korsmeyer SJ (2005) Cyclophilin D is a component of mitochondrial permeability transition and mediates neuronal cell death after focal cerebral ischemia. Proc Natl Acad Sci U S A 102:12005–12010
40. Sullivan PG, Sebastian AH, Hall ED (2011) Therapeutic window analysis of the neuroprotective effects of cyclosporine a after traumatic brain injury. J Neurotrauma 28:311–318
41. Tanaka C, Kawai R, Rowland M (2000) Dose-dependent pharmacokinetics of cyclosporin A in rats: events in tissues. Drug Metab Dispos 28:582–589
42. Tsuji A, Tamai I, Sakata A, Tenda Y, Terasaki T (1993) Restricted transport of cyclosporin A across the blood-brain barrier by a multidrug transporter, P-glycoprotein. Biochem Pharmacol 46: 1096–1099
43. Uchino H, Elmer E, Uchino K, Li PA, He QP, Smith ML, Siesjo BK (1998) Amelioration by cyclosporin A of brain damage in transient forebrain ischemia in the rat. Brain Res 812:216–226
44. Uchino H, Elmer E, Uchino K, Lindvall O, Siesjo BK (1995) Cyclosporin A dramatically ameliorates CA1 hippocampal damage following transient forebrain ischaemia in the rat. Acta Physiol Scand 155:469–471
45. Uchino H, Minamikawa-Tachino R, Kristian T, Perkins G, Narazaki M, Siesjo BK, Shibasaki F (2002) Differential neuroprotection by cyclosporin A and FK506 following ischemia corresponds with differing abilities to inhibit calcineurin and the mitochondrial permeability transition. Neurobiol Dis 10:219–233
46. Waldmeier PC, Feldtrauer JJ, Qian T, Lemasters JJ (2002) Inhibition of the mitochondrial permeability transition by the nonimmunosuppressive cyclosporin derivative NIM811. Mol Pharmacol 62: 22–29
47. Waldmeier PC, Zimmermann K, Qian T, Tintelnot-Blomley M, Lemasters JJ (2003) Cyclophilin D as a drug target. Curr Med Chem 10:1485–1506
48. Wieckowski MR, Brdiczka D, Wojtczak L (2000) Long-chain fatty acids promote opening of the reconstituted mitochondrial permeability transition pore. FEBS Lett 484:61–64
49. Wieckowski MR, Wojtczak L (1998) Fatty acid-induced uncoupling of oxidative phosphorylation is partly due to opening of the mitochondrial permeability transition pore. FEBS Lett 423: 339–342
50. Wieloch T, Mattiasson G, Hansson M, Elmér E (2007) Mitochondrial Permeability Transition in the CNS - Composition, Regulation, and Pathophysiological Relevance. In: Gibson GE, Dienel GA (eds) Handbook of neurochemistry and molecular neurobiology. Brain energetics: integration of molecular and cellular processes, vol 5. Springer, Berlin/Heidelberg, pp 667–702
51. Yoshimoto T, Siesjo BK (1999) Posttreatment with the immunosuppressant cyclosporin A in transient focal ischemia. Brain Res 839:283–291

Cytokine Marker Measurement in Human Neuroblastoma Cells with Supersensitive and Multiplex Assay: MUSTag Technology

Ryoichi Miyashita, Li Chen, Yoshihito Morizane, Yuji Takeshita, Hidekimi Fukui, Taku Ishizaki, Kiyoshi Hatakeyama, Kiyoshige Ohseto, Futoshi Shibasaki, and Hiroyuki Uchino

Abstract *Background*: Recently, various sets of protein biomarkers have been discovered in important diseases such as cancers, brain stroke and heart attack. However, clinical validation is difficult and time-consuming by individual assays or because of very low concentrations at early stages of the diseases. We have developed assay technology through an innovative modification of the immuno-PCR method for the super-sensitive and multiplex detection of target biomarkers.

Methods: In the assay technology, each different oligo-tag simultaneously detects multiplex protein targets with extremely high-level sensitivity in a dose-dependent manner by qRT-PCR (maximum: three plexes). In this study, we measured specific secreted protein concentrations in the culture supernatant of a 24-h culture of transfected SH-SY5Y cells with MUSTag.

Results: There was a significant increase in the protein level of tumor necrosis factor (TNF)-α measured with extremely high-level sensitivity (≥10 pg/mL). Compared with negative controls, the levels of TNF-α increased from 16.9 to 28.1 pg/mL ($p = 0.011$).

Conclusion: We suggest that our assay technology might be of clinical value in treating patients with cancer, cerebral ischemia, or patients who need a prompt and predictive diagnosis for adequate treatment.

Keywords Protein biomarker • MUSTag (multiple simultaneous tag) • Immuno-PCR • Cytokine • Supersensitive

R. Miyashita (✉), Y. Takeshita, H. Fukui, T. Ishizaki, K. Hatakeyama, K. Ohseto, and H. Uchino
Department of Anesthesiology, Tokyo Medical University, 6-7-1 Nishishinjuku, Shinjuku-ku, Tokyo 160-0023, Japan
e-mail: miyamiya717@hotmail.co.jp

L. Chen, Y. Morizane, and F. Shibasaki
Department of Molecular Medical Research, Tokyo Metropolitan Institute of Medical Science, Tokyo, Japan

Introduction

Clinical proteomic research is aimed at the identification of biomarkers that can aid in diagnosing disease, monitoring treatment, and estimating prognosis [2]. Large numbers of candidate biomarkers are typically identified in the discovery phase of a proteomic screen, and many candidate biomarkers have been reported in the literature [5]. However, the conventional protein assay methods have poor sensitivity and there remain problems; it is not possible to detect infinitesimal target proteins in the blood, and one needs specialized knowledge and techniques to conduct procedures such as 2-D electrophoresis and mass analysis. With that background, based on the concept of (1) ultrasensitivity, (2) the simultaneous measurement of multiple items and (3) a rapid result, we proceeded with the development of a new base technology of diagnosis and succeeded in developing the ultrasensitive multiple simultaneous tag (MUSTag). With the MUSTag technique, each different oligo-tag simultaneously detects multiplex protein targets with extremely high-level sensitivity (more than 10 fg(10^{-15} g)/mL) in a dose-dependent manner by qRT-PCR (maximum: three plexes).

In this report, we measured specific secreted protein concentrations in the culture supernatant of a 24-h culture of transfected human neuroblastoma cell line SH-SY5Y with MUSTag. These results revealed that the MUSTag method is applicable to the cytokine marker measurement in much the same way as the conventional ELISA method. We have employed the MUSTag method for cancer, ischemic brain samples, and an even broader range of applications can be expected in the future such as early diagnosis and therapeutic effect prediction.

Materials and Methods

The Int6 gene was first identified as a frequent integration site of the mouse mammary tumor virus in preneoplastic and neoplastic mammary lesions [6], and was later characterized

Y. Katayama et al. (eds.), *Brain Edema XV*, Acta Neurochirurgica Supplement, Vol. 118,
DOI 10.1007/978-3-7091-1434-6_62, © Springer-Verlag Wien 2013

as the translation initiation factor subunit e (eIF3e) in rabbits [1]. An siRNA against Int6 (siRNA-Int6) induced several angiogenic factors via HIF2α stabilization, even under normoxic conditions [3]. Moreover, we reported that siRNA-Int6 led to promotion of neoangiogenesis in subcutaneous regions and in the tissues surrounding a wound in adult mice [4]. The siRNA-Int6 constructs were prepared according to the manufacturer's instructions. Briefly, three sequences were used: human siRNA-Int6-1, 5′-AAgAACCACAgTggTTgCA-3′; human rat common sequence int6-siRNA-2, 5′-gATAGAAATgCTTTAAgTT-3′; and a green fluorescent protein sequence or non-coding siRNA as the controls. These siRNAs were individually expressed under the control of the U6promoter in the pSilencer vector (Ambion). The human neuroblastoma cell line SH-SY5Y (ATCC) was grown in DMEM (Sigma-Aldrich) supplemented with 10 % fetal bovine serum (Hyclon), 1 % penicillin/streptomycin (Invitrogen) at 37 °C and 5 % CO_2. SH-SY5Y cells were seeded in a six-well plate at a density of 4×10^5 cells/well the day before transfection. The cells were transiently cotransfected with either 1.0 μg of siRNA-Int6, or in negative controls using either 1.5 μL of lipofectamine 2000 (Invitrogen) per well in six plates, according to the manufacturer's instructions. The transfection efficiency of these cells was observed by green fluorescent protein using fluorescence microscopy (BIOREVO BZ9000, Keyence). Cells were harvested at the indicated times after transfection.

Total RNA from transfected SH-SY5Y cells was obtained using ISOGEN (Nippon Gene). First-strand cDNAs were prepared from the total RNA extract using SuperScript VILO reverse transcriptase and random hexamer primer (Invitrogen). Quantitative reverse transcription-PCR was performed using the ABI PRISM7000 Sequence Detection System (Applied Biosystems). A standard curve for a serial dilution of β-actin was generated. The abundance of mRNA of TNF-α, transforming growth factor-beta (TGF-β), and angiopoietin-1 (Ang-1) was calculated in relation to a master reference by using standard curves.

The protein levels of TNF-α, TGF-β, and Ang-1 in the supernatant samples of SH-SY5Y-transfected cells were analyzed using the MUSTag assay (Fig. 1). Briefly, recombinant TNF-α was serially diluted fivefold from 10 ng/mL to 1.6 pg/mL; then, TGF-β were serially diluted five-fold from 10 ng/mL to 3.2 pg/mL, and Ang-1 was serially diluted five-fold from 10 ng/mL to 3.2 pg/mL as the standard curves. The supernatant samples were diluted two-fold in a sample dilution buffer. After washing, the DNA-conjugated detection antibody (MUSTag Ab) was added and incubated for 1 h. MUSTag-DNA was cut by the EcoRI restriction enzyme for 10 min; 3 μL of EcoRI-cut MUSTag solution in the wells was subjected to quantitative PCR (qPCR) analysis with the Mx3005P Real-time PCR System (Agilent Technologies) using the FastStart Universal SYBR Green Master with 6-carboxy-X-rhodamine (ROX) reference dye (Roche Diagnostics).

Data were calculated as means ± the standard deviation (SD). Statistical analyses were performed with the commercially available software Prism version 5 (GraphPad Software, San Diego, CA, USA). Comparisons of two parameters were analyzed using a two-tailed Student's *t* test. The results were considered to be statistically significant when *p* values were less than 0.05.

Results

First, we examined whether siRNA-Int6 at the mRNA level influences the expression of TNF-α, TGF-β, and Ang-1 in SH-SY5Y cells. The siRNA-Int6 mRNA resulted in significant up-regulation of TNF-α mRNA at 24 h after transfection (Fig. 2a). In contrast, there was no significant difference in the mRNA expression of TGF-β and Ang-1 between the two groups (Fig. 2b, c).

We also measured secreted protein concentrations in the culture supernatant of a 24-h culture of transfected SH-SY5Y cells with MUSTag. The levels of TNF-α significantly increased after Int6 silencing (Fig. 3a). On the other hand, TGF-β and Ang-1 levels did not change significantly (Fig. 3b, c).

The protein level of TNF-α measured with extremely high-level sensitivity was significantly increased (≥10 pg/mL). Compared with negative controls, the levels of TNF-α increased from 16.9 to 28.1 pg/mL ($p = 0.011$).

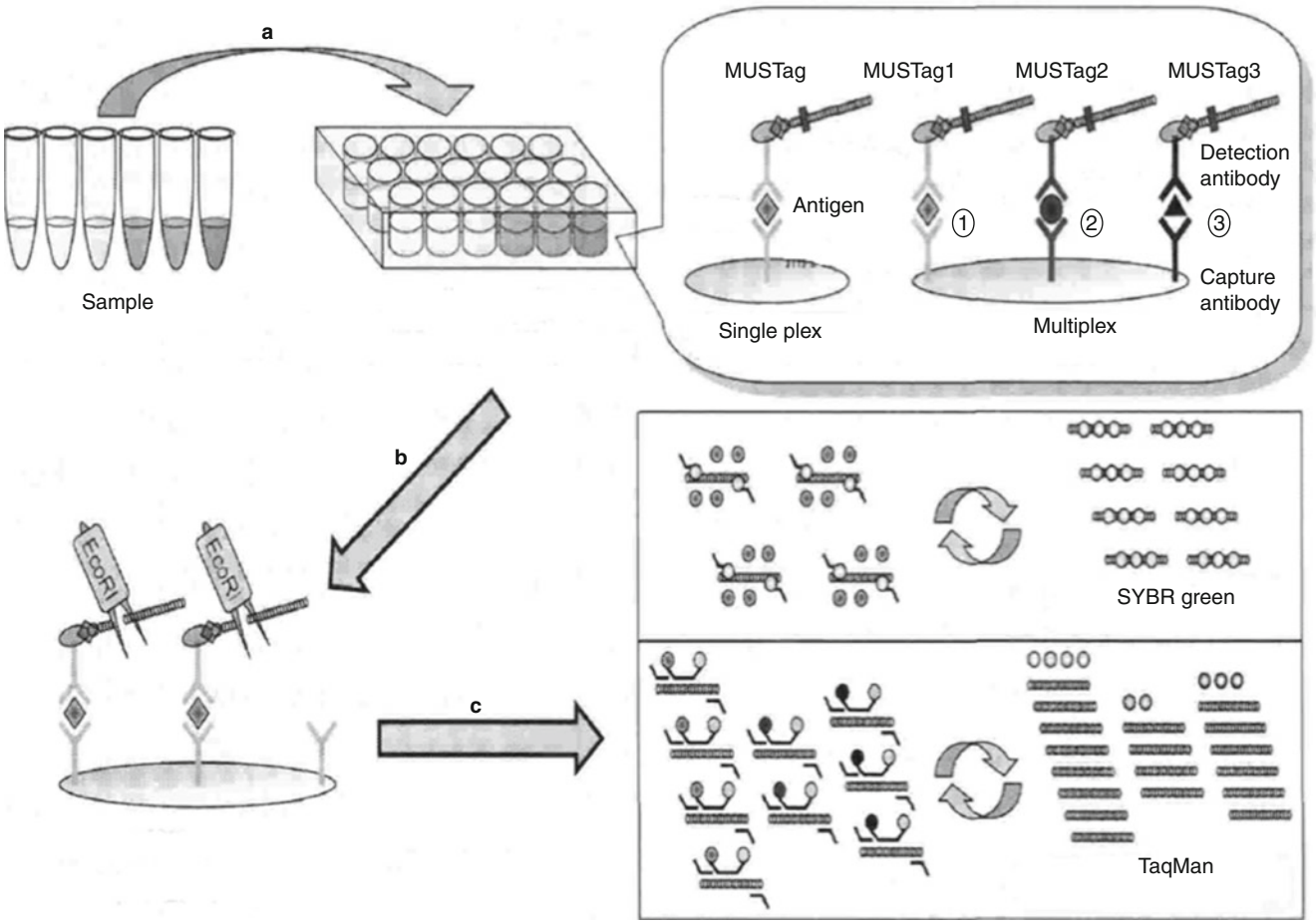

Fig. 1 Immuno-PCR (MUSTag) assays. (**a**) 96-well immunoplates were coated with each mouse monoclonal capture antibody. The plates were followed by incubation with standards and unknown samples. The DNA-conjugated detection antibody (MUSTag Ab) was added. (**b**) After washing, EcoRI in MUSTag digestion buffer was added, resulting in the DNA fragment being cut out from the detection antibody and bound to the captured antigens, and subsequently being released into the EcoRI solution. (**c**) The EcoRI-cut MUSTag solution in the wells was subjected to quantitative PCR (qPCR) analysis with a real-time PCR system using the SYBR Green or TaqMan method

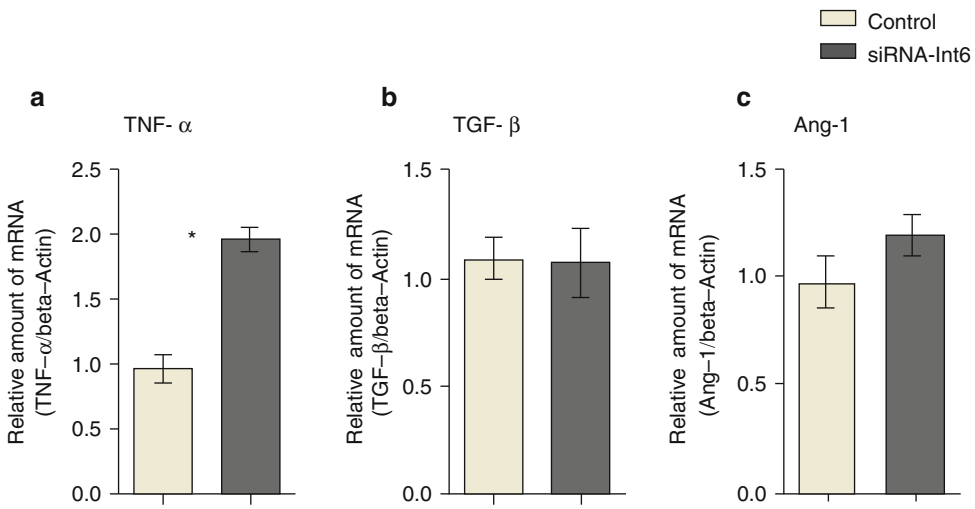

Fig. 2 Effects of the up-regulation of cytokine and angiogenic factor mRNA by siRNA-Int6 at 24 h after transfection. Data were calculated as means ± standard deviation (SD). *$p < 0.001$ vs. the control group, $n = 3$

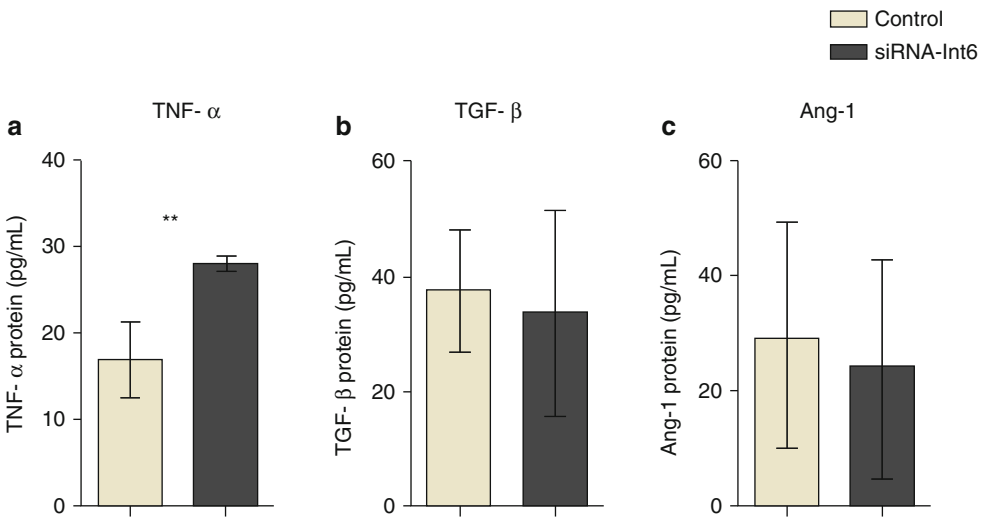

Fig. 3 Effects of up-regulation of cytokine and angiogenic factor proteins by siRNA-Int6 24 h after transfection. Data were calculated as means ± SD. $^{**}p=0.011$ vs. the control group, $n=3$

Conclusion

In our previous experiments with the MUSTag method [7, 8], sensitivity increased 110- to 740- fold for IL-6, IL-8, and EGF compared with those with the conventional ELISA. On the other hand, regarding each factor of bFGF, HGF, and VEGF, which could not be detected by ELISA, it was confirmed that the values obtained were within the measurable range.

In the present study, we demonstrated that it is possible to detect cytokine markers in human neuroblastoma cells with the measurement of pg/mL levels.

With regard to the clinical application of the MUSTag method, we have been working on the following: (1) Identifying the core protein of the hepatitis C virus by using blood serum. (2) The diagnosis of Fabry disease, a hereditary disease, by determining the quantity of α-galactosidase extracted from the blood on filter paper. (3) The early diagnosis of uterine cervix carcinoma by using the mucus of the cervix. (4) Therapeutic effect prediction of bladder carcinoma by using urine. Additionally, we have started developments such as therapeutic effect prediction and the early diagnosis of other diseases, such as Alzheimer's disease using spinal fluid, and cerebral apoplexy and emergency disease by using blood serum. These results have revealed that the MUSTag method is applicable to almost all clinical samples including body fluids and tissue specimens, in much the same way as the conventional ELISA method. However, a remaining issue is that it takes the ELISA +qRT-PCR at least 2 h or longer, and has thus not yet reached a satisfactory level of rapidity. Speeding up qRT-PCR is the most important current issue.

In conclusion, we suggest that the MUSTag method is applicable to the cytokine marker measurement of pg/mL level or below. The application of MUSTag might be of clinical value in treating patients with cancer, or ischemic brain lesions, who need a prompt and predictive diagnosis for adequate treatment.

Acknowledgments We are grateful to A. Sakurai, T. Hashimoto, and A. Endler for suggestions and critical reading of the manuscript; N. Makisaka for technical assistance; and all the members of our laboratory for their input during the course of this work.

Conflict of Interest We declare that we have no conflict of interest.

References

1. Asano K, Merrick WC, Hershey JW (1997) The translation initiation factor eIF3-p48 subunit is encoded by int-6, a site of frequent integration by the mouse mammary tumor virus genome. J Biol Chem 272(38):23477–23480
2. Banks RE, Dunn MJ, Hochstrasser DF, Sanchez JC, Blackstock W, Pappin DJ, Selby PJ (2000) Proteomics: new perspectives, new biomedical opportunities. Lancet 356(9243):1749–1756
3. Chen L, Uchida K, Endler A, Shibasaki F (2007) Mammalian tumor suppressor Int6 specifically targets hypoxia inducible factor 2 alpha for degradation by hypoxia- and pVHL-independent regulation. J Biol Chem 282(17):12707–12716
4. Chen L, Endler A, Uchida K, Horiguchi S, Morizane Y, Iijima O, Toi M, Shibasaki F (2010) Int6/eIF3e Silencing promotes functional blood vessel outgrowth and enhances wound healing by upregulating hypoxia-induced factor 2alpha expression. Circulation 122(9):910–919
5. Kingsmore SF (2006) Multiplexed protein measurement: technologies and applications of protein and antibody arrays. Nat Rev Drug Discov 5(4):310–320
6. Marchetti A, Buttitta F, Miyazaki S, Gallahan D, Smith GH, Callahan R (1995) Int-6, a highly conserved, widely expressed gene, is mutated by mouse mammary tumor virus in mammary preneoplasia. J Virol 69(3):1932–1938
7. Shibasaki F, Morizane Y, Ishikawa Y, Makisaka N, Komata Y, Chen L, Uchida K (2008) Clinical application of supersensitive and multiplex assay, MUSTag technology. Rinsho Byori 56(9):802–810
8. Shibasaki F, Morizane Y, Makisaka N (2009) Protein biomarker measurement and simple/rapid diagnostics with supersensitive and multiplex assay, MUSTag technology. Rinsho Byori 57(11):1104–1112

Cerebral Venous Thrombosis Associated with Micro-Abscesses: Case Report

Wataru Katayama, Keishi Fujita, Kuniyuki Onuma, Takao Kamezaki, Shingo Sakashita, and Shintarou Sugita

Abstract We present a case that is most likely Lemierre's syndrome. A 19-year-old man presented to us with common-cold-like symptoms, which he had had for 2 days, such as slight fever, general malaise, anorexia, sore throat, and headache. Eight days after the onset of these symptoms, he died of brain herniation due to cerebral venous thrombosis associated with micro-abscesses detected in pathological examination.

Keywords Lemierre's syndrome • Cerebral venous thrombosis • Micro-abscesses

Introduction

Many risk factors of cerebral venous thrombosis (CVT) have been reported, such as thrombophilia, malignancy, inflammatory systemic disorders, pregnancy, infection, and drug use, and the death rate of CVT at discharge is approximately 4 % [1]. In the manuscript, we report a patient who died of brain herniation due to CVT associated with micro-abscesses detected in a pathological examination.

W. Katayama, M.D. (✉), K. Fujita,
K. Onuma, and T. Kamezaki
Department of Neurosurgery,
Ibaraki Seinan Medical Center Hospital,
2190 Sakai, Sashima, Ibaraki 306-0433, Japan
e-mail: katayama_w@yahoo.co.jp

S. Sakashita and S. Sugita
Department of Pathology,
Institute of Basic Medical Science,
Graduate School of Comprehensive Human Science,
University of Tsukuba,
Tsukuba, Ibaraki, Japan

Case Report

A previously healthy 19-year-old man initially presented to our emergency room with a 2-day history of sore throat, general malaise, anorexia, headache, and slight fever. His temperature was 37.4 °C. He was diagnosed with a viral illness and discharged home with symptomatic treatment because signs of pharyngitis were seen without enlargement of the tonsils. On the next day, he presented to our neurosurgical department with persistent headache and anorexia. He denied habitual use of any drugs, although he had a medical history of bronchial asthma and of allergy to cold remedies and foods such as eggplant, cucumber, Yamato potato, and kiwi.

At the time of that second examination, his Glasgow Coma Scale (GCS) score was 15, and he had no neurological deficit. His temperature was 36.8 °C, pulse 60 bpm, blood pressure 110/60 mmHg, and pulse oximetry 99 % on room air. A stiff neck was not recognized. The rest of the physical examination was unremarkable. Blood test results revealed a C-reactive protein (CRP) level of 1.6 mg/dL and a white blood cell (WBC) count of 10,600/μL. The rest of the blood test results, including renal and liver function, were unremarkable. His chest radiograph and electrocardiograph findings were normal. No abnormal findings were found on computed tomography (CT) of the head. We diagnosed his illness as a viral infection and continued symptomatic treatment after his hospitalization.

On the next day of his hospitalization, he became febrile (38.5 °C) with neurological deterioration. His GCS score was nine points: scores for visual, verbal, and motor functions were one, two, and six points respectively. Repeated CT of the head showed a low-density lesion, including a small high-density area indicating hemorrhage in the left parietal lobe (Fig. 1a). CT with contrast medium showed cortical venous congestion indicating cerebral venous thrombosis (CVT) (Fig. 1b). Blood test results revealed a C-reactive protein (CRP) level of 5.4 mg/dL and a white blood cell (WBC) count of 16,800/μL. A lumbar puncture was performed, revealing that the cerebrospinal

Y. Katayama et al. (eds.), *Brain Edema XV*, Acta Neurochirurgica Supplement, Vol. 118,
DOI 10.1007/978-3-7091-1434-6_63, © Springer-Verlag Wien 2013

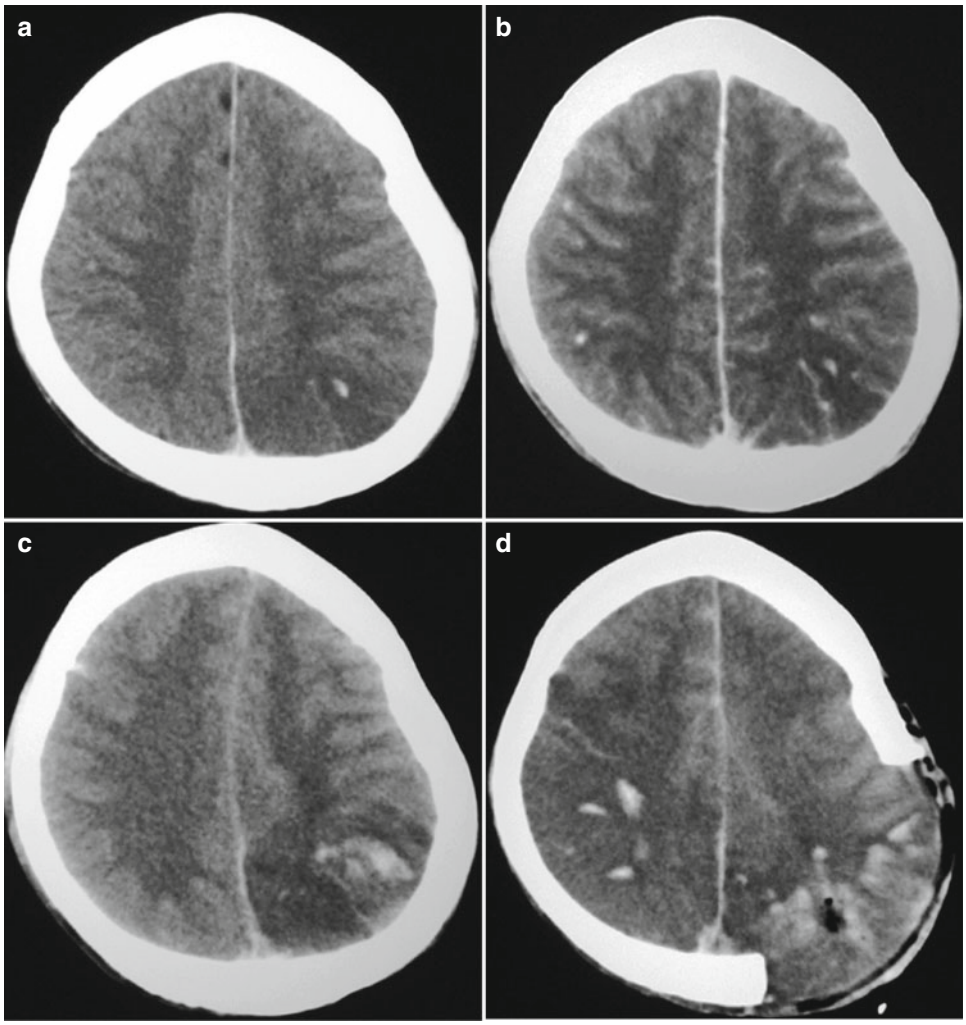

Fig. 1 (**a**) Repeated CT of the head showing a low-density lesion including a small high-density area indicating hemorrhage in the left parietal lobe. (**b**) CT with contrast medium showing cortical venous congestion indicating cerebral venous thrombosis. (**c**) Repeated CT showing midline shift due to the progression of brain edema and hemorrhage. (**d**) Repeated CT showing the swelling of the right cerebral hemisphere

fluid (CSF) contained 14 WBCs/μL (five neutrophils), total protein of 185 mg/dL, and glucose of 75 mg/dL. We made a diagnosis of CVT caused by viral meningitis and started administration of acyclovir, steroid, and hypertonic diuretic. We did not start anticoagulant therapy because the patient's prothrombin time was 17.1 s (normal values, 11.0–12.5 s) and we had found a hemorrhage in the cerebral lesion. CSF culture later proved to be negative. Repeated CT, which was performed 12 h later because anisocoria of the enlarged left pupil had been found, showed impending brain herniation due to the progression of the brain edema and hemorrhage (Fig. 1c). Emergency external decompression and evacuation of hematoma and damaged brain were performed. The brain was disrupted by the hematoma and swelled up remarkably owing to the congestion of the cortical veins occluded with thrombus (Fig. 2). Although the anisocoria disappeared immediately after the surgery, his right pupil was enlarged 5 h later, because of the swelling of the right cerebral hemisphere (Fig. 1d). We recommended a contralateral external decompression to save his life, even though his functional prognosis would be poor, but his family did not

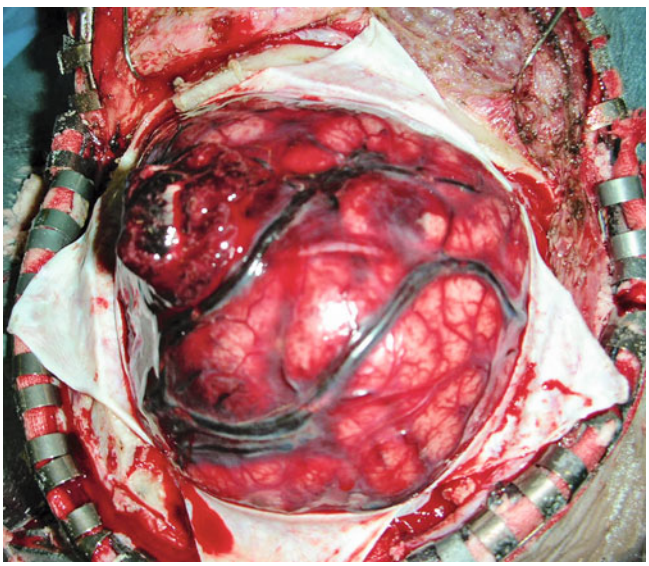

Fig. 2 Perioperative photograph showing hematoma disrupting the brain and a remarkably swollen brain due to congestion of the cortical veins occluded with thrombus

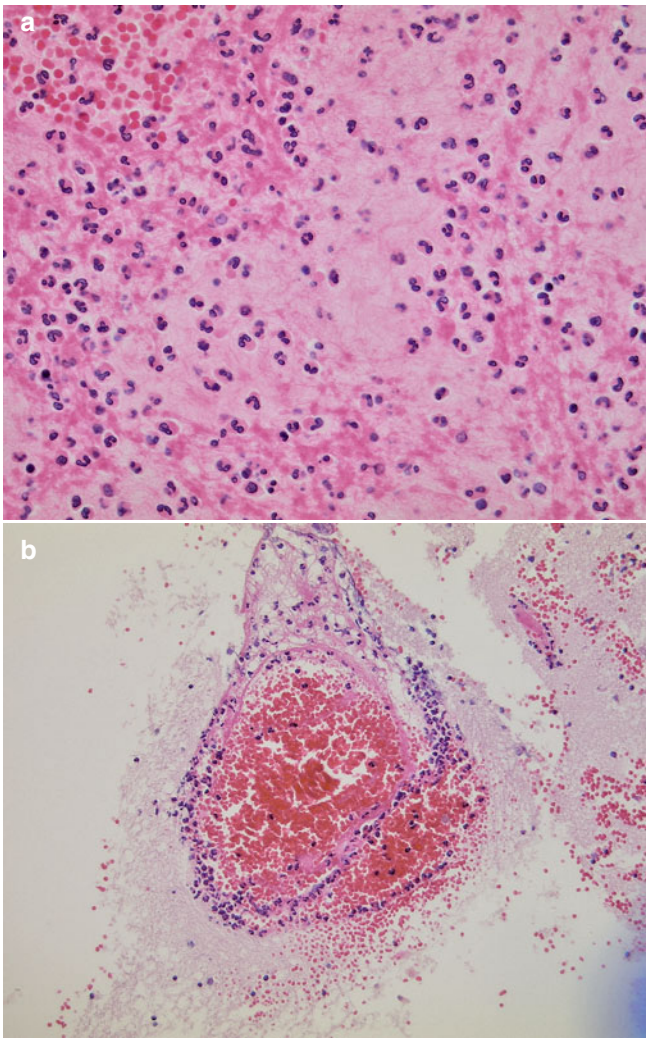

Fig. 3 Photomicrographs of a brain sample. (**a**) Hematoxylin and eosin staining (×400) showing a large number of neutrophils in the hematoma. (**b**) Hematoxylin and eosin staining (×100) showing infiltration of neutrophils into the venous walls and Virchow–Robin spaces, which were considered micro-abscesses

grant permission for this. He died of brain herniation on the seventh hospital day in spite of life support.

The surgical specimens were examined pathologically. A large number of neutrophils were found in the hematoma (Fig. 3a) and infiltration of neutrophils into the venous walls and Virchow–Robin spaces, which were considered micro-abscesses, was found. Eosinophils were not found, and fibrinoid necrosis of the venous walls was unremarkable (Fig. 3b).

Conclusion

Infiltration of neutrophils into the vessel walls suggested anti-neutrophil cytoplasmic antibody (ANCA)-associated vasculitis or bacterial vasculitis.

In the present case, however, renal dysfunction, which suggests ANCA-associated nephritis, was negative and fibrinoid necrosis, which is a characteristic of ANCA-associated vasculitides, was not found pathologically [2].

Sinusitis, otitis media, and mastoiditis can be the primary sources of intracranial bacterial infection [3, 4]. In the present case, however, there were no findings of sinusitis, otitis media, or mastoiditis in CT on admission.

Infiltration of neutrophils into Virchow–Robin spaces indicated bacterial meningitis [5]. However, a stiff neck was not recognized, and the CSF test and culture were negative. In addition, a large number of neutrophils were found in the hematoma, whereas they were not seen in the cerebral tissue. This suggested that neutrophils infiltrated the Virchow–Robin spaces from veins.

Lemierre's syndrome, first reported by Dr. Andre Lemierre in 1936, is caused by an acute oropharyngeal infection with secondary septic thrombophlebitis of the internal jugular vein (IJV) and frequent metastatic infections such as abscesses. The disease progresses in several stages. The first stage is the primary infection, which is usually pharyngitis. This is followed by local invasion of the lateral pharyngeal space, resulting in septic thrombophlebitis of the IJV, and finally the occurrence of metastatic complications. A sore throat is the most common symptom during the primary infection. During invasion of the lateral pharyngeal space, a swollen and/or tender neck is the most common finding [6]. In addition to the lungs, the brain has been reported to be a site of metastatic infection [7]. Lemierre's syndrome occurs most often in adolescents and young adults (aged 15–30 years), and *Fusobacterium* pharyngitis occurs predominantly in the same age group [8].

The advent of beta-lactam antibiotics has reduced the incidence of Lemierre's syndrome to 0.8–1.5 cases per one million persons/year, leading it to be called a "forgotten disease" [9], although mortality is still estimated at 8–15 %, despite antibiotic therapy [10]. In the present case, a sore throat was a typical initial symptom that is found in 82.5 % of patients, but a swollen and/or tender neck, which was the most common finding (52.2 % of patients) during invasion of the lateral pharyngeal space and IJV septic thrombophlebitis, was absent [6]. However, the pathological findings mentioned above indicated hematogenous metastatic infection of some kind of bacteria, which were not identified in this case.

To our knowledge, the literature shows 15 cases in which the interval from initial symptoms to central nervous system complications were described [11–25]. The average interval was 10 days, while the interval from sore throat to neurological deterioration in our patient was only 3 days. Although Lemierre's syndrome has been called a "forgotten disease" in the antibiotic era, it remains a life-threatening disease especially since the 1990s, because of restrictions on the use of antibiotics for viral pharyngitis [26].

Conflict of Interest We declare that we have no conflict of interest.

References

1. Ferro JM, Canhão P, Stam J, Bousser MG, Barinagarrementeria F (2004) Prognosis of cerebral vein and dural sinus thrombosis: results of the Internal Study on Cerebral Vein and Dural Sinus Thrombosis (ISCVT). Stroke 35:664–670
2. Calabrese LH, Molloy ES, Duna GF (2009) Antineutrophil cytoplasmic antibody-associated vasculitis. In: Firestein GS, Budd RC, Harris ED Jr, McInnes IB, Ruddy S, Sergent JS (eds) Kelley's textbook of rheumatology, 8th edn. Saunders/Elsevier, Philadelphia, pp 1429–1451
3. Ferris EJ, Levine HL (1973) Cerebral arteritis: classification. Radiology 109:327–341
4. Gerber O, Roque C, Coyle PK (1997) Vasculitis owing to infection. Neurol Clin 15:903–925
5. Gordon M, Parmar H, Ibrahim M (2009) Spread of infection to Virchow-Robin spaces in a patient with Streptococcus pneumonia meningitis. J Comput Assist Tomogr 33:562–564
6. Chirinos JA, Lichtstein DM, Garcia J, Tamariz LJ (2002) The evolution of Lemierre syndrome: report of 2 cases and review of the literature. Medicine 81:458–465
7. Karkos PD, Asrani S, Karkos CD, Leong SC, Theochari EG, Alexopoulou TD, Assimakopoulos AD (2009) Lemierre's syndrome: a systematic review. Laryngoscope 119:1552–1559
8. Centor RM (2009) Expand the pharyngitis paradigm for adolescents and young adults. Ann Intern Med 151:812–815
9. Weesner CL, Cisek JE (1993) Lemierre syndrome: the forgotten disease. Ann Emerg Med 22:256–258
10. Aouad R, Melkane A, Rassi S (2010) Lemierre syndrome: unusual cause and presentation. Pediatr Emerg Care 26:376–377
11. Vogel LC, Boyer KM (1980) Metastatic complications of Fusobacterium necrophorum sepsis. Two cases of Lemierre's postanginal septicemia. Am J Dis Child 134:356–358
12. Rathore MH, Barton LL, Dunkle LM (1990) The spectrum of fusobacterial infections in children. Pediatr Infect Dis J 9: 505–508
13. Meis JF, Polder TW, van de Kar P, Hoogkamp-Korstanje JA (1993) Multiple brain abscesses and bacteremia in a child due to Fusobacterium necrophorum. Infection 21:174–176
14. Larsen PD, Chartrand SA, Adickes ED (1997) Fusobacterium necrophorum meningitis associated with cerebral vessel thrombosis. Pediatr Infect Dis J 16:330–331
15. Agarwal R, Arunachalam PS, Bosman DA (2000) Lemierre's syndrome: a complication of acute oropharyngitis. J Laryngol Otol 114:545–547
16. Maalikjy Akkawi N, Borroni B, Magoni M, Vignolo LA, Padovani A (2001) Lemierre's syndrome complicated by carotid thrombosis. Neurol Sci 22:403–404
17. Bentham JR, Pollard AJ, Milford CA, Anslow P, Pike MG (2004) Cerebral infarct and meningitis secondary to Lemierre's syndrome. Pediatr Neurol 30:281–283
18. Aliyu SH, Yong PF, Newport MJ, Zhang H, Marriott RK, Curran MD, Ludlam H (2005) Molecular diagnosis of Fusobacterium necrophorum infection (Lemierre's syndrome). Eur J Clin Microbiol Infect Dis 24:226–229
19. Shibasaki Warabi Y, Yoshikawa H, Idezuka J, Yamazaki M, Onishi Y (2005) Cerebral infarctions and brain abscess due to Lemierre syndrome. Intern Med 44:653–656
20. Jones C, Siva TM, Seymour FK, O'Reilly BJ (2006) Lemierre's syndrome presenting with peritonsillar abscess and VIth cranial nerve palsy. J Laryngol Otol 120:502–504
21. Westhout F, Hasso A, Jalili M, Afghani B, Armstrong W, Nwagwu C, Ackerman LL (2007) Lemierre syndrome complicated by cavernous sinus thrombosis, the development of subdural empyemas, and internal carotid artery narrowing without cerebral infarction. Case report. J Neurosurg 106(1 Suppl):53–56
22. Shivashankar GH, Murukesh N, Varma MP, Sharif IM, Glynn G (2008) Infection by Panton-Valentine leukocidin-producing Staphylococcus aureus clinically mimicking Lemierre's syndrome. J Med Microbiol 57:118–120
23. van Dijk EJ, van Swieten JC, Koudstaal PJ (2008) Meningitis, cranial nerve palsies and bilateral cerebral infarcts: a neurological variant of Lemierre's syndrome. J Neurol 255:1588–1589
24. Goyal MK, Kumar G, Burger R (2009) Necrobacillosis resulting in isolated carotid thrombosis and massive stroke: a unique Lemierre variant? J Neurol Sci 287(1–2):108–110
25. Aijohaney A, McCarthy A (2010) Lemierre's syndrome with paradoxical emboli. Intern Med 49:1433–1436
26. Ramirez S, Hild TG, Rudolph CN, Sty JR, Kepl SC, Havens P, Henrickson K, Chusid MJ (2003) Increased diagnosis of Lemierre syndrome and other Fusobacterium necrophorum infections at a Children's Hospital. Pediatrics 112:380–385

Author Index

Y. Katayama et al. (eds.), *Brain Edema XV*, Acta Neurochirurgica Supplement, Vol. 118,
DOI 10.1007/978-3-7091-1434-6, © Springer-Verlag Wien 2013

Subject Index

T